1. Workshop on:

New opportunities and challenges with DANCE

February 2-4, 2004, Santa Fe, NM

Editors: R. Reifarth, T.A. Bredeweg, J.L. Ullmann, D.J. Vieira

Introduction

The Detector for Advanced Neutron Capture Experiments (DANCE), a 160-element BaF_2 detector array called DANCE, was recently commissioned at the Manuel Lujan Center at the Los Alamos National Laboratory. DANCE provides a unique capability to measure low-energy neutron capture cross sections of radioactive targets as small as ~1 mg (up to ~1 Ci). In this workshop new opportunities and challenges made possible with DANCE were explored.

The workshop was held at the La Fonda hotel in Santa Fe, NM. 51 participants contributed with talks and discussions. A list of participants including their affiliation and e-mail address is included at the end of this introduction. A summary of the two discussion sessions on astrophysics and fission at DANCE follows. The last part consists of copies of all talks held at the workshop. An extensive system of bookmarks is included in the electronic version of this document.

Astrophysics

One of the most interesting nuclear physics challenges is obtaining a detailed understanding of the nucleosynthesis processes of the elements. Knowledge about the stellar sites, and how they are governed by stellar evolution and cosmology are a crucial in understanding the overall picture. Information on reaction rates for neutron and charged-particle induced reactions have a direct impact on existing stellar models. Except for the stable isotopes, very few neutron-induced reactions in the astrophysically interesting energy range of 1 to 300 keV have been measured to date. DANCE measurements on radioactive isotopes will provide many of the missing key reactions that are needed to understand the nucleosynthesis of the heavy elements.
The slow neutron capture process ("s-process"), which provides about half of the nuclides with mass greater than iron, branches at radioactive isotopes with moderate half-lives, on the order of days to years. The competition between neutron capture and beta decay at the s-process branch point isotopes depends strongly on the dynamic properties at the stellar site. In particular information about the stellar temperature and neutron density as well as time scales can be gained, provided the neutron capture cross sections of the radioactive isotopes are known for the whole energy range of interest. Modern stellar models can calculate the production of isotopes around the s-process branch points, but they strongly rely on laboratory data to constrain the assumptions of these models. Precise measurements of these cross sections have been desired for many years, and many of them can now be carried out using DANCE.

Measurements using the DANCE array can also improve the knowledge of more exotic or less understood stellar nucleosynthesis processes. These are for instance (n,γ) measurements at light nuclei – motivated by the possibility of a "light rapid neutron capture process" and on heavy, proton-rich isotopes – investigating the stellar environment of the "(rapid) proton capture process". Furthermore, the investigation of (n,α) properties with DANCE allows to determine valuable nuclear structure data, like spin assignments of resonances etc. Those information are important for the extrapolation of measured data to the astrophysical region of interest.

Fission-Gamma Studies Session

As one moves up to the isotopes of the actinide elements, low-energy neutron-induced fission competes with neutron capture. The competition between these two channels and its dependence on incident neutron energy is of great interest for Stockpile Stewardship and nuclear attribution as well as for nuclear astrophysics, advanced reactor design and the advanced fuel cycle initiative. Measurements on ^{235}U already performed at DANCE have shown that we can partially resolved capture from fission events based on total photon calorimetry (i.e. total γ energy and γ multiplicity), but not completely. To completely separate these two processes, the idea of adding a fission-tagging detector to the DANCE array was explored.
In several talks we heard about different fission experiments using detector systems ranging from solar cells and gas counters to thin plastic scintillators. If DANCE can tolerate some increase in background, one may consider placing the fission detector directly into the neutron beam. In this case the actinide target may be incorporated into the fission detector system such that nearly 2π coverage is obtained. With a suitably thin actinide target backing one may approach 4π coverage. However, most of these actinide targets are highly α active (i.e. 1 mg of ^{239}Pu has an α disintegration rate of 2 MBq). Consequently such an in-beam fission-tagging detector must be highly neutron insensitive, distinguish between α and fission events, and be capable of tolerating high alpha rates. Solar cells and gas avalanche detectors naturally come to mind. Using such a simple fission-tagging detector with DANCE we could determine capture/fission cross sections, total photon energy release per fission, total γ multiplicity per fission, and average γ-ray energies as a function of incident neutron energy. This information already goes a long way to solving our needs. With a more sophisticated fission detector array located out of the beam, we could determine additional information such as fission fragment kinetic energies, fission fragment masses and fission fragment angular distributions. An active discussion of the pros and cons of different detector system and space constraints associated with DANCE ensued.

List of participants

LASTNAME	**FIRST**	**ORGANIZATION**	**EMAIL**
Agvaanluvsan	Undraa	North Carolina State University / LLNL	agvaanluvsan1@llnl.gov
Arbanas	Goran	Oak Ridge Natl. Lab.	arbanasg@ornl.gov

Bacrania	Minesh	University of Washington	minesh@u.washington.edu
Becker	John	Lawrence Livermore Natl. Lab.	jabecker@llnl.gov
Bernstein	Lee	Lawrence Livermore Natl. Lab.	bernstein2@llnl.gov
Bredeweg	Todd	Los Alamos Natl. Lab.	toddb@lanl.gov
Chadwick	Mark	Los Alamos Natl. Lab.	mbchadwick@lanl.gov
Danon	Yaron	Rensselaer Polytechnic Inst.	danony@rip.edu
Dietrich	Frank	Lawrence Livermore Natl. Lab.	dietrich2@llnl.gov
Drake	Darrell		ddrake@cybermesa.com
Esch	Ernst	Los Alamos Natl. Lab.	ernst@lanl.gov
Ethvignot	Thierry	CEA	thierry.ethvignot@cea.fr
Fowler	Malcolm	LANL/Summer Associates	malcolm-fowler@zianet.com
Gallino	Roberto	Universita' di Torino	gallino@ph.unito.it
Greife	Uwe	Colorado School of Mines	ugreife@mines.edu
Guber	Klaus	ORNL	guberkh@ornl.gov
Haight	Robert	Los Alamos Natl. Lab.	haight@lanl.gov
Heger	Alexander	Los Alamos Natl. Lab.	aheger@lanl.gov
Heil	Michael	Forschungszentrum Karlsruhe	michael.heil@ik.fzk.de
Herwig	Falk	Los Alamos Natl. Lab.	fherwig@lanl.gov
Hill	Tony	Los Alamos Natl. Lab.	tony.hill@lanl.gov
Hoffman	Darleane	Lawrence Berkeley Natl. Lab.	dchoffman@lbl.gov
Kaeppeler	Franz	Forschungszentrum Karlsruhe, IK	franz.kaeppeler@ik.fzk.de
Kawano	Toshihiko	Los Alamos Natl. Lab.	kawano@lanl.gov
Kerman	Arthur	MIT	kerman@lns.mit.edu
Koehler	Paul	Oak Ridge Natl. Lab.	koehlerpe@ornl.gov
Kronenberg	Andreas	Los Alamos Natl. Lab.	kronenberg@lanl.gov
Lemaire	Sebastien	Los Alamos Natl. Lab.	lemaire@lanl.gov
Lugaro	Maria	University of Cambridge	mal@ast.cam.ac.uk
Lynn	Eric		
Mengoni	Alberto	CERN	alberto.mengoni@cern.ch
Mihaila	Bogdan	Los Alamos Natl. Lab.	bmihaila@lanl.gov
Mitchell	Gary	NC State University	mitchell@tnul.duke.edu
Moller	Peter	Los Alamos Natl. Lab.	moller@lanl.gov
Nelson	Ron	Los Alamos Natl. Lab.	rnelson@lanl.gov
O'Donnell	John	Los Alamos Natl. Lab.	odonnell@lanl.gov
Paul	Michael	Racah Inst. of Physics	paul@vms.huji.ac.il
Petit	Michael	CEA	michael.petit@cea.fr
Pignatari	Marco	University of Torino	cygno1@yahoo.it
Reifarth	Rene	Los Alamos Natl. Lab.	reifarth@lanl.gov
Rundberg	Robert	Los Alamos Natl. Lab.	rundberg@lanl.gov
Sarantites	Demetrios	Washington University	dgs@wuchem.wustl.edu
Schwantes	Jon	LBL/University of California	jmschwantes@lbl.gov
Talou	Patrick	Los Alamos Natl. Lab.	talou@lanl.gov
Ullmann	John	Los Alamos Natl. Lab.	ullmann@lanl.gov
Vieira	David	Los Alamos Natl. Lab.	vieira@lanl.gov
Wender	Steve	Los Alamos Natl. Lab.	wender@lanl.gov
Wiescher	Michael	University of Notre Dame	wiescher.1@nd.edu
Wilhelmy	Jerry	Los Alamos Natl. Lab.	j_wilhelmy@lanl.gov
Wouters	Jan	Los Alamos Natl. Lab.	jwouters@lanl.gov
Zinner	Ernst	Washington University	ekz@wustl.edu

Summary of the discussion sessions

Astrophysics

The discussions on astrophysics were focused on the availability of radioactive samples. The results are summarized in the table below.

Isotope	amount	Institute	Contact	Production	Comments
Samples available or in production					
^{10}Be	?	LLNL / ORNL	D. Goosman / P. Koehler		Not available as of Feb. 2003
^{79}Se	~10 mg	ORNL / LANL	P. Koehler / R. Reifarth	long lived fission	Needs to be prepared
^{81}Kr	~10 mg	LLNL	L. Bernstein	^{81}Br(p,n)	Needs to be prepared
^{85}Kr	0.4 mg / 0.18 Ci	LLNL	L. Bernstein		High activity: 26 10^6 γ/s
^{93}Zn	2 g	FZK	F. Kaeppeler		
^{99}Tc	~10 mg	ORNL / LANL	P. Koehler / R. Reifarth	long lived fission	Needs to be prepared
^{107}Pd	?	ORNL	R. Macklin/ P. Koehler ?		R. Macklin, Nucl. Sci. Eng. **89**, 79 (1985).
^{147}Pm	~ 1 mg	LANL	R. Reifarth / R. Rundberg	n-irradation	Needs to be prepared
^{151}Sm	0.5 mg	LANL	R. Reifarth / R. Rundberg	n-irradation	
^{151}Sm	~ 200 mg	ORNL			
^{155}Eu	~ 1mg	LANL	R. Reifarth / R. Rundberg	n-irradation	Needs to be prepared
^{171}Tm	~ 1mg	LANL	R. Reifarth / R. Rundberg	n-irradation	Needs to be prepared
Ideas for future projects					
^{7}Be				???, maybe TRIUMF	Poss. Detection of (n,γ): ^{7}Be(n,γ)^{8}Be->2α
^{179}Ta				^{179}Hf(p,n)	
^{185}W				???, maybe ^{184}W(n,g)	
^{204}Tl				^{204}Hg(p,n)	
^{205}Pb				^{205}Tl(p,n)	

A promising new facility is the **I**sotope **P**roduction **F**acility at LANL, which is able to produce isotopes via (p,xn) reactions. The following information are kindly provided by Jerry Wilhelmy:

IPF Production Capabilities

The IPF will provide up to 250 μA of 100 MeV protons. Three irradiation positions are available along the flight path. Each will be limited to effective target thicknesses that degrade the beam energy by ~ 20 MeV. The proton energy range and major reactions for the target positions are:

Position	Proton Energy Range	Major Reaction Channel
1	70-90 MeV	(p,5-8n)
2	45-65 MeV	(p,3-5n)
3	10-30 MeV	(p,1-3n)

The (p,xn) reactions, in general, produce neutron deficient isotopes that will decay by β^+/EC. It is often possible to irradiate targets that are of higher Z than the production isotope desired and rely on decays through the β^+/EC chain to produce isotopically enriched production materials.

Fission at DANCE Discussion

The Fission at DANCE discussion session focused on the development of a fission-tagging detector, for the study of fissionable actinide targets, that could be incorporated into the DANCE array. An obvious first consideration for such a detector is that it not introduce too much additional capture/scatter background. A second consideration is the limited space available inside the DANCE array. Finally, the detector must tolerate and distinguish between fission and α events since the actinide targets generally have high α activity (i.e. 1 mg of ^{239}Pu has an α disintegration rate of 2 MBq).
With these two criteria in mind, the discussion centered on two fundamentally different design concepts. The first concept is a modification of two detector designs that have already been used with great success in other experiments at LANSCE, namely a solar cell [1] or a fission gas counter [2]. Both involve deposition of the target material directly onto an active component of the detector. The resulting drawback for both designs is that the detector must be placed directly in the neutron flight path. This would lead to an

increase in the capture/scatter background, which may be unacceptable. The advantages of these two designs are their simplicity as well as providing excellent, nearly 2π coverage with a minimum of equipment (with suitably thin detector components the coverage could approach 4π). Also, solar cells do not register α background. Gas avalanche counters can also be operated in a mode such that alphas do not generate an appreciable signal while fission events do. However, a gas ionization or proportional counter might suffer from charge build-up that could eventually overwhelm the counter.
The second design concept was for an external (i.e. out of the neutron flight path) mini-array placed a small distance away from the target. Several basic detector types were discussed for this array, including gas ionization, Si (active or passive) and thin plastic scintillators [3,4]. The advantages here are that no additional material is placed in the flight path and the resulting increased flexibility might allow for more than a simple fission trigger. Drawbacks would include increased size/complexity (both in terms of equipment and signal processing) and probably reduced angular coverage. The design of such a mini-array would also be hindered by the space limitations inside the DANCE array. In most cases the 6LiH neutron absorber would need to be removed or significantly modified.

Several action items were identified at the end of the discussion session:

1. A solar cell detector should be tested in DANCE before the end of the current LANSCE run cycle. The test would focus on evaluating detector performance and quantifying the added background.
2. A gas counter design that would fit within the existing beam line was discussed as the possible step. Further discussions are needed to decide what design is best. A 252Cf source should be obtained for off-line testing.
3. Finally, an out-of-beam fission detector needs to be further explored for the long term.

[1] T. Ethvignot, et.al., Nucl. Instr. and Meth. A490, 559 (2002)
[2] S.A. Wender, et.al., Nucl. Instr. and Meth. A336, 226 (1993)
[3] W. Reviol, et.al., Phys. Rev. C68, 054317 (2003)
[4] W. Reviol, et.al., submitted to Nucl. Instr. and Meth. A

Contribution by

John L. Ullmann

Los Alamos National Laboratory

ullmann@lanl.gov

24 pages

Details

- Workshop Format
  - Questions and Discussion after each talk
- Proceedings
  - Web-based, copy of slides
- Discussion on Tuesday
  - What are the outstanding problems?
  - How can they be addressed
  - How can DANCE be of use?
- Tour of LANSCE: Wed, 10 AM
  - Sign up!
- Computer/email Access

Detector for Advanced Neutron Capture Experiments (DANCE)

John Ullmann
LANSCE-3
Los Alamos National Laboratory

LANSCE-3 (LANL)
R.C. Haight
R. Reifarth
J.M. O'Donnell
E-I. Esch
L. Hunt

C-INC (LANL)
R.S. Rundberg
T. Bredeweg
J.B. Wilhelmy
M.M. Fowler
E.P. Chamberlin
D.J. Vieira
A. Kronenberg

T-DO (LANL):
D.D. Strottman

IM-8(LANL):
J.M. Wouters

Col. Sc. Mines
U. Greife
R. Hatarik
A. Alpizar

Forschungszentrum Karlsruhe
F. Kaeppeler
M. Heil

LANSCE
Los Alamos Neutron Science Center

Los Alamos Neutron Science Center *(LANSCE)*

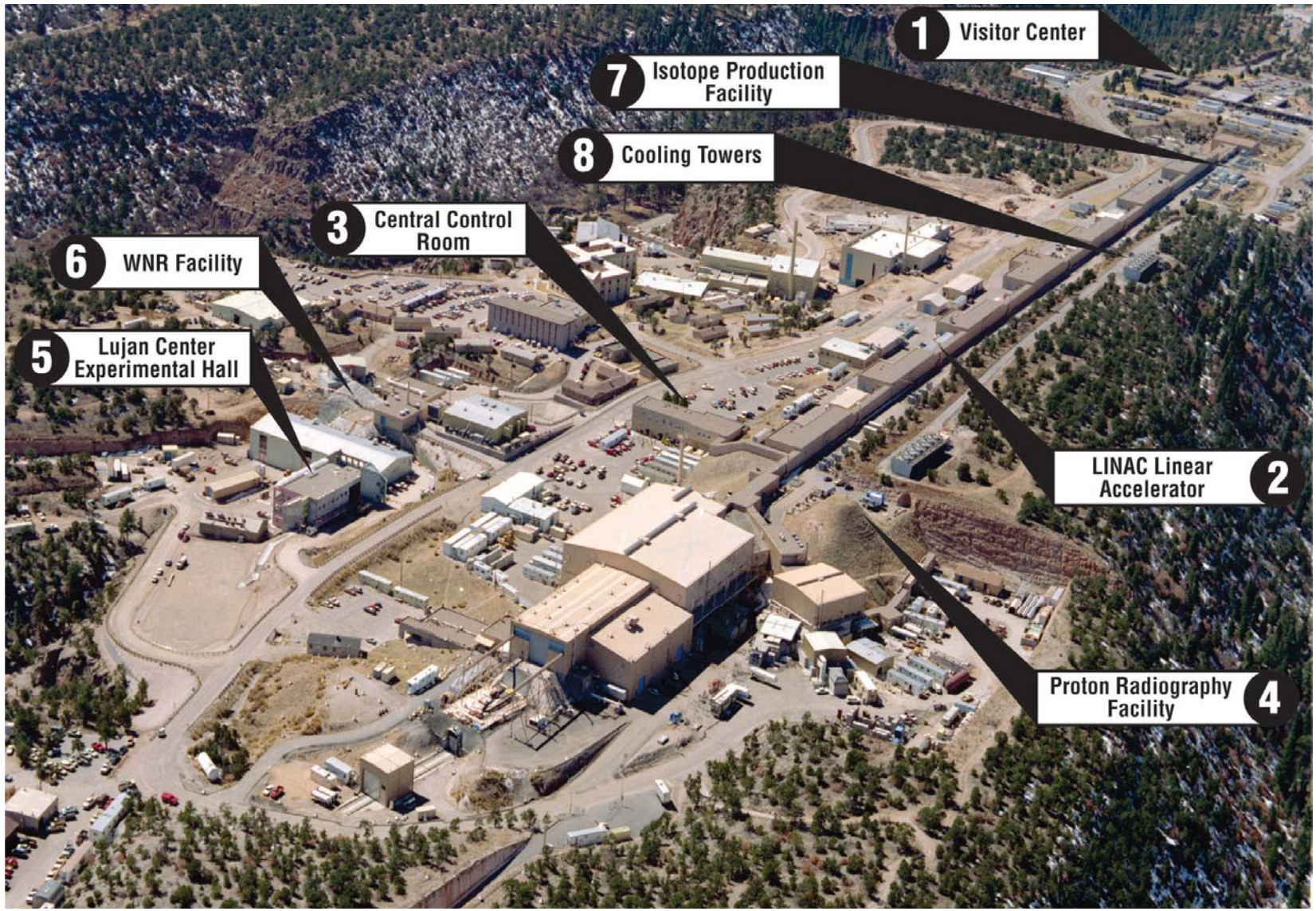

DANCE is located on Flight Path 14 at the Lujan Center.

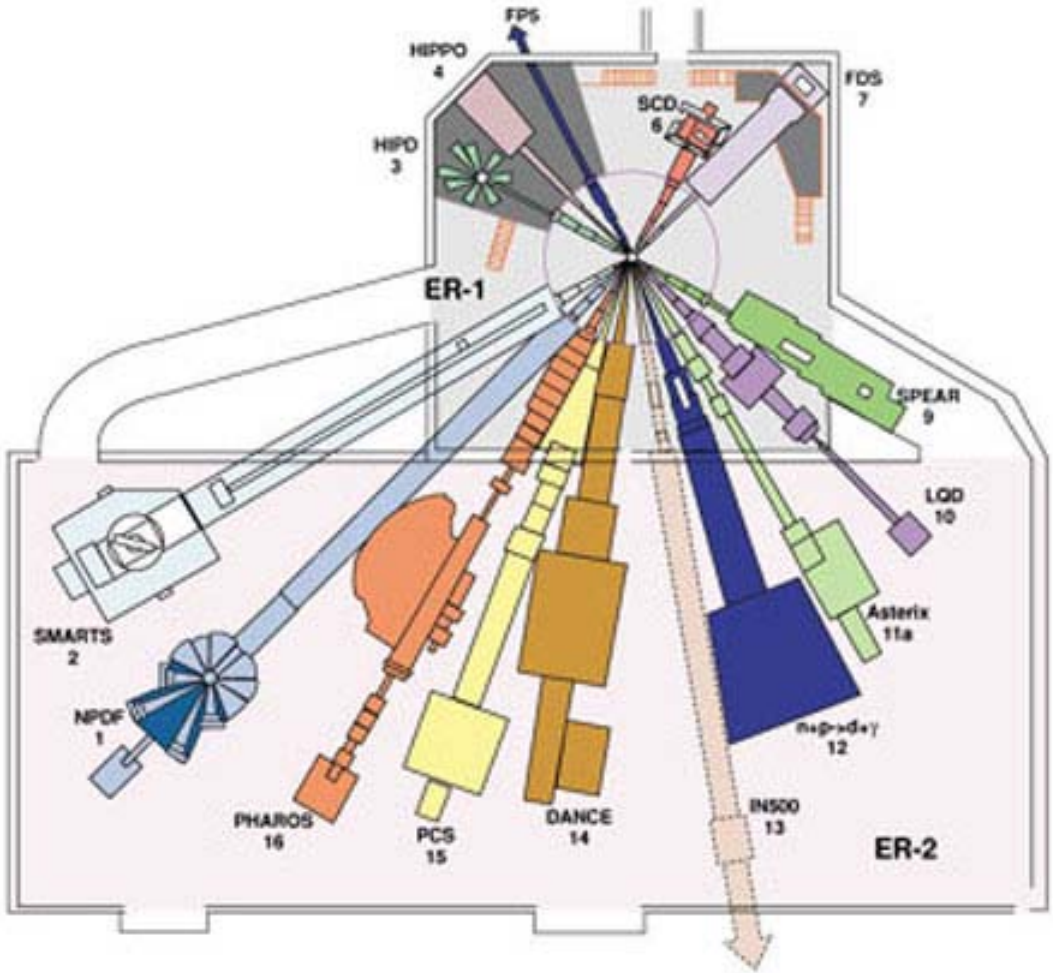

FP 14 views the second-tier coupled water moderator.

DANCE / Flight Path 14 at the Lujan Center

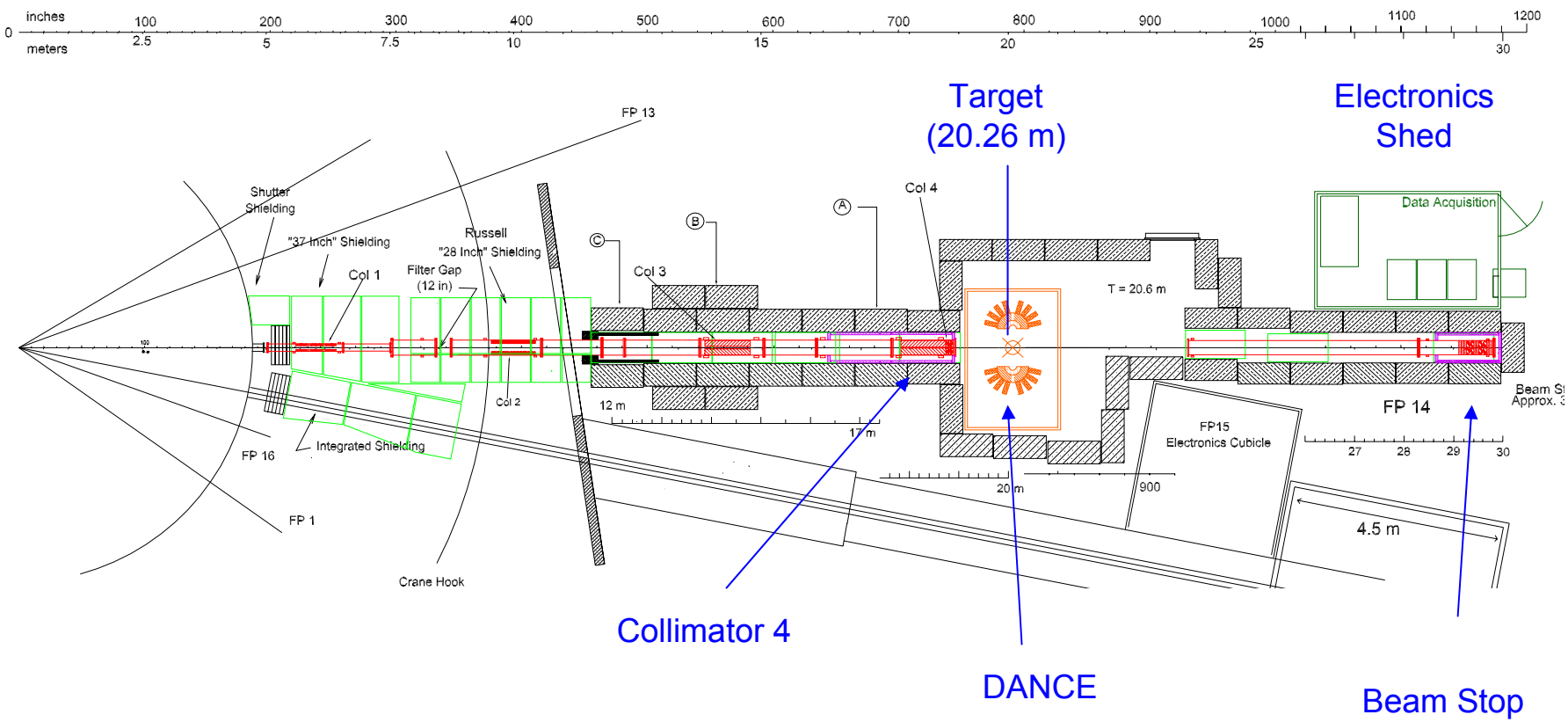

The DANCE barium fluoride array

- Calorimeter
  - identifies capture by total energy in gamma rays
- Less sensitive to neutrons
  - Scattering cross section > capture in our energy range of interest (1 keV < En < 100 keV)
- Fast
  - 1 Ci is 37 decays/nanosecond
  - 10^{12} MeV/sec (?) of radioactive decay (30 Ci)
- Segmented

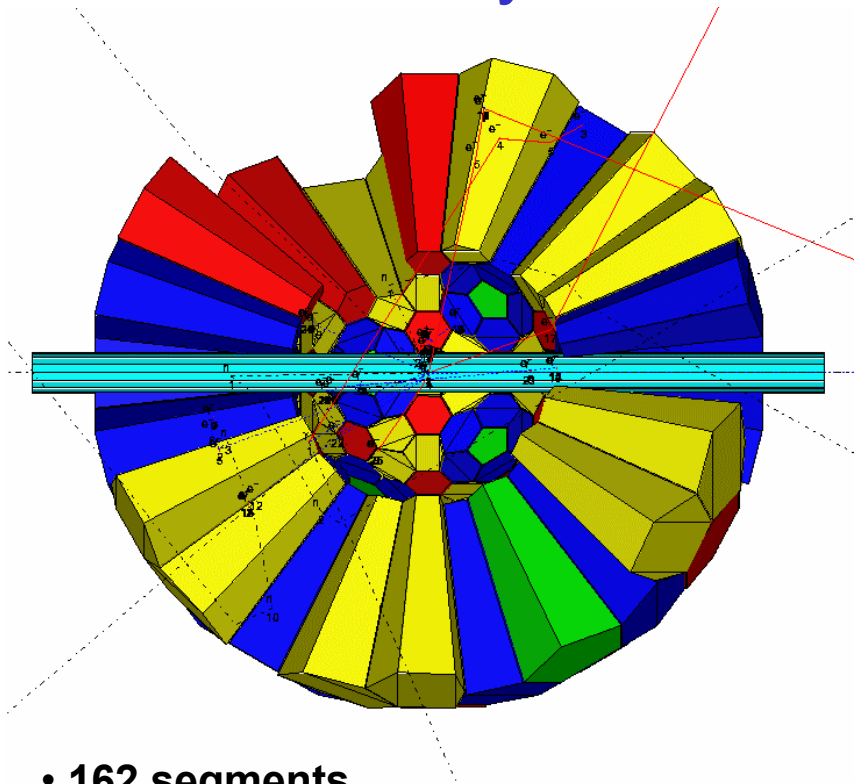

- **162 segments**
  (160 segments with crystals)
- **4 different crystal shapes**
- **Inner radius = 17 cm**
  - **18 cm actual $\Rightarrow$ 3.52π**
- **Crystal depth = 15 cm**
- **6 cm thick ^{6}LiH neutron shield**
  (Inner radius = 10.5 cm)

LANSCE
Los Alamos Neutron Science Center

DANCE crystals and assembly

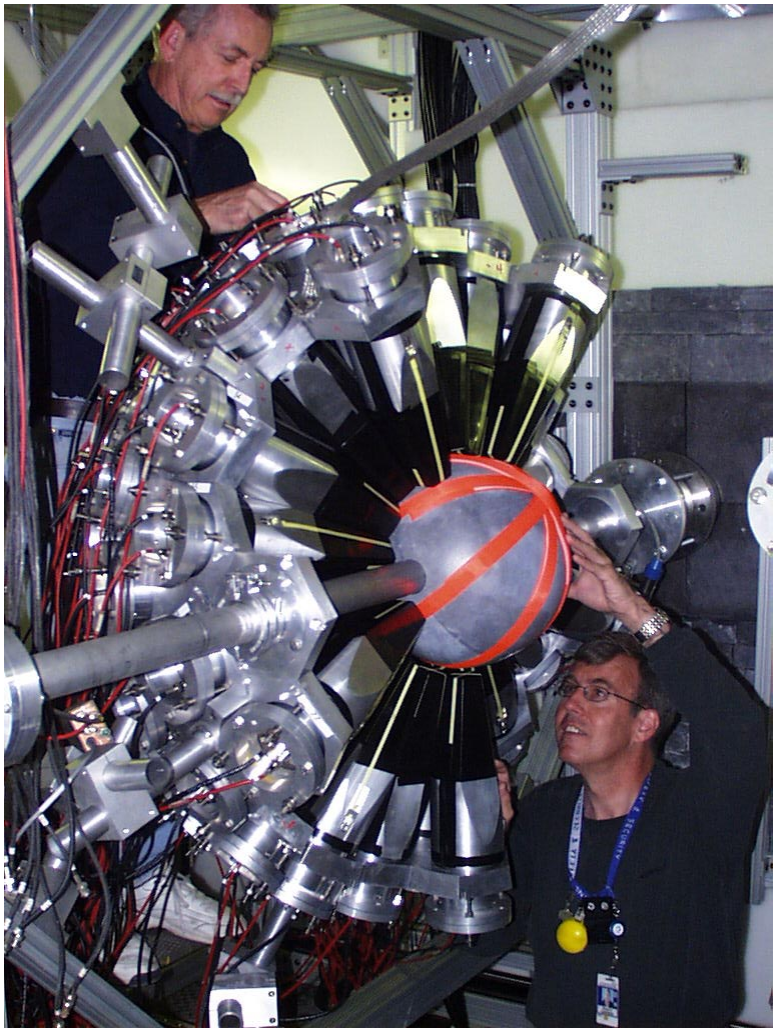

Half of DANCE array with ^{6}LiH ball

BaF_2 Crystal

Crystal mounted on 3 in phototube

DANCE Uses 324 fast waveform digitizers for acquisition

CAMAC / VME not adequate

- Need >2ms multi-hit time digitization
- ADC conversion times long
- High rate => buffered ADC,TDC
- Camac transfer rates slow

DANCE Solution- Waveform digitizers

- 8-bit, 500 Msample/sec (300 MHz bandwidth)
- Two digitizers/crystal (hi and low gain) for adequate dynamic range
- 128 kpoints/channel
- Acqiris DC-265
- 14 Compact PCI crates, 24 channels/crate
  Each crate has onboard computer for digitizer control and distributed analysis of waveforms between beam bursts (50 msec)
- Central computer (2 GHz PC)/ethernet
  CAMAC crate for control and scalers
- 1- Tbyte RAID for event-mode storage

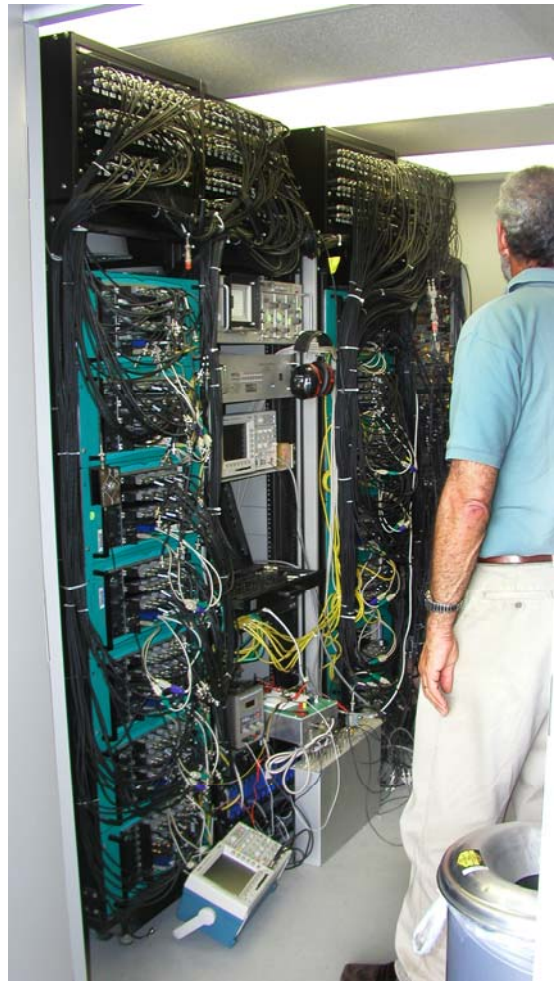

DANCE Acquisition Hut

Some details on waveform digitizer use at DANCE

Acquisition Modes

Segment Mode

- Trigger for each event
  Requires external electronics
- 1000 channels (2 μsec) per segment
- Only "hit" channels digitized
- Approx 100 events/channel per To
- 3.0 μsec fixed deadtime

Continuous Mode

- One trigger for each To
- "No" deadtime – analyze overlapping waveforms observed at higher rates
- Limited energy range -
  Current trial T_{neut} > 215 eV

Waveform analysis in 50 msec

Timing Algorithm (Segment)

- Segment time at segment trigger (recorded in segment time stamp)
- Reference event trigger sent to all channel at To
- TOF = difference in time stamps + (small) correction for leading edge

Sample Waveforms

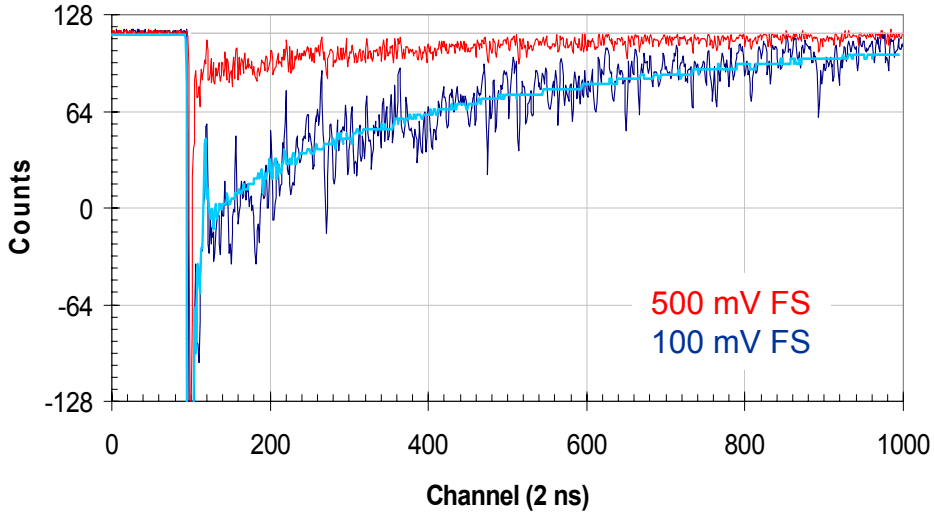

Peak Area Algorithm (Segment)

- Single peak per segment
  (If 2nd pulse – reject 2nd)
- Background ahead of leading edge
  Look back 200 ns before trigger
- Leading edge, >25 mV/chan
- Fast component – integrate low-gain waveform for 20 chan (40 ns)
- Total area (fast + slow)
  Compare to reference waveform
  (equiv. To least-squares)

Flight Path 14 Neutron Flux

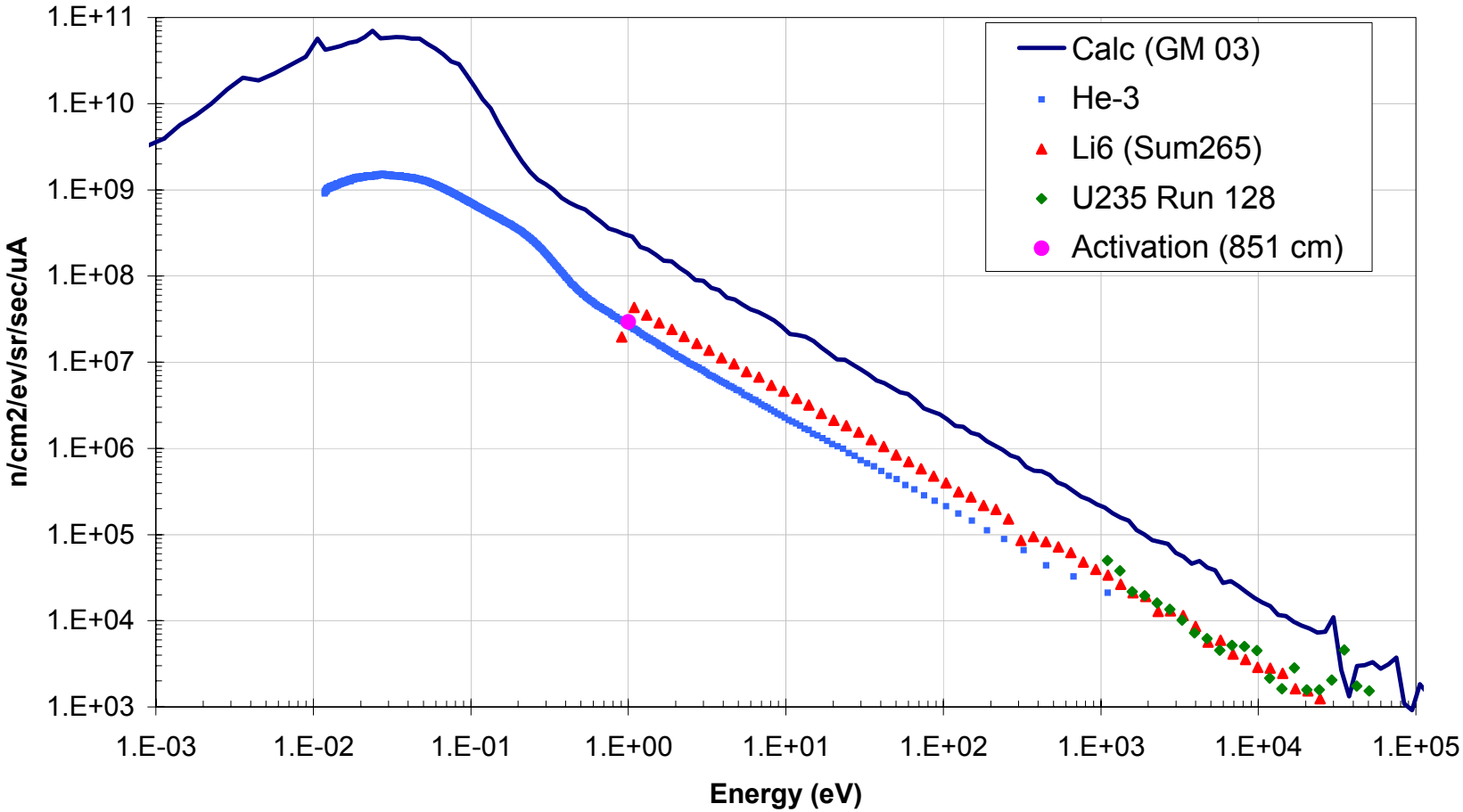

Fluxes adjusted to "moderator current" for comparison

$I \approx (2.78\text{x } 10^7 \text{ N/cm}^2\text{/sr/ev/sec/}\mu\text{A}) \text{ / E (eV)}$

$\Phi \approx (127 \text{ N/cm}^2\text{/ev/sec/}\mu\text{A}) \text{) / E (eV)}$

Summed gamma cascade energy identifies target nucleus

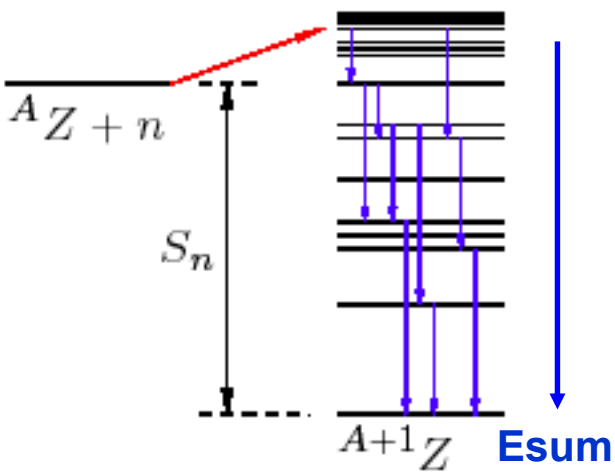

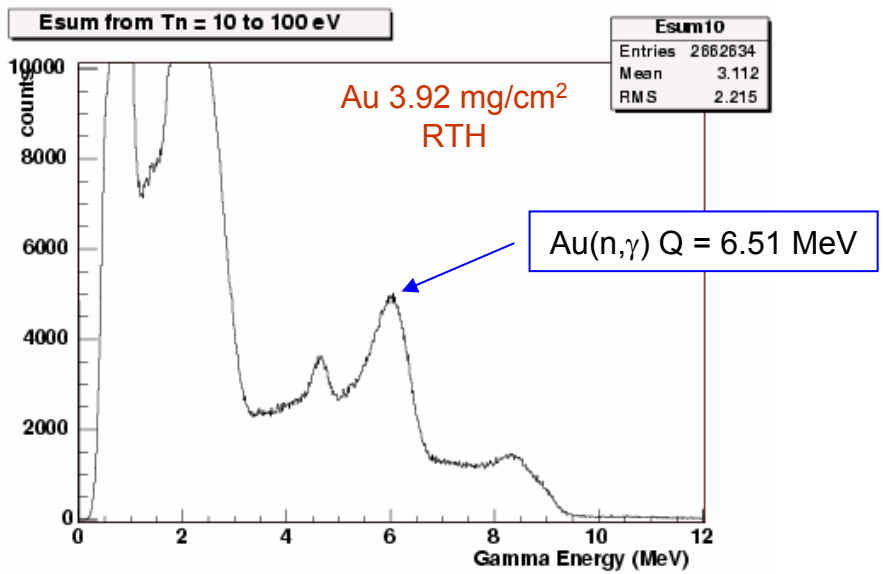

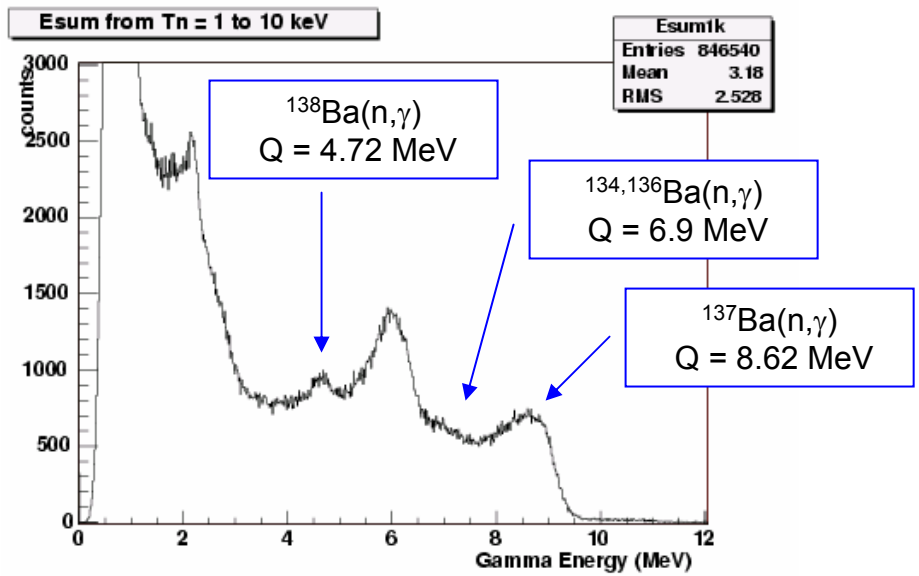

- Summed gamma energy = Q value
- Energy sum from 160 crystals
- Events due to scattered neutrons capturing in BaF_2 become more important at high energies
- Gate on Esum peak

Summed Gamma Energy as function of Neutron Energy

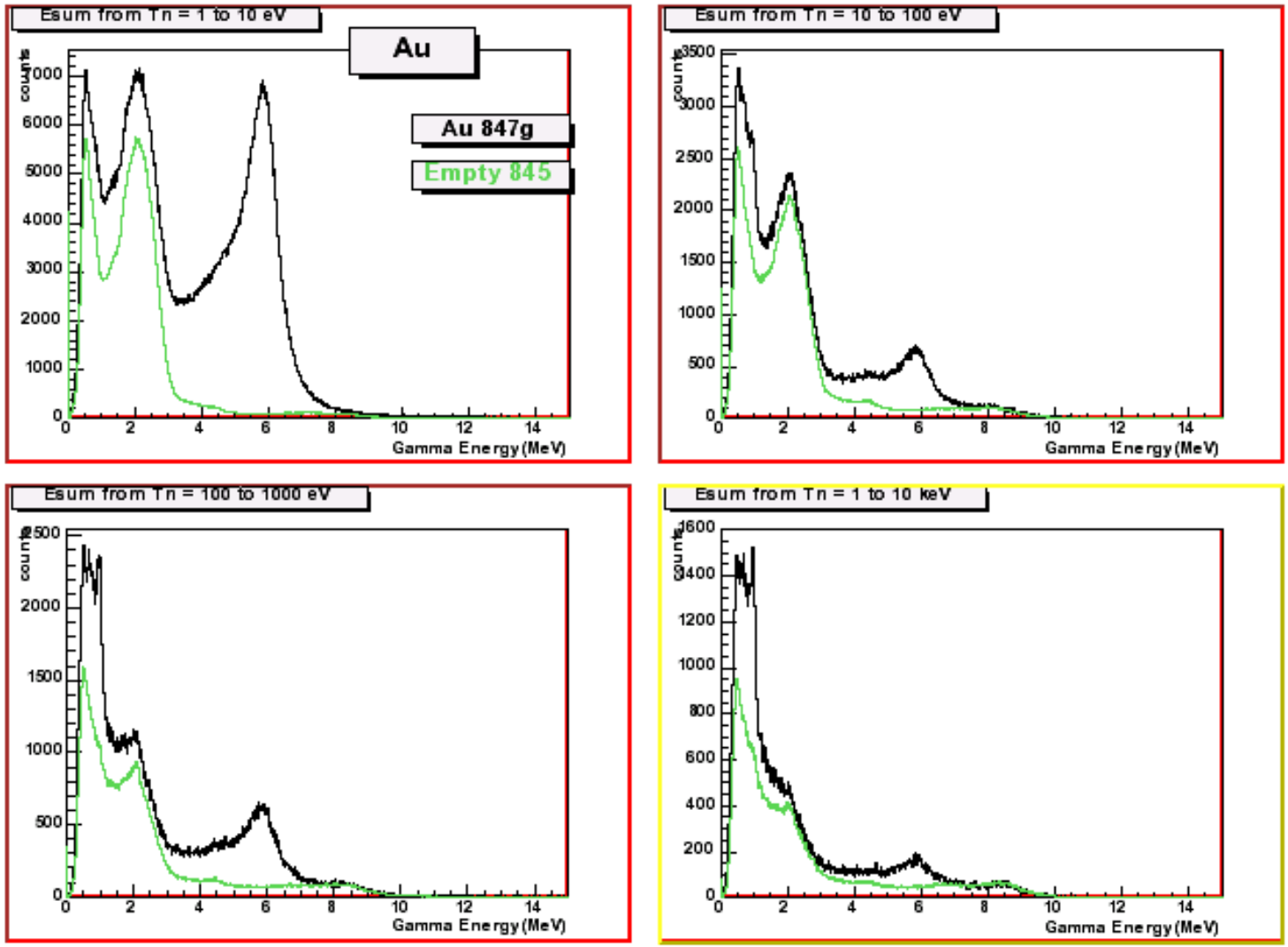

Au (3.92 mg/cm^2) Q = 6.51 MeV

Crystal Multiplicity = 2

Summed Energy: The story to now.

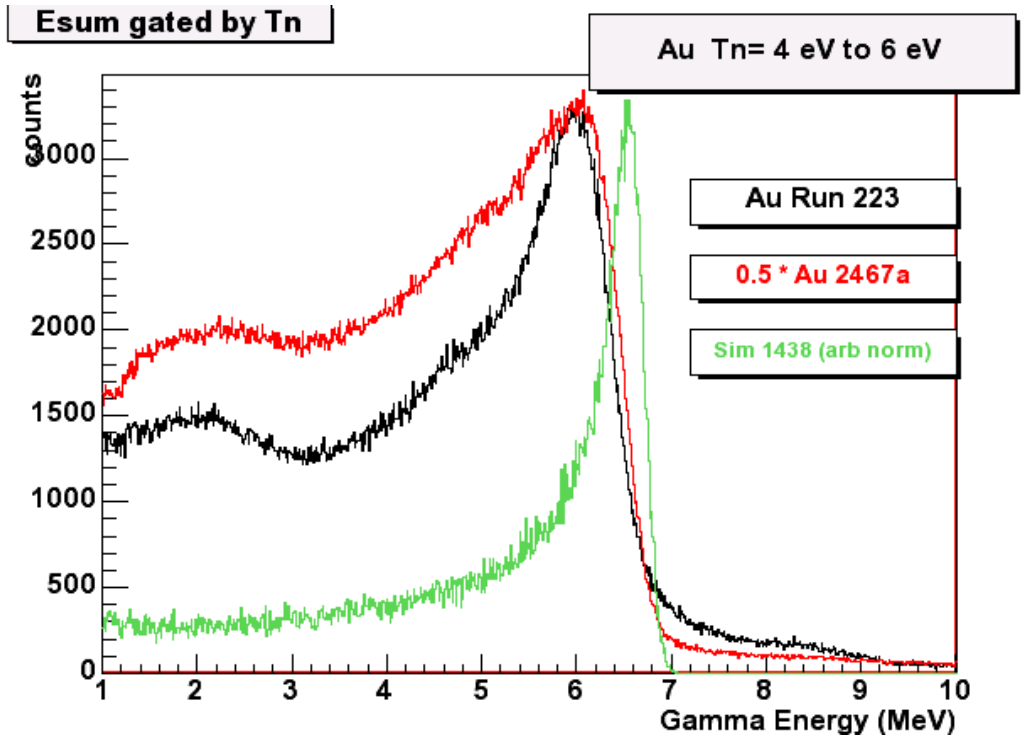

Green: Calculated Au gamma “Esum” spectrum
Red: 141 Crystals, 50 mV threshold per crystal
Black: 159 crystals, 25 mV threshold per crystal

Cluster Multiplicity provides an additional means of neutron discrimination

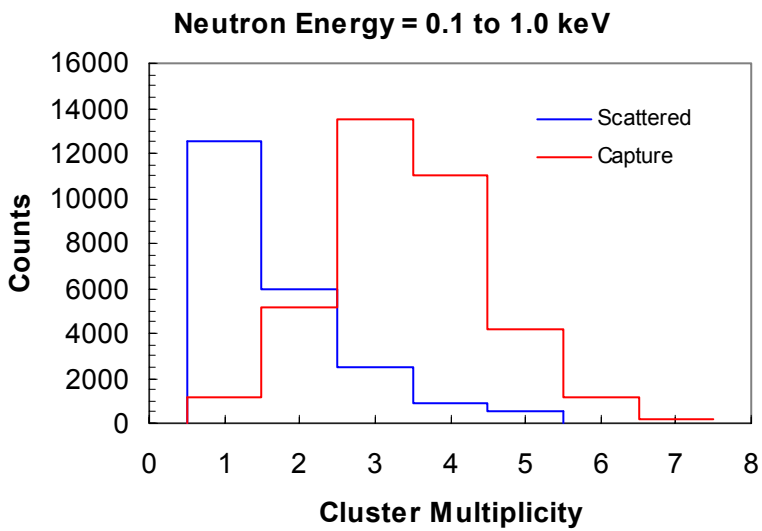

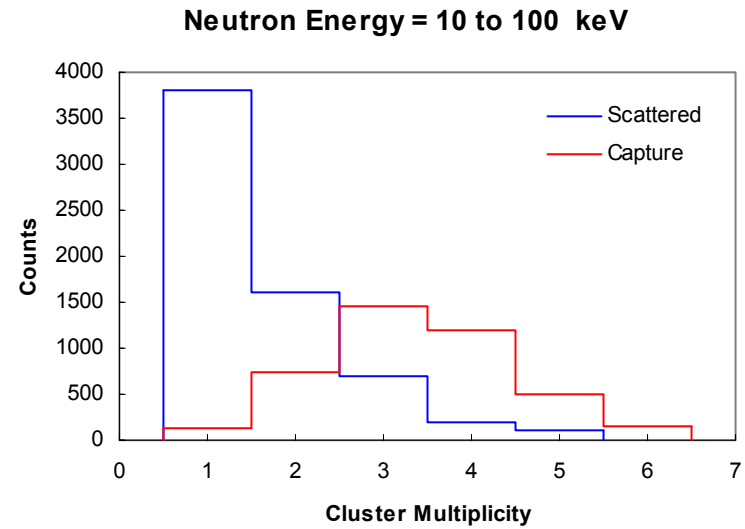

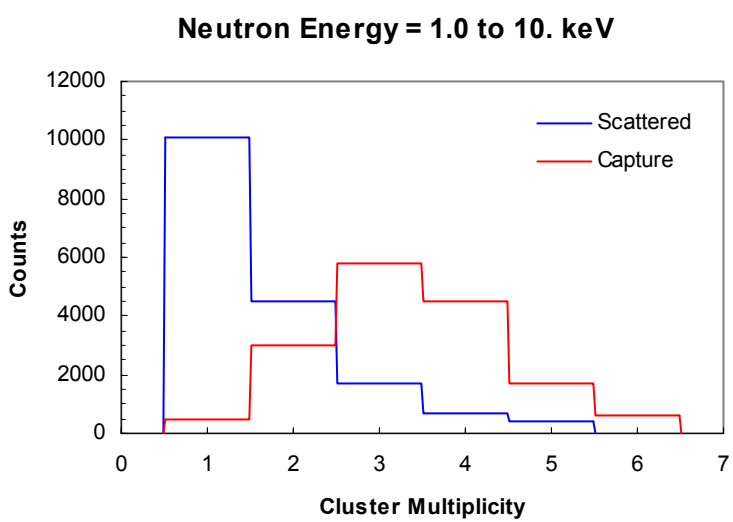

Cluster multiplicity for scattered neutrons interacting in array (blue) and for gammas from true captures in an Au target (red). This parameter also provides a means of discrimination. A cluster is a set of adjacent “hit” crystals.

Cluster Multiplicity vs. Summed Energy (Au)

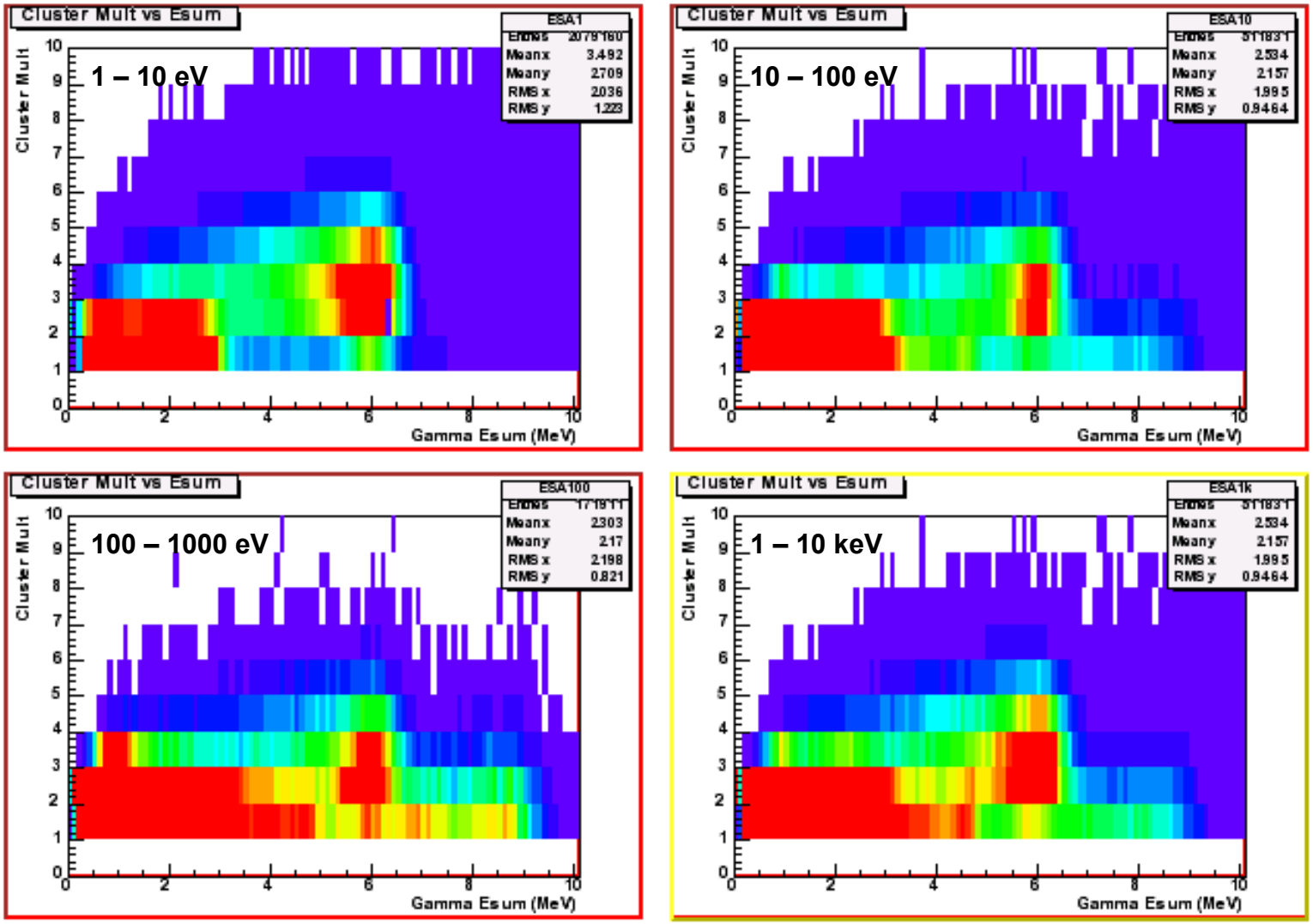

Projected Counts – different cluster multiplicity thresholds

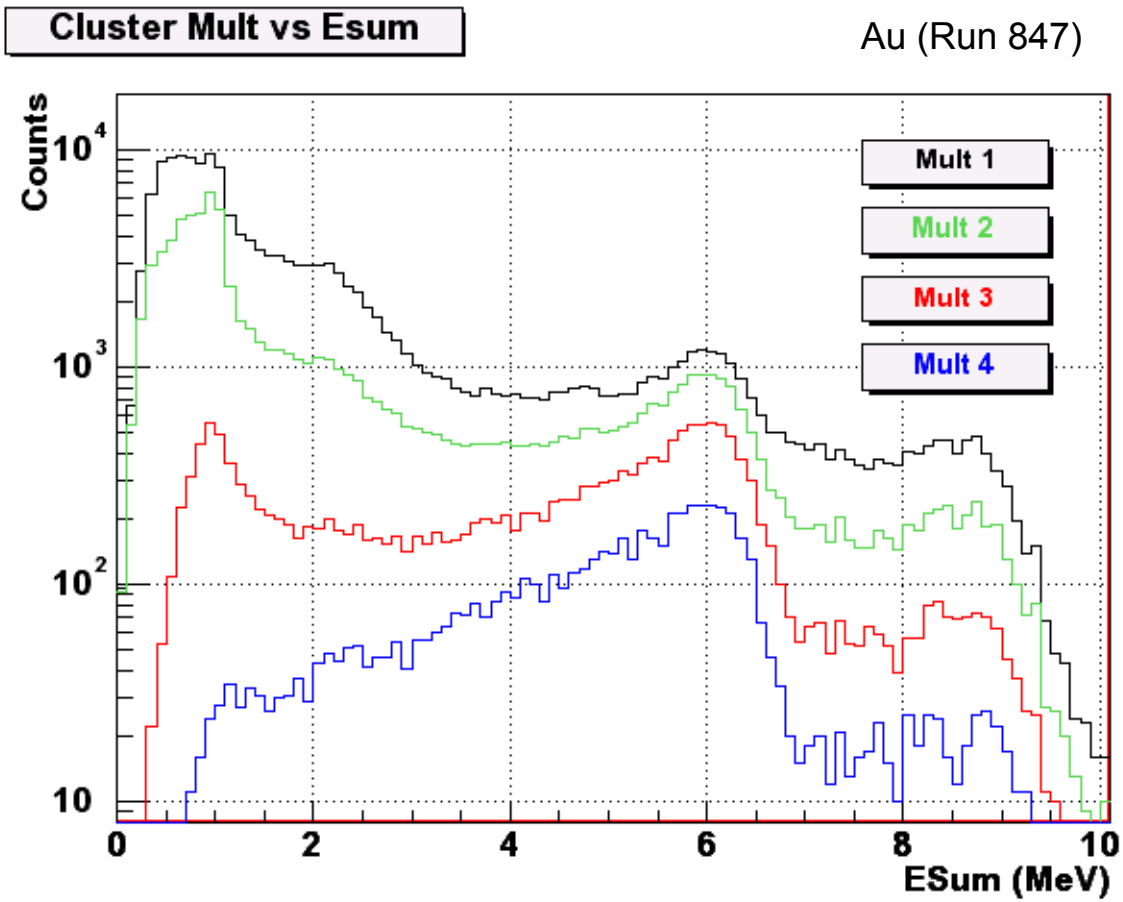

Au (3.92 mg/cm2) Spectrum with Background

Cluster Multiplicity ≥ 4 5.0 MeV < Esum < 7.0 MeV 50 bins/decade

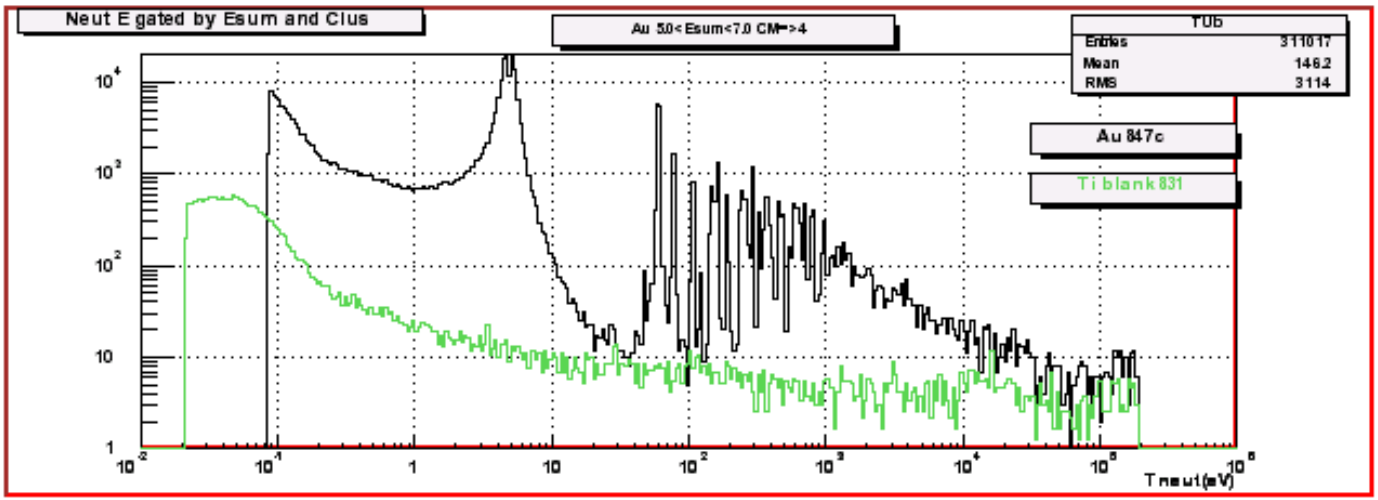

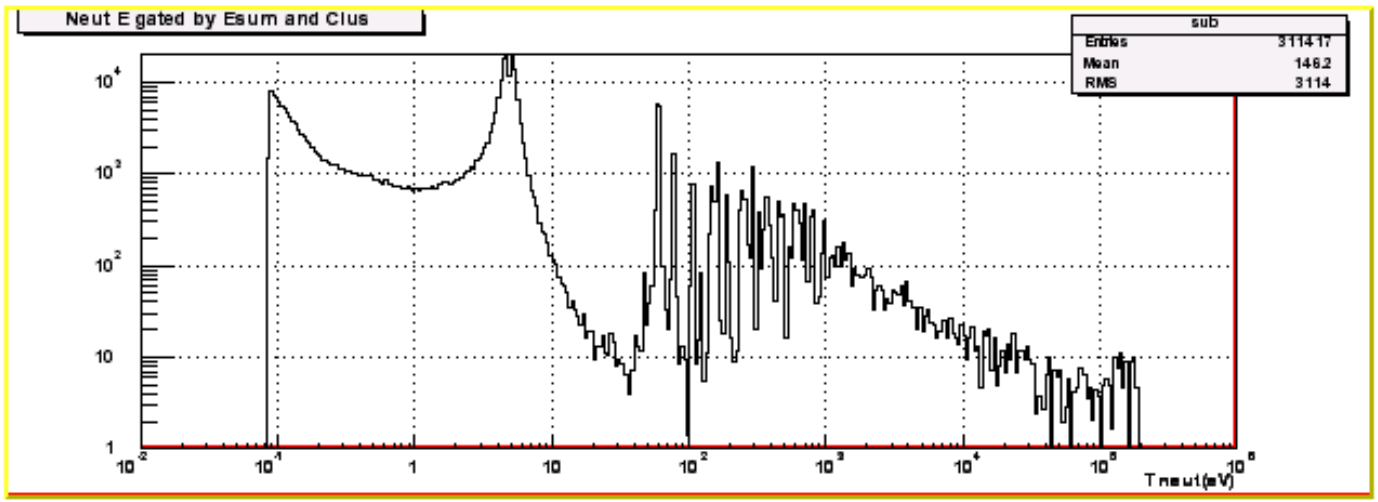

Time of flight spectra and Deadtime correction

Au (3.92 mg/cm^2)

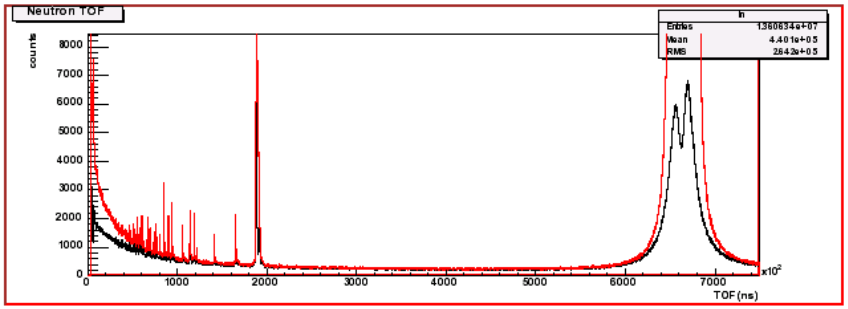

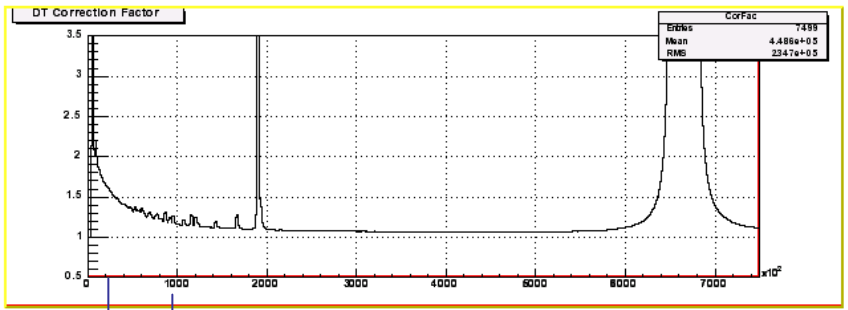

Empty holder

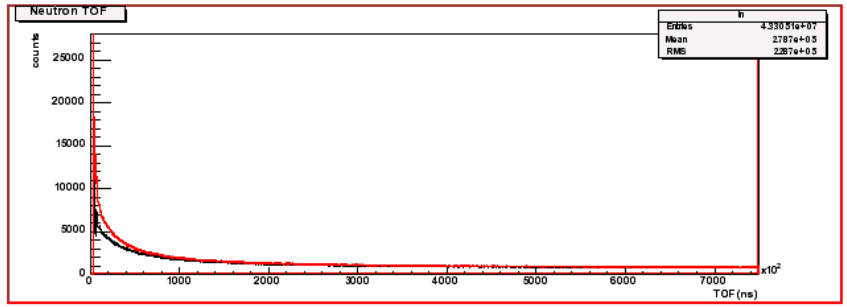

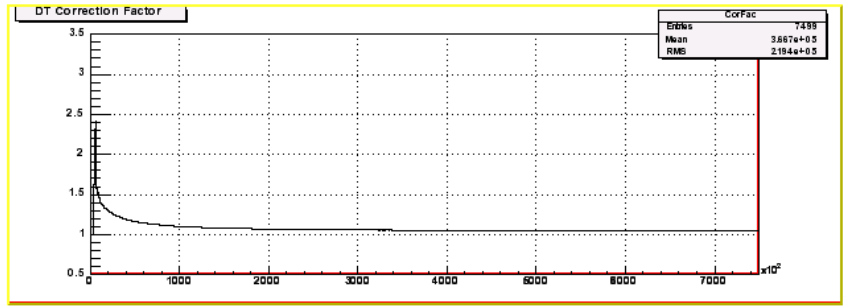

100 μsec = 214 eV

14.6 μsec = 10 keV

Deadtime correction: C..D. Bowman and R.L. Bramblett, LLNL LINAC-21, 91962).
See also P.B. Coates,J. Phys. E Sci. Instr **1**, 878 (1968).

Fixed deadtime = 3.00 μsec ^{6}LiH absorber in place

Plans 2003 - 2004

Experiments

Stable Targets:

- ^{139}La,^{45}Sc,^{55}Mn,^{59}Co,Cu,V,Rb,Sr (Gaps in s-process)
- ^{102}Pd (rp process)
- ^{151}Eu rad-chem diagnostic

Radioactive Targets

- ^{237}Np AFCI
- ^{234,235,236,238}U better targets and statistics
- ^{151}Sm Key s-process branch (largely completed)
- ^{147}Pm s process branch - target irradiated, needs chemistry
- ^{171}Tm,^{155}Eu rad-chem diagnostics, target irradiated, needs chemistry

Development

- Improved hardware handshaking
- Further work on resolution and backgrounds
- Development of “continuous” data acquisition
- Ge detector in concidence for fission studies (??)

Simulations of $^{197}Au(n, \gamma)$

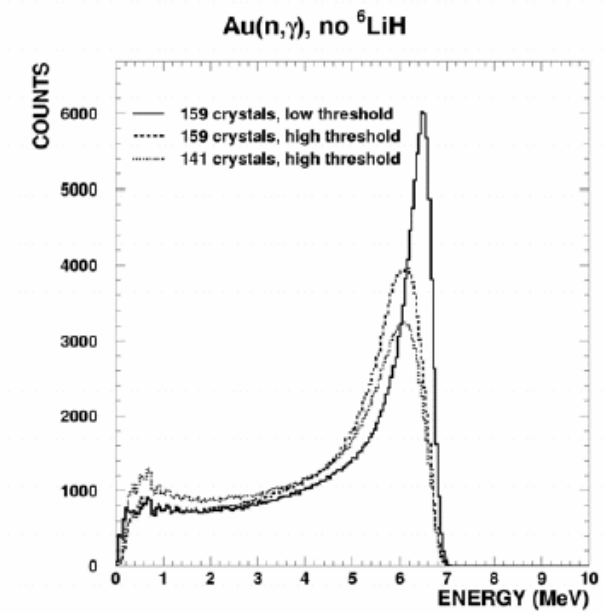

Comparison of Au summed-energy peak

* 2002/2003 Setup (141 Crystals)
* Full Array (151 crystals)

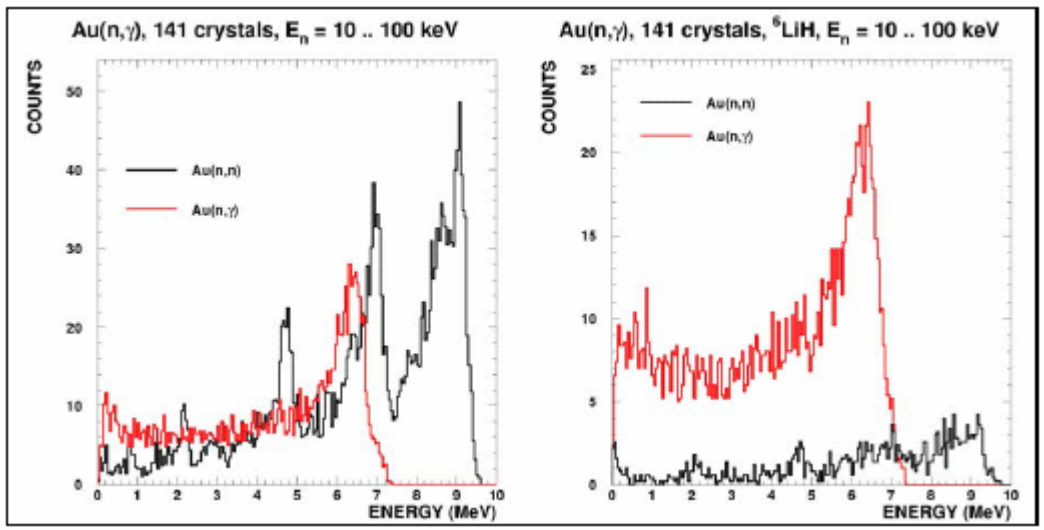

Simulation of Au summed-energy peak and background from scattered neutrons.

* 141 Crystals
* With and without LiH

Sample spectra using waveform digitizers

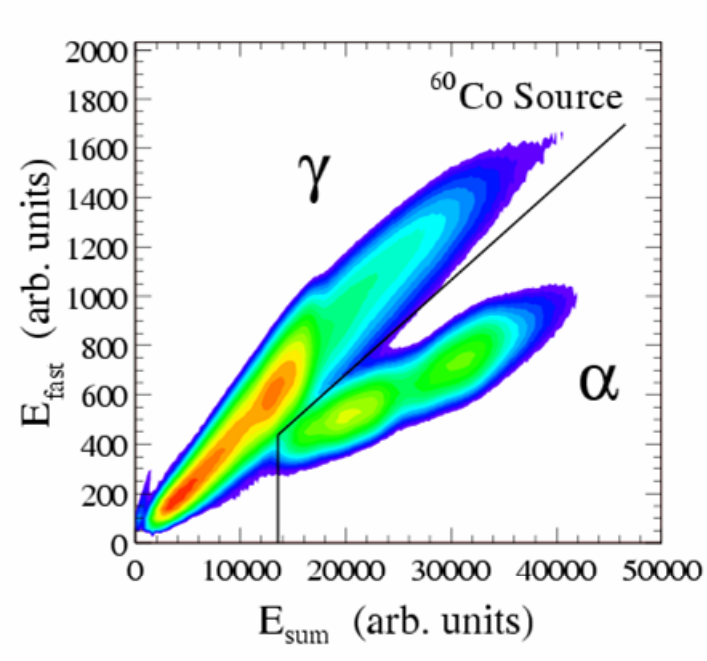

Alpha – gamma discrimination;
Fast component (vertical) vs
Total energy (horiz)

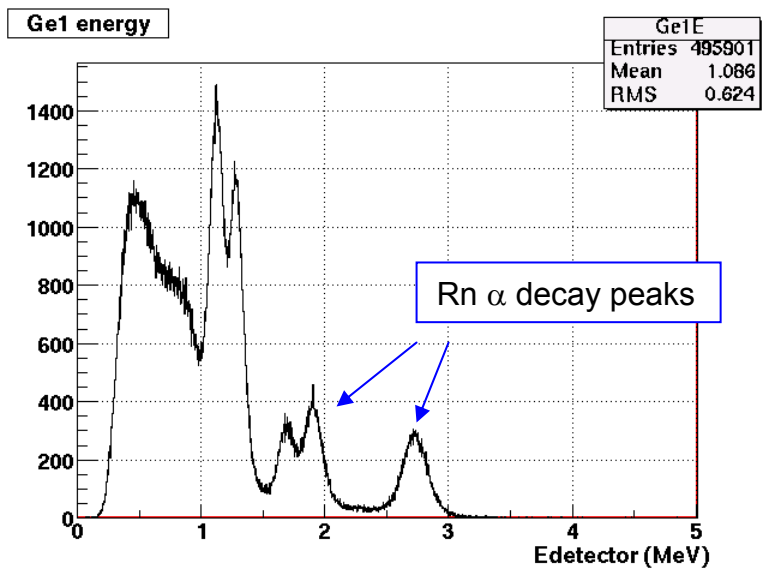

^{60}Co Source spectrum

Beam Spot at Filter Box in FP14 (8.xx m)

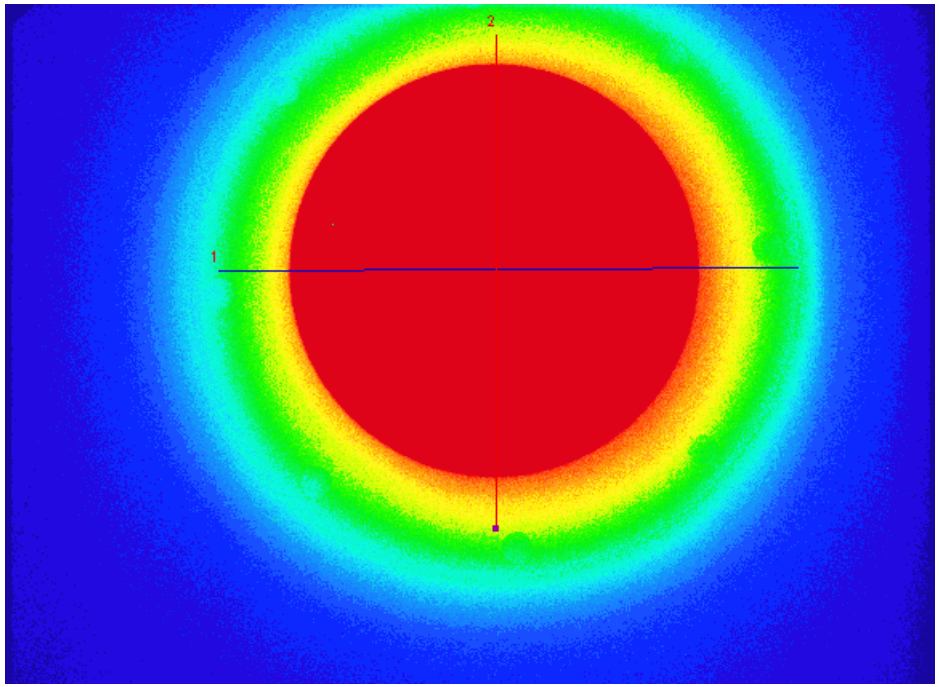

Approx 100 mm

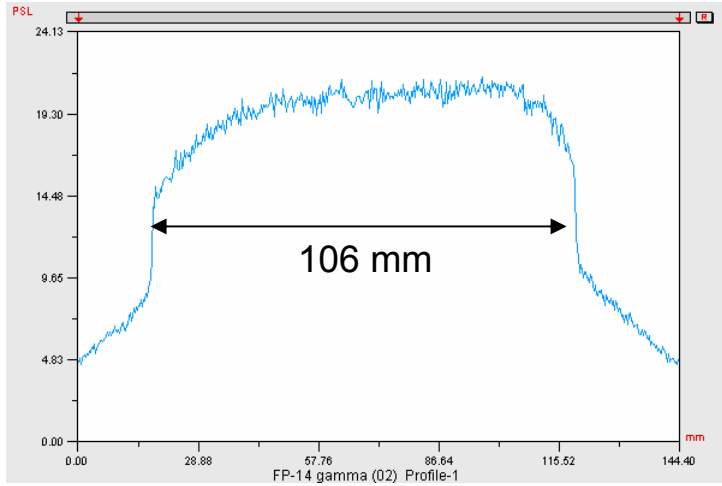

Profile – Left/right

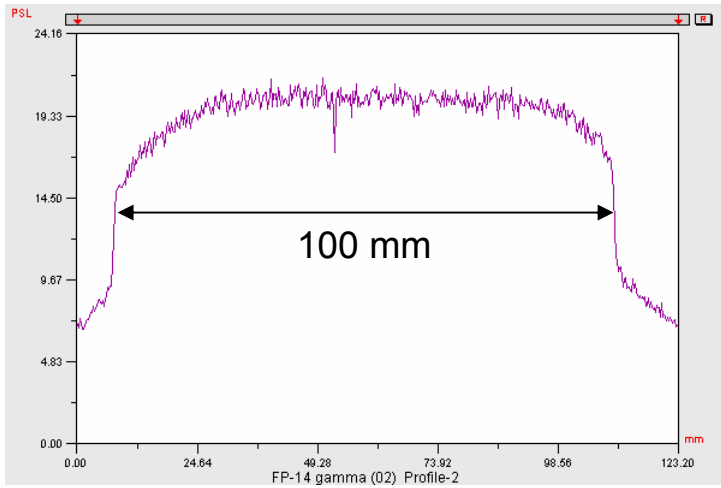

Profile: up/down

Activation: 2.5 X 2.5 cm Au foil

Beam flux measurements on FP14

Differential measurements

- ^{6}Li(n,αt) monitor
- ^{235}U(n,f)
- ^{3}He (Luke Daemen)

Au activation measurements

- In filter box (8.51 m)
- Target location (20.25 m)
- Analysis: “Westcotte convention”
  - With and without Cd filter
  - Assume 1/E spectrum shape

Preliminary Results: $^{234,236}U$ Resonances

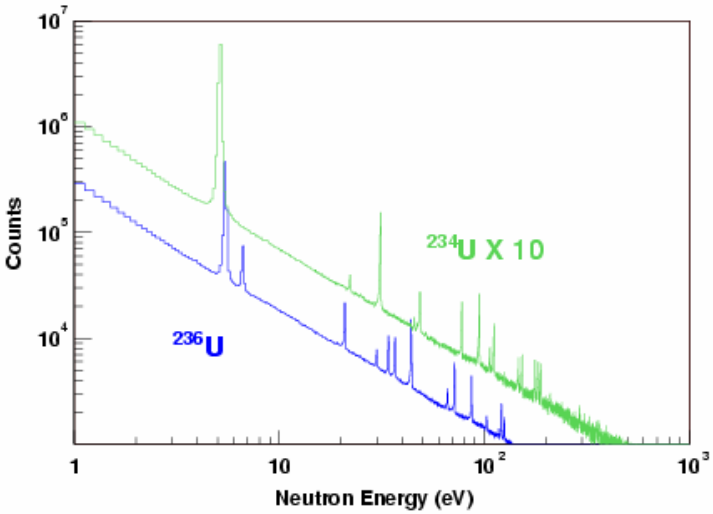

Raw Energy Spectra

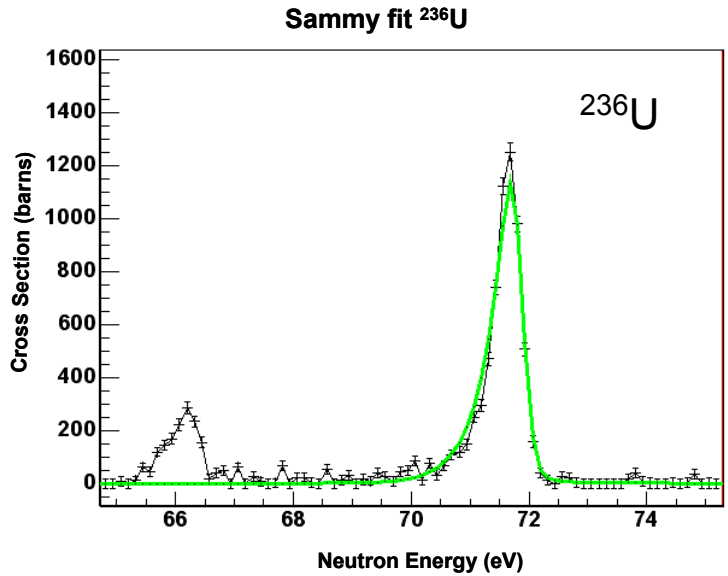

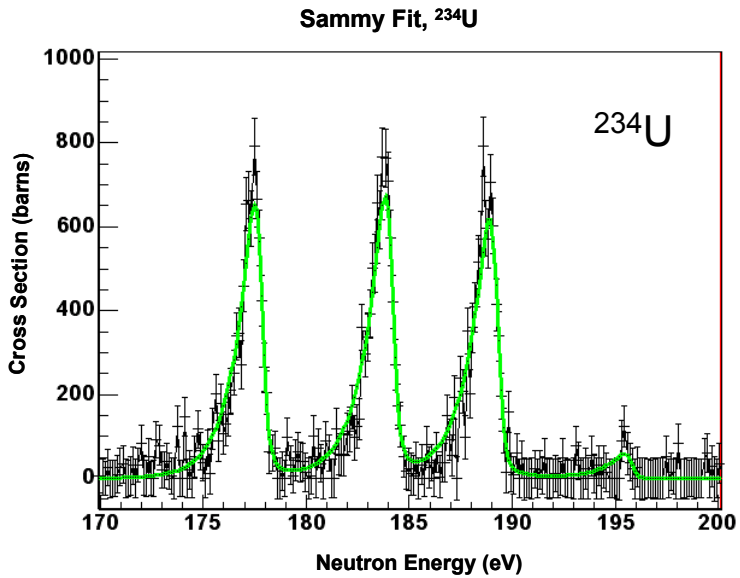

Resonances fit using SAMMY code

- Parameters determined from Au resonances
- T_{eff} = 300° (Doppler Broadening)
- ΔL = 0.0109 m (Moderator thickness)
- ΔT_x = 0.390 μsec (Exp. Tail parameter)
- T_E = 0.019 μsec (Gaussian width param.)

Contribution by

Franz Kaeppeler

Froschungszentrum Karlsruhe

franz.kaeppeler@fzk.de

21 pages

nucleosynthesis between iron and the actinides clues for modeling Red Giants *(and supernovae)*

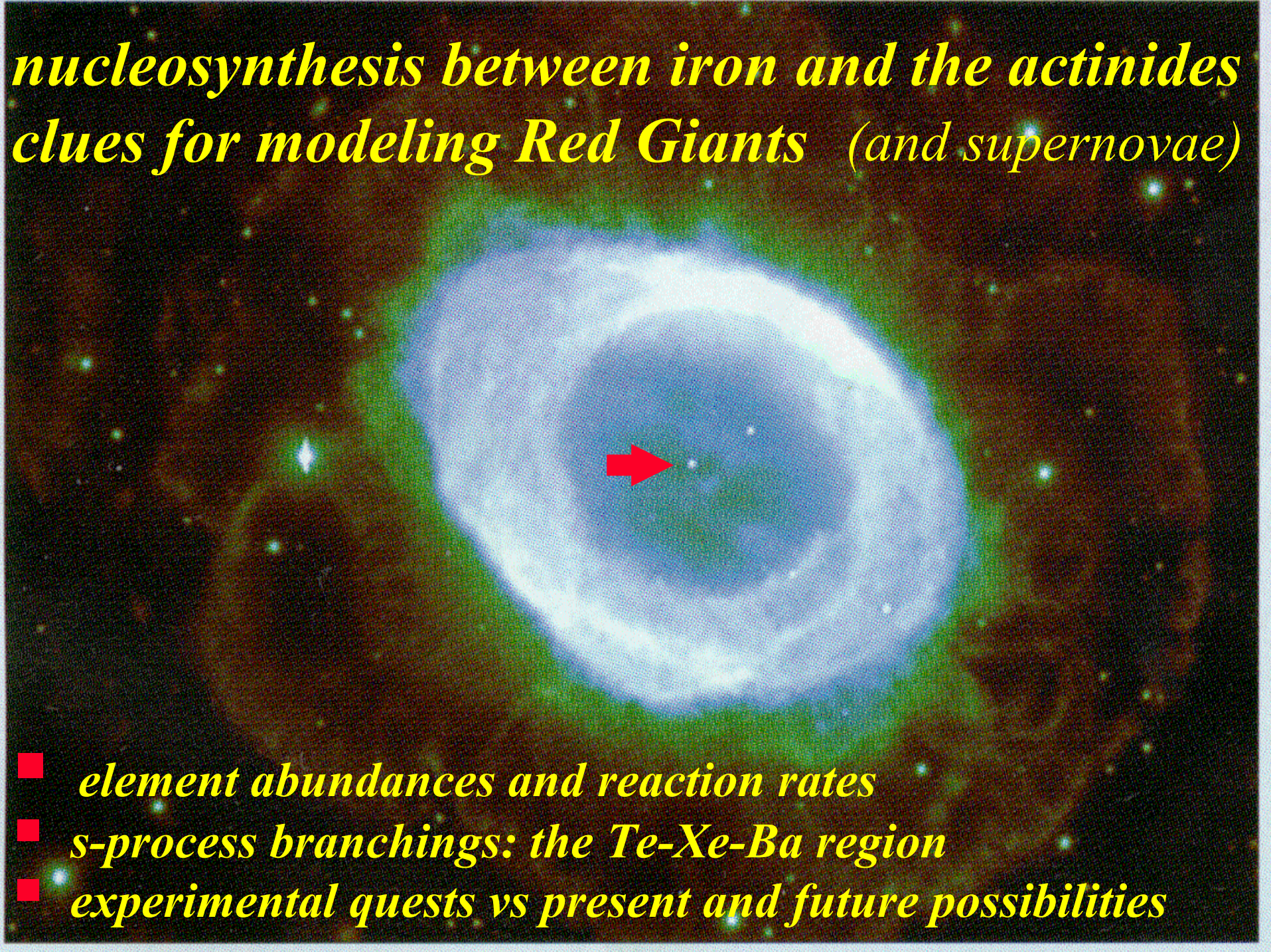

- *element abundances and reaction rates*
- *s-process branchings: the Te-Xe-Ba region*
- *experimental quests vs present and future possibilities*

the standard abundance distribution

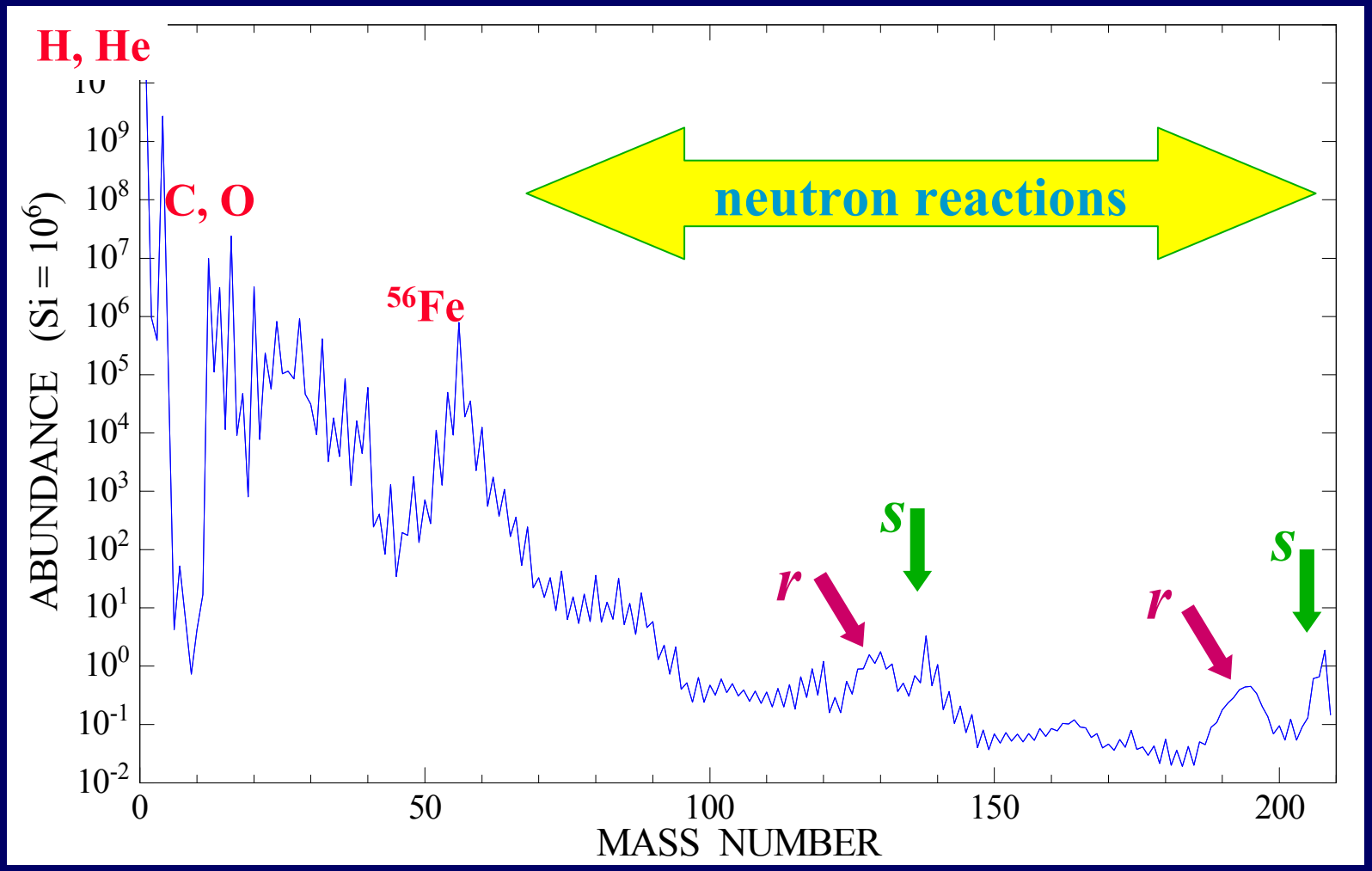

sources of abundance information

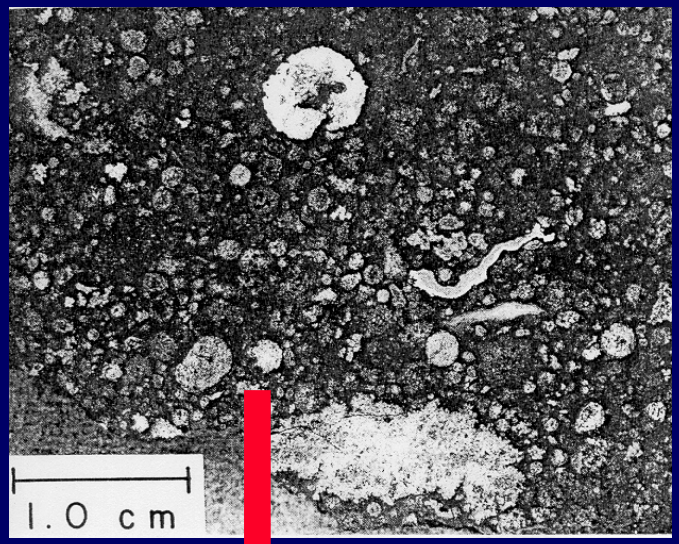

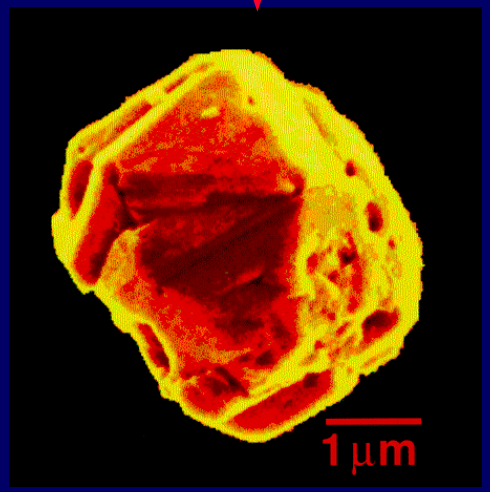

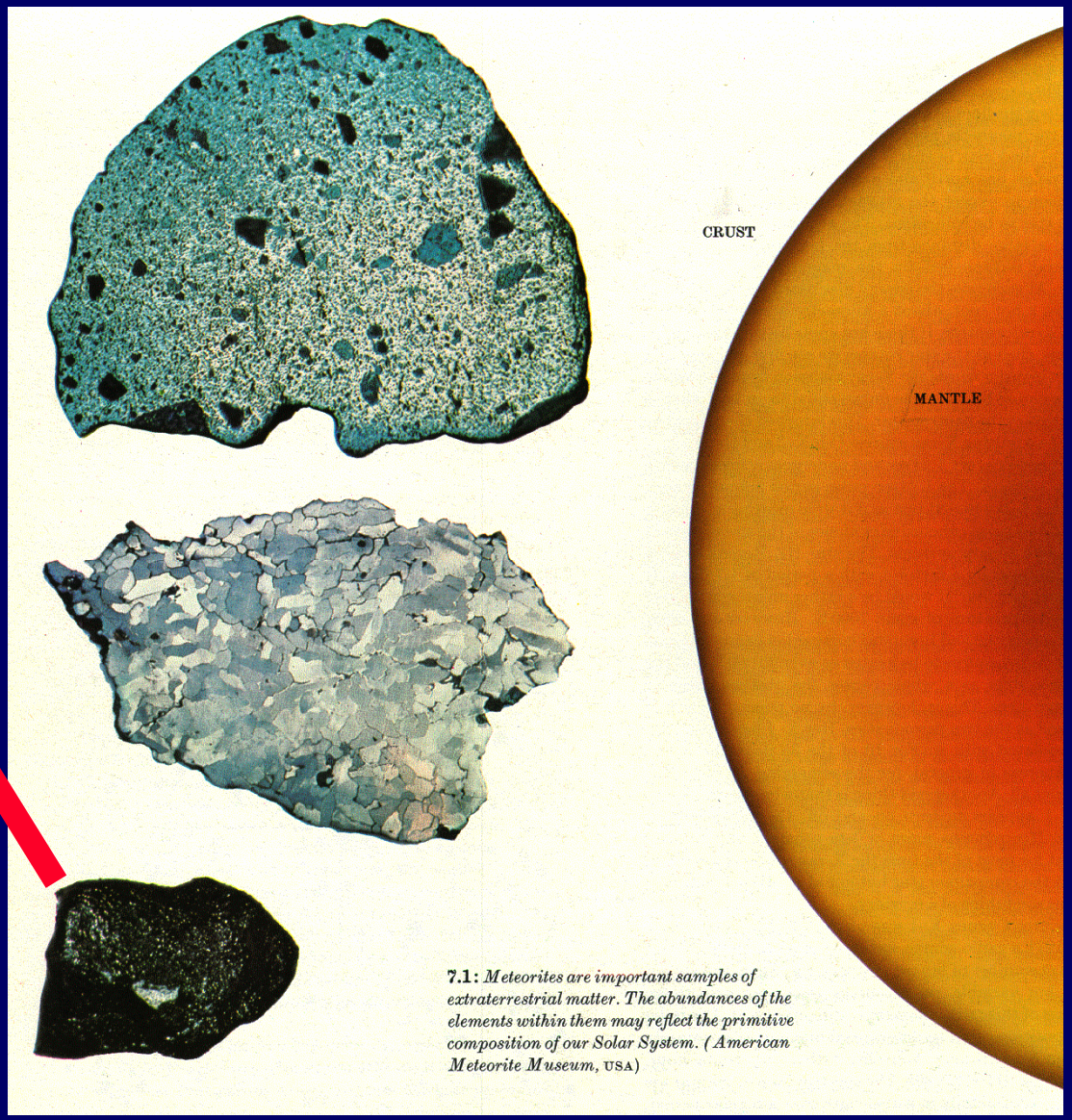

7.1: *Meteorites are important samples of extraterrestrial matter. The abundances of the elements within them may reflect the primitive composition of our Solar System. (American Meteorite Museum,* USA)

presolar grains: Xe-S and Xe-HL

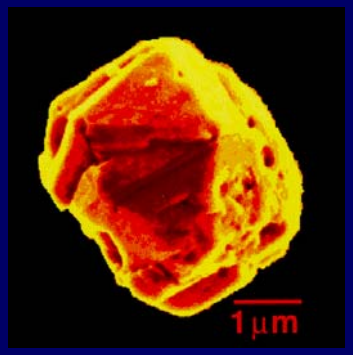

AGB stars

↓

***s* process**

↓

stellar (n,γ) cross sections

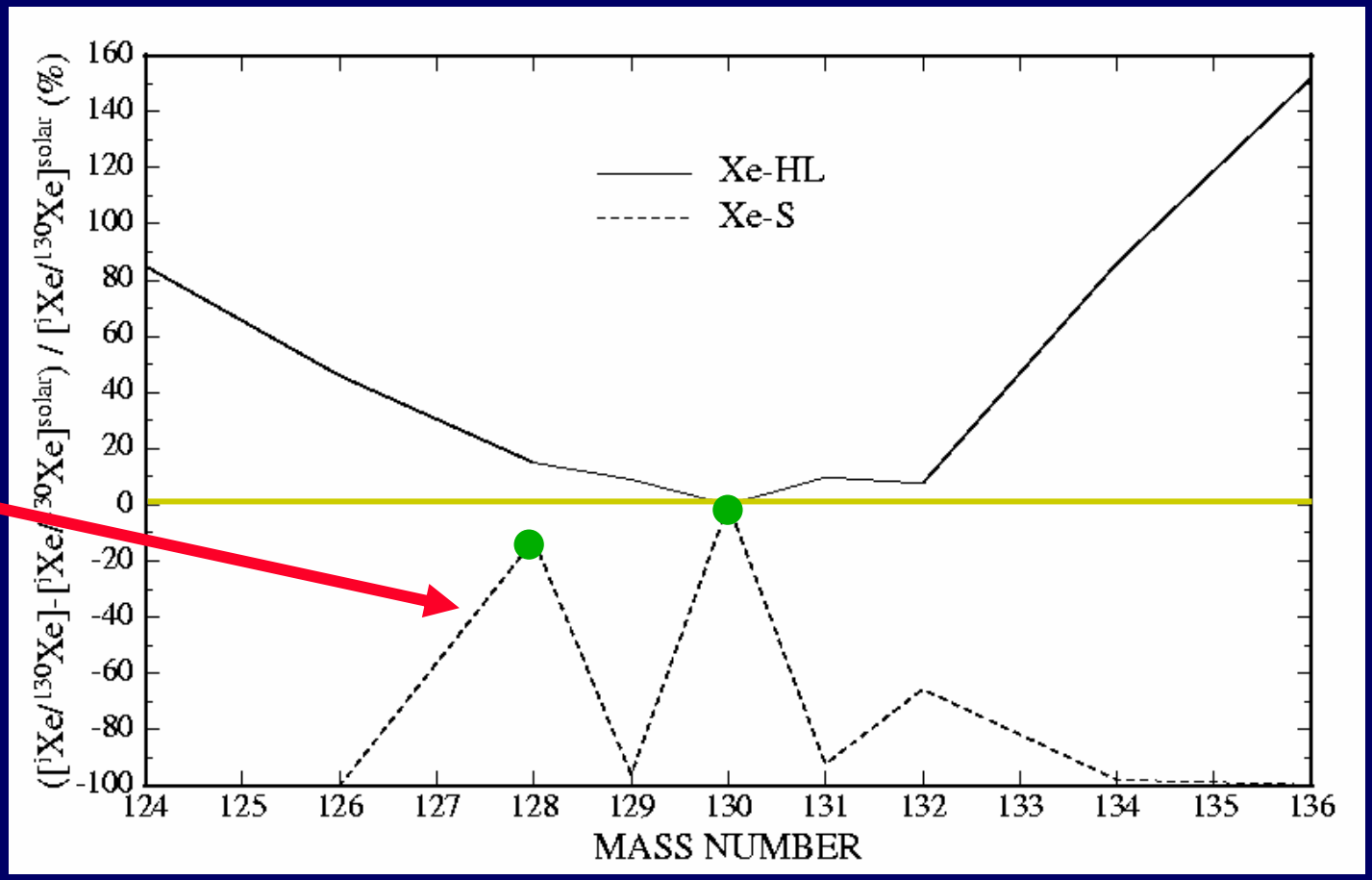

the Te-Xe-Ba region

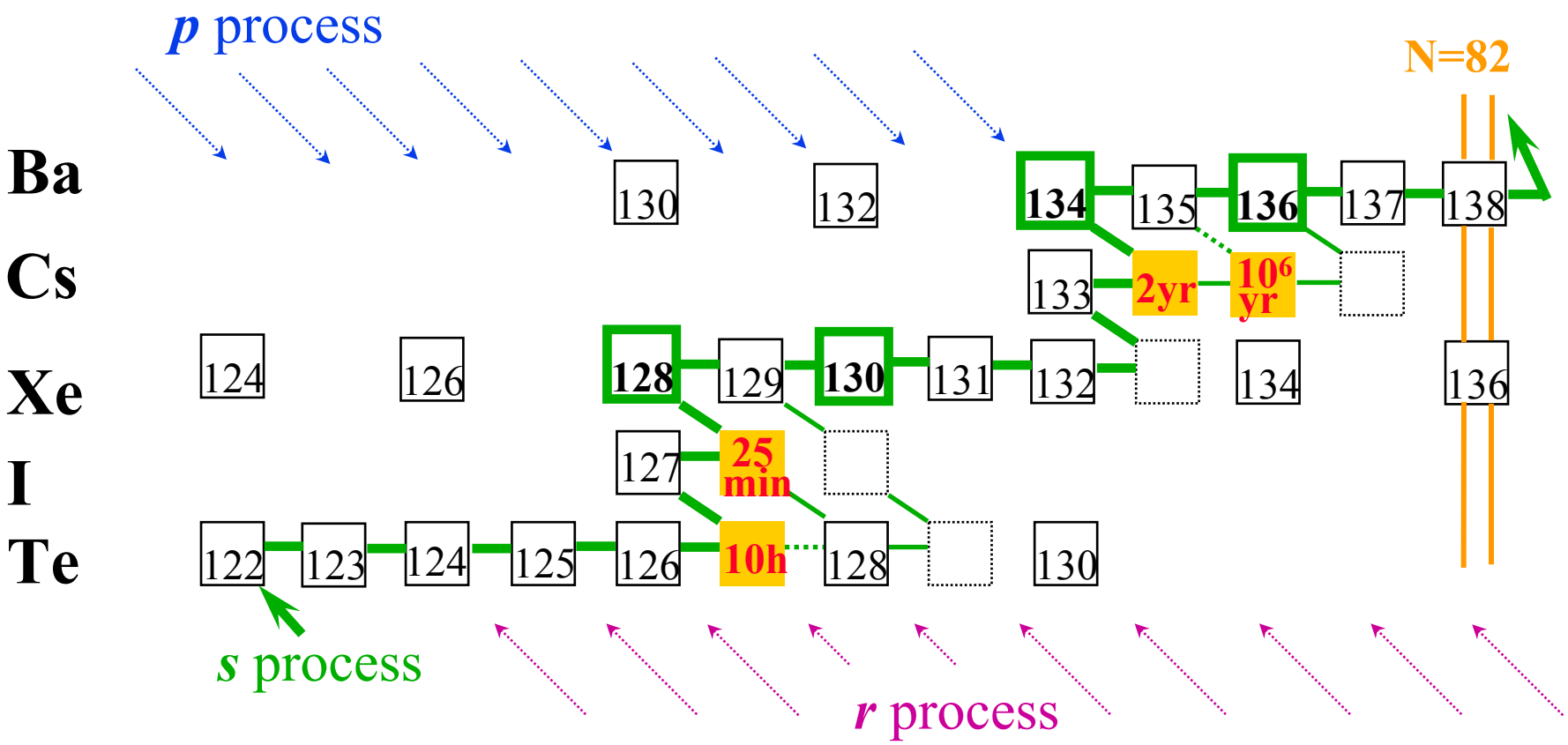

s-process flow at A=127/128 ?

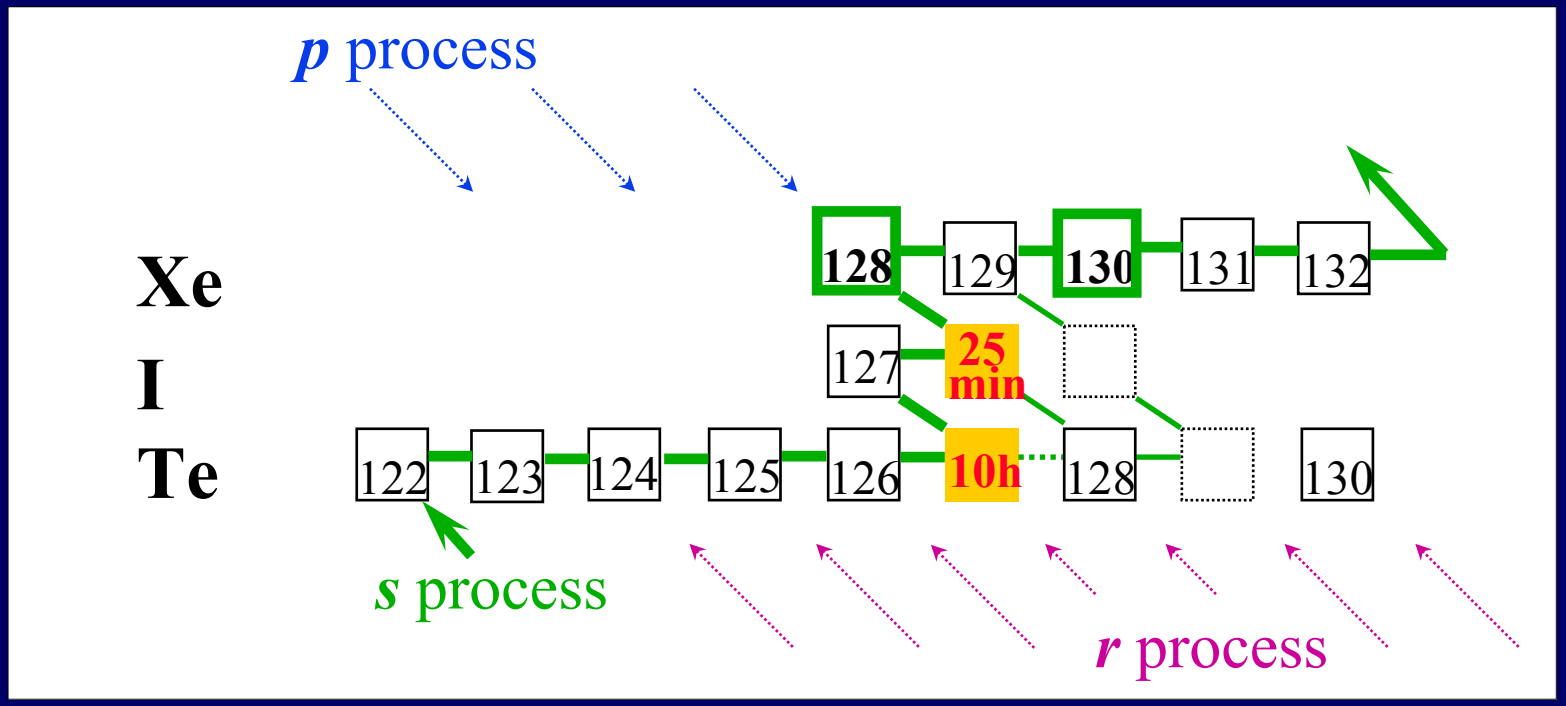

- ^{130}*Xe:* ***normalization of solar Xe abundance***
- ***branching?:***

answer only via σN test,
requires accurate (n,γ) cross sections

detection of neutron capture events

(n,γ):

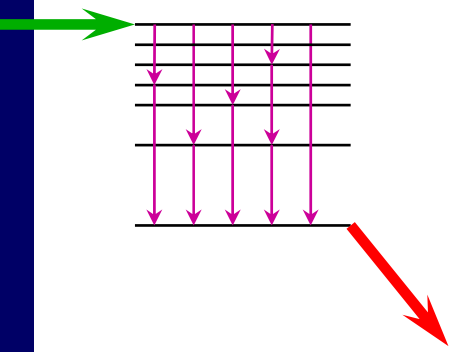

prompt γ–rays + TOF-method

single γ´s	* Moxon-Rae	$\varepsilon_\gamma \sim 1\%$
	* PH-weighting	$\sim 20\%$
	* Ge, NaI	$< 1\%$
all cascade γ´s * 4π BaF_2		**~100%**

activation in quasi-stellar spectrum

most sensitive	* small cross sections, **10^{14}** atoms sufficient
selective	* natural samples or low enrichment

the Karlsruhe 4π BaF_2 array

ε_γ >90% up to 10 MeV

$\Delta E/E$ = 6% at 6 MeV

Δt = 500 ps

ε_{casc} > 98%

clear signatures

good TOF resolution

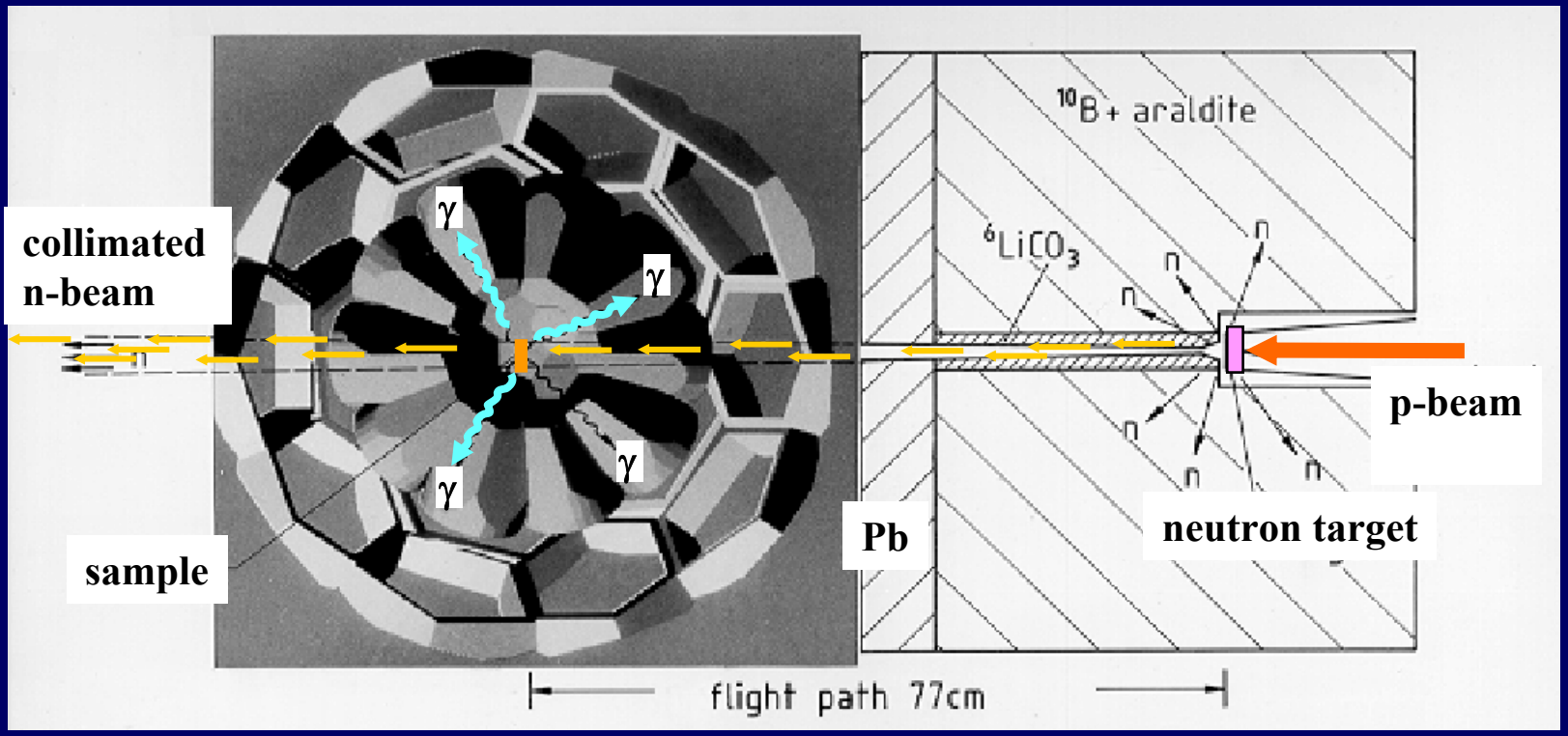

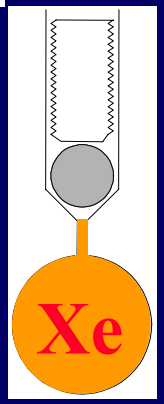

samples, spectra & cross sections

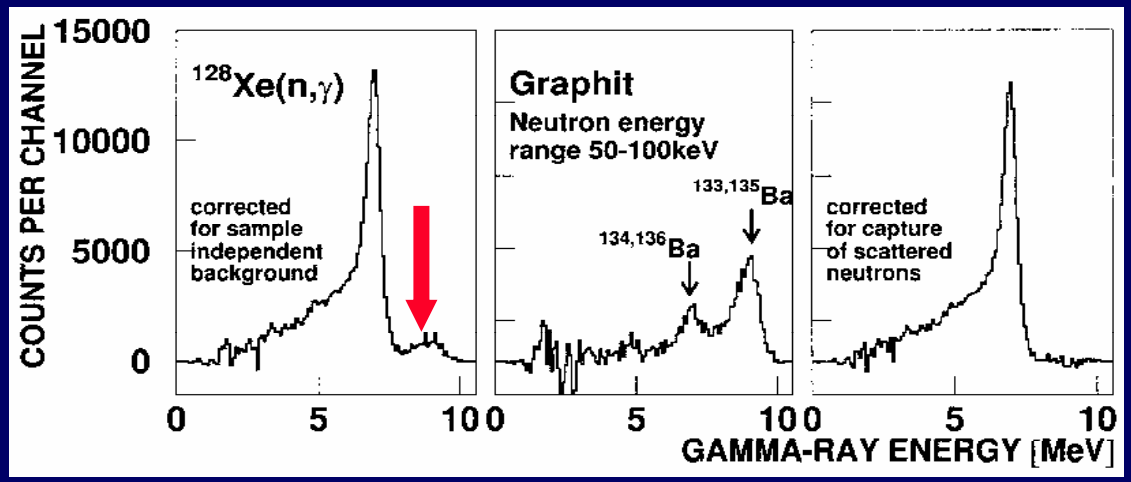

	previous	measured
^{128}Xe	248 ±66	**262.5 ±3.7**
^{129}Xe	472 ±71	**617 ±12**
^{130}Xe	141 ±51	**132.0 ±2.1**

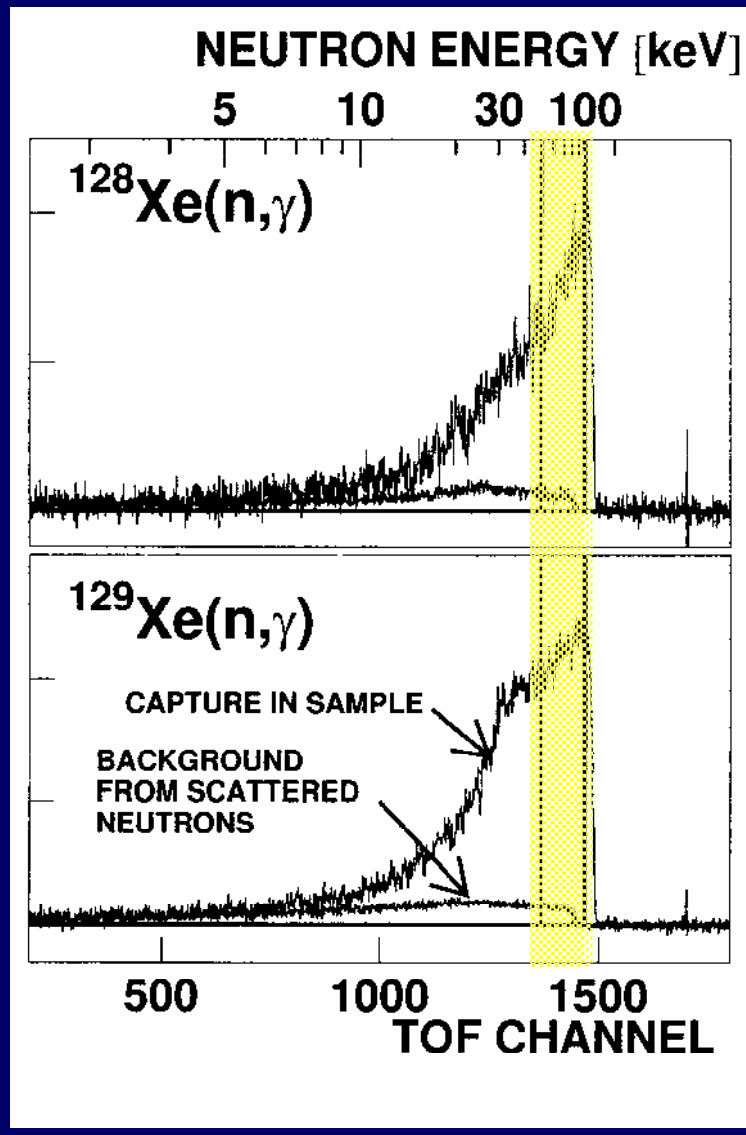

s-process branchings at A=127/128 confirmed by 8% difference in σN !

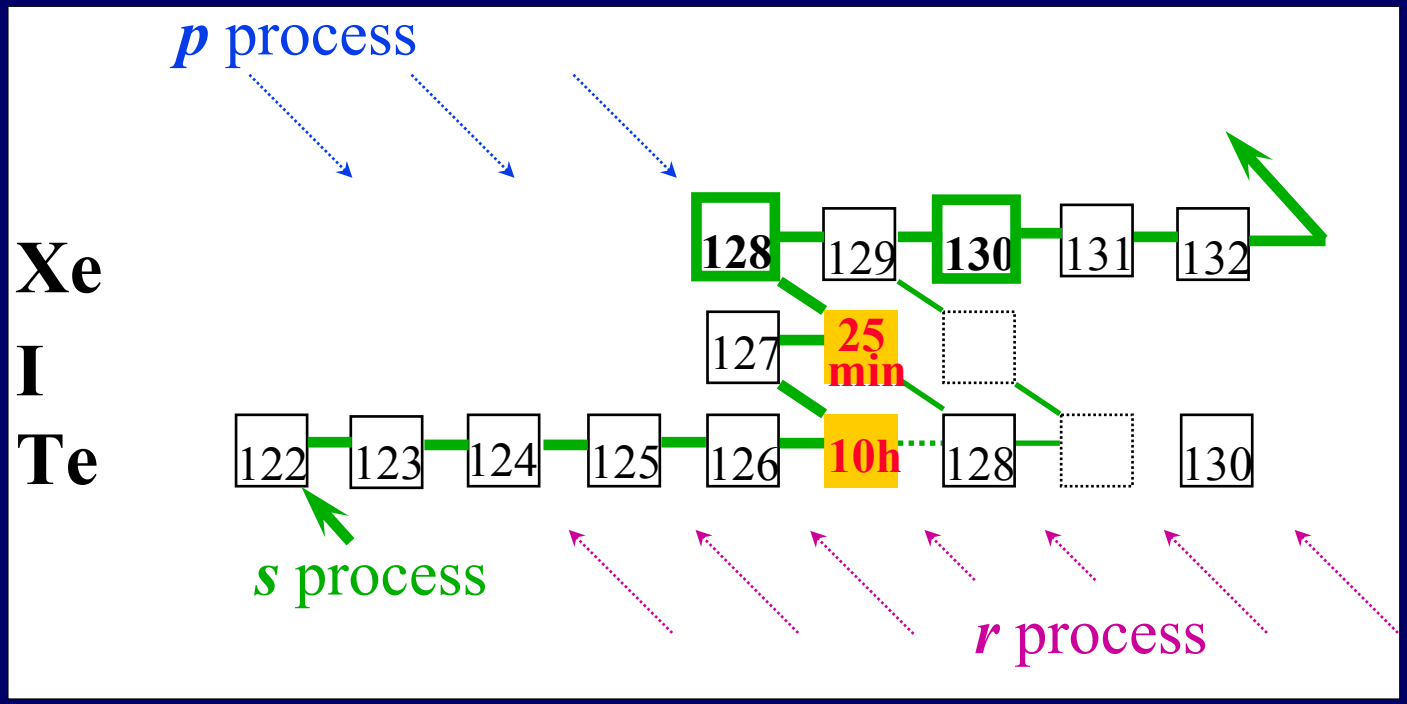

- ***branching independent of stellar neutron flux!!***
- ***β^-/ EC = 94% at T_8 = 1 .....but 99% at T_8 = 3***

the s process in AGB stars

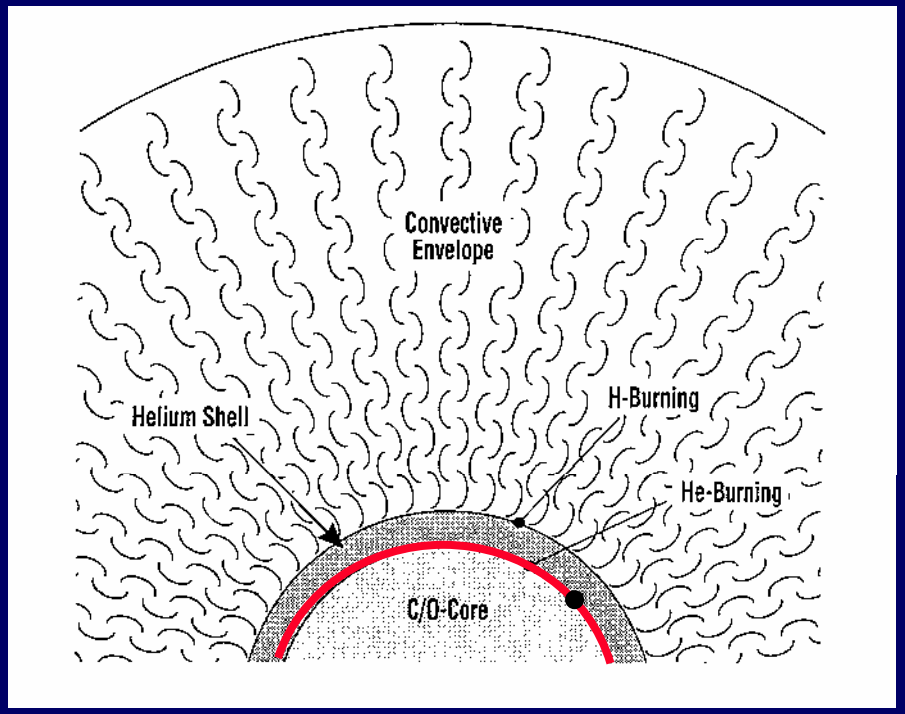

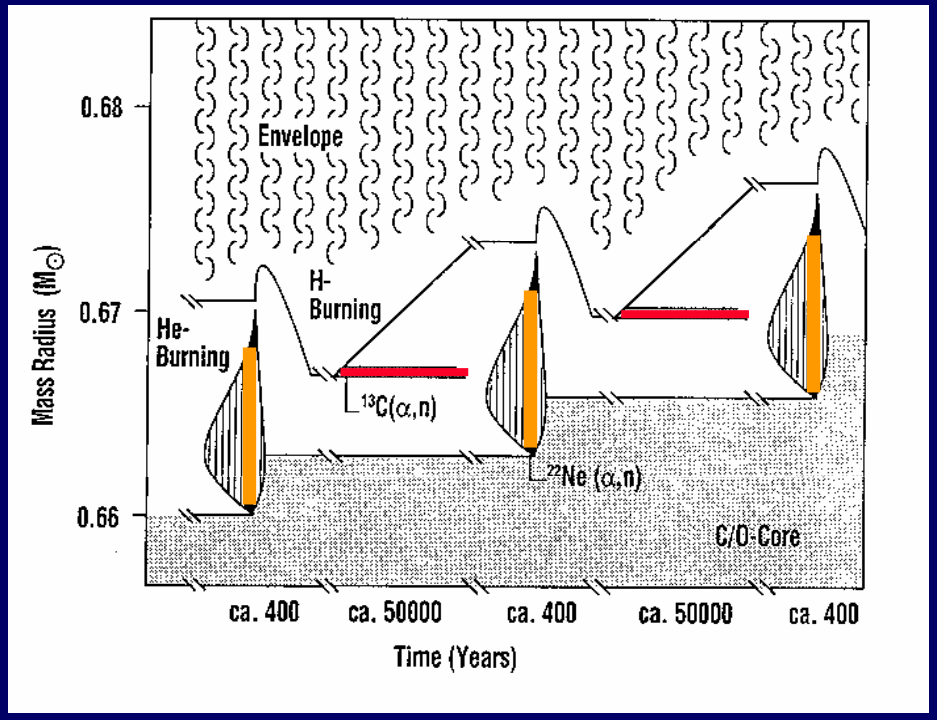

$^{13}C(\alpha,n)$ source operates during H-burning phase
kT=8 keV, $\beta^-/EC = 94\%$

final abundance patterns formed by $^{22}Ne(\alpha,n)$ during He shell flash
kT=23 keV, $\beta^-/EC = 99\%$

no branching!?

short convective turnover:

A = 128 branching works by fast mixing!

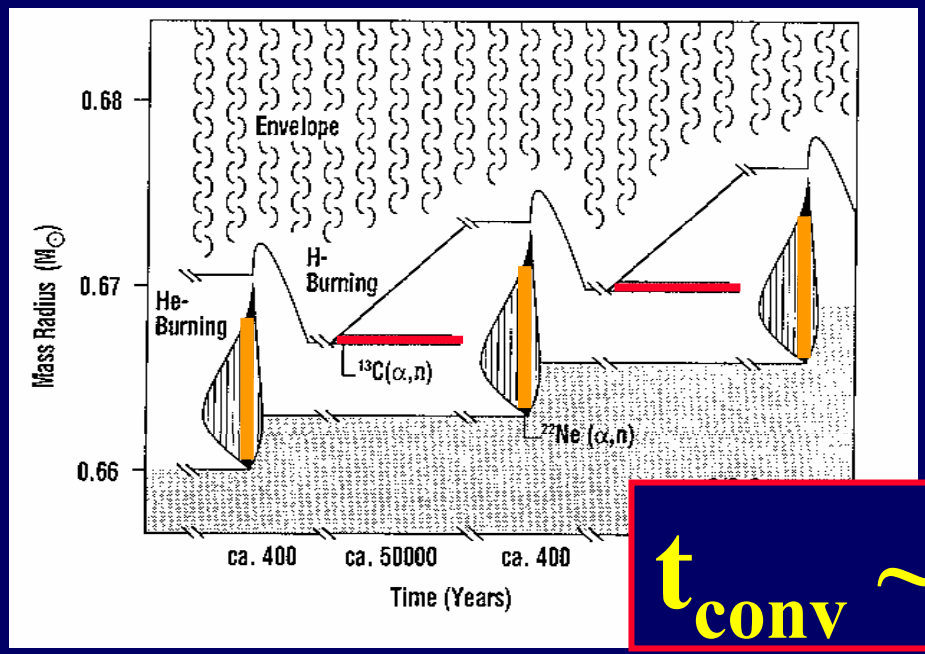

$t_{conv} \sim 1$ h

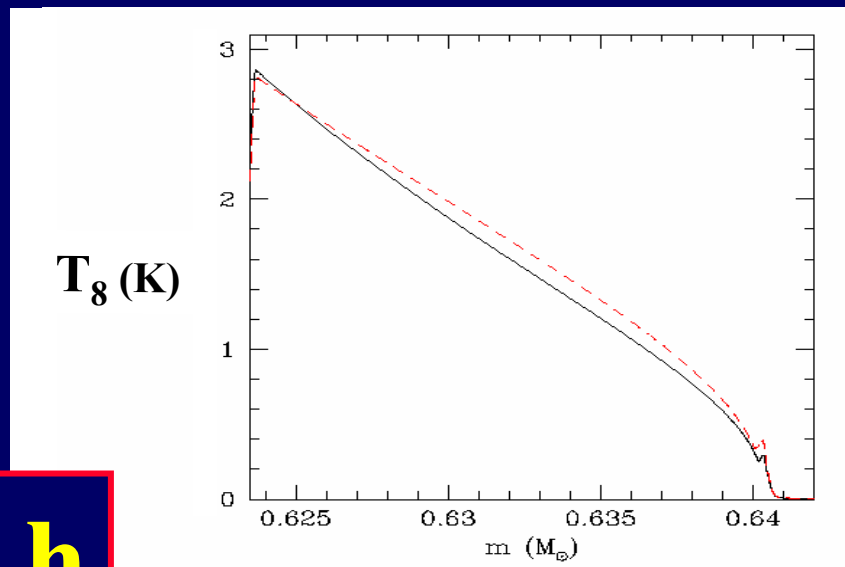

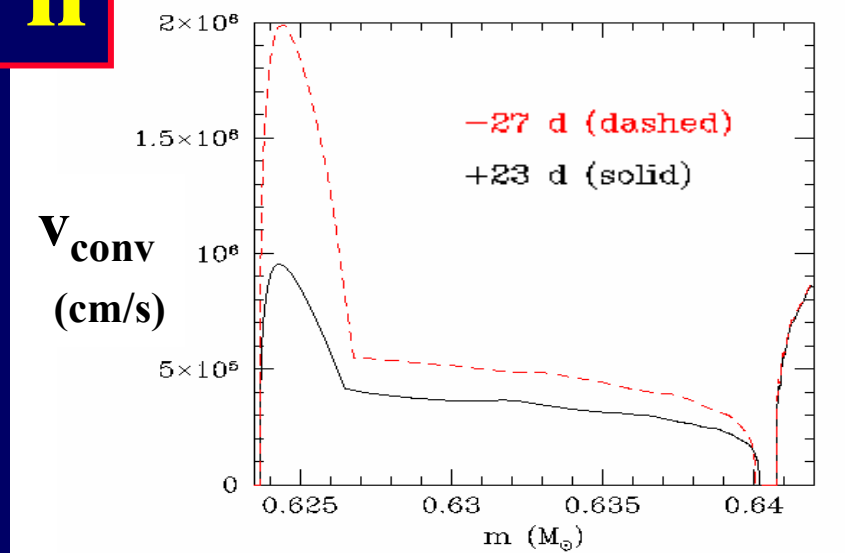

$T_8 = 0$	1	2	3
$f_{\beta^-} = 94$	95	99	100

the s-process branching at A=134

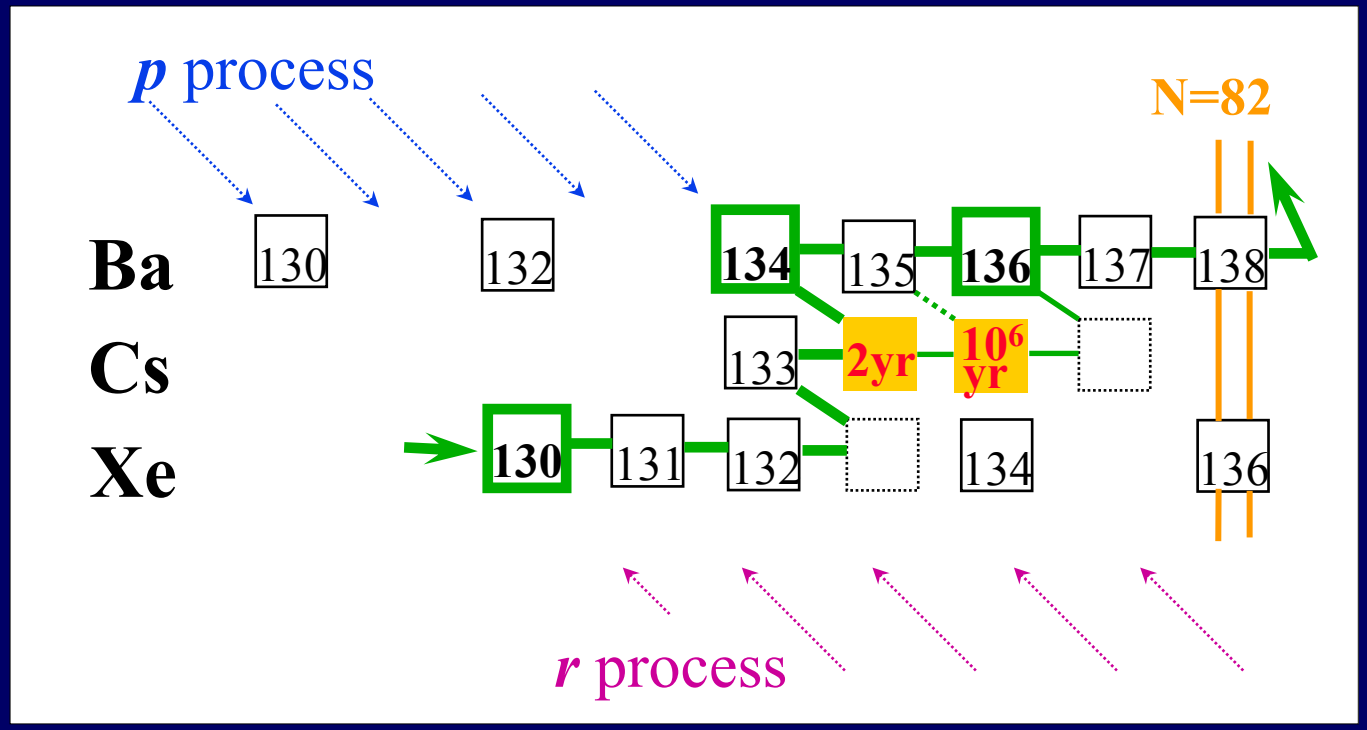

^{134}Cs tough: ***beta decay rate enhanced***
cross section difficult to measure → ***DANCE !?***

1 μg ^{134}Cs are N=4.5 10^{15} atoms
activity/ μg = Nλ = 5 10^{7} Bq
each module of DANCE sees R = 6. 10^{5} (600+700keV γ/s
corresponding to a signal rate of 1/μs/module

perhaps possible by restriction to fast component

the easy way to $\sigma(^{134}Cs)$
activation of ^{135}Cs ($t_{1/2}$=2 10^6 yr)

$^7Li(p,n)^7Be$, neutron energies 30 and 500 keV, $\Phi_n \approx 3\ 10^9$ n/s

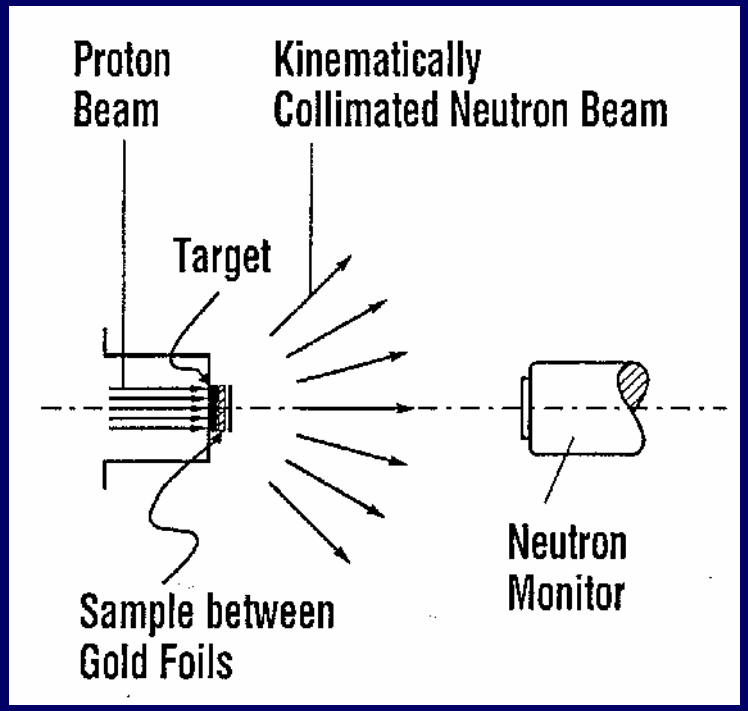

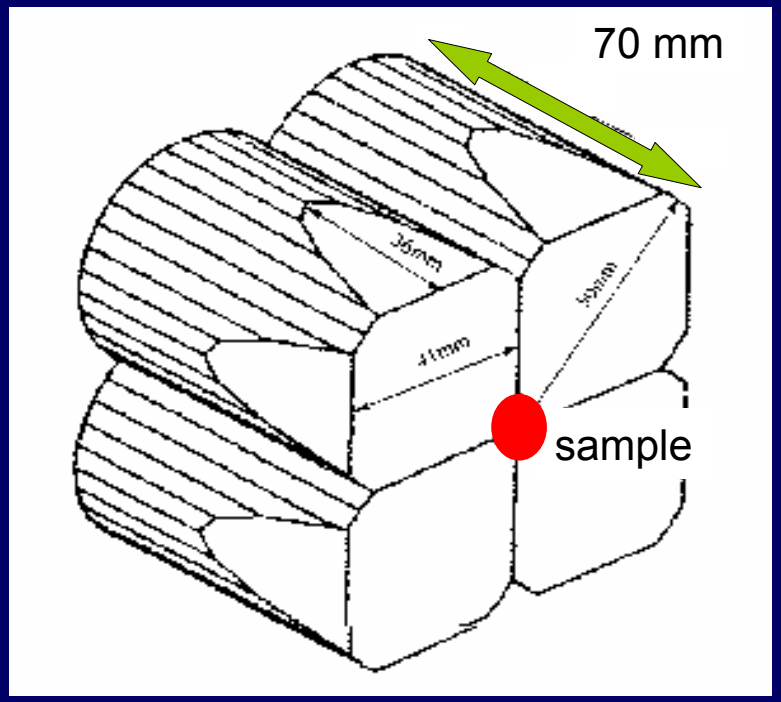

➡ **measurement with sample of 400 ng ^{135}Cs**

$\sigma(^{134}Cs)$ by model normalization

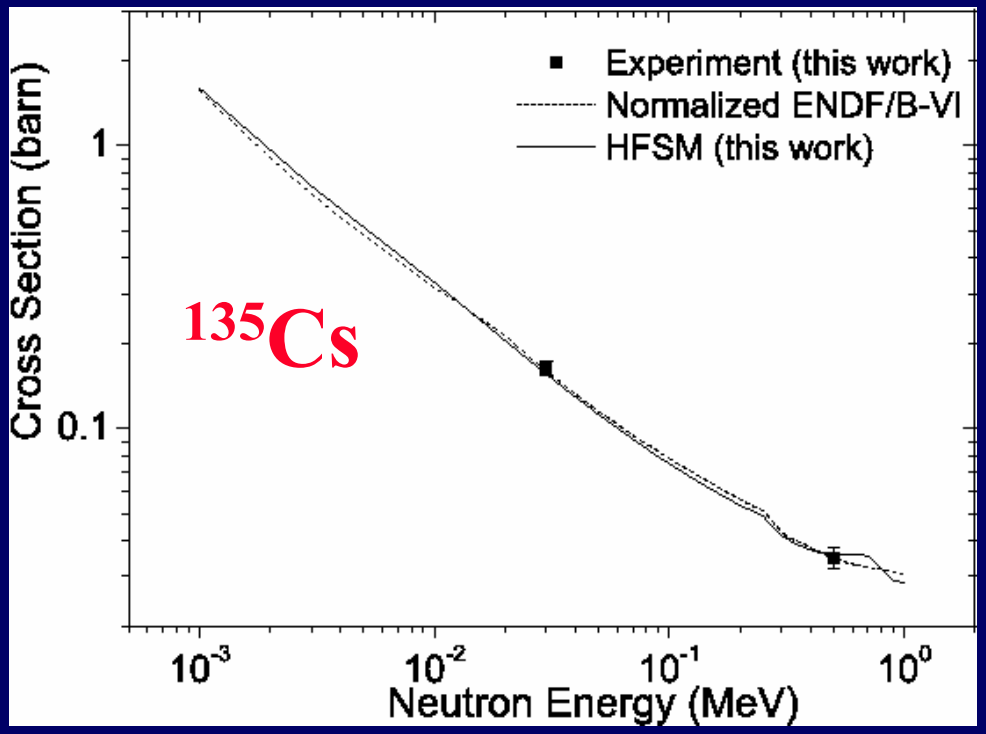

$^{134}Cs/^{135}Cs$ and $^{134}Cs/^{133}Cs$ ratios well reproduced by statistical model calculations

↓

^{134}Cs cross section via measured cross sections of neighbors

↓

$\sigma_{(134)}$ = 724 ± 65 mb at kT=30 keV

BUT: in general, direct cross section measurements necessary, e.g. for explosive nucleosynthesis

possible approaches
for samples with high specific γ–ray activities

- **further reduction of sample mass:** **requires higher fluxes**
  SNS
  short n_TOF flight path,
  minimized flight path & fast timing

- **storage ring experiments:** **RIB intersected with n-beam**
  periods of $\approx$ 1 μs → gain of 10^6 !

n_TOF improvements

D_2O moderator

- eliminates in-beam γ-rays
- boosts fast flux

more shielding

- eliminates in-beam bkgd

new vertical flight path

- further background reduction
- 100 times higher flux
- 10 times better duty factor

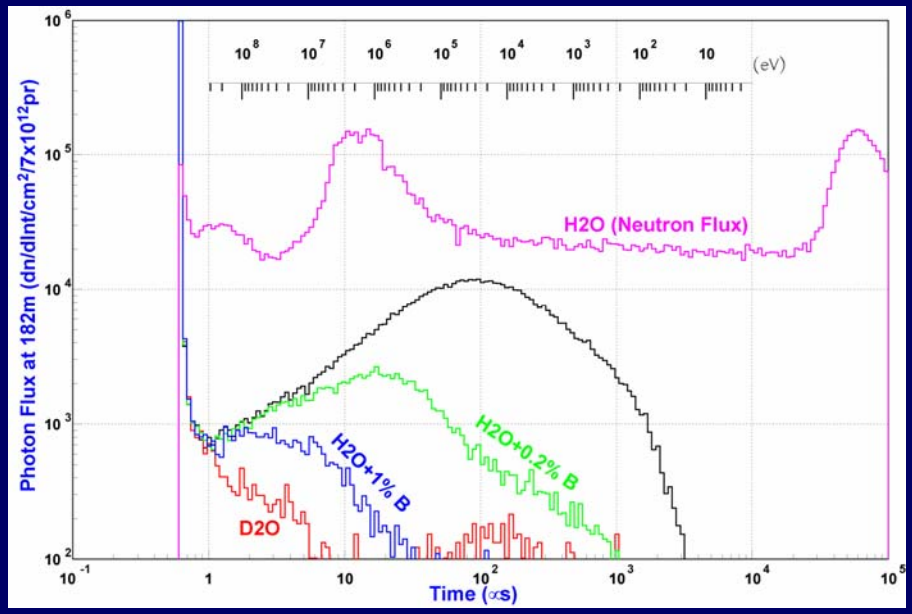

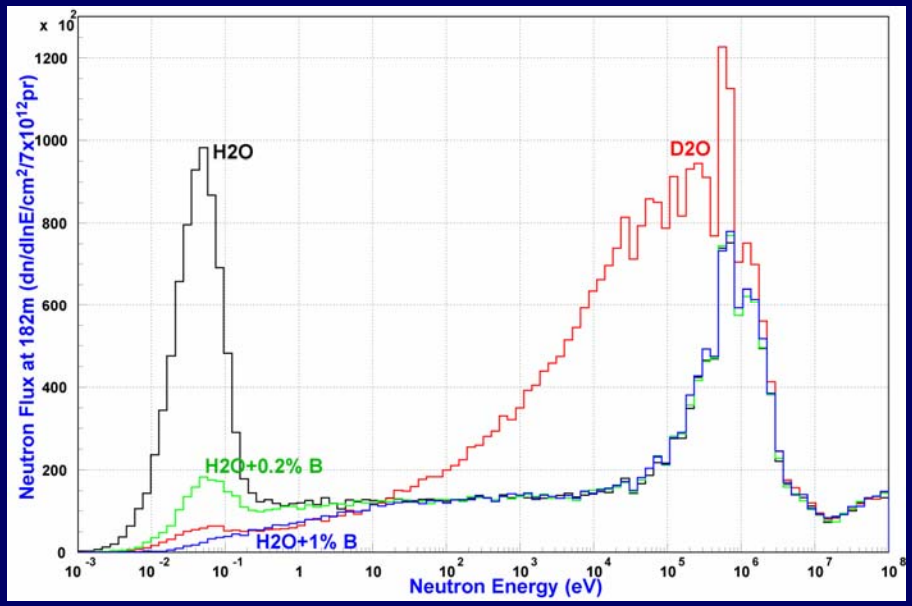

minimized flight path

enhancement of sensitivity in TOF measurements by shorter flight path

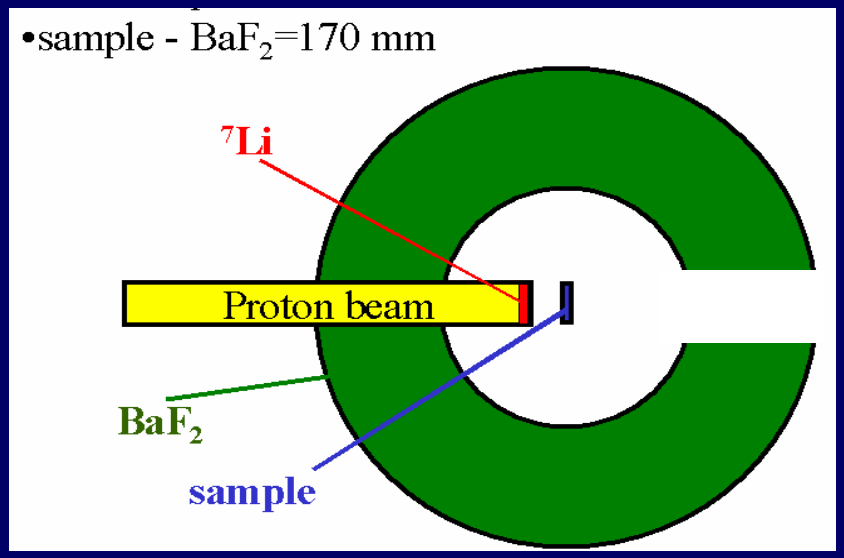

➡ TOF measurements with samples of 10^{15} atoms short lived isotopes ($t_{1/2}$> 10 d)

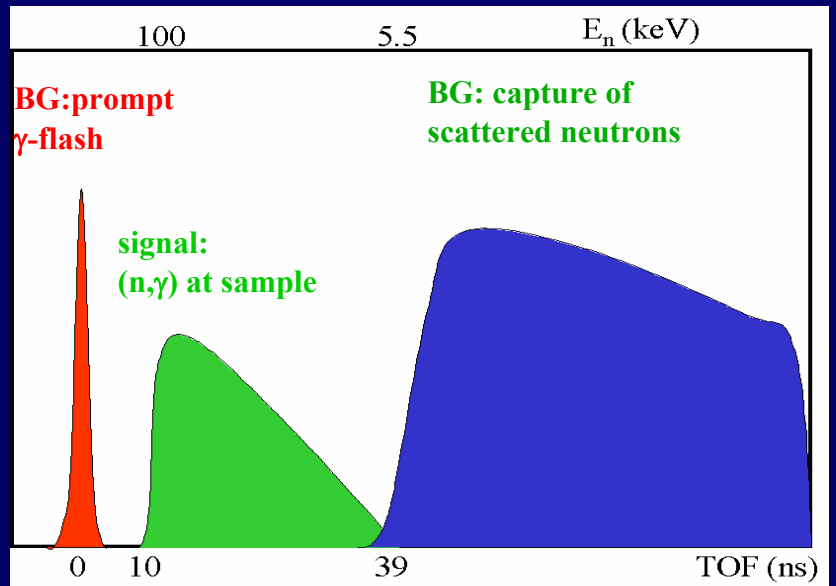

storage ring approach

(n,γ)➡Masuda, KEK)

(γ,n)➡Mohr, GSI)

(p,γ) .....

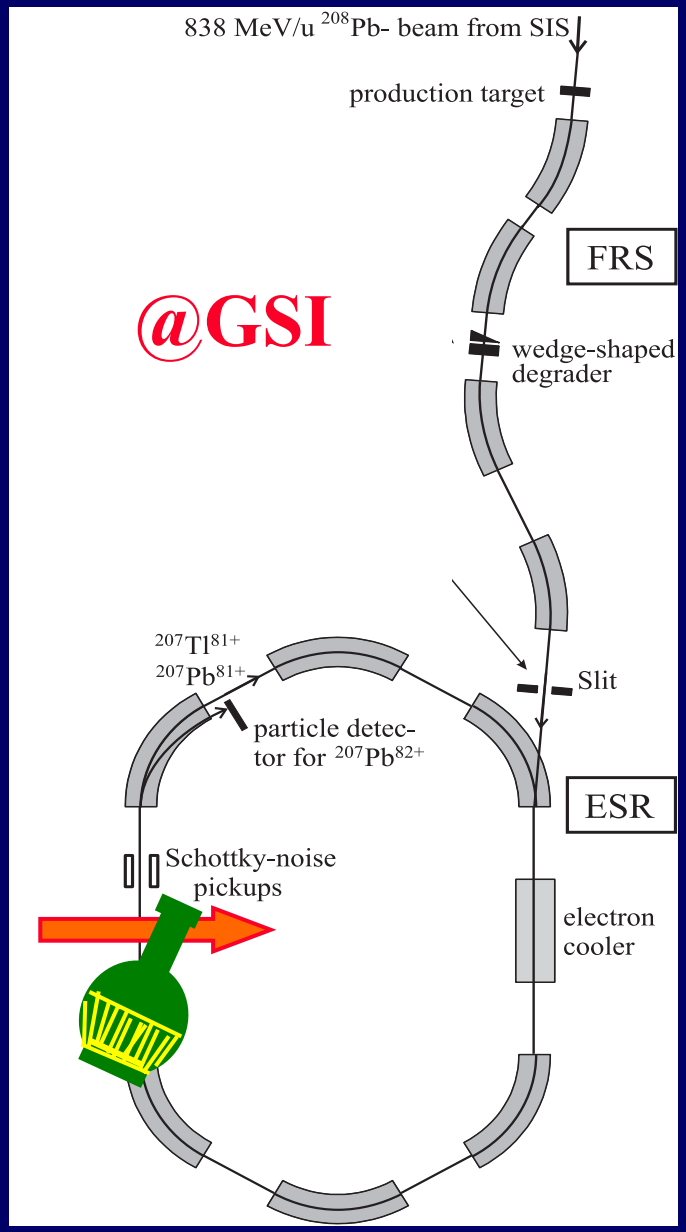

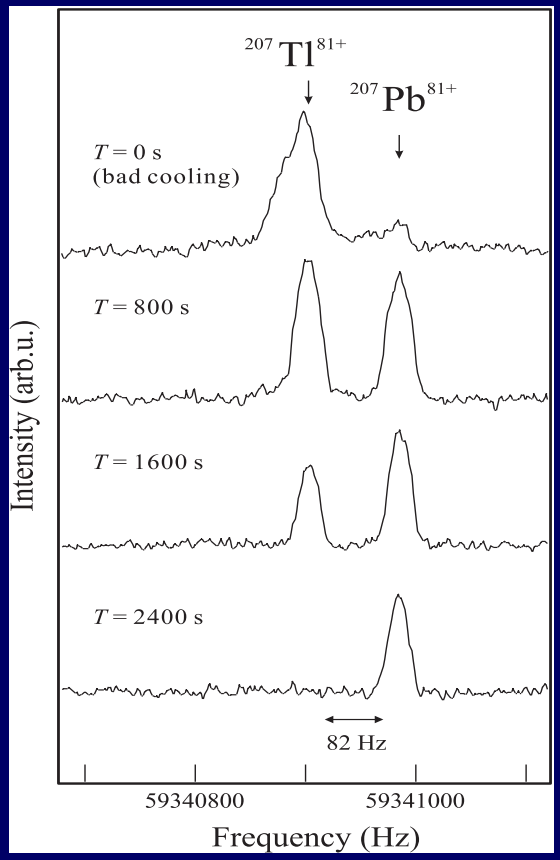

wide range of applications once that intense RIBs available

the s process in AGB stars:

the overall abundance distribution

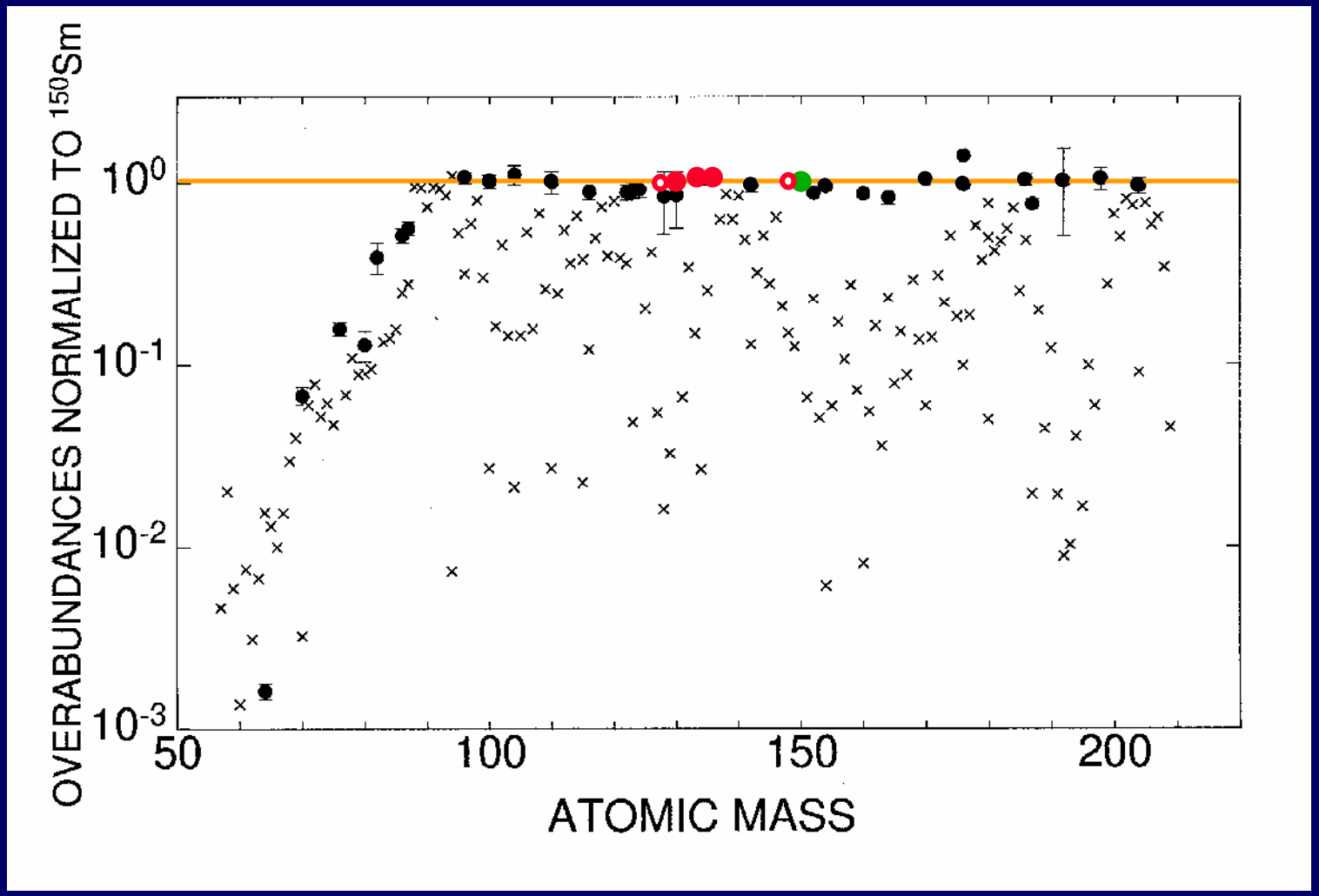

summary

- *s*-process branchings represent unique windows to the deep interior of Red Giants but require reliable neutron capture rates
- present facilities and detectors need to be used intensively for improving these rates in a number of areas (presolar grains, massive stars, optimizing HF prescriptions)
- the direct measurement of such rates for radioactive samples leads to the limits of present techniques
- promising options are expected at RIB facilities

→ ***important for quantitative picture of galactic chemical evolution***

Contribution by

Michael Wiescher

University of Notre Dame

michael.c.wiescher.1@nd.edu

29 pages

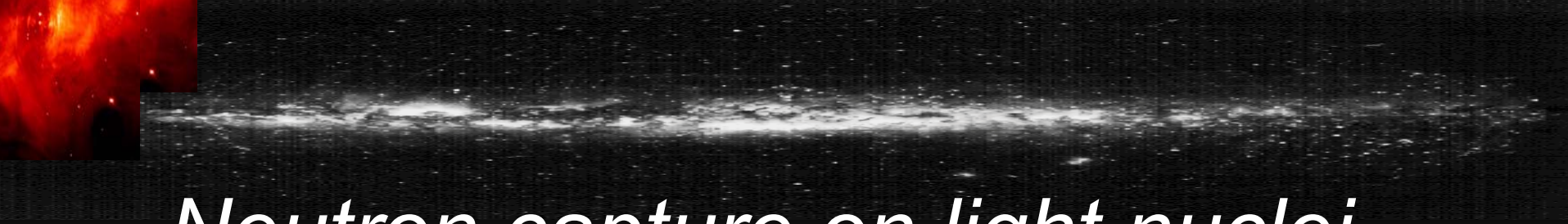

Neutron capture on light nuclei - is there a light r-process?

Michael Wiescher
University of Notre Dame

- Ignition of nucleosynthesis in the early SN shock
- Three-particle fusion processes as trigger reactions
- n-capture on halo nuclei; the light r-process?
- Experiments?

Supported by he Joint Institute of Nuclear Astrophysics;
www.JINAweb.org

Temperature and Density Development

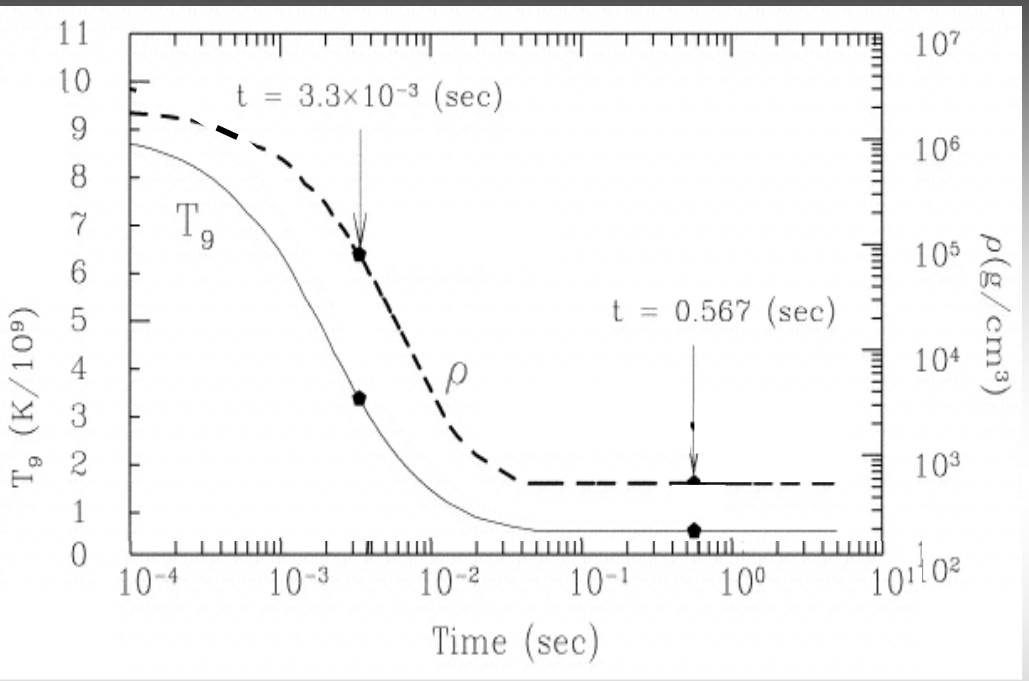

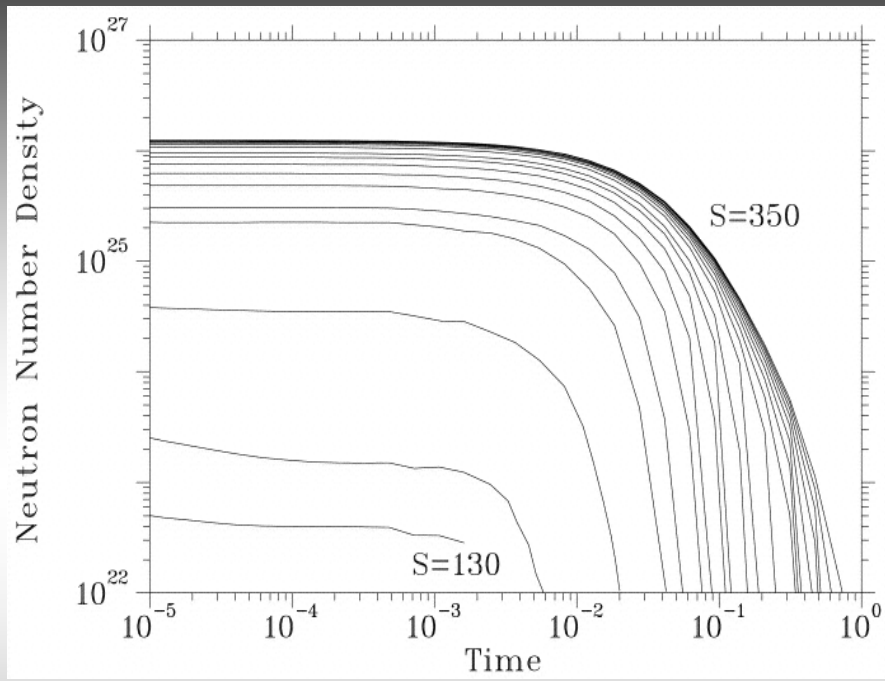

Adiabatic expansion on millisecond time scale $S \approx \frac{T_9}{\rho_5}$

Explosive burning in expanding shock

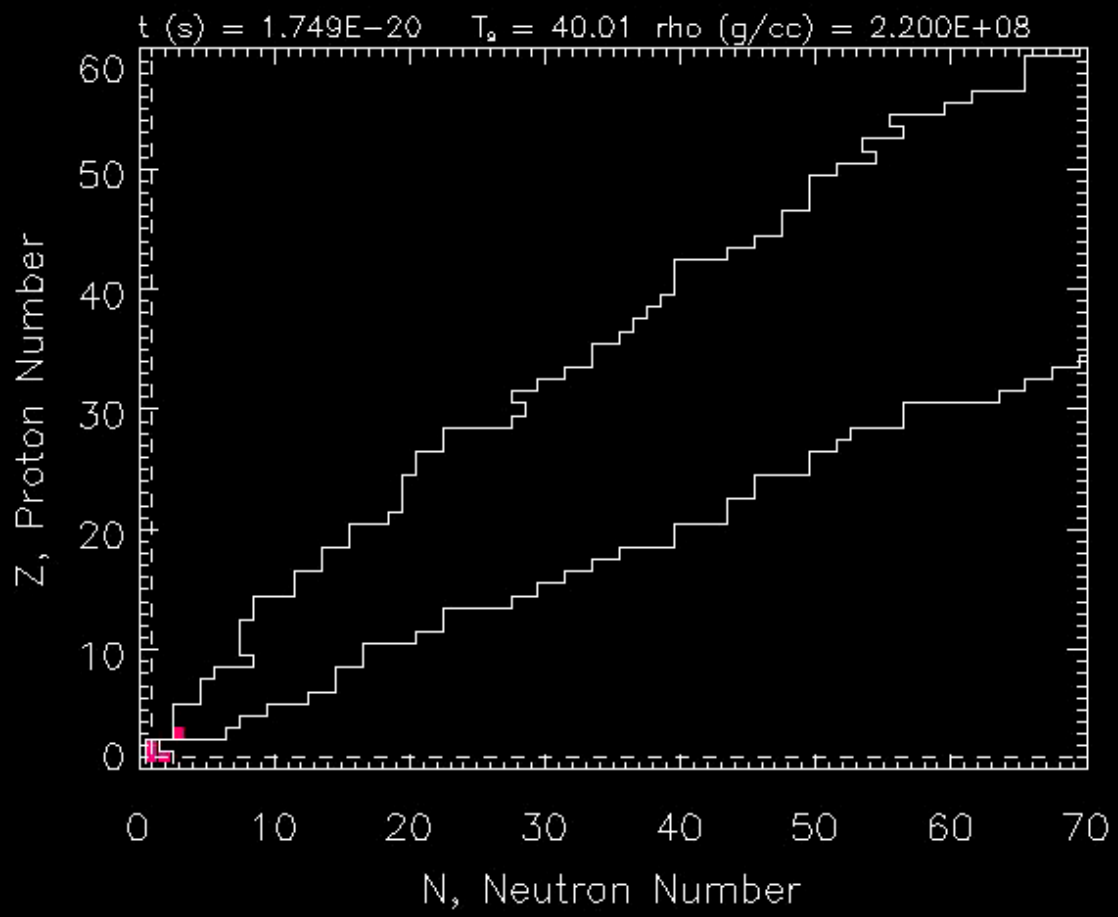

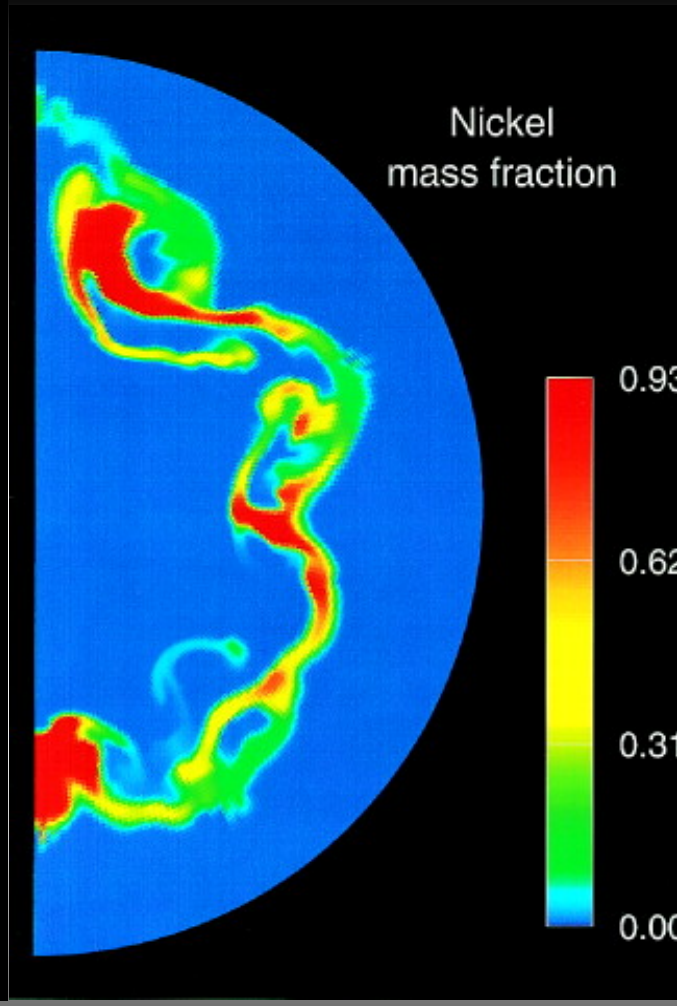

Initial NSE conditions: only p, n, ^{4}He, abundances
with decline in T $\Rightarrow$ re-association in NSE towards ^{56}Ni

Network simulations of early SN shock-front nucleosynthesis

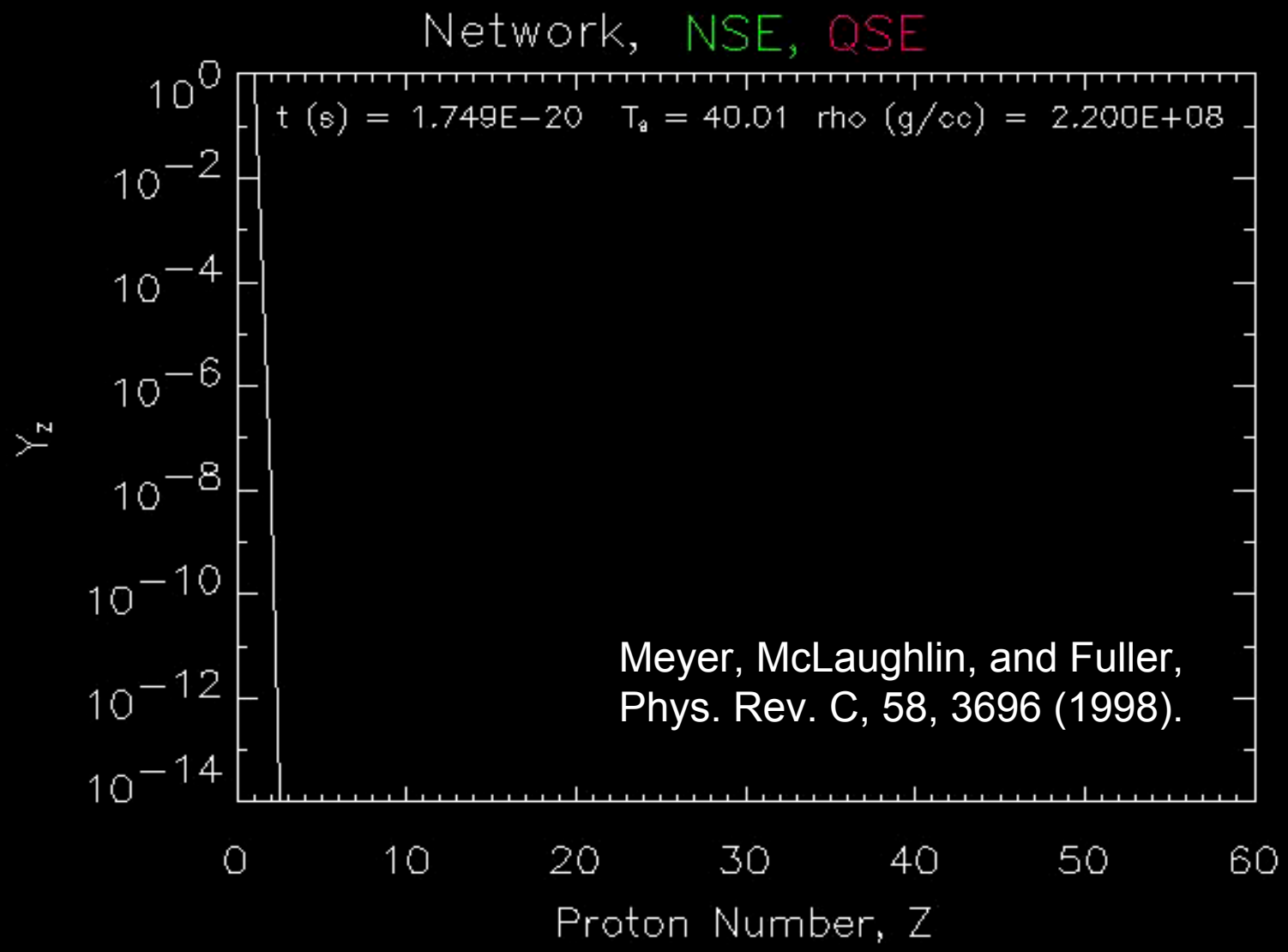

Meyer, McLaughlin, and Fuller, Phys. Rev. C, 58, 3696 (1998).

Dynamical Reaction Network

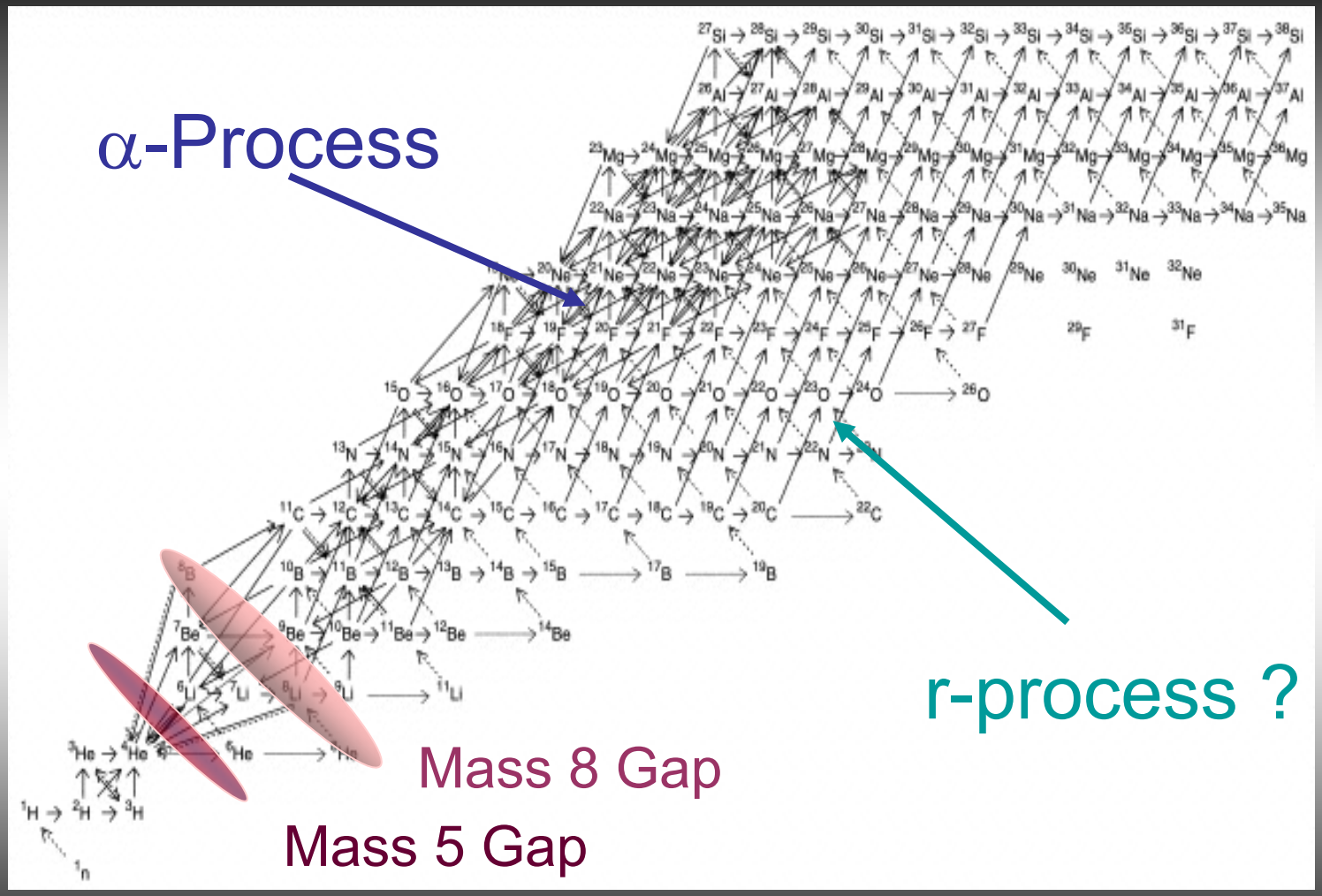

Build-Up of Seed Nuclei

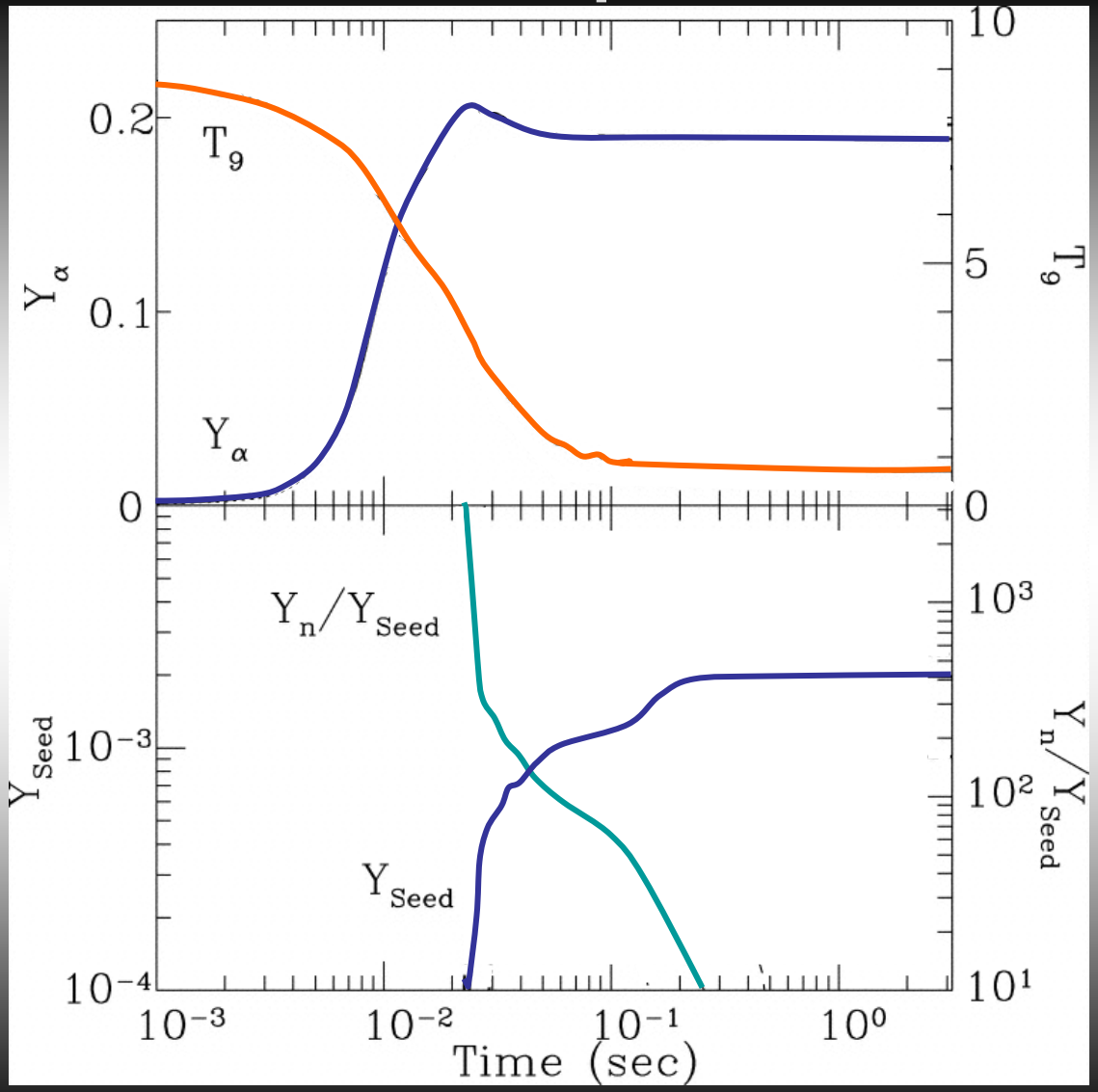

Conversion of initial p, n, ^{4}He abundance into seed nuclei is controlled by three particle reactions involving ^{4}He, this maintains high ^{4}He abundance

Terasawa et al. ApJ 562, 2001 & ApJ 578, 2002

Bridging the A=5 (8) Gap

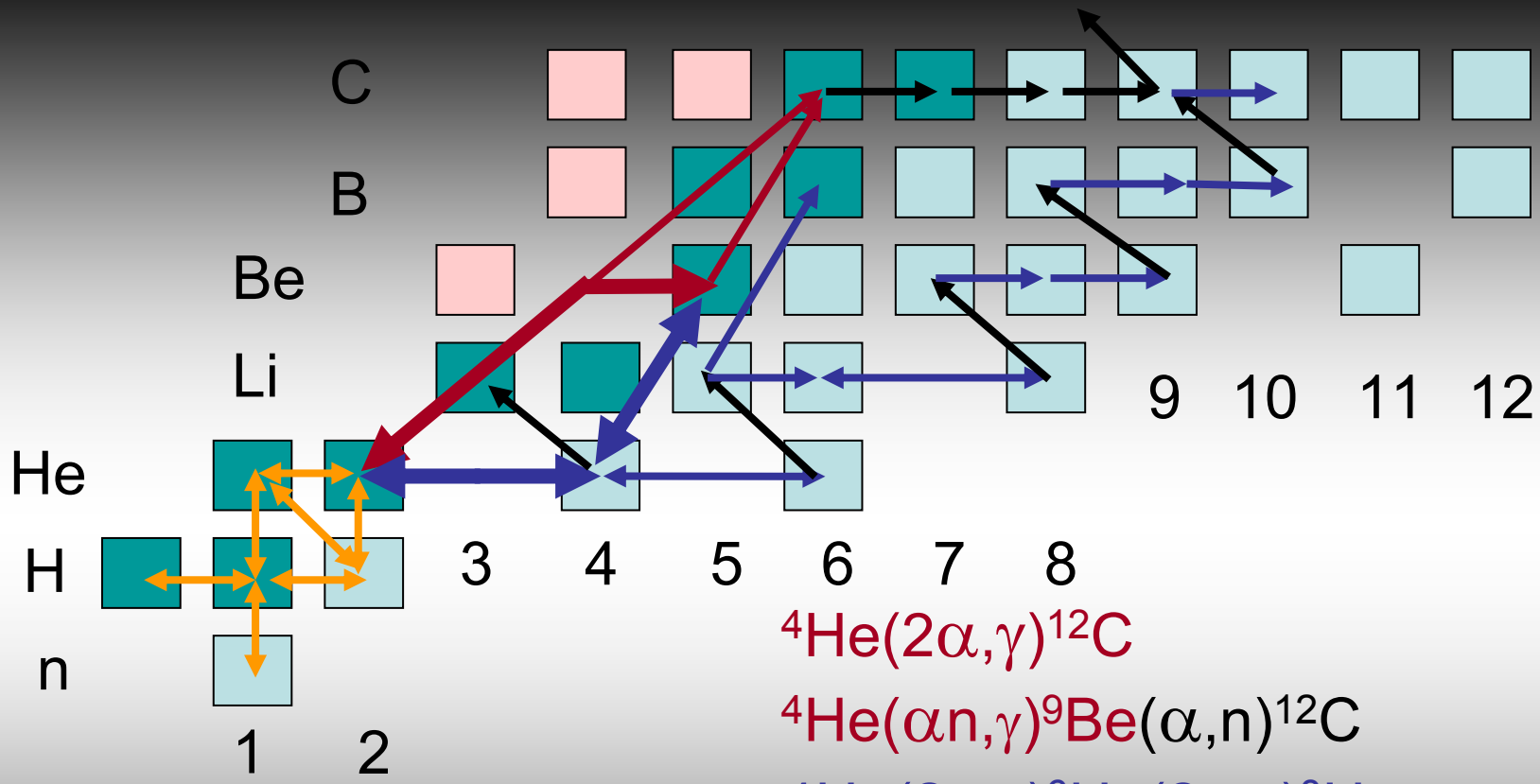

$^{4}He(2\alpha,\gamma)^{12}C$

$^{4}He(\alpha n,\gamma)^{9}Be(\alpha,n)^{12}C$

$4He(2n,\gamma)^{6}He(2n,\gamma)^{8}He$

$^{4}He(2n,\gamma)^{6}He(\alpha,n)^{9}Be\ (\alpha,n)^{12}C$

Feeding of r-process seed depends on 3-particle reaction rates

The triple α Reaction

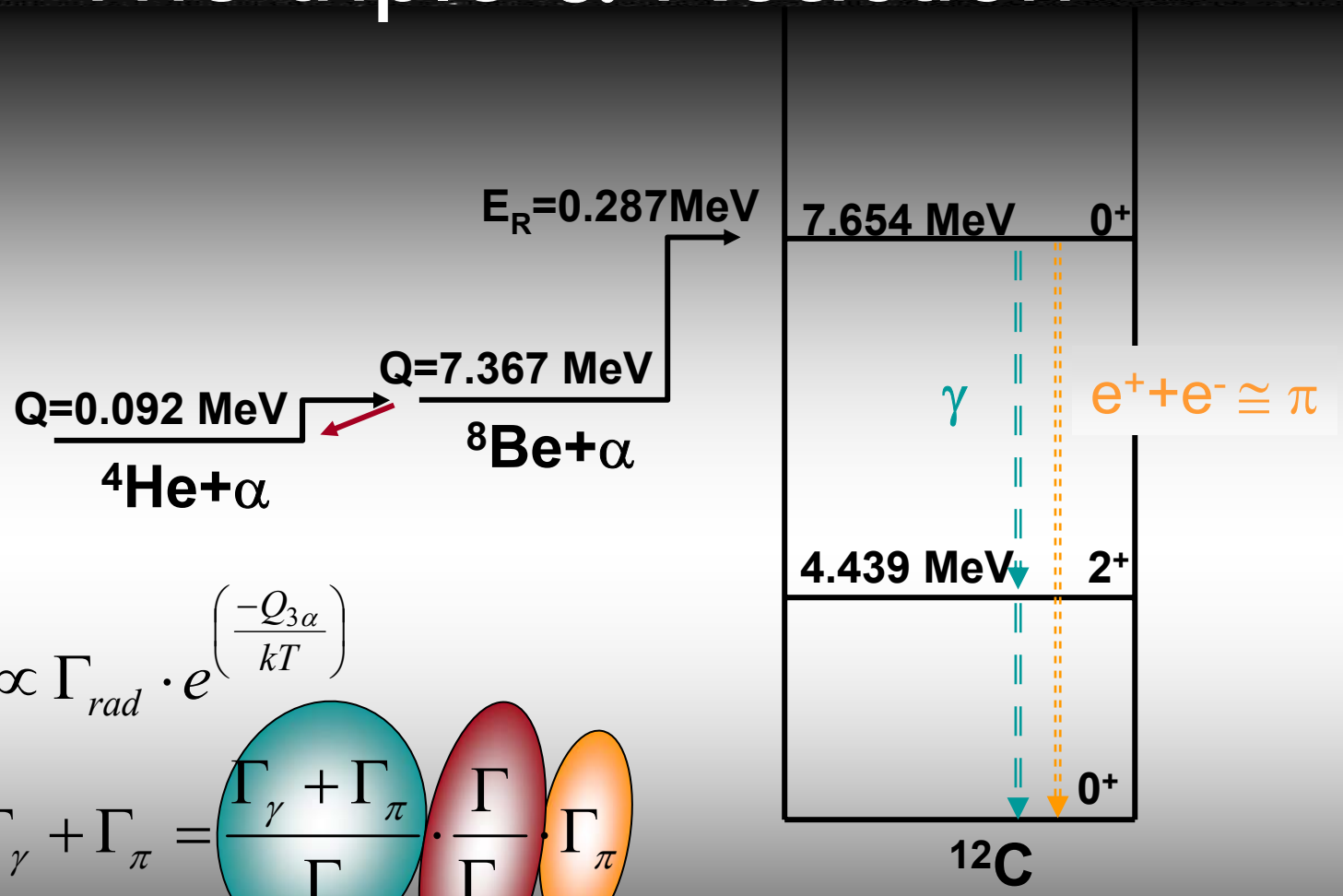

$$\langle \alpha\alpha\alpha \rangle \propto \Gamma_{rad} \cdot e^{\left(\frac{-Q_{3\alpha}}{kT}\right)}$$

$$\Gamma_{rad} = \Gamma_\gamma + \Gamma_\pi = \frac{\Gamma_\gamma + \Gamma_\pi}{\Gamma} \cdot \frac{\Gamma}{\Gamma_\pi} \cdot \Gamma_\pi$$

present values are based on different experiments ±12%

The (ααn) Reaction

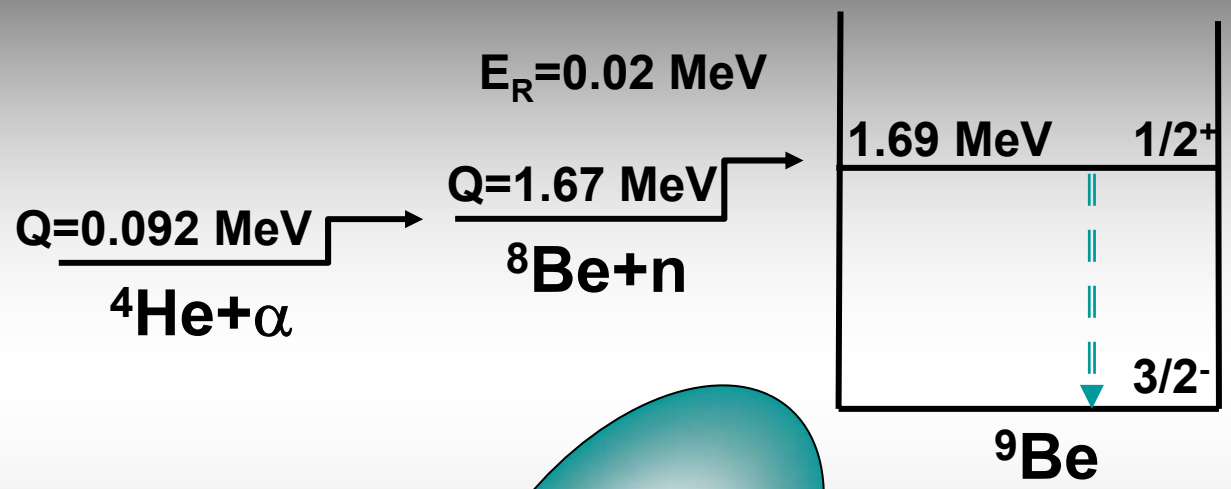

$$\langle \alpha\alpha n \rangle \propto e^{\frac{-Q_{\alpha\alpha}}{kT}} \cdot \left(\Gamma_\gamma \cdot e^{\frac{-E_R}{kT}} + \sigma_{DC_s} \cdot v \right)$$

Uncertainties are in the DC calculation and in s-wave interference

Three Particle Reactions

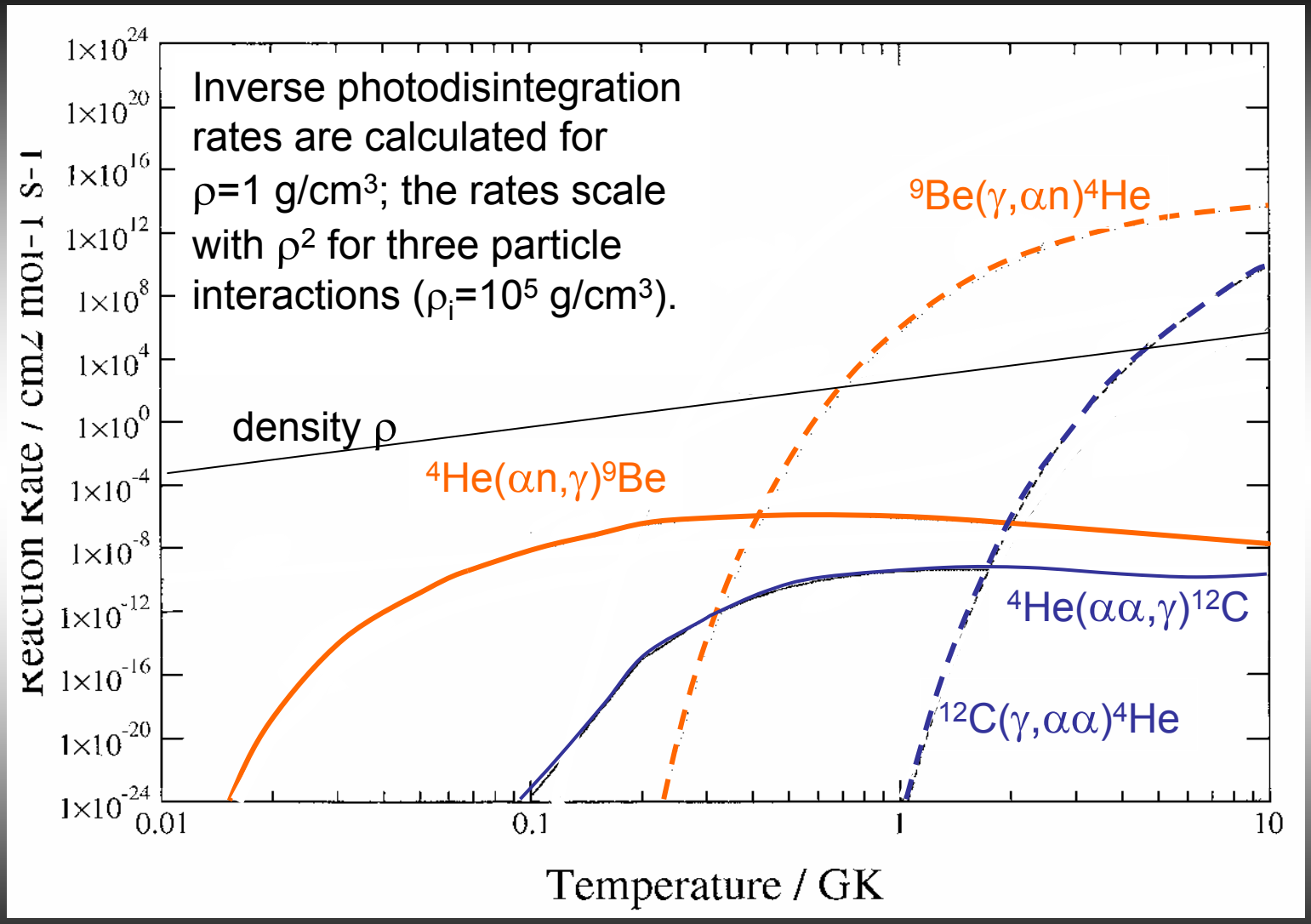

2n-capture processes

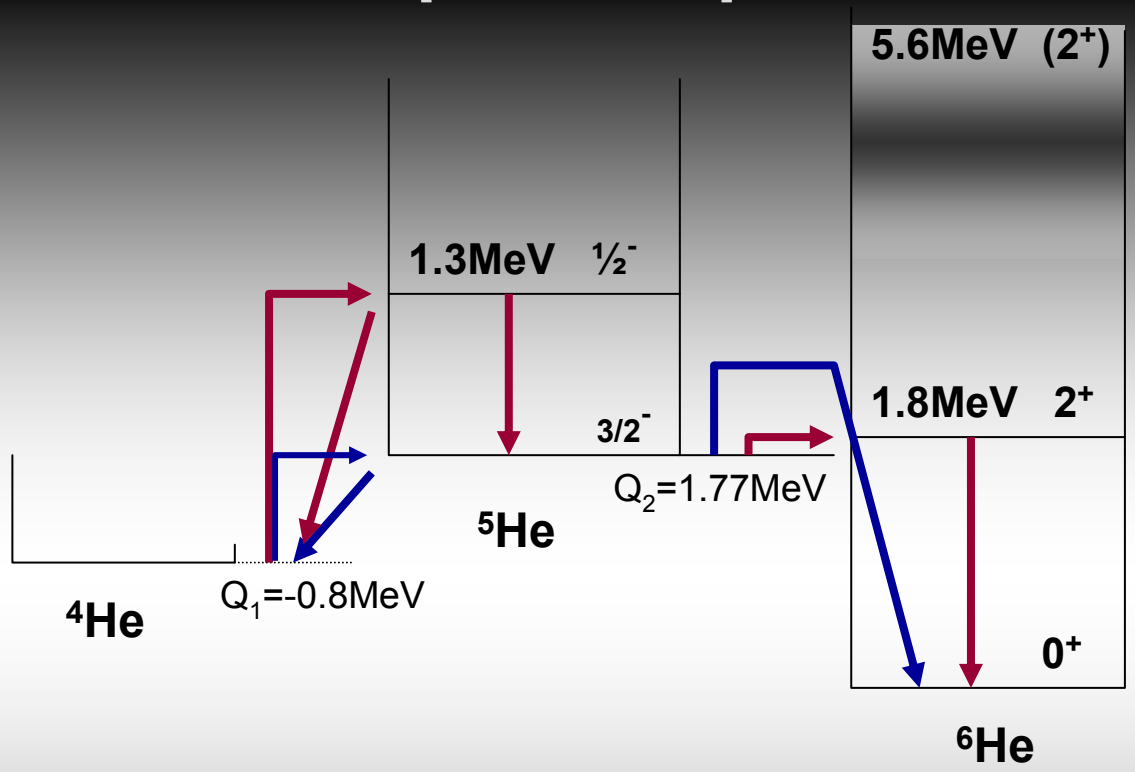

$$\langle \sigma v \rangle_{2n} = c \cdot T^{-3/2} \cdot e^{\left(\frac{Q_1}{k \cdot T}\right)} \cdot \langle \sigma v \rangle_2$$

$$\langle \sigma v \rangle_2^{res} \propto \Gamma_{1.8MeV}(E2)$$

$$\langle \sigma v \rangle_2^{dc} \propto \sigma_{PD}(E1)$$

Di-neutron capture

$$N_A^2\langle \alpha nn\rangle = N_A^2 \int_{E_1} \frac{d\langle pp\rangle(E_1)}{dE_1}\cdot\frac{2\eta}{\Gamma(E_1)}\left[\int_{E_2}\frac{\langle p\gamma\rangle(E_1,E_2)}{dE_2}dE_2\right]dE_1$$

$$\frac{d\langle \sigma\upsilon\rangle}{dE} = \sqrt{\frac{8}{\pi\mu}}\cdot\frac{1}{(kT)^{3/2}}\cdot\sigma(E)\cdot e^{\left(-\frac{E}{kT}\right)}$$

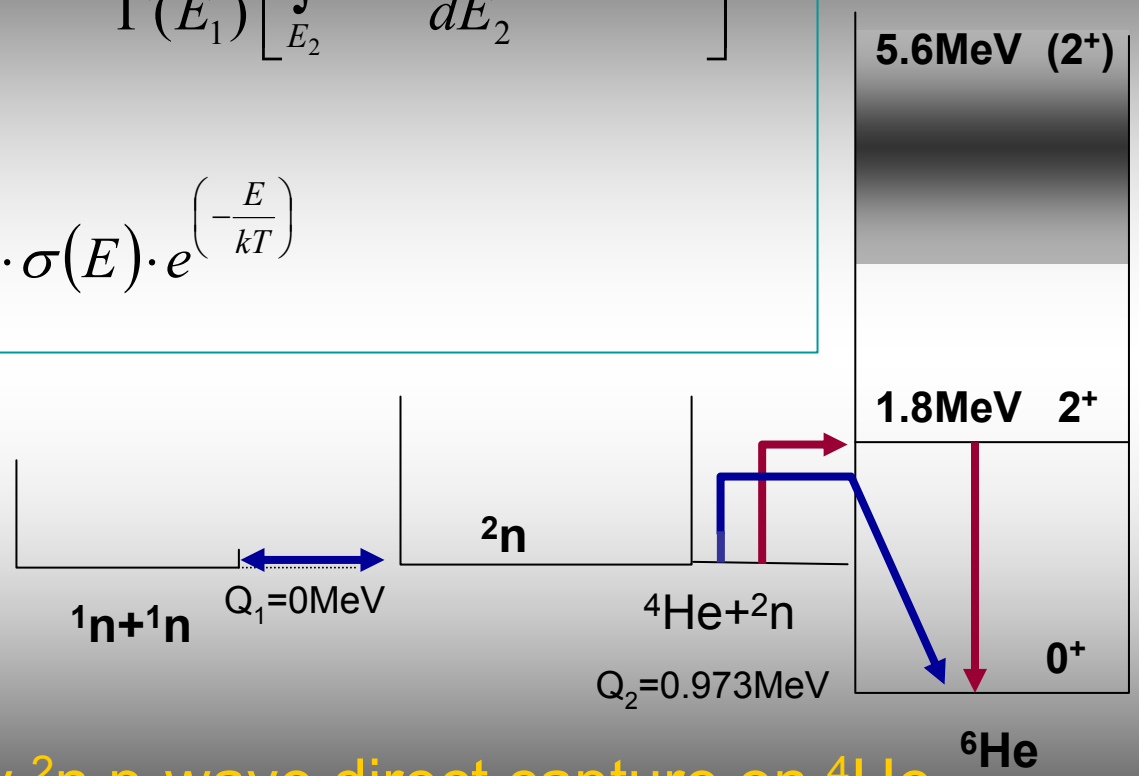

Mainly ^{2}n p-wave direct capture on ^{4}He
the 830 keV resonance is negligible!

Probability of di-neutron formation and di-neutron capture

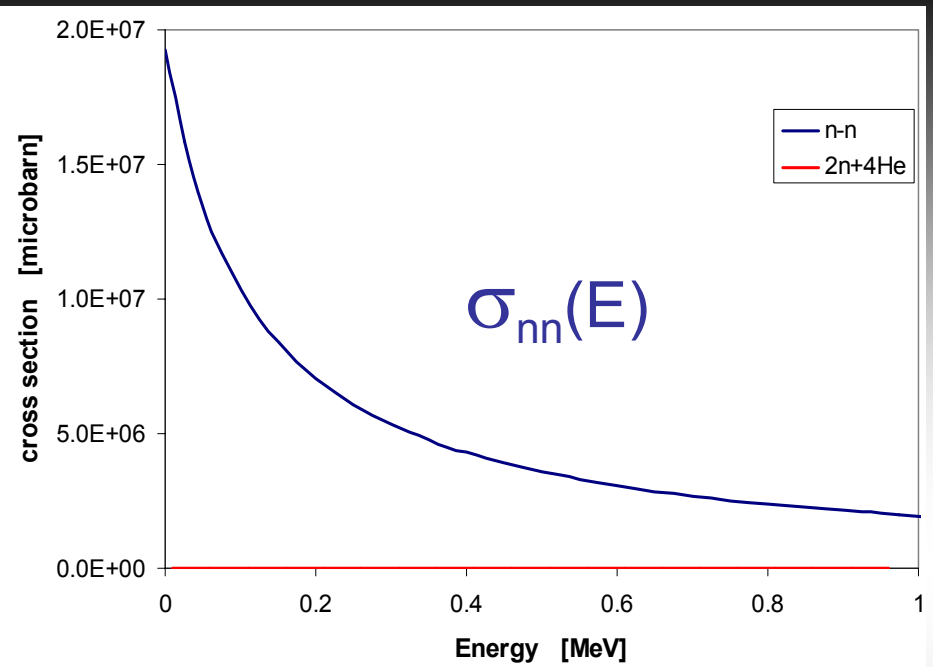

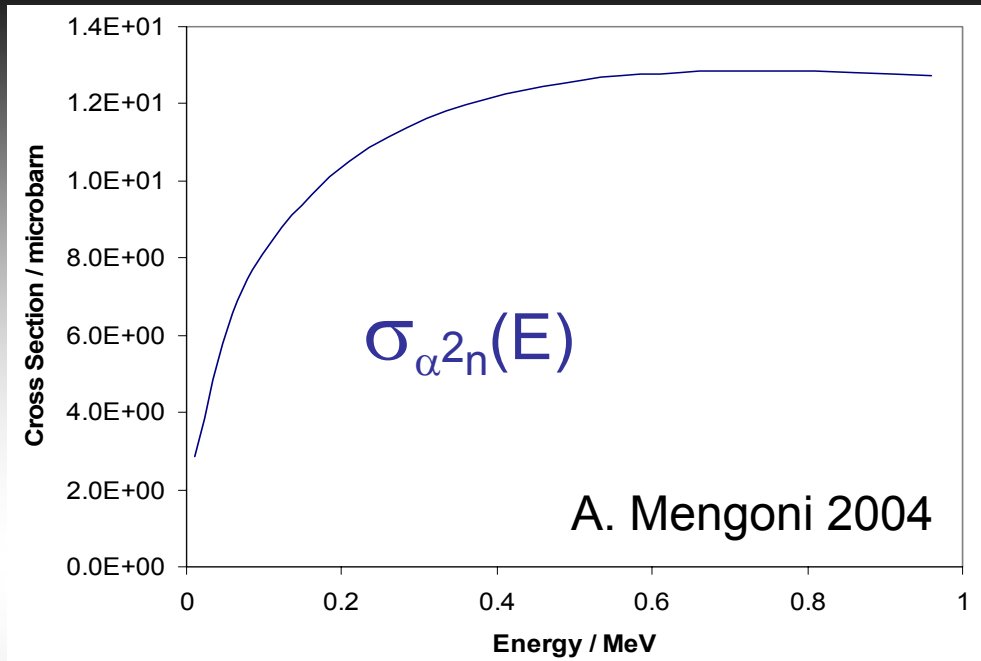

$$N_A^2\langle \alpha nn\rangle = N_A^2 \int_{E_1} \frac{d\langle pp\rangle(E_1)}{dE_1}\cdot\frac{2\eta}{\Gamma(E_1)}\left[\int_{E_2}\frac{\langle p\gamma\rangle(E_1,E_2)}{dE_2}dE_2\right]dE_1$$

$$\frac{d\langle \sigma\upsilon\rangle}{dE} = \sqrt{\frac{8}{\pi\mu}}\cdot\frac{1}{(kT)^{3/2}}\cdot\sigma(E)\cdot e^{\left(-\frac{E}{kT}\right)}$$

The $^{6}He(\alpha,n)^{10}Be$ Reaction

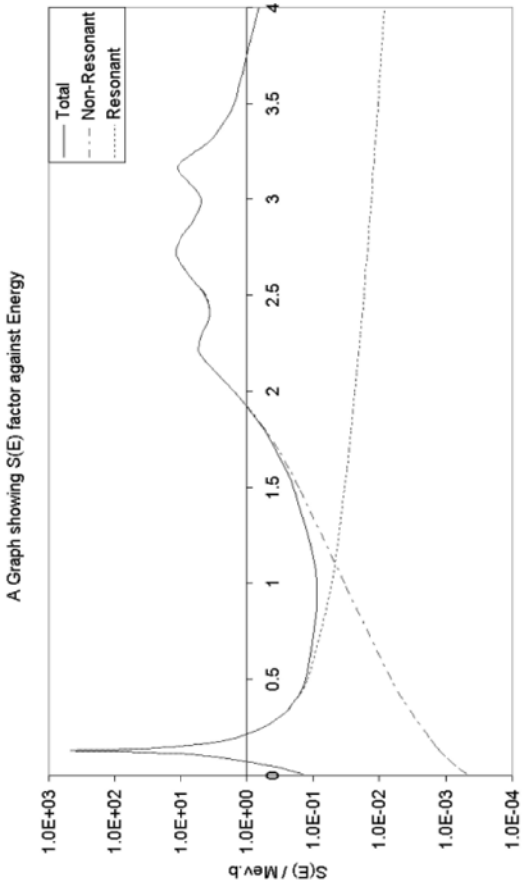

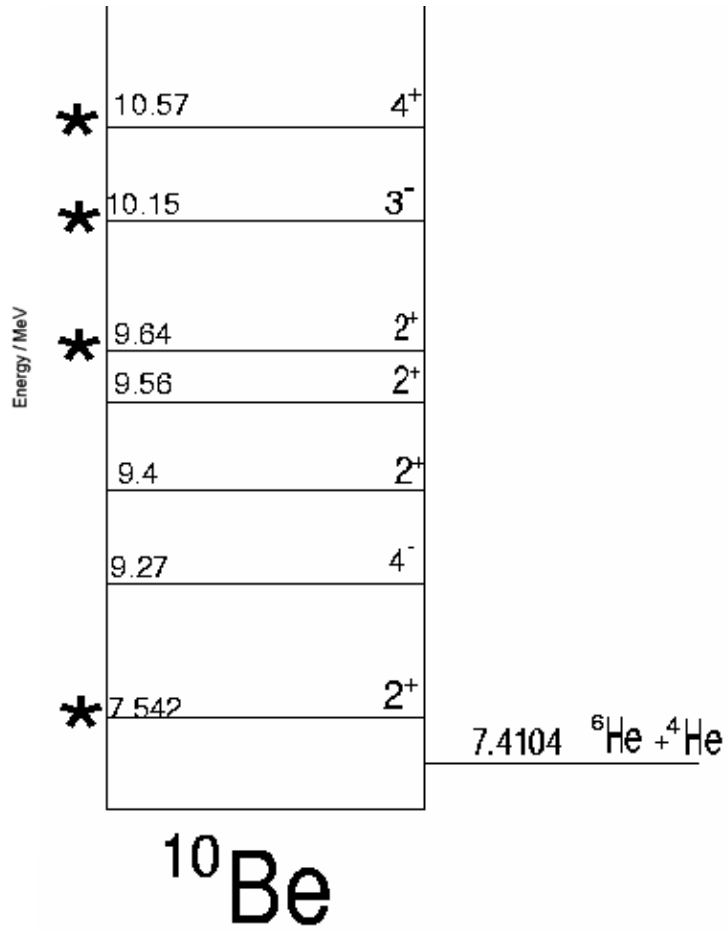

Reaction rates

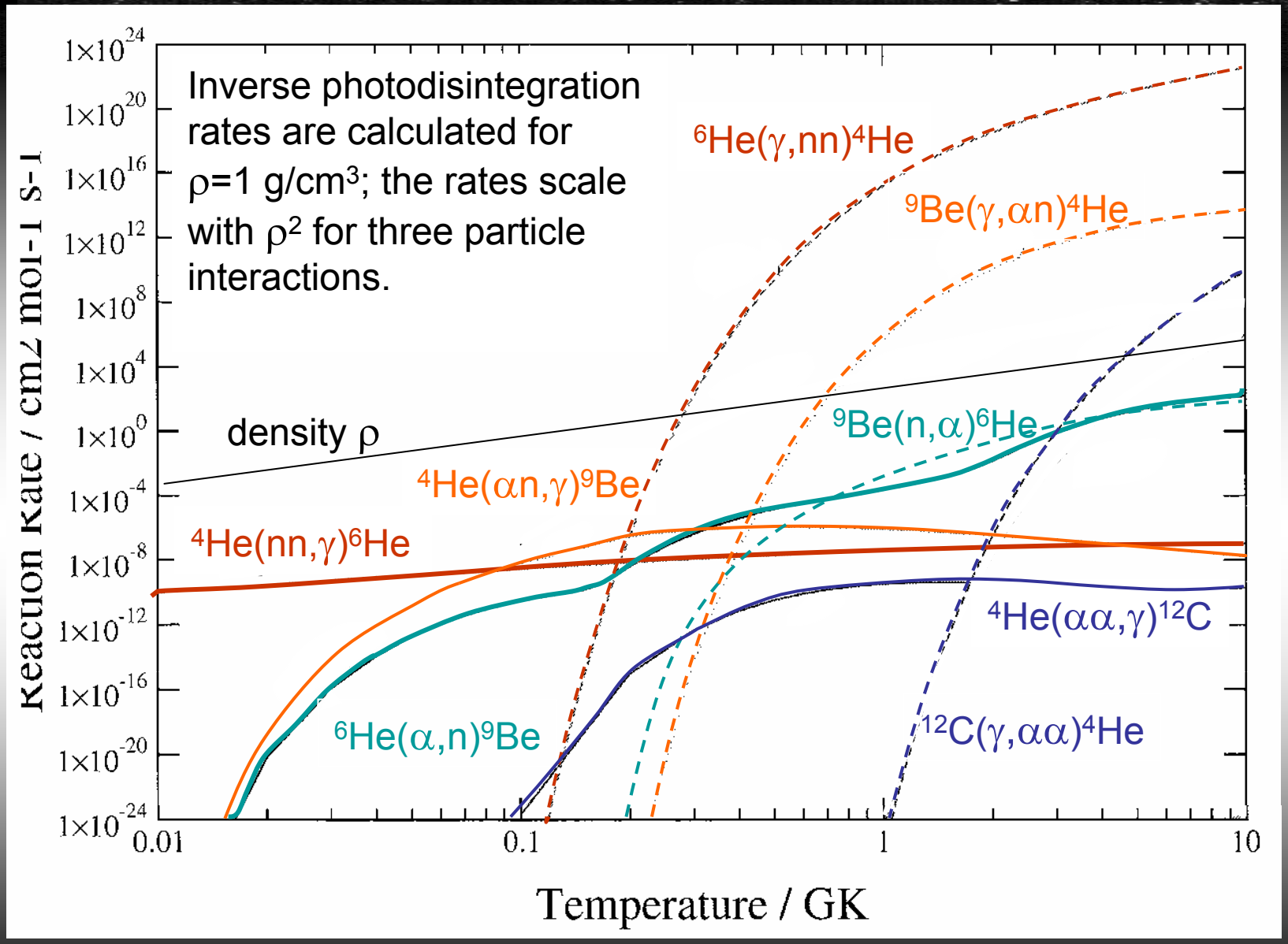

Fate of ^{9}Be

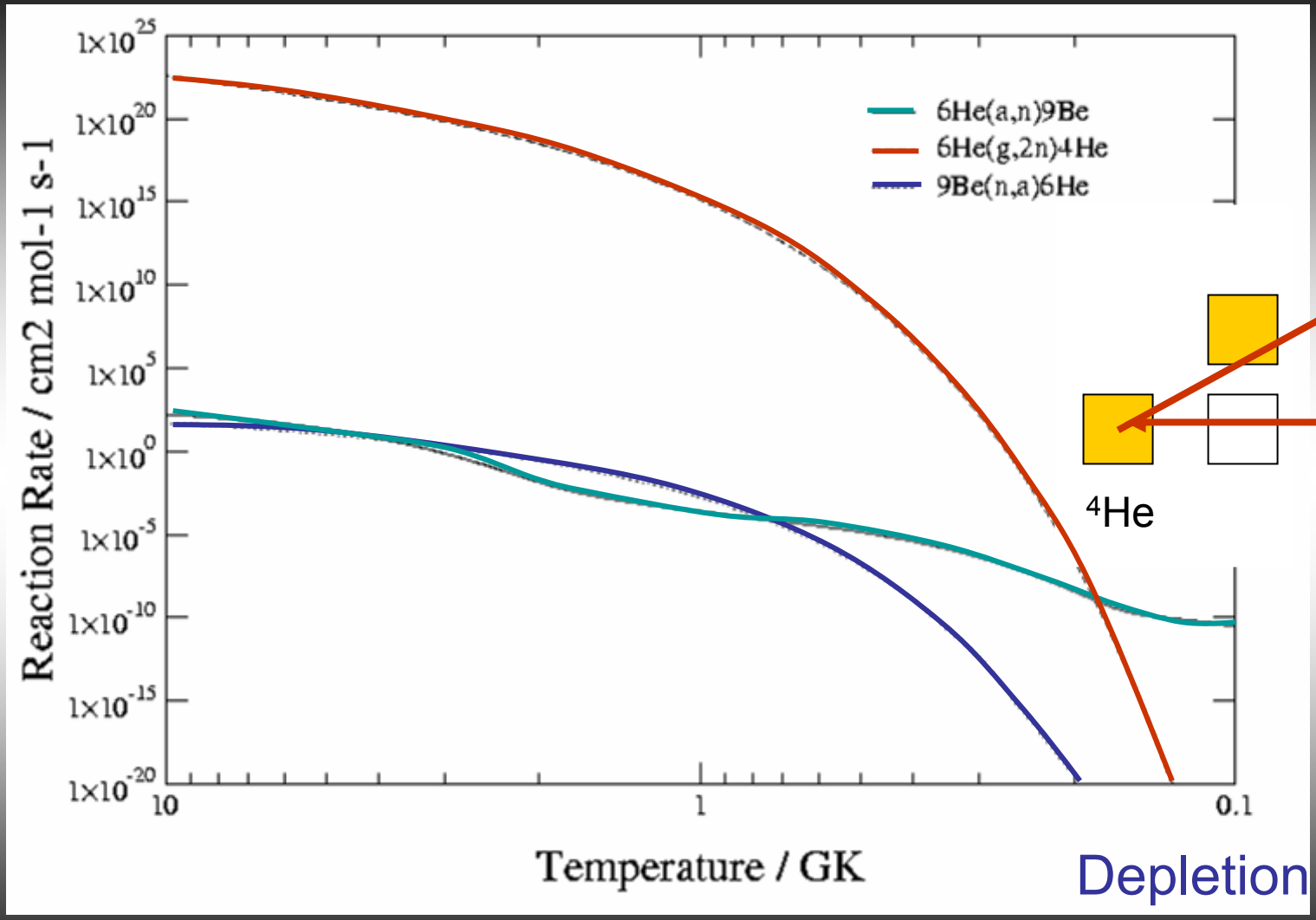

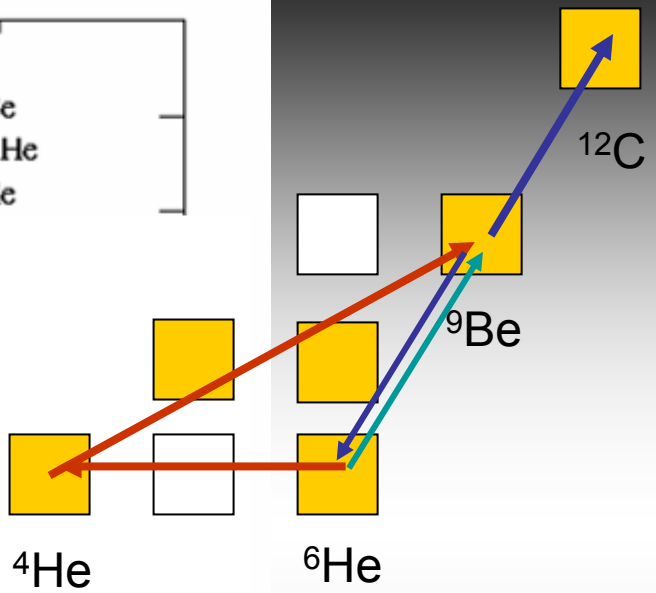

Depletion of the ^{9}Be equilibrium abundance

Nucleosynthesis of light isotopes

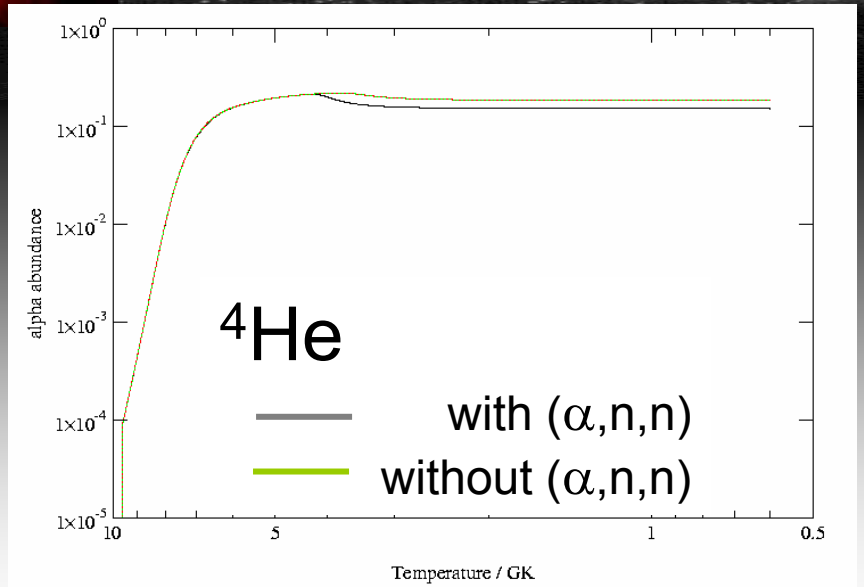

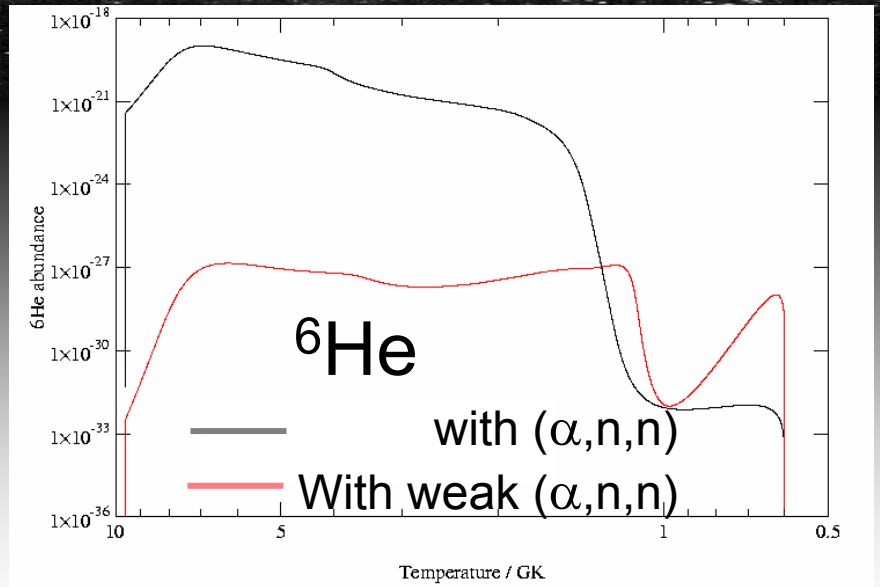

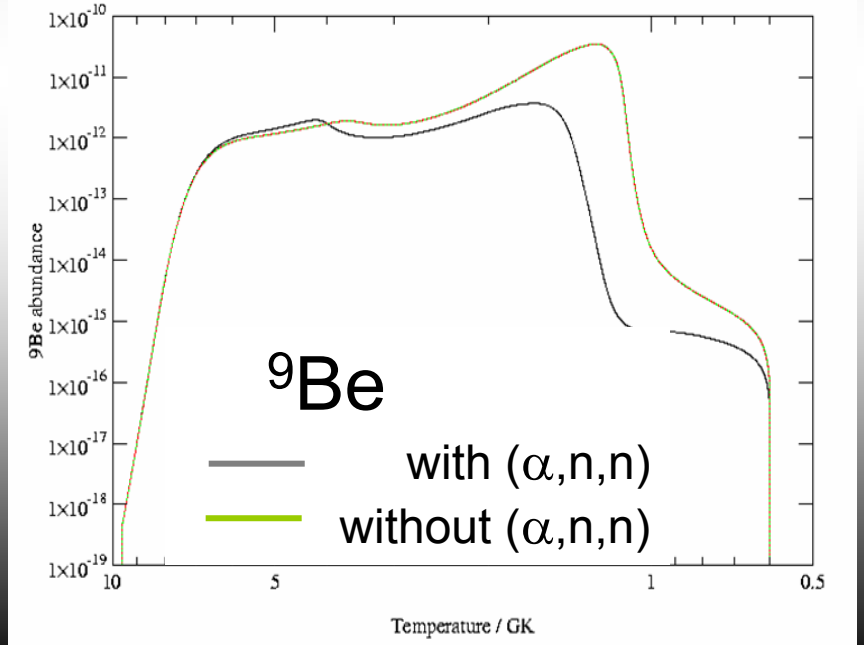

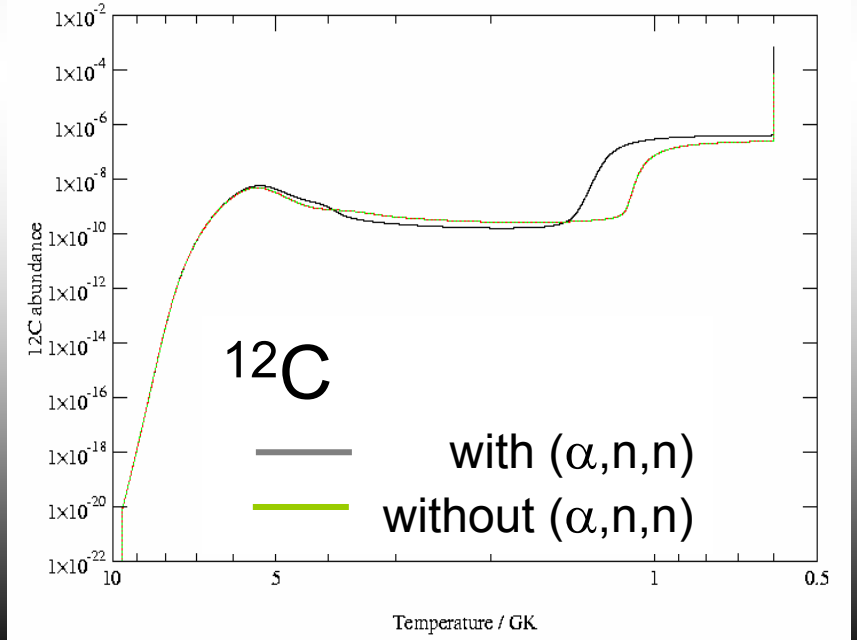

Neutron budget & alpha process

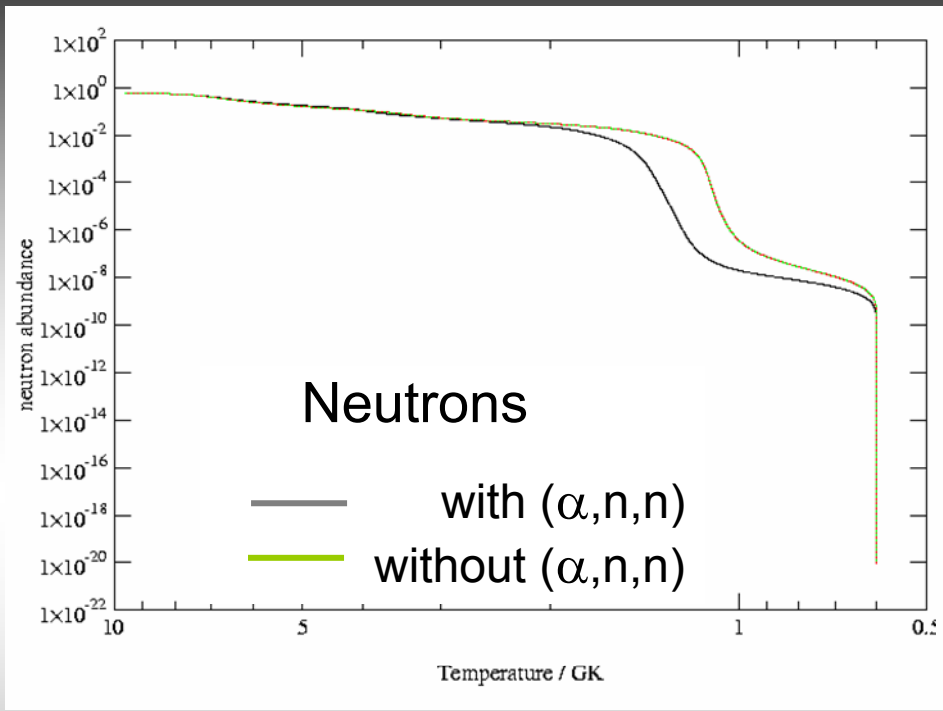

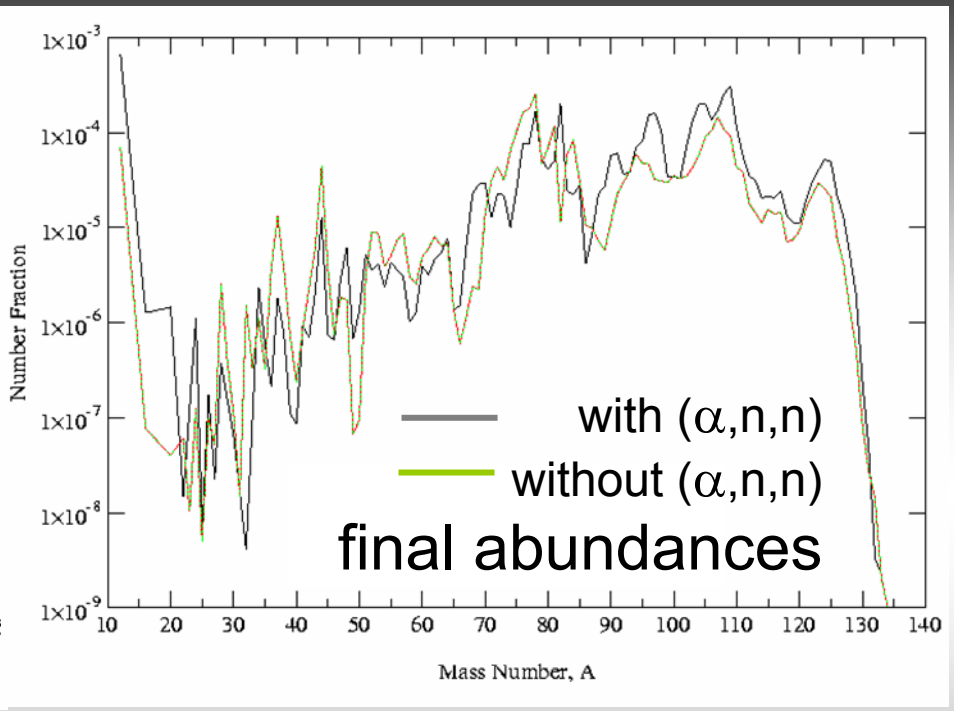

⇒ less flow towards heavier elements

⇒ more back-processing via $^{9}Be(n,\alpha)^{6}He(\gamma,nn)^{4}He$

⇒ less neutrons for r-process?

Dynamical r-process simulation

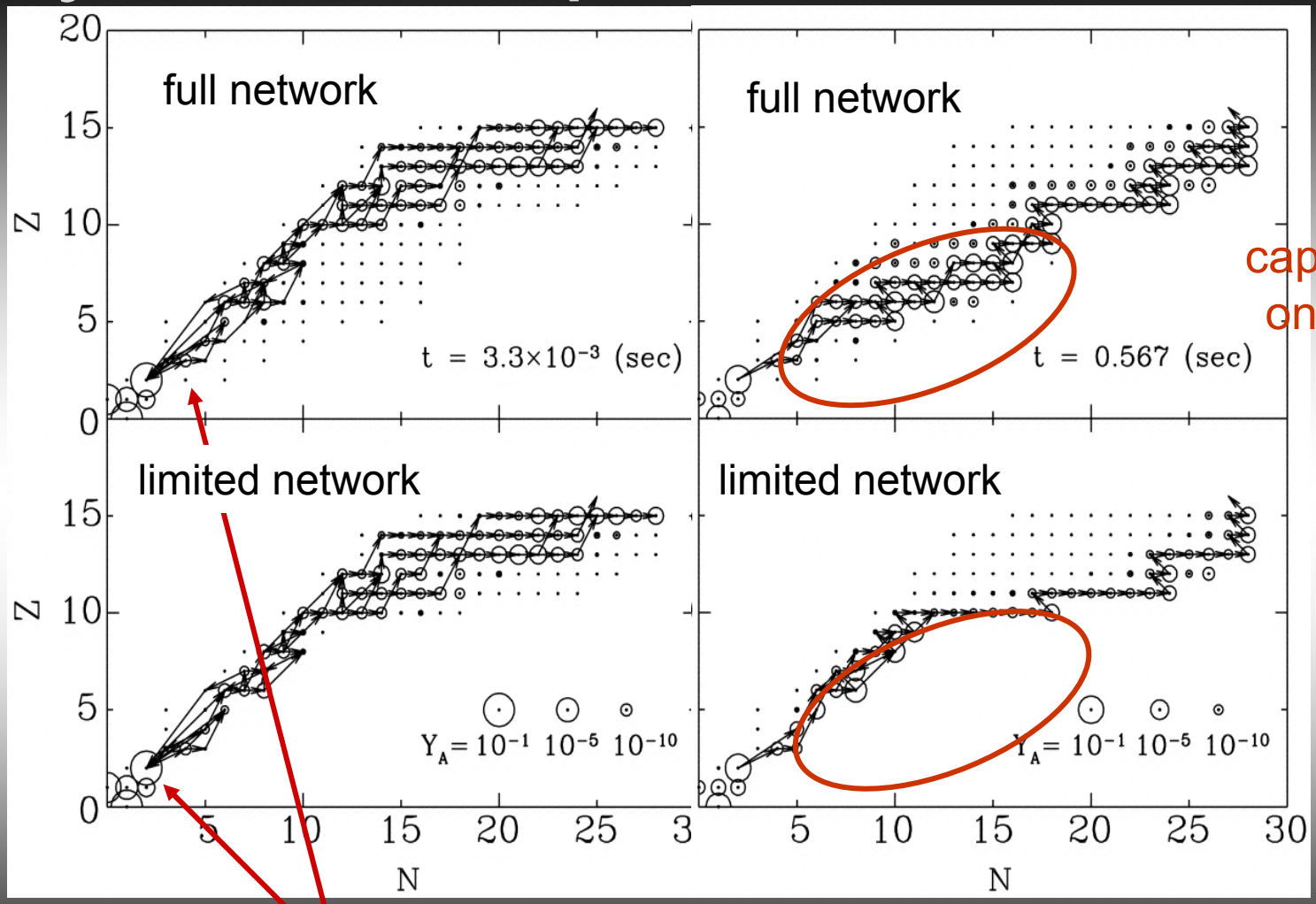

neutron capture rates on light halo nuclei?

α-capture dominated

Terasawa et al. ApJ562, 2001

(n,γ) ⇔ (γ,n) equilibrium

(n,γ)⇔(γ,n) equilibrium reached if $Q_{(n,\gamma)} \leq 2 \cdot T_9$

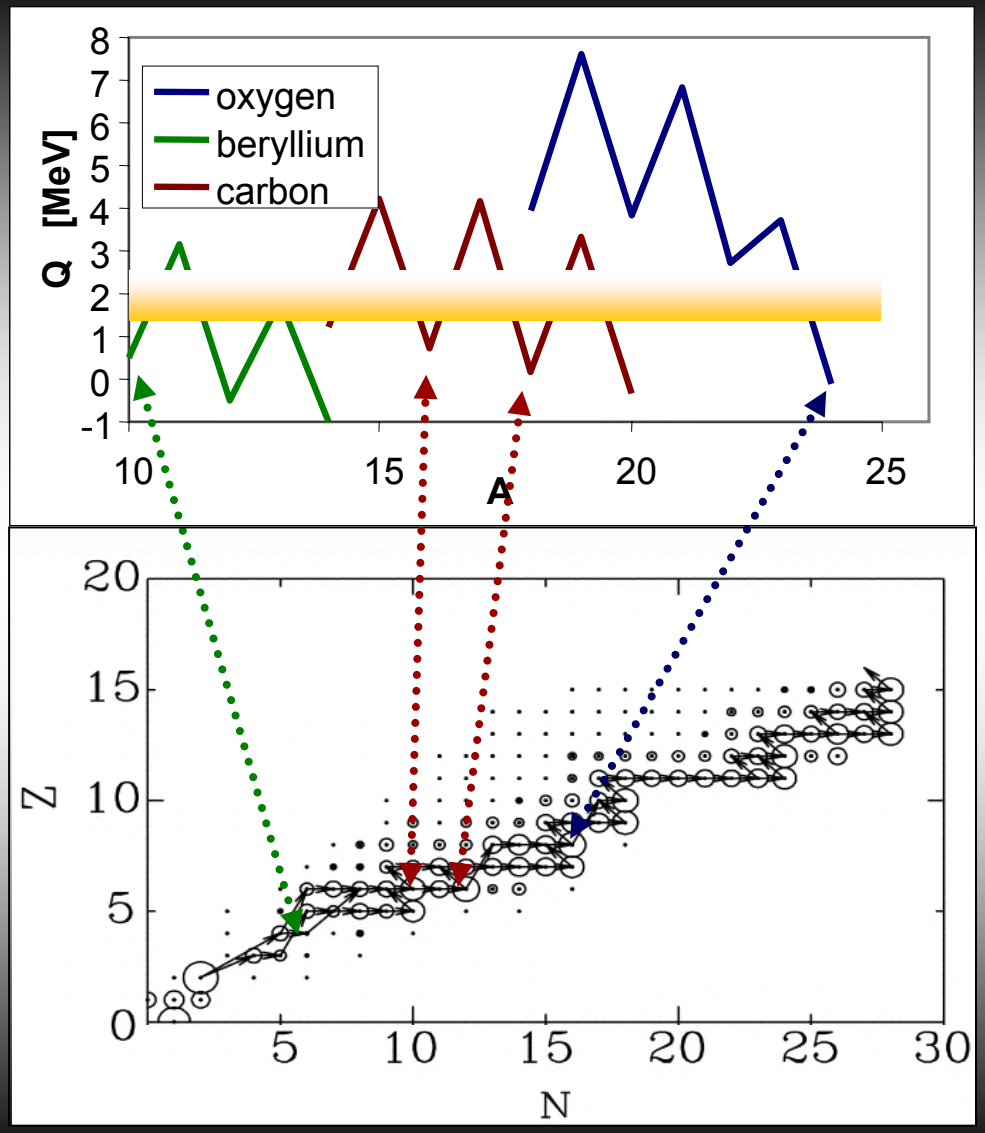

'light' r-process path limited by low Q-value (n,γ) reactions

C, O (n,γ) reaction rates

Present shell model based calculations; Herndl et al. PRC, 2002 includes single resonances but the rates are dominated by direct capture contributions

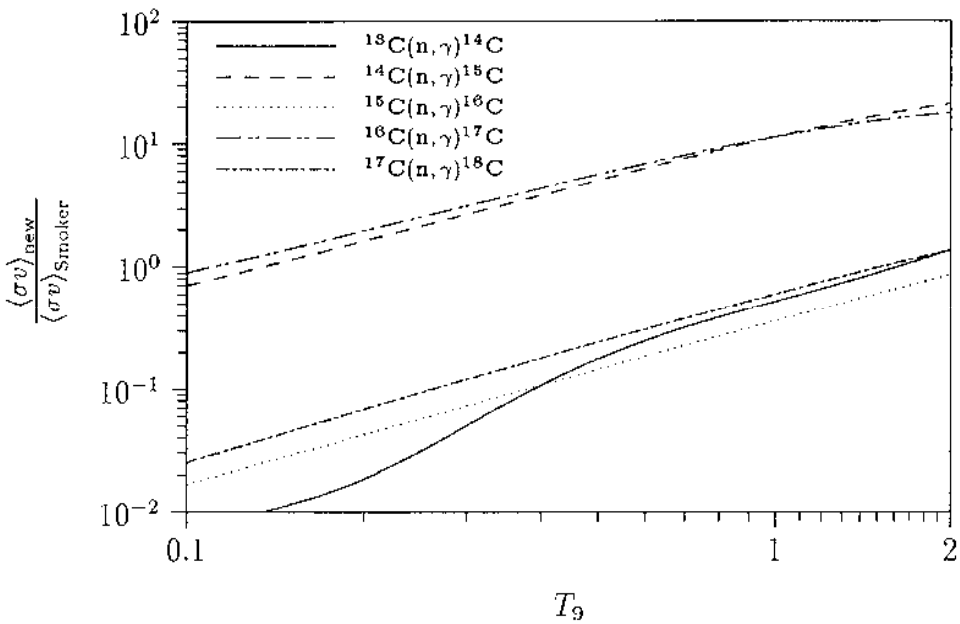

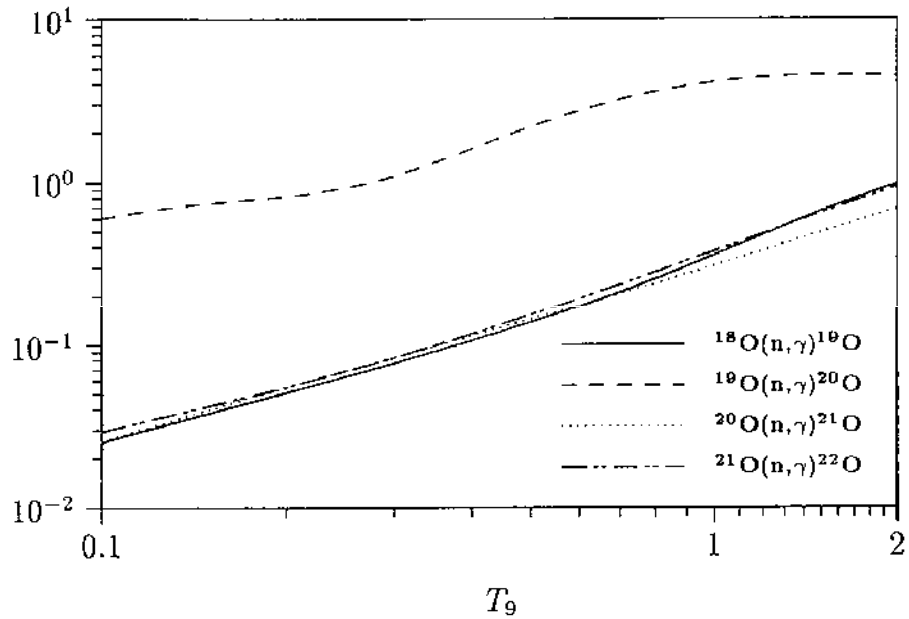

Significant deviations from HF calculations!

Halo in neutron capture

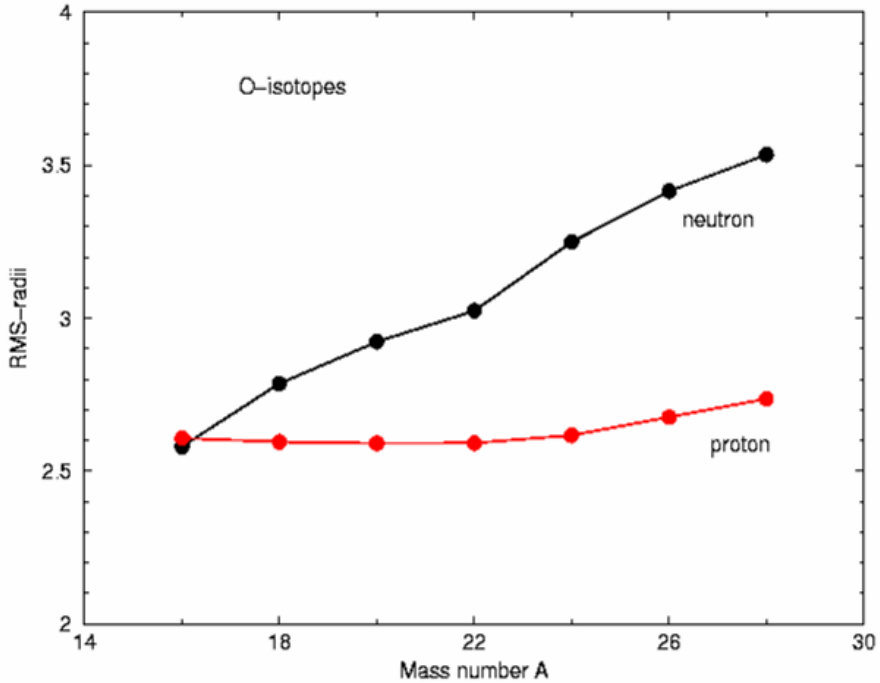

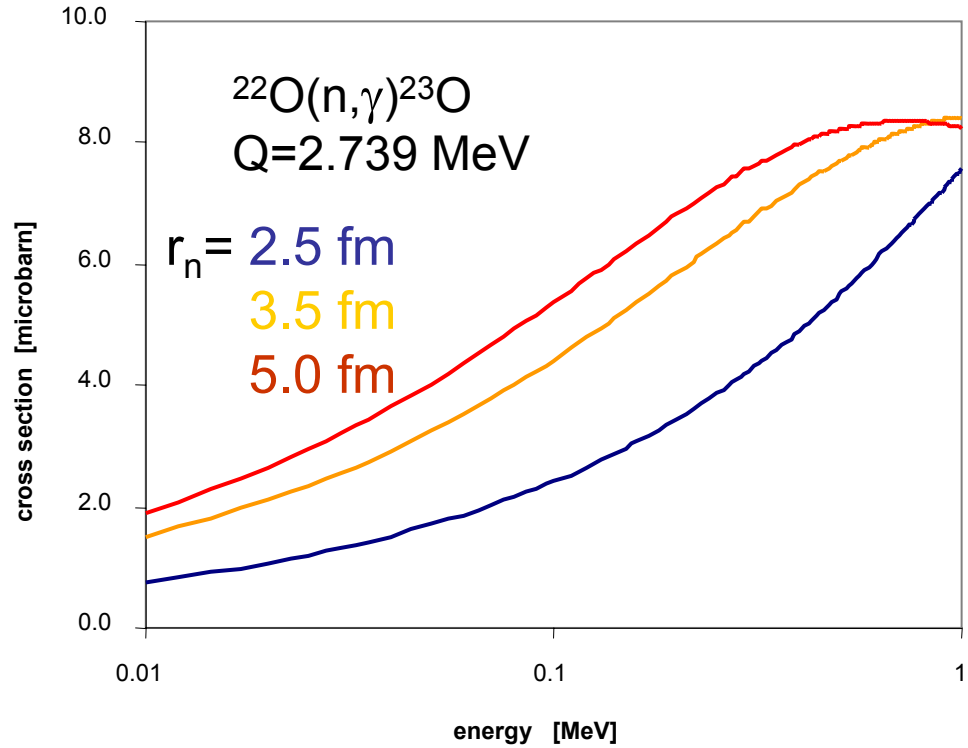

Capture on extended neutron halo may have significant impact on cross sections and therefore on neutron capture reaction rates!

Are neutron capture measurements on radioactive targets possible?

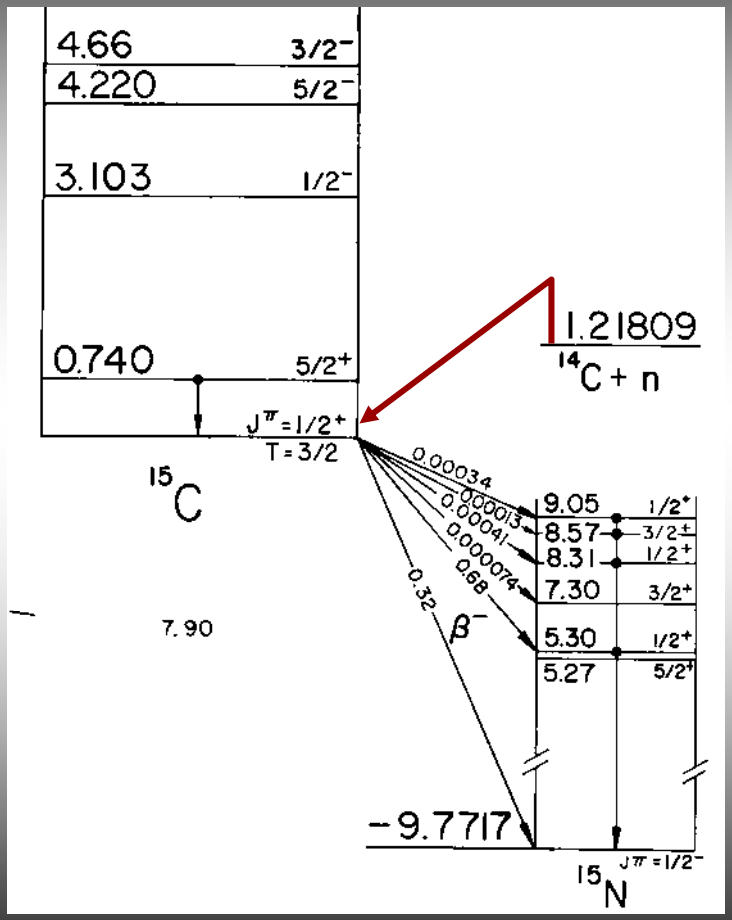

Neutron capture measurements are possible for long-lived radioactive isotopes, e.g. $^{14}C(n,\gamma)^{15}C$

Mainly p-wave direct capture to s-wave ground state in ^{15}C!

activation method with 15N γ-decay as signature

10 years of $^{14}C(n,\gamma)^{15}C$

Experiment was performed at FZ Karlsruhe by activation of Ni container enclosed ^{14}C target with Maxwell-Boltzmann-shaped neutron beam that was produced by $^{7}Li(p,n)$ at 1.98 MeV.

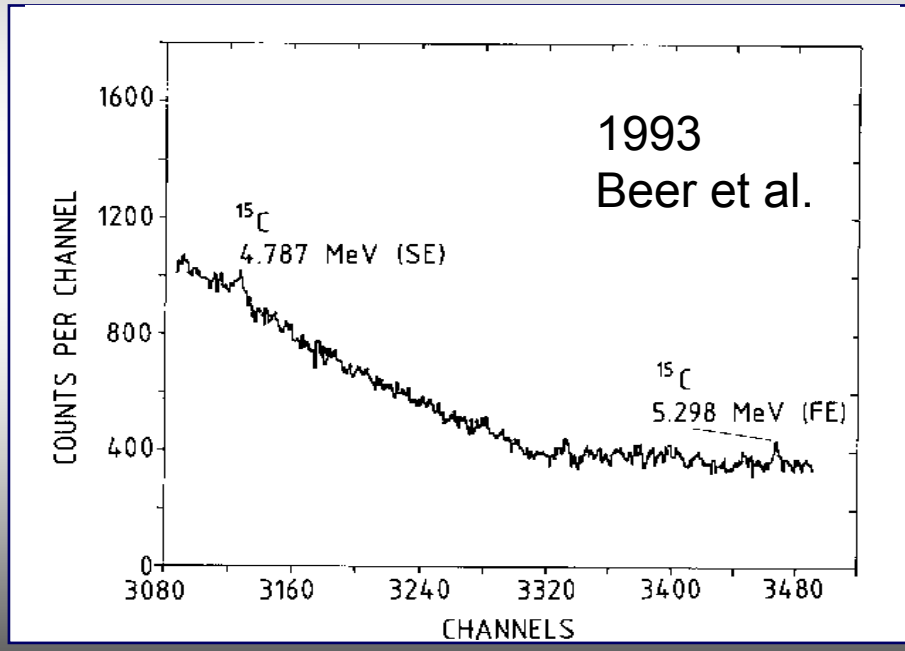

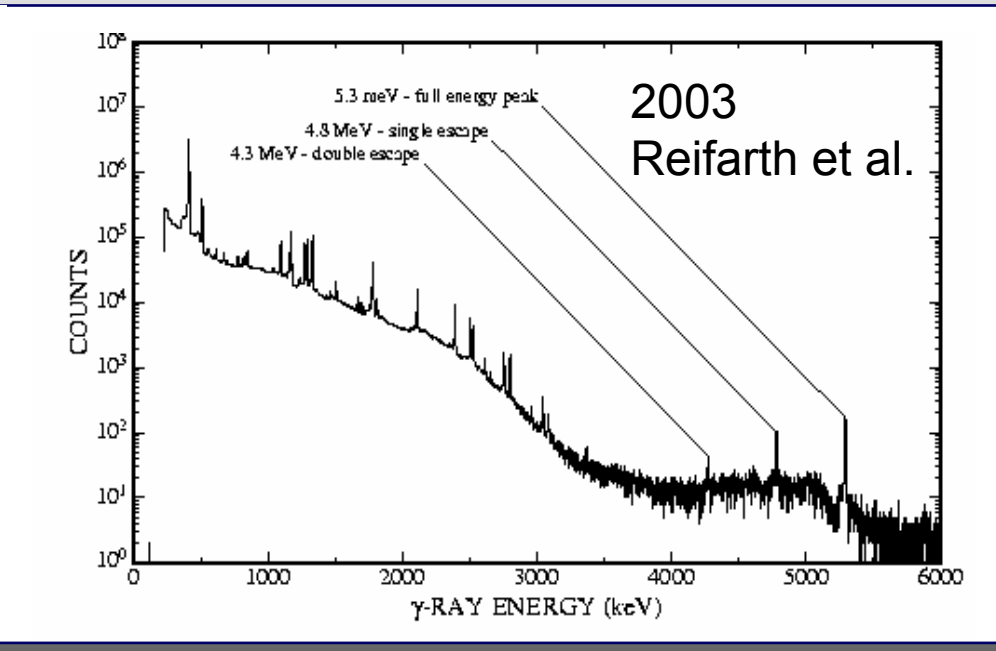

Considerable improvement due to bg reduction & efficiency improvements

RIA with neutron beams

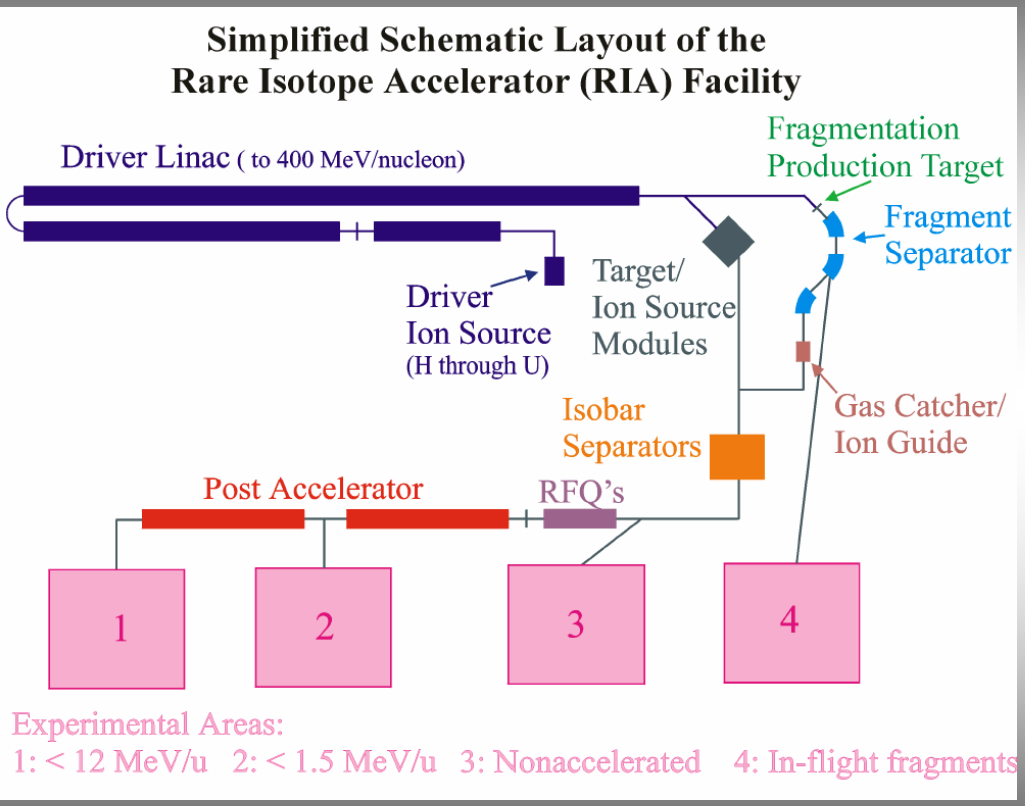

Are experimental studies with neutron beams on short-lived targets possible?

only for life times in the range of 10 days! (see F. Käppeler)

Alternatives:

- (d,p) single neutron transfer reactions?
- (γ,n) Coulomb disintegration

Example: $^{14}C(n,\gamma)^{15}C$ by $^{14}C(d,p)^{15}C$

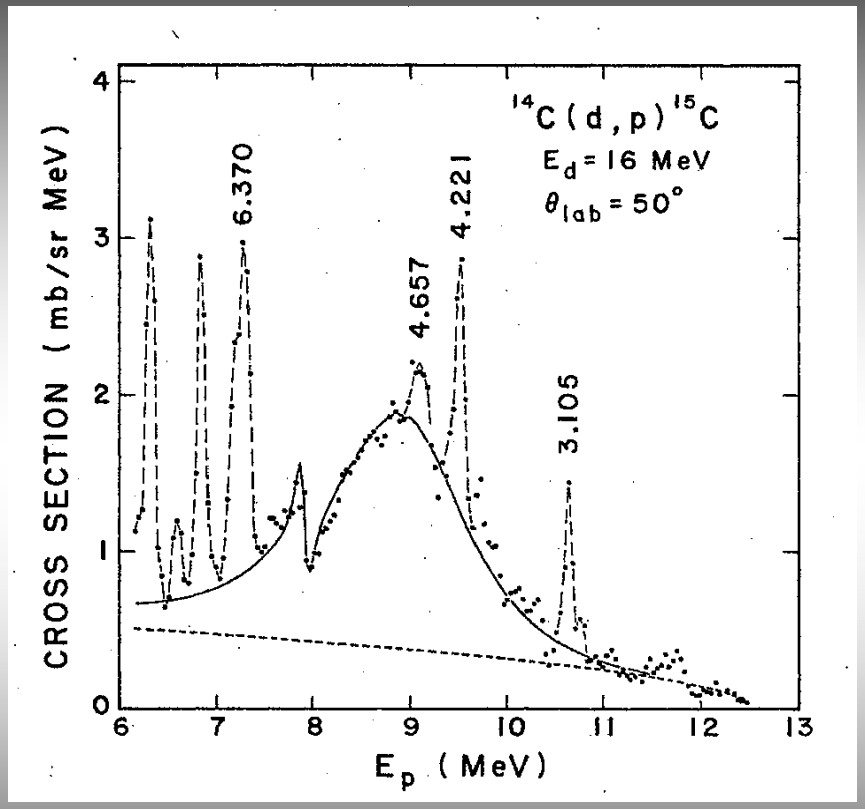

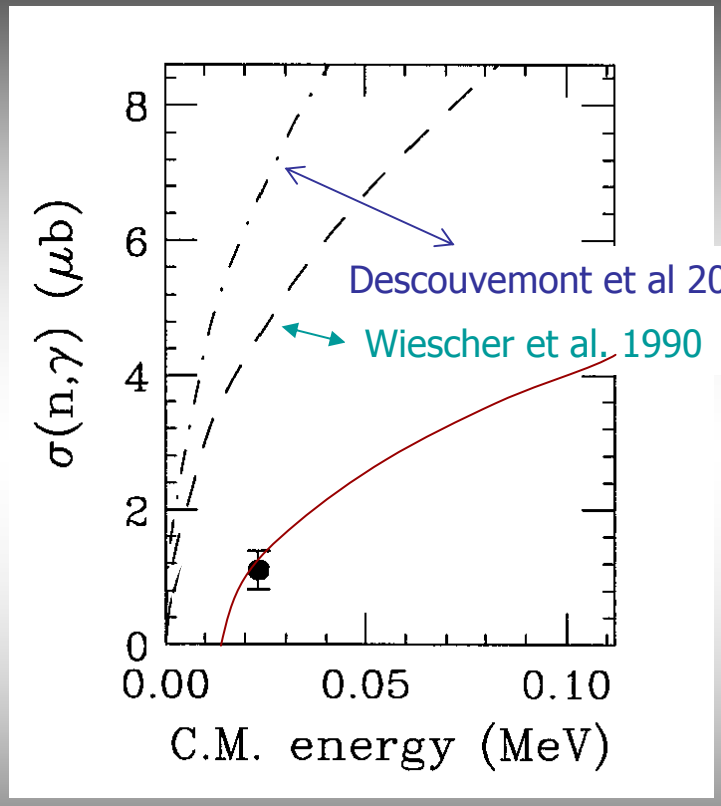

Spectroscopic information C^2S_n leads to model predictions
But the quality of result depends on model quality

Example: $^{14}C(n,\gamma)^{15}C$ by $^{15}C(\gamma,n)^{14}C$

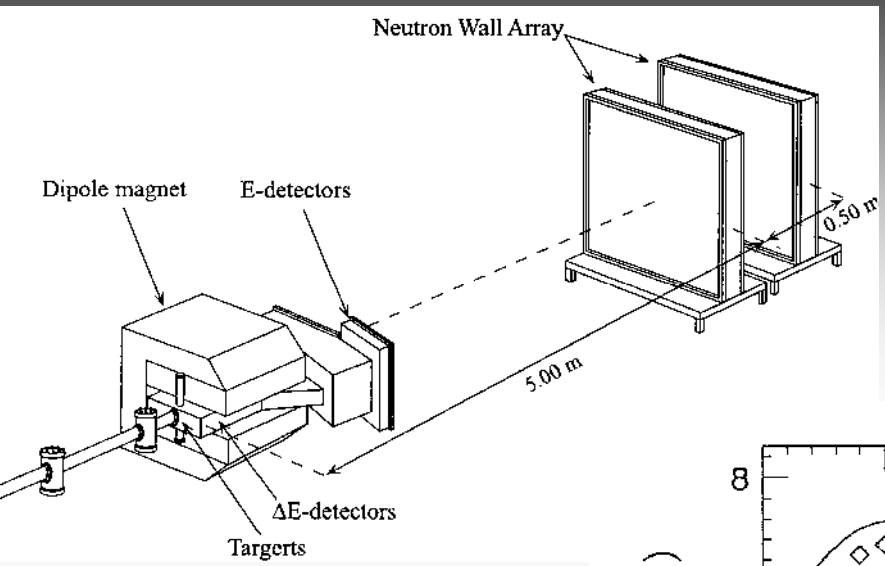

Coulomb dissociation experiment
With fast beam from NSCL/MSU
Coupled cyclotron facility

Direct capture measurement

≈ Factor 2 difference

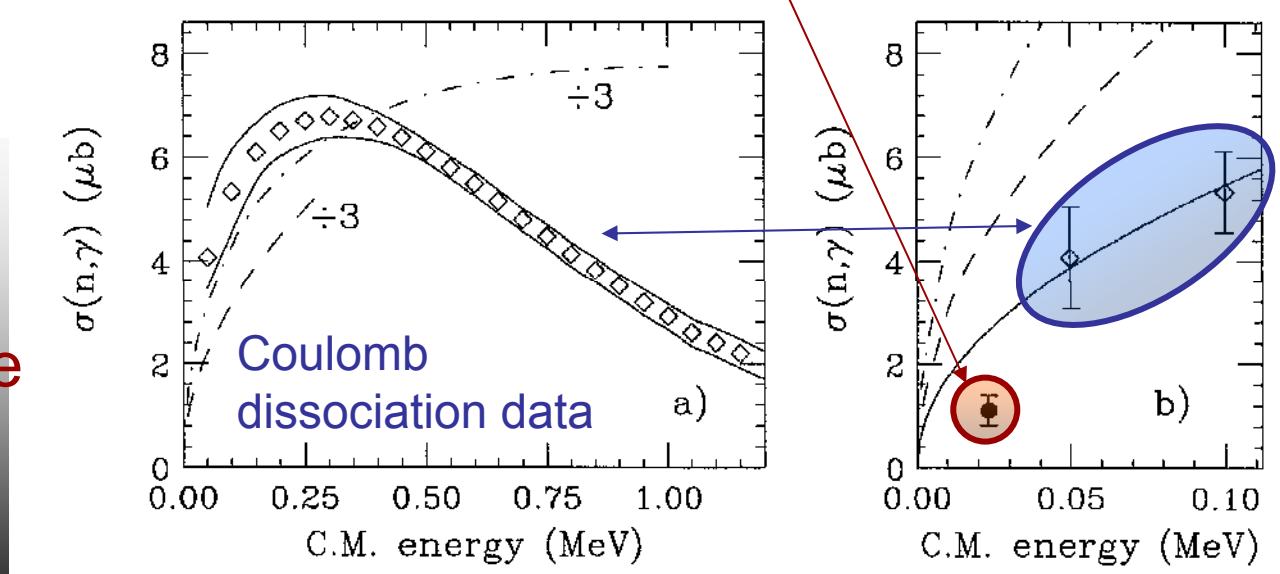

Conclusions

- Complexity of reaction networks (and temperature conditions) requires often more detailed reaction rate information than appreciated by model community! All reaction links need to be included!
- Light r-process seems possible if sufficient n-flux is available at cooling conditions. Halo structure of nuclei may enhance n-capture rates!
- new & reliable experimental methods need to be developed for measuring neutron capture rates for short-lived radioactive nuclei!

Acknowledgements

- Amy Bartlett — University of Surrey, UK
- Joachim Görres — University of Notre Dame
- Michael Heil — FZK, Germany
- Franz Käppeler — FZK, Germany
- Alberto Mengoni — CERN, Switzerland
- Kaori Otsuki — University of Notre Dame
- Rene Reifarth — LANL

Contribution by

Paul E. Koehler

Oak Ridge National Laboratory

koehlerpe@ornl.gov

20 pages

Improving Explosive Nucleosynthesis Rates for Reactions Involving Alpha Particles: The DANCE Connection

Paul Koehler

Oak Ridge National Laboratory

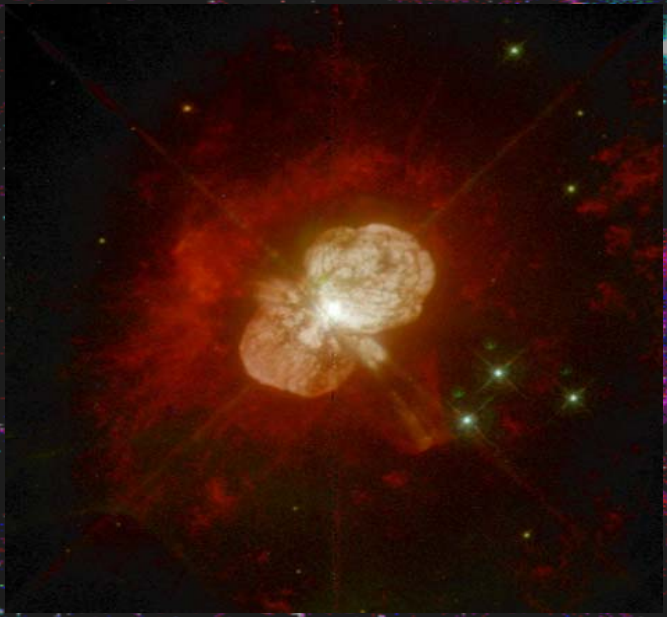

Motivation Roadmap

(n,α) Measurements

Nuclear Models

Constraints on Astro. Models

What's needed: Global improvement in α+nucleus potential.

Better (γ,α) and (α,p) Rates

Better Understanding of Supernovae, Origin of Elements,…

(n,α) Measurements are Difficult but Doable

- Cross sections (~10 μb), fluxes ("I_n" ~ 7 ppA), and samples (~ 50 μg/cm^2 - ~1 mg/cm^2) are small, backgrounds (from "flash") can be large. Compensated Ion Chamber (CIC) overcomes these problems).
- Several (n,α) measurements completed (blue) or planned (red) at ORELA and proof-of-principle experiments demonstrated that LANSCE will be ~20x better (green).

Isotope	$\langle\sigma\rangle_{30}$	% Abundance	ORELA (mg)
^{32}S	8.7	95.02	36
^{36}Ar	49	0.337	7.2
^{43}Ca	1.4	0.135	300
^{44}Ti	560	60 yr	0.78
^{59}Ni	6400	75000 yr	0.090
^{61}Ni	3.5	1.13	1700
^{64}Zn	240	48.6	26
^{67}Zn	310	4.1	21
^{73}Ge	0.11	7.8	6500
^{77}Se	2.8	7.6	270
^{91}Zr	3.7	11.32	240
^{94}Mo	0.18	9.25	5200
^{95}Mo	19	15.92	50
^{97}Mo	0.15	9.55	6400
^{96}Ru	15	5.52	60
^{99}Ru	43	12.7	20
^{101}Ru	0.21	17.0	4700
^{105}Pd	0.73	23.33	1400
^{106}Cd	0.12	1.25	8700
^{120}Te	0.25	0.096	4700
^{123}Te	2.6	0.908	420
^{143}Nd	24	12.18	60
^{145}Nd	1.1	8.30	1300
^{147}Sm	32	15.0	45
^{149}Sm	3.2	13.8	450
^{171}Yb	0.10	14.3	16900
^{177}Hf	0.12	18.6	14600

Comparisons as Averaged Cross Sections Leading to Improvements in α Potential

- Statistical model calculations differ from the data by ≈ 3 and from each other by ≈ 10.
- Drawback: Comparison as cross sections includes uncertainties due to neutron and γ strength functions, level densities, and width fluctuation corrections.

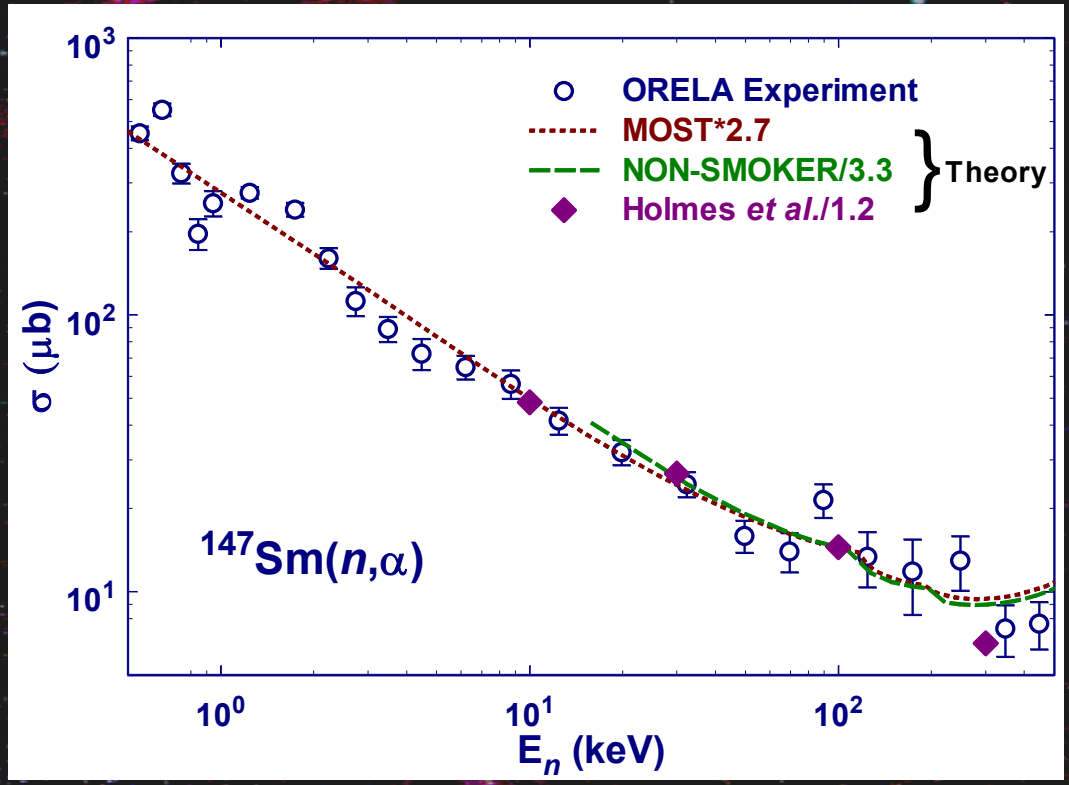

A Better Approach:
Compare Calculated Transmission Coefficient T to Measured α Strength Function S

- **Isolates effect of α potential**

$$T = 2\pi S.$$

- **Catch: requires *R*-matrix analysis and hence accurate J^{π}, Γ_n, and Γ_γ for many resonances.**

Exists for ^{147}Sm from previous neutron total and (n,γ) data.

Current resonance parameters for ^{95}Mo and ^{143}Nd not good enough.

Example: ^{147}Sm

- ^{147}Sm has $I^{\pi} = 7/2^{-}$

  s-wave neutrons on ^{147}Sm lead to 3^{-} and 4^{-} states in ^{148}Sm.

- $Q_{(n,\alpha)} = 10.127$ MeV, $E_n = 3 – 700$ eV.

  Alpha energy E_α (and hence α penetrability P_α) does not change across range of analysis.

  However, alphas emitted below the Coulomb barrier, so P_α is a steep function of E_α.

Example: ^{147}Sm

- $J^{\pi} = 4^-$ states in ^{148}Sm cannot α decay to 0^+ ground state of ^{144}Nd, but 3^- ones can.

$E_{\alpha,4} < E_{\alpha,3}$ =>

$P_{\alpha,4} < P_{\alpha,3}$ =>

$S_{\alpha,4} \approx 1/10\ S_{\alpha,3}$

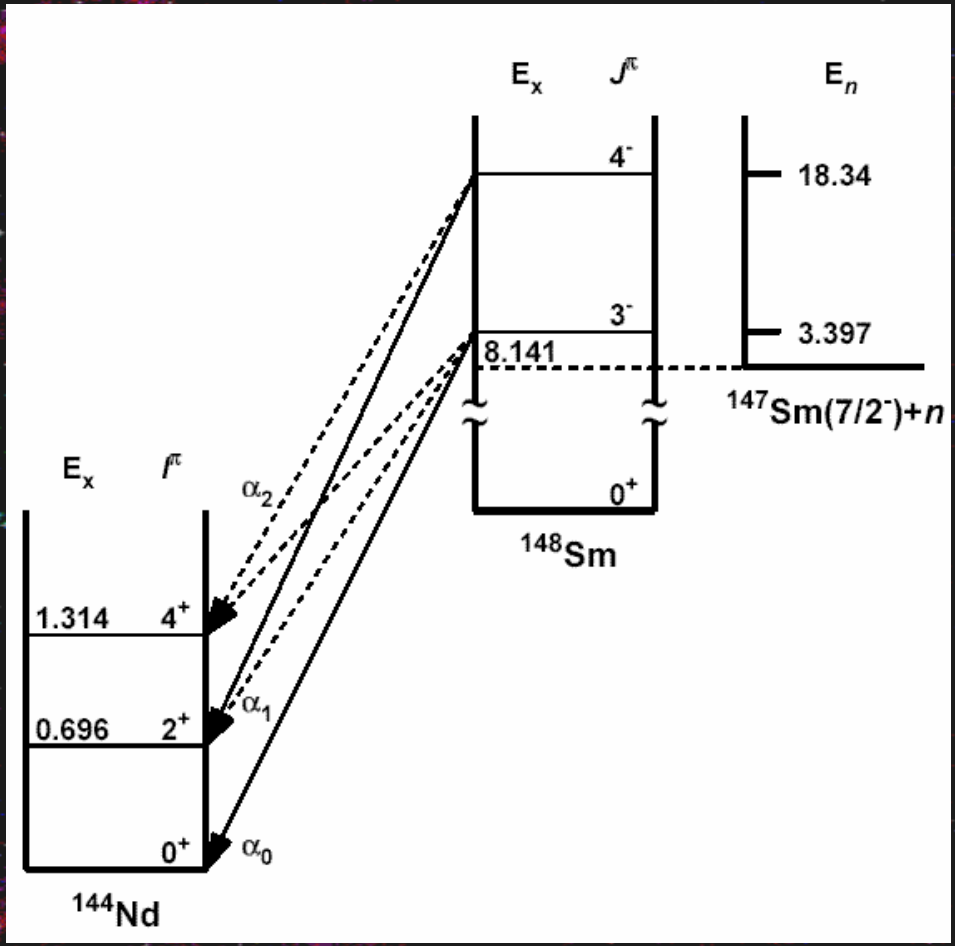

Example: ^{147}Sm, Neutron Channels

- Obtain resonance parameters (E_n, Γ_n, Γ_γ) from *R*-matrix analysis of total and capture cross sections.
- Neutron strength function S_0 determined from slope of cumulative reduced width vs. energy.

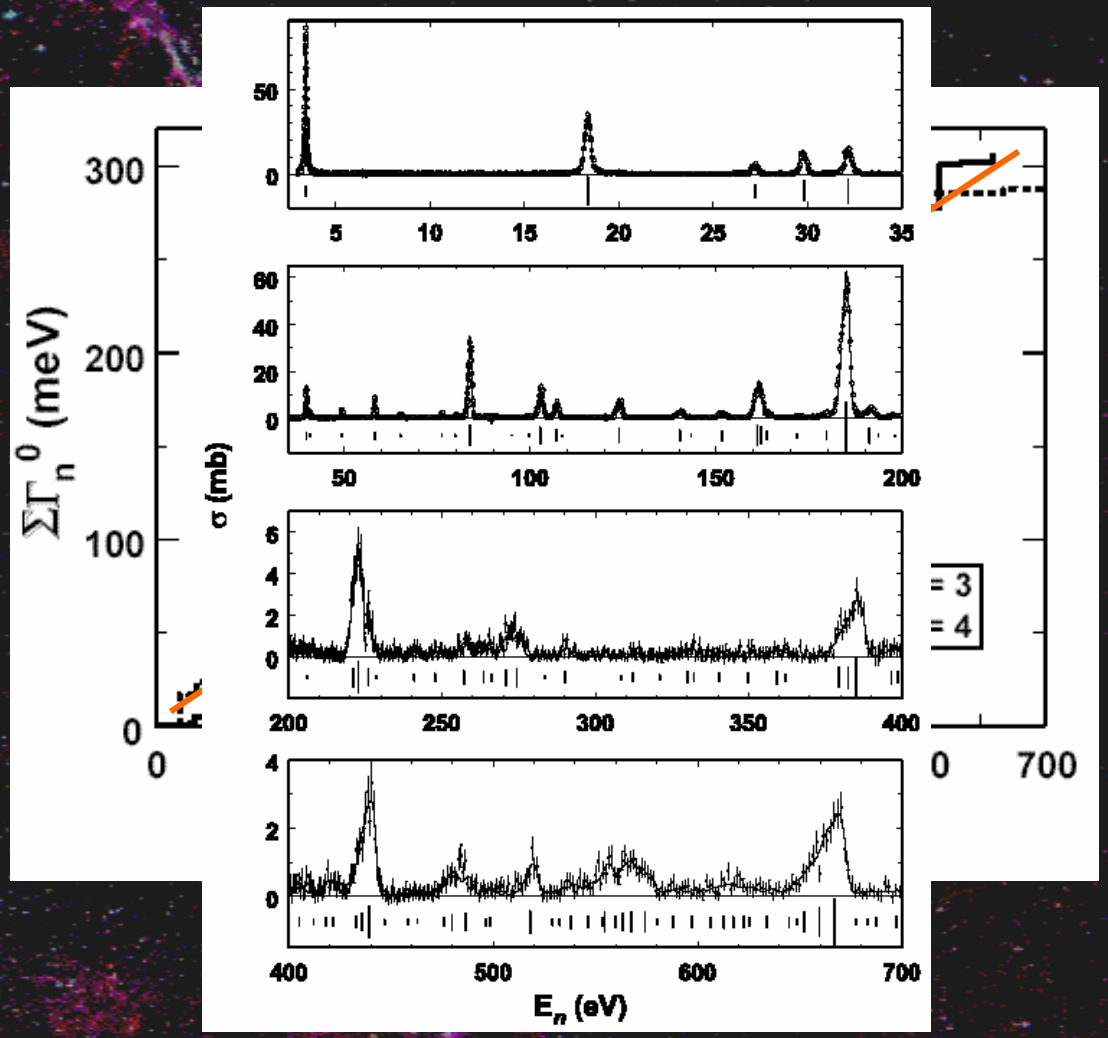

Example: ^{147}Sm , Neutron Channels

- Determine level spacing D_0 from slope of number of resonances vs. energy.
- Compare to Porter-Thomas distribution calculated from S_0 and D_0 to data.
  If consistent, S_0 should be reliable.
- Compare measured S_0 to calculated T.
  Neutron Channel: Factor of 2 difference for ^{147}Sm.
  Neutron potential needs adjustment.

	Neutrons	
J	$10^4 S_0$	
	Experiment	Optical Model
3	4.6 ± 1.0	9.2
4	4.3 ± 0.9	9.2

Number of Resonances

Example: ^{147}Sm , α Channels

- Problem: α widths show signs of being non-statistical.

  Strength function plots have steps.

  α widths do not follow expected distributions.

  Strength function ratio ($J^{\pi}=3^{-}/4^{-}$) should be constant, but changes with energy.

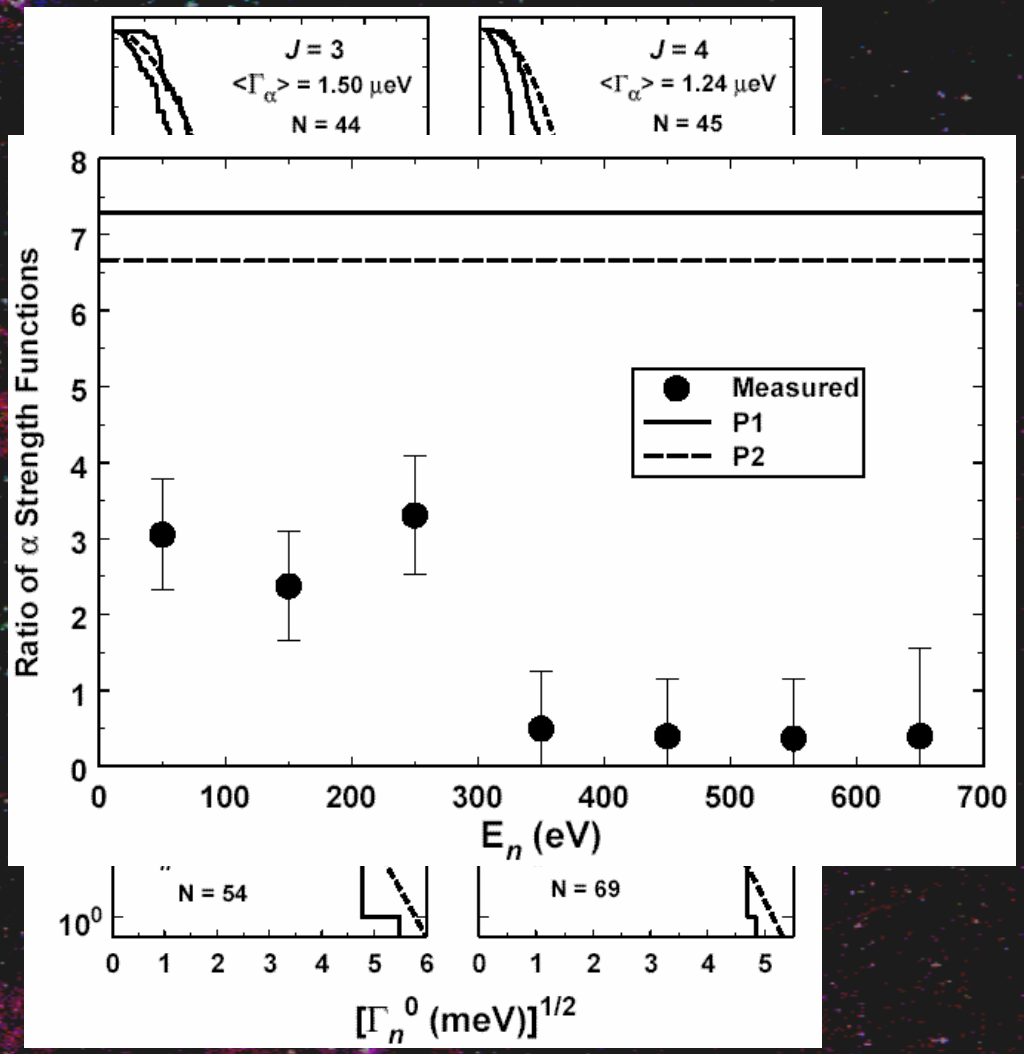

Example: ^{147}Sm , α Channels

- **Ignoring these problems:**

  Calculated α transmission coefficients ≈ 10-20 times too large.

  => α potential needs more adjustment than surmised from cross section comparison.

  Different average α energies (for 3^- and 4^- resonances) could be useful for constraining α potential.

  => Could not reproduce $3^-/4^-$ α strength function ratio with Saxon-Woods potential.

Possible Solution

- Some of the non-statistical effects might be due to erroneous J^{π} assignments.

  Changing J^{π} assignment of 4^- resonances having largest α widths to 3^- could result in better "statisticalness".

  Current evidence (crude α pulse-height information, alignment of energy scales, J^{π} from previous γ multiplicity experiment) indicates that J^{π} assignments are good.

Proposed Experiment to Check J^{π} Assignments

- New (n,α) measurement at LANSCE with thinner samples could nail down J^{π} assignments via α pulse-height information.

  The few low-energy resonances for which pulse heights have been measured are consistent with J^{π} assignments using other techniques.

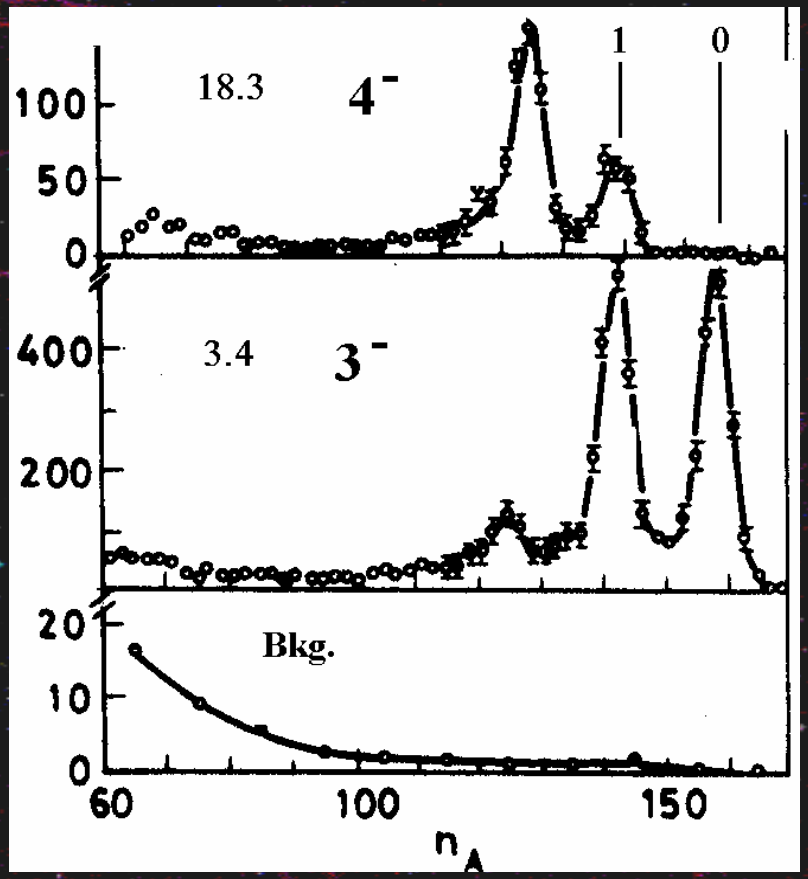

The DANCE Connection

- **Experiments to determine resonance parameters.**

  Extracted α strength functions depend on accurate J^{π}, Γ_n, and Γ_γ assignments.

  Measure $A_\alpha = g_J \Gamma_\alpha \Gamma_n / (\Gamma_n + \Gamma_\gamma) \Rightarrow \Gamma_\alpha = A_\alpha (\Gamma_n + \Gamma_\gamma) / g_J \Gamma_n$.

- **Experiments to cross-calibrate energy scales of various measurements.**

  Need to ensure that same resonances being observed in all measurements.
  Measure (n,γ) and (n,α) at same time or in "coincidence"?

Experiments to Determine E, Γ_n, Γ_γ, and J^π

- **Transmission (total cross section).**

  E, and
  Γ_n (if large enough), and/or
  Γ_γ (in special cases), and
  J^π (if Γ_n large enough and resolution good enough).

- **Neutron Capture, (*n*,γ).**

  E (usually with less precision),
  $A_\gamma = g_J\Gamma_\gamma\Gamma_n/(\Gamma_\gamma+\Gamma_n)$ => $g_J\Gamma_\gamma$ if Γ_n large, or
  $g_J\Gamma_n$, if Γ_n small, and/or
  J, if $<\Gamma_\gamma>$ known and conditions are right.

- **(*n*,γ) multiplicity.**

  E (usually with less precision), and
  J^π, and
  Γ_γ (if conditions right).

Example: DANCE Multiplicity Experiment

- **Previous experiment: Georgiev *et al*., Nucl. Phys. A565, 643 (1993).**

  16 NaI detectors (122x122x152 mm^3 each) in 4π arrangement.

  IBR-30 pulsed reactor in Dubna: d=500 m, P=10 kW, Δt=4 μs.

  Measured TOF spectrum for each detector and used to determine multiplicity for each resonance.

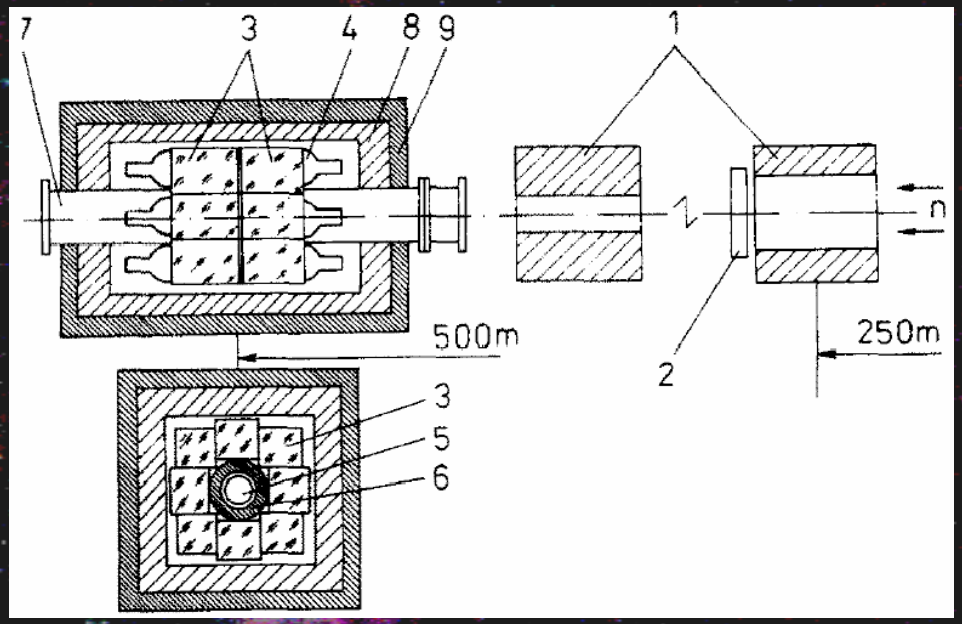

Example: DANCE Multiplicity Experiment

- **Previous experiment: Georgiev *et al.*, Nucl. Phys. A565, 643 (1993).**

$J^{\pi} = 3^{-}$ and 4^{-} resonances separated by multiplicity.

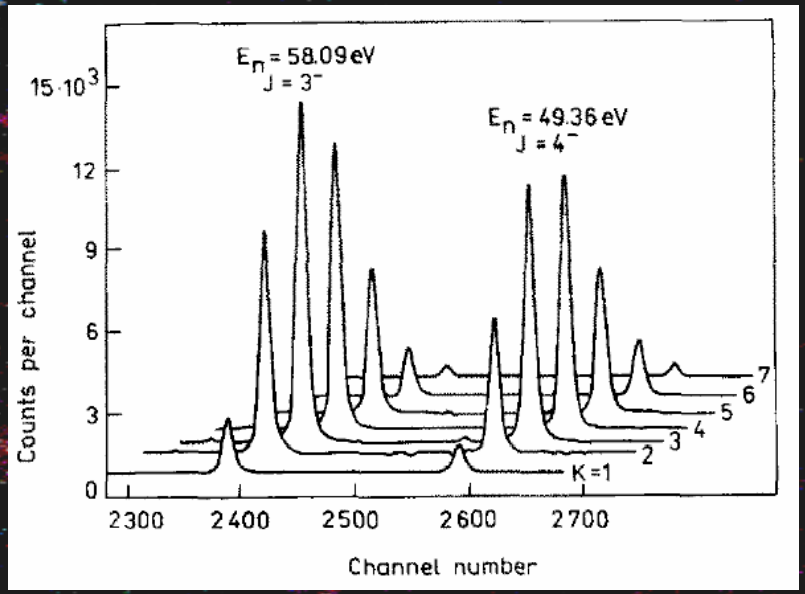

^{147}Sm resonance parameters

N	E (eV)	$\langle k \rangle$	J	Γ_γ
1	18.36 (2)	3.695 (7)	4	
2	27.16 (2)	3.445 (10)	3	84 (5)
3	29.76 (2)	3.411 (8)	3	71 (4)
4	32.14 (2)	3.684 (7)	4	70 (5)
5	39.70 (2)	3.705 (9)	4	68 (4)
6	40.72 (3)	3.444 (17)	3	
7	49.36 (2)	3.674 (9)	4	75 (4)
8	58.09 (2)	3.424 (9)	3	77 (5)
9	65.10 (3)	3.458 (23)	3	
10	65.10 (3)	3.647 (30)	4	
11	76.15 (3)	3.677 (12)	4	74 (5)
12	79.89 (3)	3.637 (26)	4	
13	83.60 (4)	3.406 (12)	3	76 (5)
14	99.54 (4)	3.705 (24)	4	79 (5)
15	102.69 (4)	3.498 (20)	3	76 (7)
16	106.93 (4)	3.687 (12)	4	82 (5)
17	108.58 (5)	3.679 (151)	4	
18	123.71 (4)	3.481 (22)	3	73 (6)
19	140.00 (4)	3.531 (14)	3	
20	143.27 (5)	3.672 (45)	4	
21	151.54 (5)	3.399 (22)	3	75 (5)
22	161.03 (5)	3.427 (26)	3	
23	161.88 (15)	3.578 (20)	4	
24	163.62 (5)	3.665 (19)	4	77 (4)
25	171.80 (5)	3.670 (23)	4	69 (4)
26	179.68 (6)	3.374 (32)	3	

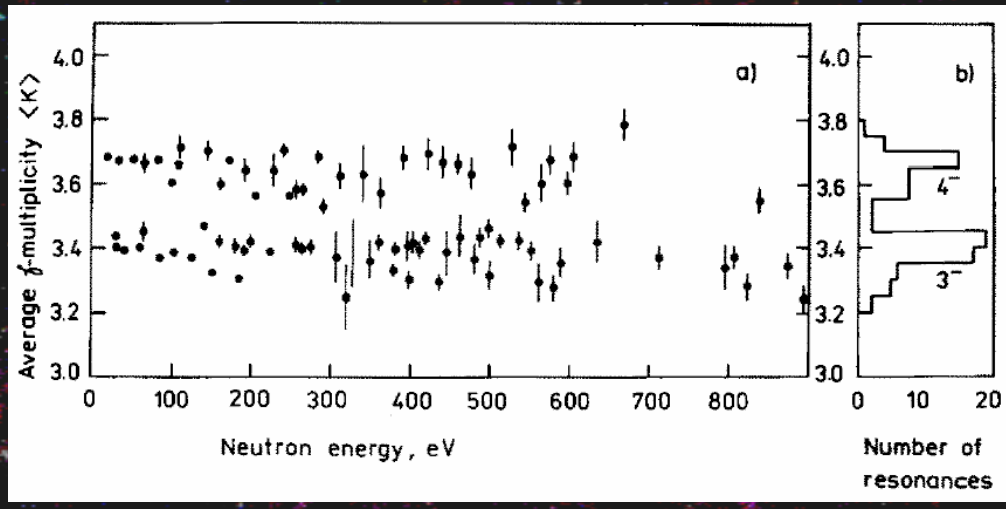

Possible DANCE Multiplicity Experiments (to improve α potential)

- Cases taken from earlier table.
- Use ^{147}Sm as test?

Several isotopes heavier than 77Se may be good candidates.

Isotope	Meas?	E_{up} (eV)	D (eV)	ΔE_{up} (eV)	Γ_n OK?	Comments
^{32}S	O	~10^6	17000	173000	Y	
^{43}Ca	L	40000	1500	1400	Y	
^{59}Ni	Y	17000	~1000	380	N	
^{64}Zn	O	369000	680	39000	Y	
^{67}Zn	O	185000	510	14000	Y	
^{77}Se	L	4000	60	44	Y	Many l=1
^{91}Zr	L	20000	213	490	Y	Many l=1
^{95}Mo	Y	2100	55	17	Y?	Several l=1
^{96}Ru	O	-	-	-	N	Nothing Known?
^{99}Ru	O	1000	25	5.5	Y	Need J, Γ_γ
^{123}Te	L	2000	25	15	Y	Need J, Γ_γ
^{143}Nd	Y	1500	45	10	Y	Need J
^{147}Sm	Y	700	5.7	3.2	Y	Calibration?
^{149}Sm	L	520	2.2	2.0	Y	Need J above 250

Example: DANCE/(n,α) Coincidence Experiment?

- Goal: determine E_n, J^π of (n,α) resonances.
- Technique: Use fact that 4^- resonances can't α decay to ground state.

$Y_{696}/Y_\alpha \approx 1$ for 4^-
$Y_{696}/Y_\alpha < 1$ for 3^-

- Problems:
  Not ironclad.
  α detector fit inside DANCE?
  $R_\gamma \approx 10^3\text{-}10^6\ R_\alpha$

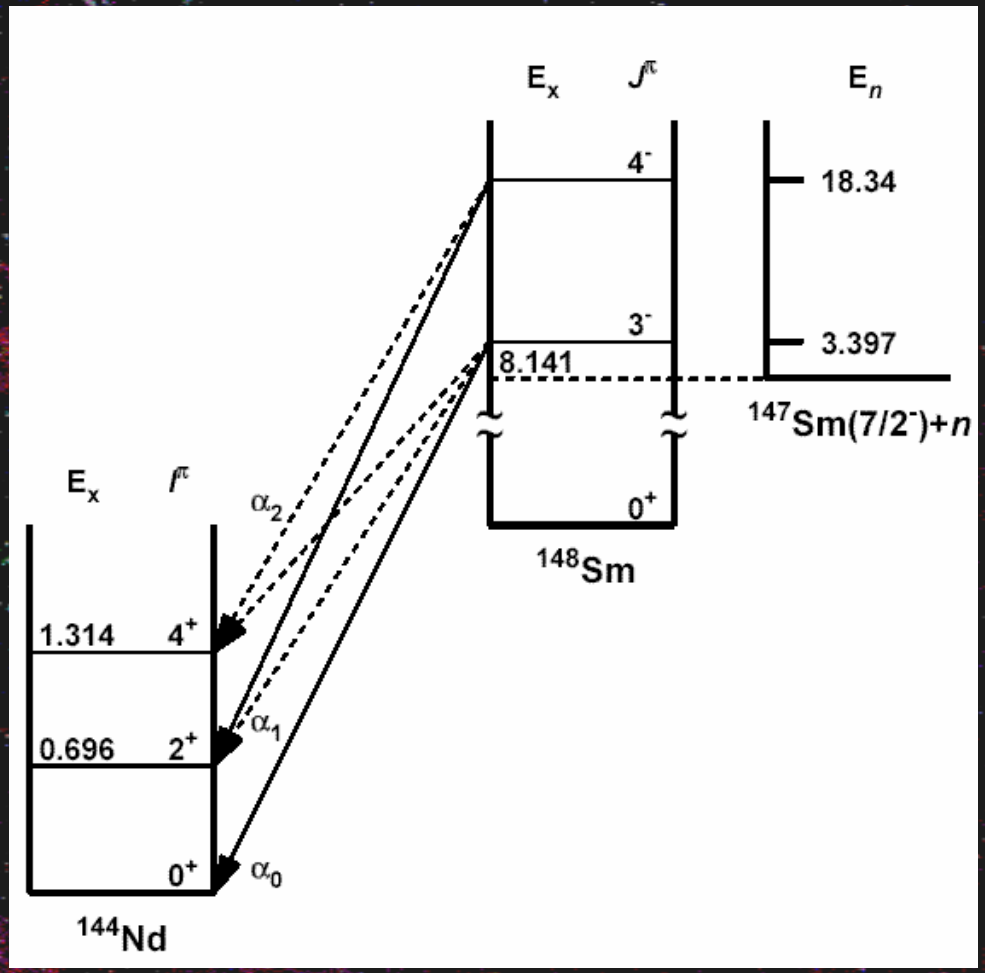

Summary

- (n,α) measurements beginning to show promise as a means to improve reaction rates for explosive nucleosynthesis.
- Comparison between theory and data as strength functions (rather than as cross sections) appears to be very useful and interesting.

Requires better resonance parameters.

DANCE experiments should be very helpful.

Contribution by

Roberto Gallino

Universita di Torino

gallino@ph.unito.it

32 pages

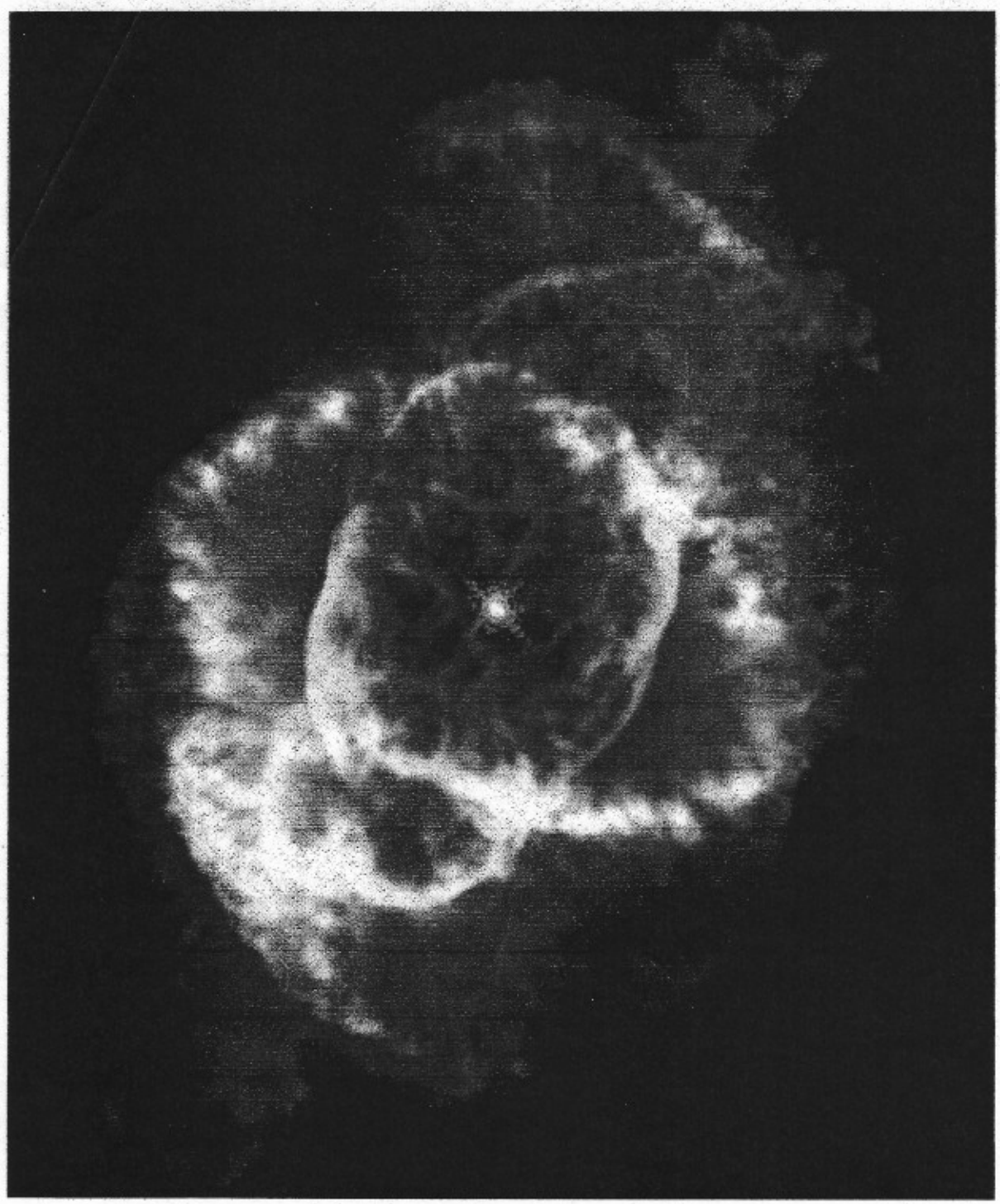

The Cat's Eye Nebulae, NGC 6543, imaged by the Hubble Space Telescope. Planetary nebulae such as NGC 6543 are believed to consist of several tenths of a solar mass of gas and dust expelled during the latter stages of the asymptotic giant branch phase of stellar evolution. Image from `http://www.astro.washington.edu/balick/WFPC2/`.

MINUTE STEPS ON THE QUEST OF THE s–PROCESS

R.Gallino, C.Travaglio, S.Masera, E.Arnone, M.Lugaro, O.Straniero, F.Kaeppeler, H.VanWinckel, M.Reyniers, A.M.Davis, D.L.Lambert, R.Reifarth, E. Zinner, S.Amari, R.S.Lewis, M.Savina, M.Heil M.Pellin, M.Busso, M.Pignatari, F.Herwig, V.Smith, D.Lattanzio, D.Delande, P.Illiadis

- AGB stars of low mass (1.5 – 8 $M_\odot$):
  ^{12}C + s-process elements producers
  Wind mass loss along the AGB
  C–O core —> WD

- The major neutron source: $^{13}C(\alpha,n)^{16}O$
  Production zone: He intershell
  Double mechanism of dilution of s-process material:
  - ^{13}C-pocket diluted into convective pulse
  - recurrent third dredge up

  Minor neutron source: $^{22}Ne(\alpha,n)^{25}Mg$

- Production of heavy s-elements A $\geq$ 88: the three s-peaks Zr-peak, Ba-peak, Pb-peak

MS–S–SC–C(N)–postAGB
Ba–CH–symbiotics

- PostAGB (21 μ) as the best indicators of intrinsic AGB stars

- The problem of Lead

- The Lead monster or peeled AGBs:
  FG Sge
  Sakurai's object
  R Corona Borealis: CrB mjority and minority classes

- Presolar grains trapped in meteorites of AGB origin: how many AGB parent stars?

- Updated nuclear network
  (Bao et al. 2000 + ...)

- The s-process is not unique
  - dependence on metallicity
  - dependence on ^{13}C–pocket

- How to make the solar system main component + strong component through the chemical evolution of the galaxy

- The r–process as the mirror image of the s–process (and vice-versa)

- The puzzle of Sr–Y-Zr in very metal poor stars

- Spectroscopic obsrevations of the chemically peculiar red giants (and their descendants):

Beer, Voss, Winters, 1992
Ap.J. Suppl 80, 403

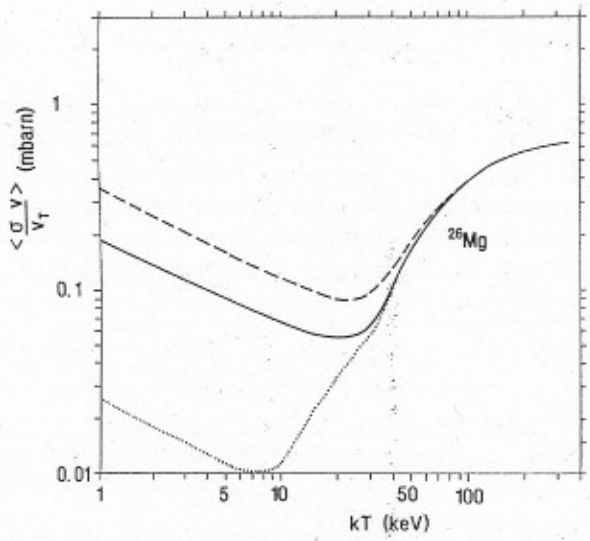

FIG. 1.—Maxwellian-averaged capture cross section of ^{26}Mg. The dashed and dotted lines illustrate the effect of erroneous assumptions.

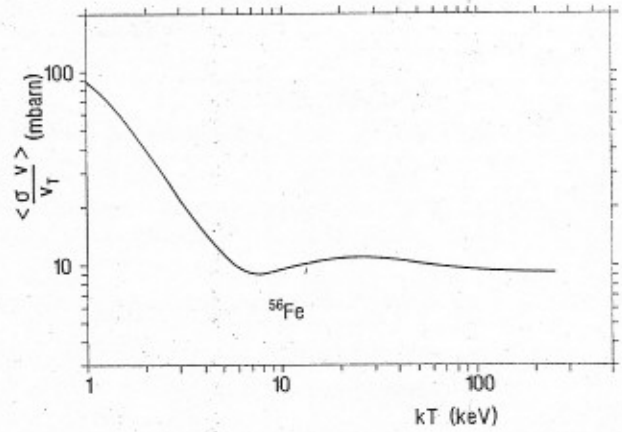

FIG. 2.—Maxwellian-averaged capture cross section of ^{56}Fe

first term in $J_{3\alpha}$ were neglected. This term is not negligible if E_r lies in the keV region.

3.4. ^{56}Fe

Maxwellian-averaged cross sections for a number of isotopes differs substantially from a temperature dependence of $\langle \sigma v \rangle / v_T \sim (kT)^{-b}$. The isotope ^{56}Fe is such a case. Due to a lack of resonances between 1.147 and 12.45 keV the Maxwellian-averaged capture cross section shows a minimum of ~7 keV (Fig. 2). This case demonstrates again that each individual isotope required special consideration of the resonance structure.

3.5. ^{76}Se

The thermal capture cross section of ^{76}Se is 85 ± 7 barn. Only 400 mbarn are due to the tails from positive resonances. The rest is associated with a negative resonance at −0.3 keV. ^{76}Se has a typical shape for a Maxwellian-averaged capture cross section: $\langle \sigma v \rangle / v_T \sim (kT)^{-0.42}$ (Fig. 3; *solid line*). The dotted curve shows what would result if direct capture were assumed instead of bound states capture for the interpretation of the thermal cross section. At $kT = 10$ keV the solid and dotted curves are different by 6%.

3.6. ^{104}Pd

The excitation function of ^{104}Pd, an s-only isotope, has been measured by Macklin & Winters (1981) and Cornelis et al. (1982) from 3 keV up to 600 and 300 keV, respectively. No data are given below the resonance at 2.7263 keV except the resonance at 0.1823 keV which can account for the thermal cross section. The excitation function must be supplemented between 0.1823 and 2.7263 keV by statistical model calculations (integral J_4). For the 0.1823 keV resonance and for resonances between 2.7263 to 3.49 keV areas A_γ are given. The calculation has to combine contributions from $J_{3\alpha}$, J_4, J_5, and J_6. For the $kT = 30$ keV Maxwellian-averaged capture cross section (288 ± 29 mbarn) J_6 and the first term in $J_{3\alpha}$ are negligible. The contributions from the resonance areas and the statistical model calculation amount to 6 mbarn.

It is important to note that ^{104}Pd is one of the isotopes measured at ORELA (Oak Ridge Electron Linear Accelerator) and published in the period 1972–1982, where a correction factor (0.7999) has to be applied to the data because of an error in the computer codes detected later. Tables of these correction factors have been published (Macklin & Winters 1981; Allen, Boldeman, & Macklin 1982).

3.7. ^{197}Au

^{197}Au is used in many measurements, activations, and time-of-flight measurements, as cross section standard. The value of its cross section is thus of particular importance. Its absolute value [$\langle \sigma v \rangle / v_T$(30 keV) = 582 ± 9 mbarn] as well as its shape are well determined (Ratynski & Käppeler 1988; Macklin 1982c). Calculations using resonance parameters in the eV and low keV range plus smooth cross section data, or statistical model calculations with experimental average parameters plus

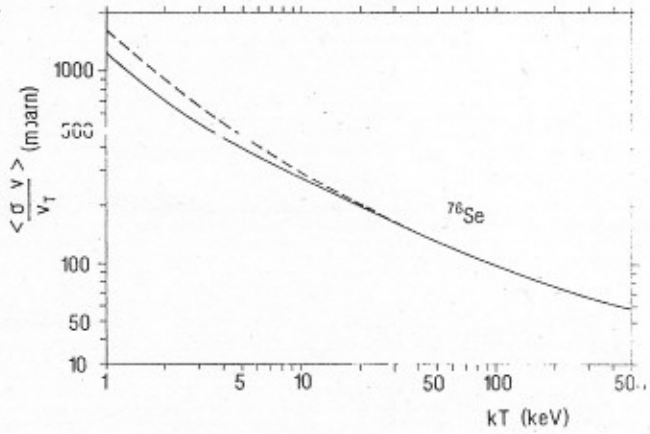

FIG. 3.—Maxwellian-averaged capture cross section of ^{76}Se. The dashed line illustrates the effect of an erroneous assumption.

The ^{22}Ne neutron source is marginally activated in low mass AGB s

($T_{max} \leq 3.1 \cdot 10^8 K$)

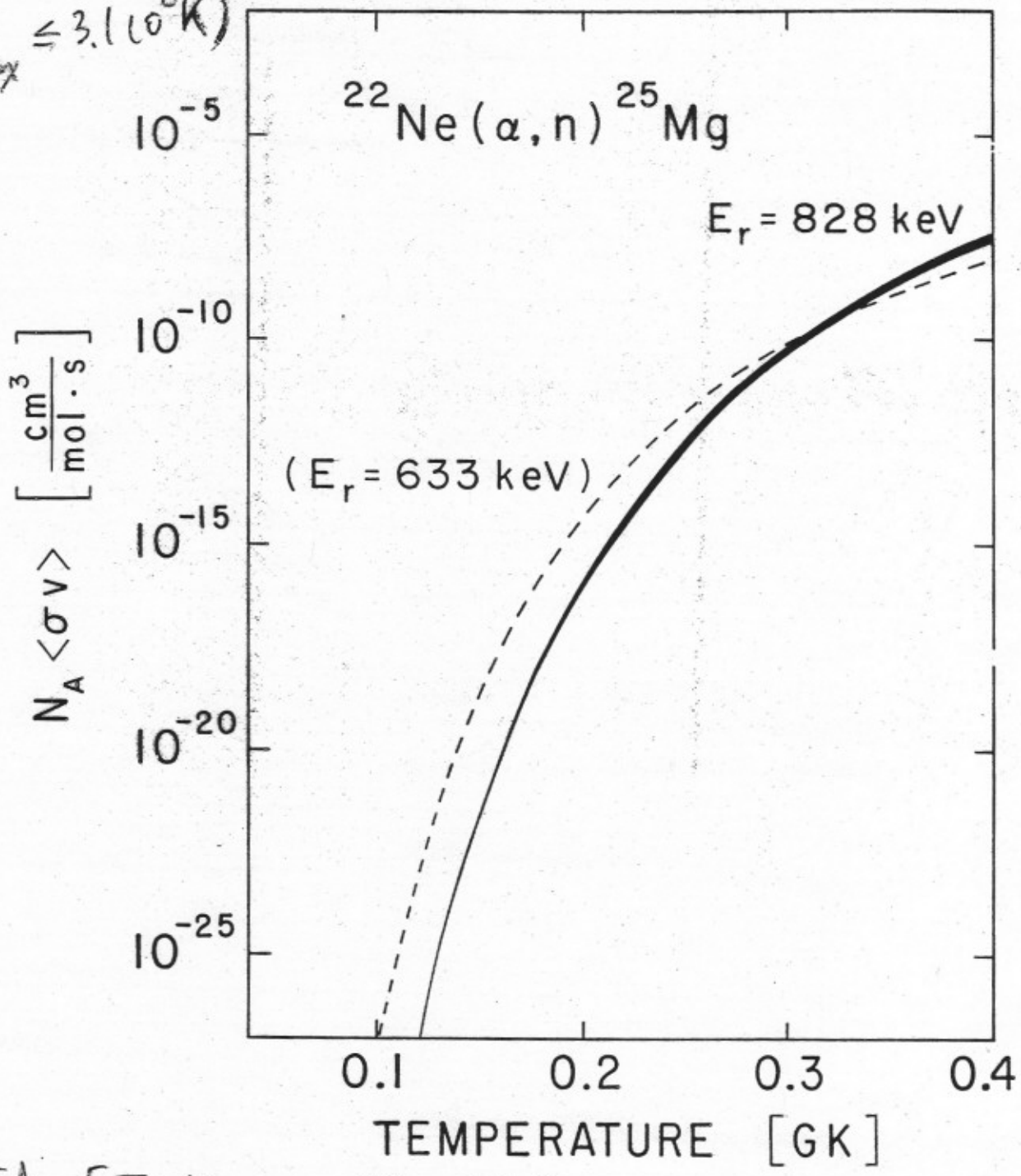

GIESEN ET AL. — PR 1993
KÄPPELER WIESCHER ET AL. — APJ 1994

Mutti et al

Mutti et al. (2002)

Kr cross sections

strong departure at low temperature

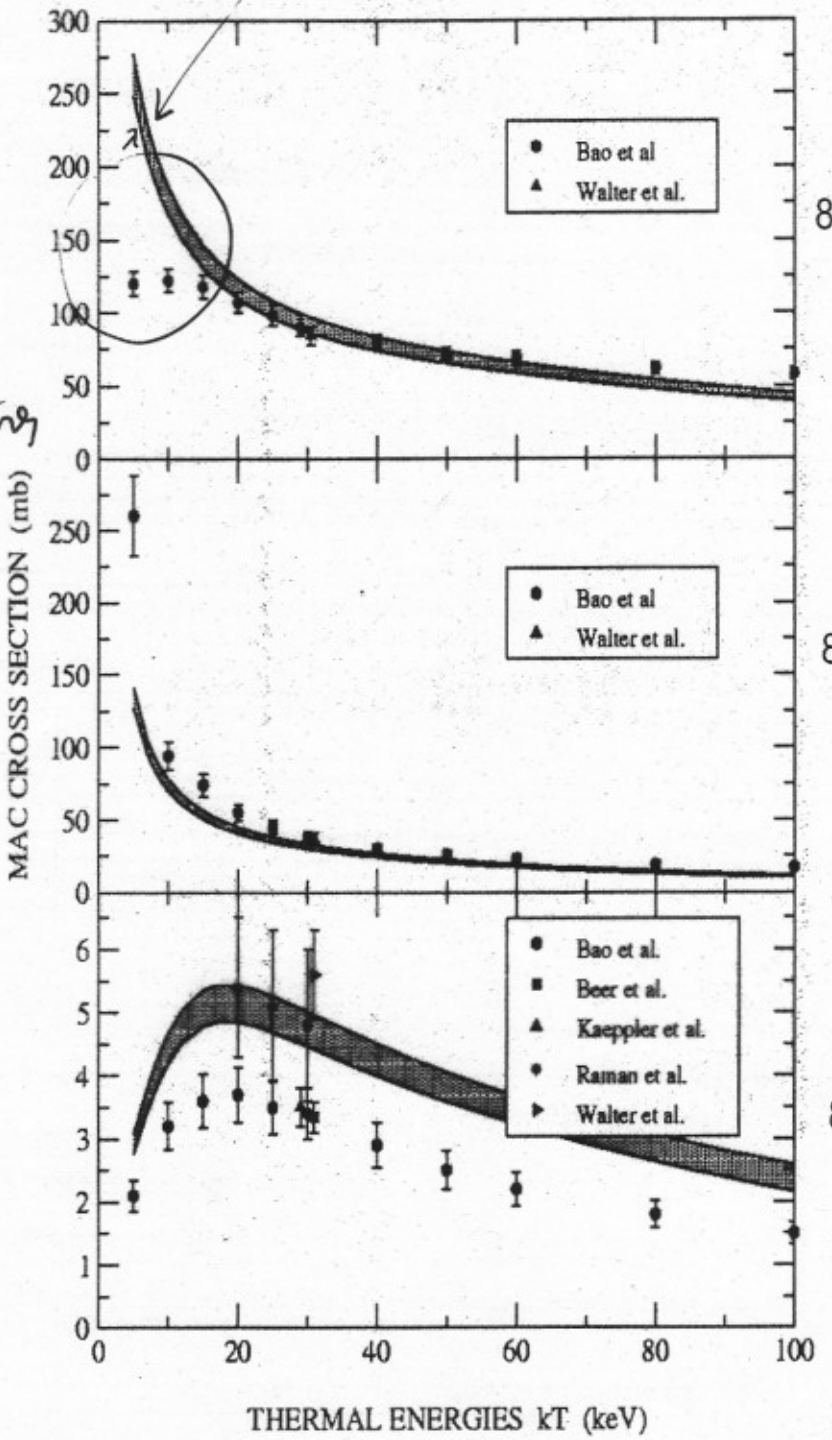

systematic discrepancy between TOF and previous activation measurements

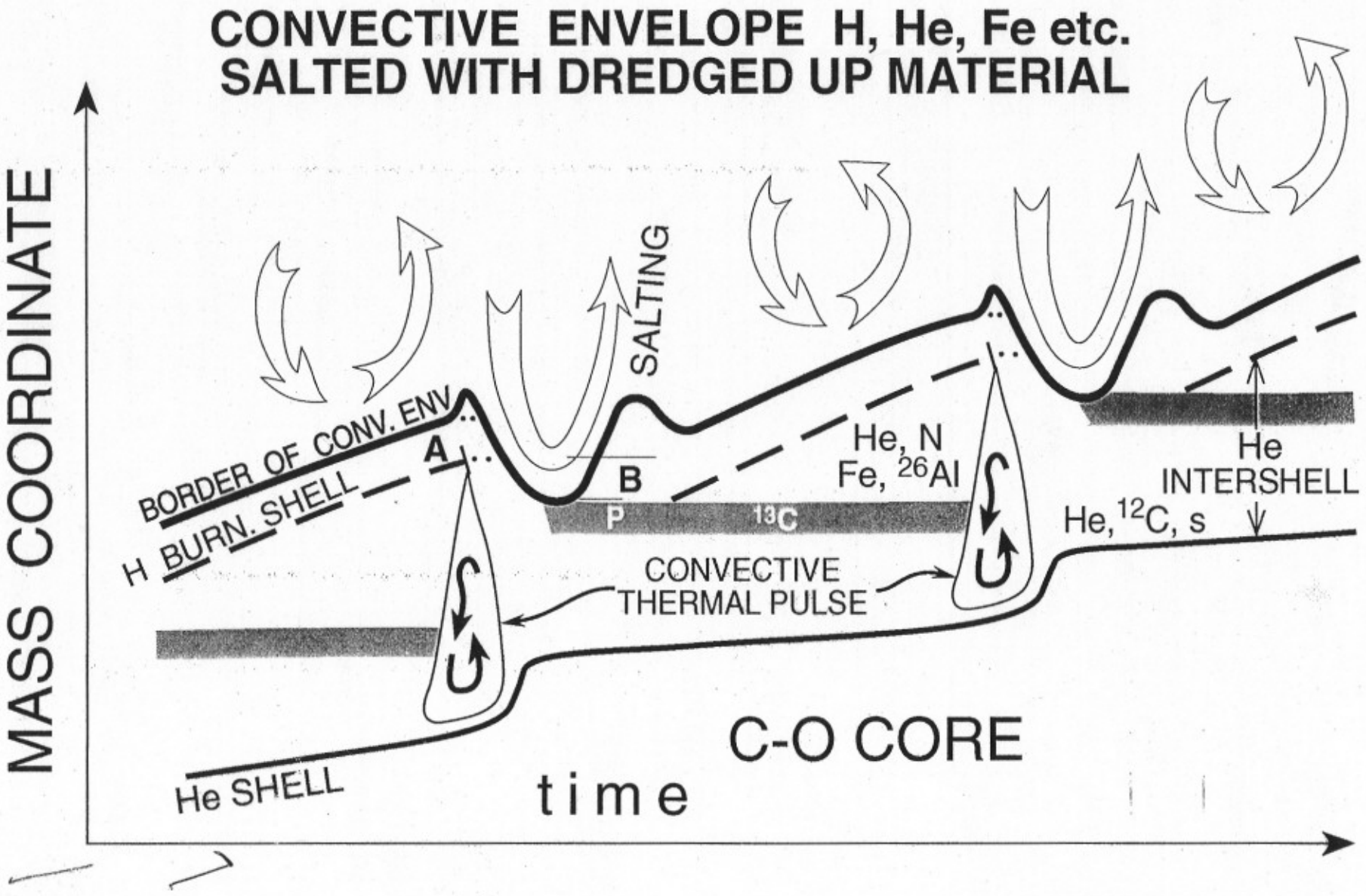
CONVECTIVE ENVELOPE H, He, Fe etc.
SALTED WITH DREDGED UP MATERIAL
MASS COORDINATE
SALTING
BORDER OF CONV. ENV
H BURN. SHELL
A
B
P
13C
He, N
Fe, 26Al
He
INTERSHELL
He, 12C, s
CONVECTIVE
THERMAL PULSE
C-O CORE
He SHELL
time

(24

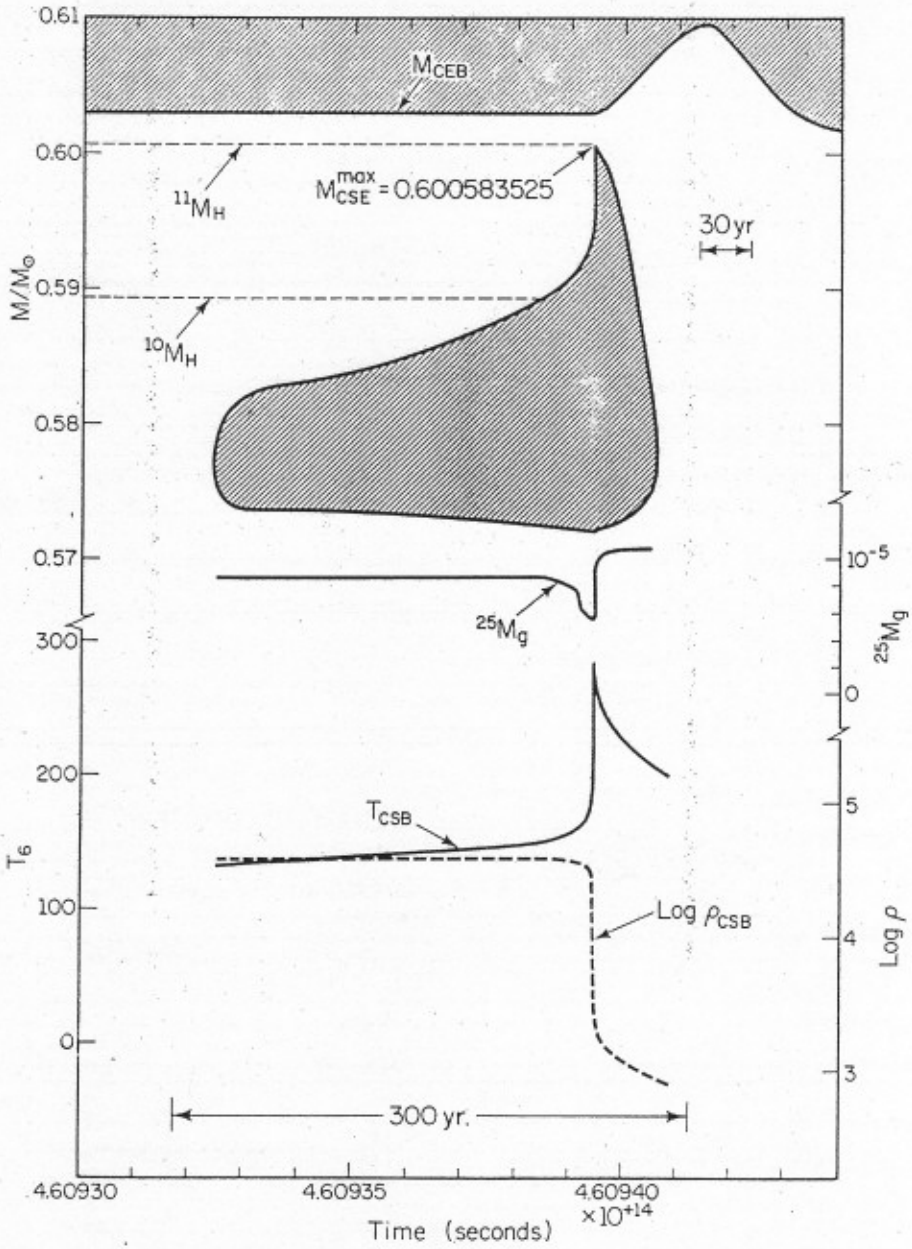

FIG. 7.—Properties of convective regions during the eleventh pulse for a model of mass $M = 0.7\ M_\odot$. The shaded regions indicate the formal presence of convection. T_{CSB} and ρ_{CSB} are, respectively, the temperature (units of 10^6 K) and density (units of g cm^{-3}) at the base of the helium burning convective shell, and ^{25}Mg is the abundance by mass of ^{25}Mg in the convective shell. The dashed lines labeled $^{10}M_H$ and $^{11}M_H$ denote the location of the hydrogen burning shell immediately prior to the tenth and eleventh pulses, respectively.

$M^* = 0.7\ M_\odot$ IBEN, Ap. J. 1982

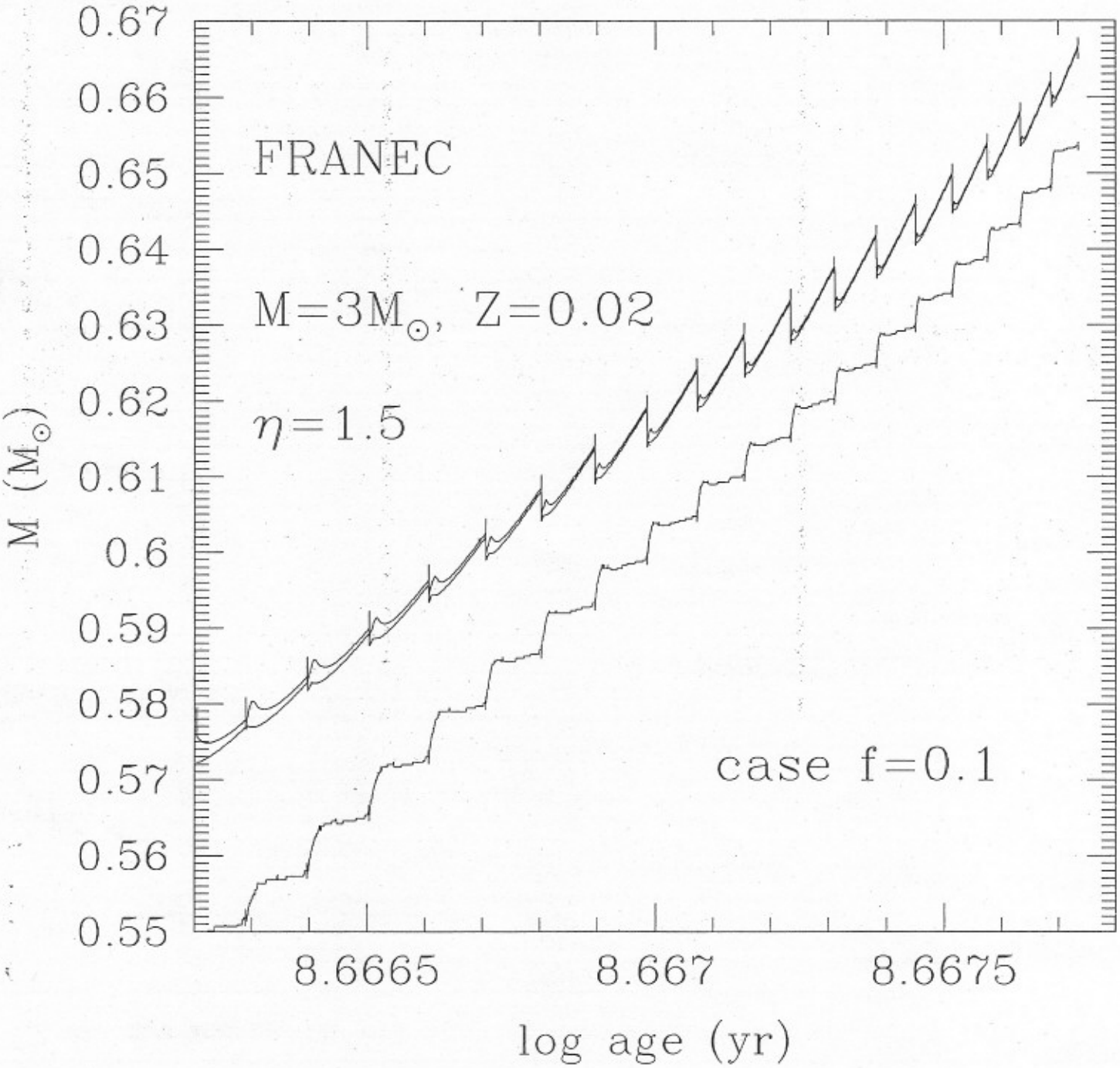
FRANEC
M=3M$_\odot$, Z=0.02
η=1.5
case f=0.1
M (M$_\odot$)
0.67
0.66
0.65
0.64
0.63
0.62
0.61
0.6
0.59
0.58
0.57
0.56
0.55
8.6665
8.667
8.6675
log age (yr)

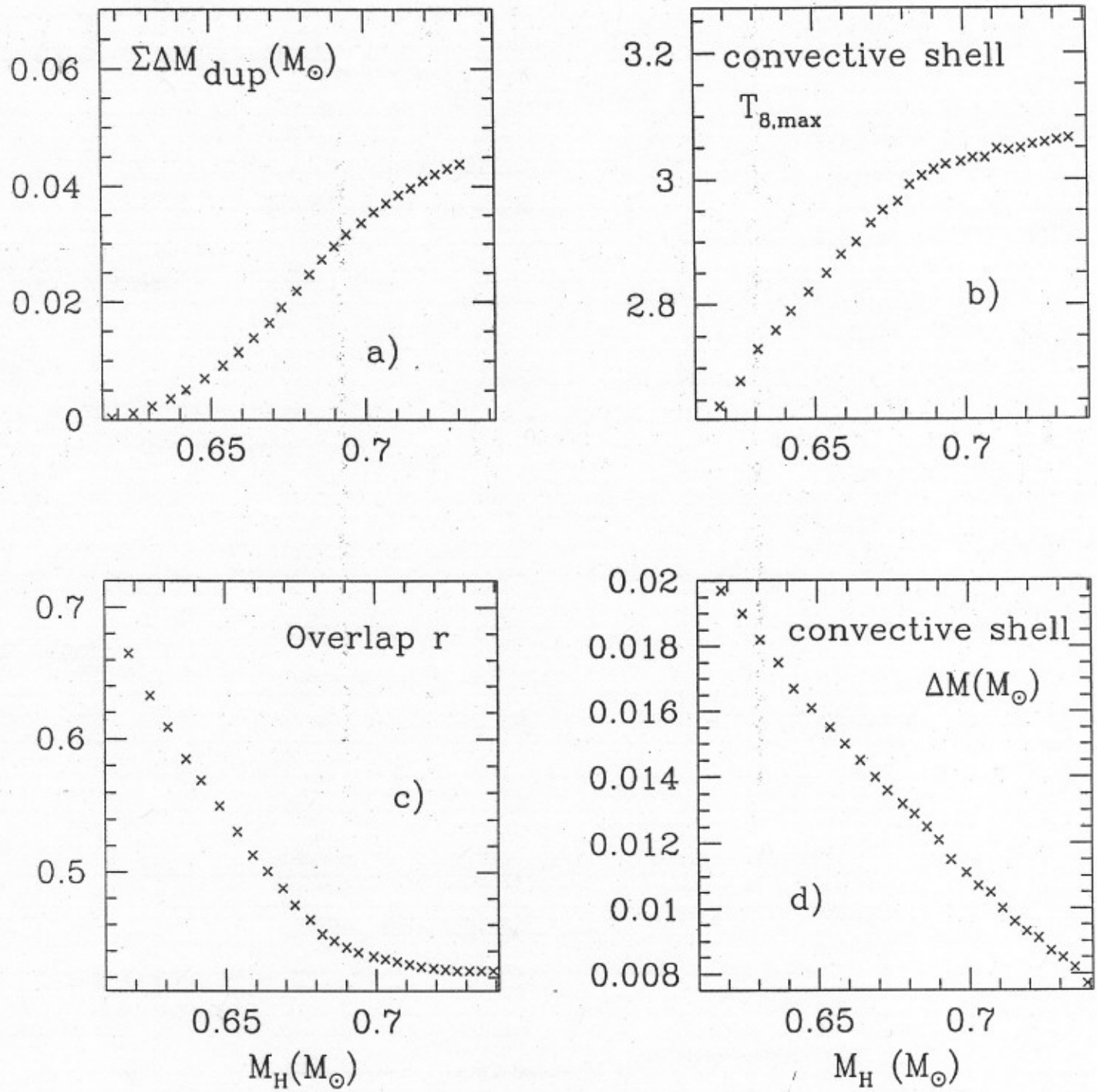

Fellin et al. ApJ. 1998

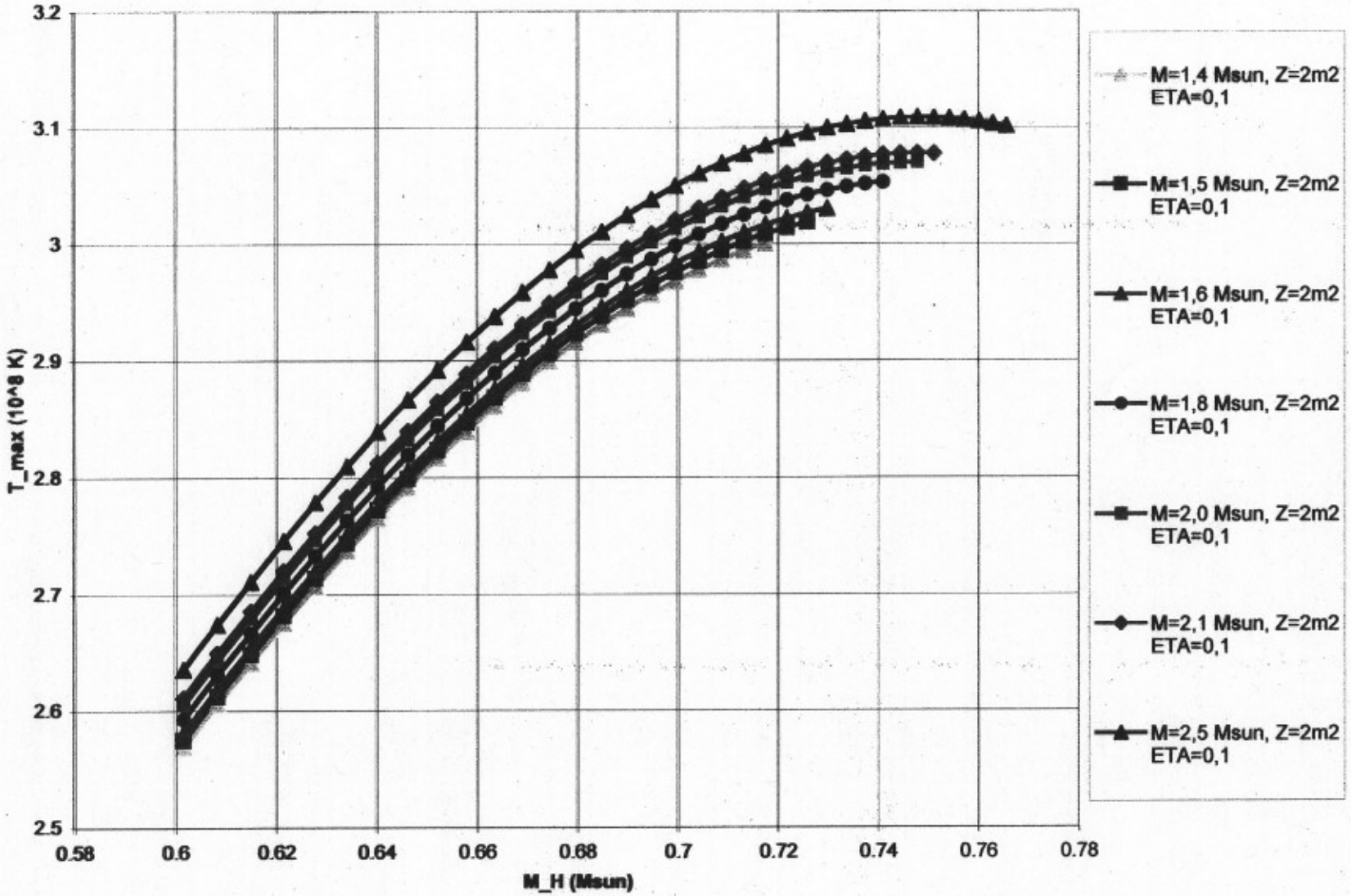
3.2
3.1
3
2.9
2.8
2.7
2.6
2.5
T_max (10^8 K)
0.58
0.6
0.62
0.64
0.66
0.68
0.7
0.72
0.74
0.76
0.78
M_H (Msun)
M=1,4 Msun, Z=2m2 ETA=0,1
M=1,5 Msun, Z=2m2 ETA=0,1
M=1,6 Msun, Z=2m2 ETA=0,1
M=1,8 Msun, Z=2m2 ETA=0,1
M=2,0 Msun, Z=2m2 ETA=0,1
M=2,1 Msun, Z=2m2 ETA=0,1
M=2,5 Msun, Z=2m2 ETA=0,1

M=1,4 Msun, Z=2mZ
ETA=0,1
M=1,5 Msun, Z=2mZ
ETA=0,1
M=1,6 Msun, Z=2mZ
ETA=0,1
M=1,8 Msun, Z=2mZ
ETA=0,1
M=2,0 Msun, Z=2mZ
ETA=0,1
M=2,1 Msun, Z=2mZ
ETA=0,1
M=2,5 Msun, Z=2mZ
ETA=0,1
0.012
0.011
0.01
0.009
0.008
0.007
0.006
0.005
0.004
0.003
0.002
0.001
0
UGT_M (nuSM)
0.58
0.6
0.62
0.64
0.66
0.68
0.7
0.72
0.74
0.76
0.78
M_H (Msun)

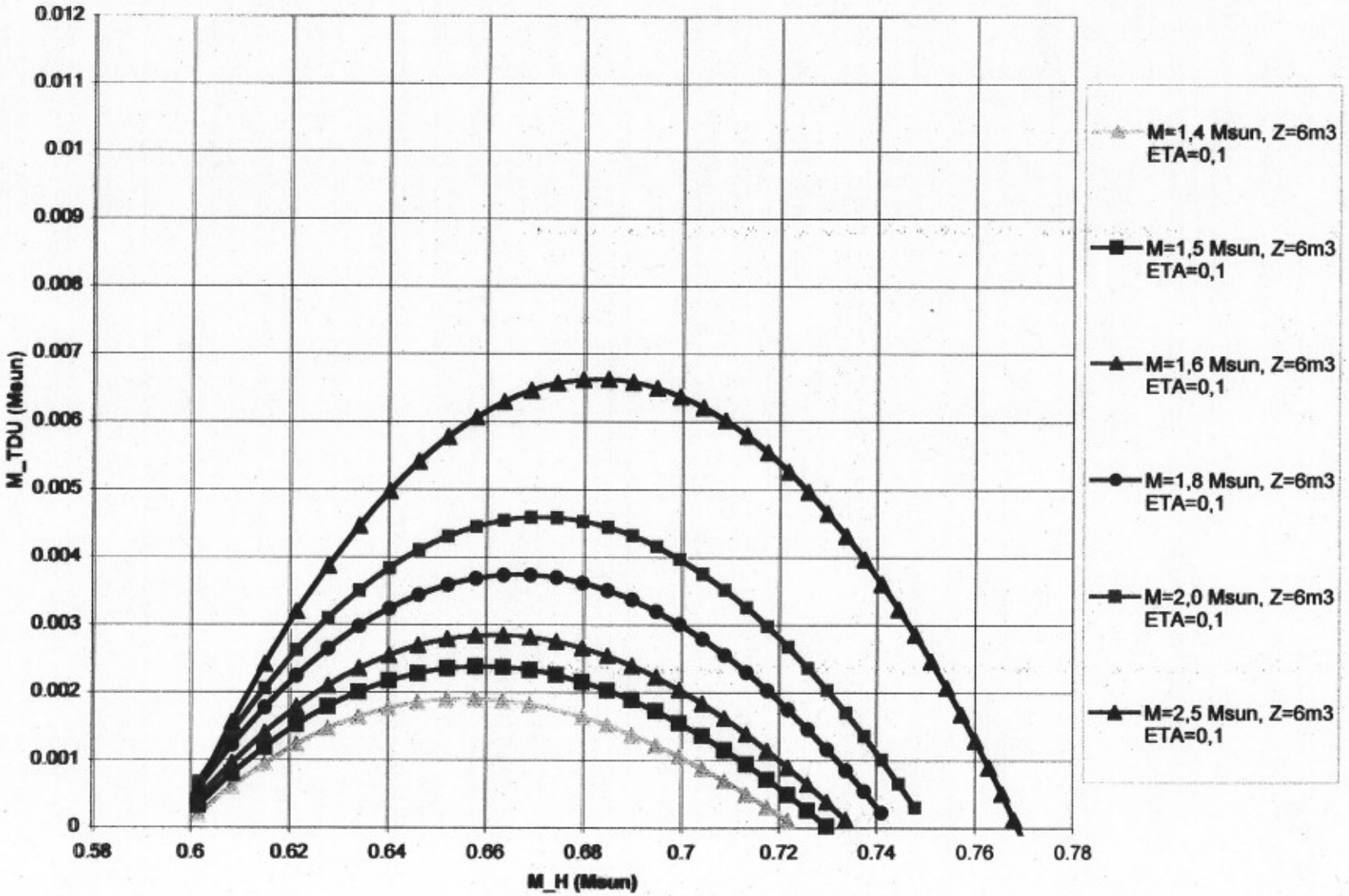
0.012
0.011
0.01
0.009
0.008
0.007
0.006
0.005
0.004
0.003
0.002
0.001
0
M_TDU (Msun)
0.58
0.6
0.62
0.64
0.66
0.68
0.7
0.72
0.74
0.76
0.78
M_H (Msun)
M=1,4 Msun, Z=6m3 ETA=0,1
M=1,5 Msun, Z=6m3 ETA=0,1
M=1,6 Msun, Z=6m3 ETA=0,1
M=1,8 Msun, Z=6m3 ETA=0,1
M=2,0 Msun, Z=6m3 ETA=0,1
M=2,5 Msun, Z=6m3 ETA=0,1

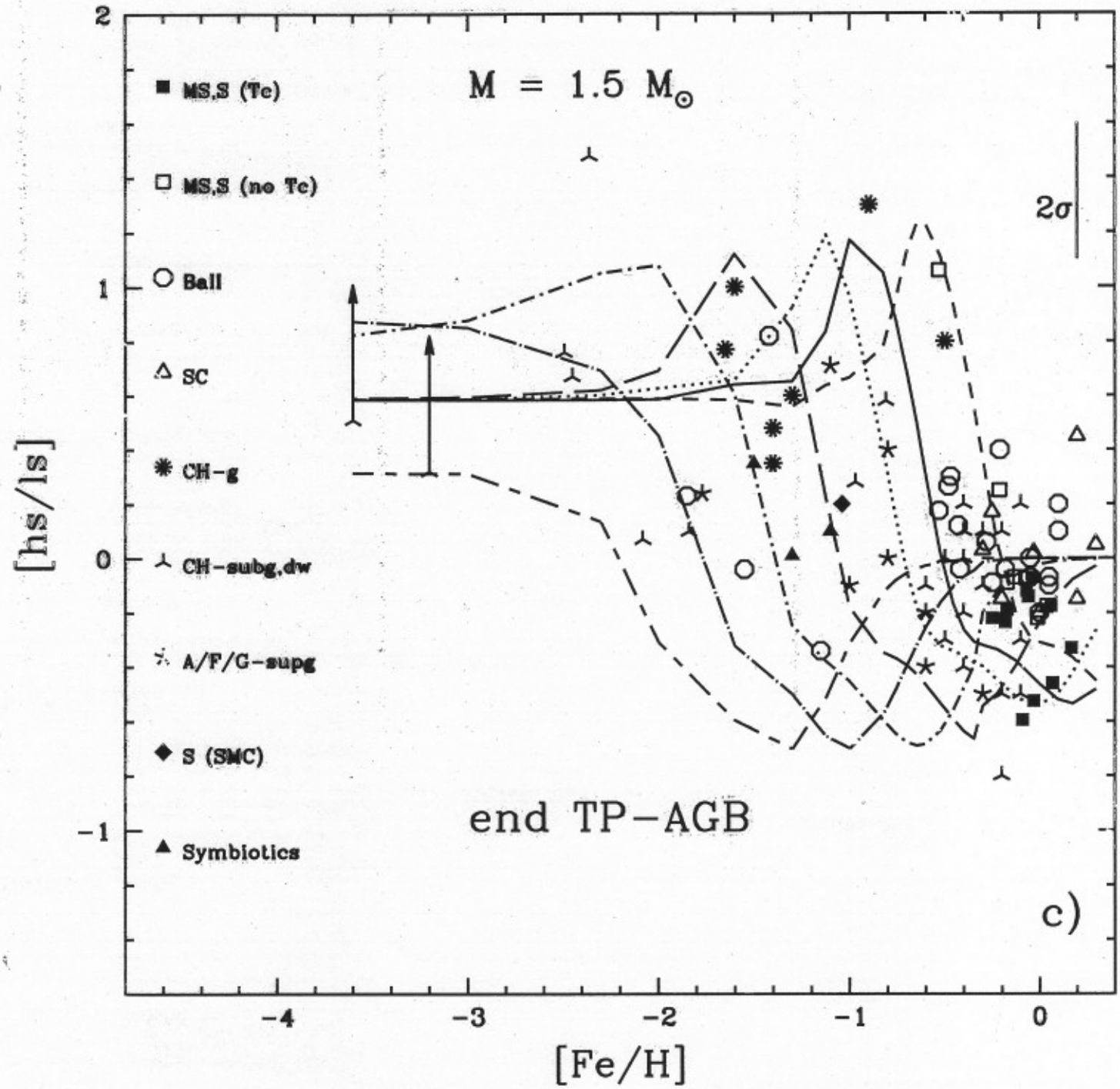

Busso et al 2001 ApJ

How to get Pb and Bi...

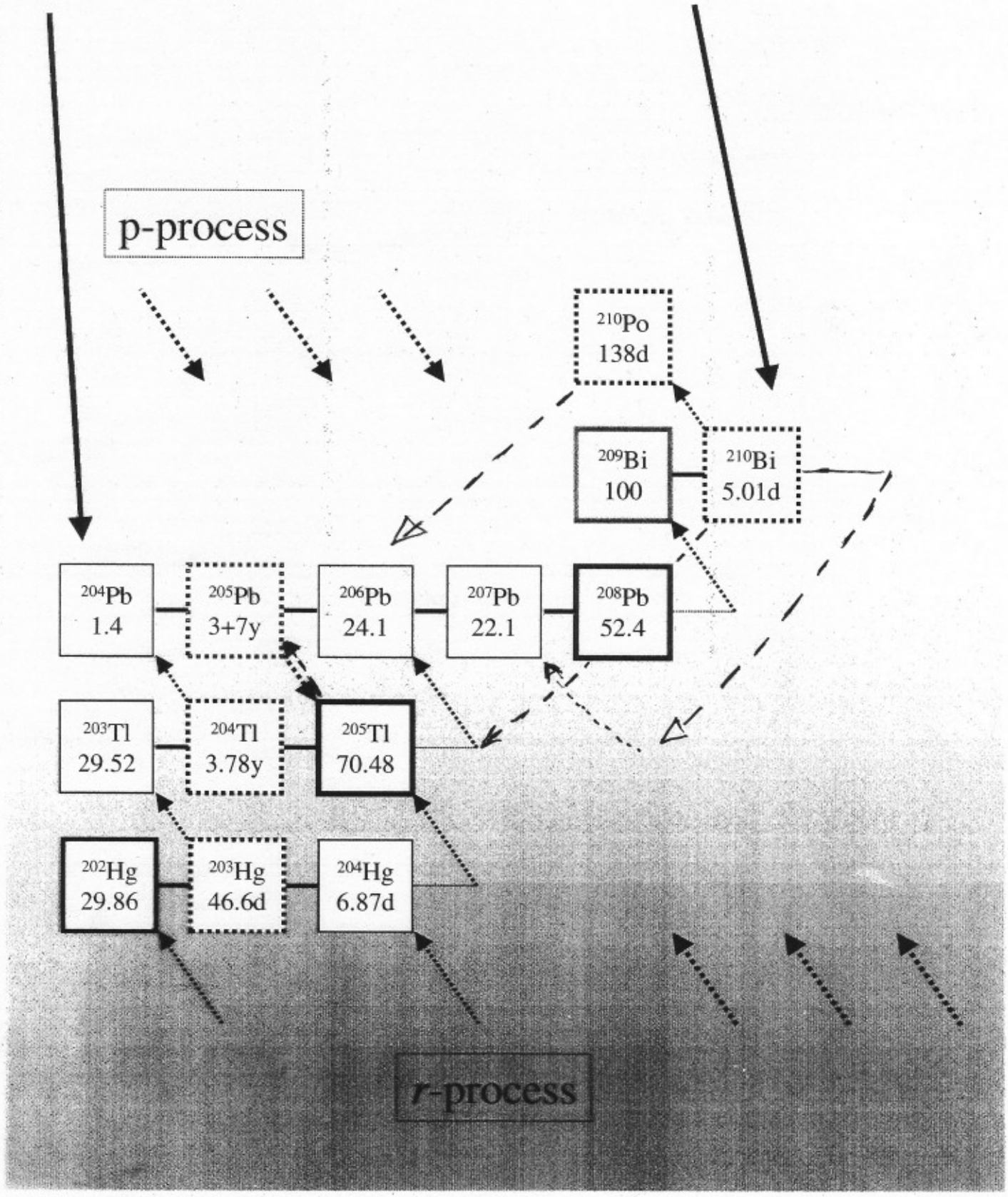

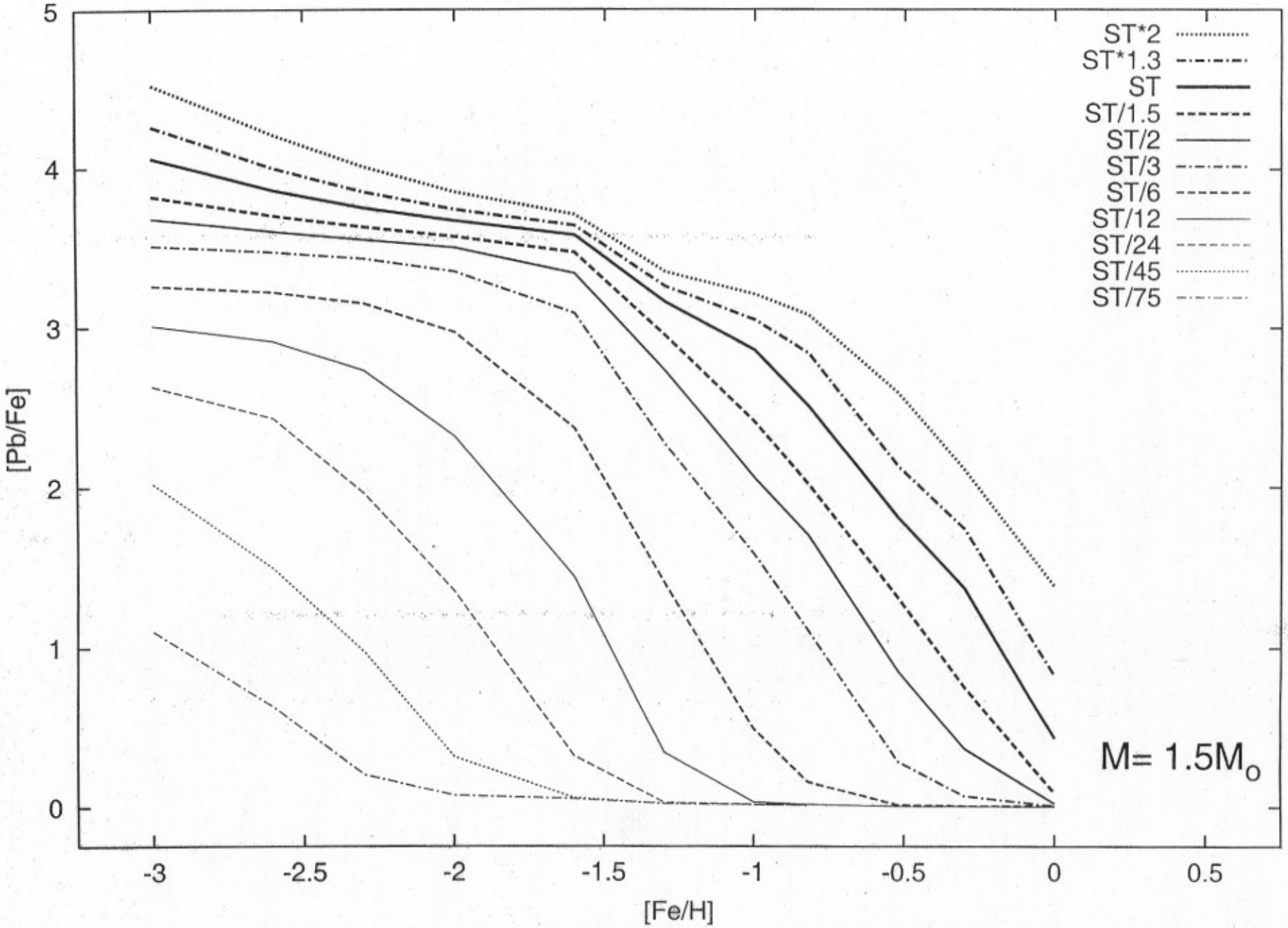
ST*2
ST*1.3
ST
ST/1.5
ST/2
ST/3
ST/6
ST/12
ST/24
ST/45
ST/75
M= 1.5M$_o$
[Pb/Fe]
[Fe/H]
5
4
3
2
1
0
-3
-2.5
-2
-1.5
-1
-0.5
0
0.5

~ 2 $M_\odot$ AGB star yields:

FRANEC code + s-process nucleosynthesis

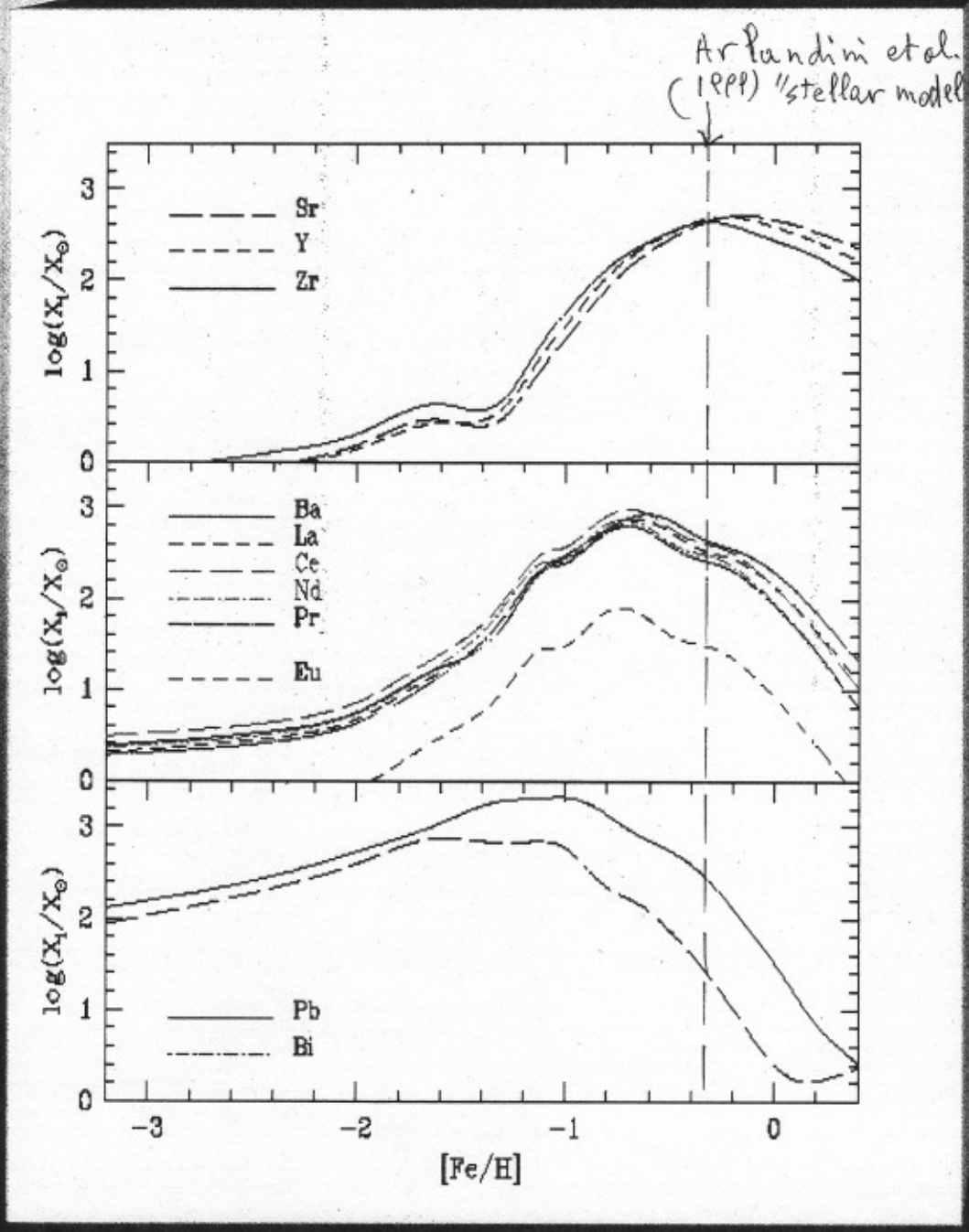

Gallino et al. 1998; Travaglio et al. 1999

Busso et al. 2001, ApJ, 557, 802

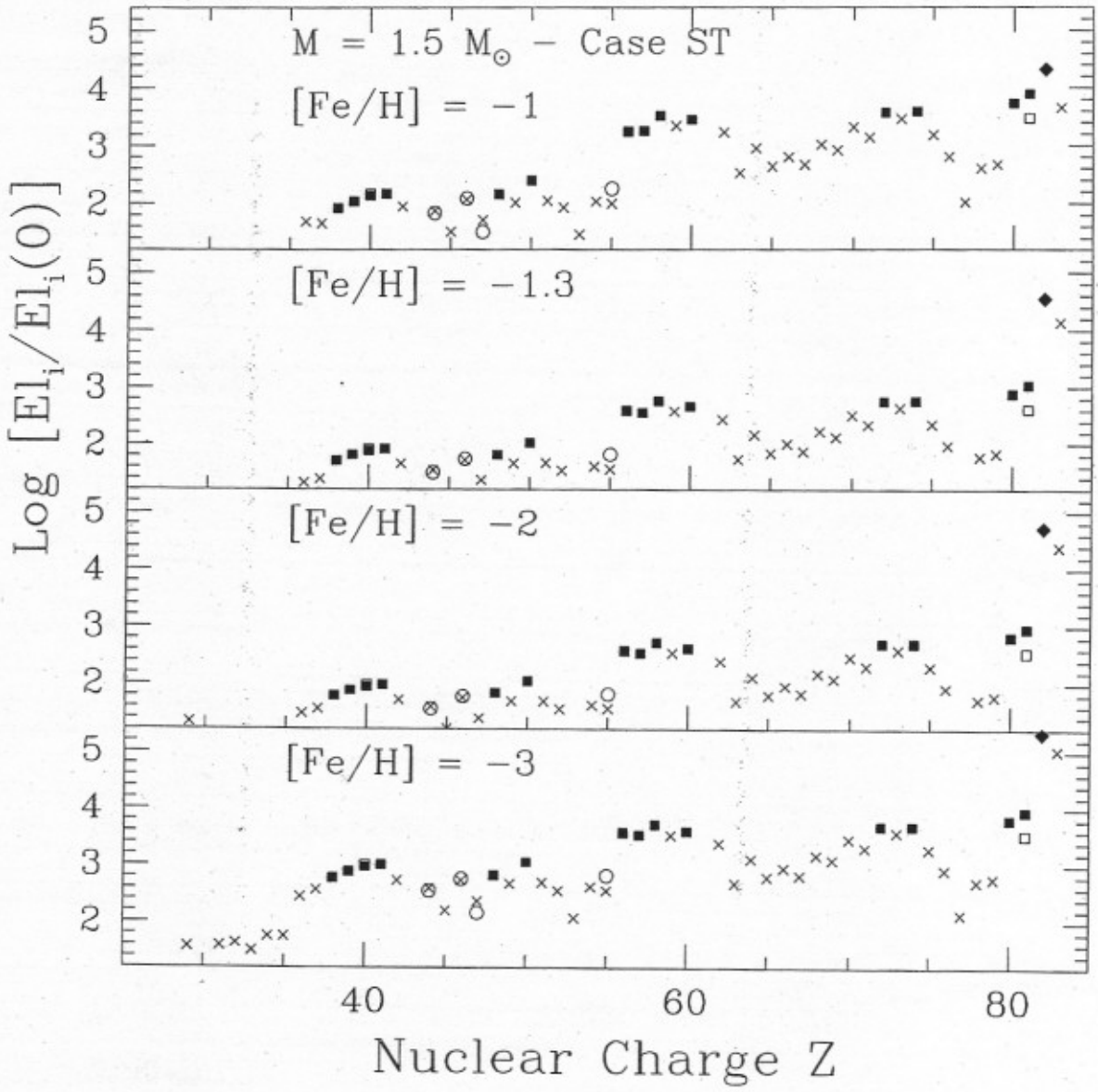

Fig. 2.— Same as Figure 1, but for metallicities from [Fe/H] = −1 down to [Fe/H] = −3.

Busso, Gallino, Lambert, Travaglio, Smith, 2001, ApJ, 557, 802

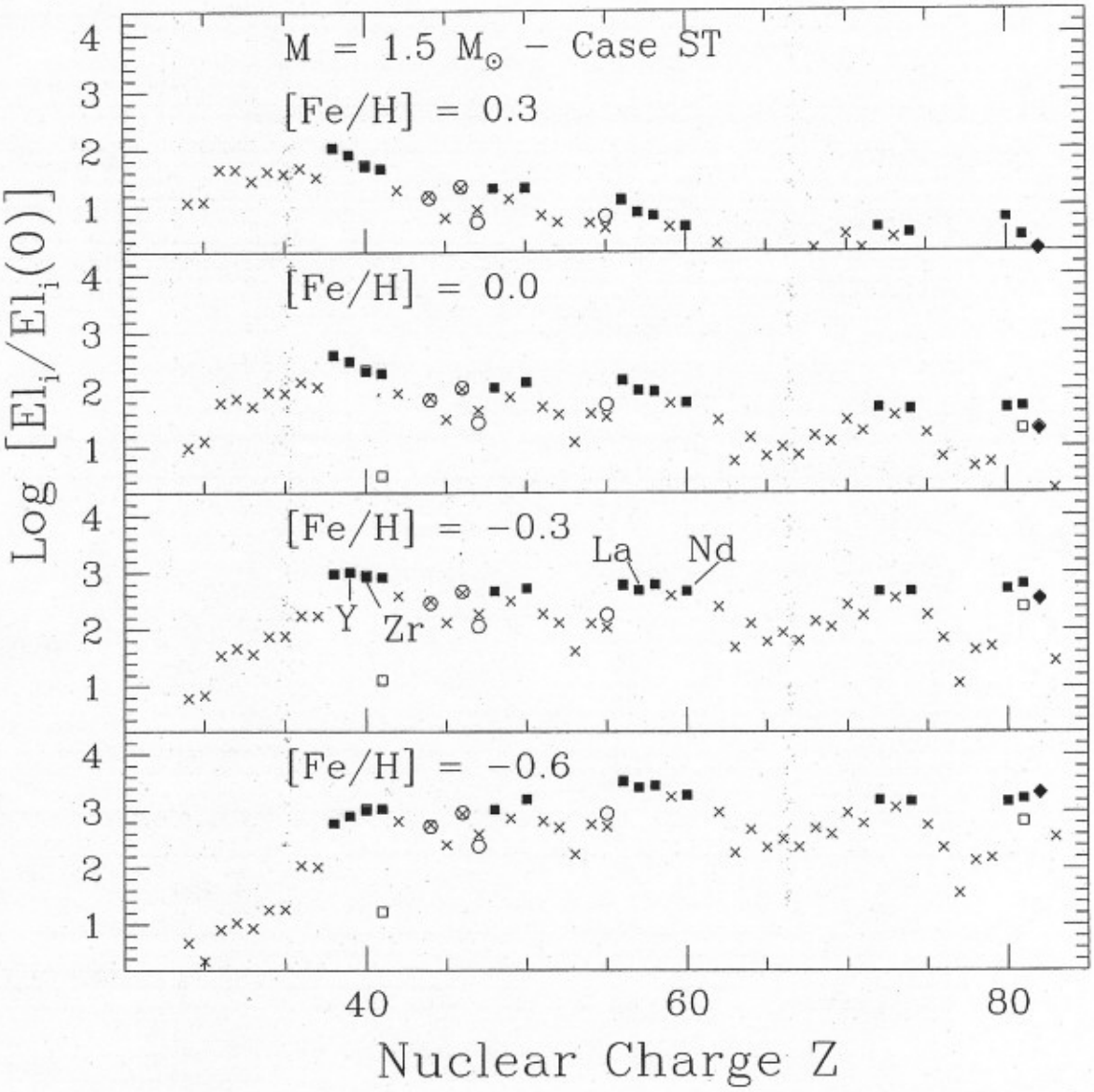

Fig. 1.— The distribution of the elements from Cu to Bi in the He intershell as a function of the initial metallicity. Elements mainly produced by the main component of the *s* process (by at least 50 % according to Arlandini et al. 1999) are shown as bold squares. Pb has a special symbol (bold diamond) because it is mainly attributed to the strong *s*-process component, deriving from AGB stars of low metallicity (Travaglio et al. 2001). The models refer to a 1.5 $M_\odot$ star, with the choice ST for the ^{13}C pocket discussed in the text, and with metallicities from [Fe/H] = +0.3 down to −0.6. For elements affected by the decay of unstable isotopes whose half-life is longer than a typical interpulse period, but shorter than 10^9 yr, open symbols refer to abundances before decay.

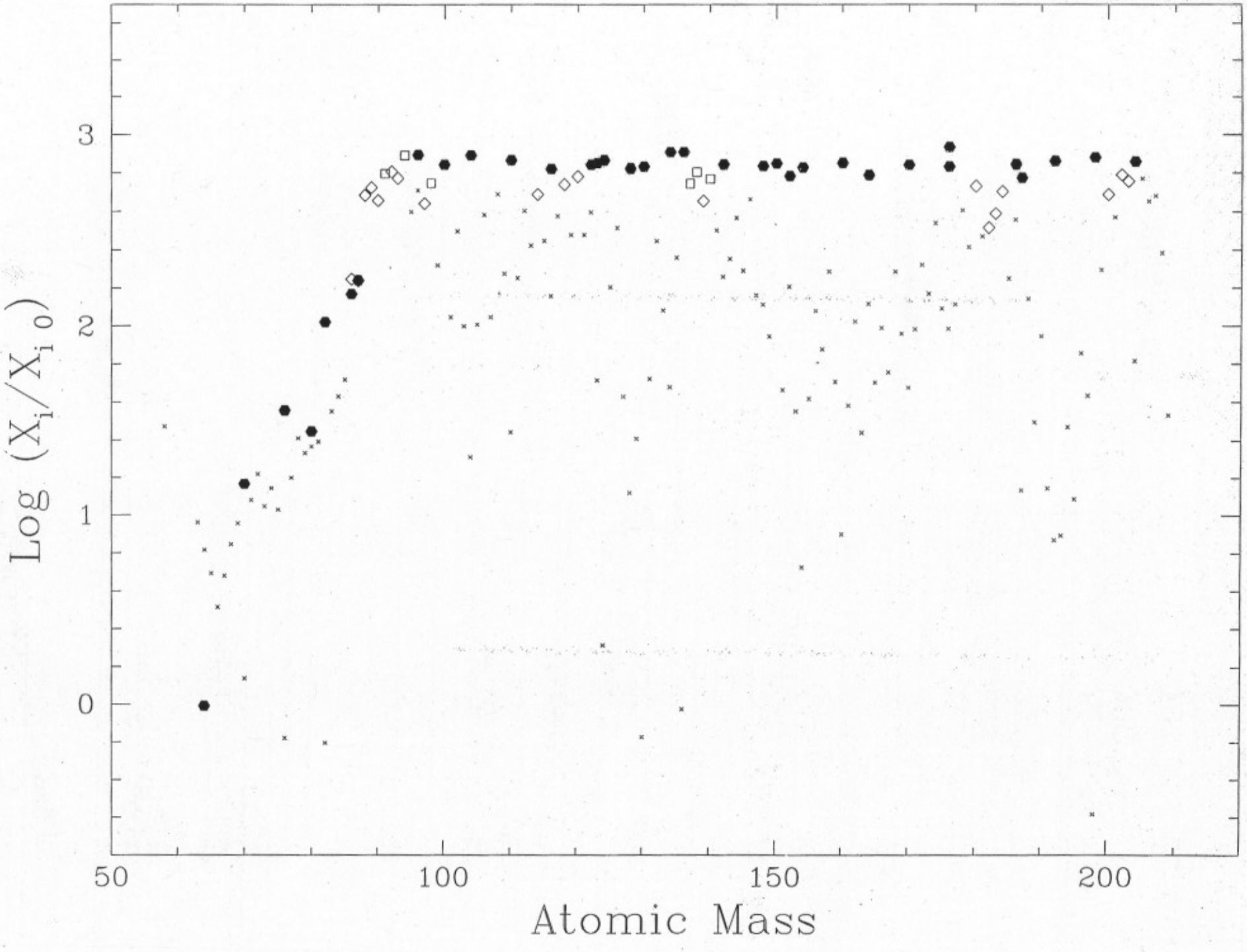
Log $(X_i/X_{i\,0})$
3
2
1
0
50
100
150
200
Atomic Mass

AGB star Z = 0.001

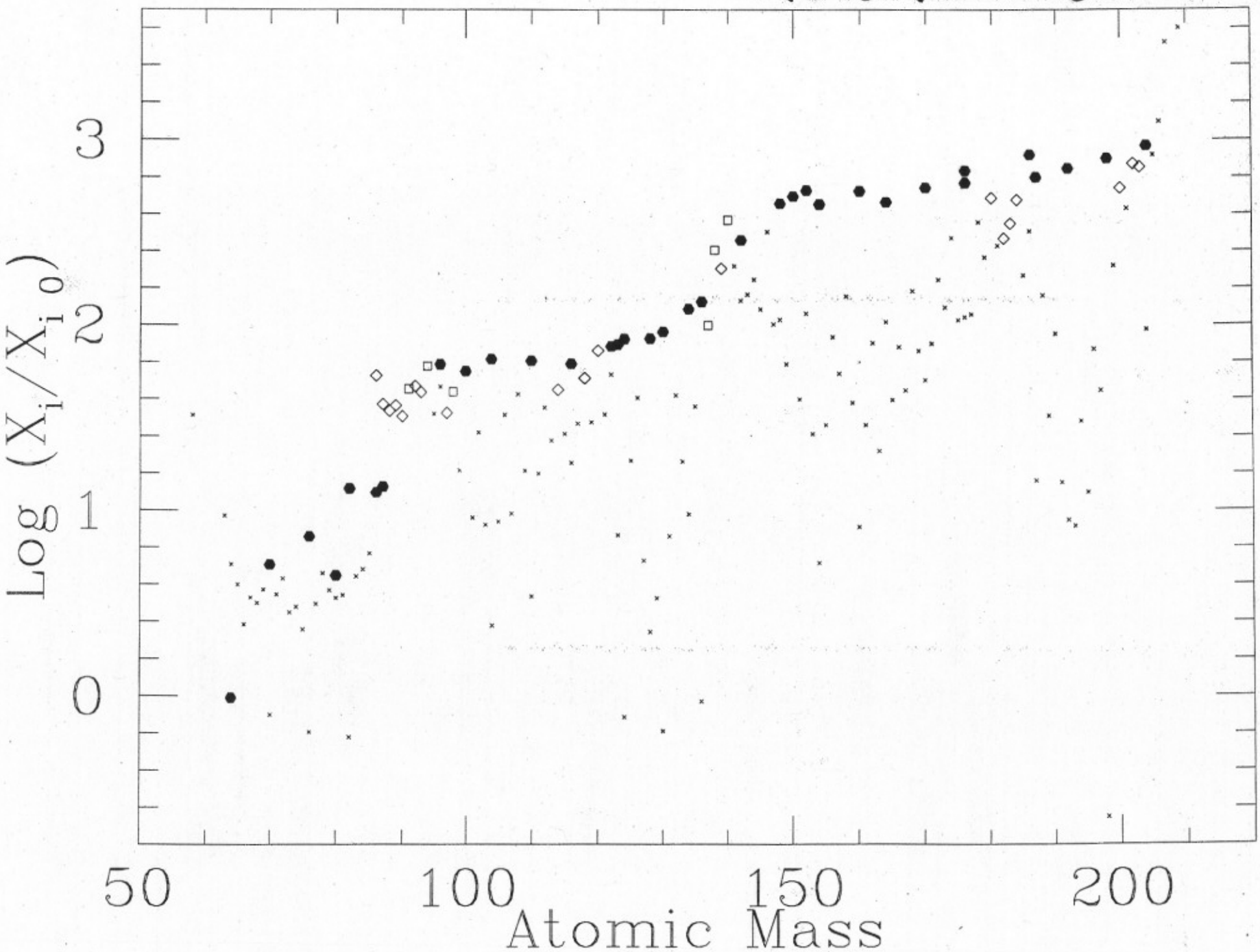

Object	T_{eff}	log g	[Fe/H]	[Pb/Fe]	Binary
CS 22183-015	5200	2.5	-3.12	3.17	...
CS 22880-074	5850	3.8	-1.93	1.9	no
CS 22892-052	4710	1.5	-3.1	1.35	...
CS 22898-027	6250	3.7	-2.26	2.84	no
CS 22942-019	5000	2.4	-2.64	$\leq$1.6	yes
CS 29497-030	6650	3.5	-2.70	3.55	yes
CS 29526-110	6500	3.2	-2.38	3.3	yes
CS 30301-015	4750	0.8	-2.64	1.7	...
CS 31062-012	6250	4.5	-2.55	2.4	...
CS 31062-050	5600	3.0	-2.31	2.9	...
LP 625-44	5500	2.8	-2.71	2.6	yes
LP 706-7	6000	3.8	-2.74	2.28	no
HD 26	5170	2.2	-1.25	1.9	...
HD 2665	5061	2.35	-1.95	< 1	...
HD 21581	4978	2.29	-1.57	< 0.5	...
HD 115444	4750	1.7	-2.77	0.30	...
HD 126238	4979	2.5	-1.7	-0.05	...
HD 187861	5320	2.3	-1.65	2.40	...
HD 189711	3500	0.5	-1.8	0.7	...
HD 196944	5250	1.8	-2.25	1.7	...
HD 198269	4800	1.3	-2.2	2.2	...
HD 201626	5190	2.25	-2.1	2.4	...
HD 201891	5991	4.30	-1.04	< 0.5	...
HD 224959	5200	2.3	-1.7	2.55	...
HD 23439A	5140	4.48	-0.99	0.6	...
HE 0024-2523	6625	4.3	-2.72	3.3	yes
HE 2148-1247	6380	3.9	-2.3	3.12	yes
V Ari	3580	-0.2	-2.4	1.0	...

Table 4.1: Summary of available data for lead in metal-poor stars. (from Sivarani et al. 2003)

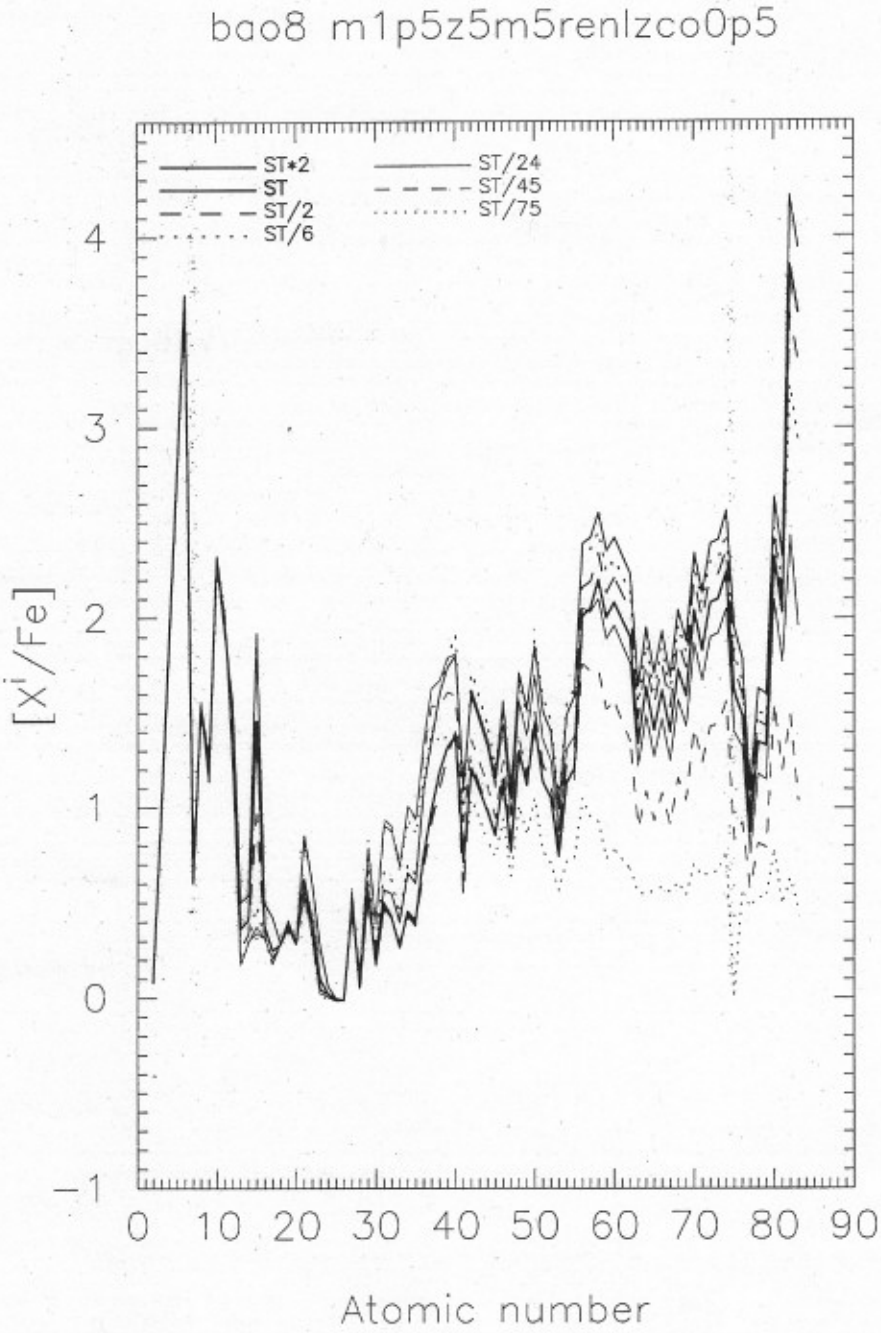

Figure 4.1: Theoretical element abundances at last pulse with TDU (pulse 17), for a 1.5 $M_\odot$ star, with $Z = 5 \times 10^{-5}$ ([Fe/H]≈ -2.6) and different choices of the ^{13}C pocket.

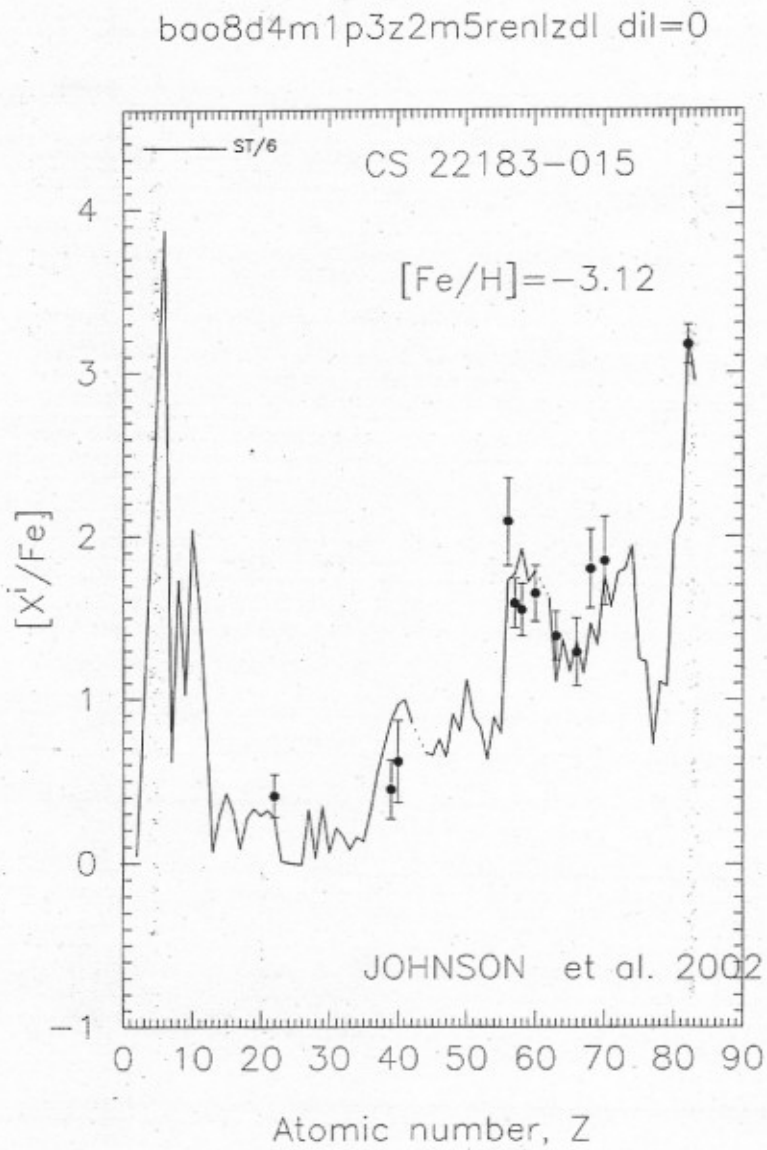

Figure 4.10: Fit for the star CS 22183-015. Considered parameters: ^{13}C pocket - $ST/6$, stellar mass - $1.3M_{\odot}$, stellar metallicity - $2 \cdot 10^{-5}$, dilution factor - 0, continuous mass transfer, long-lived nuclide decays. Observed abundances from Johnson et al. 2002 (see Table 4.3).

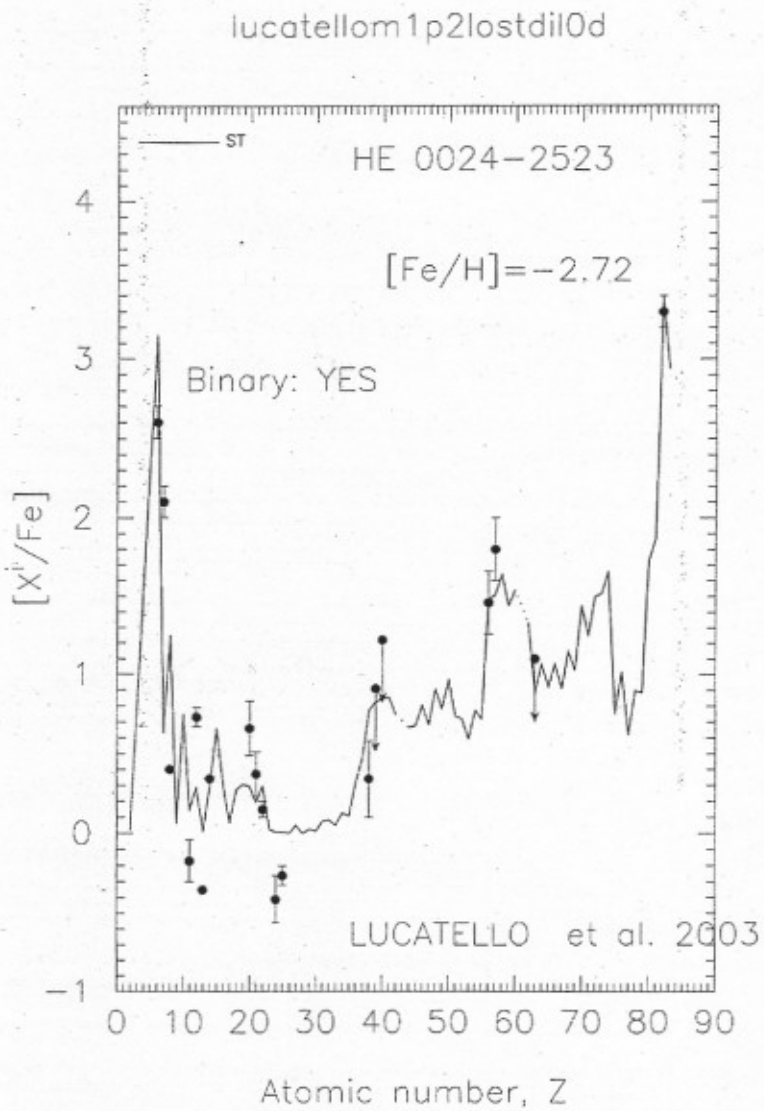

Figure 4.14: Fit for the star HE 0024-2523. Considered parameters: ^{13}C pocket - ST, stellar mass - $1.2M_{\odot}$, stellar metallicity - $5 \cdot 10^{-5}$, dilution factor - 0, continuous mass transfer, long-lived nuclide decays. Observed abundances from Lucatello et al. 2003 (see Table 4.7).

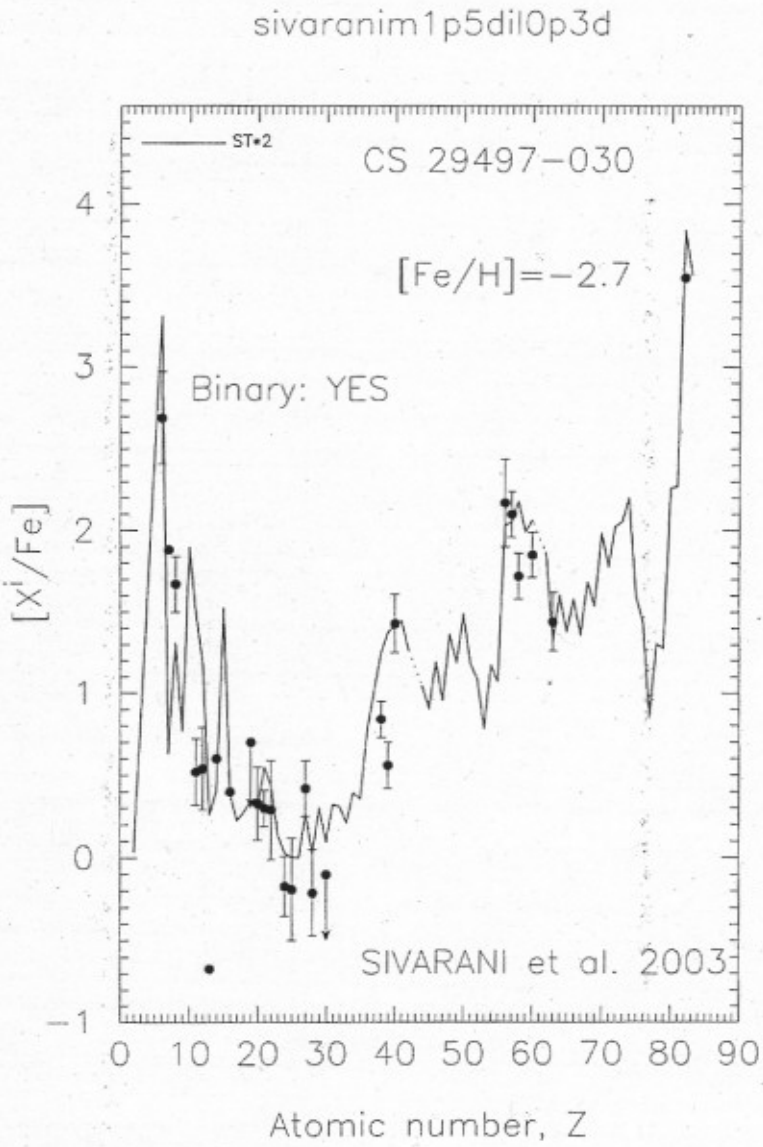

Figure 4.5: Fit for the star CS 29497-030. Considered parameters: ^{13}C pocket - $ST*2$, stellar mass - $1.5M_{\odot}$, stellar metallicity - $5 \cdot 10^{-5}$, dilution

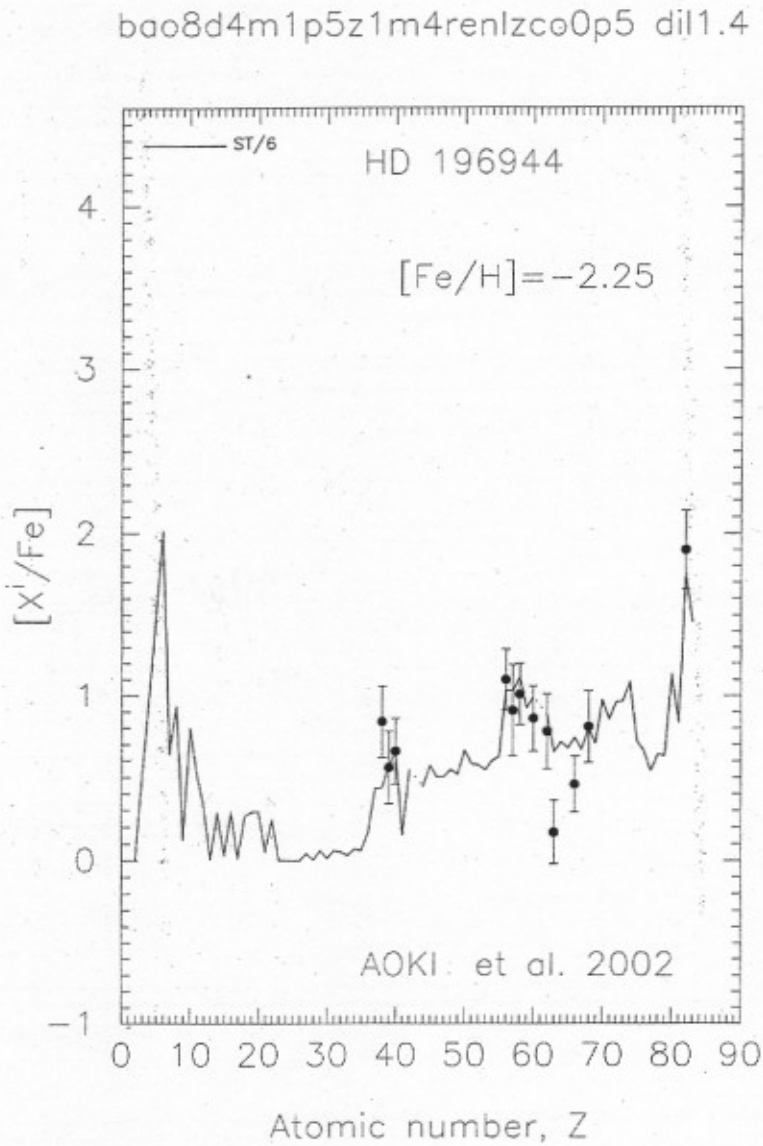

Figure 4.12: Fit for the star HD 196944. Considered parameters: ^{13}C pocket - $ST/6$, stellar mass - $1.5M_{\odot}$, stellar metallicity - $1 \cdot 10^{-4}$, dilution factor - 1.4, mass transfer at last pulse (pulse 17), no long-lived nuclide decays. Observed abundances from Aoki et al. 2002 (see Table 4.5).

How we treat galactic chemical evolution ...

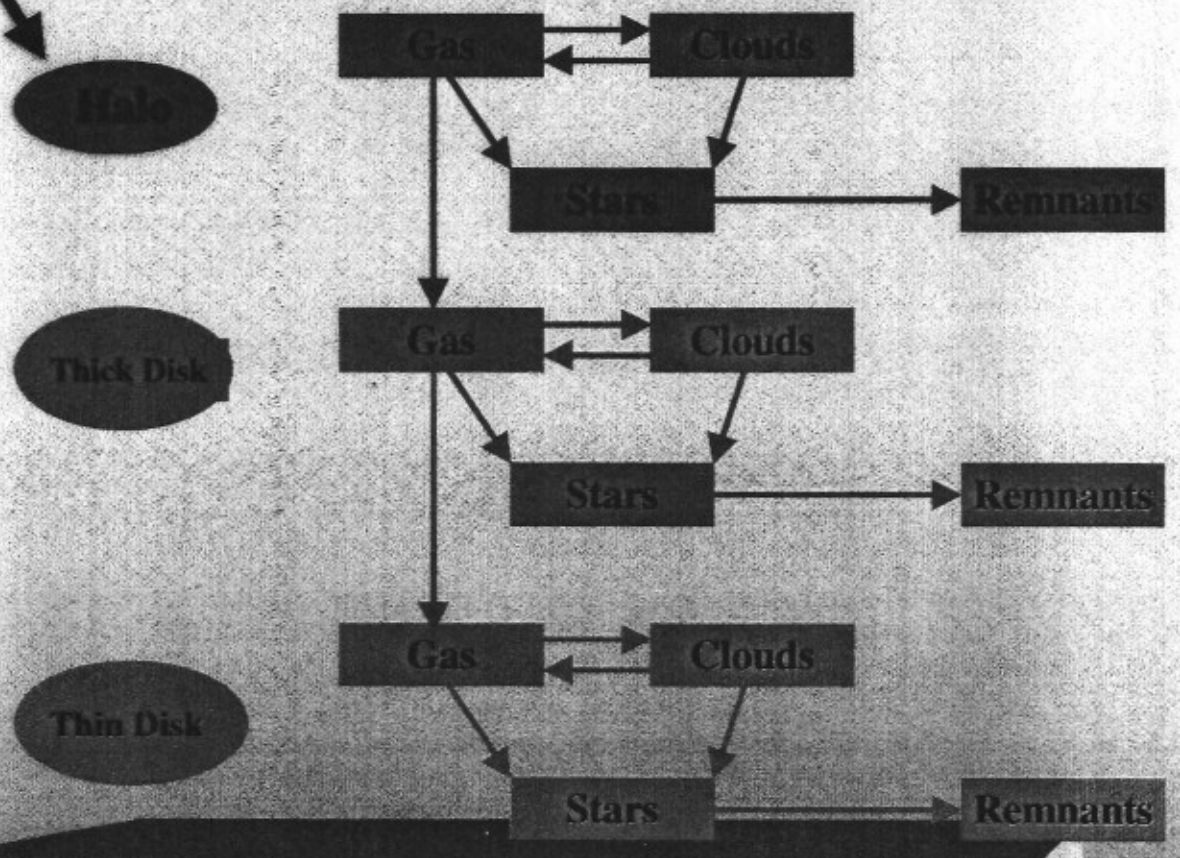

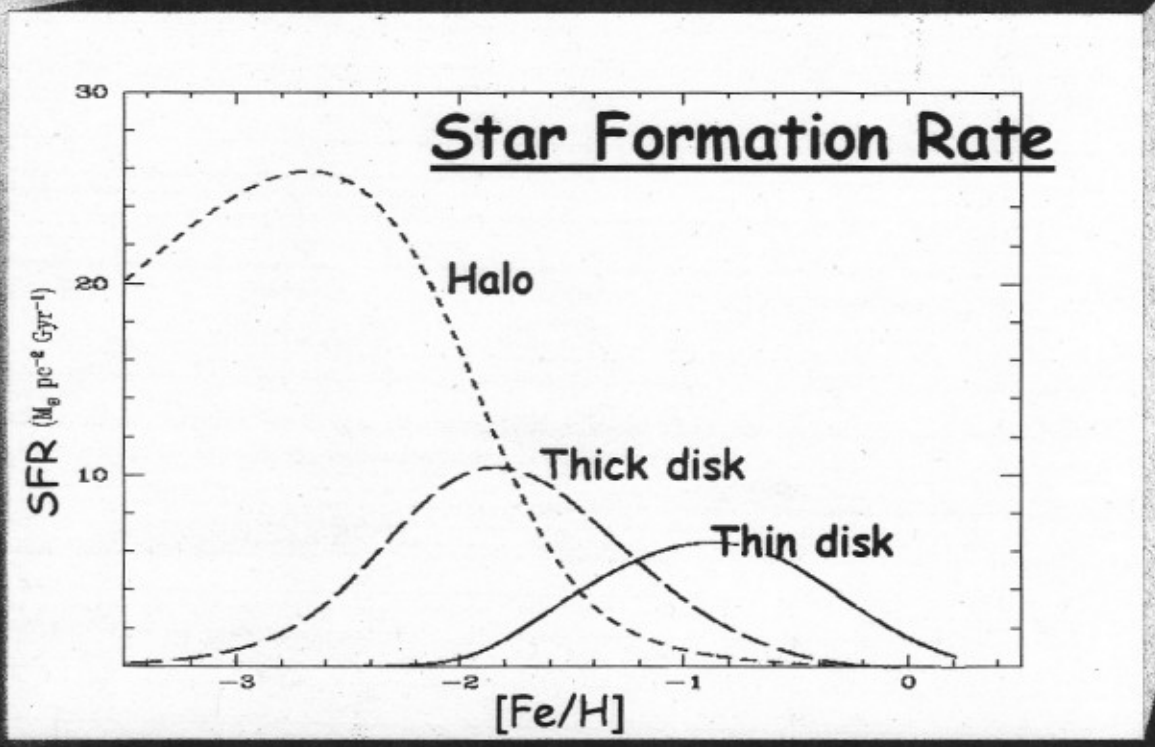

Different stellar sources for chemical evolution ...

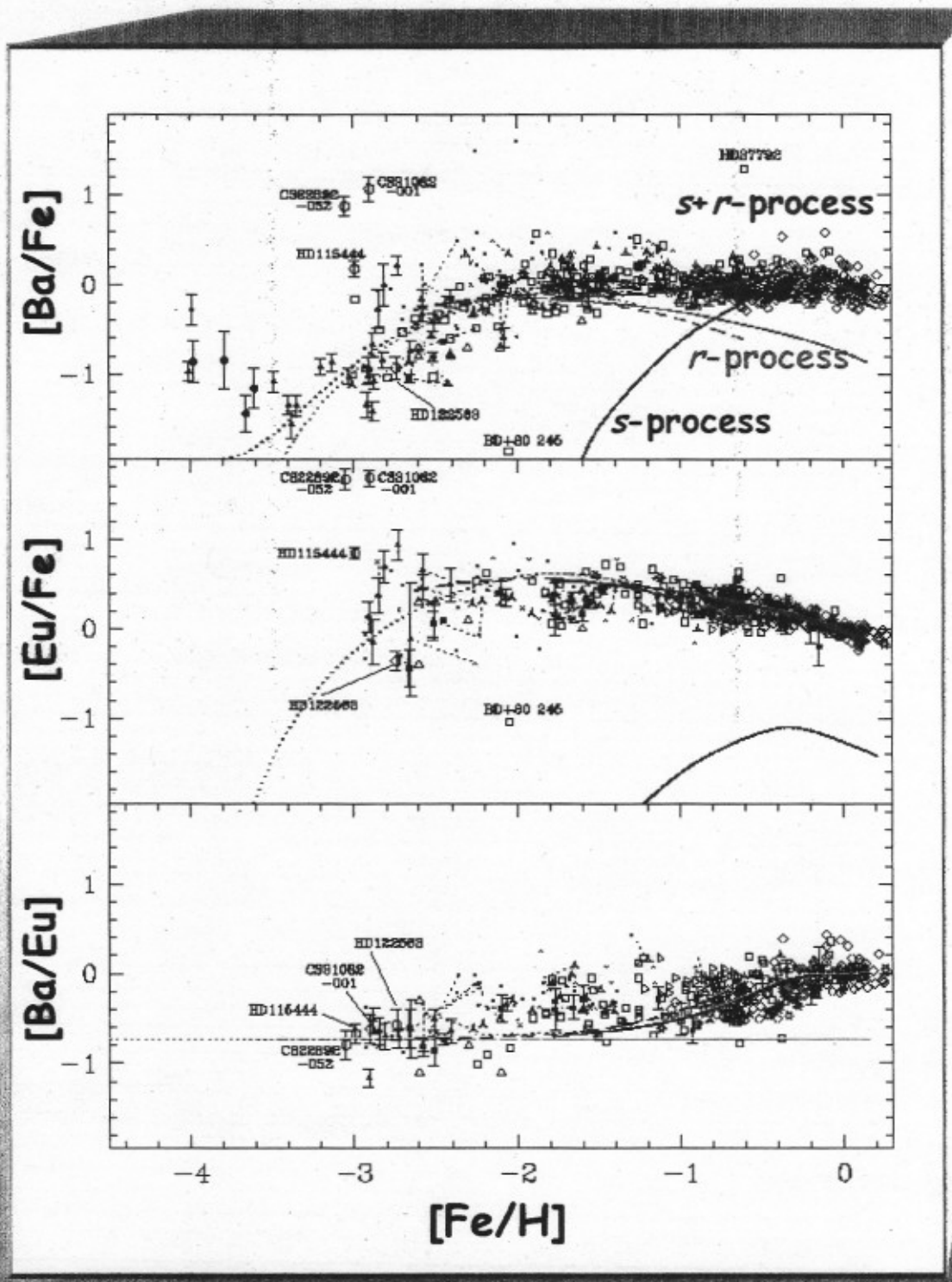

in preparazione

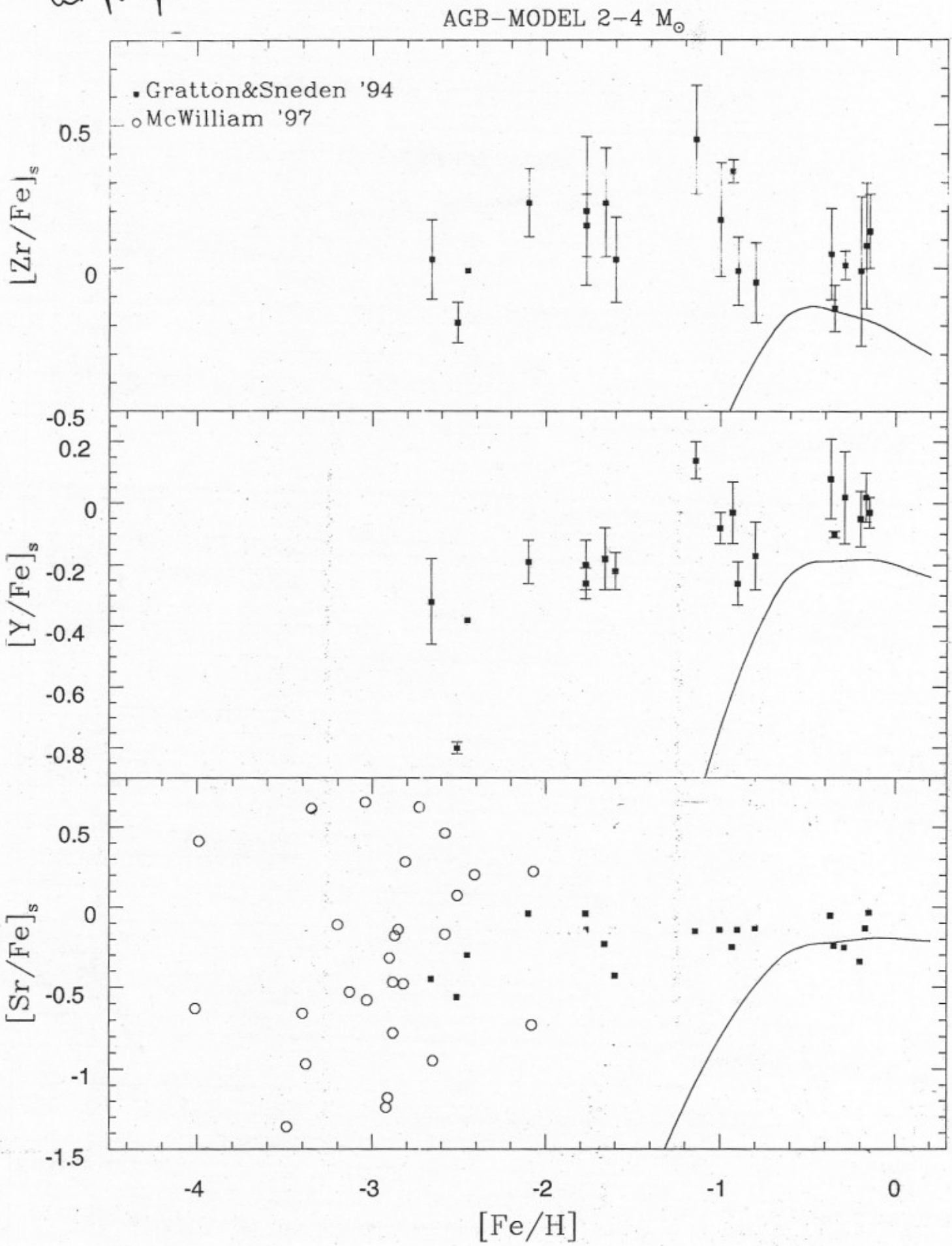

Different stellar sources for chemical evolution ...

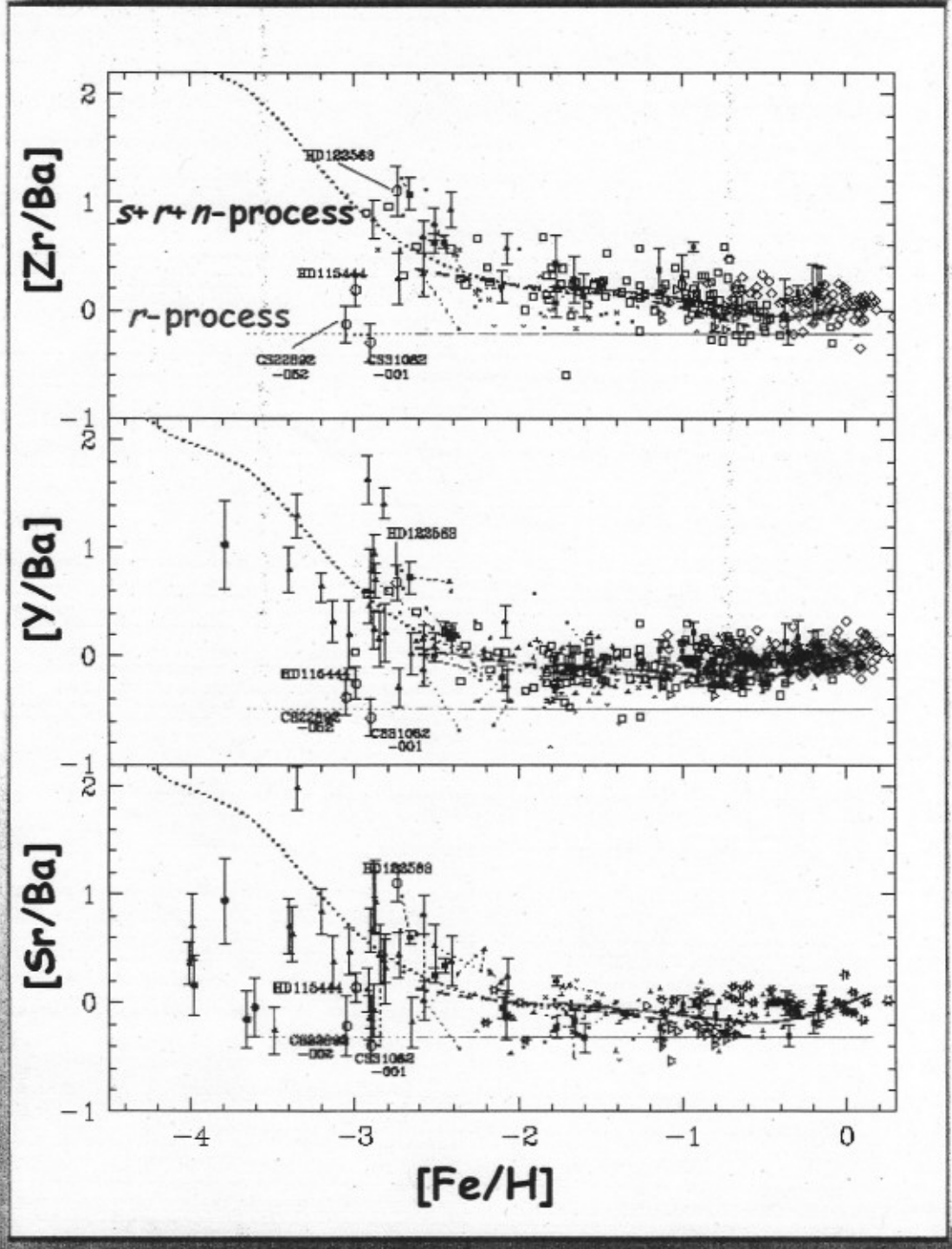

Contribution by

Rene Reifarth

Los Alamos National Laboratory

reifarth@lanl.gov

16 pages

LA-UR-04-0638

Nuclear astrophysics at DANCE

René Reifarth

1. Workshop on:
New opportunities and challenges with DANCE
Santa Fe, New Mexico, February 2-4, 2004

Outline

- Astrophysics – s-process
- DANCE
  - Setup
  - experiments

- Outlook

nucleosynthesis ingredients

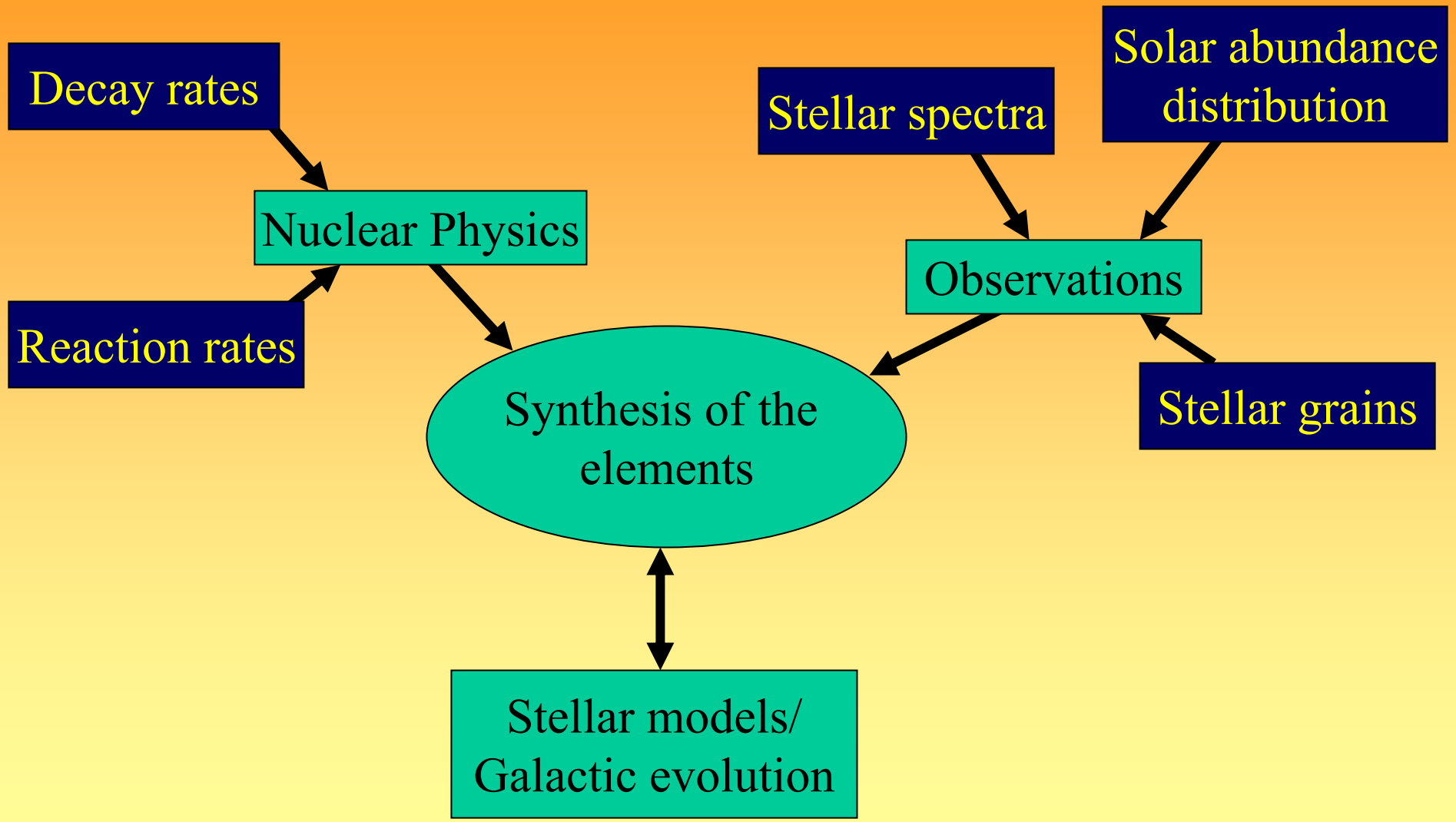

s-process ingredients

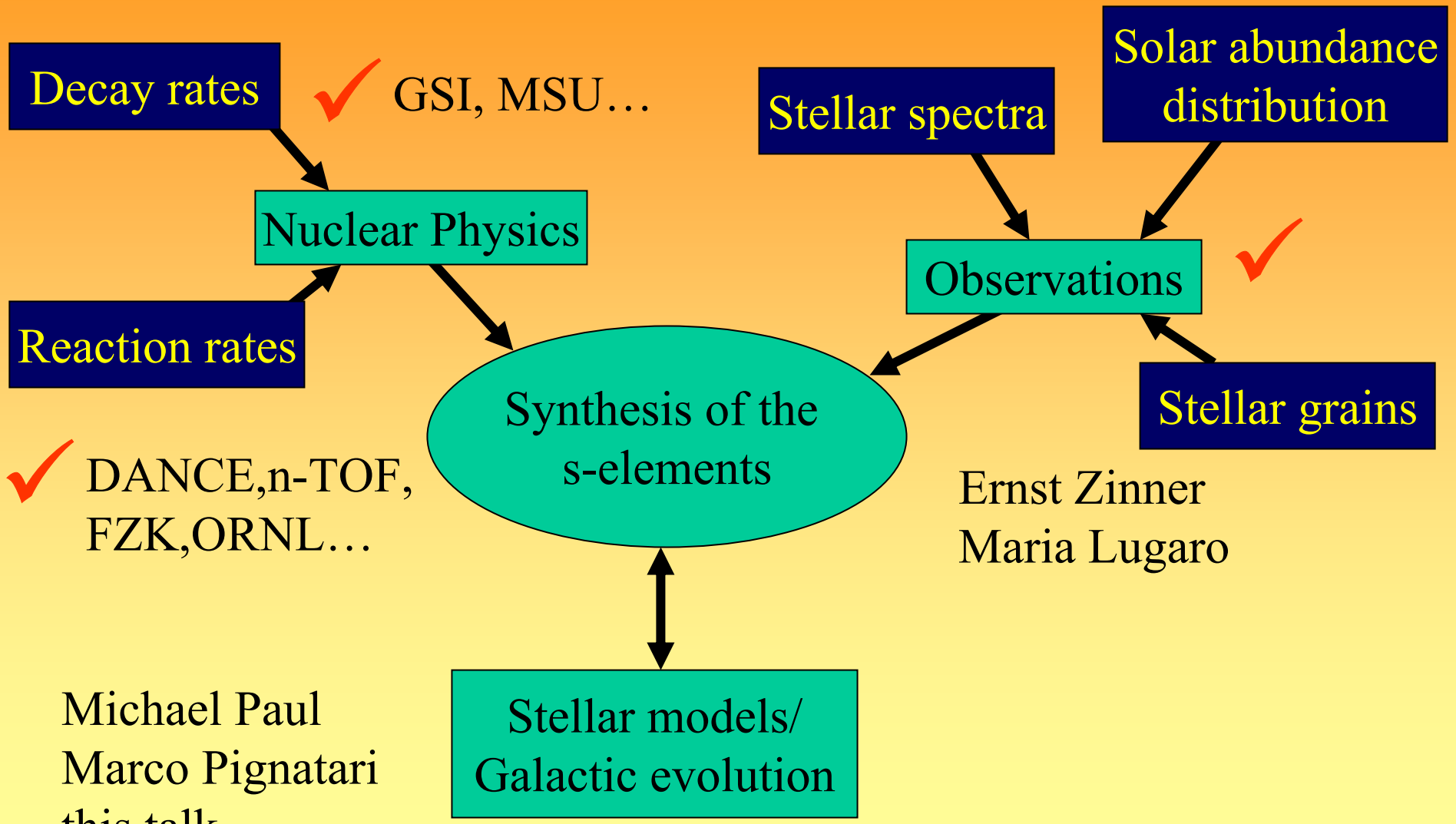

LANSCE @ LANL

1943 - 2003
os Alamos
TIONAL LABORATORY
Ideas That Change the World

DANCE / Flight Path 14 at the Lujan Center

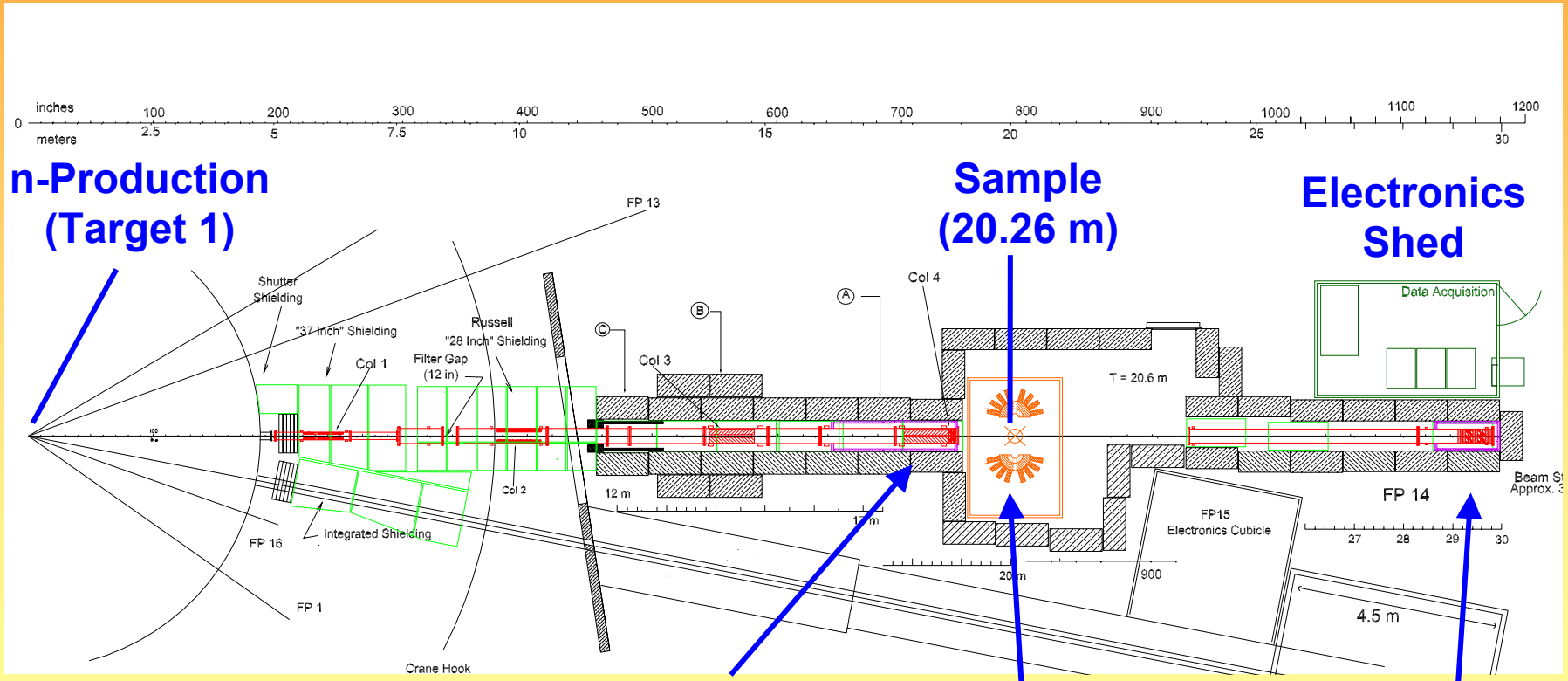

Evidence for neutron capture: PROMPT

$$^{A}X + n \Rightarrow {}^{A+1}X + Q$$

$$Q = \sum \gamma_i$$

⇨ **"monoenergetic" if 100 % efficiency**

Detector for Advanced Neutron Capture Experiments

collimated neutrons beam

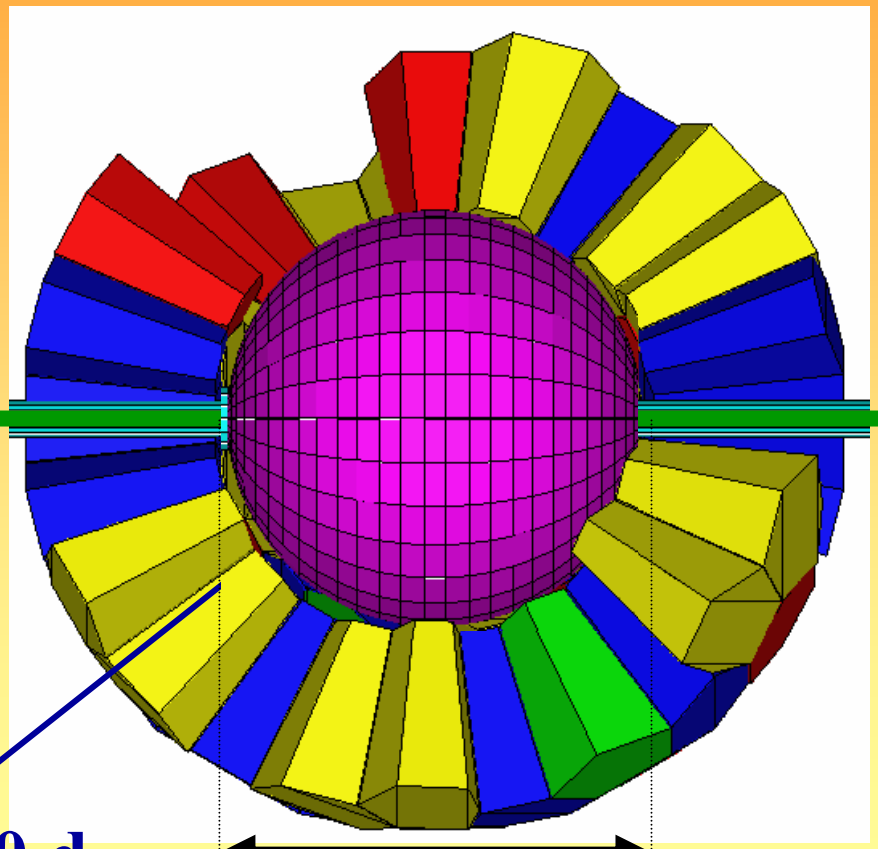

34 cm

sample

$t_{1/2}$ > 100 d

m ~ 1 mg

neutrons:

- spallation source
- thermal .. 500 keV
- 20 m flight path
- 3 10^5 n/s/cm^2/decade

γ-Detector:

- 159 BaF_2 crystals
- 4 different shapes
- R_i=17 cm, R_a=32 cm
- 7 cm ^{6}LiH inside
- $\varepsilon_\gamma \approx$ 90 %
- $\varepsilon_{casc} \approx$ 98 %

BaF_2 waveforms - linear

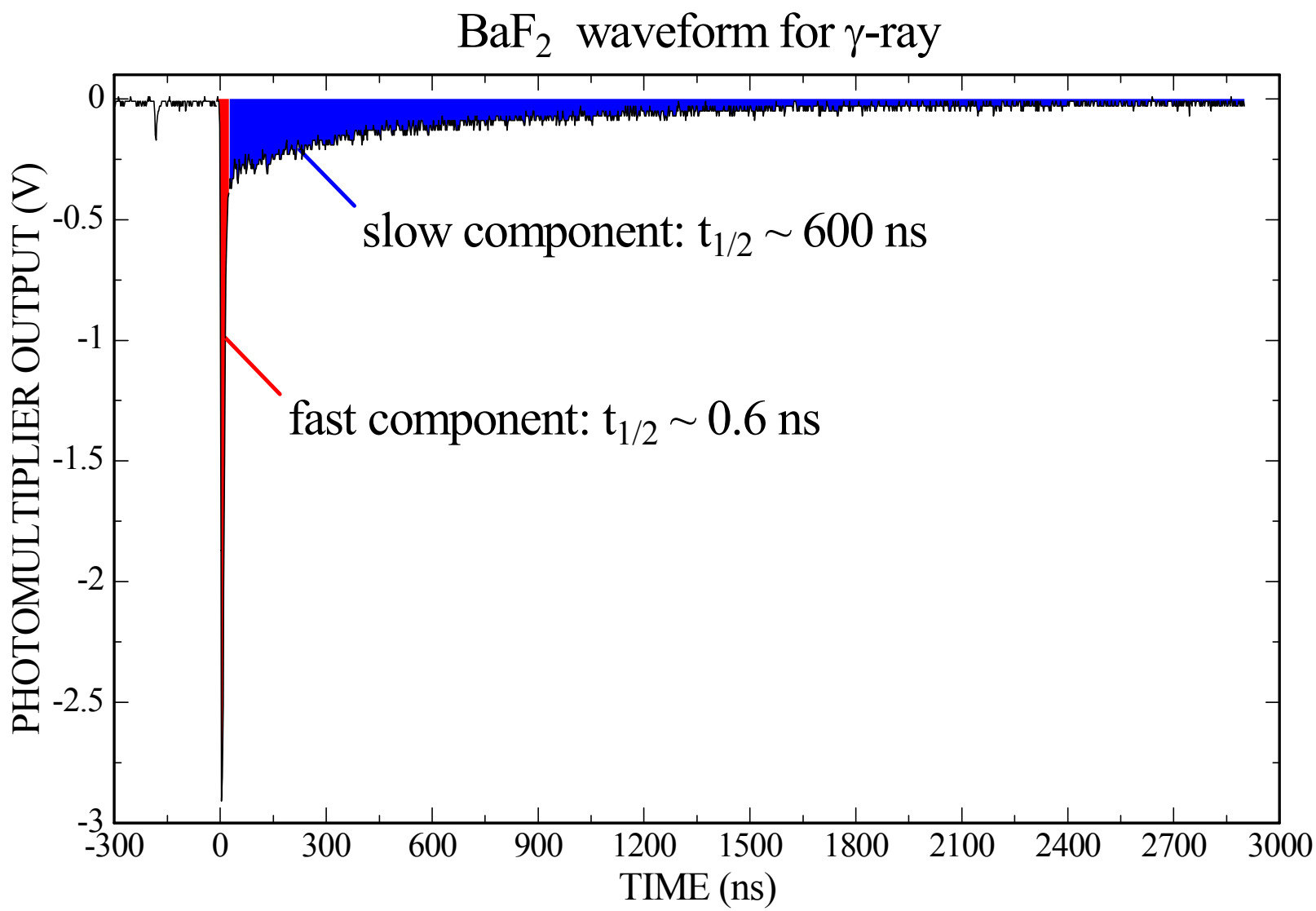

Problem with ^{151}Sm

TOF

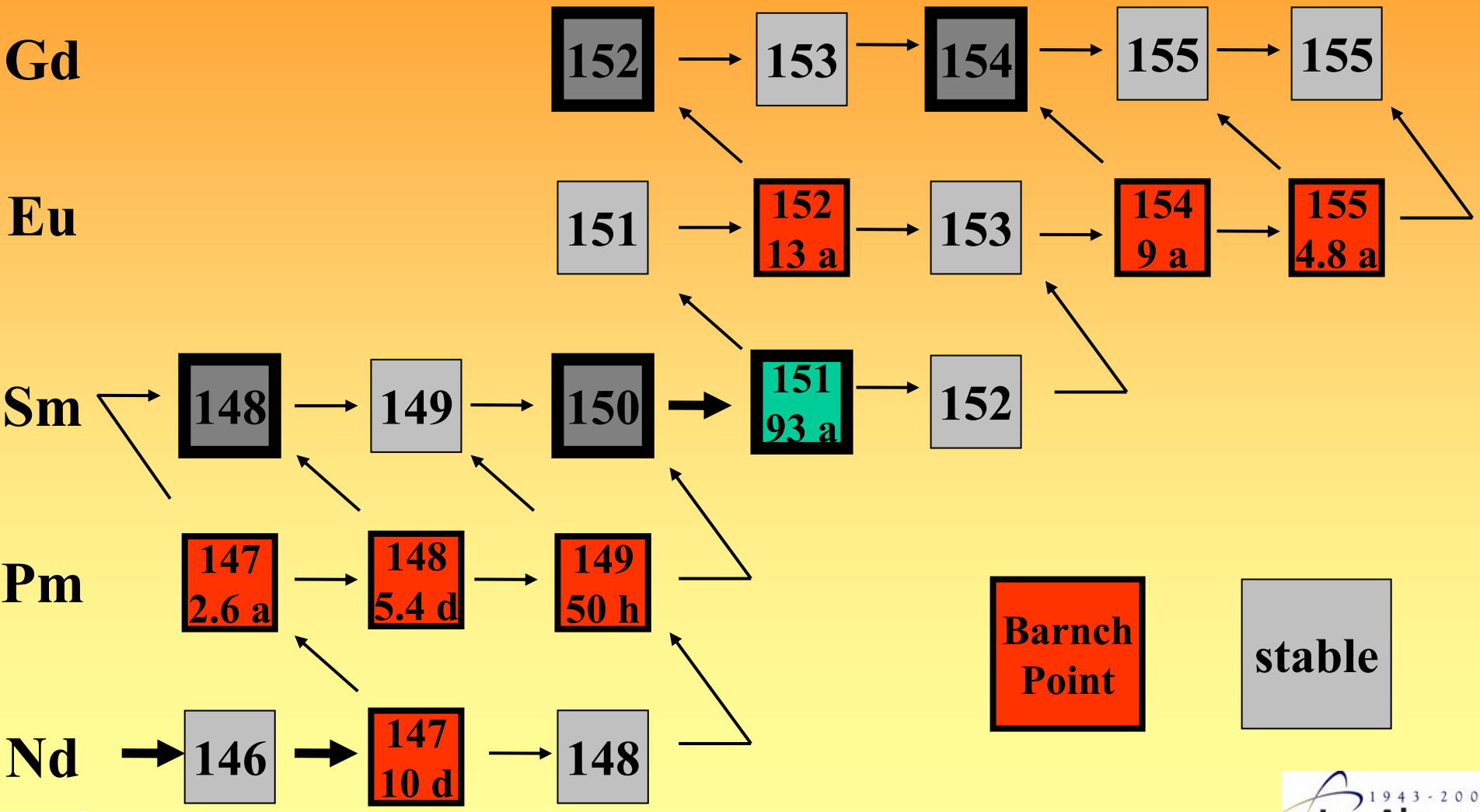

Nuclear Energy
NNSA
Office of Science
LANSCE
1943 - 2003
Los Alamos
NATIONAL LABORATORY
Ideas That Change the World

0.5 mg of $^{151}Sm(n,\gamma)$ – TOF

TOF

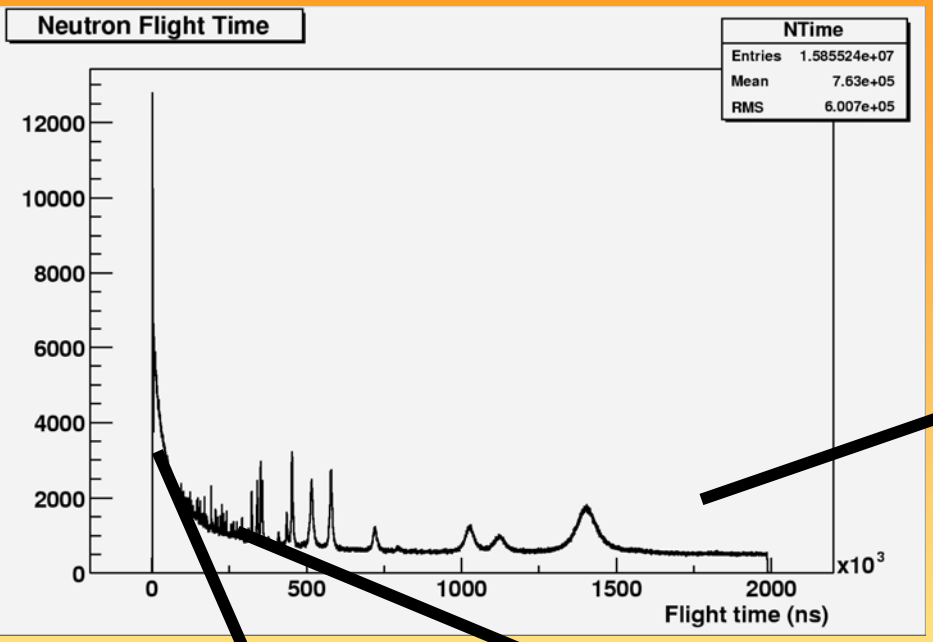

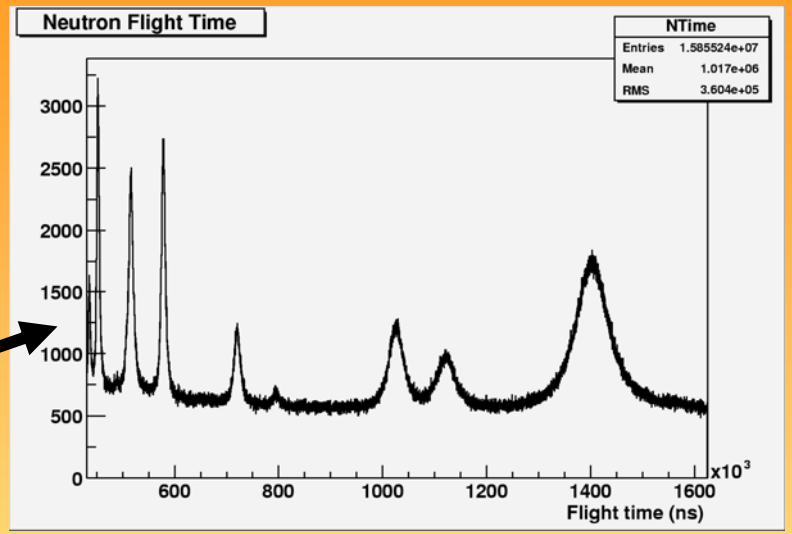

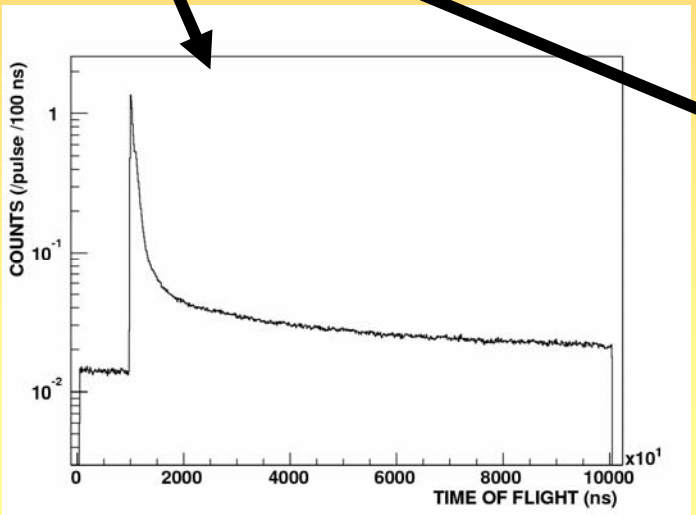

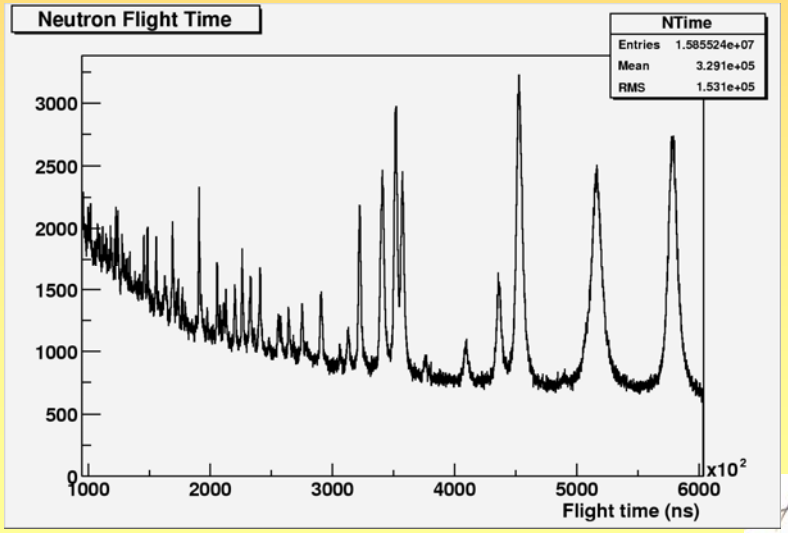

Nuclear Energy
NNSA
Office of Science
LANSCE
1943 - 2003
Los Alamos
NATIONAL LABORATORY
Ideas That Change the World

Measurements done

^{139}La

- almost mono-isotopic (99.9 %)
- closed n-shell (Z=57; **N=82**)
- easier to observe than Ba
- better suited as "s-element" than Ba
- **integrated neutron flux during s-process**
- **s/r ratio in metal poor stars**

Rb, Sr

- closed n-shell (Z=37, 38; **N=50**)
- between weak and main s-component
- r-abundance below Ba ($N_r + N_s = N_\odot$)
- **uniqueness of r-process**
- **integrated neutron flux during s-process**

Measurements planned (spring)

^{62}Ni

- stable
- only 25 % of MACS from resonances
- until recently: 75% had to rely on theory
- see talk by Michael Paul

^{102}Pd

- stable
- (n,γ) – (γ,n) equilibrium during p-process
- sample only 80% enriched

Measurements planned (12 month)

^{99}Tc

- 2 10^5 years (terr.); <100 years (s-process)
- extremely T-dependent
- potential branch point during s-process
- long-lived fission product

^{79}Se

- ~5 10^4 years (terr.); <50 years (s-process)
- extremely T-dependent
- potential branch point during s-process
- long-lived fission product
- (n,g) on ^{78}Se, ^{80}Se can be disentangled via Q-value

^{93}Zr

- 1.5 10^6 years (terr.)
- on the way to ^{95}Zr (64 days) – branch point
- long-lived fission product

Long-term program

s-process Branch Points, $t_{1/2} > 1$ yr
^{151}Sm, ^{147}Pm (FY2003)
^{63}Ni, ^{79}Se, ^{81,85}Kr, ^{93}Zr, ^{99}Tc, ^{134}Cs, ^{135}Cs, ^{152}Eu, ^{154}Eu, ^{155}Eu, ^{163}Ho, ^{171}Tm, ^{176}Lu, ^{179}Ta, ^{185}W, ^{186}Re, ^{193}Pt, ^{204}Tl, ^{205}Pb

Investigation of all (feasible) radioactive s-process nuclei.
Order determined by

- **sample availability**
- **importance for s-process models**

Thanks to:

A. Alpizar, T.A. Bredeweg, J.C. Browne, E.I. Esch, M.M. Fowler, U. Greife, R.C. Haight, R. Hatarik, M. Heil, J.M. O'Donnell, F. Kaeppeler, A. Kronenberg, R.S. Rundberg, J.L. Ullmann, D.J. Vieira, J.B. Wilhelmy, J.M. Wouters

Contribution by

Ernst Zinner

Laboratory for Space Sciences
Washington University St. Louis,MO
ekz@wustl.edu

31 pages

NanoSIMS isotopic analysis of small presolar dust grains: implications for stellar nucleosynthesis

Ernst Zinner
Laboratory for Space Sciences
Washington University
St. Louis, MO

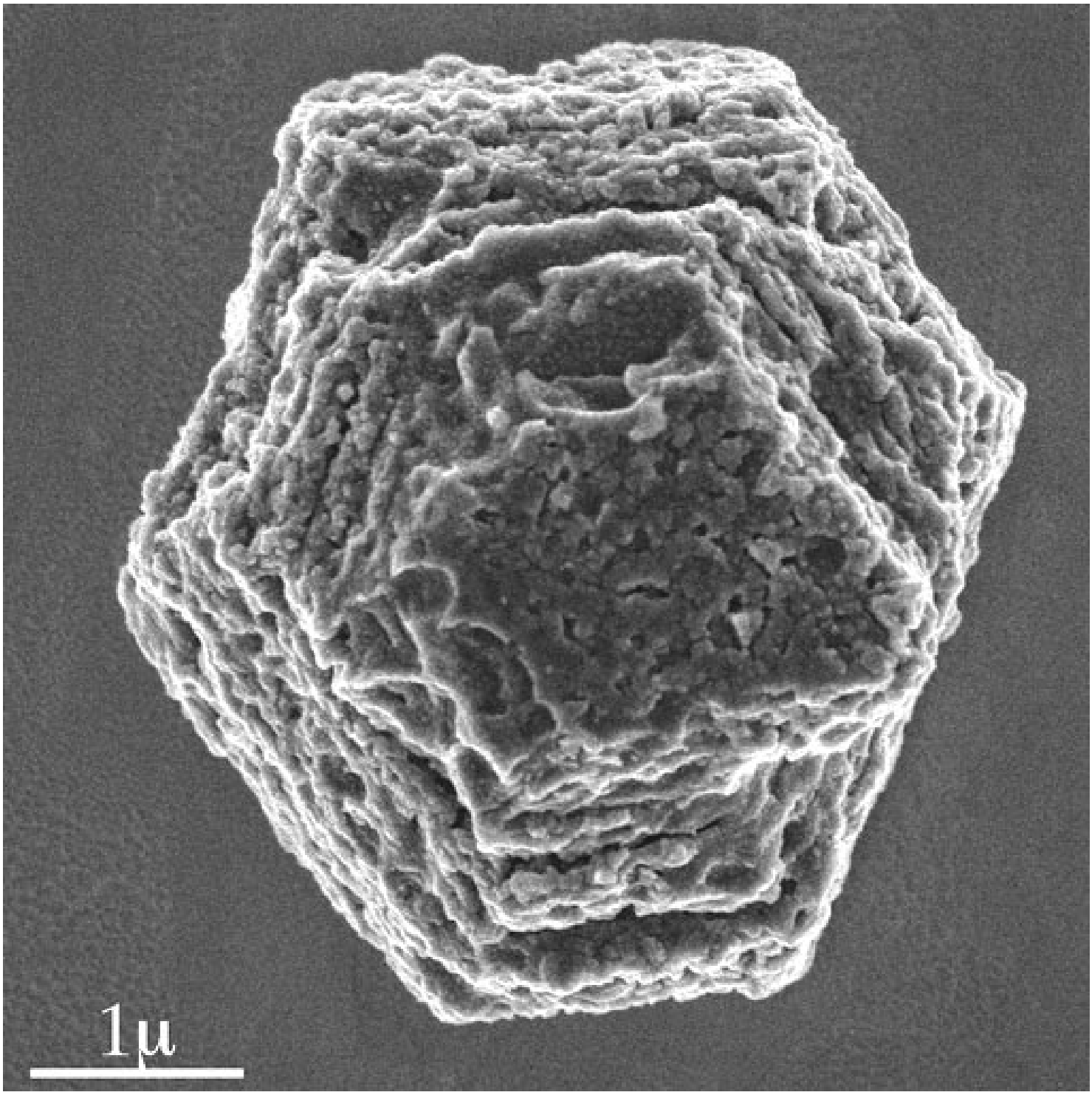
1μ

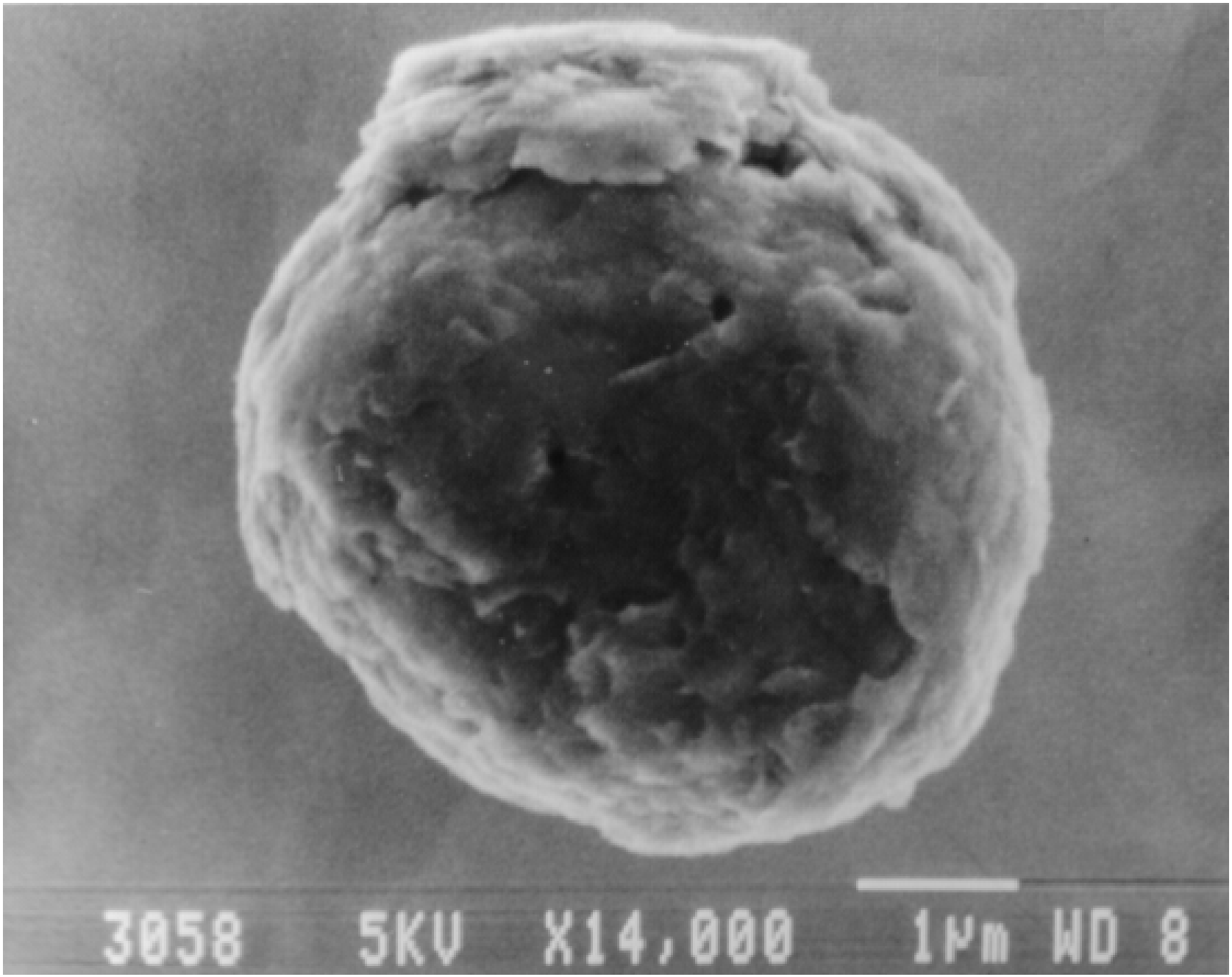
3058 5KV X14,000 1μm WD 8

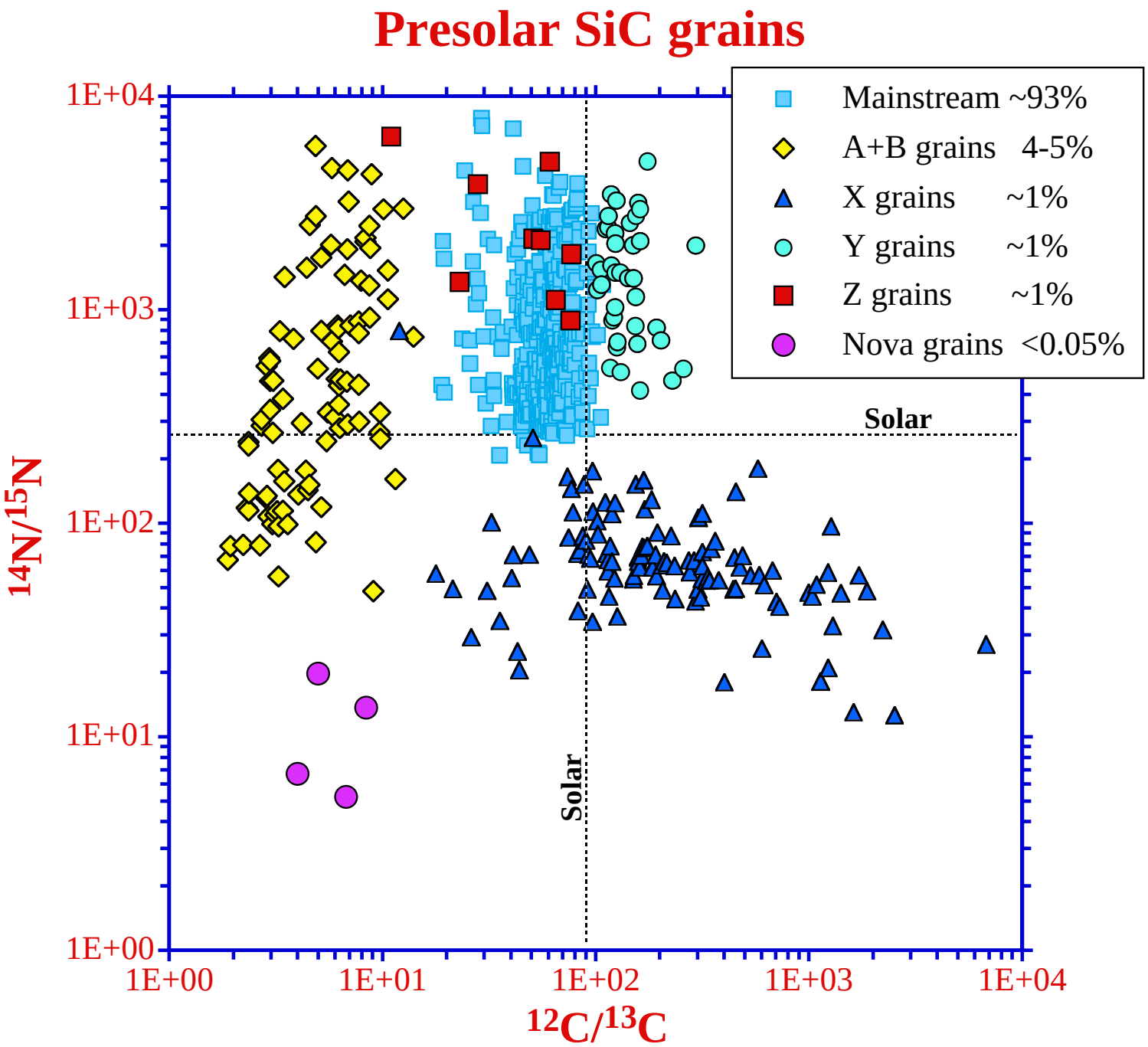
Presolar SiC grains
Mainstream ~93%
A+B grains 4-5%
X grains ~1%
Y grains ~1%
Z grains ~1%
Nova grains <0.05%
Solar
Solar
1E+04
1E+03
1E+02
1E+01
1E+00
1E+00
1E+01
1E+02
1E+03
1E+04
14N/15N
12C/13C

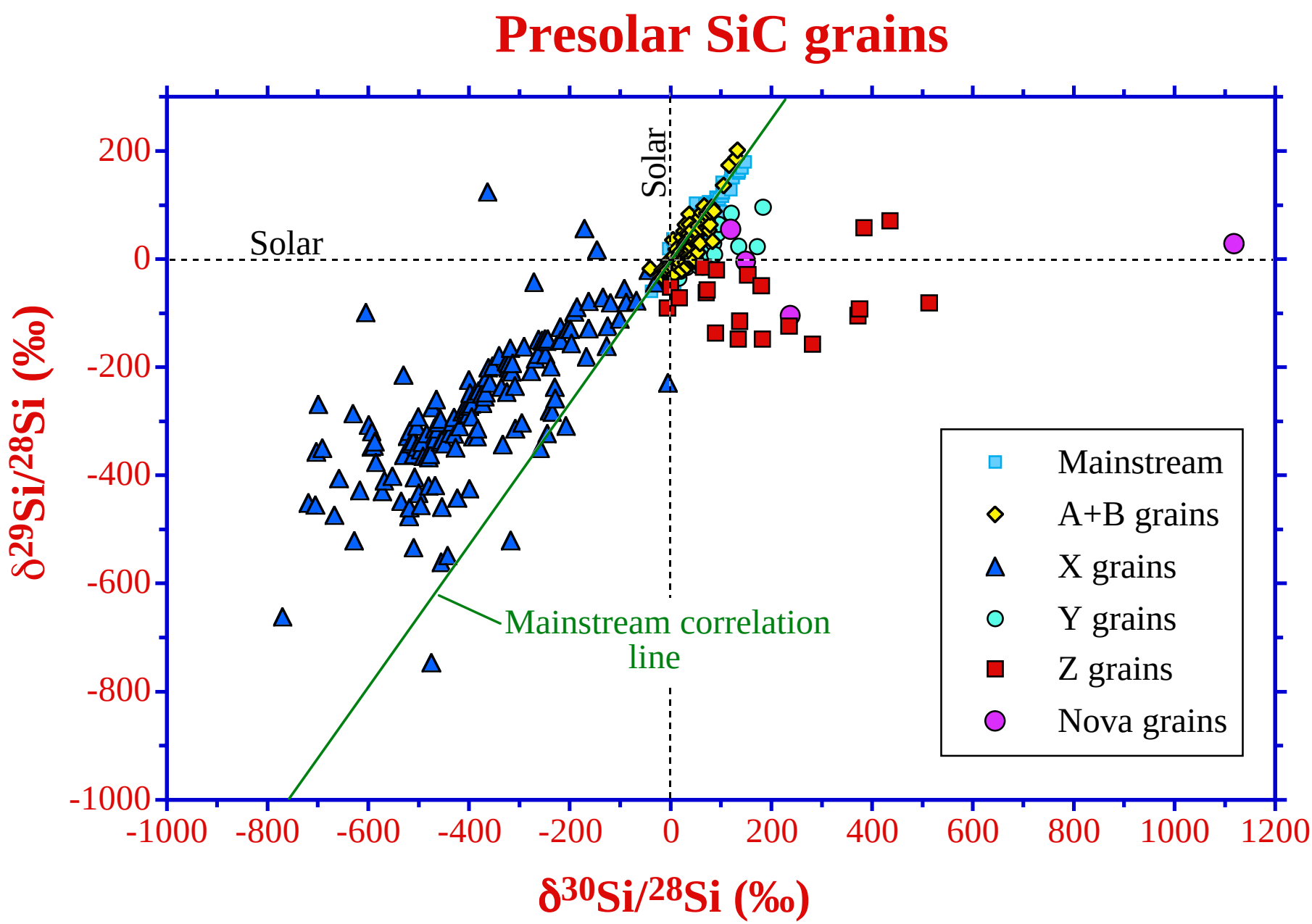
Presolar SiC grains
Solar
Solar
Mainstream correlation line
Mainstream
A+B grains
X grains
Y grains
Z grains
Nova grains
200
0
-200
-400
-600
-800
-1000
-1000
-800
-600
-400
-200
0
200
400
600
800
1000
1200
δ29Si/28Si (‰)
δ30Si/28Si (‰)

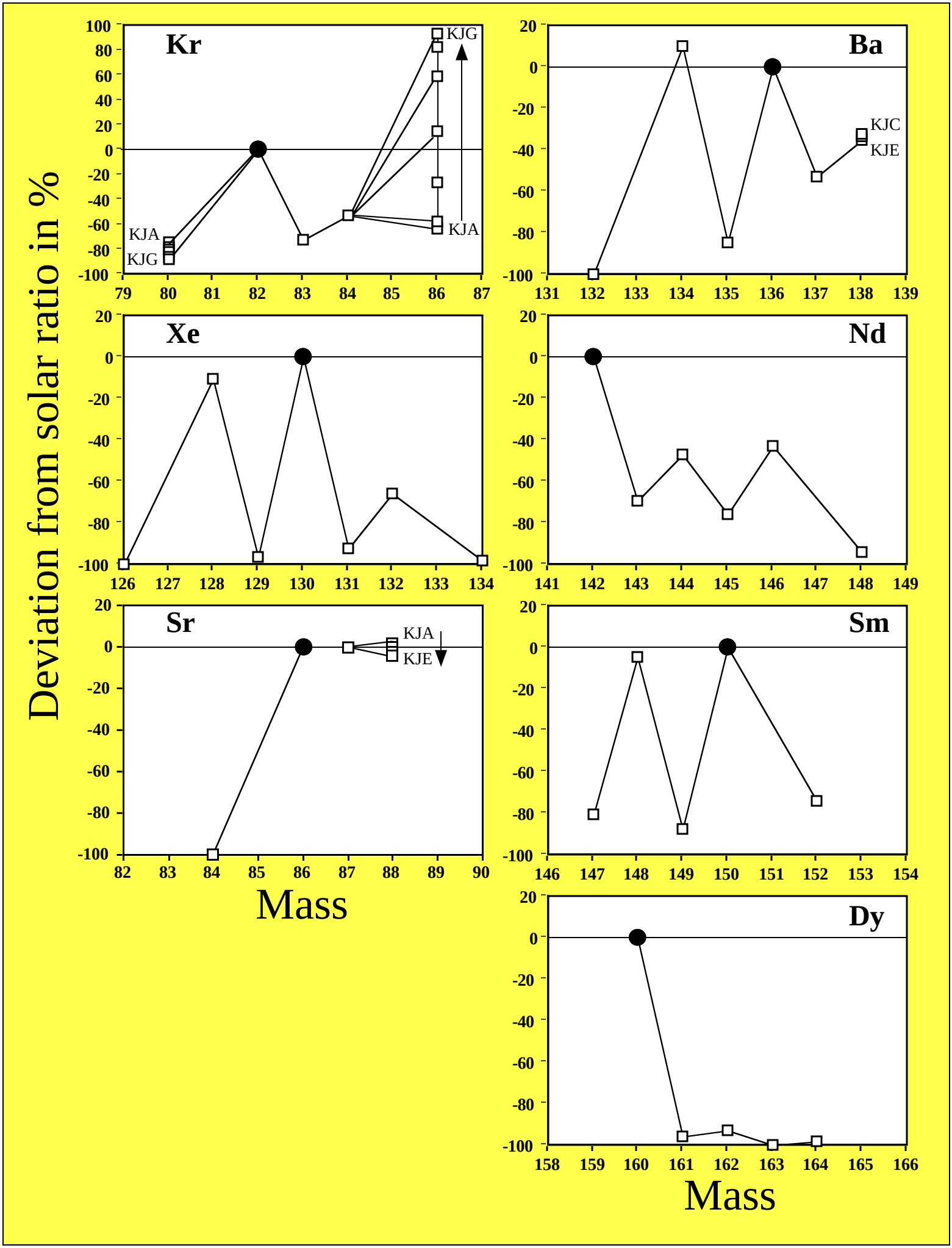
Deviation from solar ratio in %
Kr
KJG
KJA
KJG
KJA
Ba
KJC
KJE
Xe
Nd
Sr
KJA
KJE
Sm
Dy
Mass
Mass

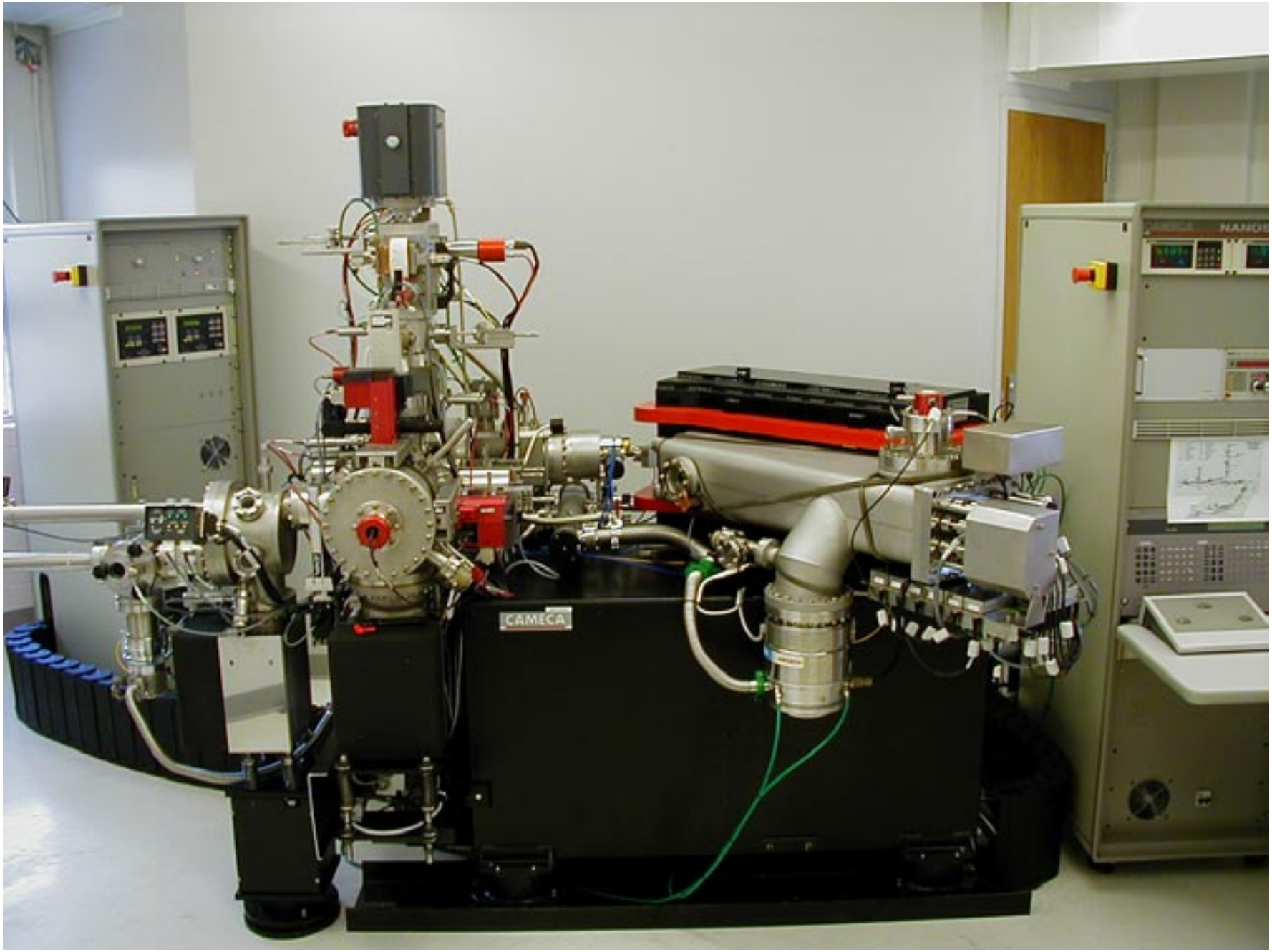
CAMECA

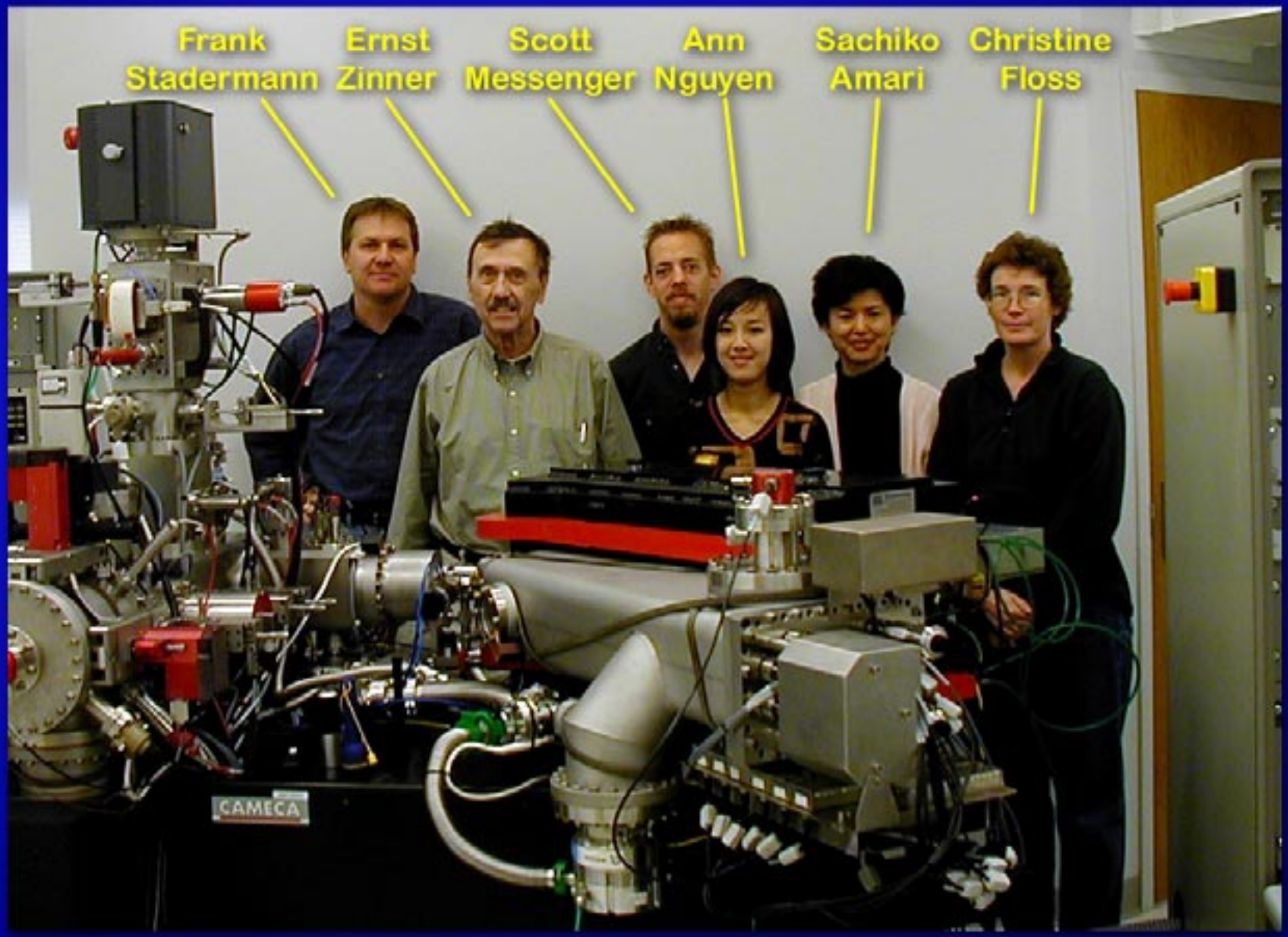
Frank Stadermann
Ernst Zinner
Scott Messenger
Ann Nguyen
Sachiko Amari
Christine Floss
CAMECA

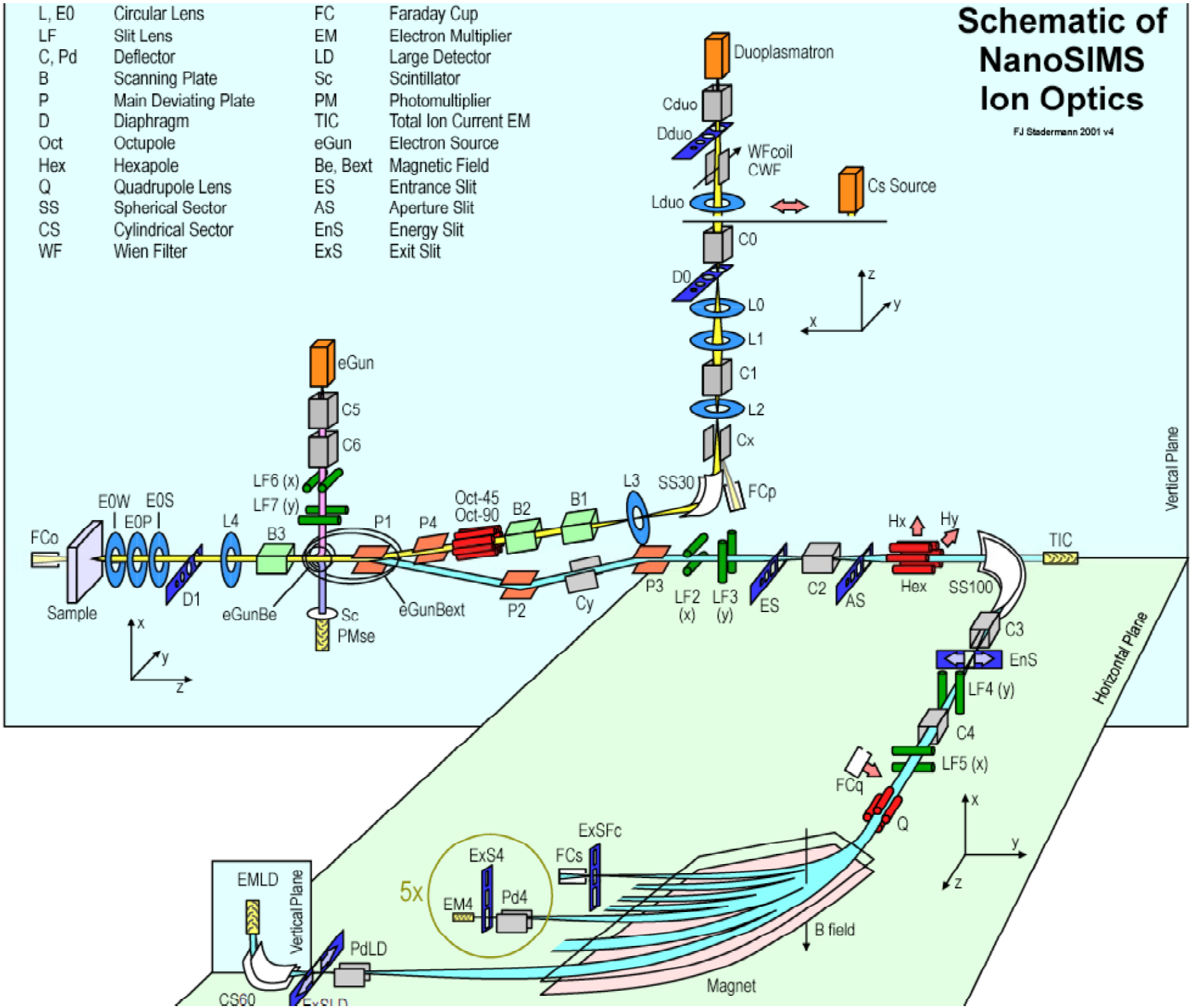
Schematic of NanoSIMS Ion Optics
FJ Stadermann 2001 v4
L, E0 Circular Lens
LF Slit Lens
C, Pd Deflector
B Scanning Plate
P Main Deviating Plate
D Diaphragm
Oct Octupole
Hex Hexapole
Q Quadrupole Lens
SS Spherical Sector
CS Cylindrical Sector
WF Wien Filter
FC Faraday Cup
EM Electron Multiplier
LD Large Detector
Sc Scintillator
PM Photomultiplier
TIC Total Ion Current EM
eGun Electron Source
Be, Bext Magnetic Field
ES Entrance Slit
AS Aperture Slit
EnS Energy Slit
ExS Exit Slit
Duoplasmatron
Cduo
Dduo
WFcoil
CWF
Cs Source
Lduo
C0
D0
L0
L1
C1
L2
Cx
FCp
SS30
L3
B1
B2
Oct-45
Oct-90
P4
P1
P2
P3
Cy
LF2 (x)
LF3 (y)
ES
C2
AS
Hx
Hy
Hex
SS100
TIC
C3
EnS
LF4 (y)
C4
LF5 (x)
FCq
Q
Vertical Plane
Horizontal Plane
eGun
C5
C6
LF6 (x)
LF7 (y)
B3
L4
E0W
E0S
E0P
FCo
Sample
D1
eGunBe
Sc
PMse
eGunBext
ExSFc
FCs
ExS4
5x
EM4
Pd4
EMLD
Vertical Plane
PdLD
CS60
ExSLD
B field
Magnet

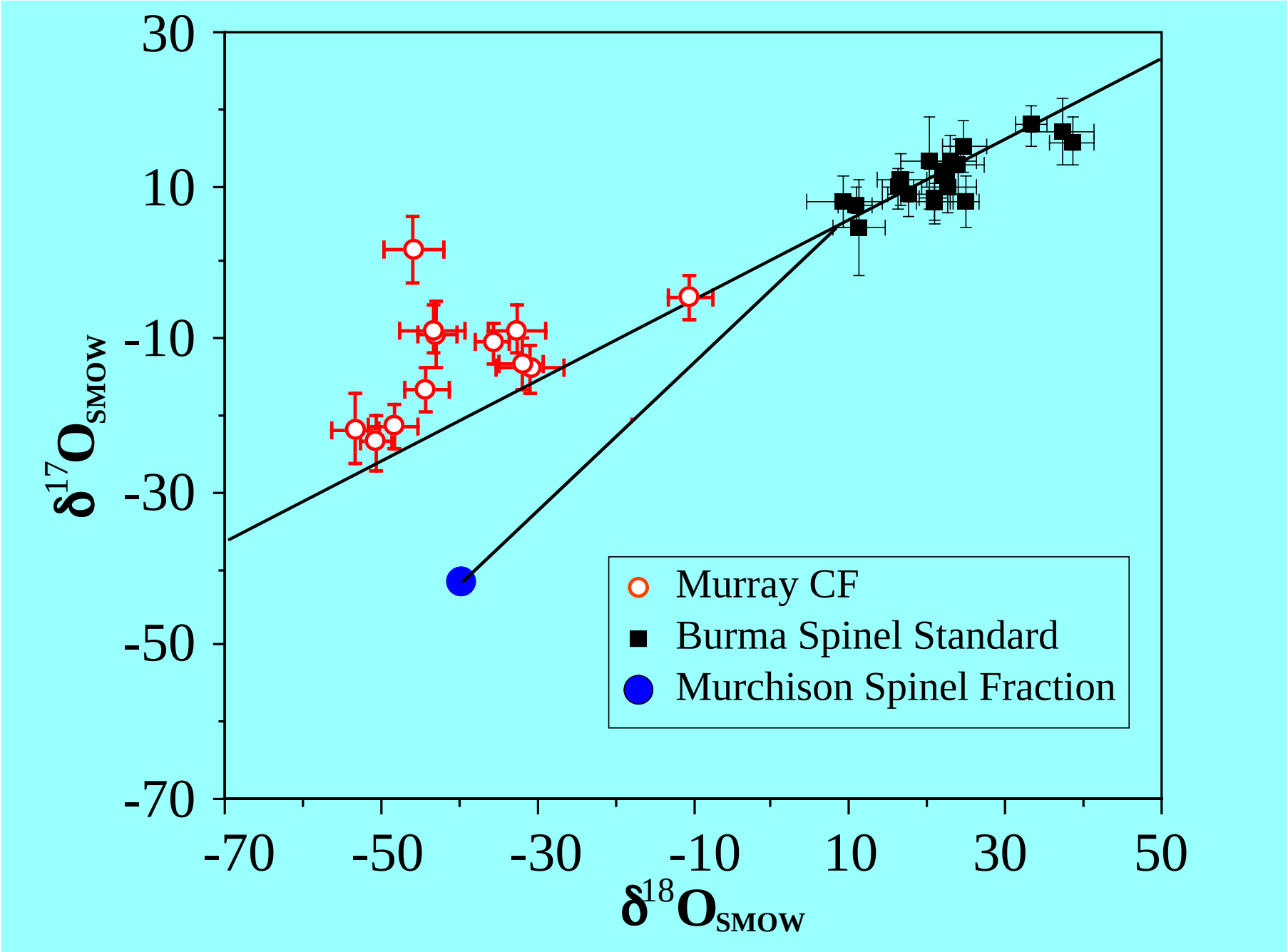
30
10
-10
-30
-50
-70
-70
-50
-30
-10
10
30
50
δ17OSMOW
δ18OSMOW
Murray CF
Burma Spinel Standard
Murchison Spinel Fraction

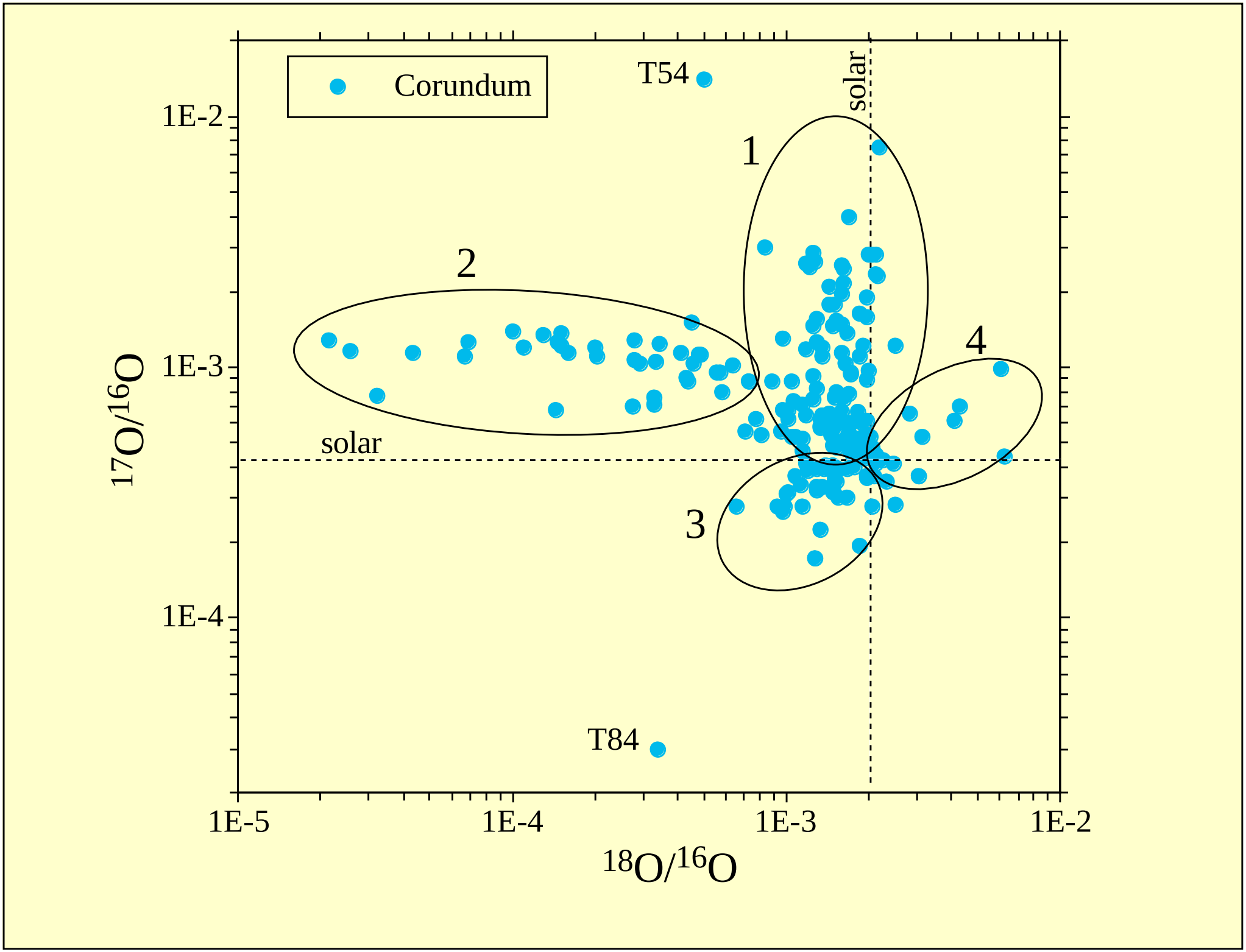
Corundum
T54
T84
solar
solar
1
2
3
4
1E-2
1E-3
1E-4
1E-5
1E-4
1E-3
1E-2
$^{17}O/^{16}O$
$^{18}O/^{16}O$

A2 mount: Murray CG

Regions marked for analysis

♦ Murchison Matrix ◊ Corundum Standard

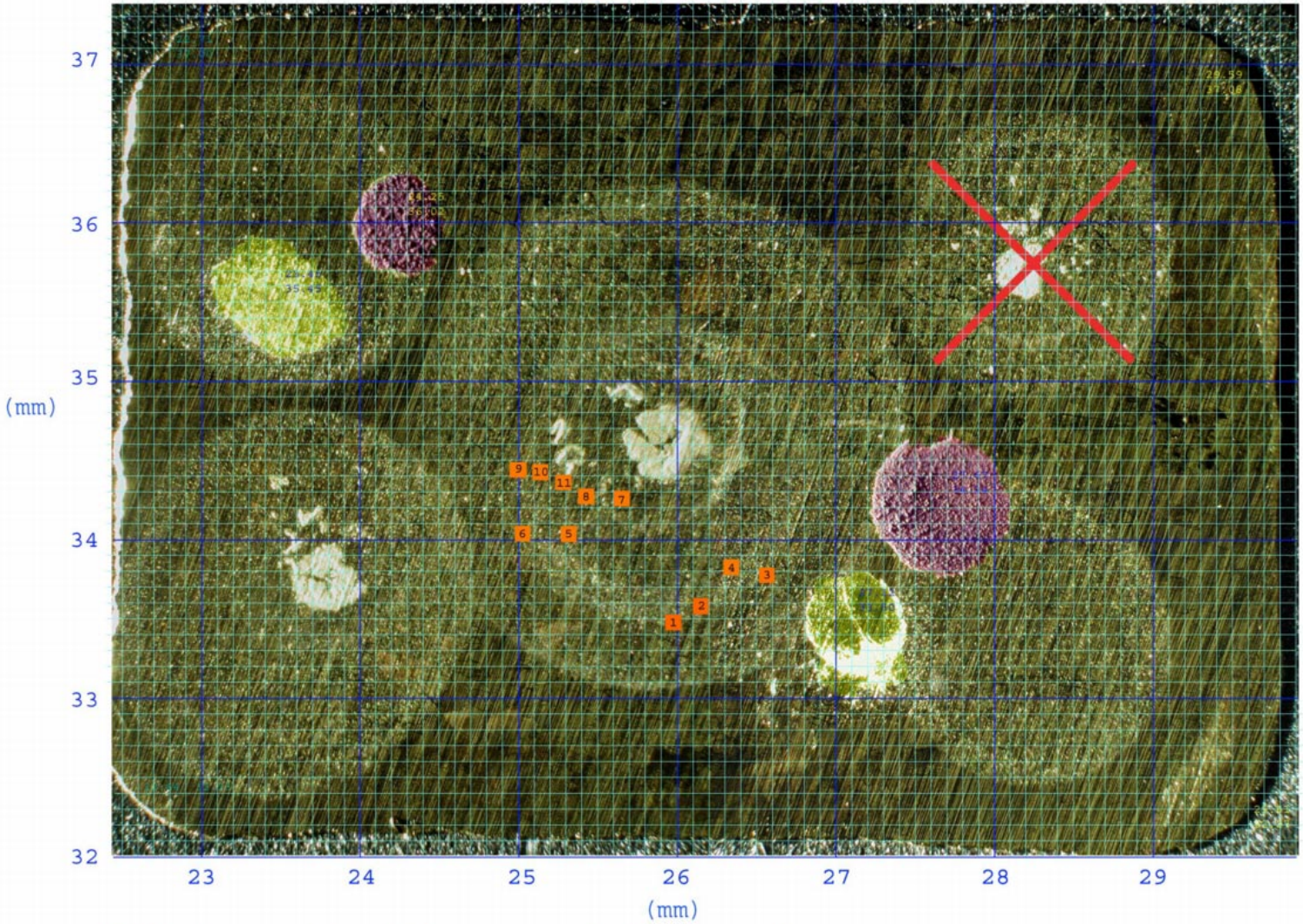

X Region accidentally sprayed with corundum

26 February 2002

Murchison KIE grains

20x20 μm^2

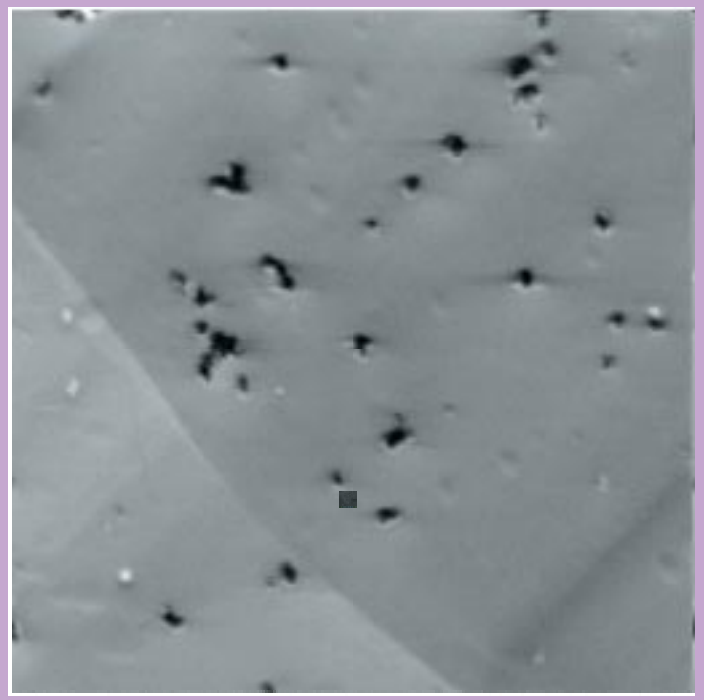

Sec. electron image

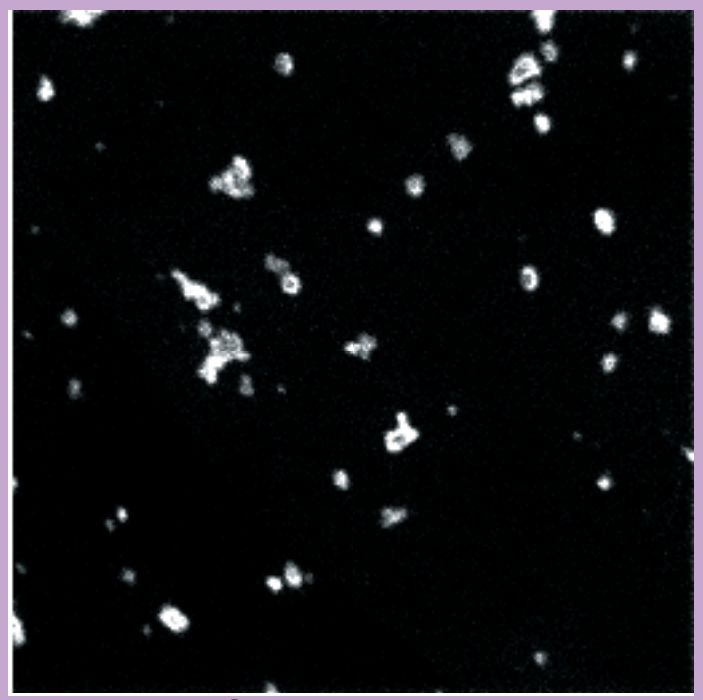

$^{16}O^-$ image

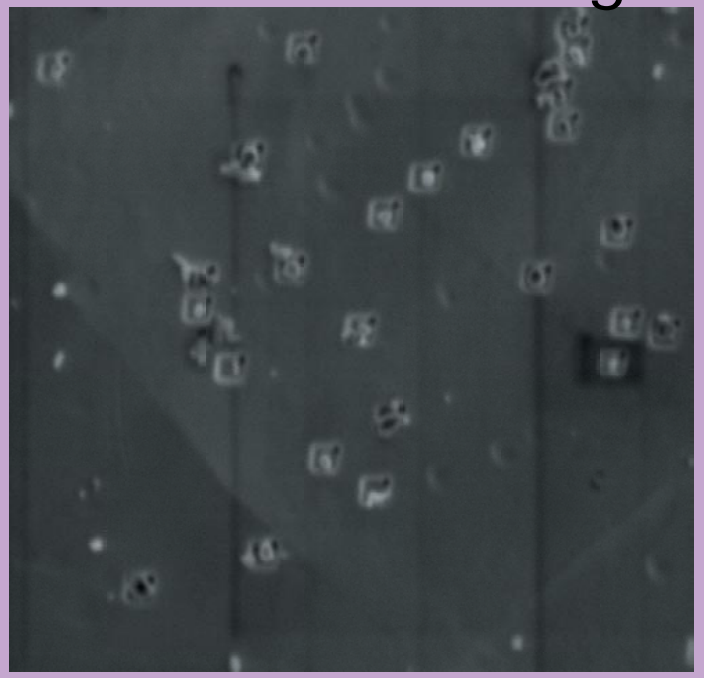

SEM image after

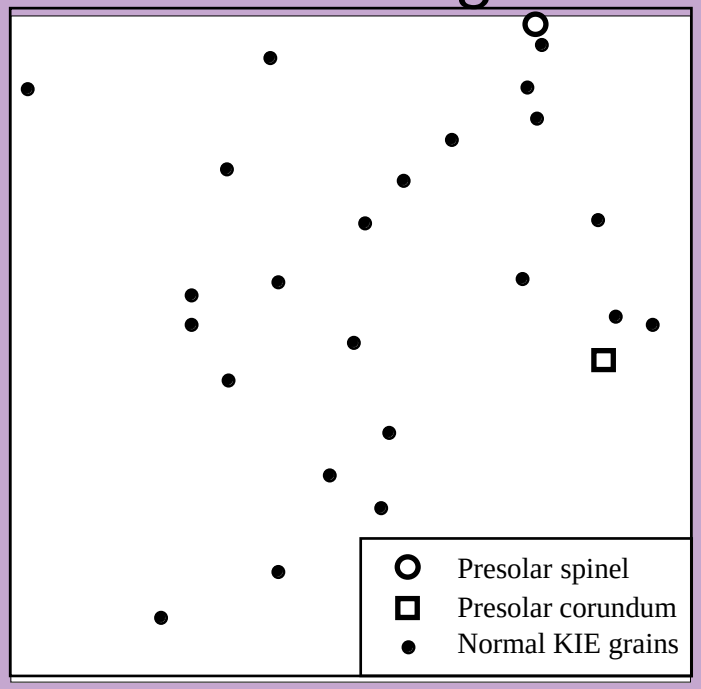

Analyzed grains

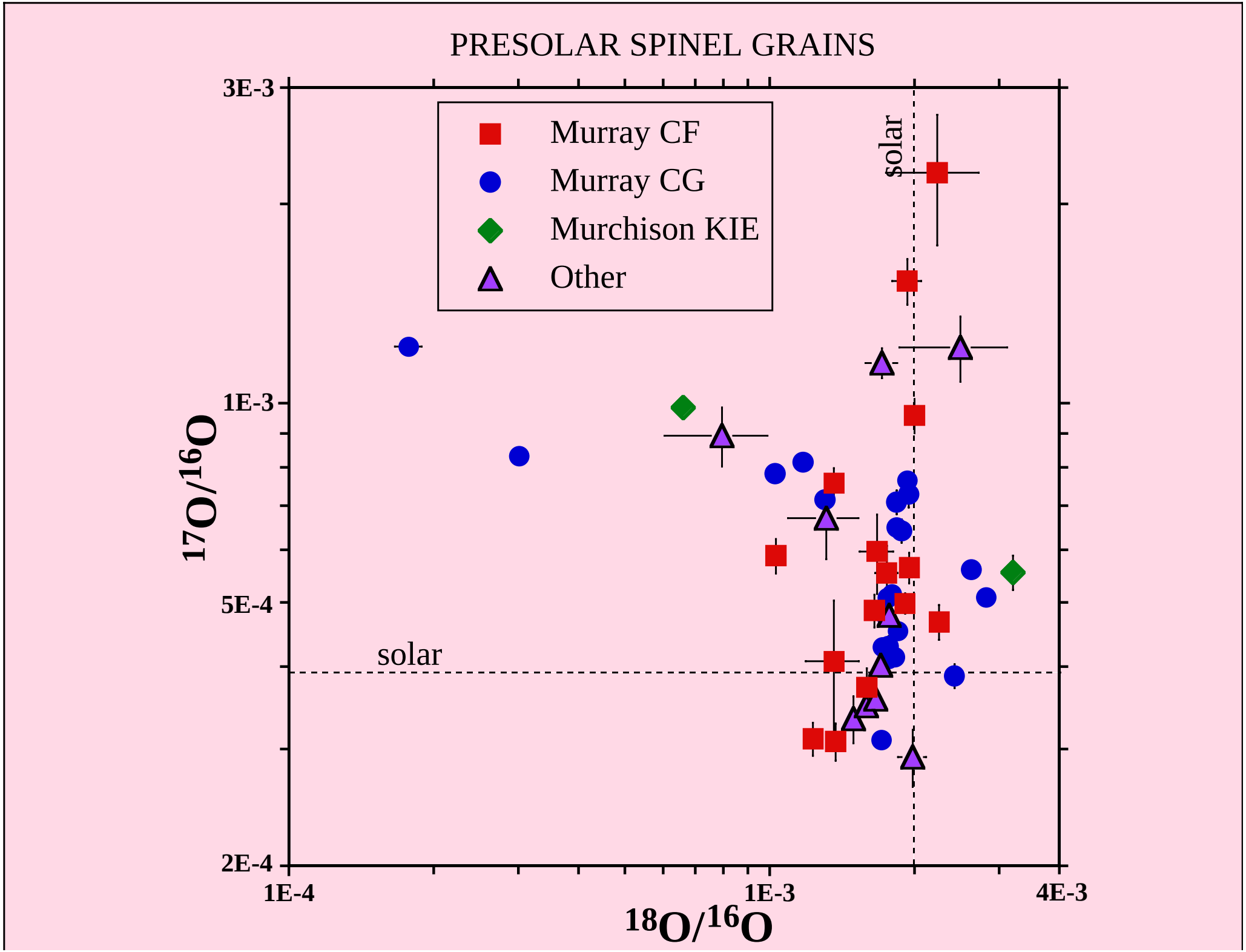
PRESOLAR SPINEL GRAINS
Murray CF
Murray CG
Murchison KIE
Other
solar
solar
3E-3
1E-3
5E-4
2E-4
1E-4
1E-3
4E-3
17O/16O
18O/16O

FRACTIONS OF PRESOLAR OXIDE GRAINS

Meteorite/residue	**Spinel/res**	**Corundum/res**
Murray CF (0.15 µm)	15/628 (2.4%)	3/628 (0.5%)
Murray CG (0.45 µm)	21/1253 (1.7%)	1/1253 (0.1%)
Murray CH (0.7-2 µm)	0/1000 (<0.1%)	0/1000 (<0.1%)
	Spinel/Murray	**Cor./Murray**
CF	**670 ppb**	**25-130 ppb**
CG	**765 ppb**	**45-130 ppb**
Total	**~1.4 ppm**	**70-260 ppb**

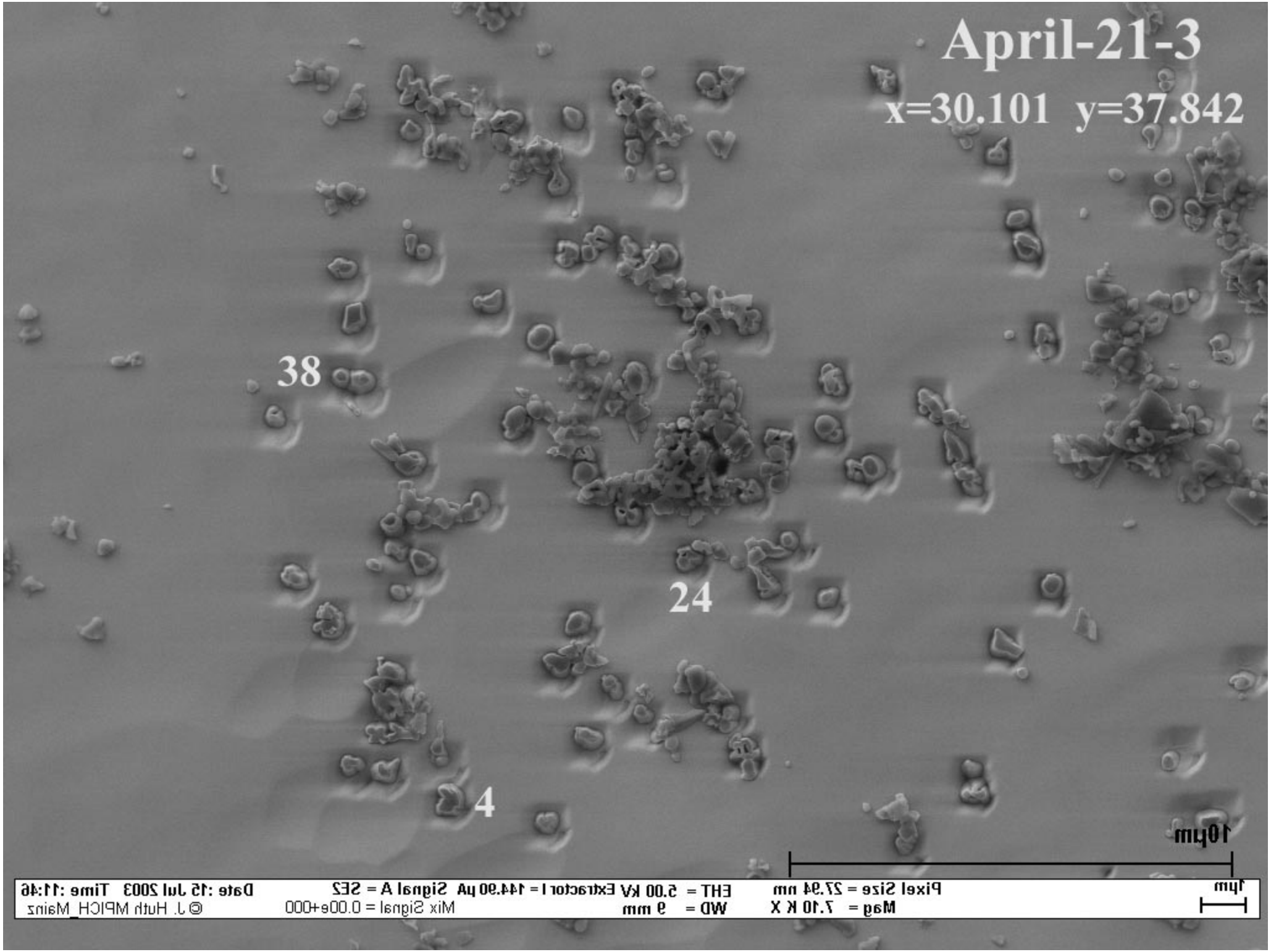
April-21-3
x=30.101 y=37.842
38
24
4
10µm
1µm
Pixel Size = 27.94 nm
Mag = 7.10 K X
EHT = 5.00 kV
WD = 9 mm
Extractor1 = 144.90 µA Signal A = SE2
Mix Signal = 0.00e+000
Date :15 Jul 2003 Time :11:46
© J. Huth MPICH_Mainz

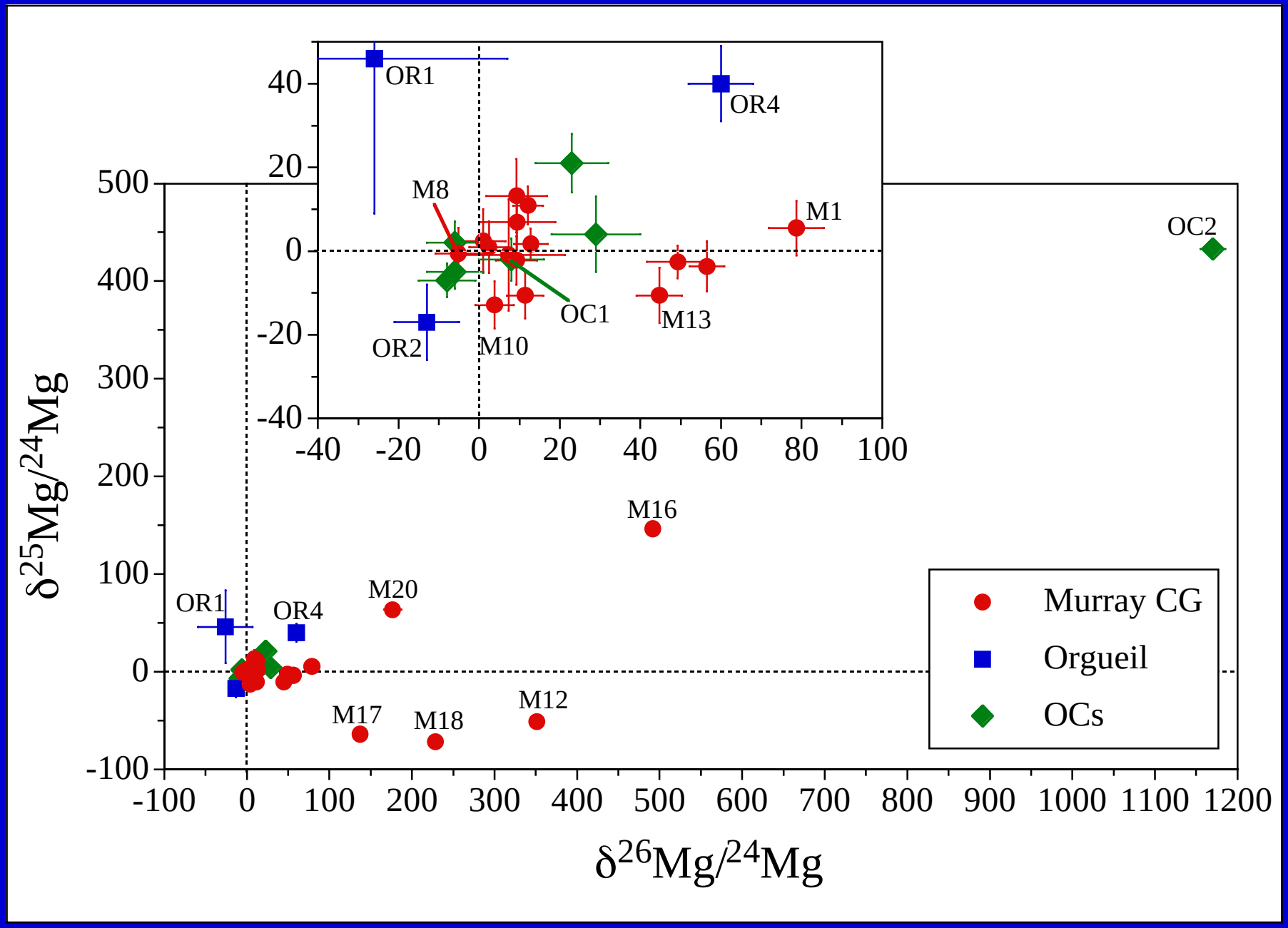
δ25Mg/24Mg
δ26Mg/24Mg
Murray CG
Orgueil
OCs
OR1
OR4
OR2
M8
M1
OC2
OC1
M13
M10
M16
M20
M17
M18
M12
500
400
300
200
100
0
-100
-100
0
100
200
300
400
500
600
700
800
900
1000
1100
1200
40
20
0
-20
-40
-40
-20
0
20
40
60
80
100

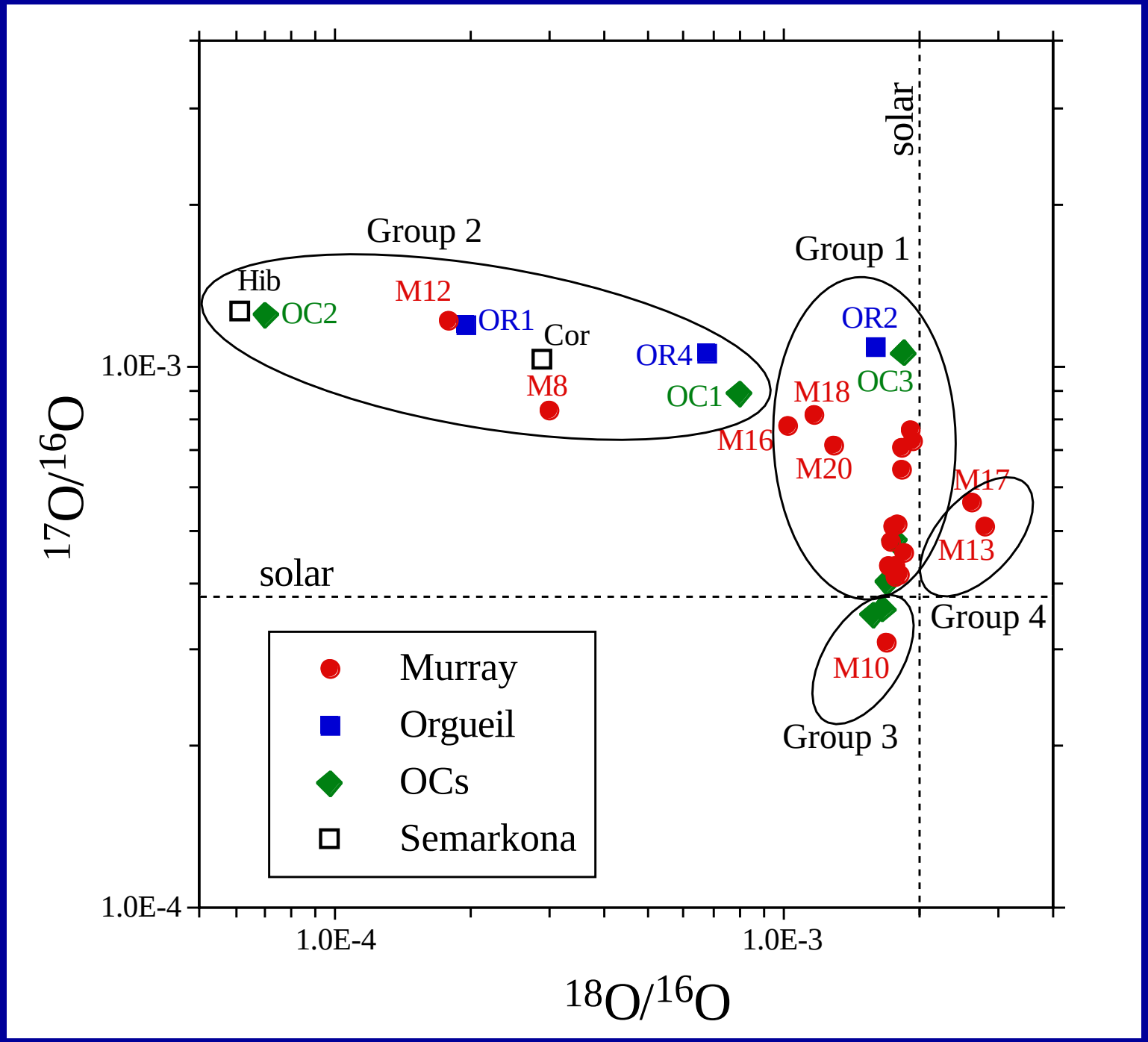
solar
Group 2
Group 1
Hib
OC2
M12
OR1
Cor
OR4
OC1
M8
OR2
OC3
M18
M16
M20
M17
M13
solar
Group 4
M10
Group 3
Murray
Orgueil
OCs
Semarkona
1.0E-3
1.0E-4
1.0E-4
1.0E-3
17O/16O
18O/16O

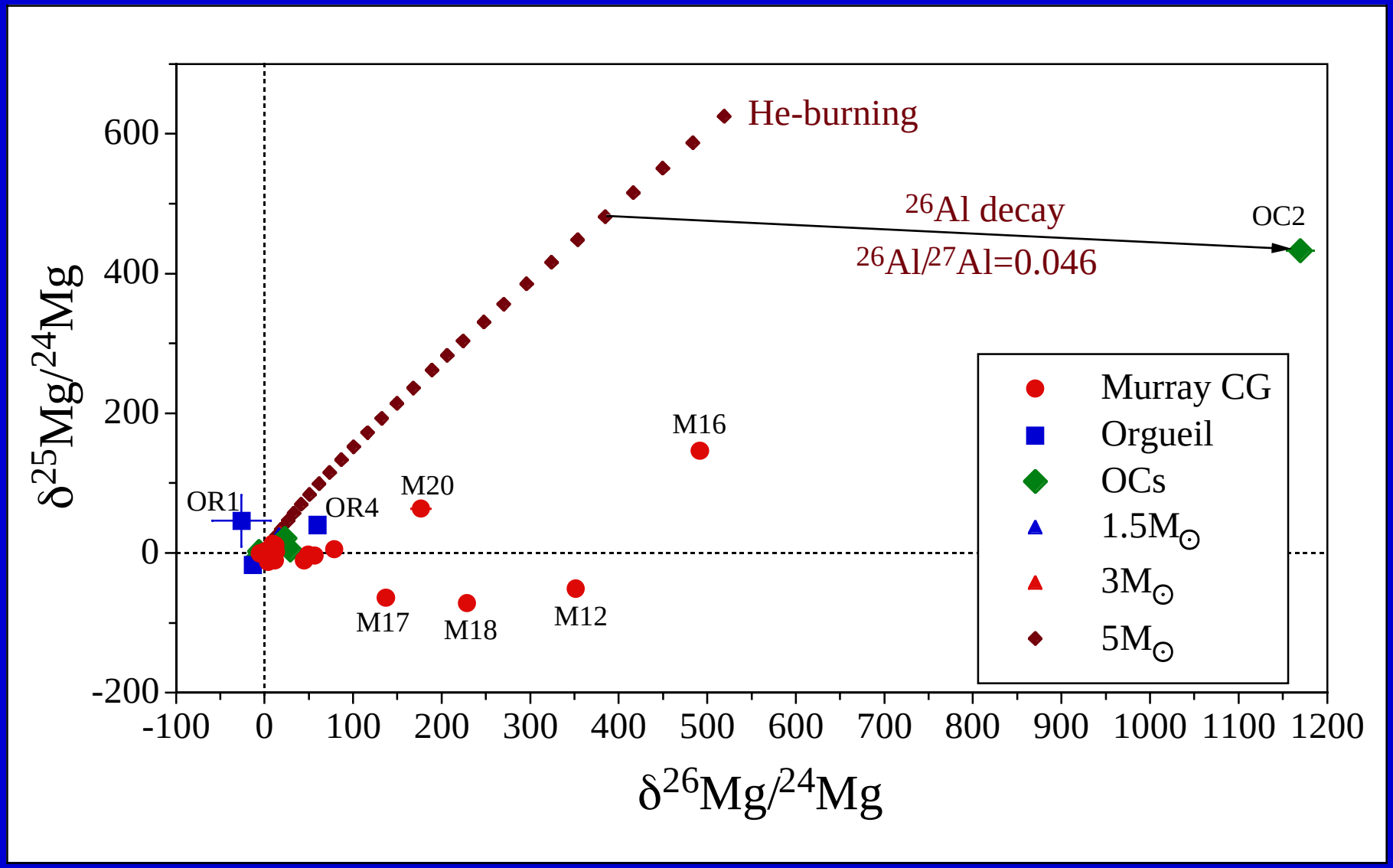
He-burning
^{26}Al decay
^{26}Al/^{27}Al=0.046
OC2
M16
M20
OR1
OR4
M17
M18
M12
Murray CG
Orgueil
OCs
1.5M$_\odot$
3M$_\odot$
5M$_\odot$
600
400
200
0
-200
-100
0
100
200
300
400
500
600
700
800
900
1000
1100
1200
δ^{25}Mg/^{24}Mg
δ^{26}Mg/^{24}Mg

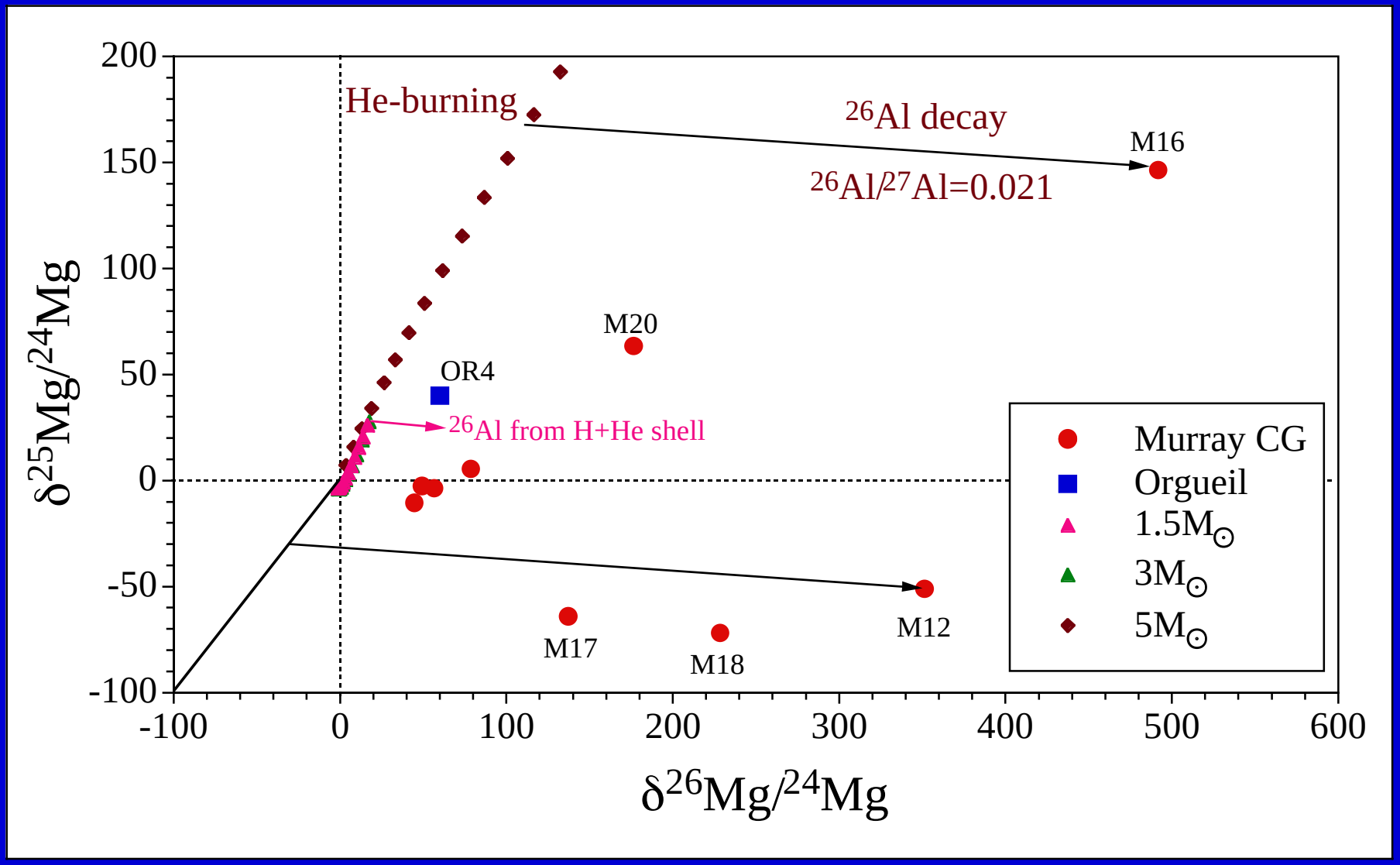
He-burning
26Al decay
26Al/27Al=0.021
M16
M20
OR4
26Al from H+He shell
M12
M17
M18
Murray CG
Orgueil
1.5M⊙
3M⊙
5M⊙
δ25Mg/24Mg
δ26Mg/24Mg
200
150
100
50
0
-50
-100
-100
0
100
200
300
400
500
600

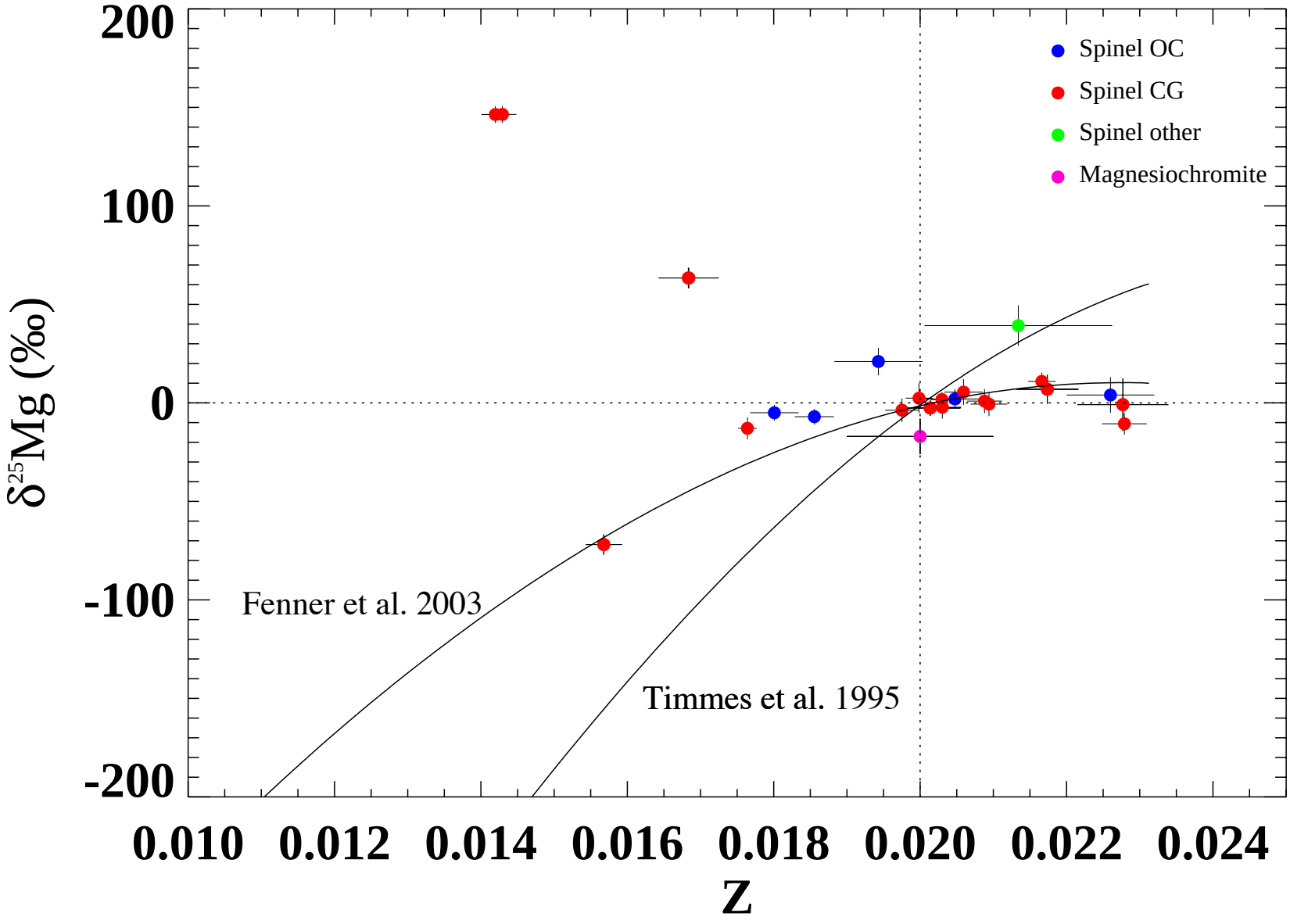
Spinel OC
Spinel CG
Spinel other
Magnesiochromite
Fenner et al. 2003
Timmes et al. 1995
200
100
0
-100
-200
0.010
0.012
0.014
0.016
0.018
0.020
0.022
0.024
Z
δ25Mg (‰)

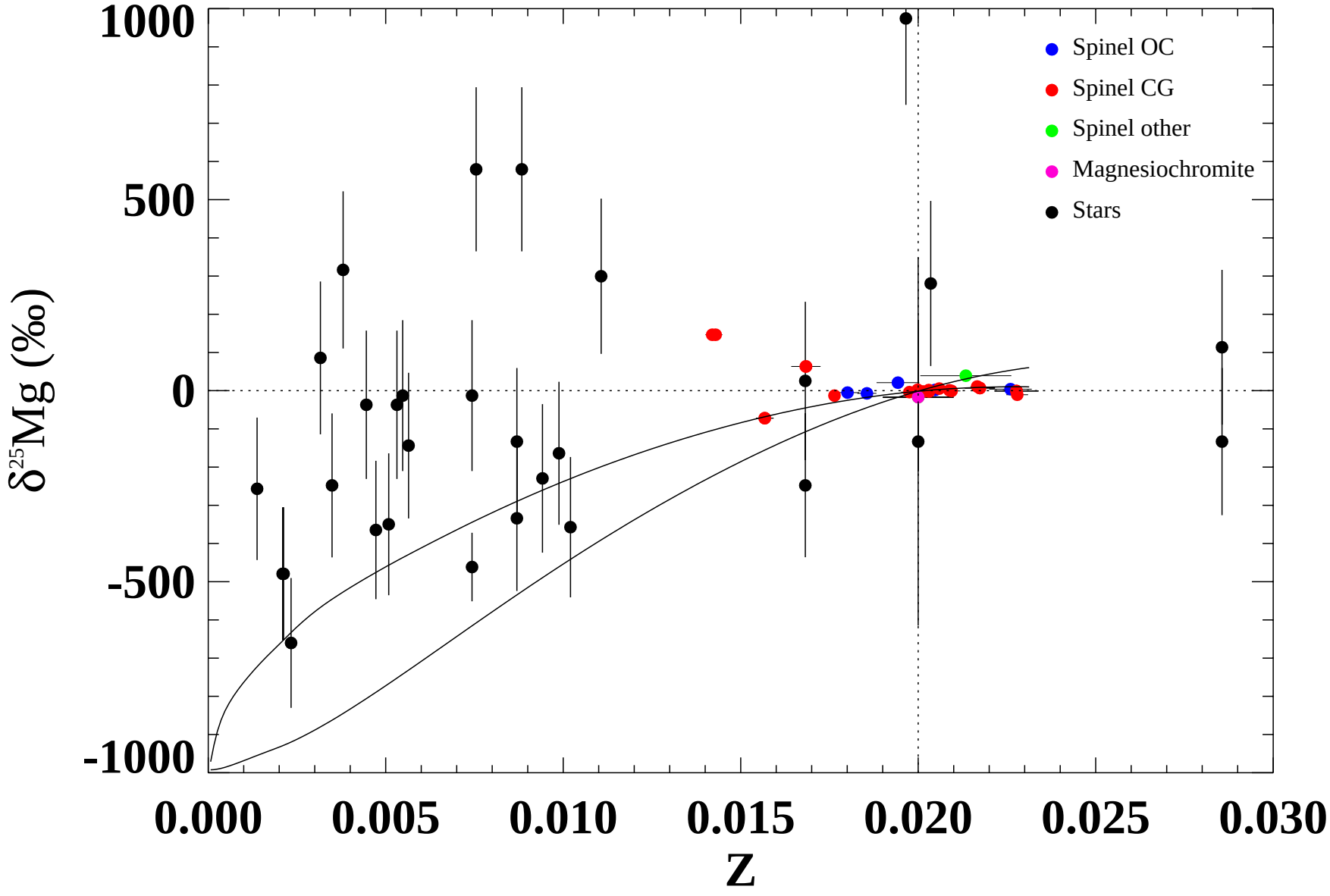
1000
500
0
-500
-1000
0.000
0.005
0.010
0.015
0.020
0.025
0.030
Z
δ25Mg (‰)
Spinel OC
Spinel CG
Spinel other
Magnesiochromite
Stars

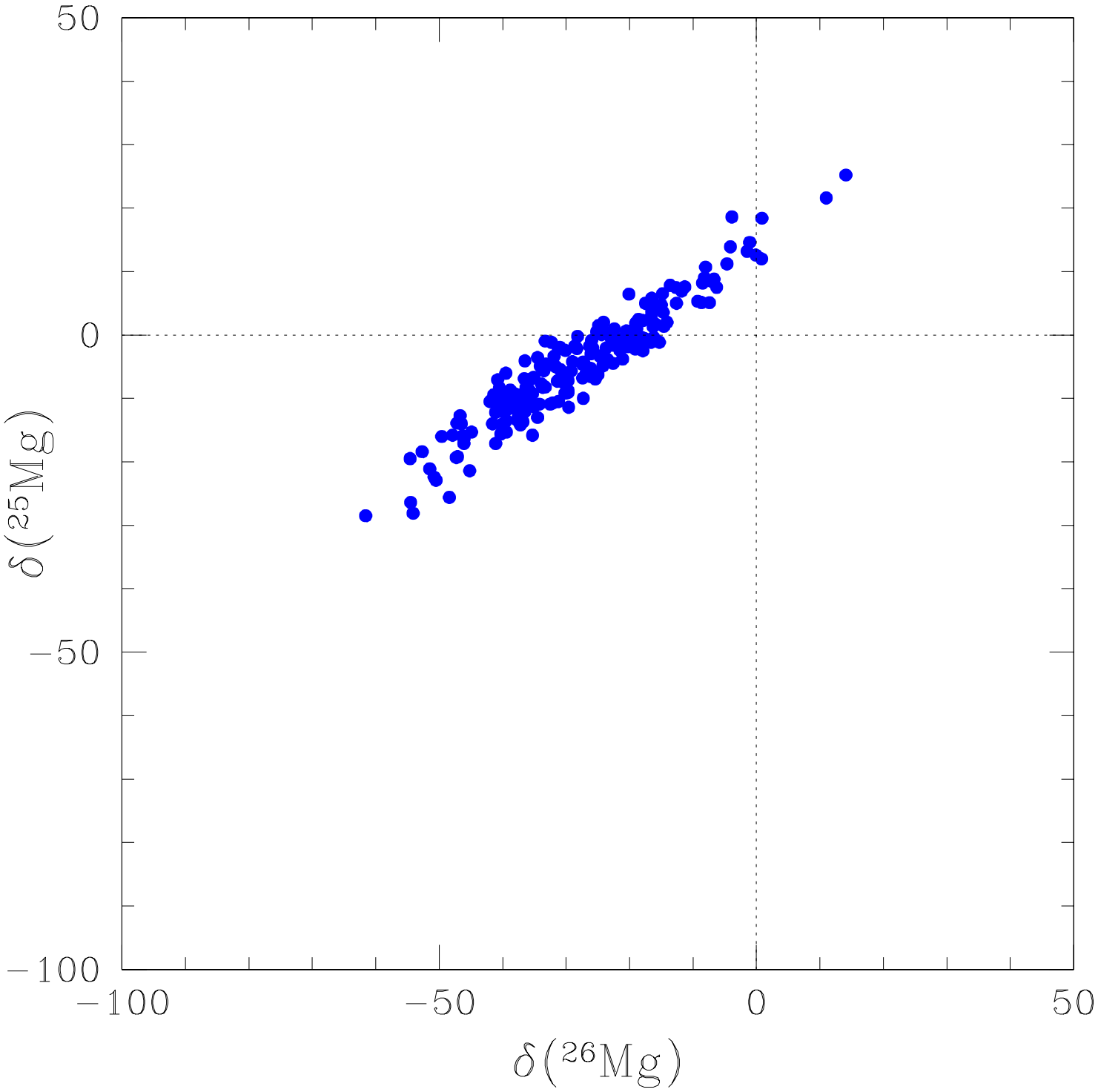

Monte Carlo model of Galactic heterogeneity
by Maria Lugaro

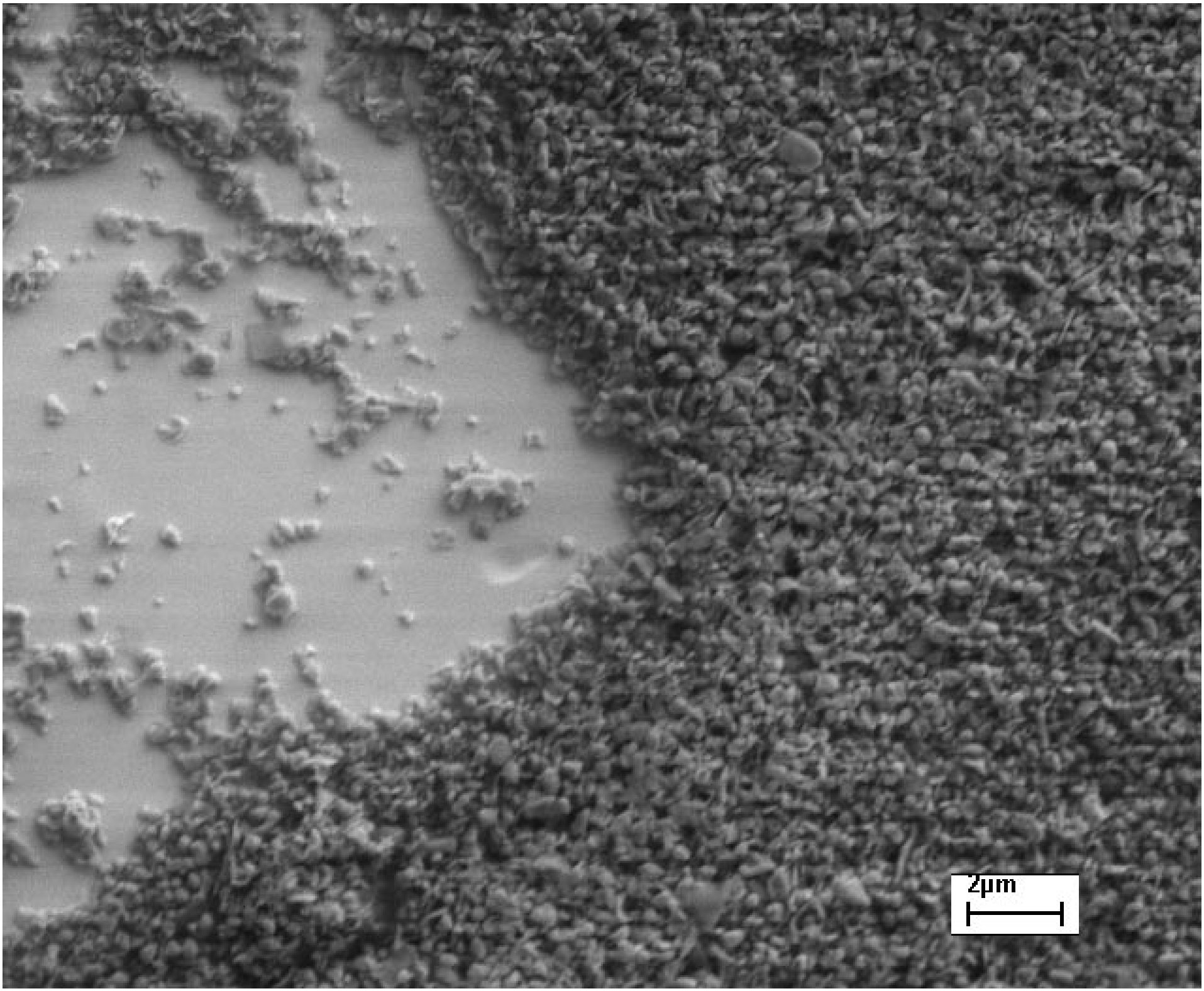
2μm

Murray CG residue

$^{16}O^-$ $^{17}O^-$ $^{18}O^-$

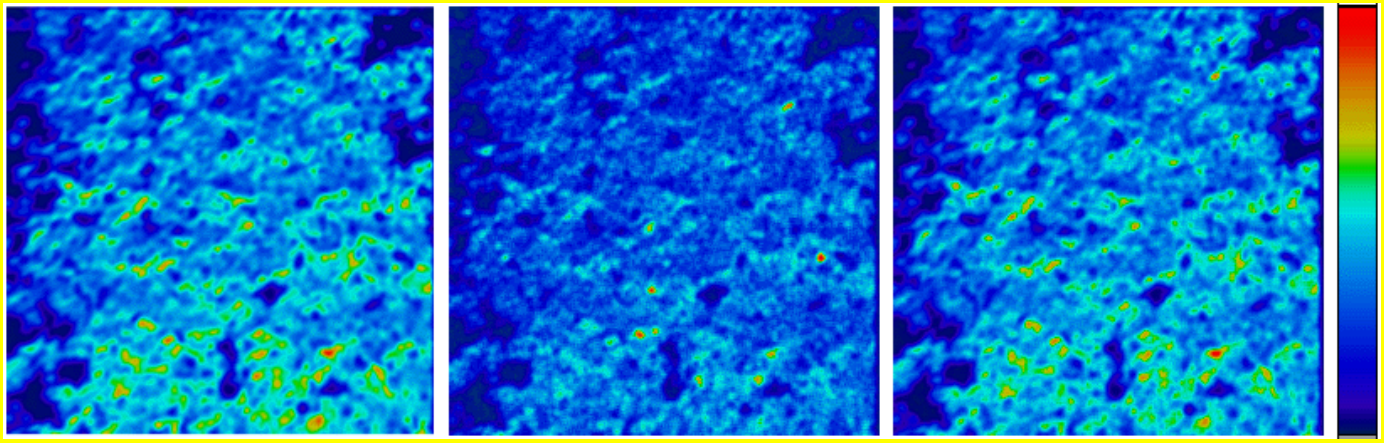

$^{17}O/^{16}O$ $^{18}O/^{16}O$

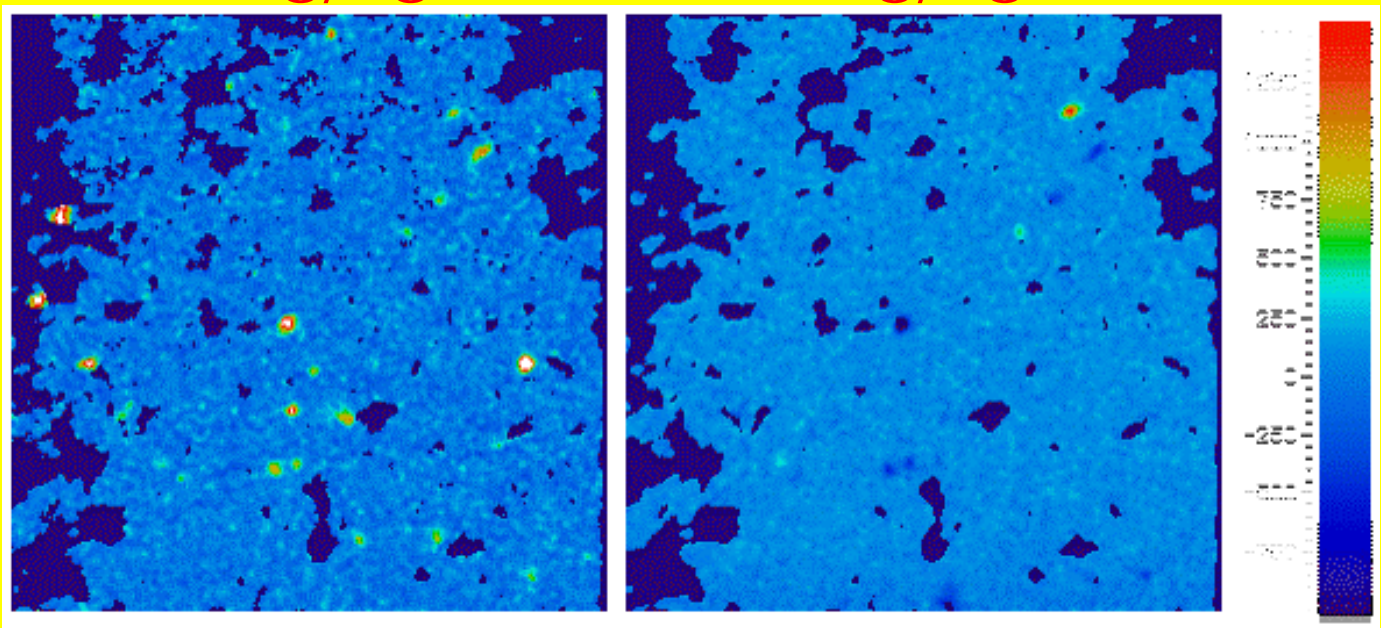

Discovery of presolar silicate in a primitive meteorite

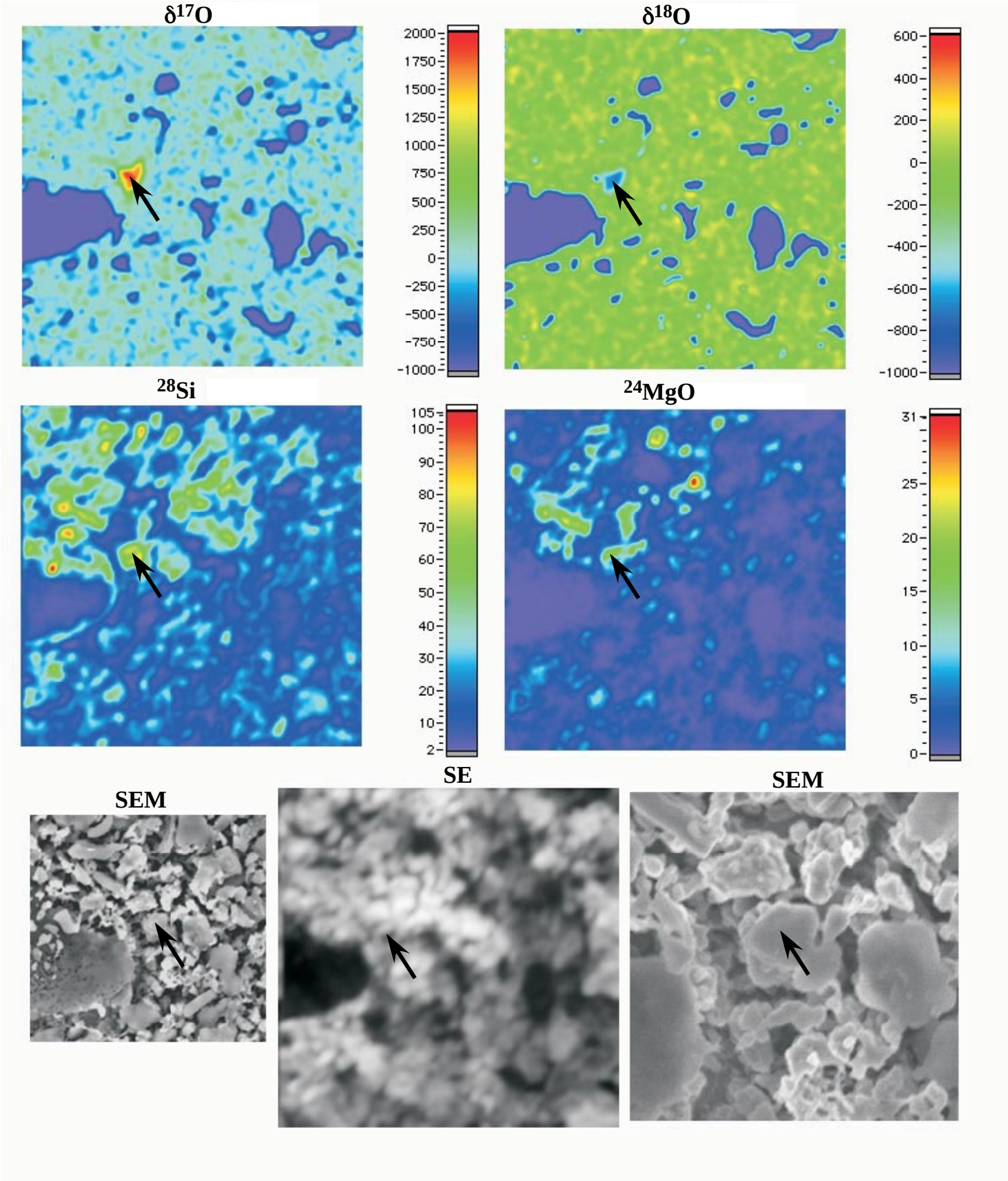

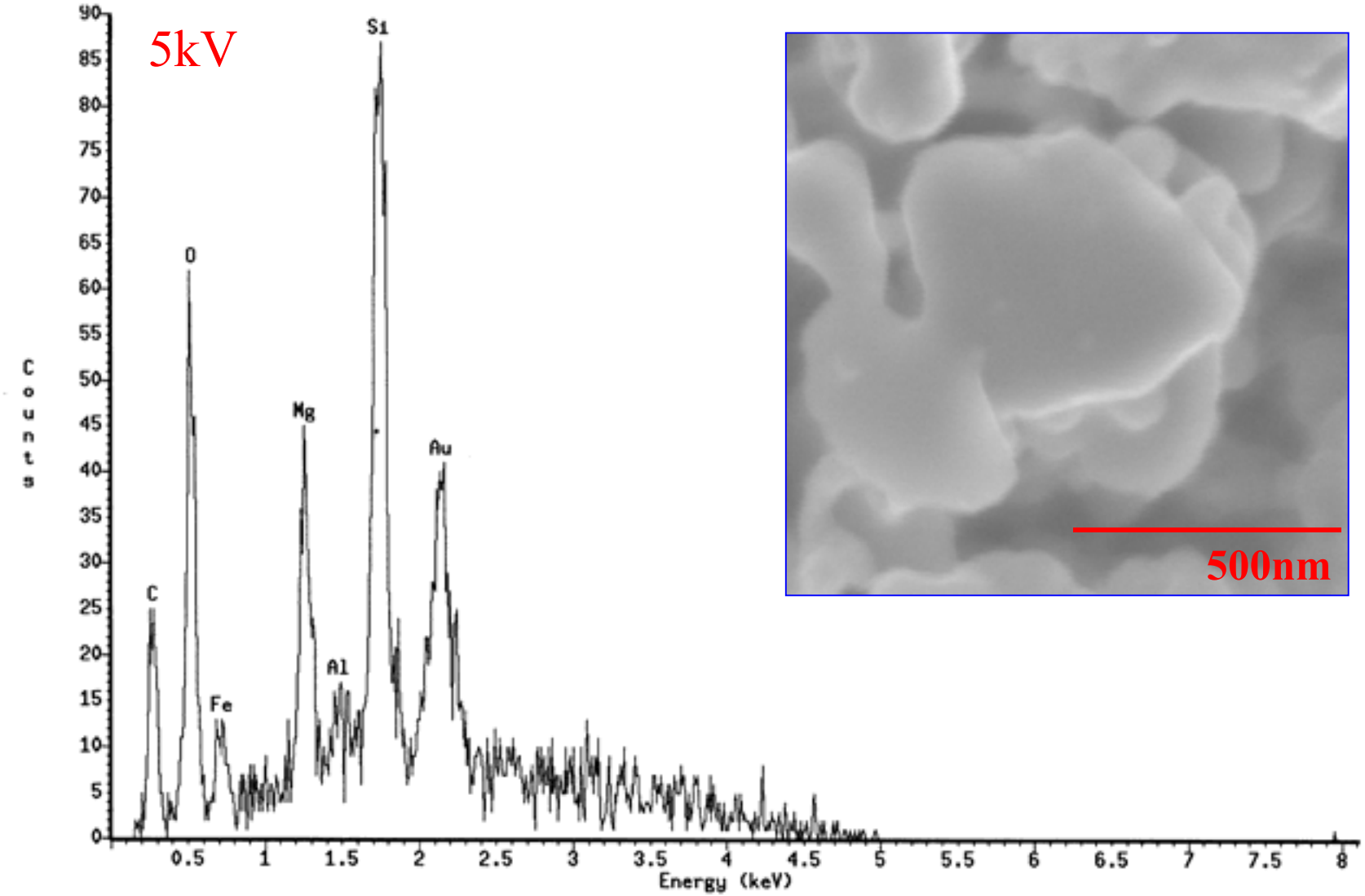
5kV
Counts
Energy (keV)
C
O
Fe
Mg
Al
Si
Au
500nm

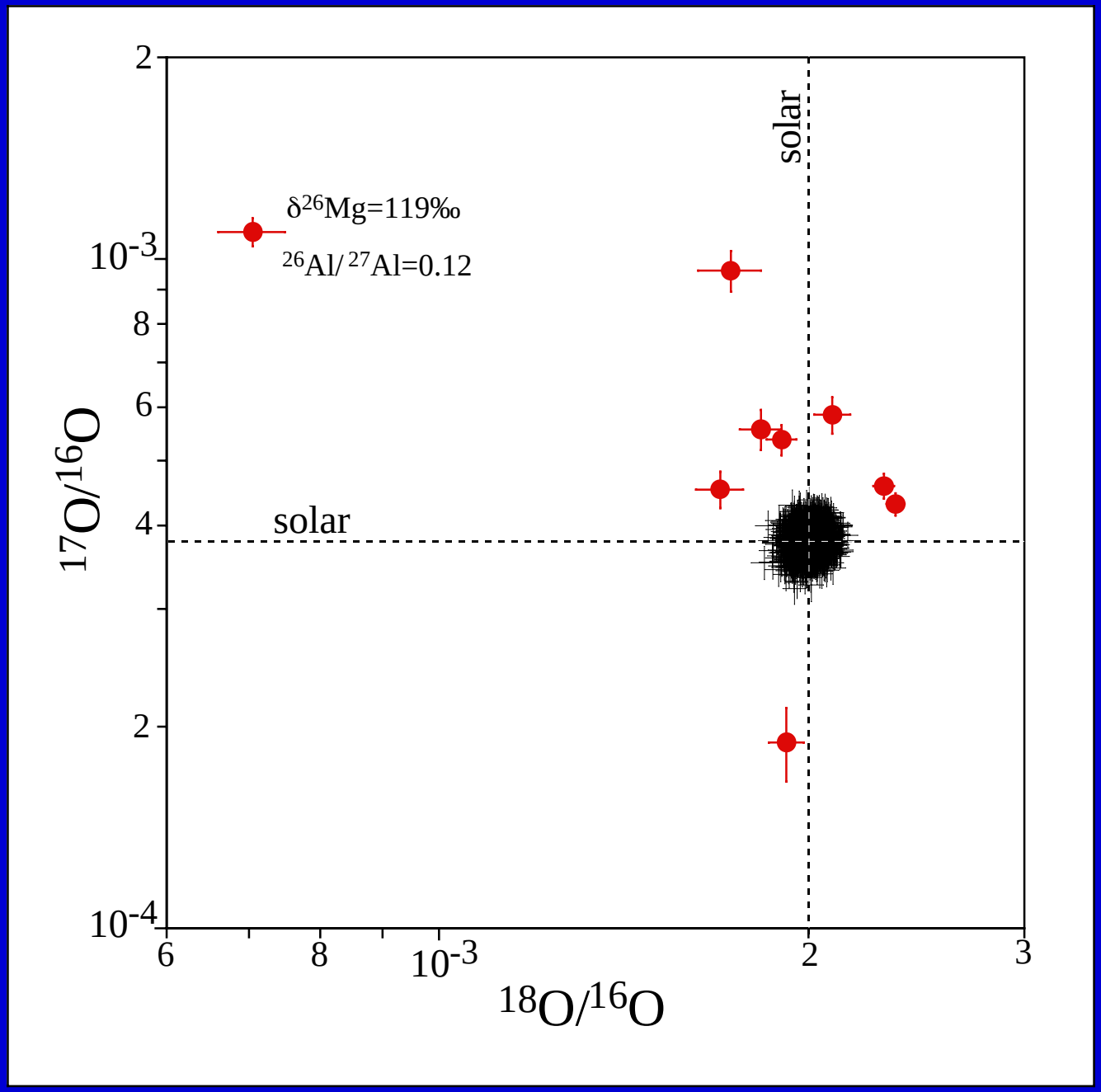
δ26Mg=119‰
26Al/27Al=0.12
solar
solar
17O/16O
18O/16O
2
10-3
8
6
4
2
10-4
6
8
10-3
2
3

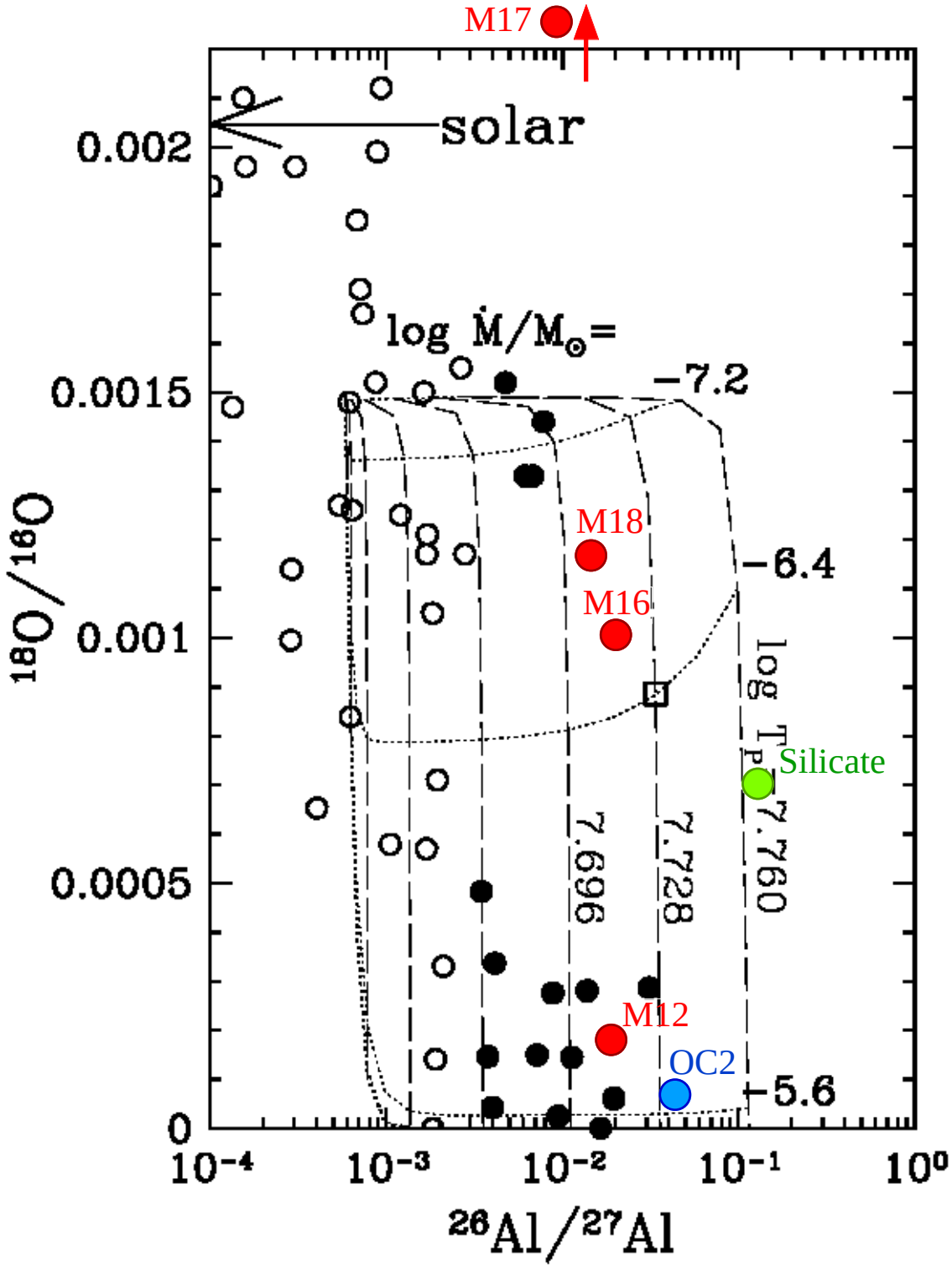

Nollet et al. 2003

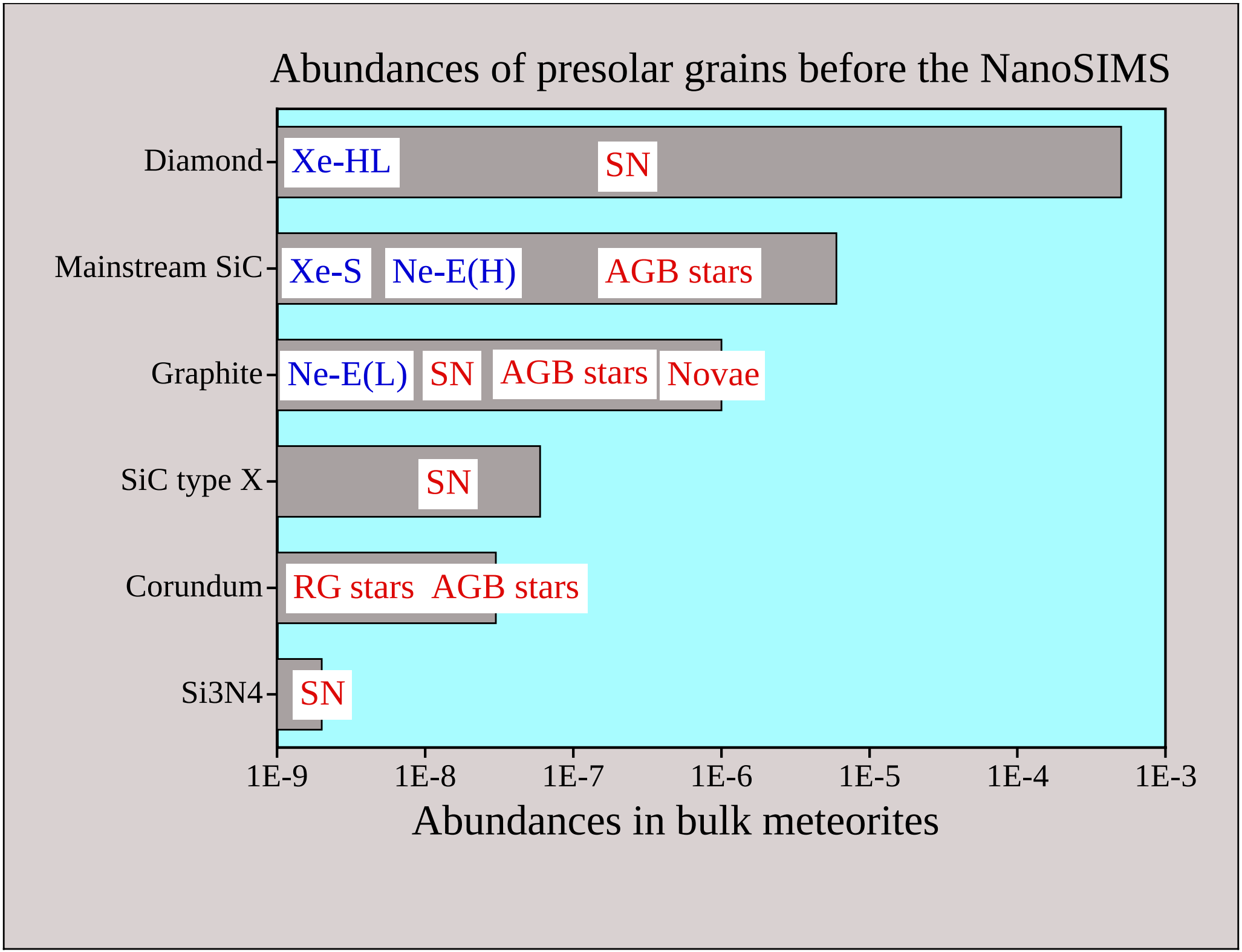
Abundances of presolar grains before the NanoSIMS
Diamond
Xe-HL
SN
Mainstream SiC
Xe-S
Ne-E(H)
AGB stars
Graphite
Ne-E(L)
SN
AGB stars
Novae
SiC type X
SN
Corundum
RG stars
AGB stars
Si3N4
SN
1E-9
1E-8
1E-7
1E-6
1E-5
1E-4
1E-3
Abundances in bulk meteorites

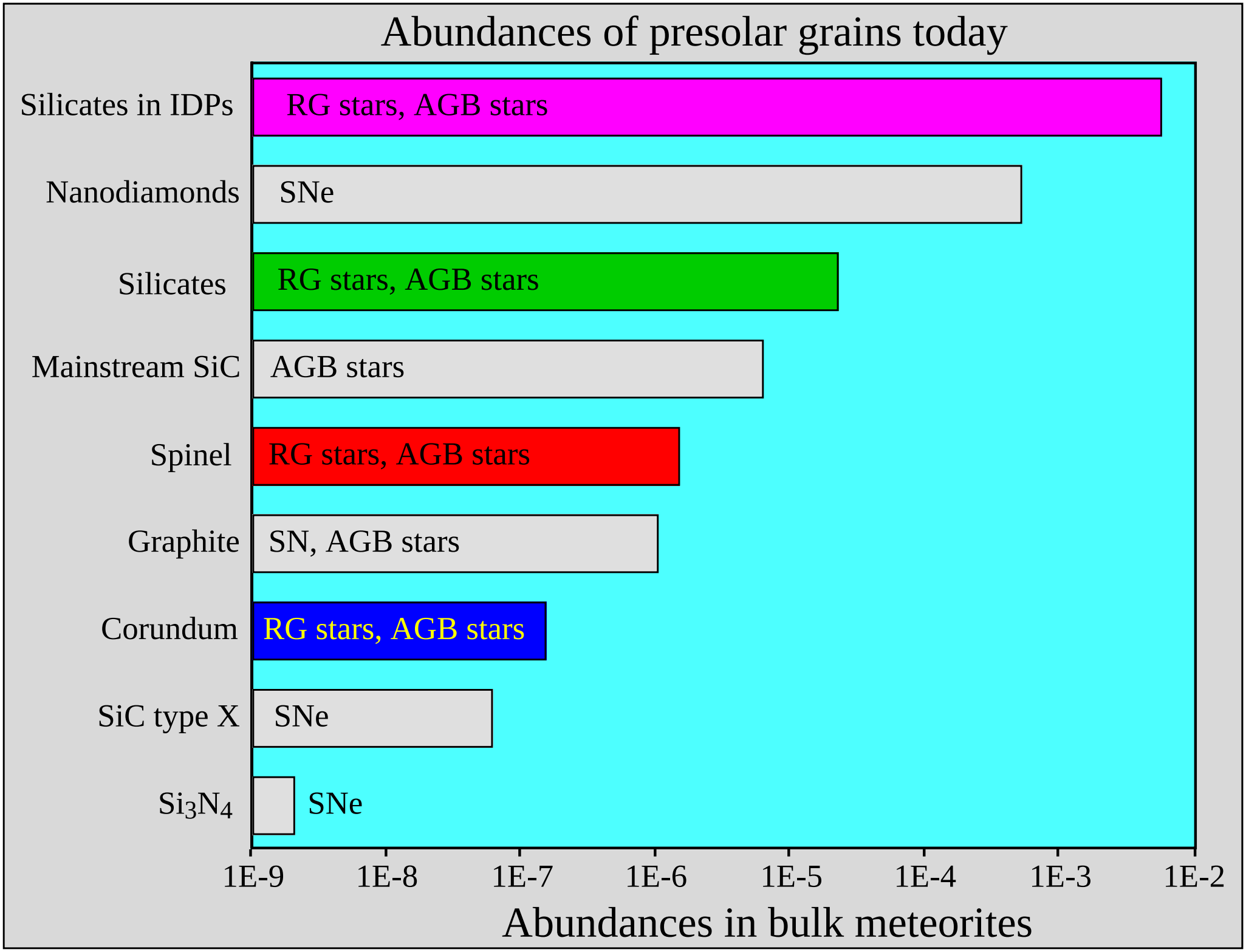
Abundances of presolar grains today
Silicates in IDPs
RG stars, AGB stars
Nanodiamonds
SNe
Silicates
RG stars, AGB stars
Mainstream SiC
AGB stars
Spinel
RG stars, AGB stars
Graphite
SN, AGB stars
Corundum
RG stars, AGB stars
SiC type X
SNe
Si_3N_4
SNe
1E-9
1E-8
1E-7
1E-6
1E-5
1E-4
1E-3
1E-2
Abundances in bulk meteorites

Contribution by

Maria Lugaro

University of Cambridge
mal@ast.cam.ac.uk

6 pages

S PROCESS in AGB STARS

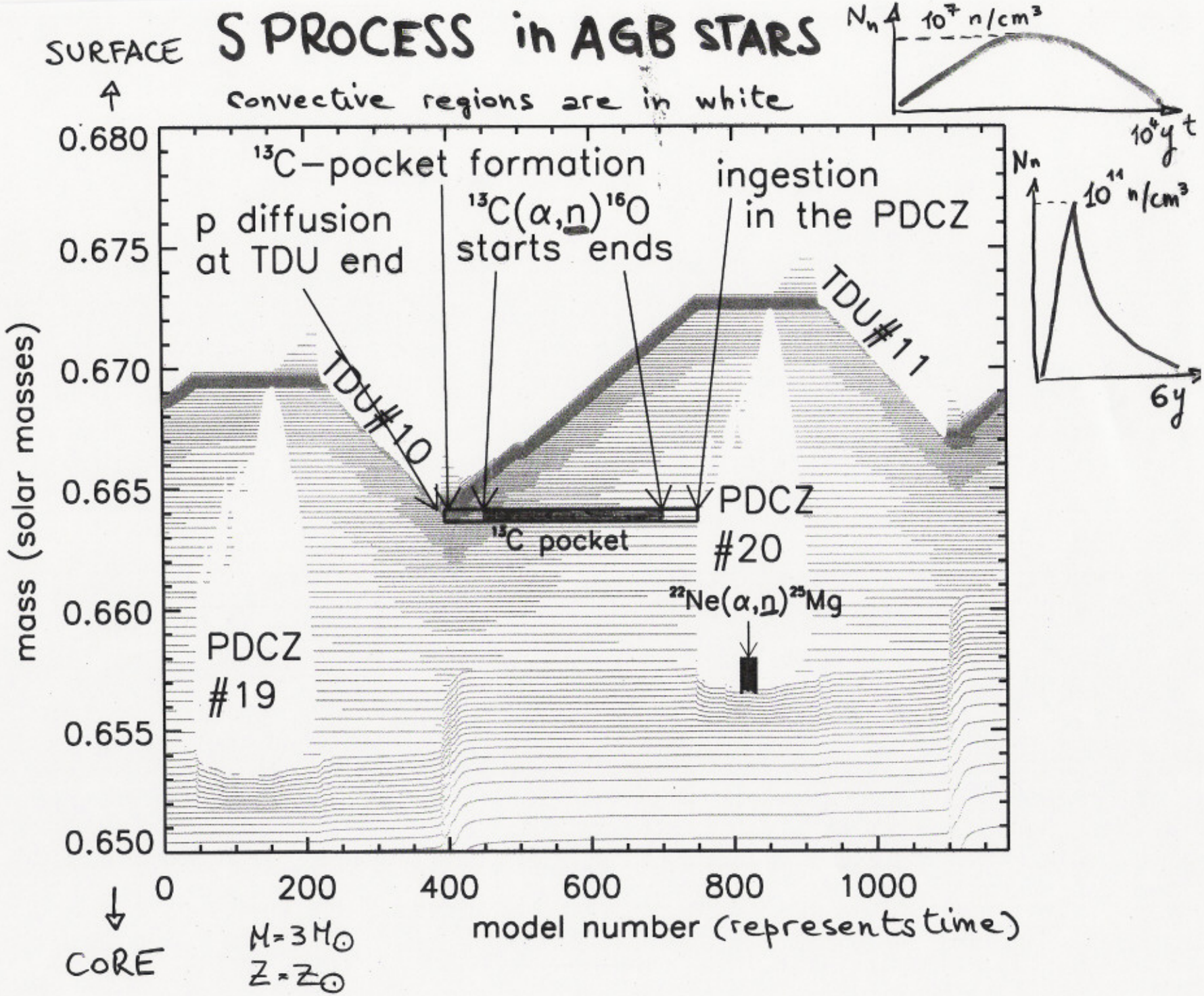

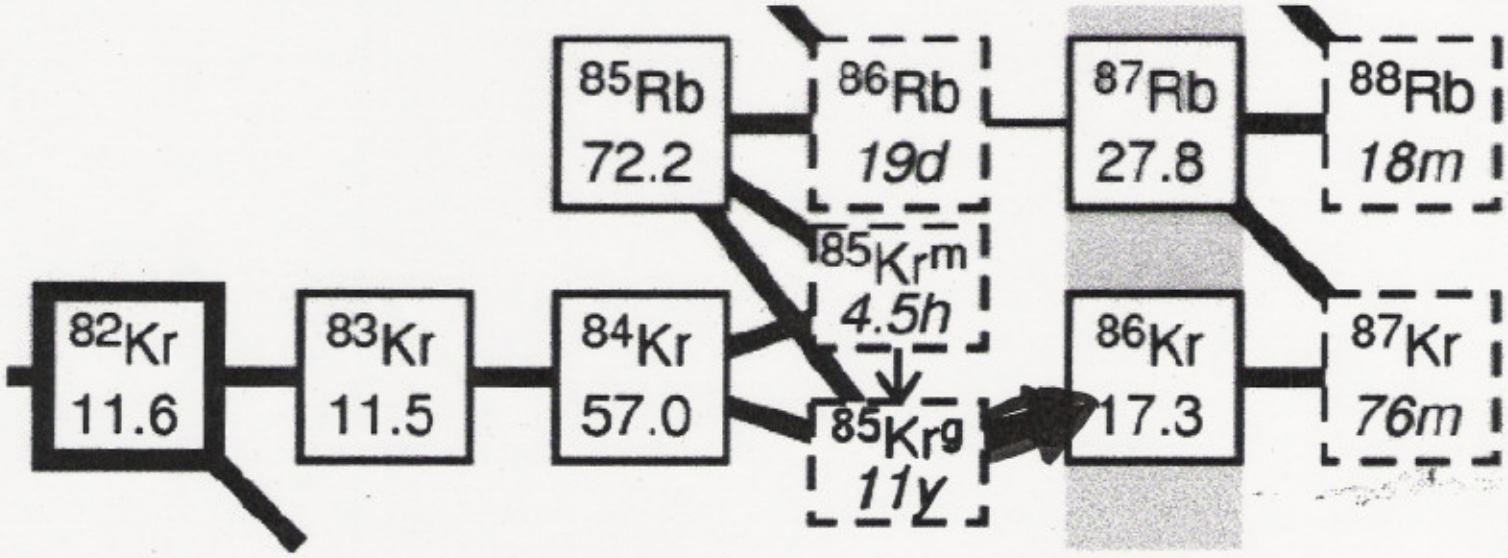

^{85}Kr	123	Rauscher & Thielemann (2000)	* only
$\frac{\langle\sigma v\rangle}{v_T}$ (mb)	67 ± 17	Walter et al. (1986)	theoretical
	25	Harris (1981)	data
at 30 KeV	150	Woosley et al. (1978)	available
	55 ± 45	Bao et al. (2000) recommended	

Kr is a noble gas. Measurements have been performed by stepped-heating combustion of the sample (Lewis et al. 1994)

BULK SiC data, G component = (only ~5% of the grains contain noble gases) = pure S-process component

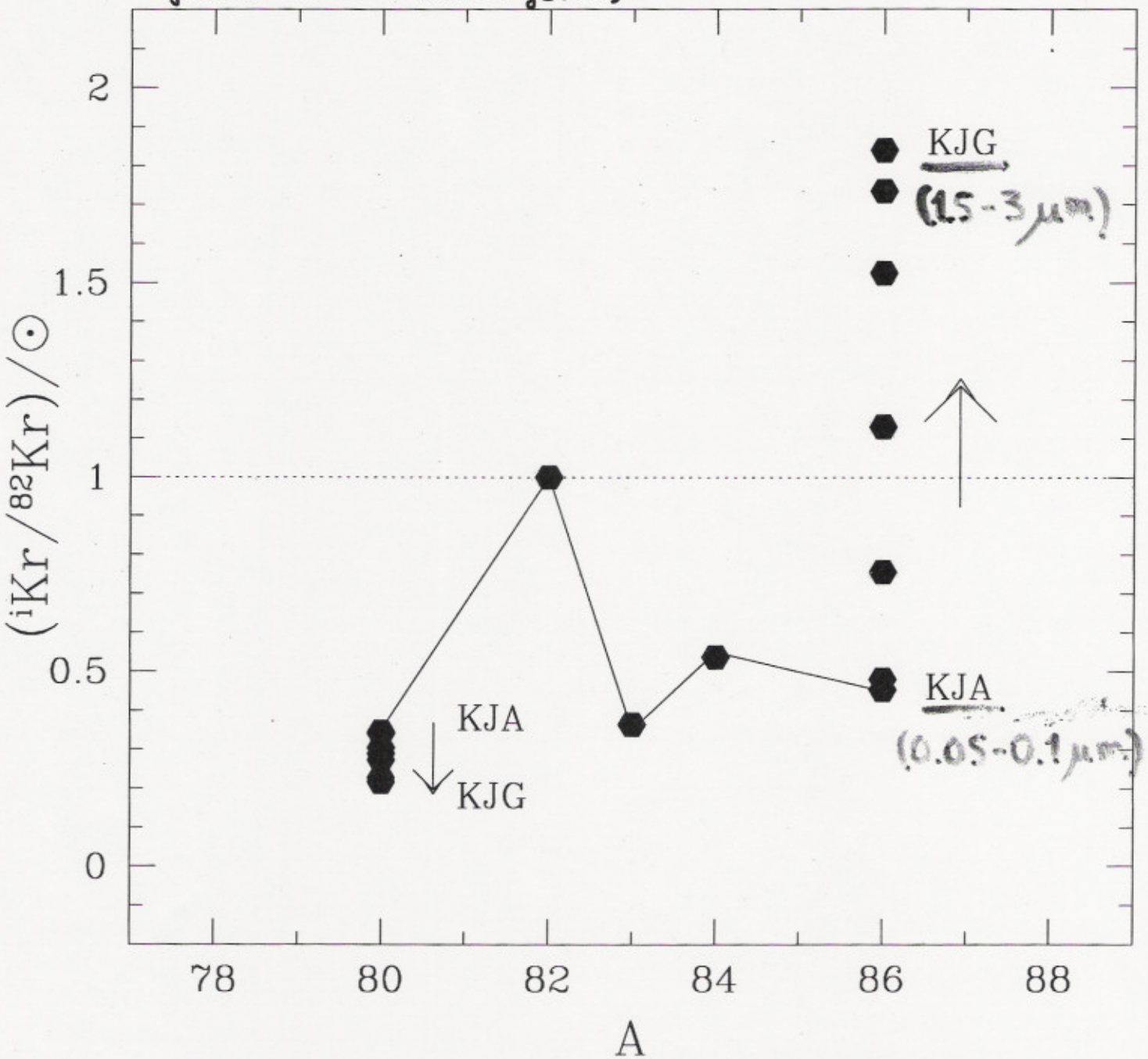

Noble gases likely were implanted in SiC after being ionized. (Verchovsky et al. 2003)
The concentration of Kr vs. grain size indicates two different patterns, i.e. components. One implanted with low energy (and with low $^{86}Kr/^{82}Kr$) the other implanted with high energy (high $^{86}Kr/^{82}Kr$).

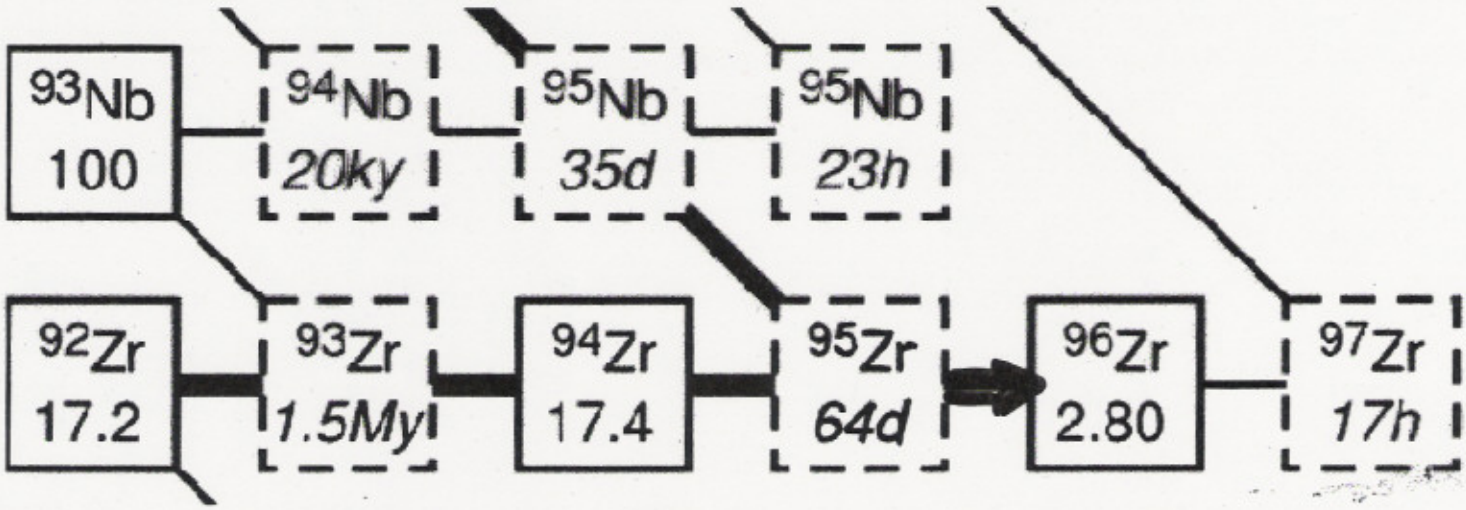

^{95}Zr	50	Toukan & Käppeler (1990)	*only theoretica data available
$\frac{\langle \sigma v \rangle}{v_T}$ (mb)	126	Rauscher & Thielemann (2000)	
	72	Holmes et al. (1976)	
at 30 keV	79±12	Bao et al. (2000) recommended	
	+23	Goriely, Nuclear Astrophysics Data Base	

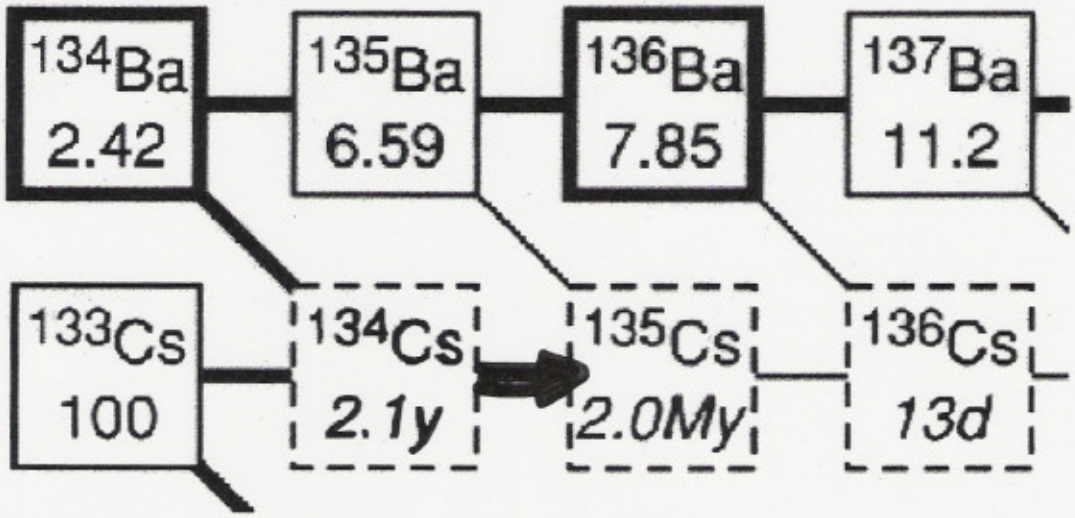

^{134}Cs				
$\frac{\langle\sigma v\rangle}{v_T}$ (mb)	894	Rauscher & Thielemann	(2000)	* only theoretical data available
	597	Harris	(1981)	
	1320	Holmes et al.	(1976)	
at 30 KeV	664 ± 174	Bao et al. (2000)	recommended	

^{134}Cs	T_8	0.5	1.	2.	3.	4.
β^- decay rate (s^{-1}) (Takahashi & Yokoi 1987)		1.02-8 (thermal pulse top temberature)	3.28-8	6.31-7	2.11-6 (thermal pulse bottom temherature)	4.81-6

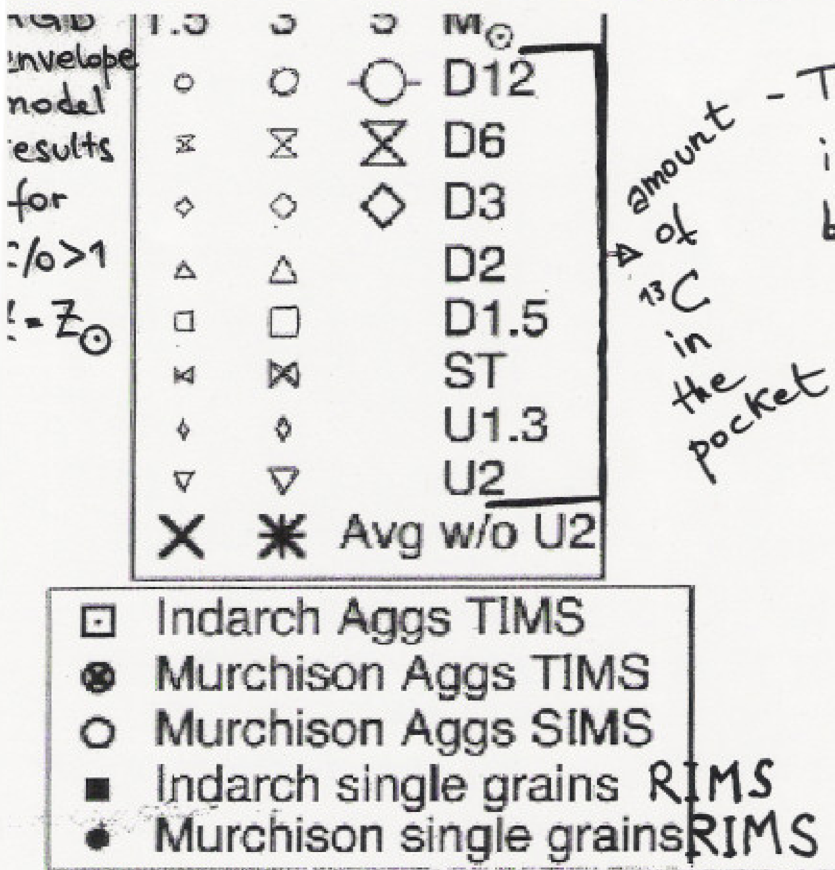

- The $^{134}Ba/^{136}Ba$ ratio is affected by the branching at ^{134}Cs

- The Temperature in the thermal pulse grow with the pulse number. Hence in later pulses the branchings are more activated (⇒ bending)

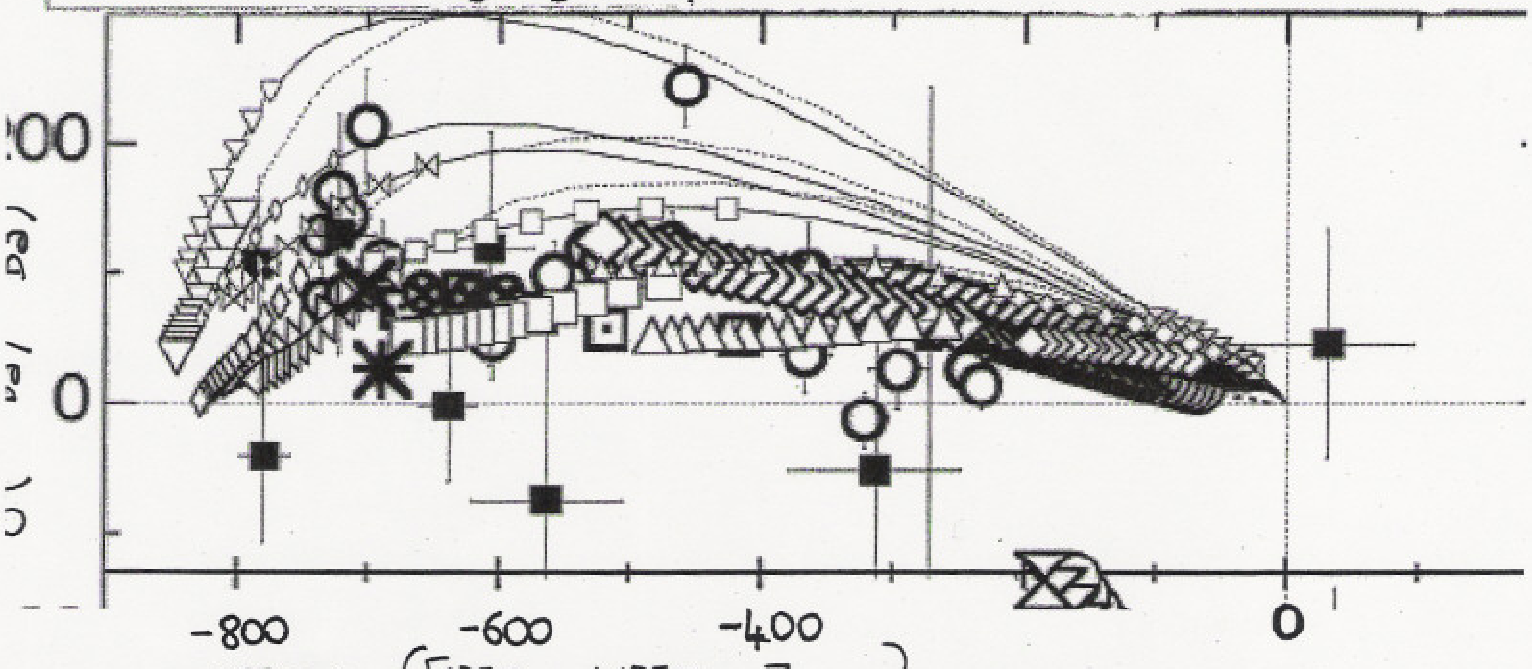

$$\delta\left(\frac{^{135}Ba}{^{136}Ba}\right) = \left\{\left[\frac{^{135}Ba}{^{136}Ba} \Big/ \frac{^{135}Ba_\odot}{^{136}Ba_\odot}\right] - 1\right\} \times 1000.$$

(Lugaro et al. 2003)

Contribution by

Falk Herwig

Los Alamos National Laboratory
fherwig@lanl.gov

28 pages

The s-process in low and intermediate mass stars

Solar and very low metallicity

Falk Herwig, LANL, T-6

2 February 2004, DANCE workshop Santa Fe, NM

Introduction

Mixing for the s-process:

- What mixing processes are responsible?
- Validation of physical concepts for mixing.

Nuclear reaction rate uncertainties:

- ^{95}Zr(n,γ), ^{13}C(α,n), ^{14}N(p,γ), tripple-α.

A new code:

- Complete s-process and multi-zone time-dependent mixing.

The first s-process:

- s-process and evolution at Z=0?
- Z=10^{-4}: Evolution, DUP, corrosive H-shell burning.

Stellar evolution for different masses

Massive stars: C, O, α-elements
Fe-group elements

Low- and intermediate mass: C, N, Li, s-process (half of all elements with A>90)

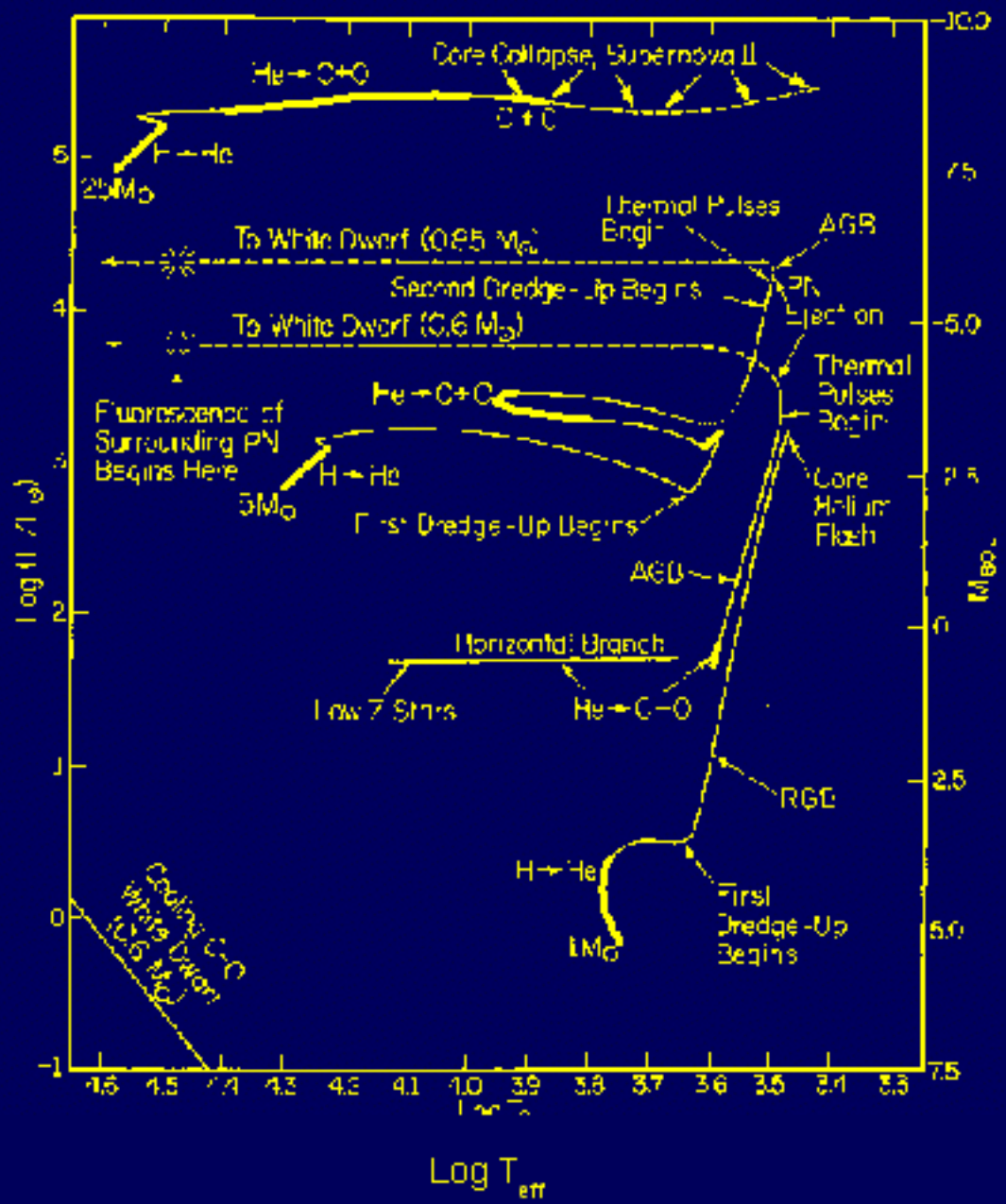

s-Process Mind Map

Pre-solar grains:
- Isotopic ratios

Physical processes in stars:
- Convection
- Rotation
- Magnetic Fields

Spectroscopic observables:
- Solar-like metallicity stars
- Extremely metal-poor stars
- Central stars of PN

N-capture nuclear physics:
- X-sections
- T-dependence

Predicting observables

Computational modelling:
- Large network and mixing codes
- High-resolution stellar structre and evolution
- Hydrodynamic processes in stars

- ✓Model the first s-process in the Early Universe
- ✓Decipher the information locked in the EMP stars

The *s*-process components

Weak component
from He-core burning
in massive stars

Main component
from double shell
burning in low-mass
giants (AGB stars)

Indices [hs/ls], [s/Fe], [Pb/hs]
-> τ n-exposure

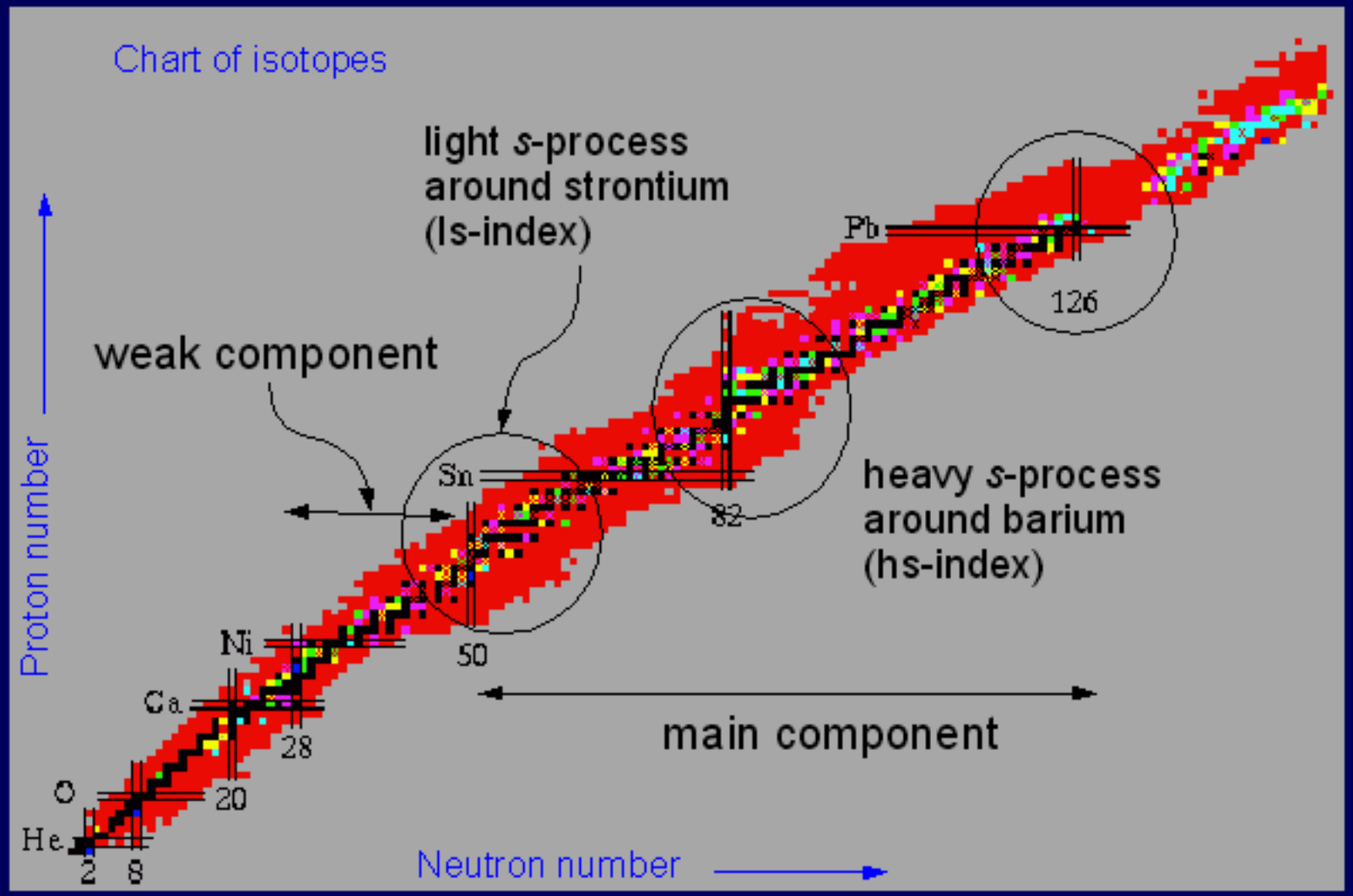

The Asymptotic Giant Branch stars

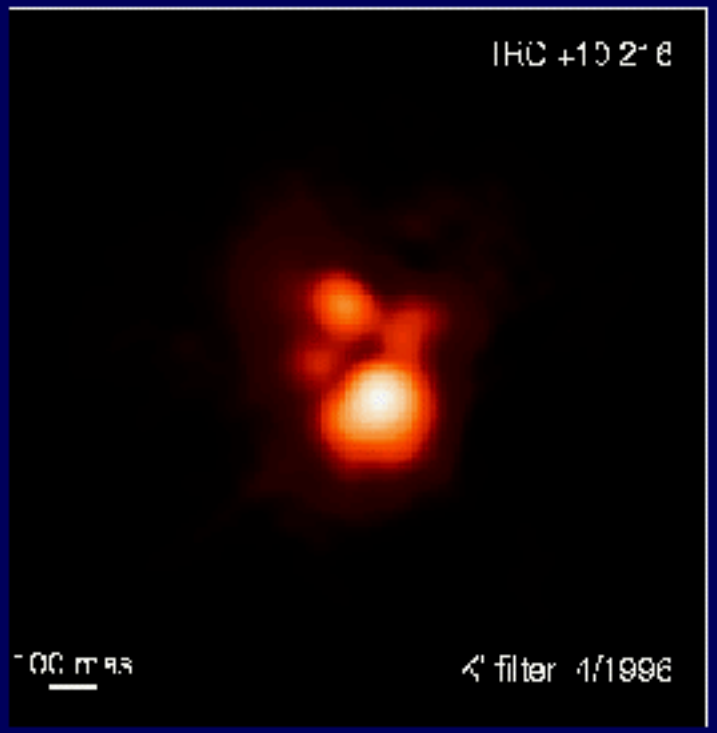

Speckle interferometric image of carbon AGB stars IRC+10216: clouds with separation of 16 - 34 AU and velocity of 3 AU/yr
Weigelt etal (1998)

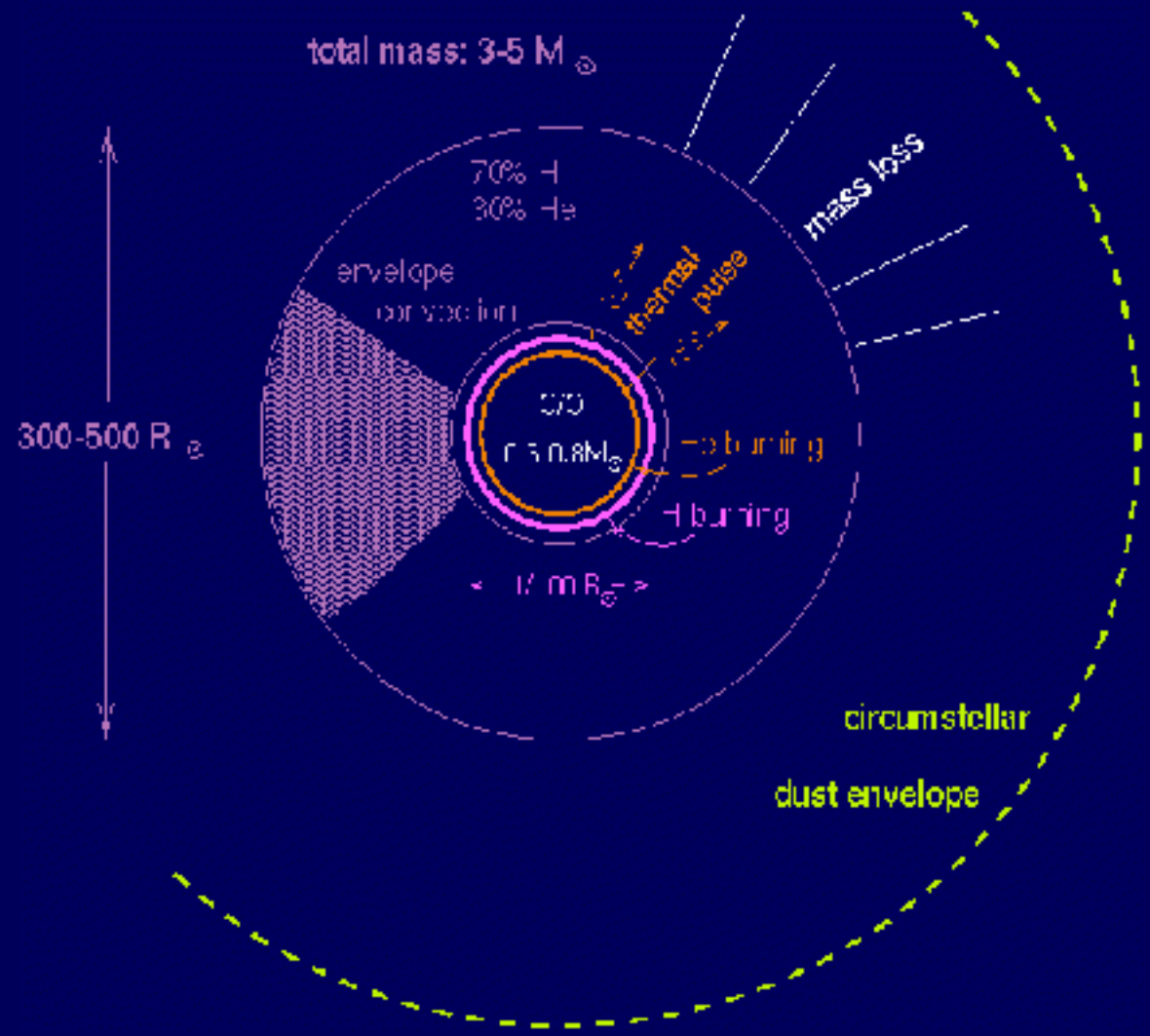

The standard model of the s-process in TP-AGB stars (thanks to Gallino and his group)

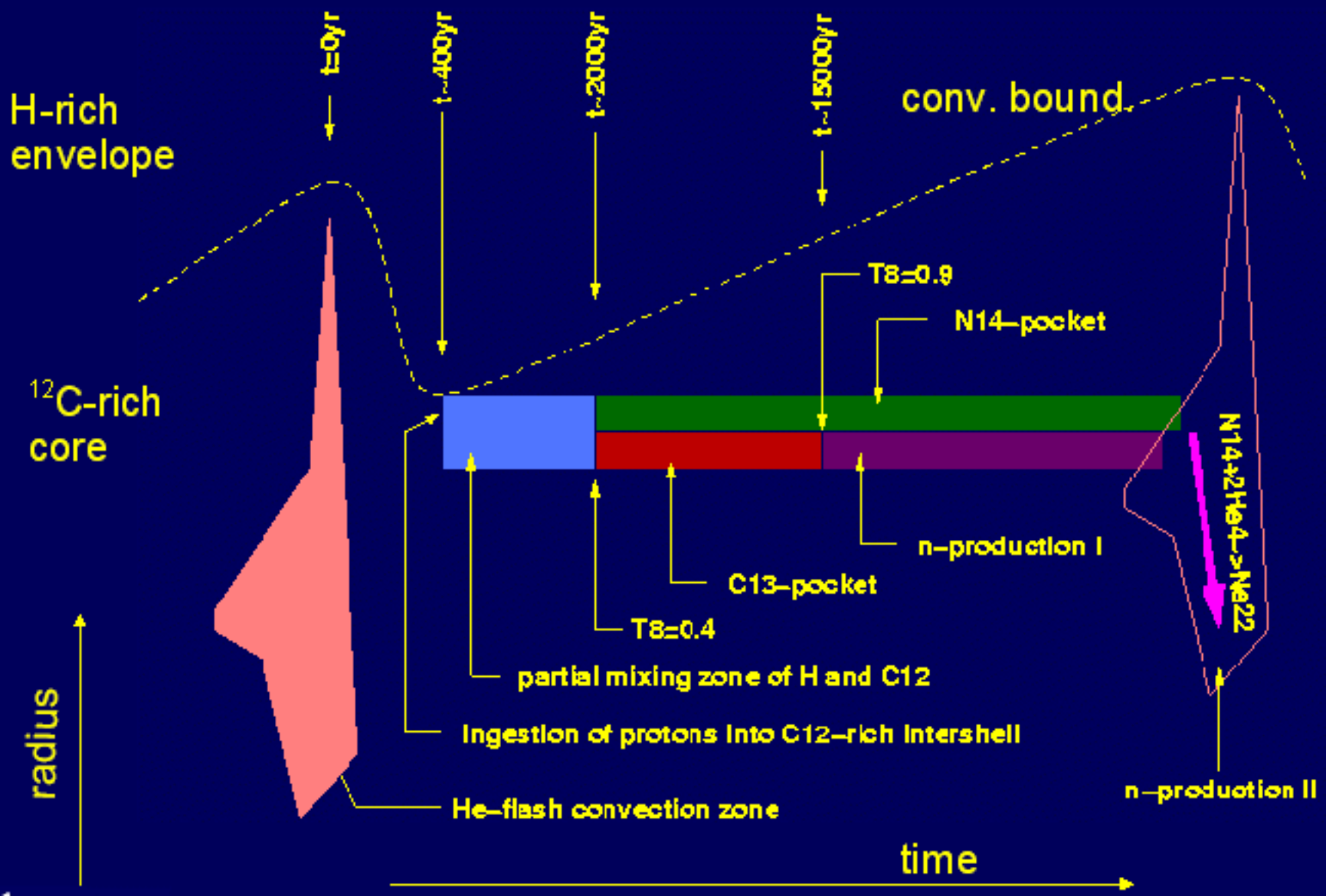

The most simple parameterization:
No ^{14}N; only one free parameter

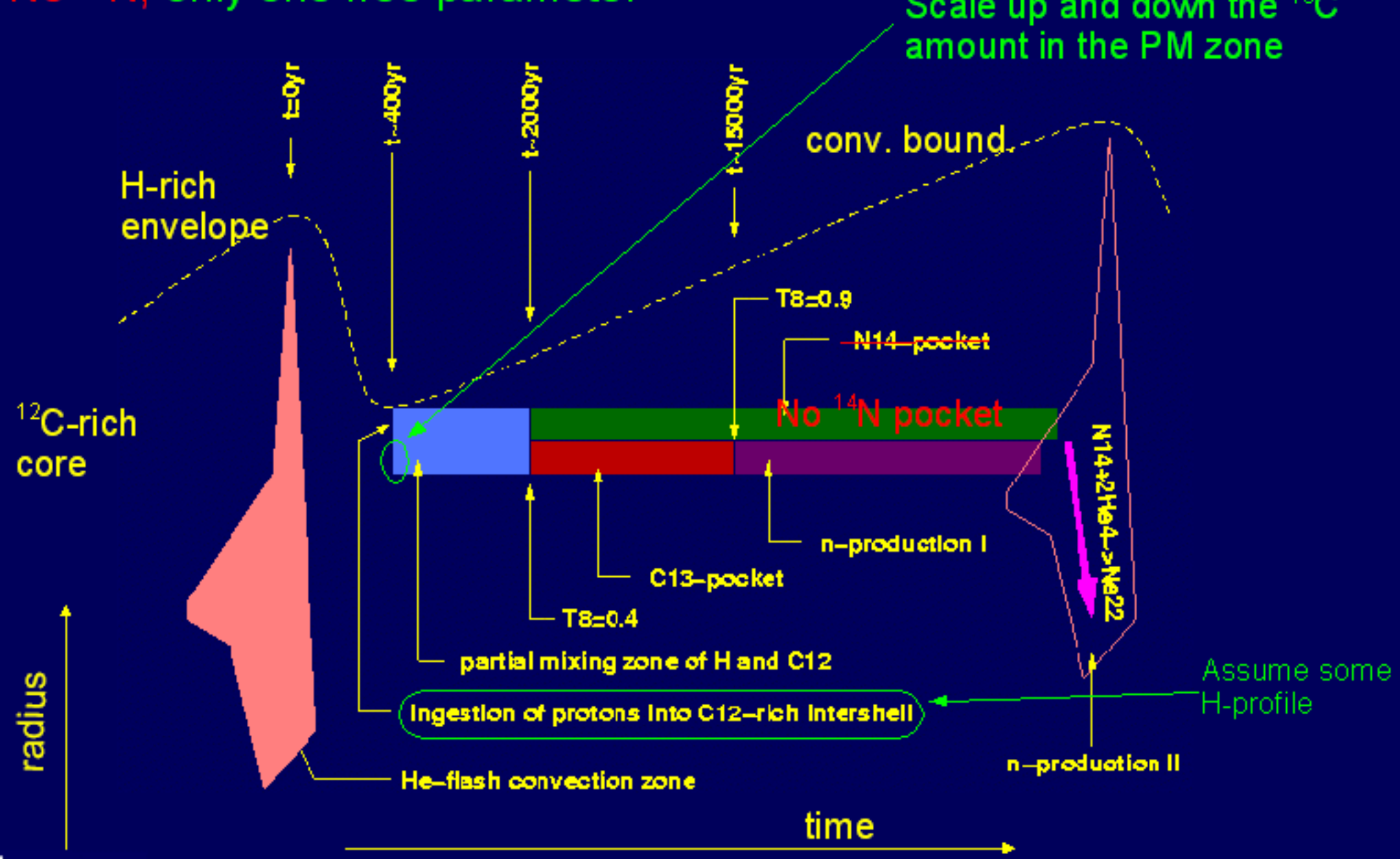

Key Mixing Hot Spots:

1. Dependence of IS abundance on OV
2. DUP dependence of OV, corrosive H-shell burnging in massive EMP stars
3. Mixing for ^{13}C pocket (GW/rot/OV picture)
4. Mixing during IP phase: rotation? Magnetic fields?

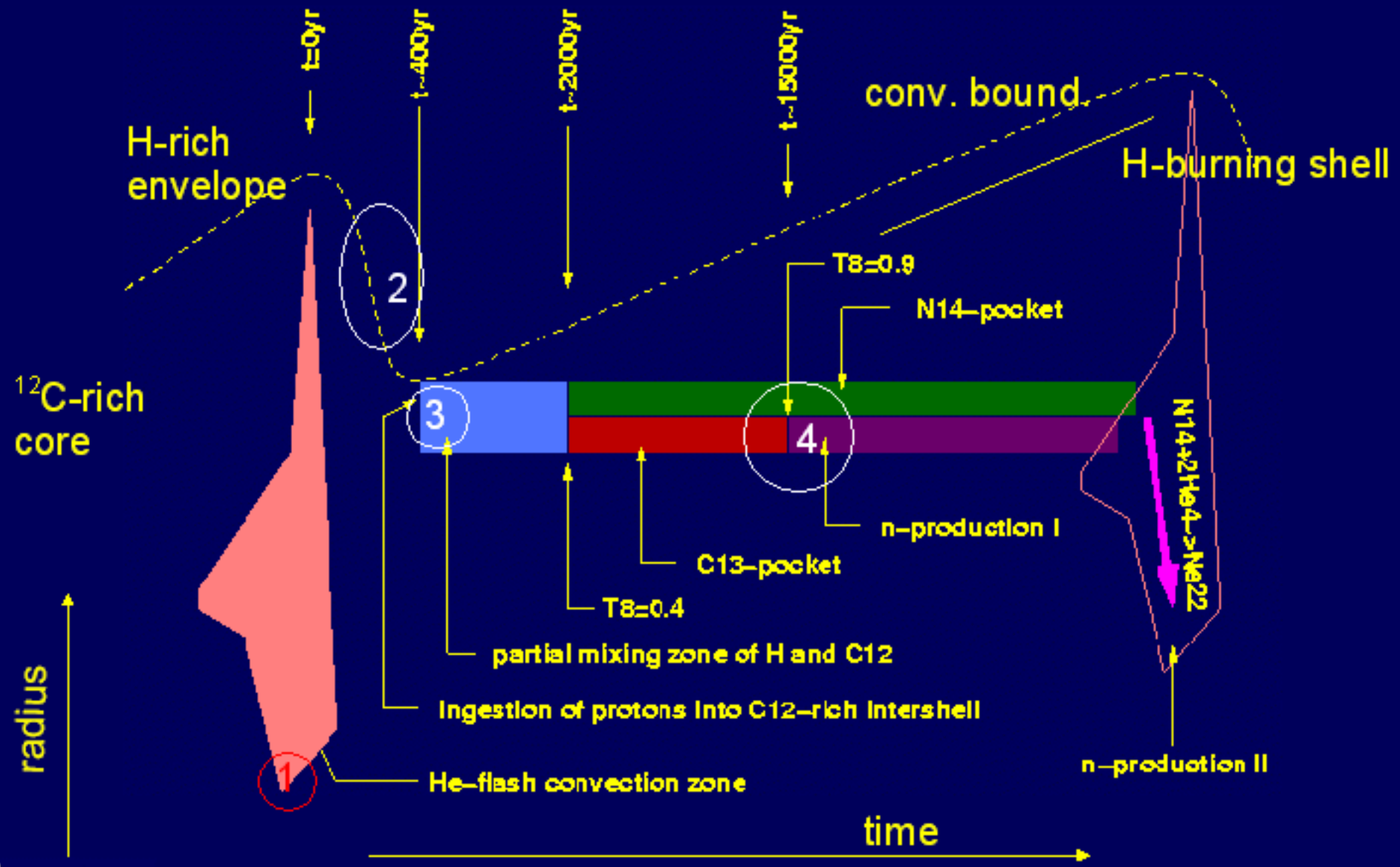

1. Dependence of IS abundance on OV

Intershell abundance vs. overshoot efficiency at He-flash convection zone bottom

Intershell ^{12}C abundance vs. neutron exposure in s-process layer

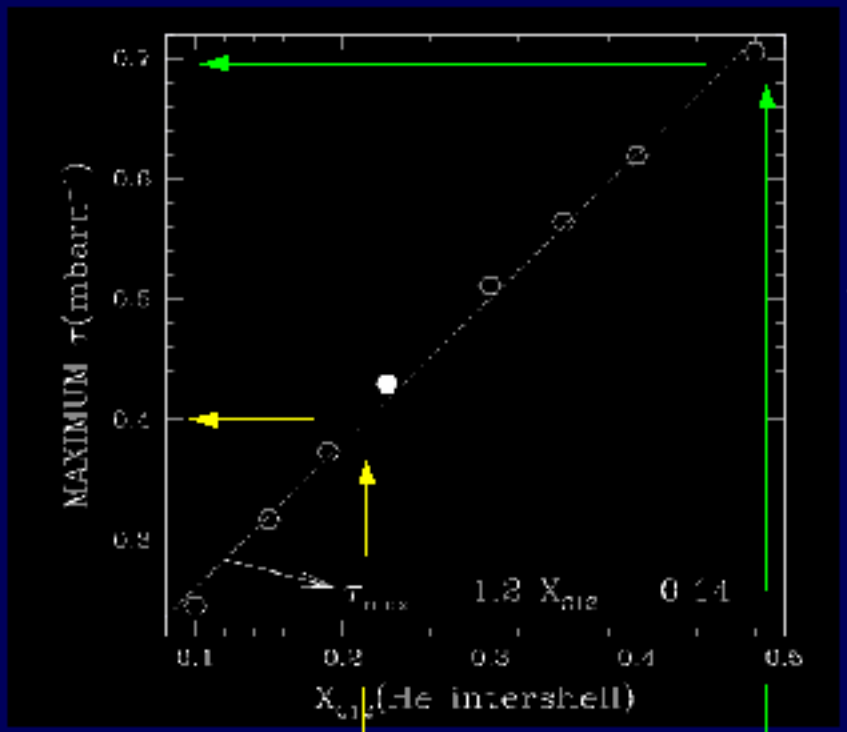

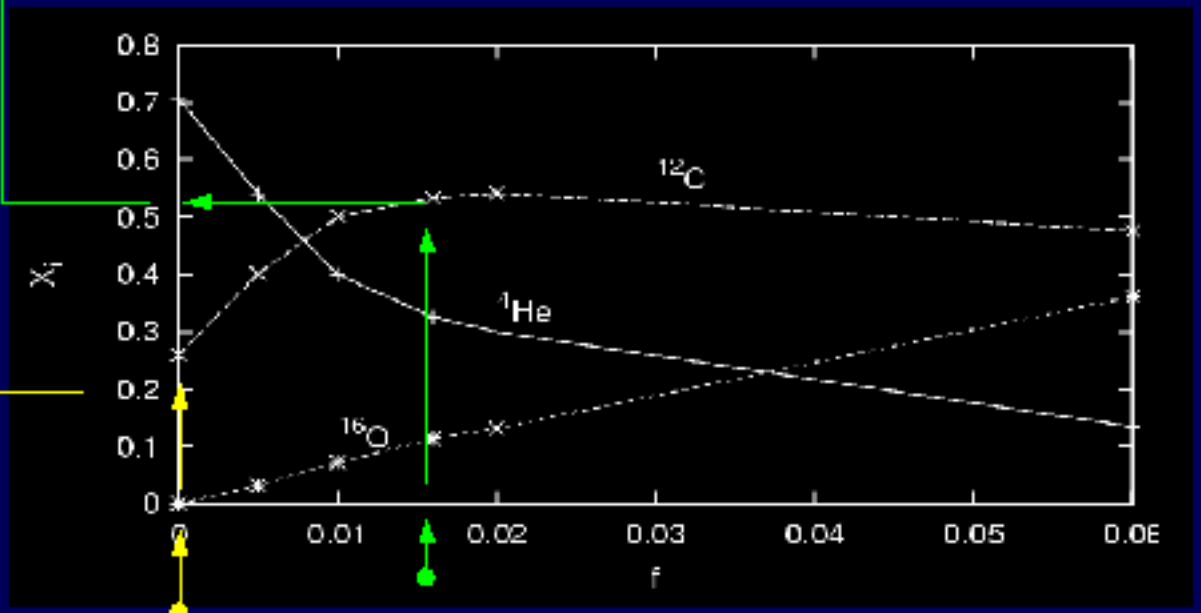

Lugaro etal (2003, ApJ)
Herwig (2000, A&A)

Neutron exposure vs
s-process distribution in
s-process production site

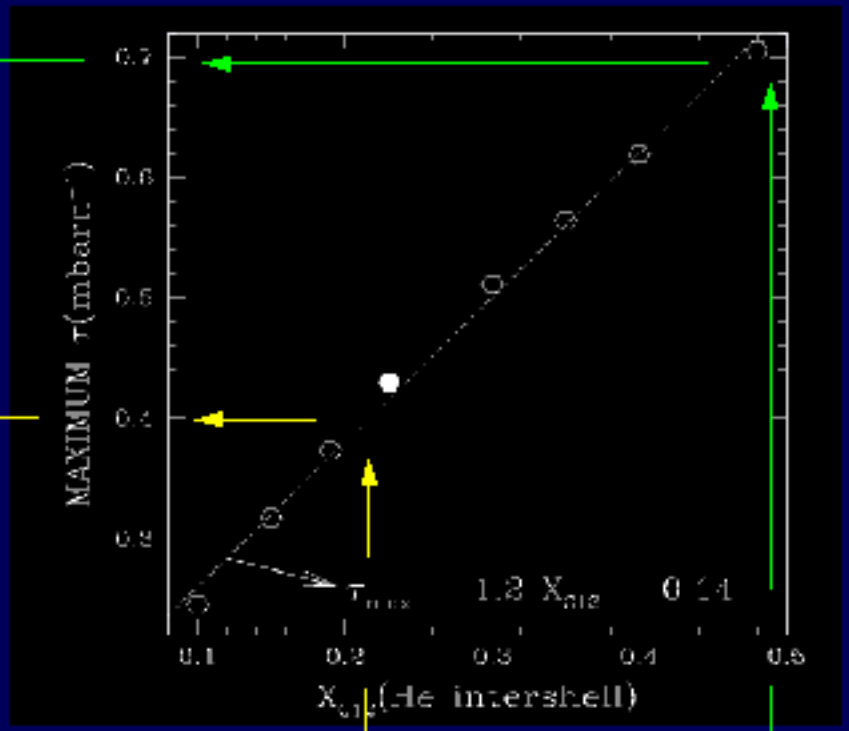

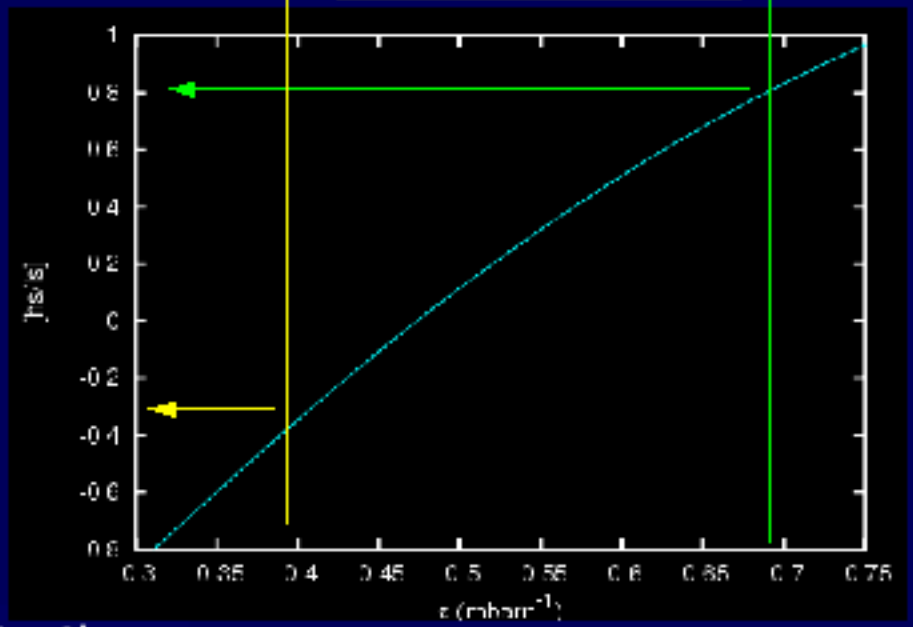

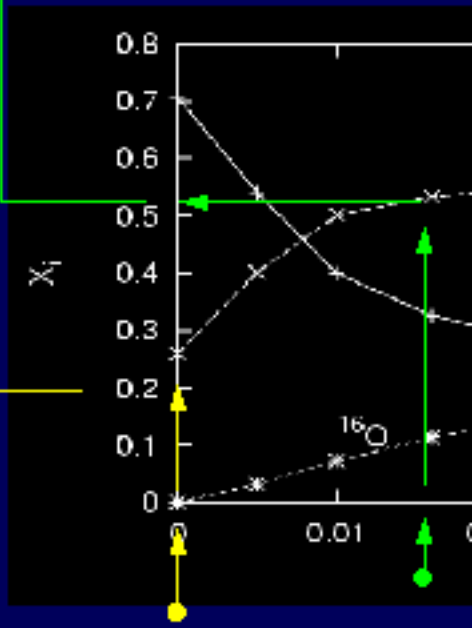

Lugaro etal (2003, ApJ 586, 1305)

Observations:

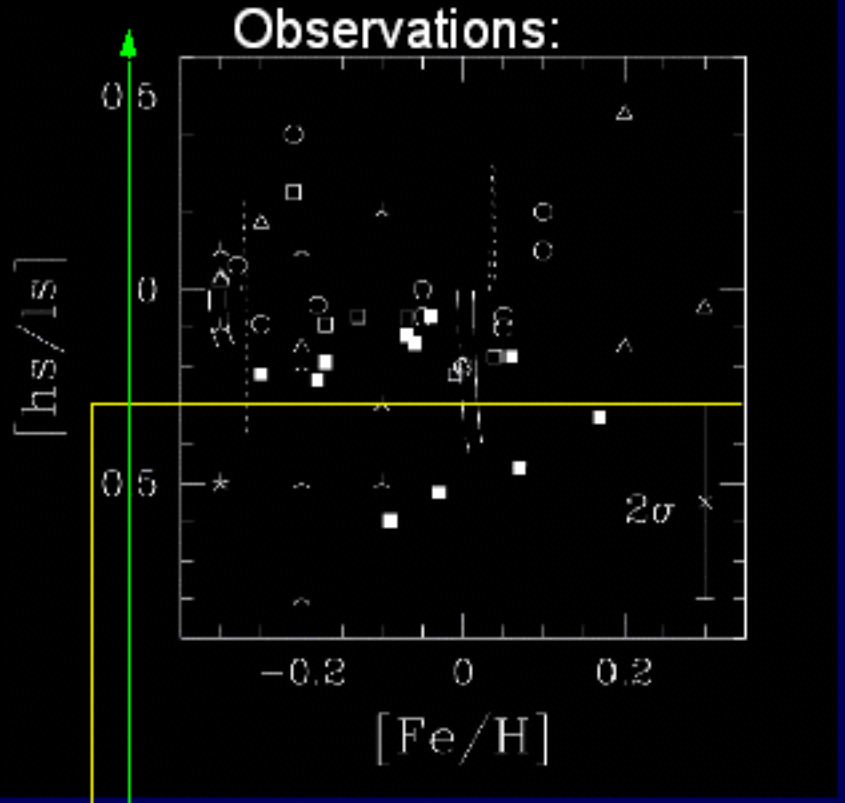

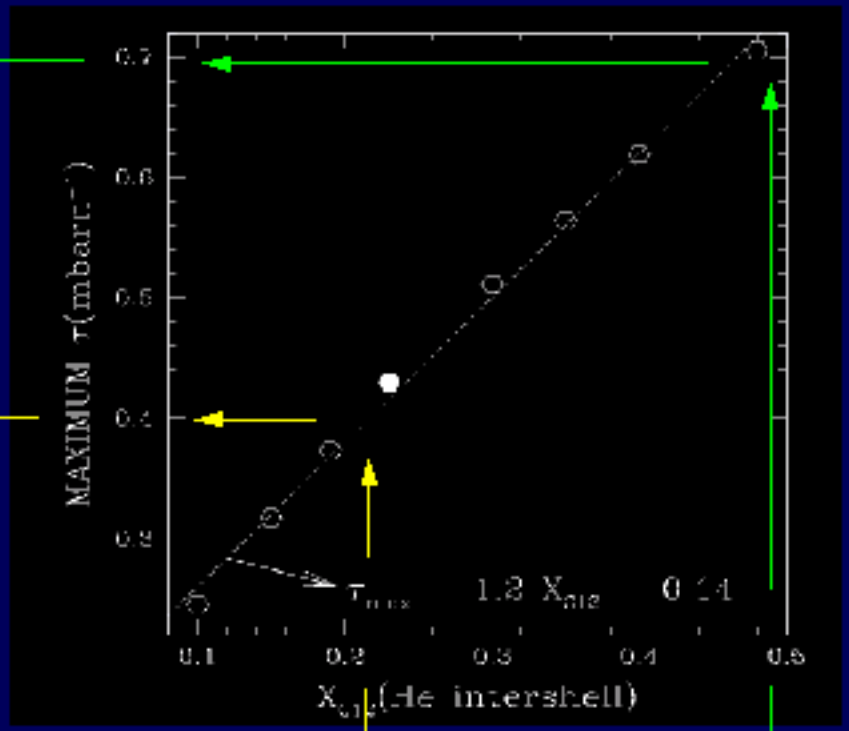

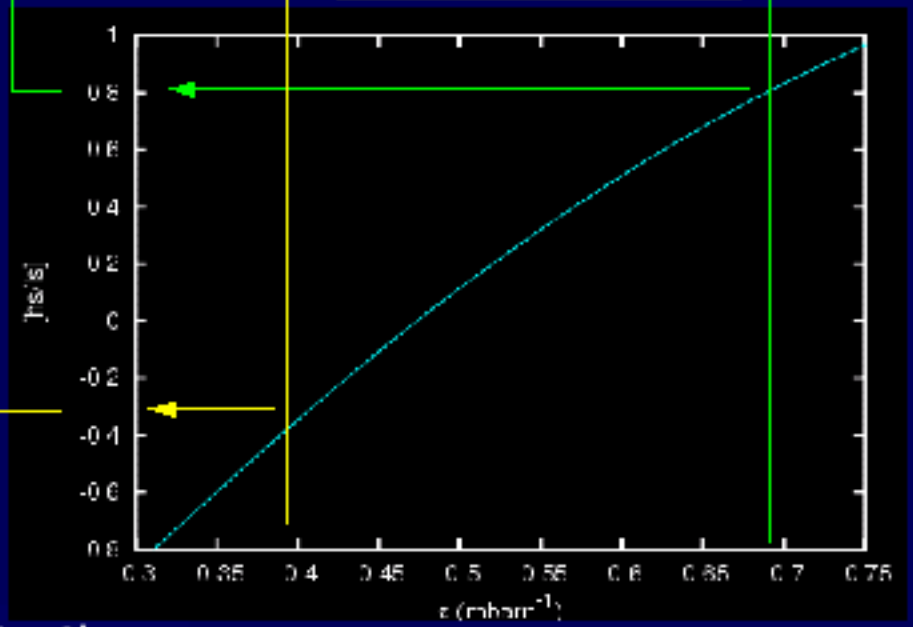

Model of convection:

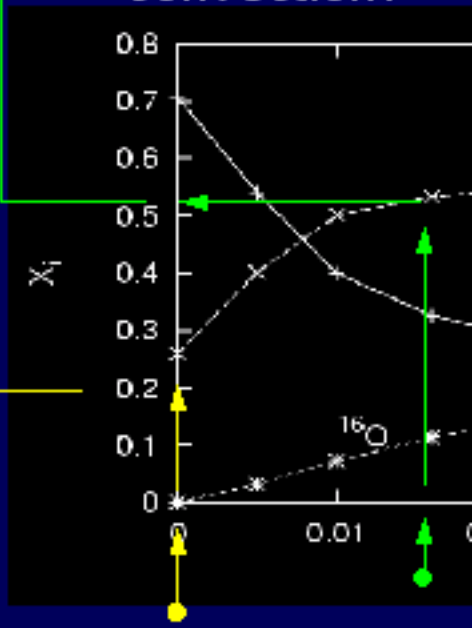

Large C abundance in intershell abundance of AGB stars implies too large neutron exposure in standard s-process model.

Is this the full story? *Stars rotate!*

The sun rotates!

White Dwarf rotation velocities: 0.1 … 1km/s (from asterio-seismology).

Is this fast or slow?

Rigidly rotating sun would die as WD with rotation $v \sim 10^{-4}$ km/s.

Large C abundance in intershell abundance of AGB stars implies too large neutron exposure in standard s-process model.

Something is missing: *Stars rotate!*

Rotating AGB stellar models (Langer etal 1999)

- 1D angular velocity evolution, angular momentum transport
- mixing due to rotionally induced instabilities
- Endal & Sofia (1976), Maeder &Meynet (2000), Heger etal (2000)

s-process in rotating AGB stellar models (Herwig etal 2003)

- shear mixing at envelope-core interface, i.e. in ^{13}C-pocket layer
- *s-process inhibited due to ^{14}N-neutron poison*

Key Mixing Hot Spots:

1. Dependence of IS abundance on OV
2. DUP dependence of OV, corrosive H-shell burnging in massive EMP stars
3. Mixing for ^{13}C pocket (GW/rot/OV picture)
4. Mixing during IP phase: rotation? Magnetic fields?

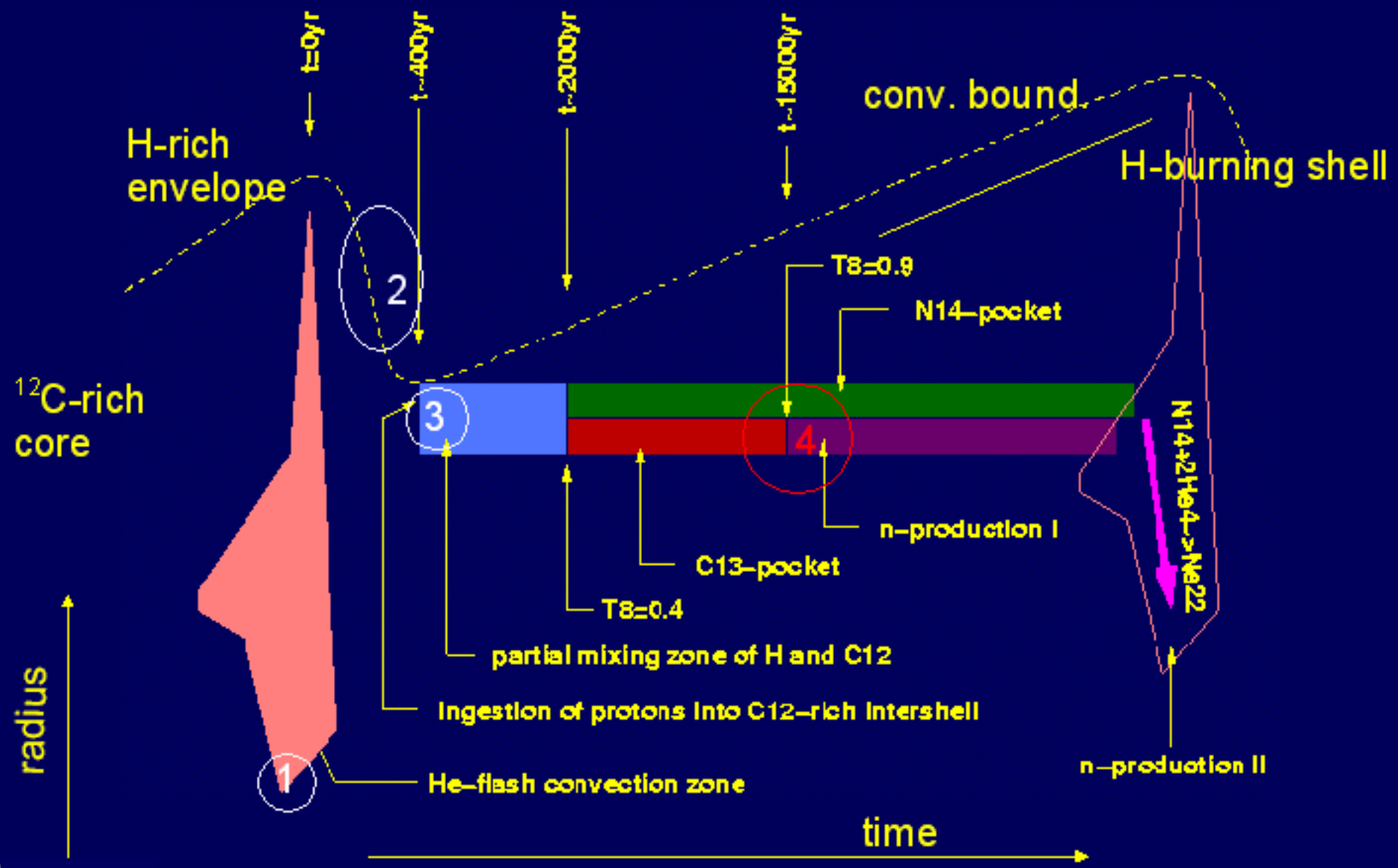

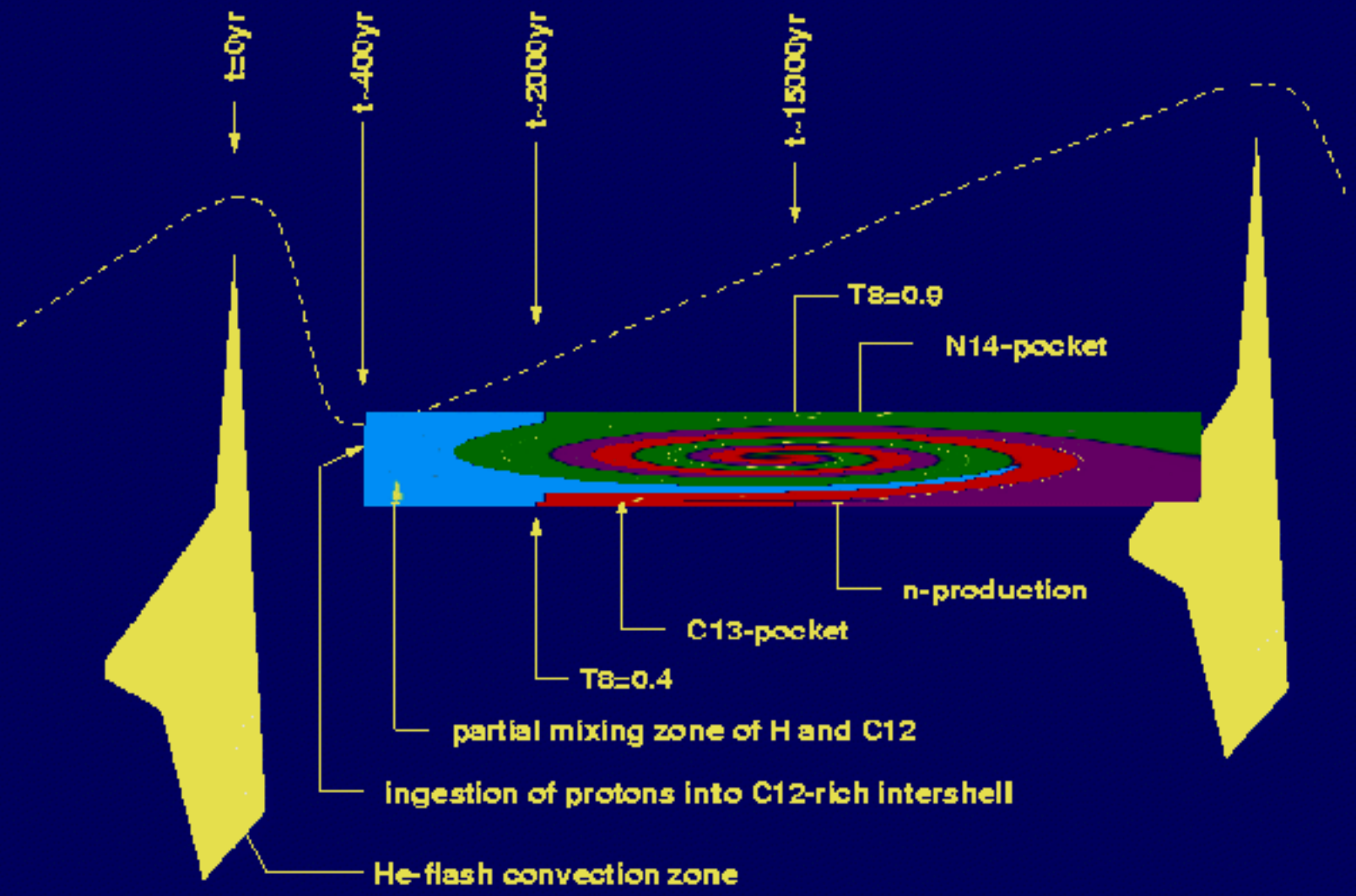

$^{14}N(n,p)^{14}C$ neutron poison

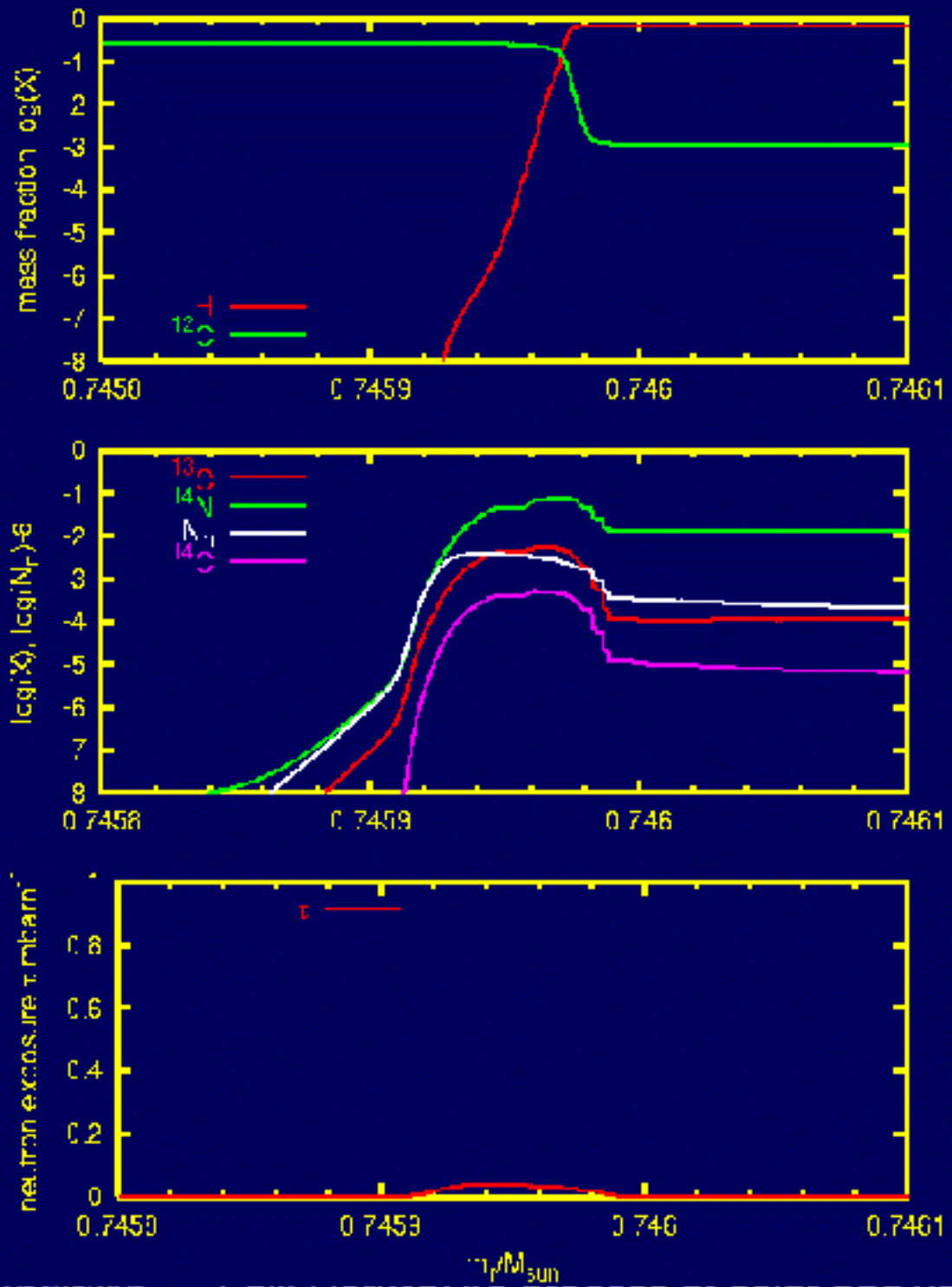

Rotating AGB model:

beginning of interpulse phase: formation of PM zone

^{13}C and ^{14}N pocket has formed, beginning of neutron release, ^{13}C pocket covered with ^{14}N, ^{14}N(n,p) reaction keeps τ down

final neutron exposure: very much too small, pocket a little too narrow

Herwig etal (2003)

Models with rotation ...

✗ Predicted rotation induced mixing inhibits the s-process.
✗ Predict core rotation rates ~30km/s larger than observed in WDs!

➔ angular momentum transport during progenitor evolution is more efficient than predicted

Hypothesis: Magnetic fields introduce friction and reduce angular velocity gradients -> Shear mixing at core-envelope interface may be reduced.

Synthetic models: start with PM zone from hydrodynamic overshooting model and apply constant slow mixing throughout interpulse phase (IP)

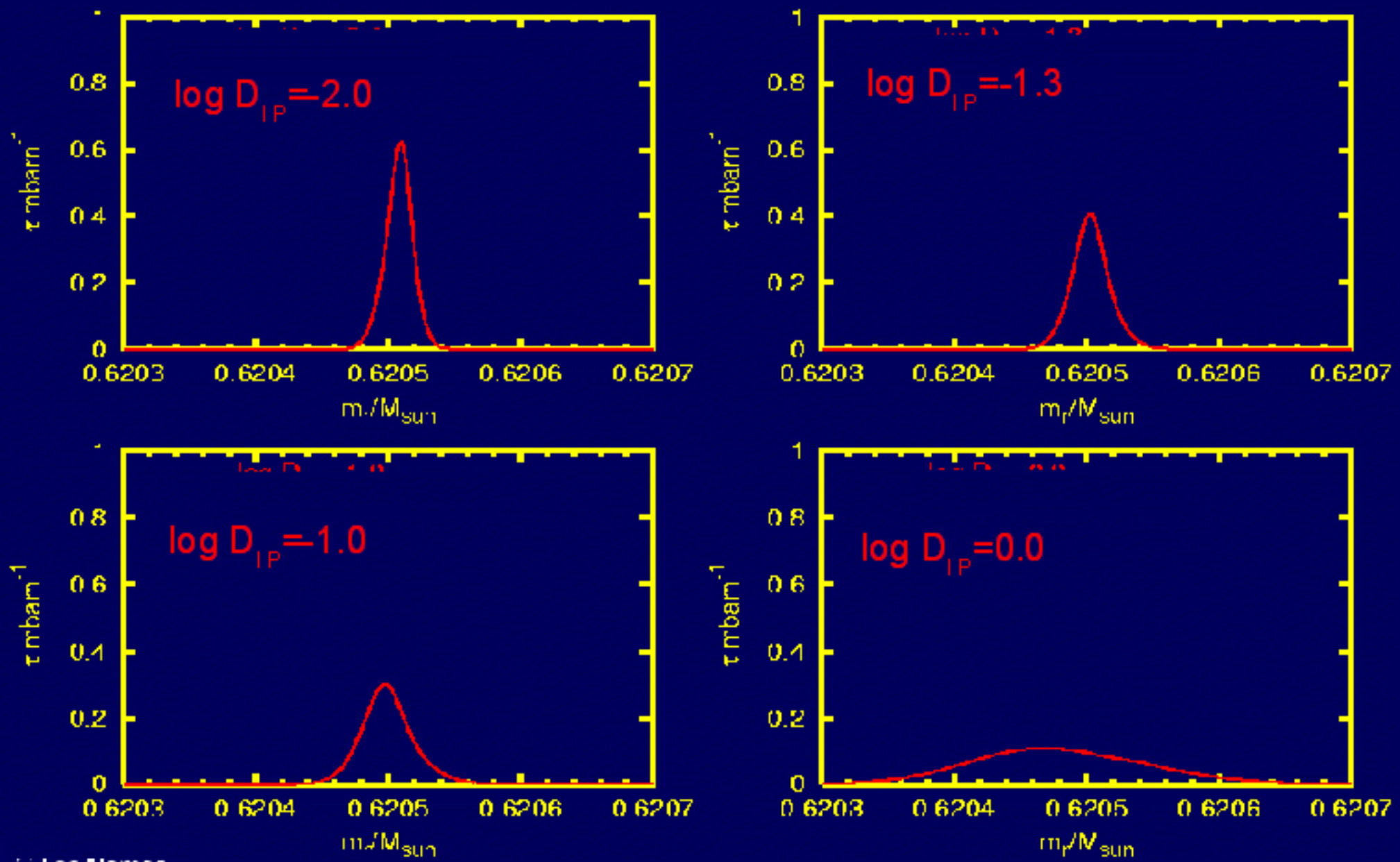

Isotopic studies on presolar grains

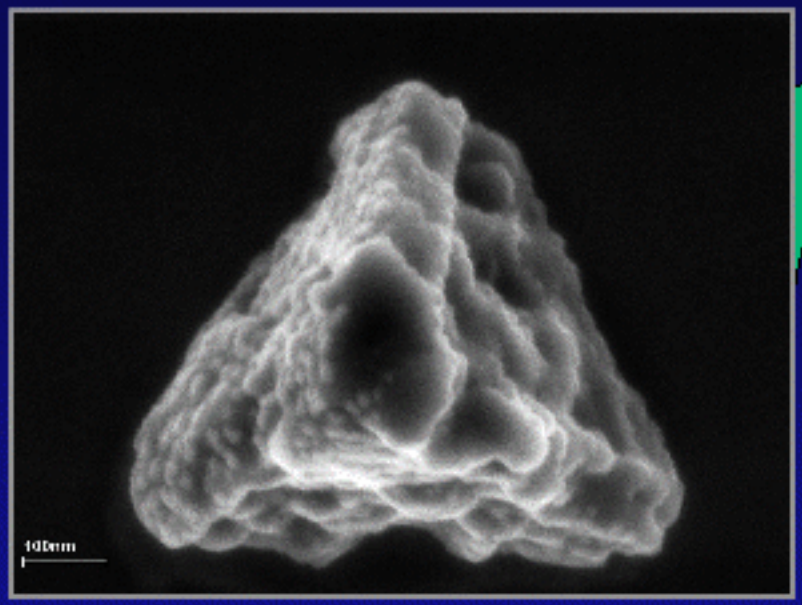

Presolar SiC

NanoSIMS 50 ion microprobe

(Slide from P. Hoppe, Max-Planck Institute for Chemistry, Mainz, Germany)

He-shell flash convection and branching at ^{95}Zr

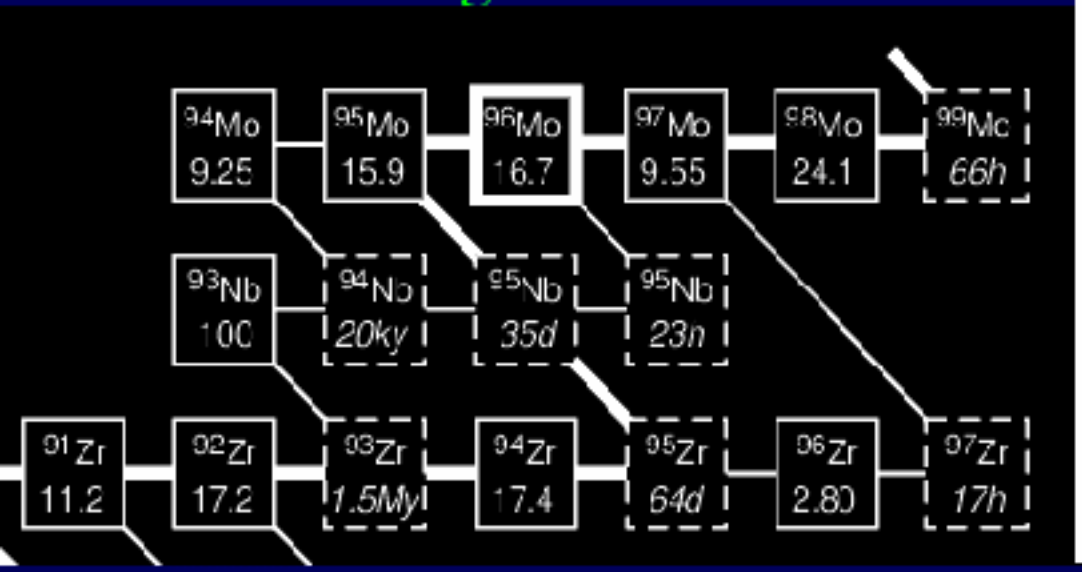

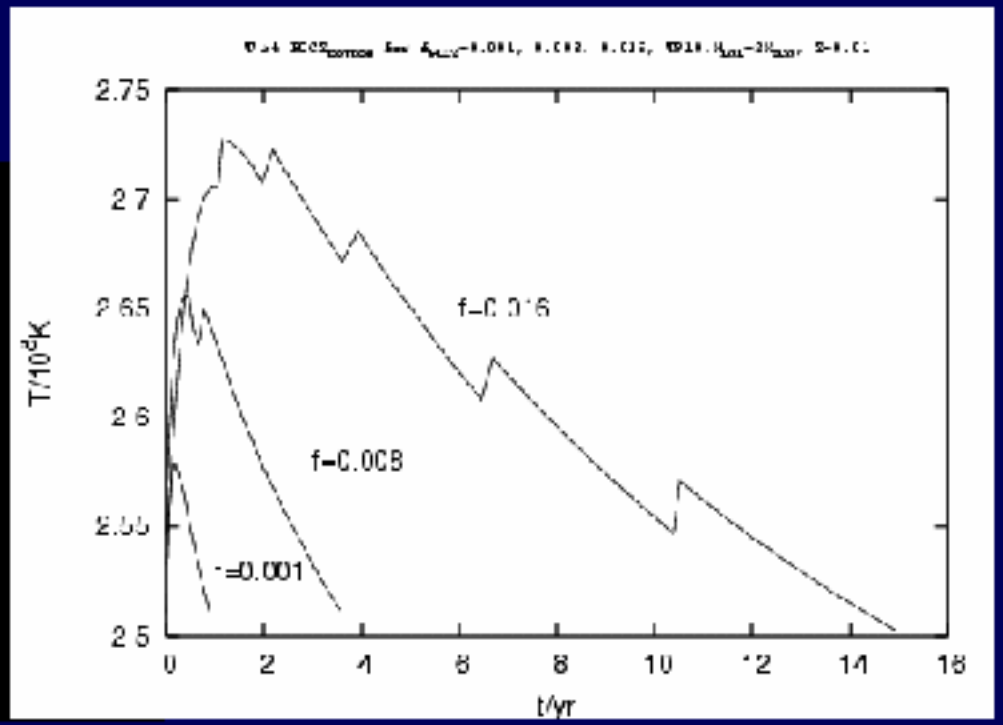

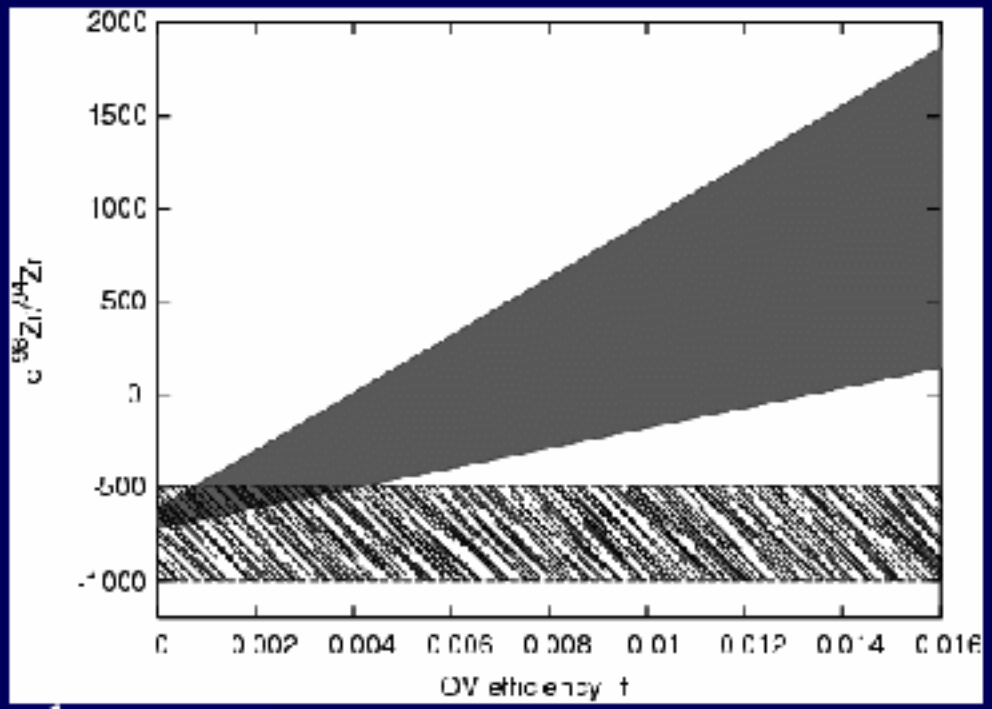

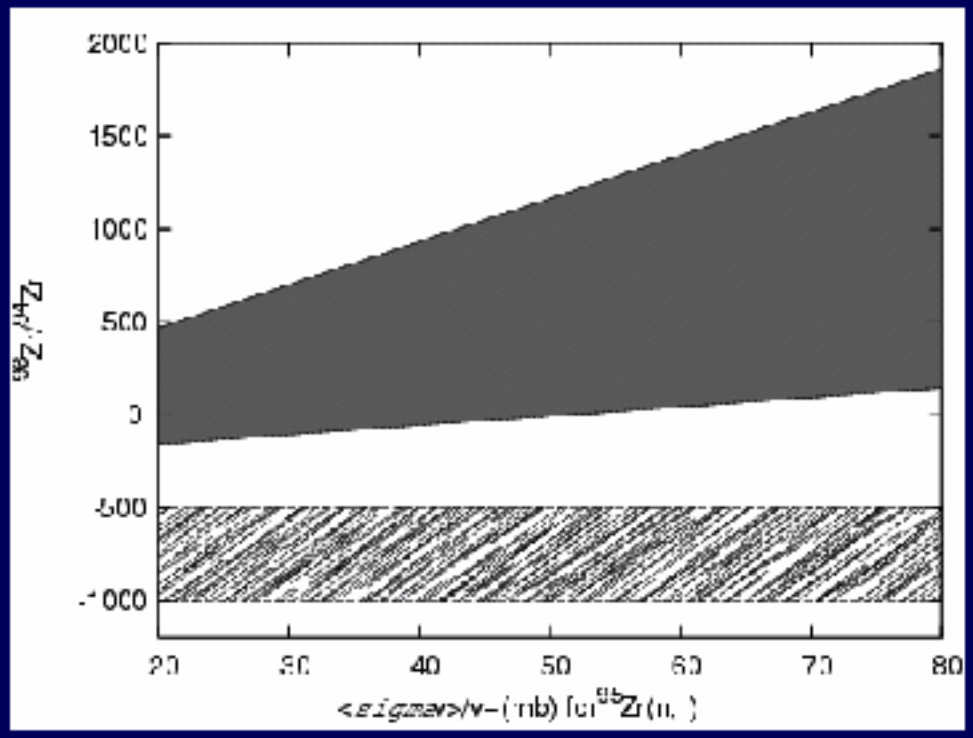

Yield uncertainty of AGB stars due to nuclear reaction rate uncertainty:

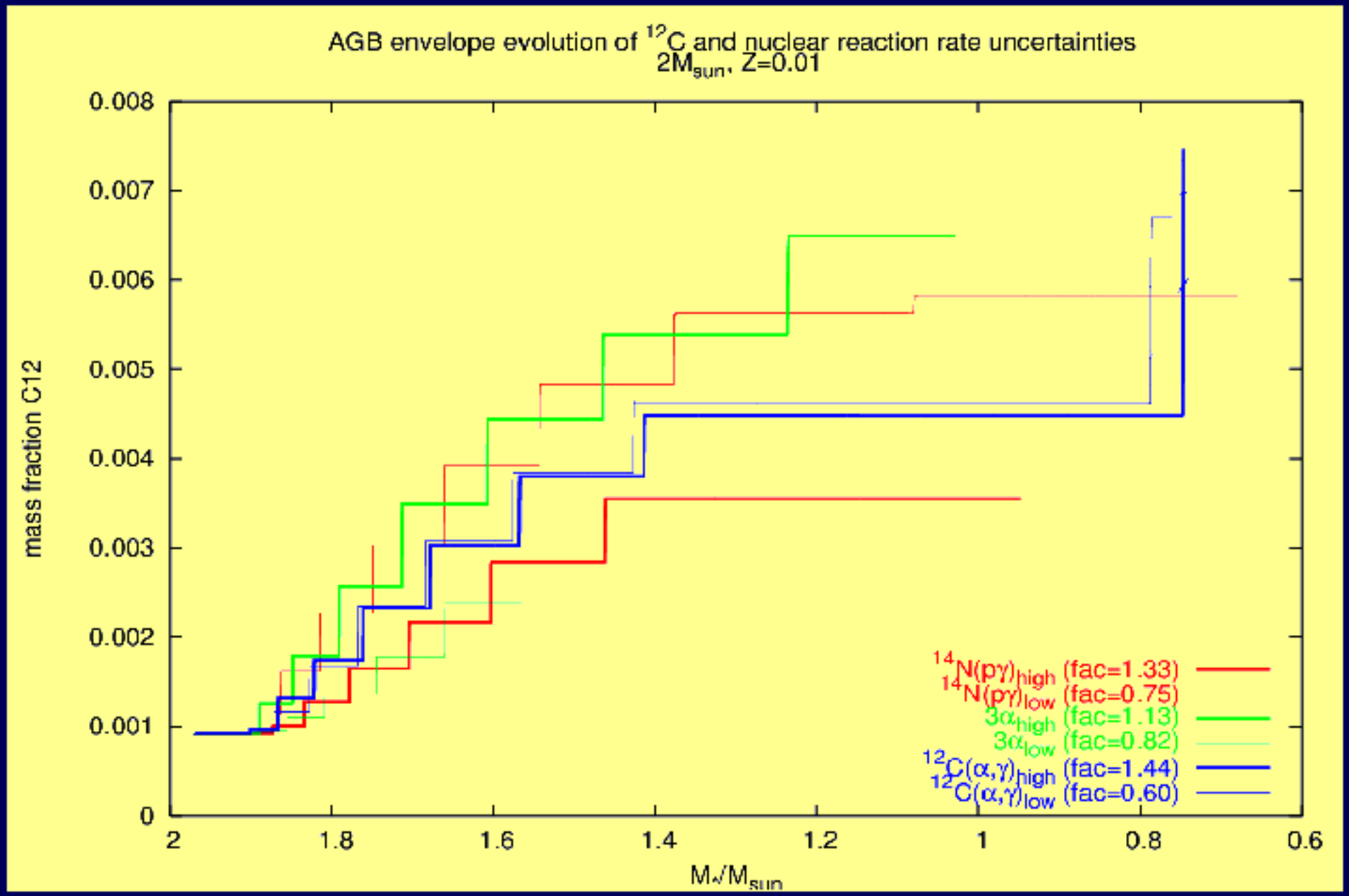

s-process and $^{13}C(\alpha,n)$ uncertainty in rotating and non-rotating AGB models:

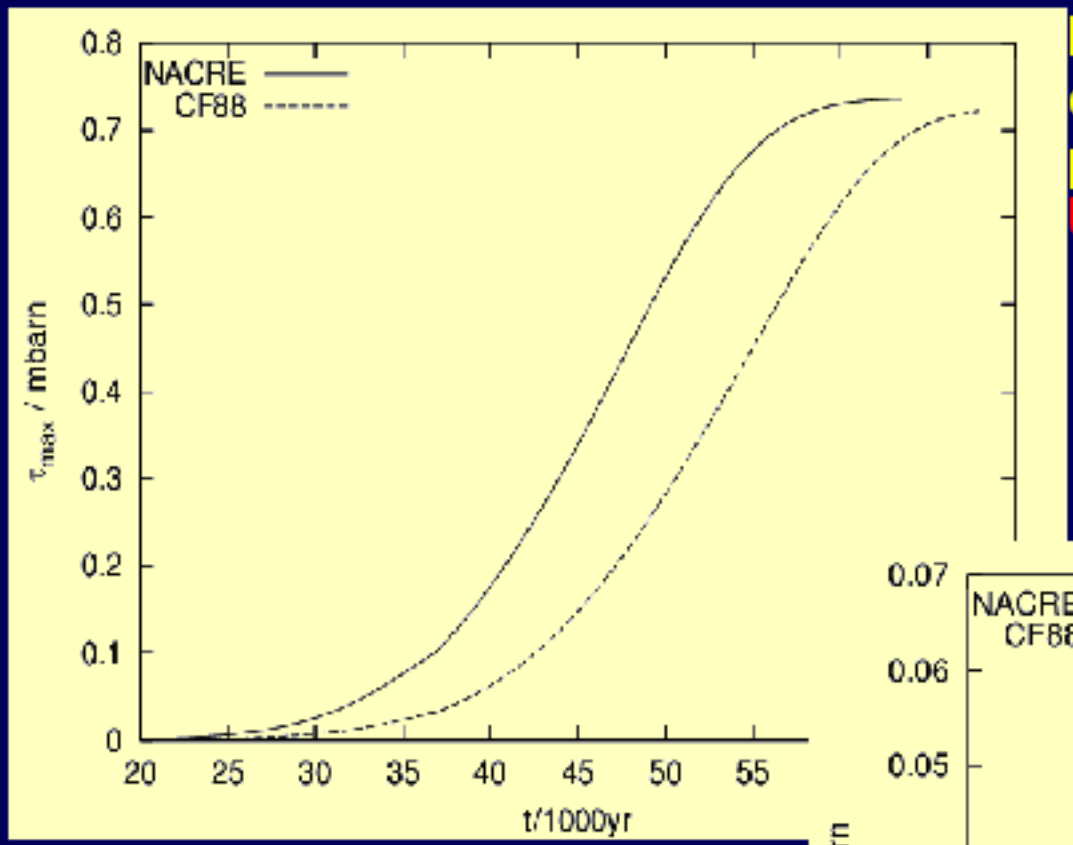

Non-rotating model: no mixing of ^{13}C-pocket during interpulse phase --->
Uncertainty not important.

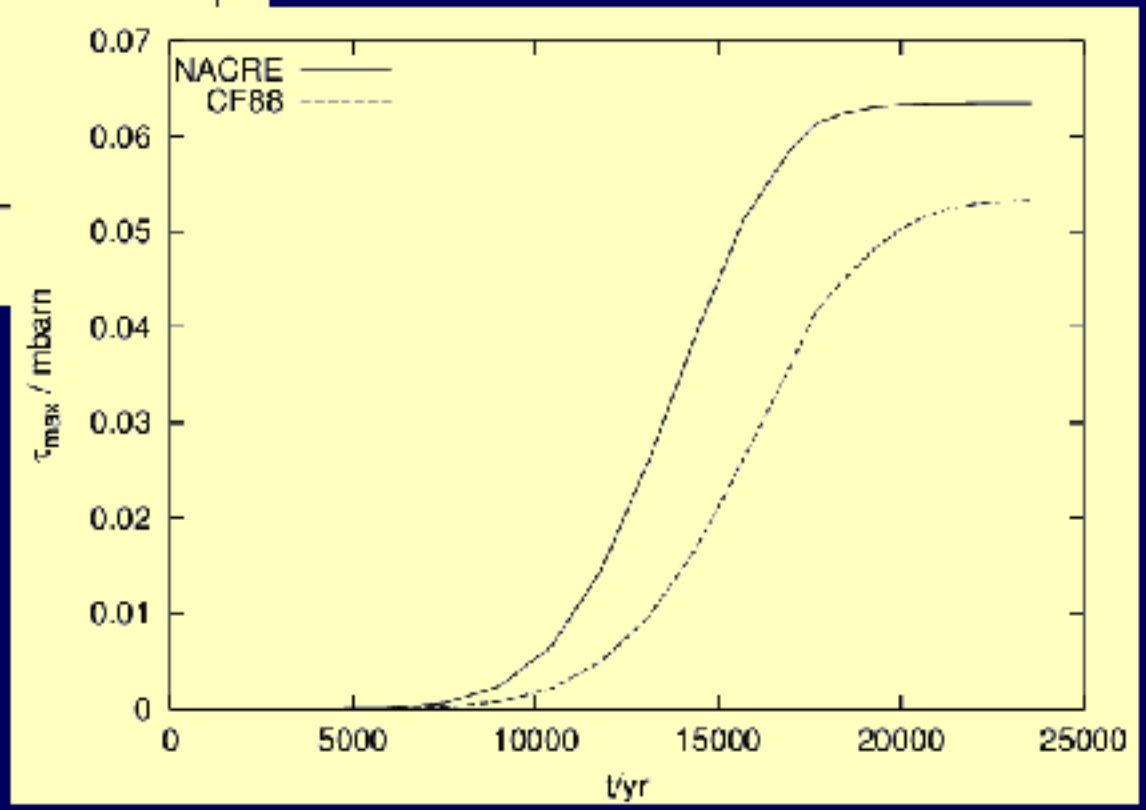

Rotating model: mixing of ^{13}C-pocket during interpulse phase.
---> Uncertainty important!

A new s-process and mixing code:

- multi-zone time-dependent mixing and full network from H to Pb
- simultaneous fully-implicit solution
- e.g. for s-process in He-shell flash convection zone
- T-dependent capture rates and β-decays,
- short life times comparable to t_{conv}

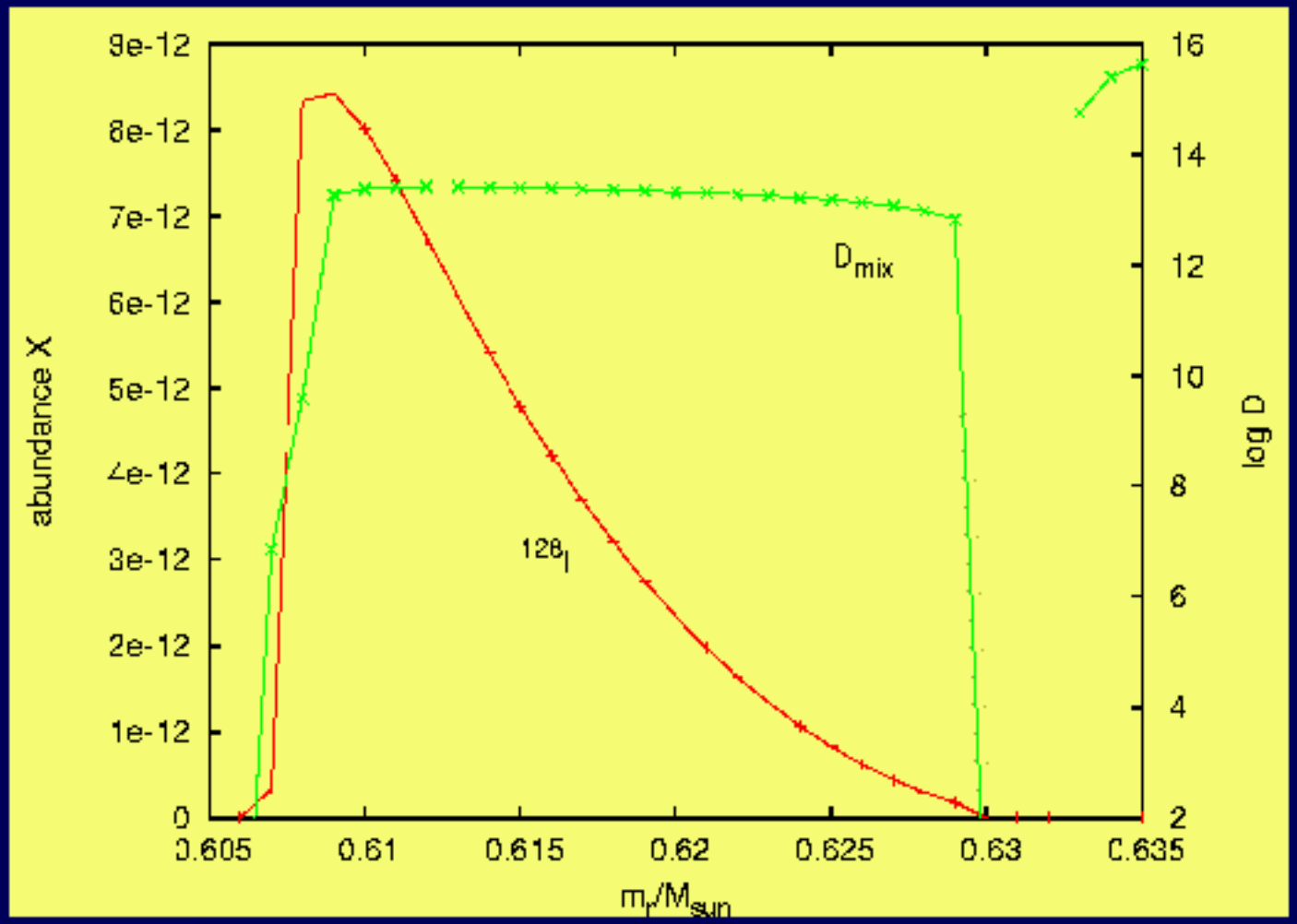

Example (remember Kaeppeler talk!):

^{128}I, $t_{1/2}$=25min

snapshot in advanced TP $2M_{sun}$, Z=0.01 sequence

Z=0: s-process

- no Fe-seed
- in He-shell plenty of primary ^{12}C, can act as seed
- Neutron source (both ^{12}C and ^{22}Ne) primary

one-zone calculation, initial abundance:

$X(^{4}He)=0.72$

$X(^{12}C)=0.23$

$X(^{13}C)=0.03$

$X(^{16}O)=0.02$

all other X=0

$T_8=0.9$

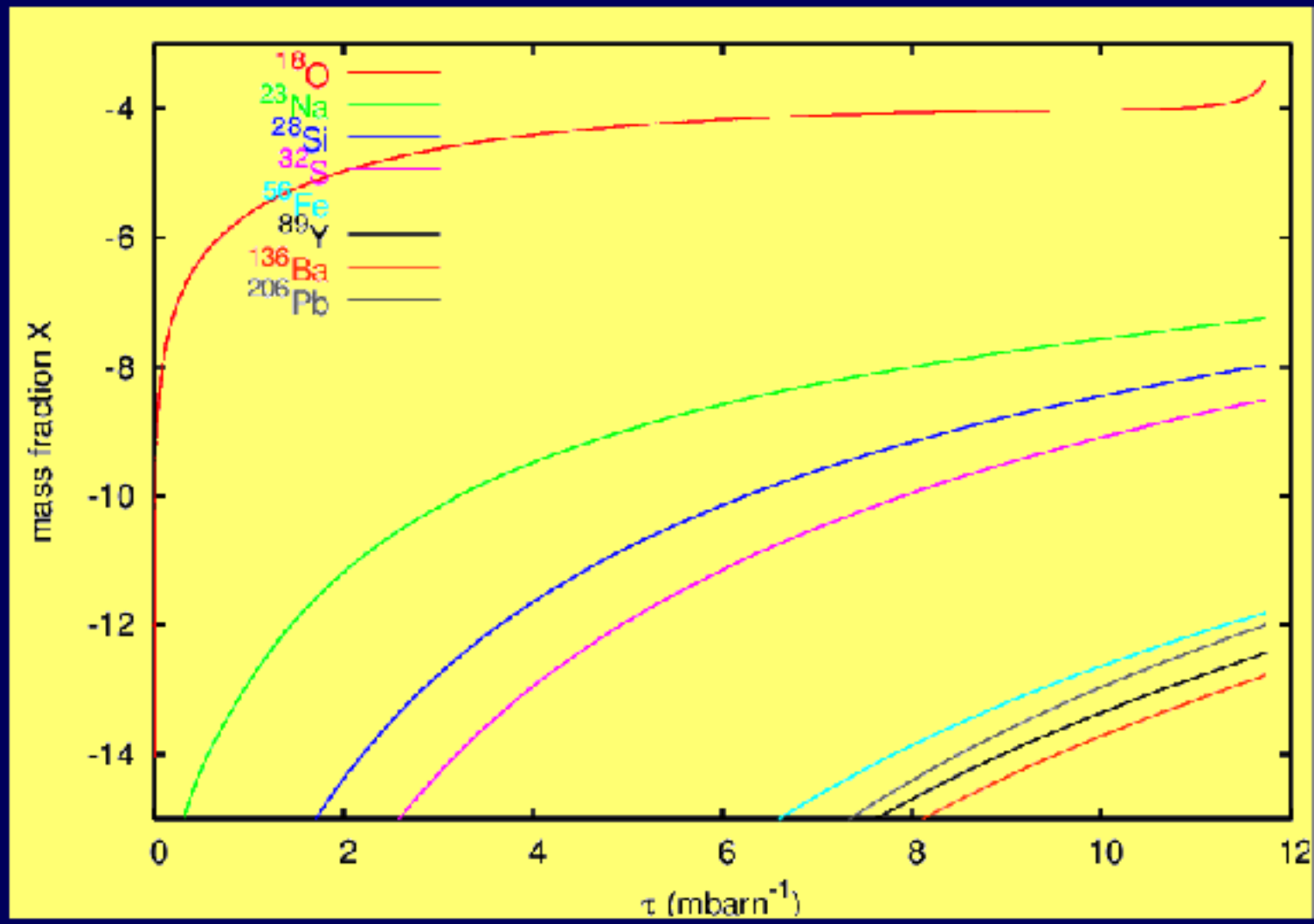

Z=0: evolution

- no CNO for CNO cycle
- H-shell very hot
- may show HIF (Hydrogen-ingestion flash)

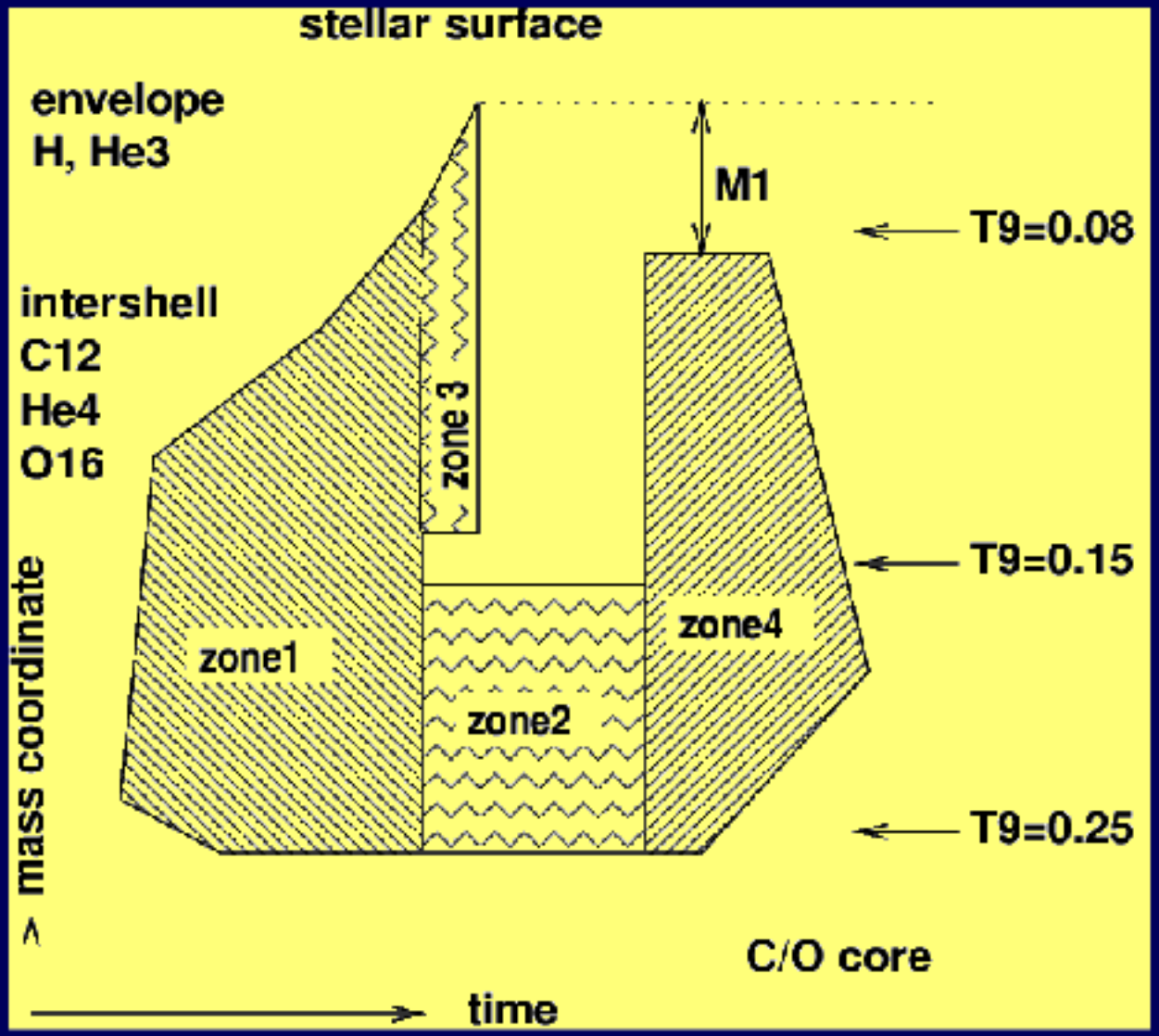

Ingestion of H into He-flash convection (Fujimoto etal 2000)

Known or suspected to happen in several other situations, e.g. young WDs (born again AGB stars)
Herwig etal 1999, Herwig 2001

- whether or not HIF occurs depends on excact interplay of convection, rotation and likely also magnetic fields
- and so does the exact morphology of the different zone
- this determines the nuclear evolution

$M=5M_{sun}$, Z=0.0, time sequence of profiles in H-flash region (on top of He-shell flash convection zone)

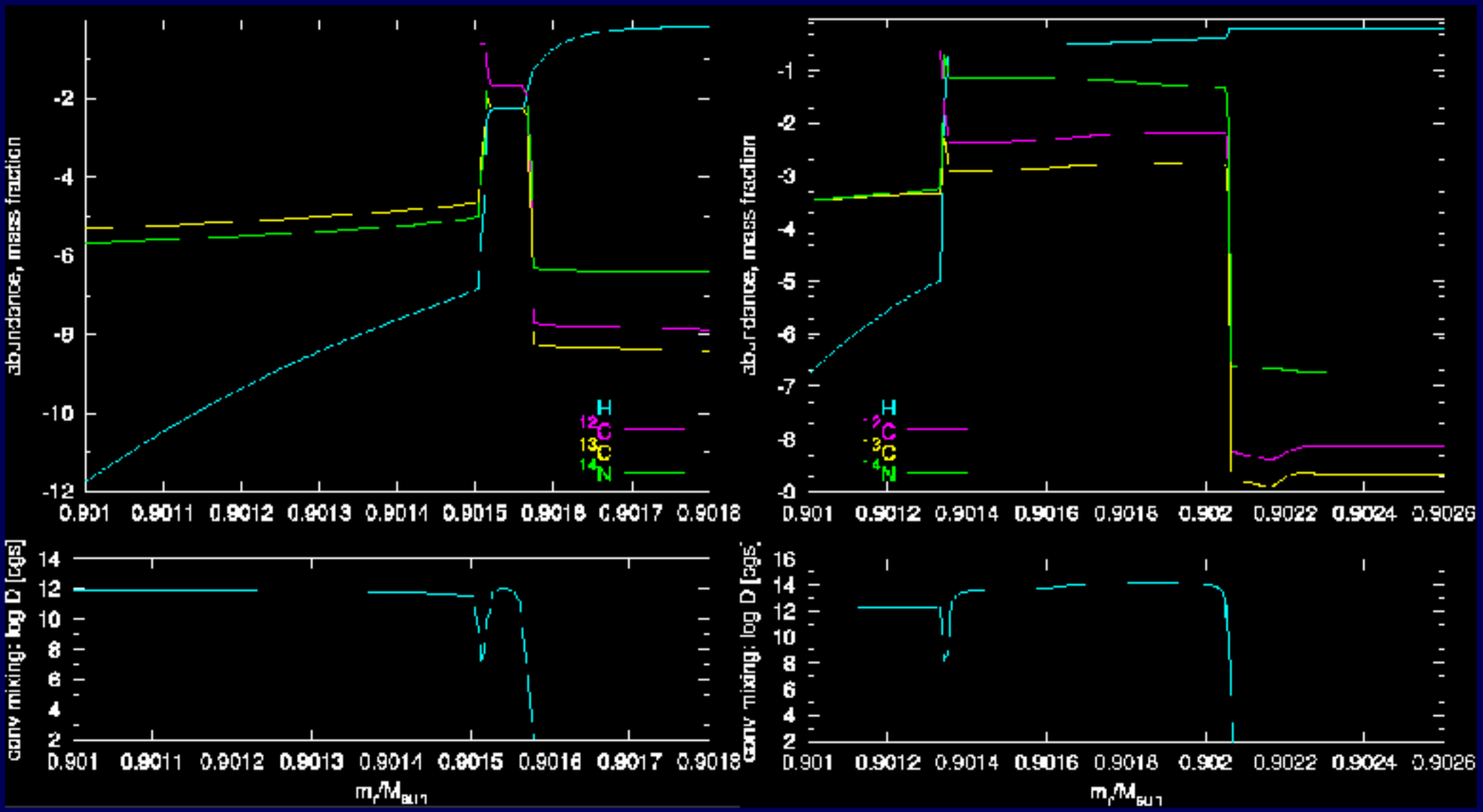

$Z=10^{-4}$: evolution

- Herwig 2003, ApJ in press, ApJS in prep
- overal *normal* AGB evolution, TPs etc
- corrosive H-burning during DUP phase
  -> may lead to termination of AGB phase

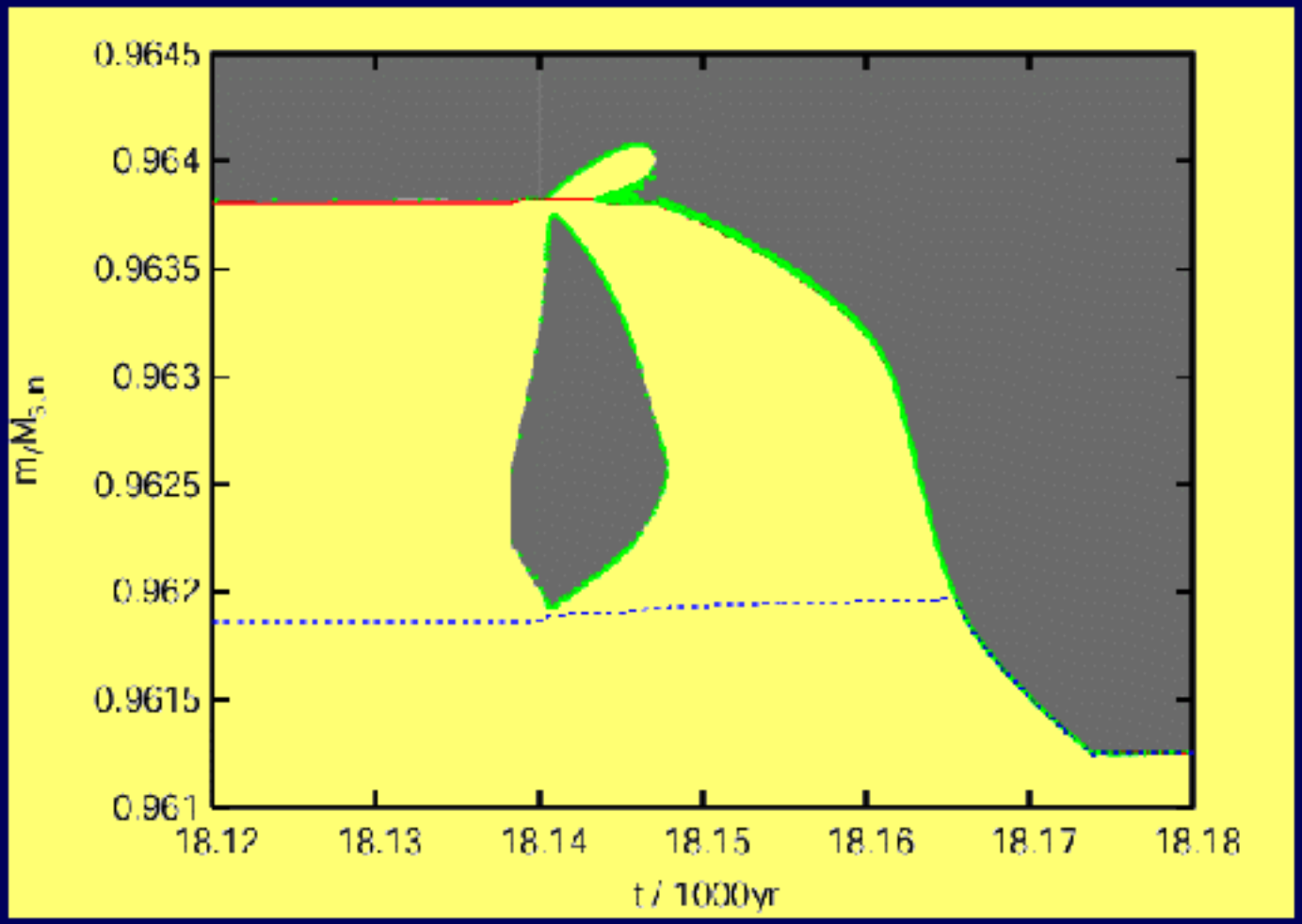

Early TP during $5M_{sun}$ sequence.

f_{OV}=0.016 (=10x smaller than what would be required for ^{13}C-pocket).

Conclusions

I. Use grains and other observables to verify modelling of physical processes (convection, rotation, magnetic fields).

II. With this knowledge: The first s-process.

III. Accurate nuclear reaction for validation and model prediction.

IV. New mixing and network s-process codes.

Contribution by

Alexander Heger

Los Alamos National Laboratory
aheger@lanl.gov

34 pages

s- and p-process in massive stars

Alexander Heger
Stan Woosley
Rob Hoffman
Tommy Rauscher
Karlheinz Langanke

http://nucleosynthesis.org

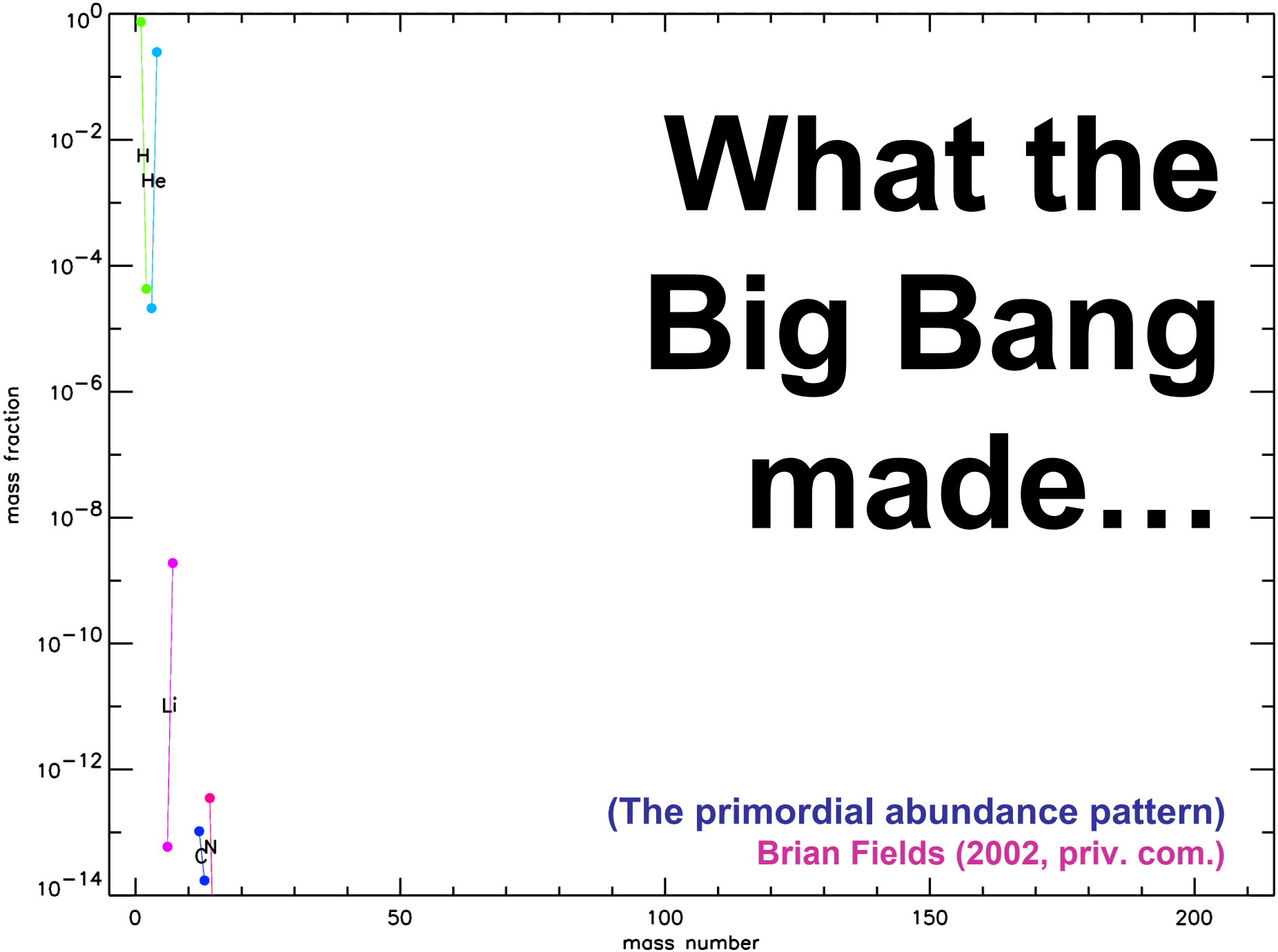

What the Big Bang made…

(The primordial abundance pattern)

Brian Fields (2002, priv. com.)

What We Find Today

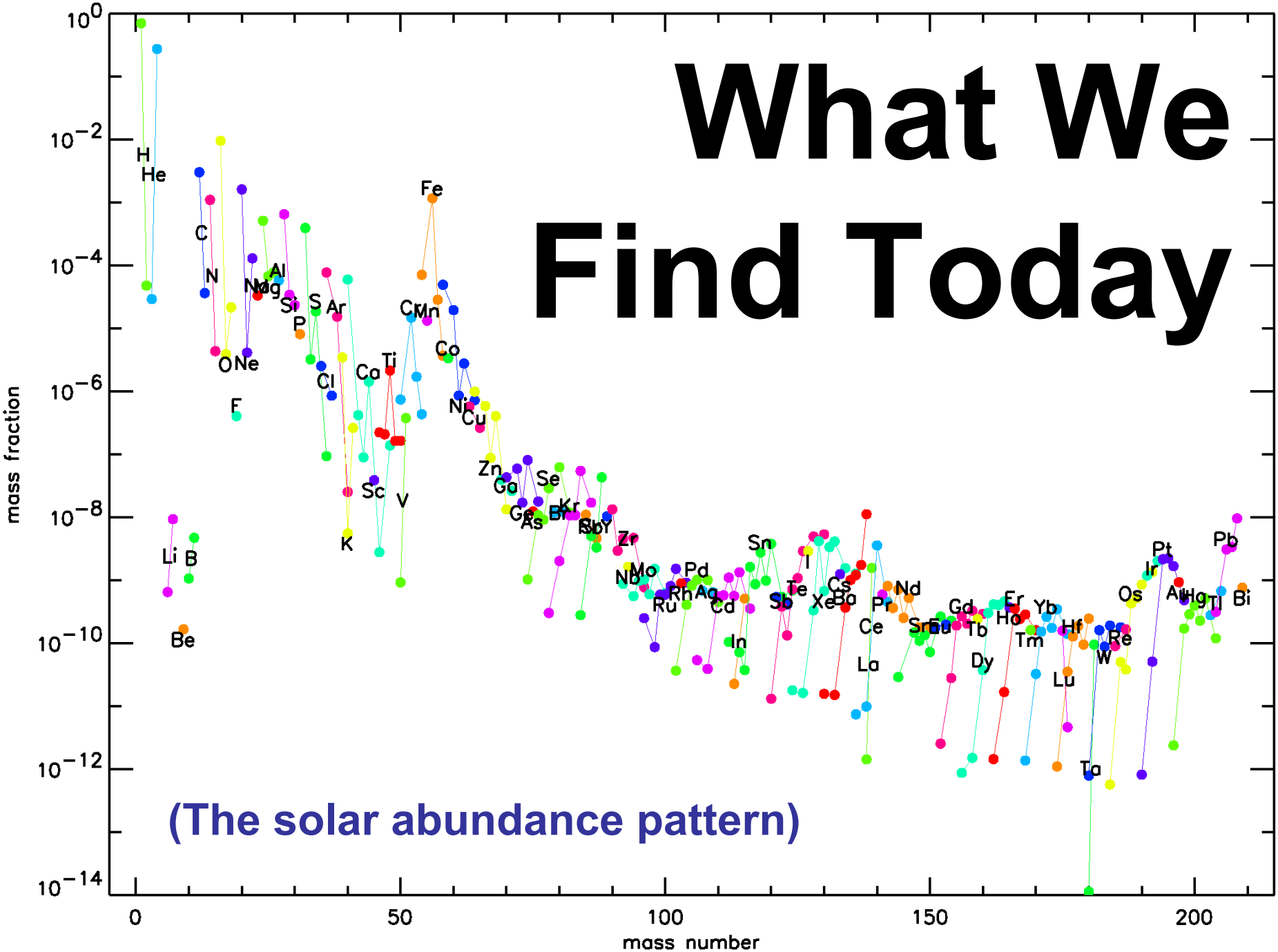

(The solar abundance pattern)

Relative Abundance by Weight

Universe

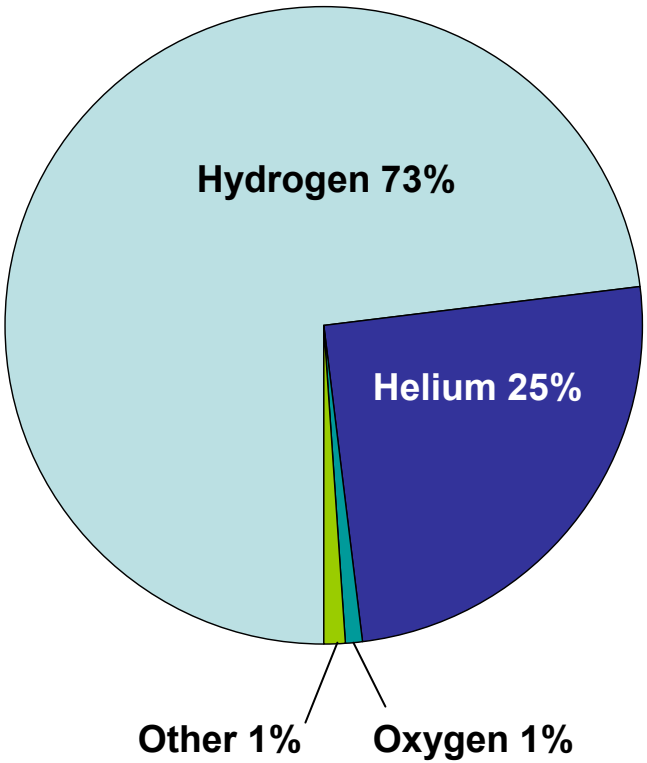

Humans

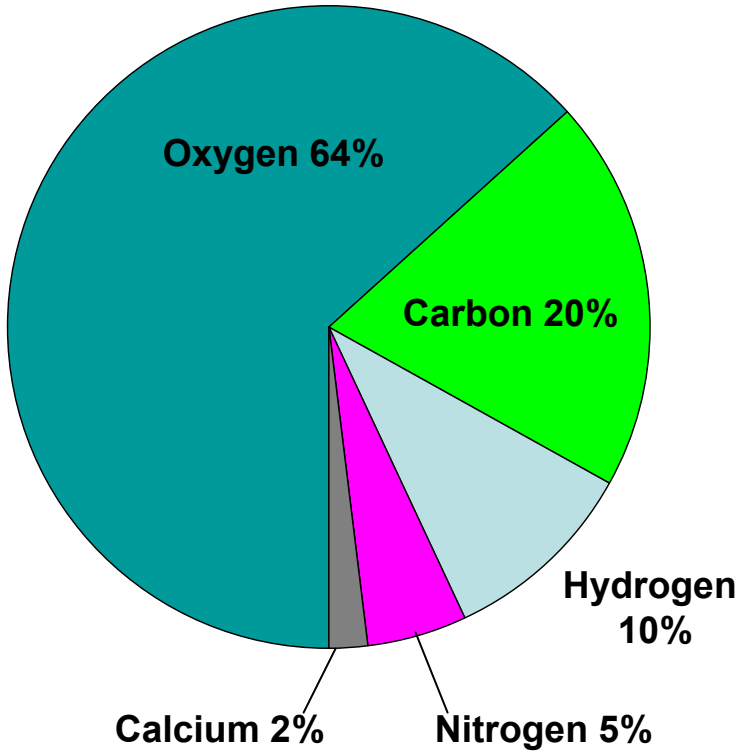

Overview

- Introduction
- Evolution of massive stars
- Nucleosynthesis in core collapse supernovae
- **s-Process** in massive stars
- **p-Process:** ν-process & γ-process
- Conclusions

Massive Stars

Once formed, the evolution of a star is governed by gravity:

continuing contraction

to higher central densities and temperatures

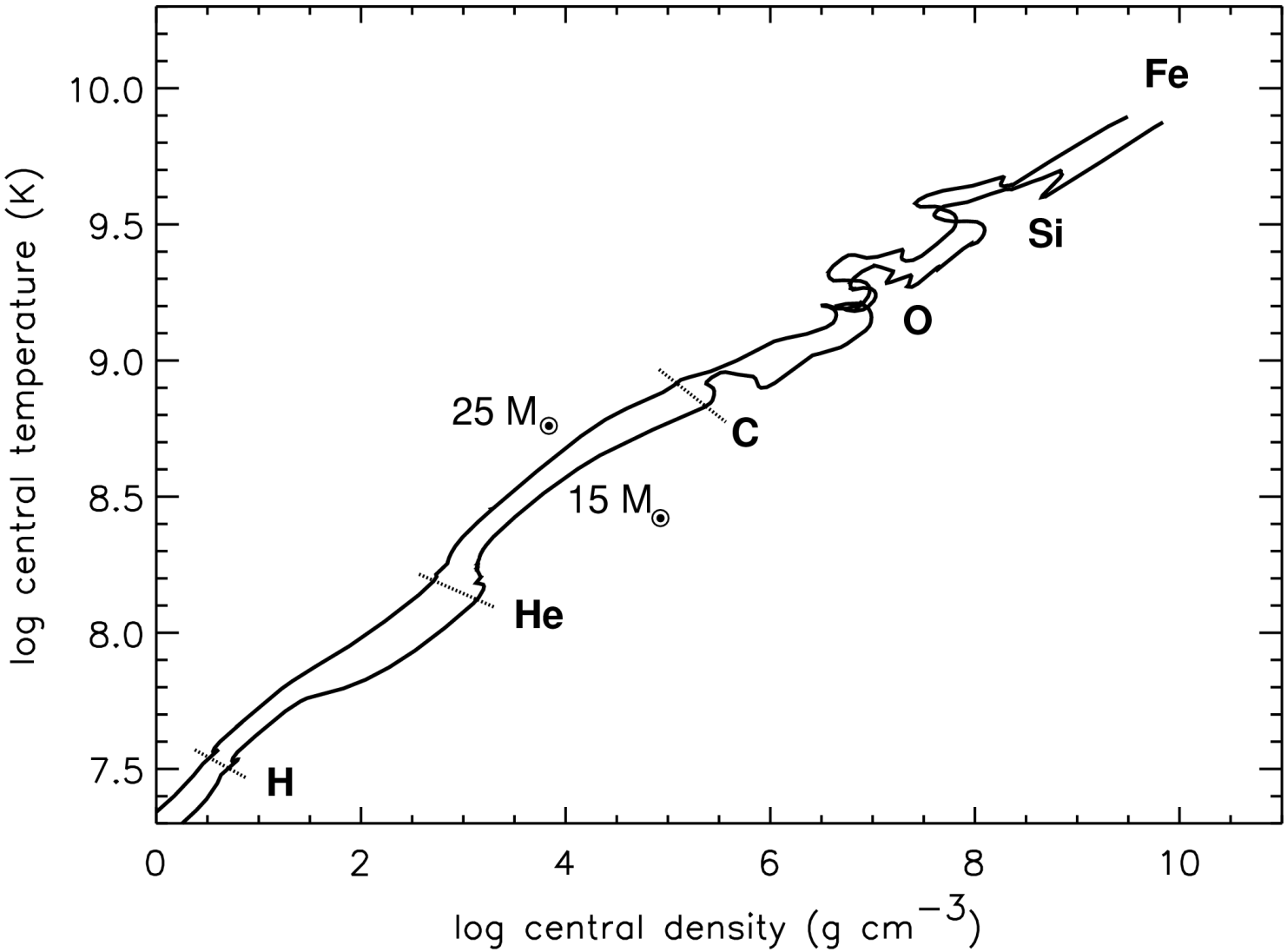

Evolution of central density and temperature of 15 $M_\odot$ and 25 $M_\odot$ stars

Nuclear burning stages

(e.g., 20 solar mass star)

Fuel	Main Product	Secondary Product	T (10^9 K)	Time (yr)	Main Reaction
H	He	^{14}N	0.02	10^7	$4\ H \xrightarrow{CNO} {}^4He$
He	O, C	^{18}O, ^{22}Ne s-process	0.2	10^6	$3\ He^4 \rightarrow {}^{12}C$ ${}^{12}C(\alpha,\gamma){}^{16}O$
C	Ne, Mg	Na	0.8	10^3	${}^{12}C + {}^{12}C$
Ne	O, Mg	Al, P	1.5	3	${}^{20}Ne(\gamma,\alpha){}^{16}O$ ${}^{20}Ne(\alpha,\gamma){}^{24}Mg$
O	Si, S	Cl, Ar, K, Ca	2.0	0.8	${}^{16}O + {}^{16}O$
Si	Fe	Ti, V, Cr, Mn, Co, Ni	3.5	0.02	${}^{28}Si(\gamma,\alpha)\ldots$

Neutrino losses from electron/positron pair annihilation

- Important for carbon burning and beyond

- For $T>10^9$ K (about 100 keV), occasionally:

  $$\gamma \rightarrow e^+ + e^-$$

  and usually

  $$e^+ + e^- \rightarrow 2\gamma$$

  but sometimes

  $$e^+ + e^- \rightarrow \nu_e + \overline{\nu}_e$$

- The neutrinos exit the stars at the speed of light while the e^+, e^-, and the γ's all stay trapped.

- This is an important energy loss with $\varepsilon_\nu \approx -10^{15}\,(T/10^9\mathrm{K})^9$ erg g^{-1} s^{-1}

- For carbon buring and beyond, each burning stage gives about the same energy per nucleon, thus the lifetime goes down as T^{-9}

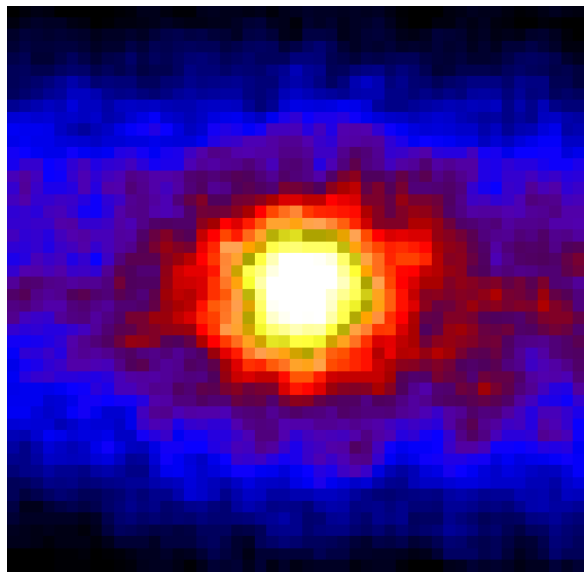

The sun as seen by Kamiokande

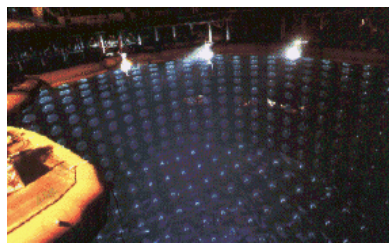

Explosive Nucleosynthesis

in supernovae

Fuel	Main Product	Secondary Product	T (10^9 K)	Time (s)	Main Reaction
Innermost ejecta	*r*-process	-	>10 low Y_e	1	(n,γ), β^-
Si, O	^{56}Ni	iron group	>4	0.1	(α,γ)
O	Si, S	Cl, Ar, K, Ca	3 - 4	1	^{16}O + ^{16}O
O, Ne	O, Mg, Ne	Na, Al, P	2 - 3	5	(γ,α)
		p-process ^{11}B, ^{19}F, ^{138}La, ^{180}Ta	2 - 3	5	(γ,n)
		ν-process		5	(ν, ν'), (ν, e$^-$)

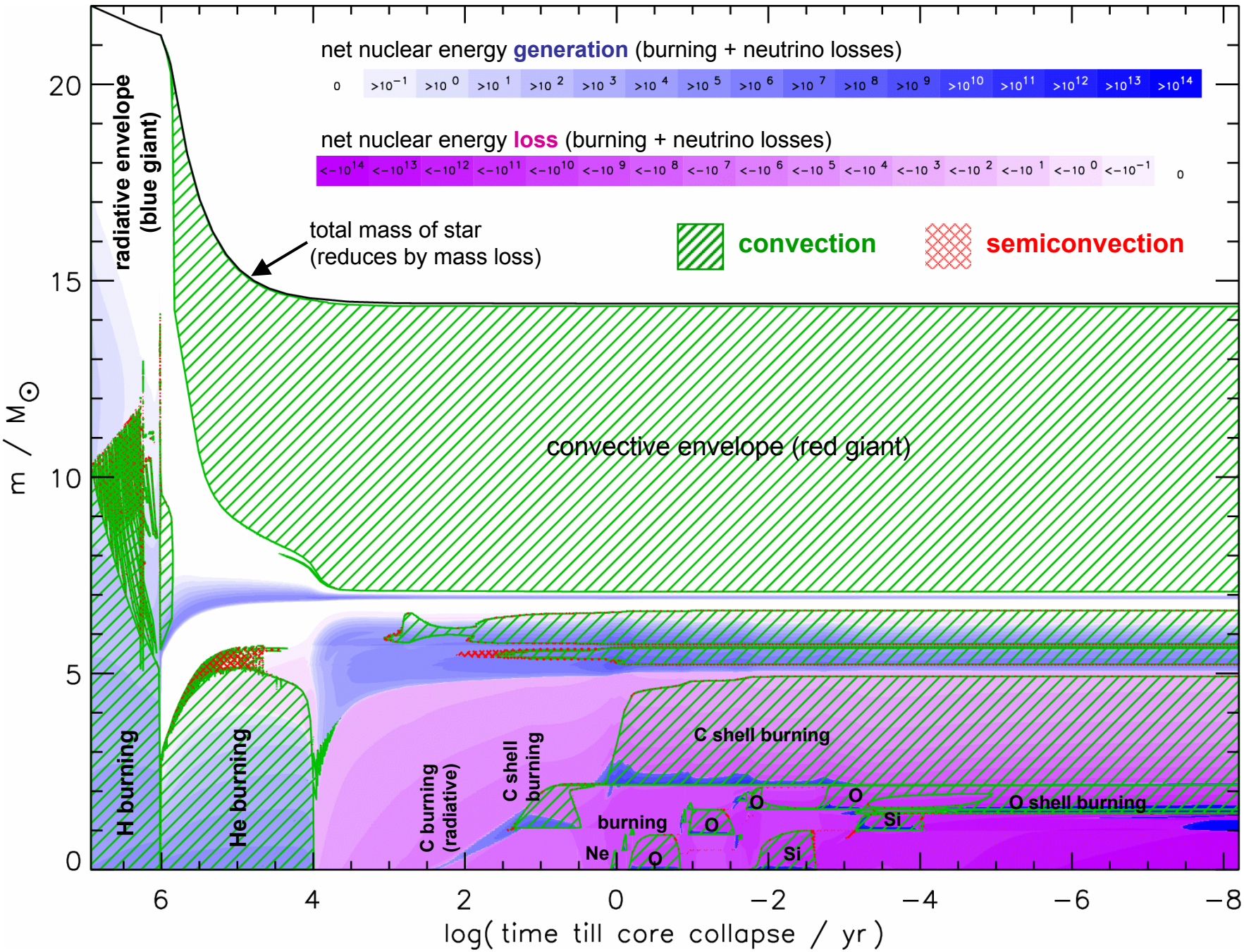
net nuclear energy generation (burning + neutrino losses)
0
>10^−1
>10^0
>10^1
>10^2
>10^3
>10^4
>10^5
>10^6
>10^7
>10^8
>10^9
>10^10
>10^11
>10^12
>10^13
>10^14
net nuclear energy loss (burning + neutrino losses)
<−10^14
<−10^13
<−10^12
<−10^11
<−10^10
<−10^9
<−10^8
<−10^7
<−10^6
<−10^5
<−10^4
<−10^3
<−10^2
<−10^1
<−10^0
<−10^−1
0
total mass of star
(reduces by mass loss)
convection
semiconvection
radiative envelope
(blue giant)
convective envelope (red giant)
H burning
He burning
C burning
(radiative)
C shell
burning
C shell burning
burning
Ne
O
O
O
Si
Si
O shell burning
m / M⊙
log(time till core collapse / yr)
20
15
10
5
0
6
4
2
0
−2
−4
−6
−8

Change of the stellar structure as a function of initial mass

- Mass loss becomes more important
- The “cores” becomes bigger,
  the density gradients more shallow
- The evolution time-scale of all burning phases accelerates
- Central carbon burning becomes radiative, central entropy and Y_e increase

The Calculations

- Complete stellar evolution calculations including all relevant isotopes up to bismuth
- We include most recent experimental and theoretical nuclear reaction rates
- Supernova explosion and explosive nucleosynthesis is followed in (one-dimensional) hydrodynamic calculation (explosion model parameterized)
- Nucleosynthesis by “hot” neutrinos form the proto-neutron star is included

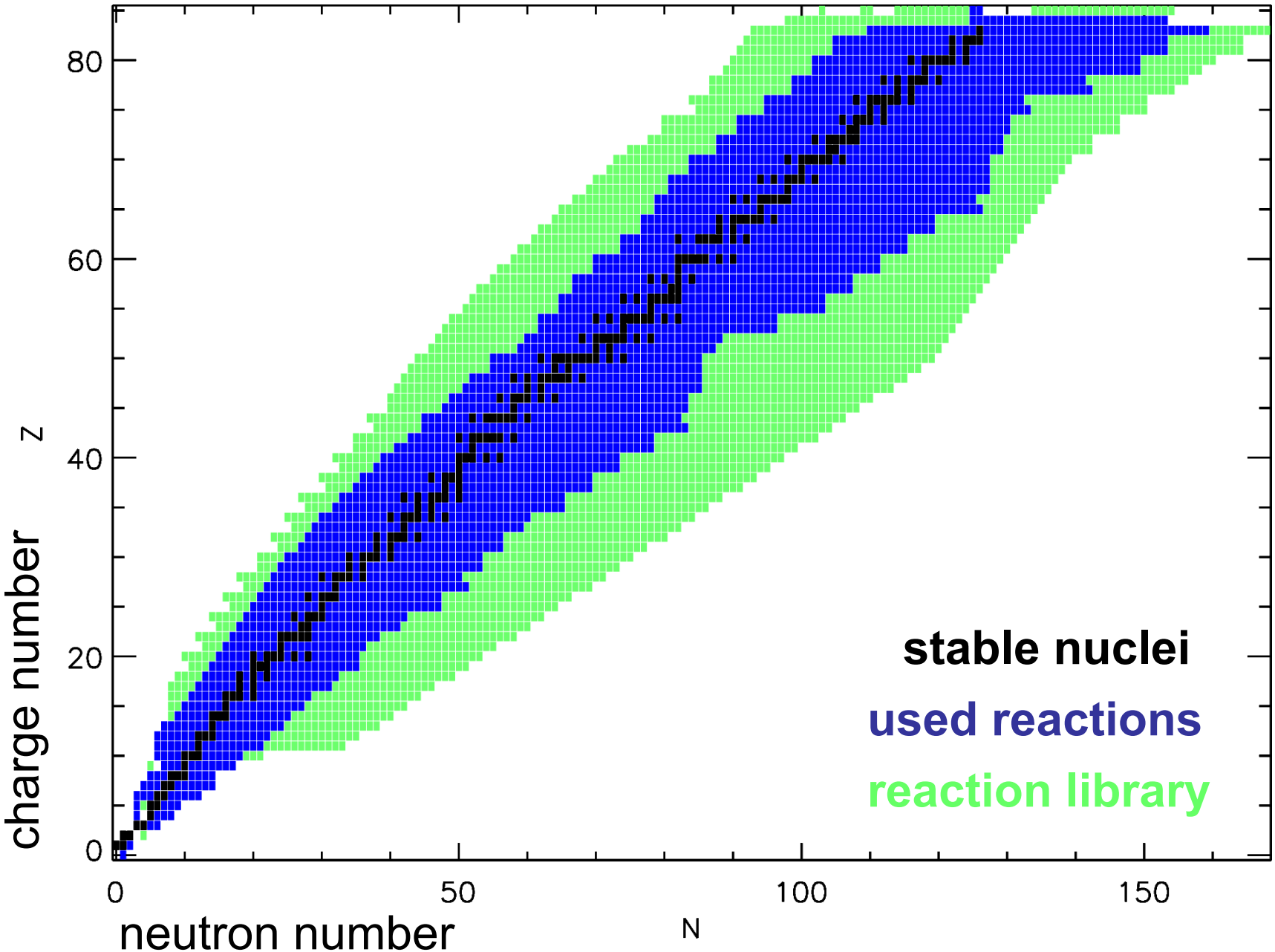
stable nuclei
used reactions
reaction library
charge number
Z
neutron number
N
0
20
40
60
80
0
50
100
150

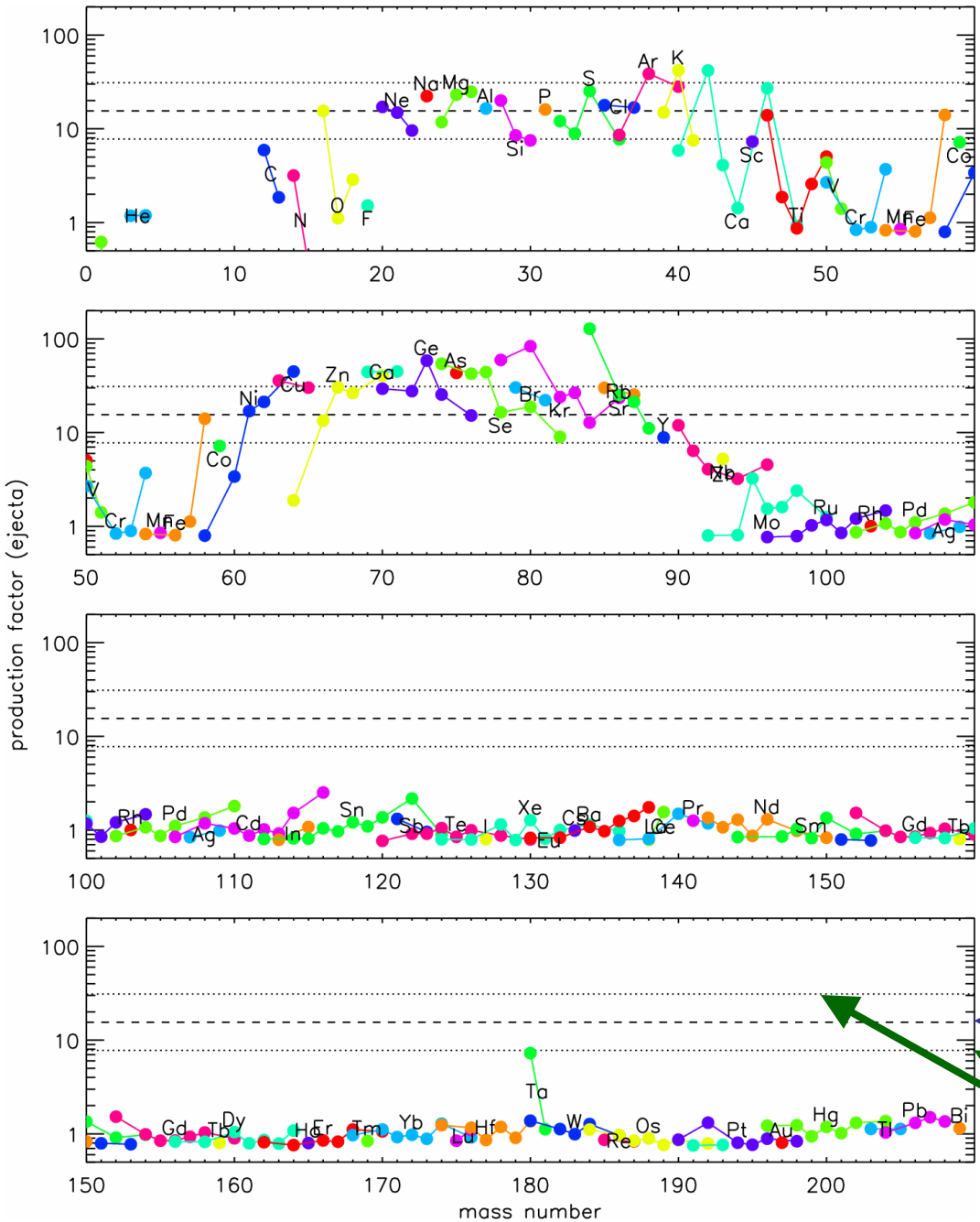

25 $M_\odot$ star

Presupernova production factors relative to solar composition

"band of acceptable co-production" defined by

← ^{16}O production

(± a factor 2)

Explosive Nucleosynthesis contribution

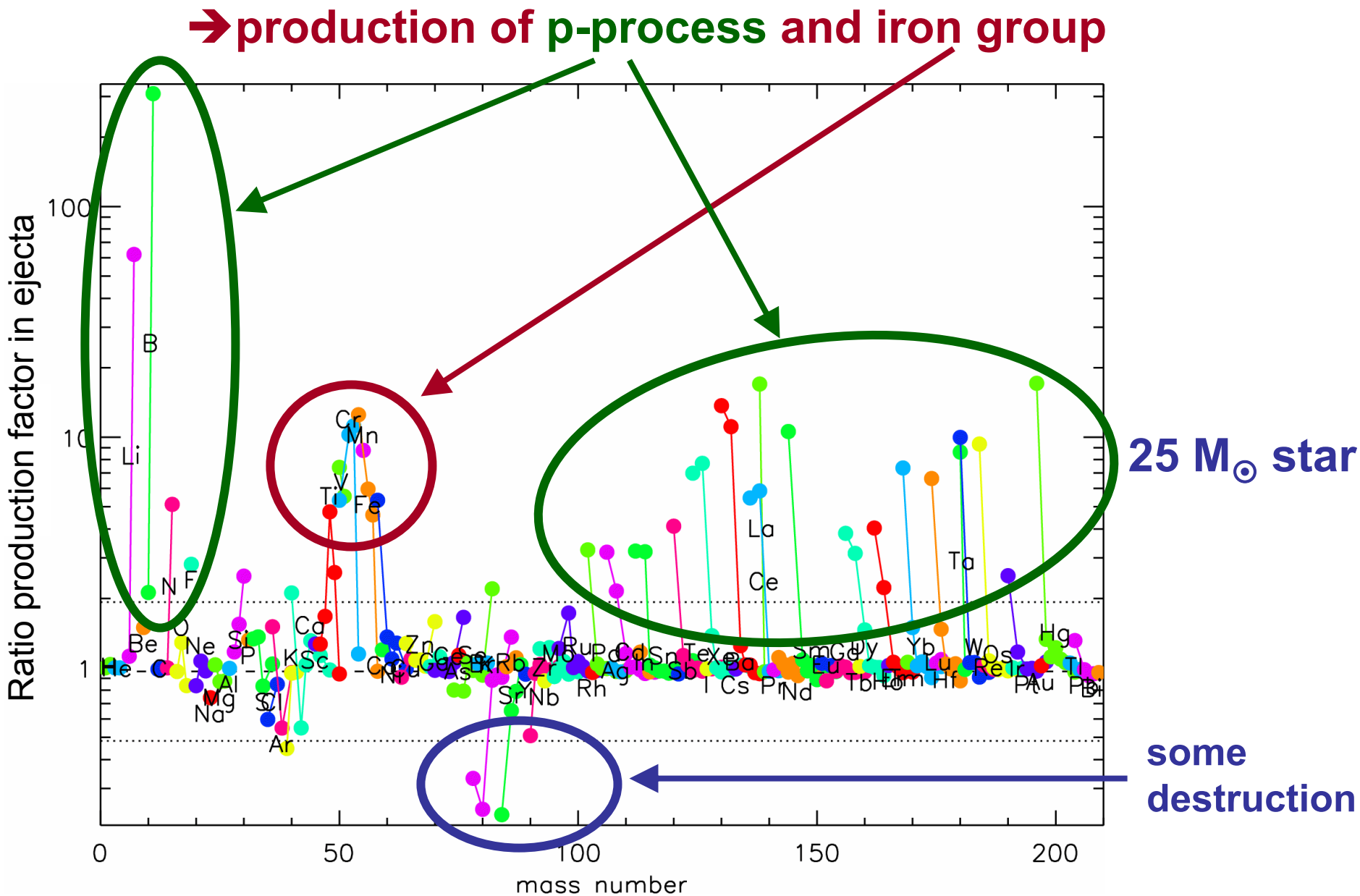

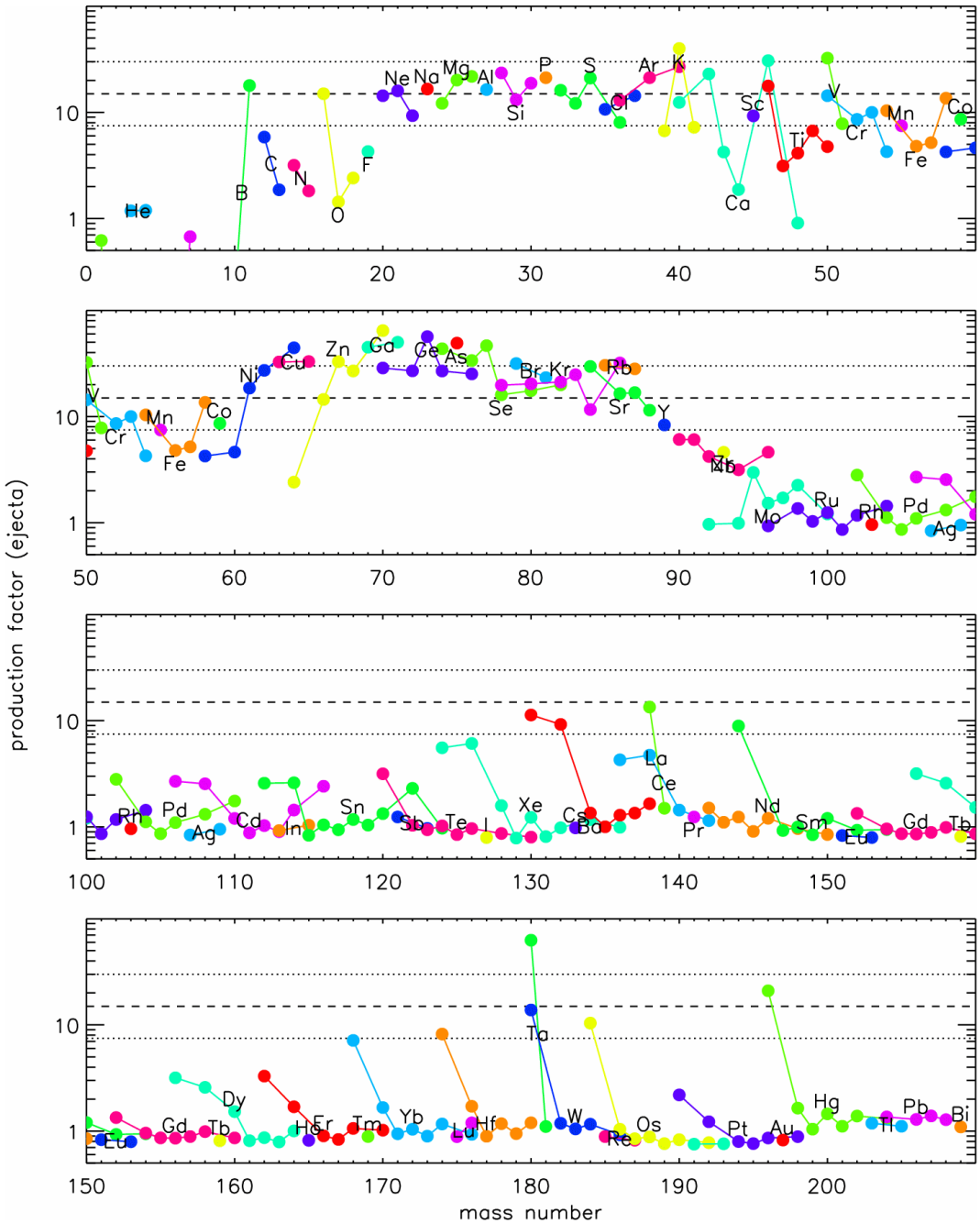

25 $M_\odot$ star

Production factors relative to solar composition

"band of acceptable co-production" defined by ^{16}O production (± a factor 2)

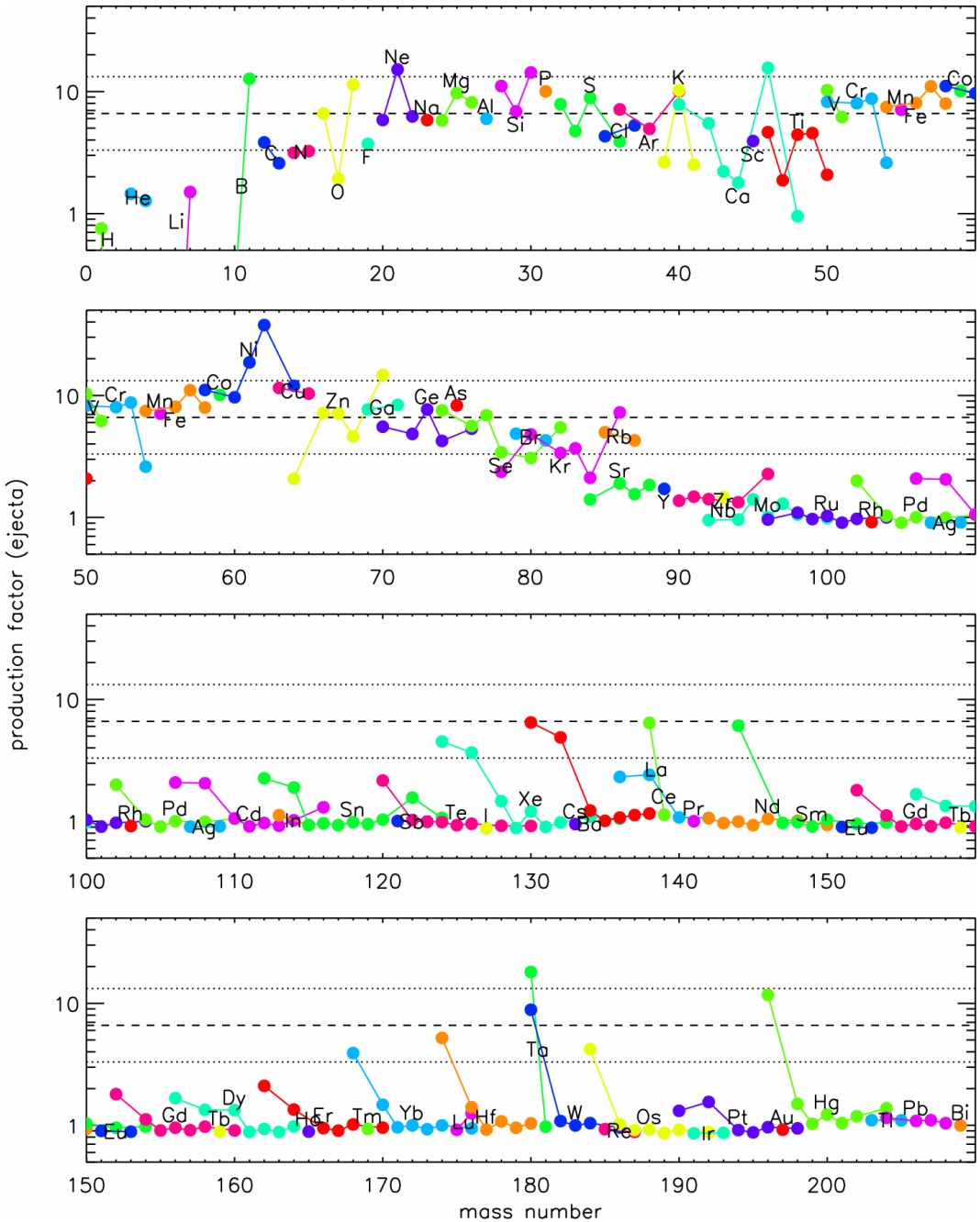

15 $M_\odot$ star

Production factors relative to solar composition

"band of acceptable co-production" defined by ^{16}O production (± a factor 2)

The Results

- Current stellar model can produce most of the elements up to a mass number of $A \approx 85$ in about solar abundances (relative to oxygen)
- many proton-rich heavy elements ("*p*-process elements") are also well co-produced in about solar abundance ratio by the γ-process and the ν-process
- some light isotopes are also produced (^{11}B, ^{19}F)
- some "critical" isotopes we do not find (e.g., ^{92}Mo)

Nuclear Reaction Rate Uncertainties for the s-process

…are some of the key uncertainties in current stellar evolution and nucleosynthesis modeling

Example:

$^{22}Ne(\alpha,n)^{25}Mg$, $^{22}Ne(\alpha,\gamma)^{26}Mg$

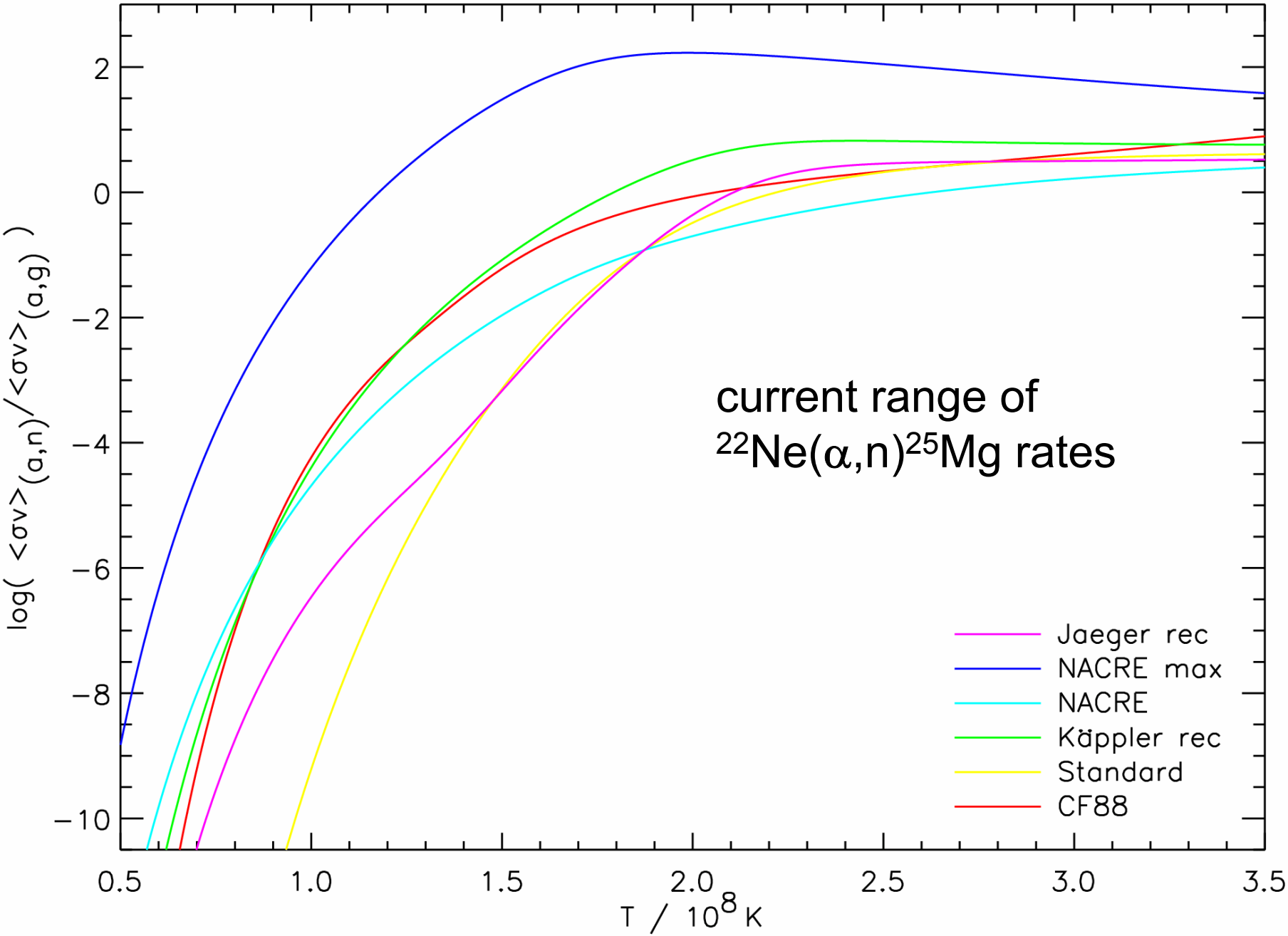
current range of
$^{22}Ne(\alpha,n)^{25}Mg$ rates
Jaeger rec
NACRE max
NACRE
Käppler rec
Standard
CF88
$\log(\langle\sigma v\rangle_{(\alpha,n)}/\langle\sigma v\rangle_{(\alpha,g)})$
$T / 10^8$ K
2
0
−2
−4
−6
−8
−10
0.5
1.0
1.5
2.0
2.5
3.0
3.5

Final Abundances 25 Msun

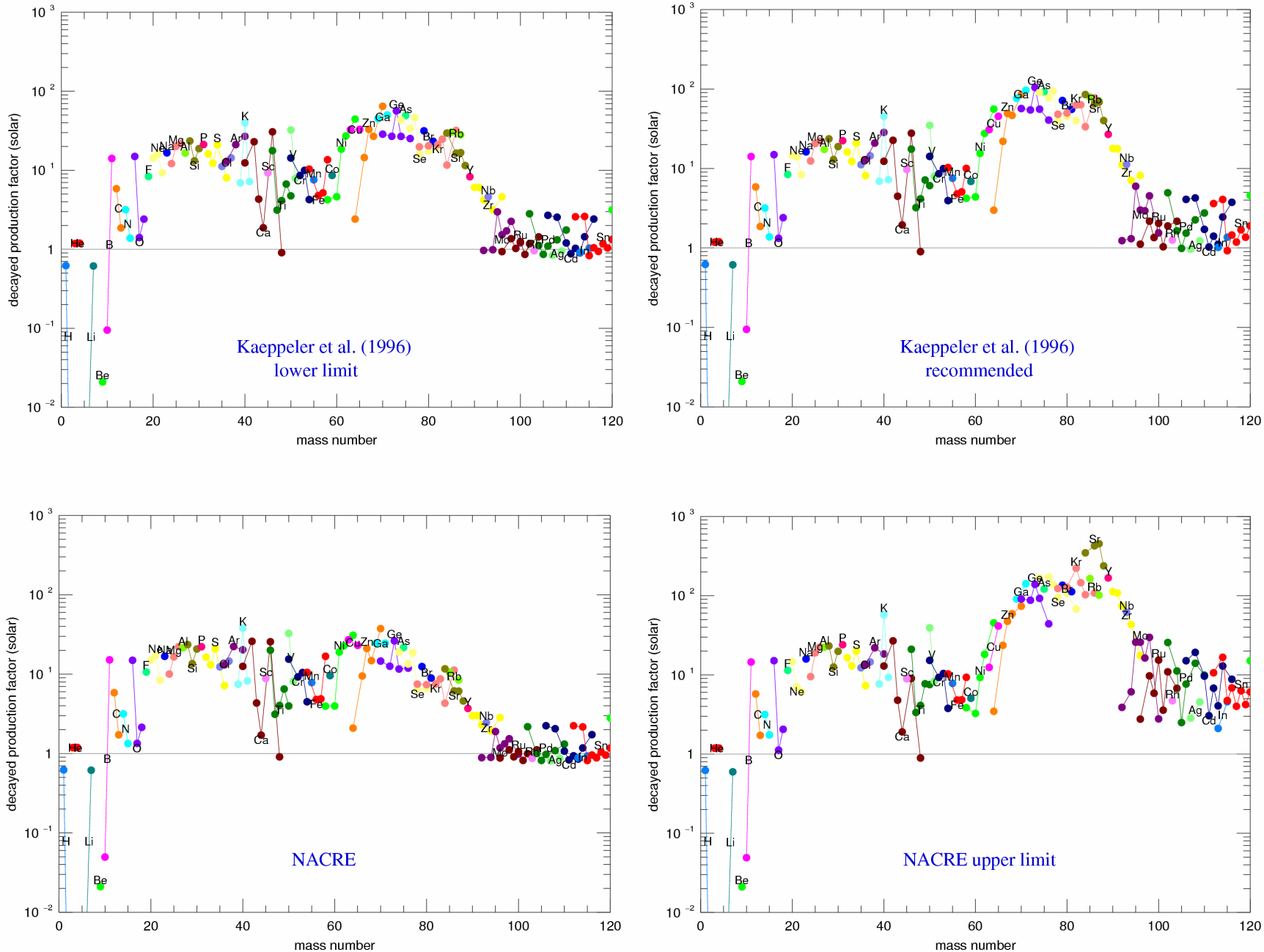

^{60}Fe Production in Supernova

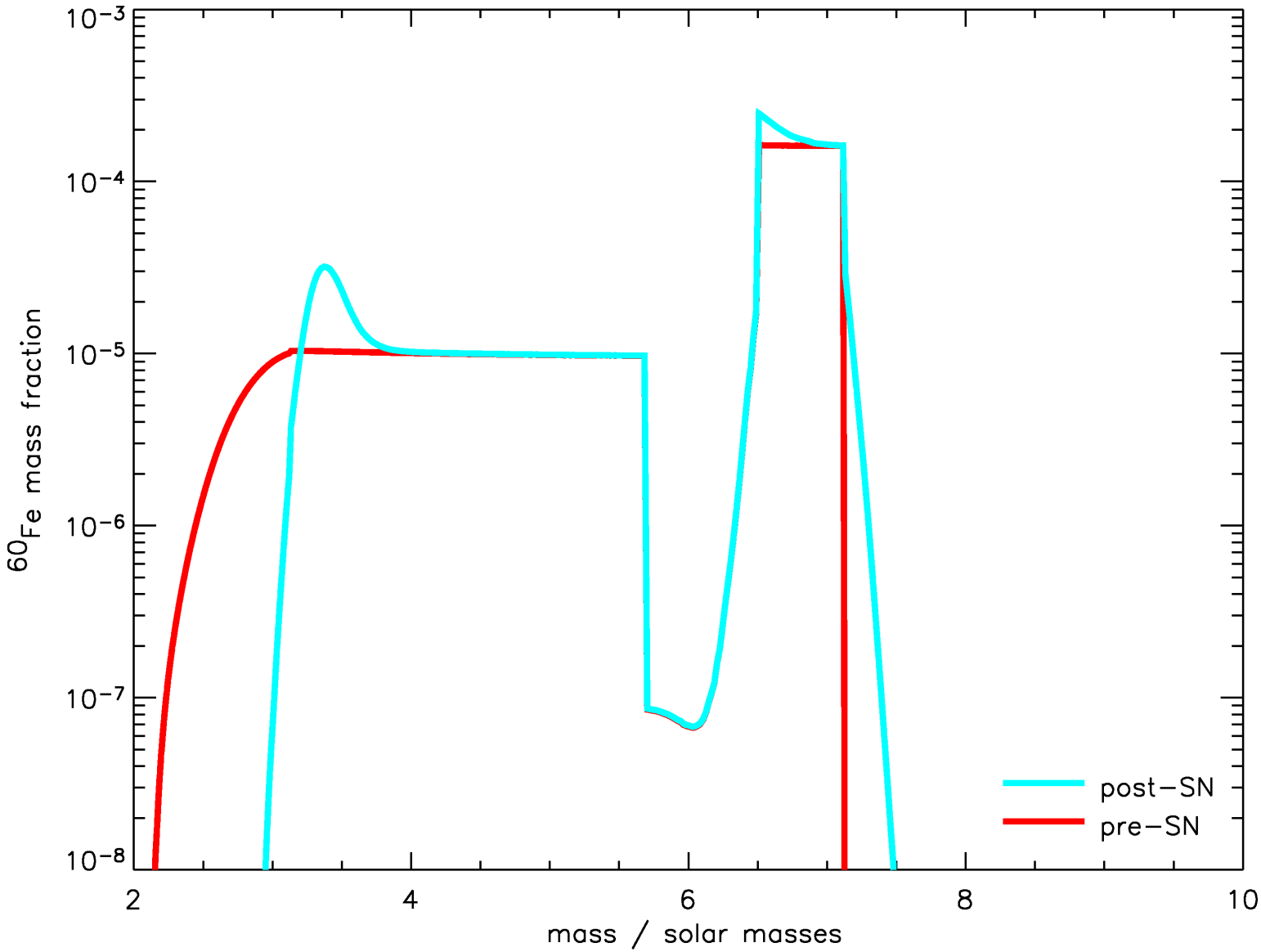

^{60}Fe Production for different ^{59}Fe(n,γ) cross sections

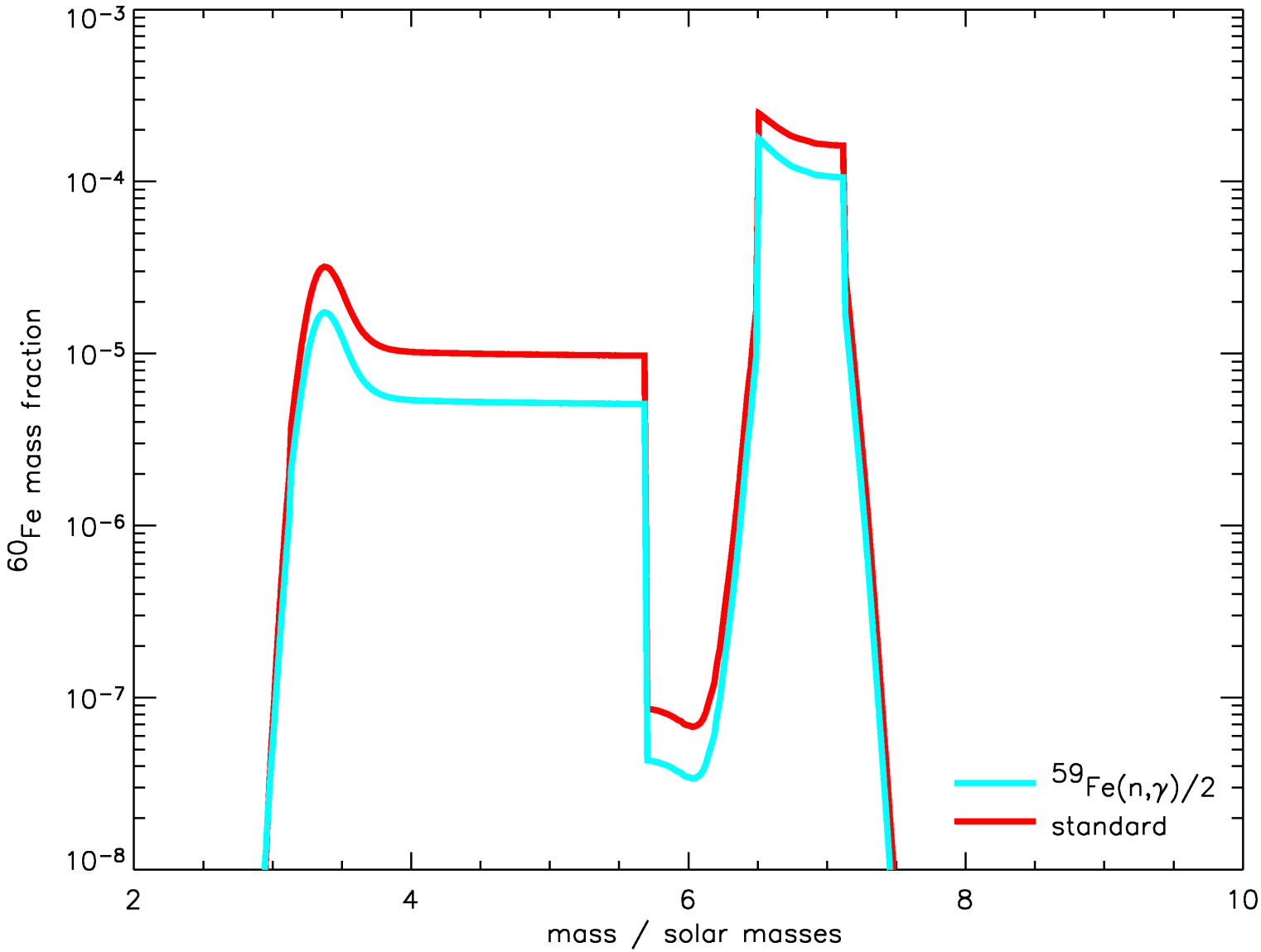

The p-process

- Production of (mostly rare) proton-rich nuclei from **abundant** neighbors
- γ-process: photo-sublimation,
  mostly (γ,n) reactions close to valley of stability
- ν-process:
  - neutral current (ν,ν') scattering to excited nucleus that decays by particle emission
  - charges current (ν,e^-), (ν,e^+); excited daughter nucleus can *also* decay by particle emission {γ, n, p, a}*

“Relocation” of the p-process

p-process can be made in implosive O shell burning,
but peak abundance is destroyed by SN and recreated further out

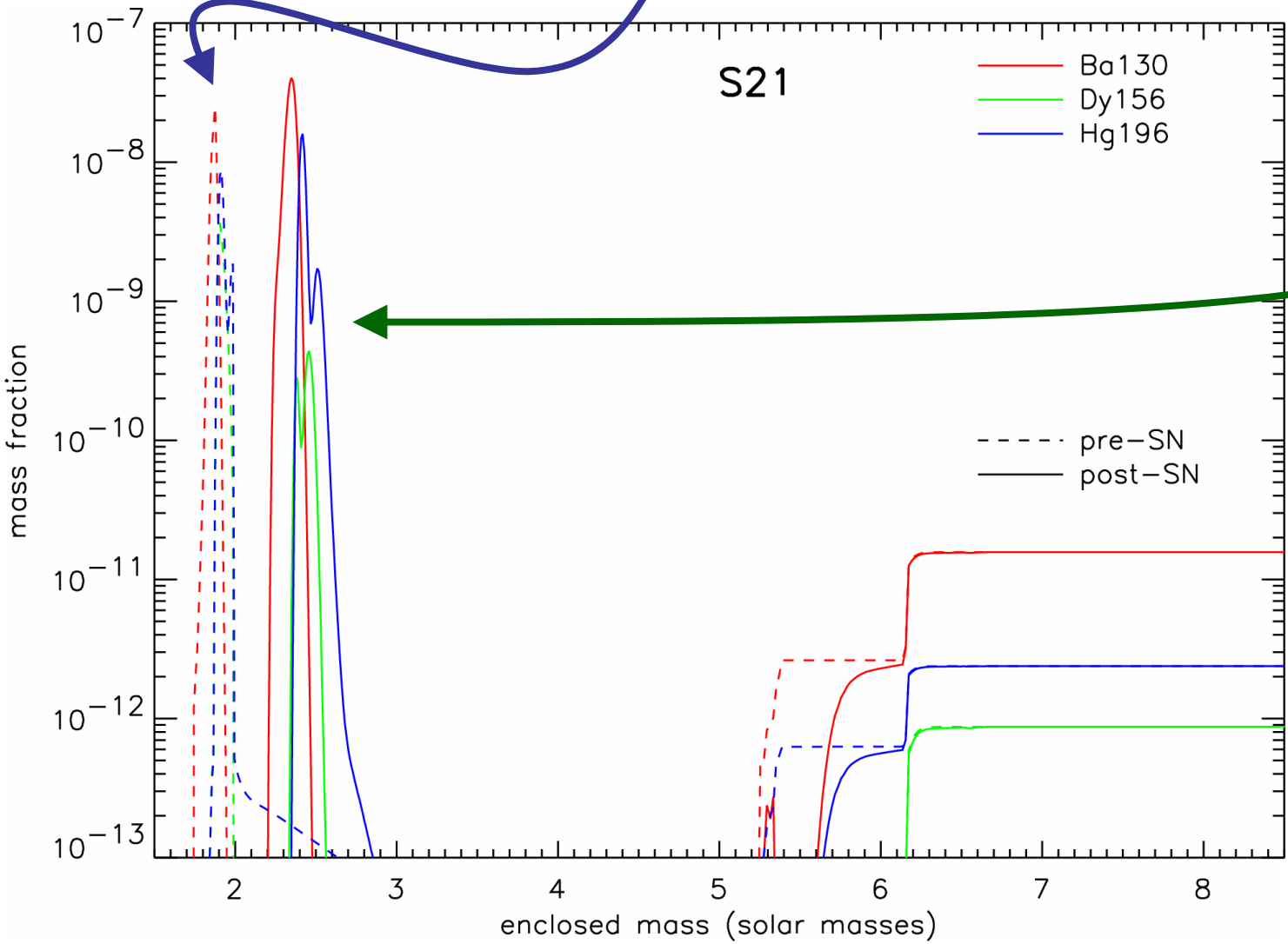

21 $M_\odot$ star

The Impact of $^{138}Ba(\nu,e^-)^{138}La$

➔ ^{138}La is coproduced in solar ratio

with respect to ^{16}O

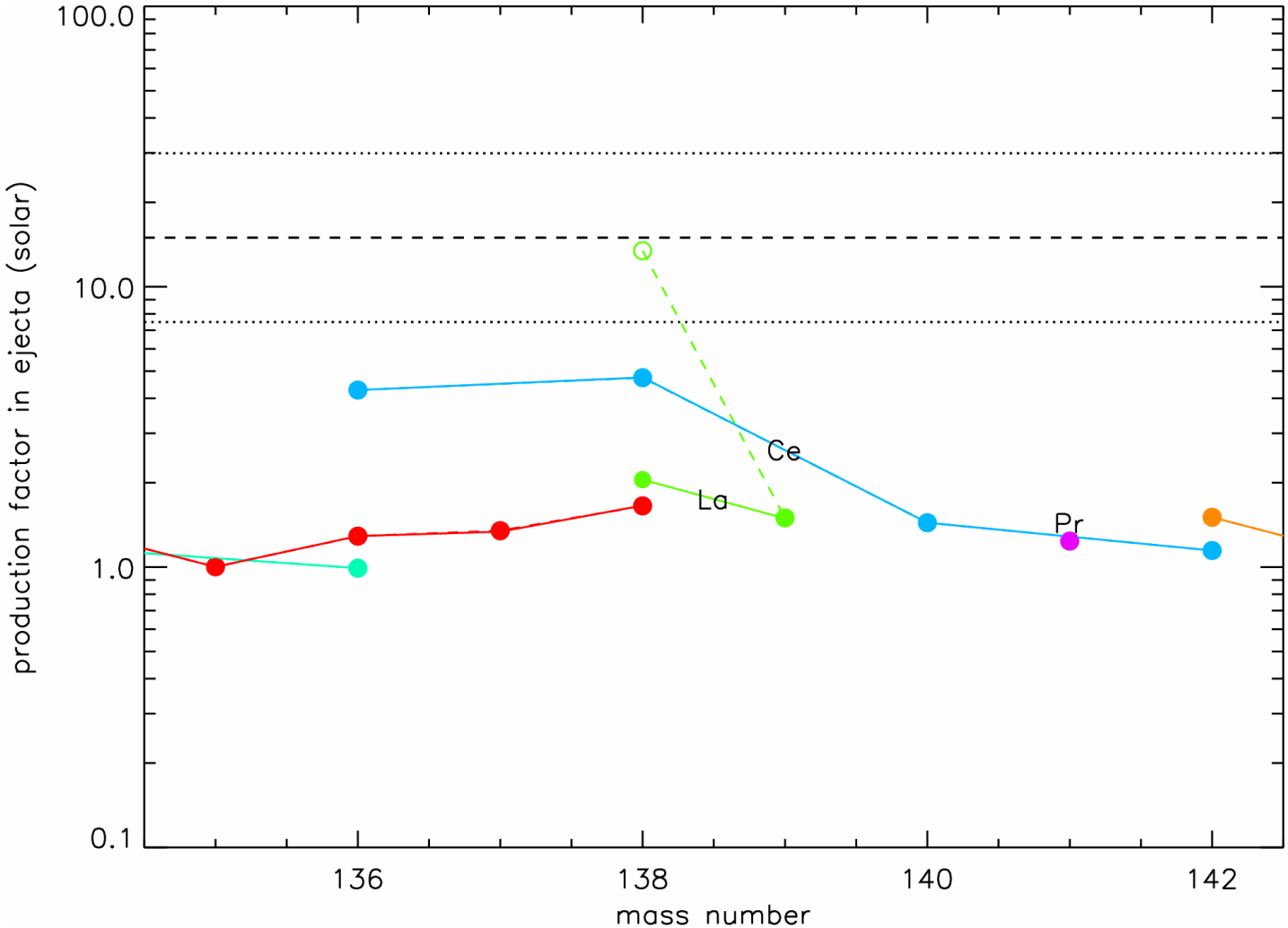

ν-process production of ^{180}Ta

little production by ^{181}Ta(ν,ν' n)^{180}Ta

➔production dominated by ^{181}Ta(γ,n)^{180}Ta and ^{180}Hf(ν_e,e$^-$)^{180}Ta

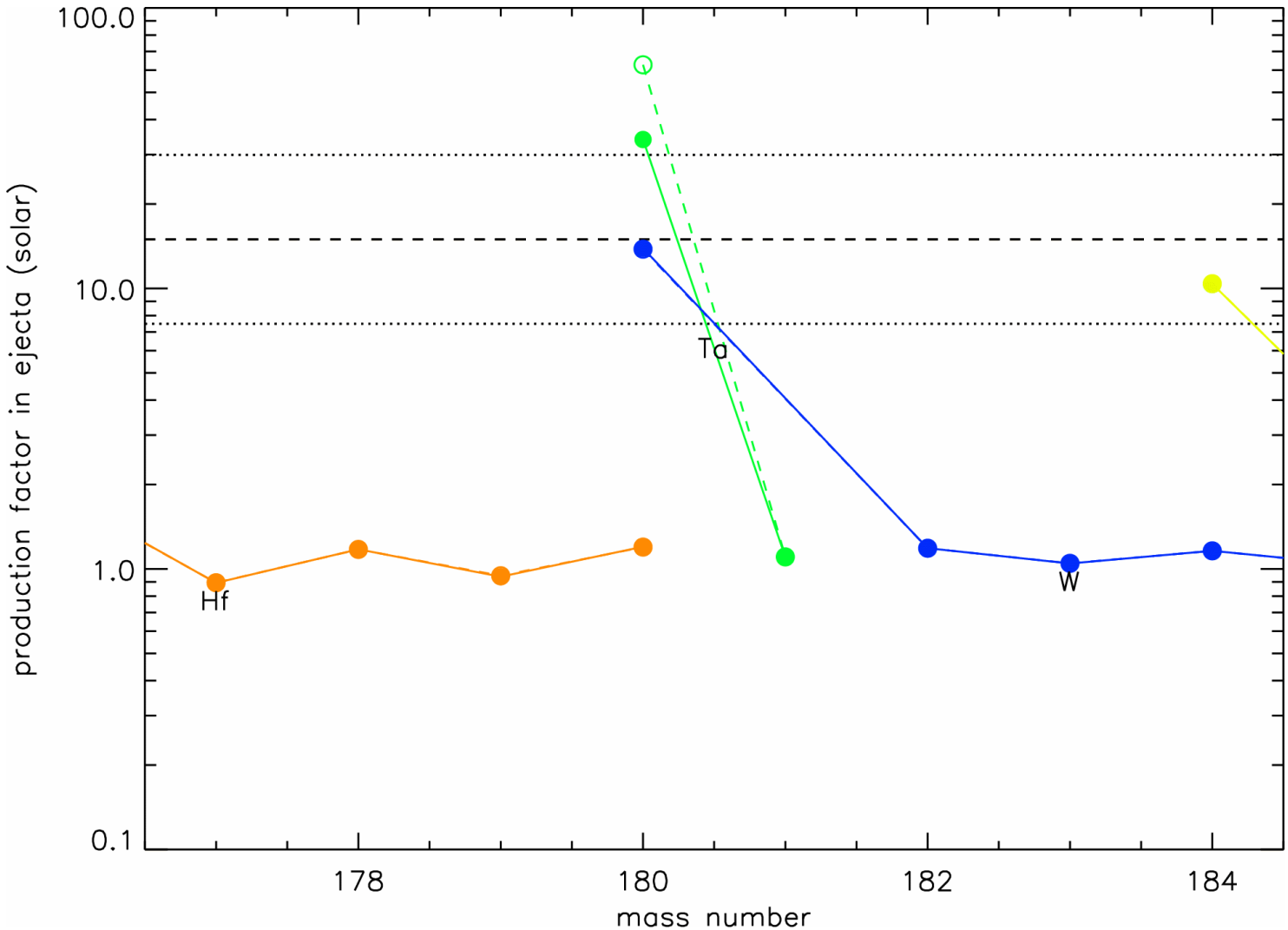

The Production of ^{138}La

by γ-process and ν-process

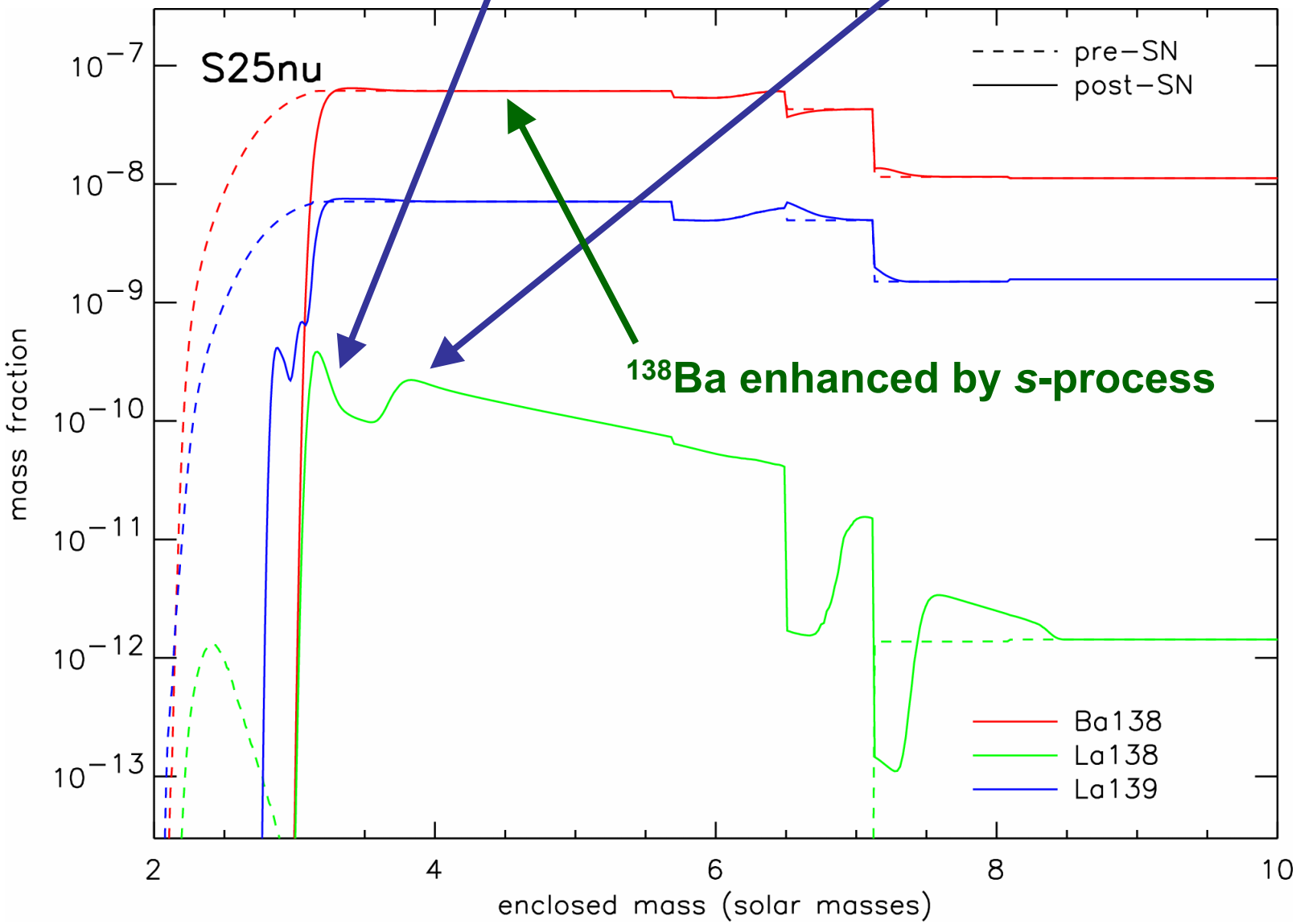

The Production of ^{138}La

by γ-process and ν-process

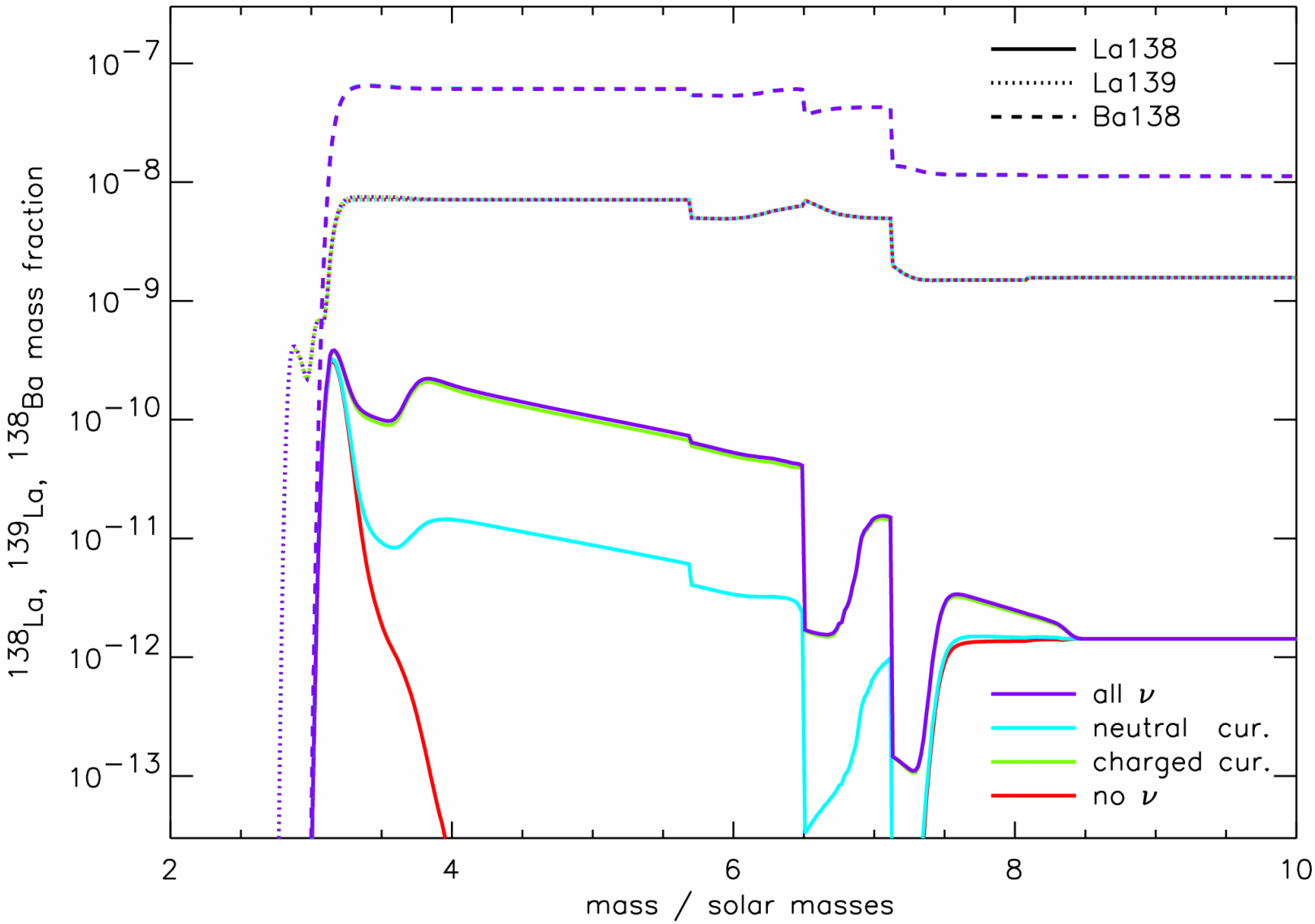

The Production of ^{180}Ta

by γ-process and ν-process

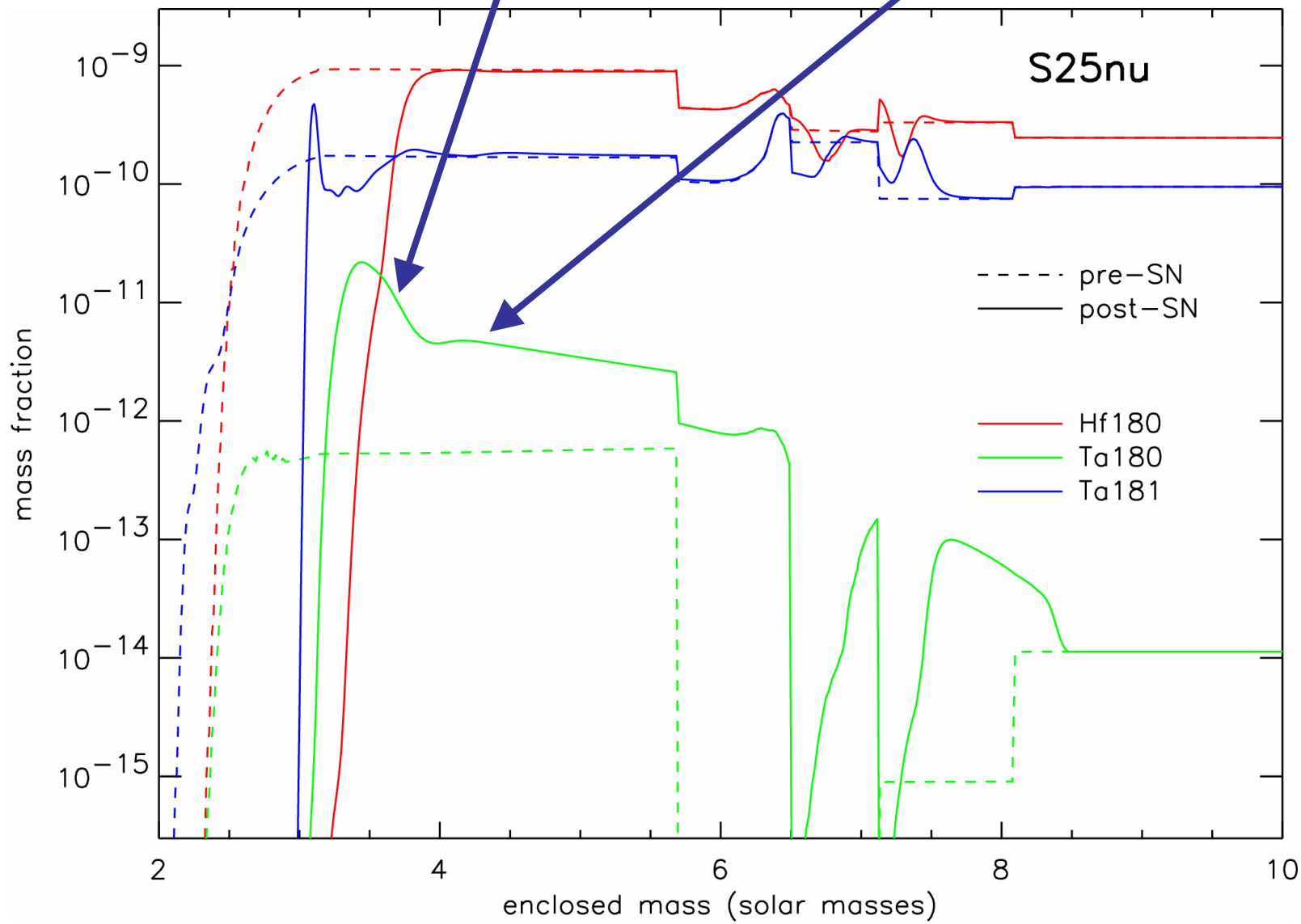

The Production of ^{180}Ta

by γ-process and ν-process

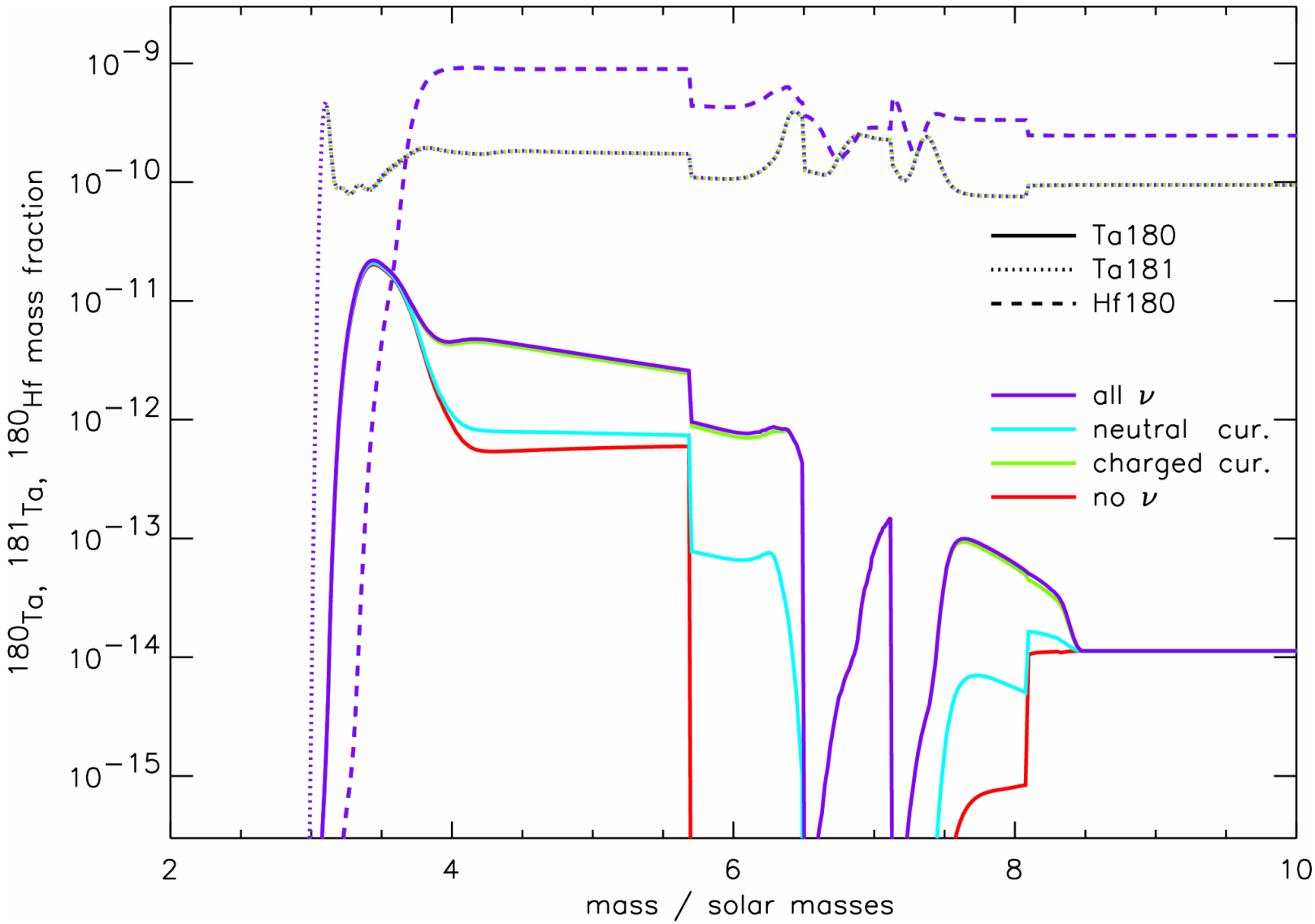

Neutrino Nucleosynthesis

- ^{138}La consistently produced by ^{138}Ba(ν,e$^-$)^{138}La for T(ν_e) = 4 MeV
- Very sensitive to neutrino temperature:
  - for T(ν_e) = 6 MeV: **2**× higher ^{138}La yield (too high)
  - for T(ν_e) = 8 MeV: **5**× higher ^{138}La yield (too high)

➔Fossil ν-process abundances in the sun *may* constrain ν temperature (and oscillations?)
(combination of ^{11}B, ^{19}F, ^{138}La, ^{180}Ta, …)
while *current* solar neutrinos constrain Δm^2

Conclusions

- **Massive stars can account for most of the heavy elements up to the end of the *weak s-process* at A~90.**
  (We do not find production of the very abundant p-nuclei ^{92}Mo, ^{94}Mo, and ^{96}Ru.)
- The uncertainty of the ^{22}Ne(α,n) and ^{22}Ne(α,γ) rates has significant impact on the s-process in massive stars
- Many p-process nuclei are made in explosion of massive stars
- The ν-process can well account all of ^{138}La and contributes about half to ^{180}Ta
- **The pre-explosive enrichment/depletion of nuclei by the s-process is crucial for the p-process.**
- ν-process is probe for SN ν temperature and ν oscillations
- We need good ν cross sections and BRs for light elements producing ^{11}B, ^{15}N, ^{19}F, the A~50 region, ^{138}La, and ^{180}Ta

Contribution by

Marco Pignatari

Universita di Torino

cygno1@yahoo.it

25 pages

Effects of uncertainties of ^{22}Ne(α, n)^{25}Mg rate

Marco Pignatari

Roberto Gallino

Dance Workshop 2004

In the low mass stars AGB phase the ^{22}Ne(α, n) neutron source is marginally activated during convective instabilities.

$$kT \simeq 23 \text{ keV}$$
$$n_n \leq 10^{10} \text{ n cm}^{-3}$$

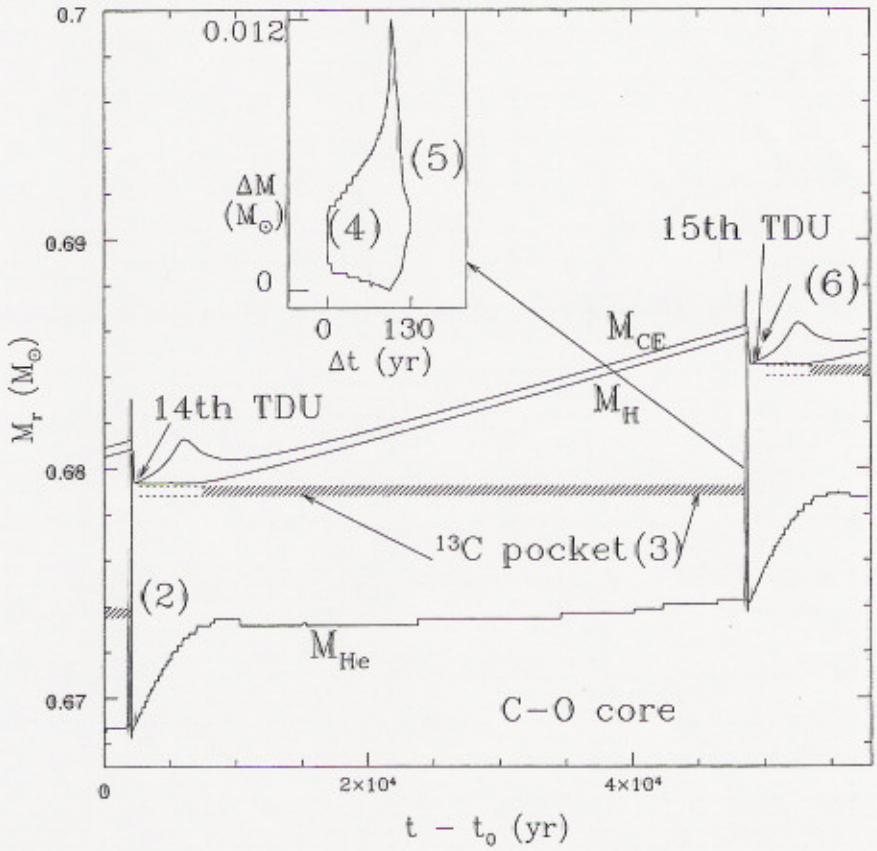

Figure 1: From Kahane et al. (2000).

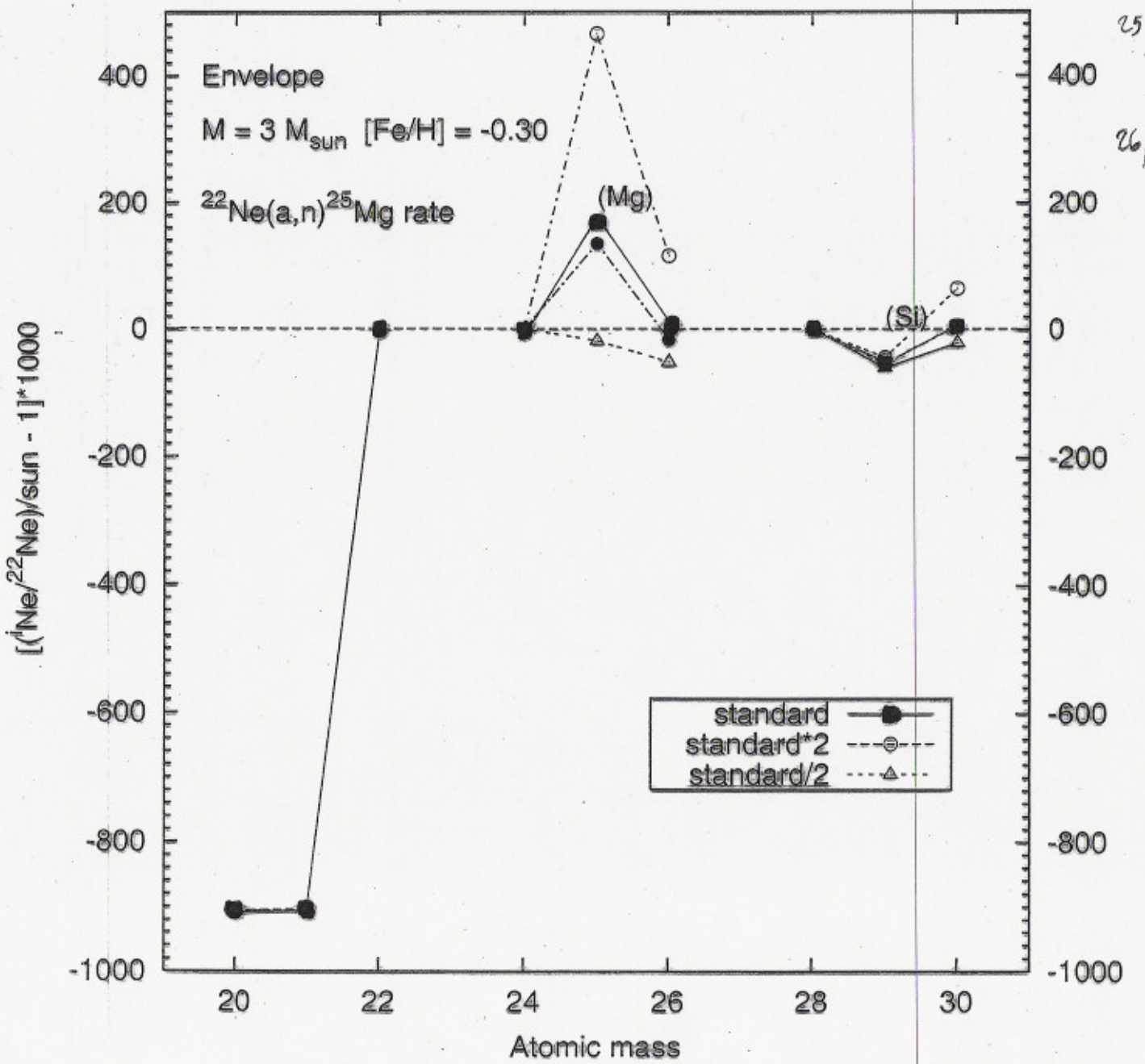

$^{25}Mg \rightarrow$ +26% (rate * 2)
−15% (rate / 2)

$^{26}Mg \rightarrow$ +18,4% (rate * 2)
−5% (rate / 2)

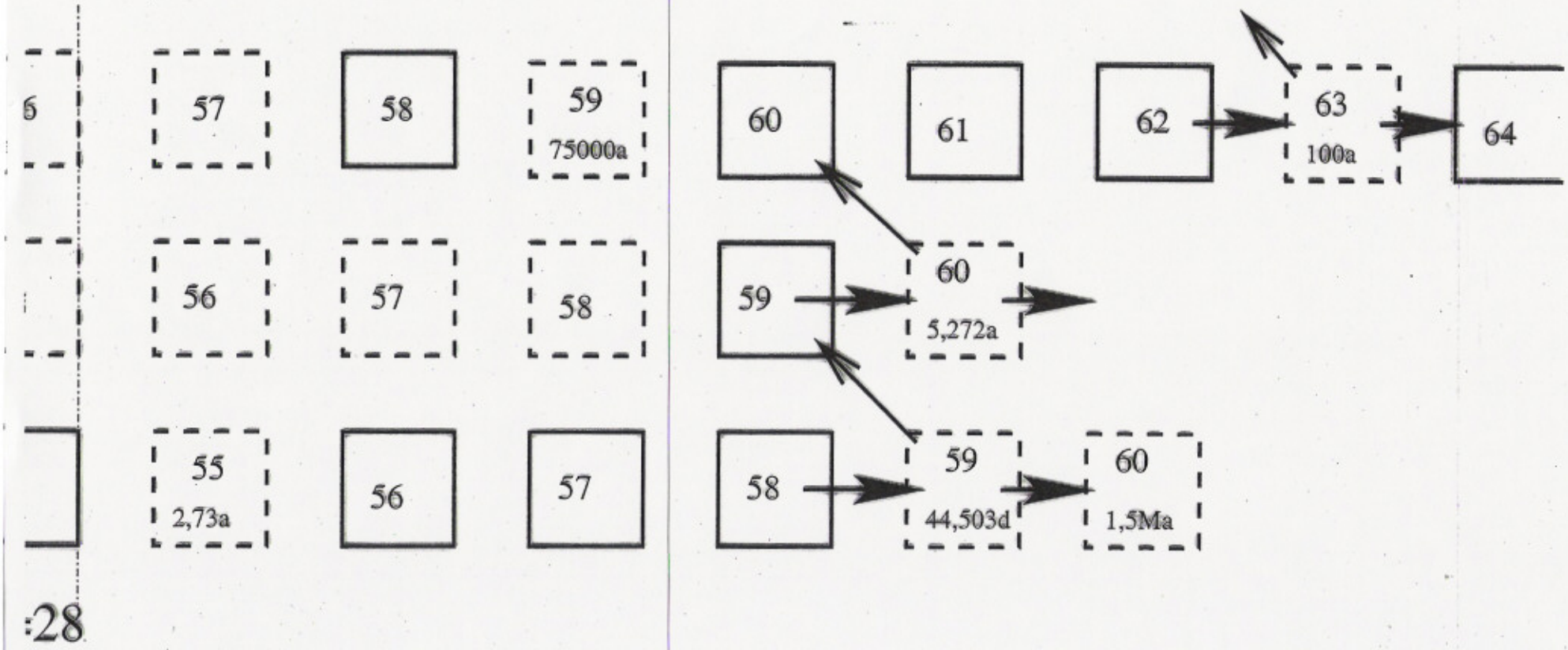
6
57
58
59
75000a
60
61
62
63
100a
64
56
57
58
59
60
5,272a
55
2,73a
56
57
58
59
44,503d
60
1,5Ma

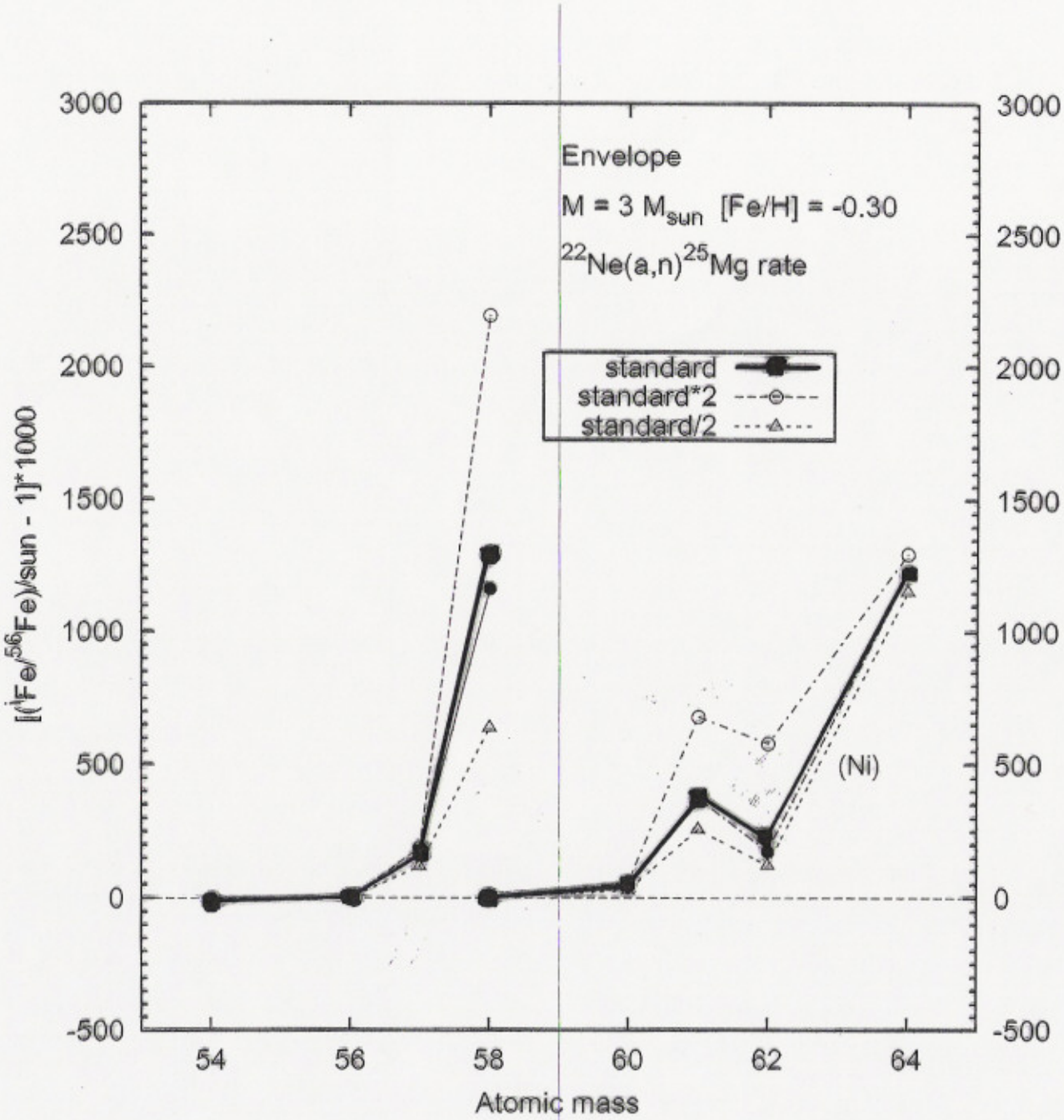

^{58}Fe → +41% (rate * 2)
−27% (rate/2)

^{61}Ni → +18% (rate * 2)
−9% (rate/2)

^{62}Ni → +34% (rate * 2)
−5% (rate/2)

The s-process path through the first s-peak

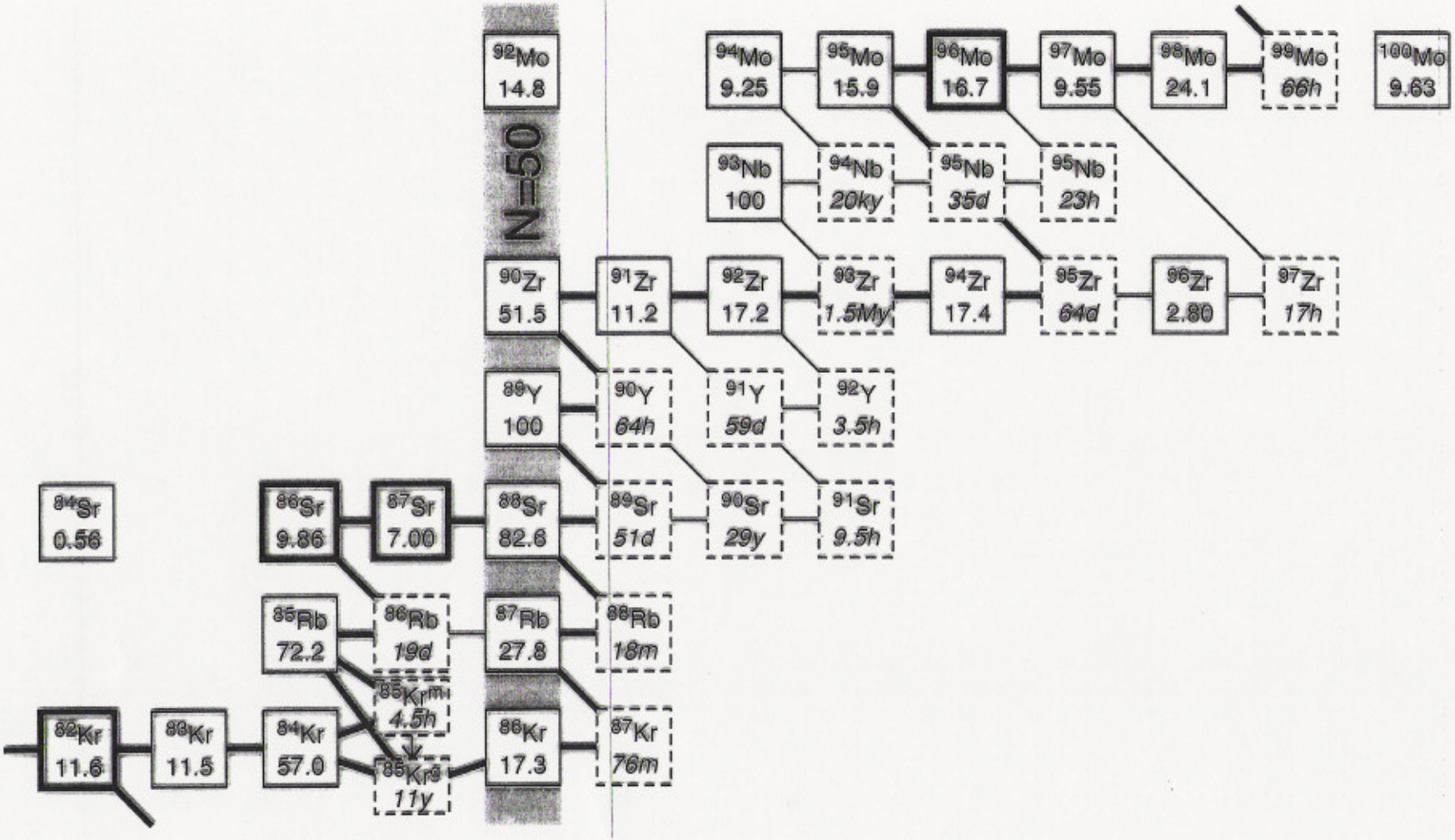

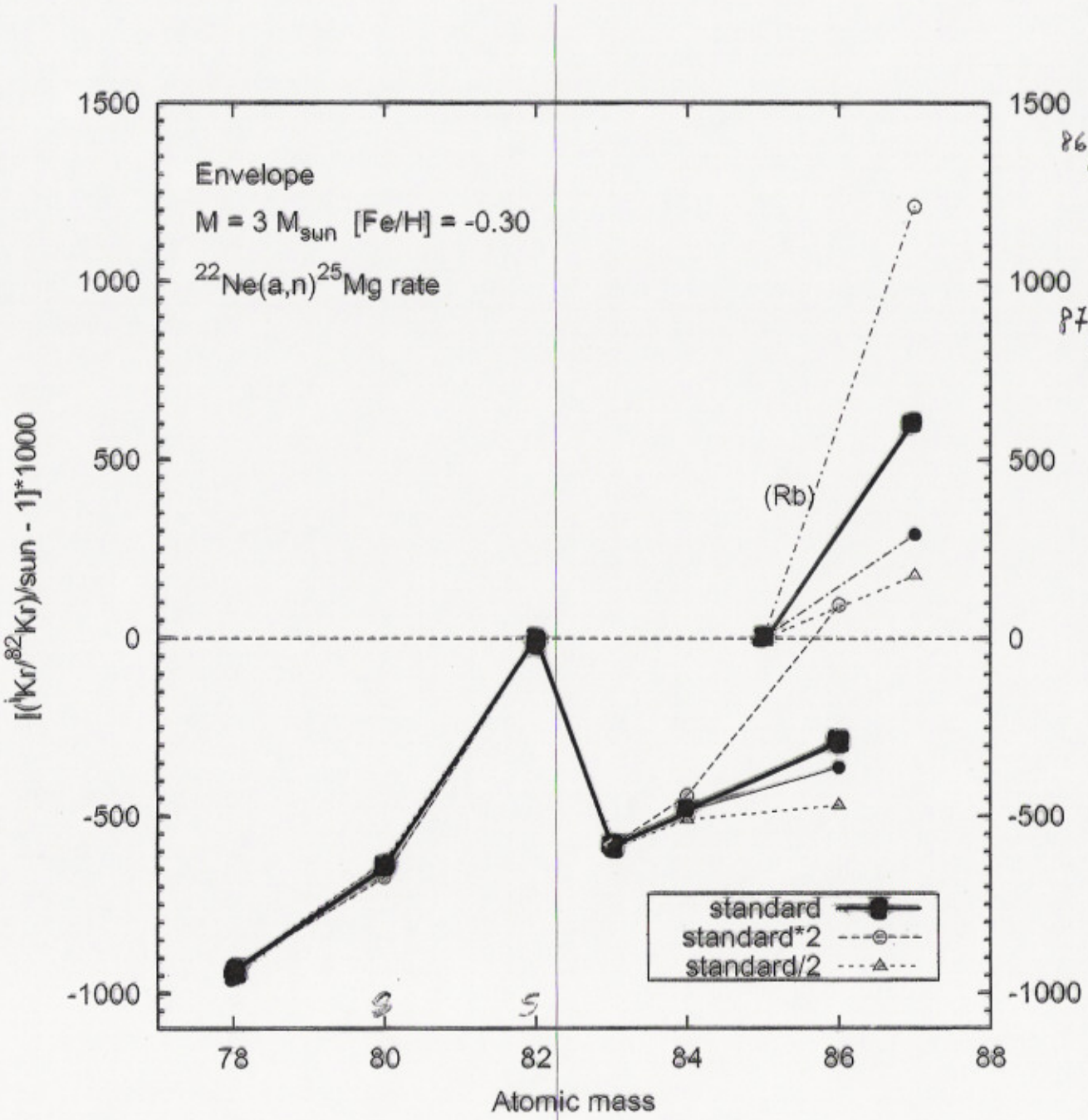

$^{86}Kr \rightarrow$ +54% (rate *2)
−34% (rate/2)

$^{87}Rb \rightarrow$ +38% (rate *2)
−26% (rate/2)

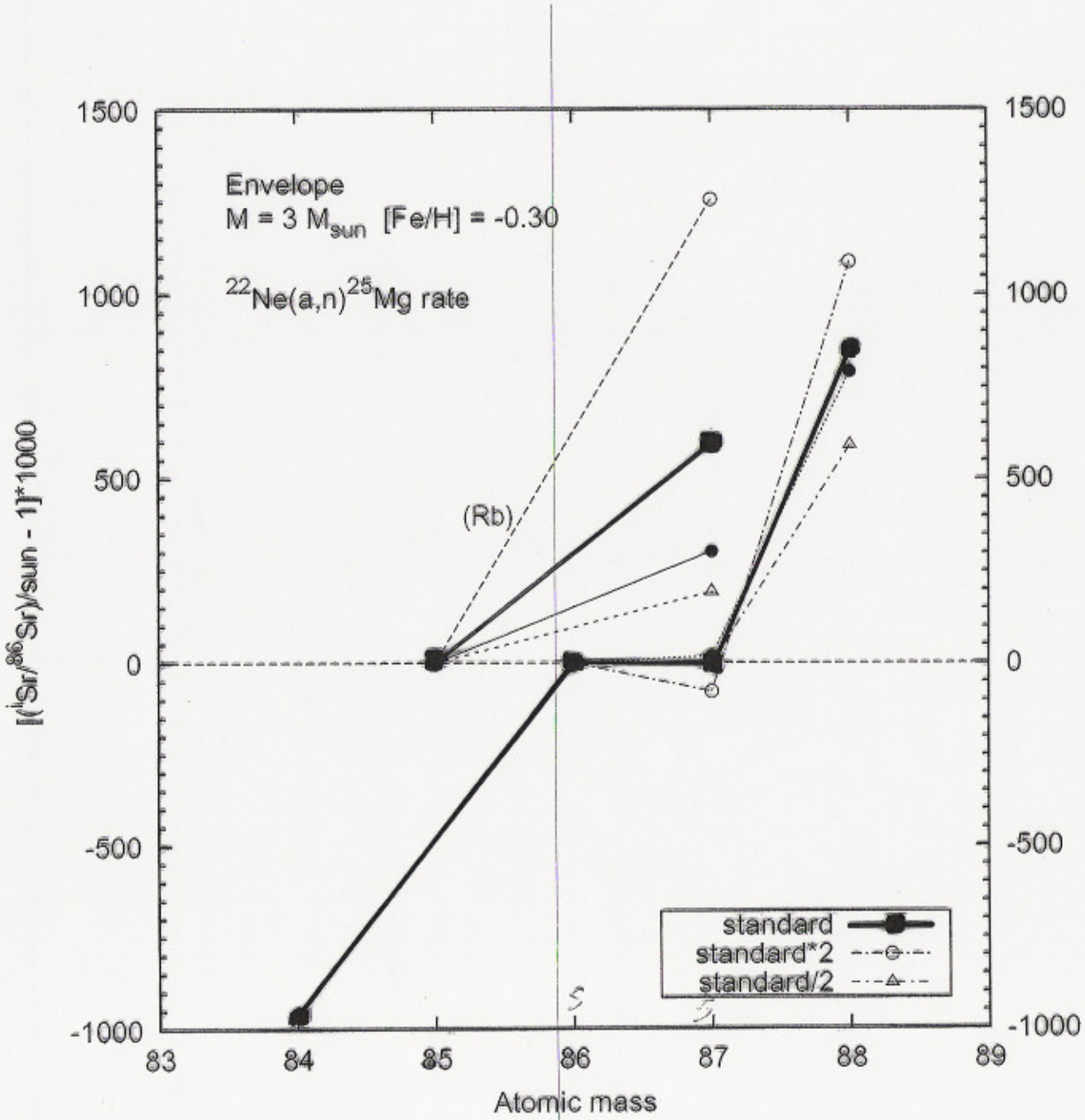

^{88}Sr → + 13% (rate * 2)
− 14% (rate / 2)

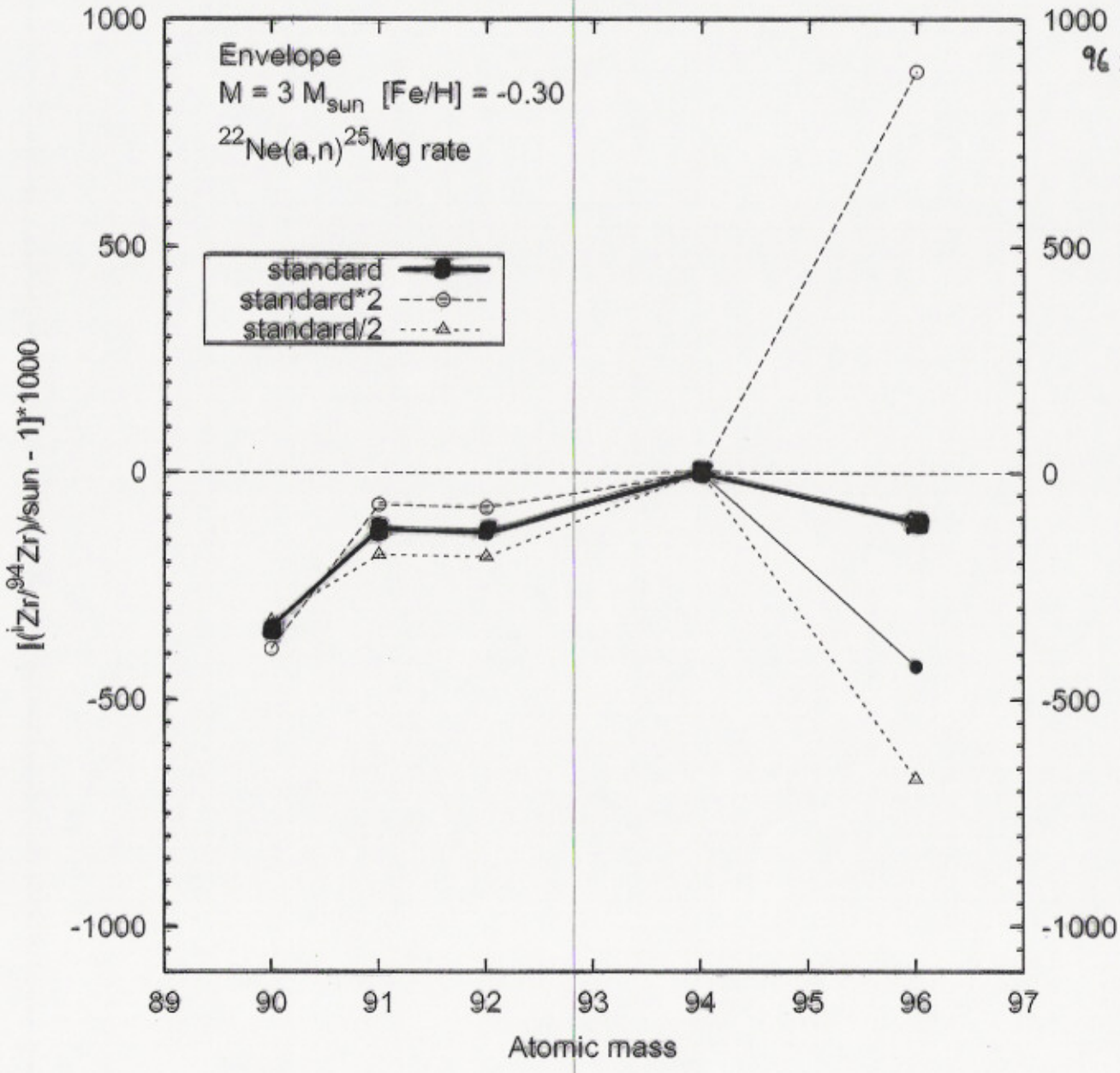

^{96}Zr → +110 % (rate*2)
−62 % (rate/2)

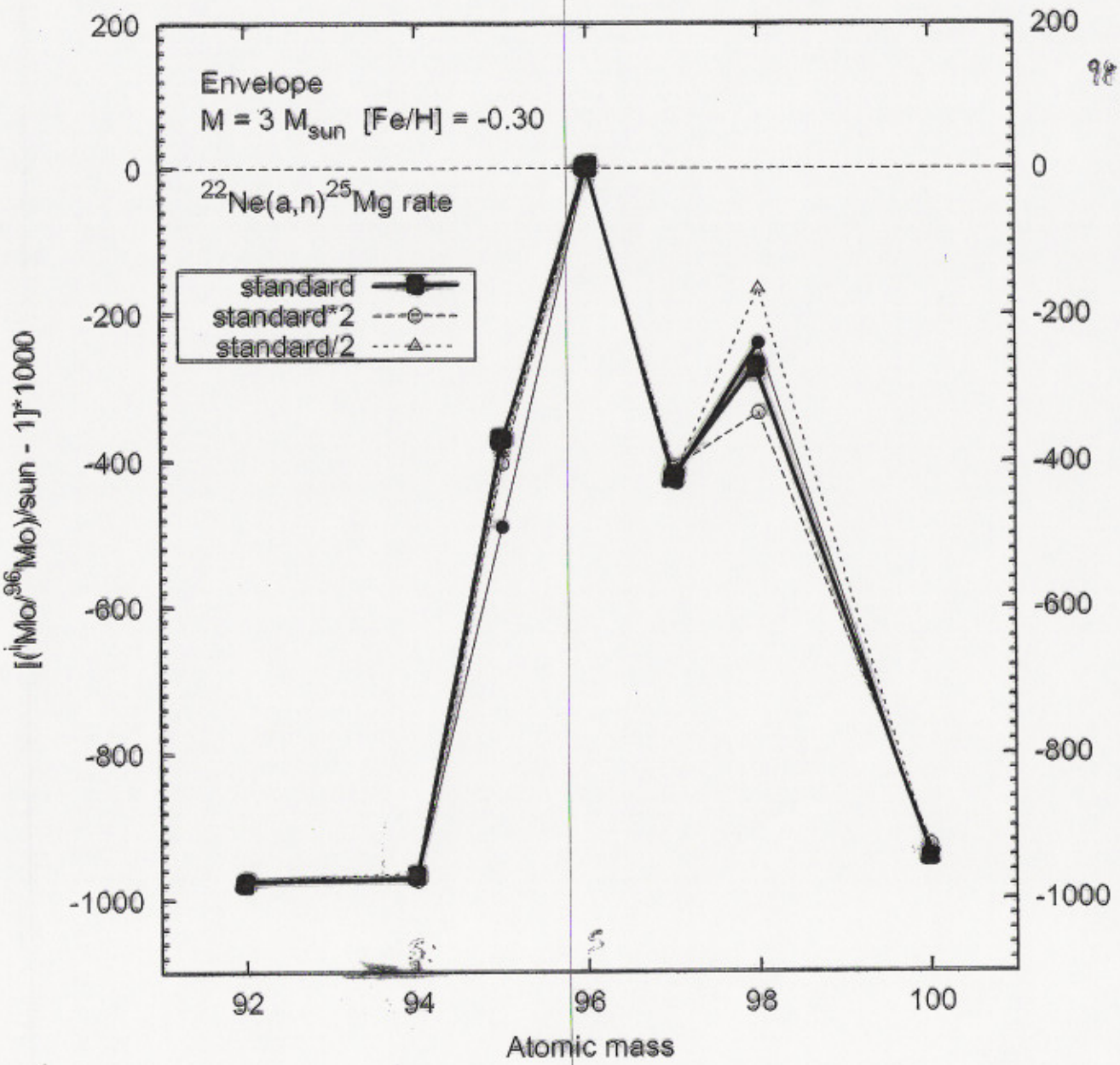

^{98}Mo → −10% (rate * 2)
+14% (rate/2)

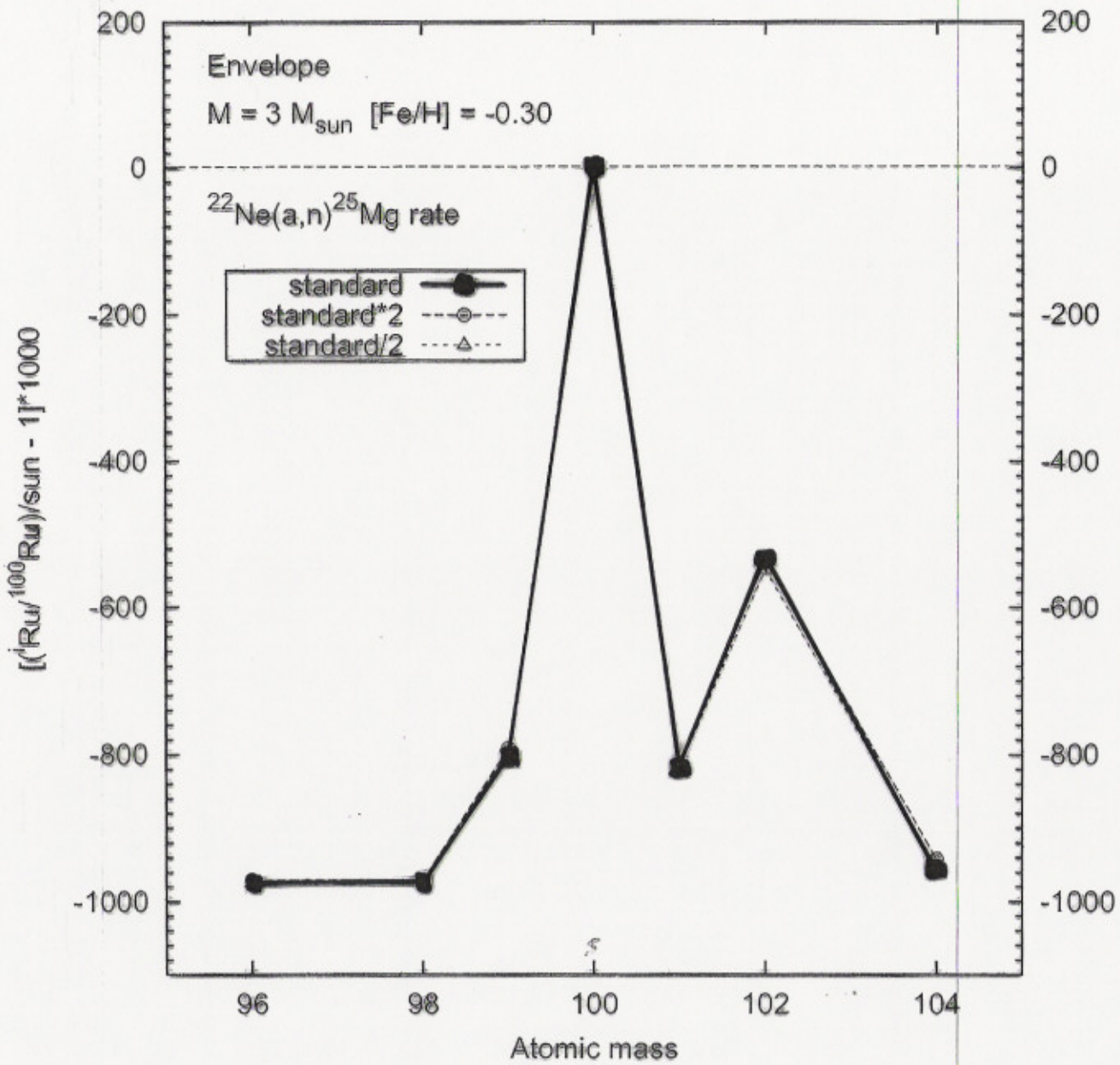
Envelope
M = 3 M_sun [Fe/H] = -0.30
22Ne(a,n)25Mg rate
standard
standard*2
standard/2
[(iRu/100Ru)/sun - 1]*1000
Atomic mass
200
0
-200
-400
-600
-800
-1000
96
98
100
102
104

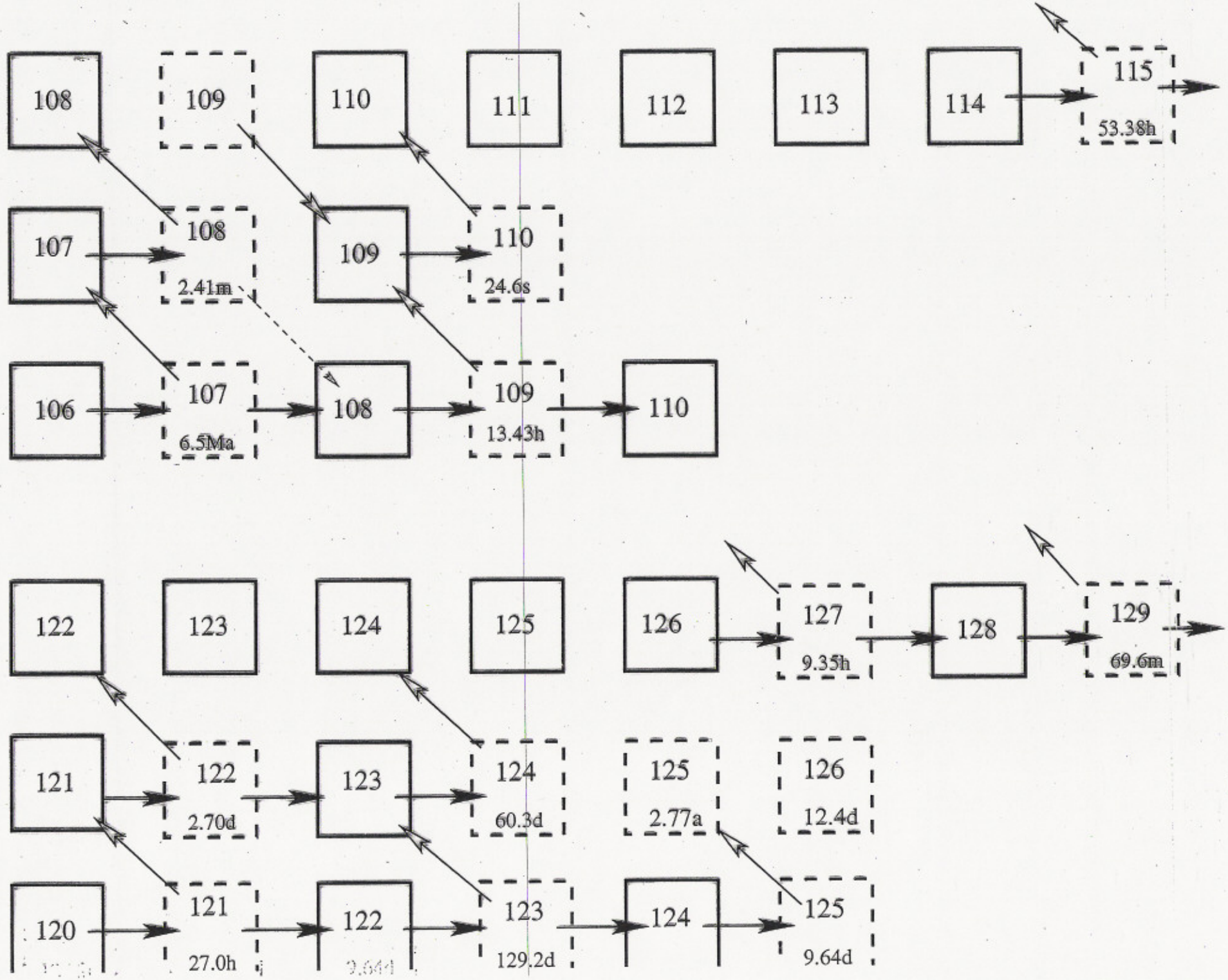
108
109
110
111
112
113
114
115
53.38h
107
108
2.41m
109
110
24.6s
106
107
6.5Ma
108
109
13.43h
110
122
123
124
125
126
127
9.35h
128
129
69.6m
121
122
2.70d
123
124
60.3d
125
2.77a
126
12.4d
120
121
27.0h
122
123
129.2d
124
125
9.64d

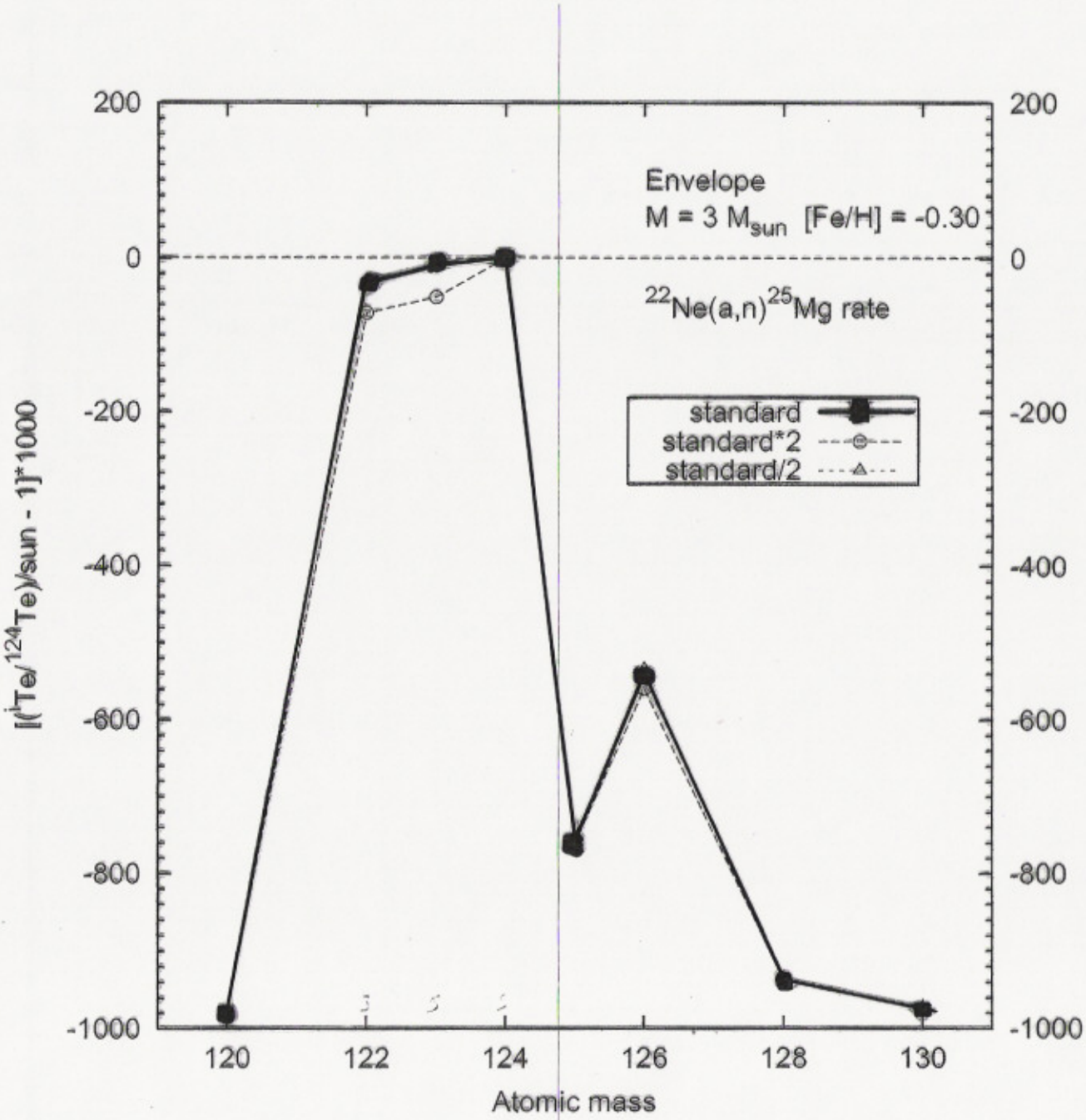
Envelope
M = 3 M_sun [Fe/H] = -0.30
22Ne(a,n)25Mg rate
standard
standard*2
standard/2
[(iTe/124Te)/sun - 1]*1000
Atomic mass
200
0
-200
-400
-600
-800
-1000
120
122
124
126
128
130

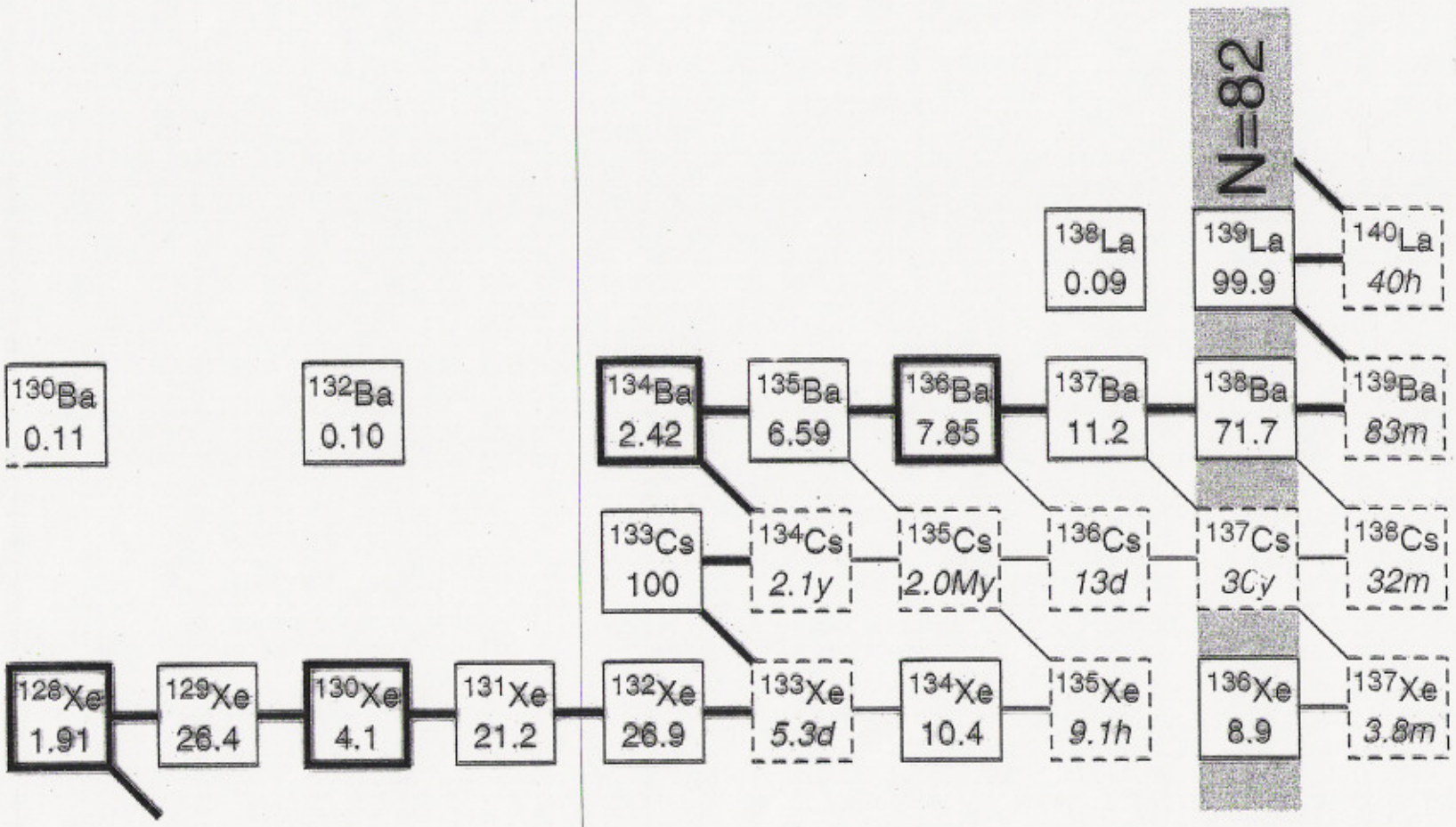
N=82
130Ba 0.11
132Ba 0.10
134Ba 2.42
135Ba 6.59
136Ba 7.85
137Ba 11.2
138Ba 71.7
139Ba 83m
138La 0.09
139La 99.9
140La 40h
133Cs 100
134Cs 2.1y
135Cs 2.0My
136Cs 13d
137Cs 30y
138Cs 32m
128Xe 1.91
129Xe 26.4
130Xe 4.1
131Xe 21.2
132Xe 26.9
133Xe 5.3d
134Xe 10.4
135Xe 9.1h
136Xe 8.9
137Xe 3.8m

Figure 1

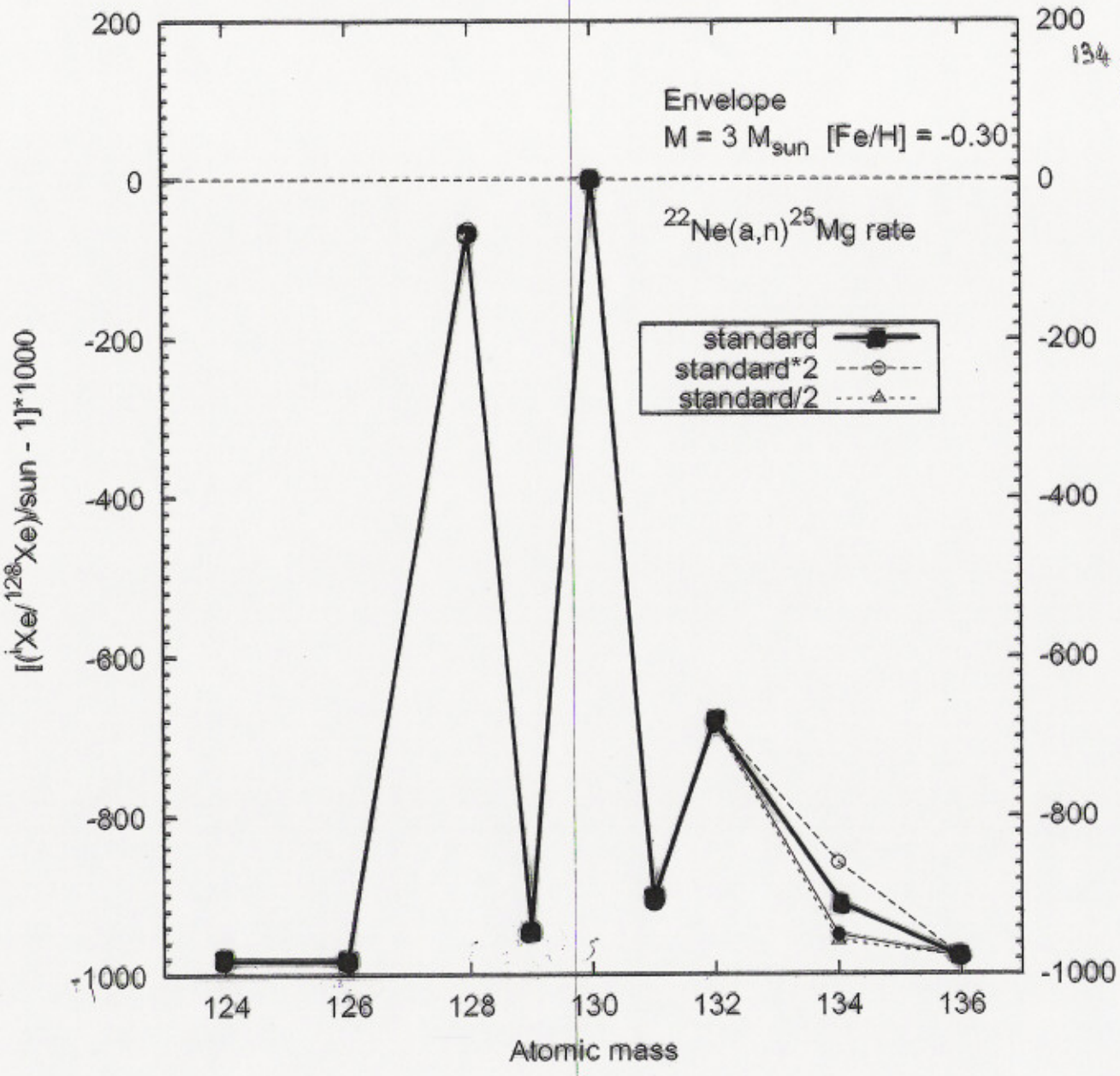

^{134}Xe → +86% (rate*2)
−47% (rate/2)

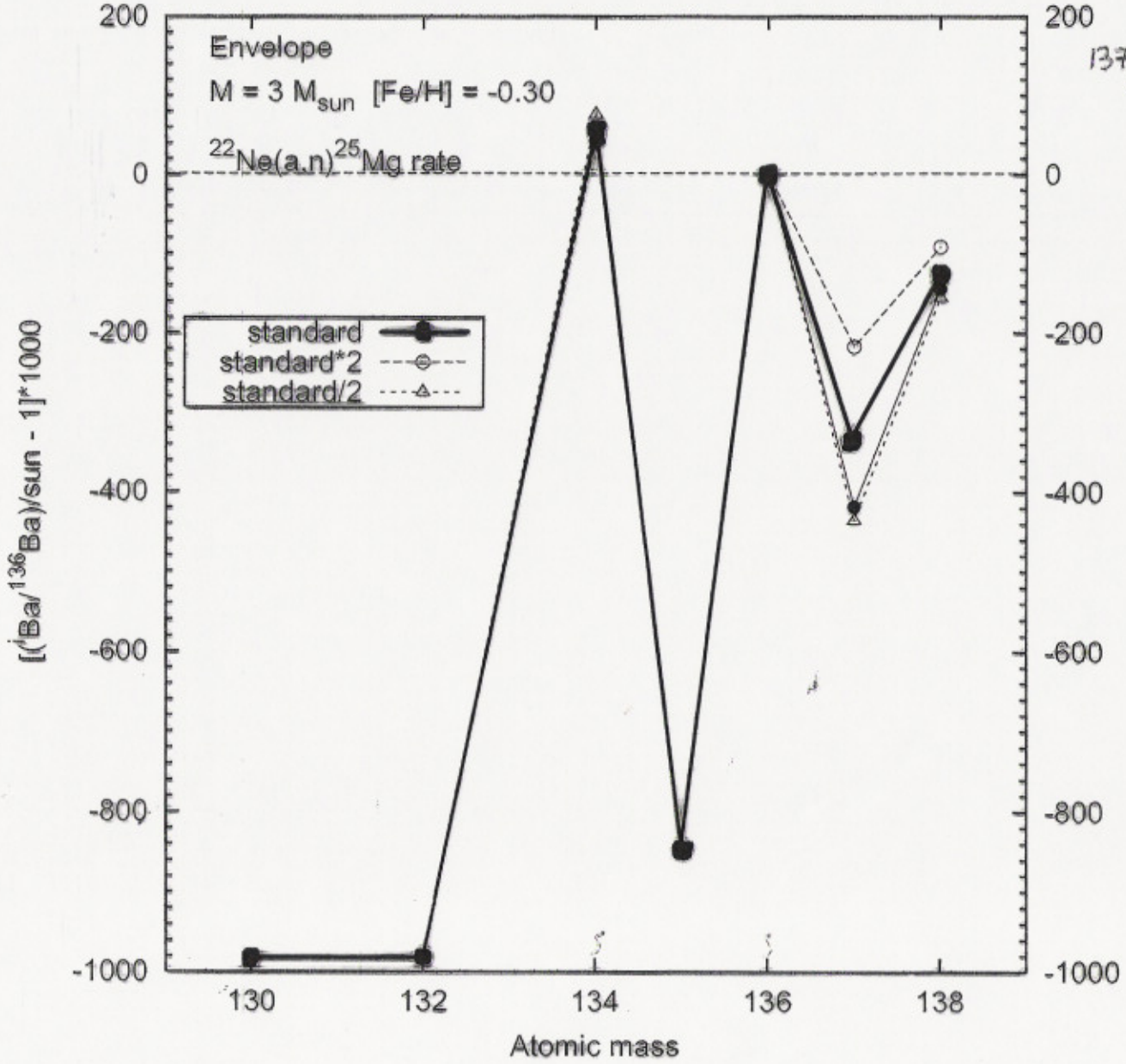

^{137}Ba → +23% (rate *2)
−11% (rate/2)

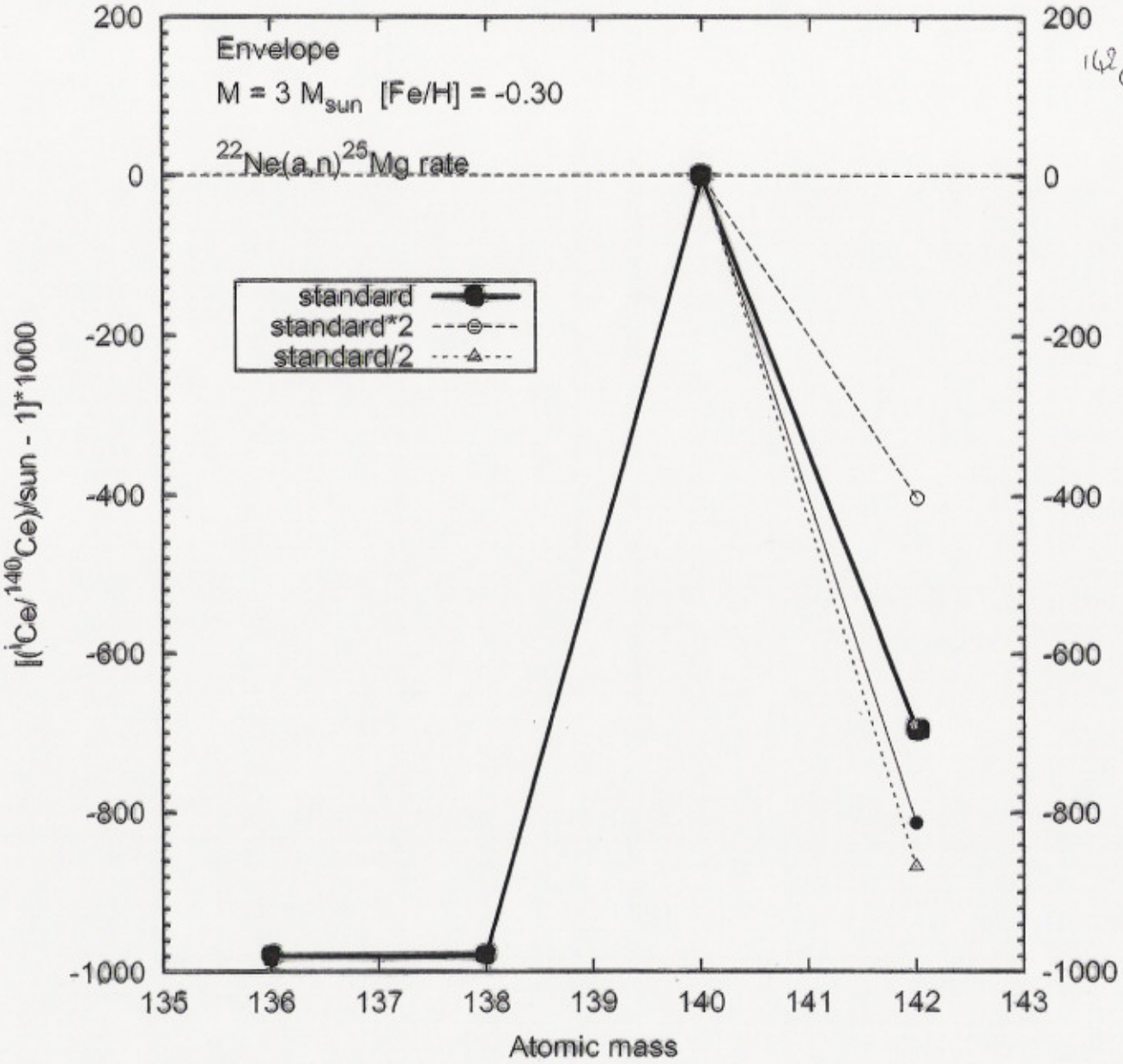

^{142}Ce → +96% (rate*2)
−54% (rate/2)

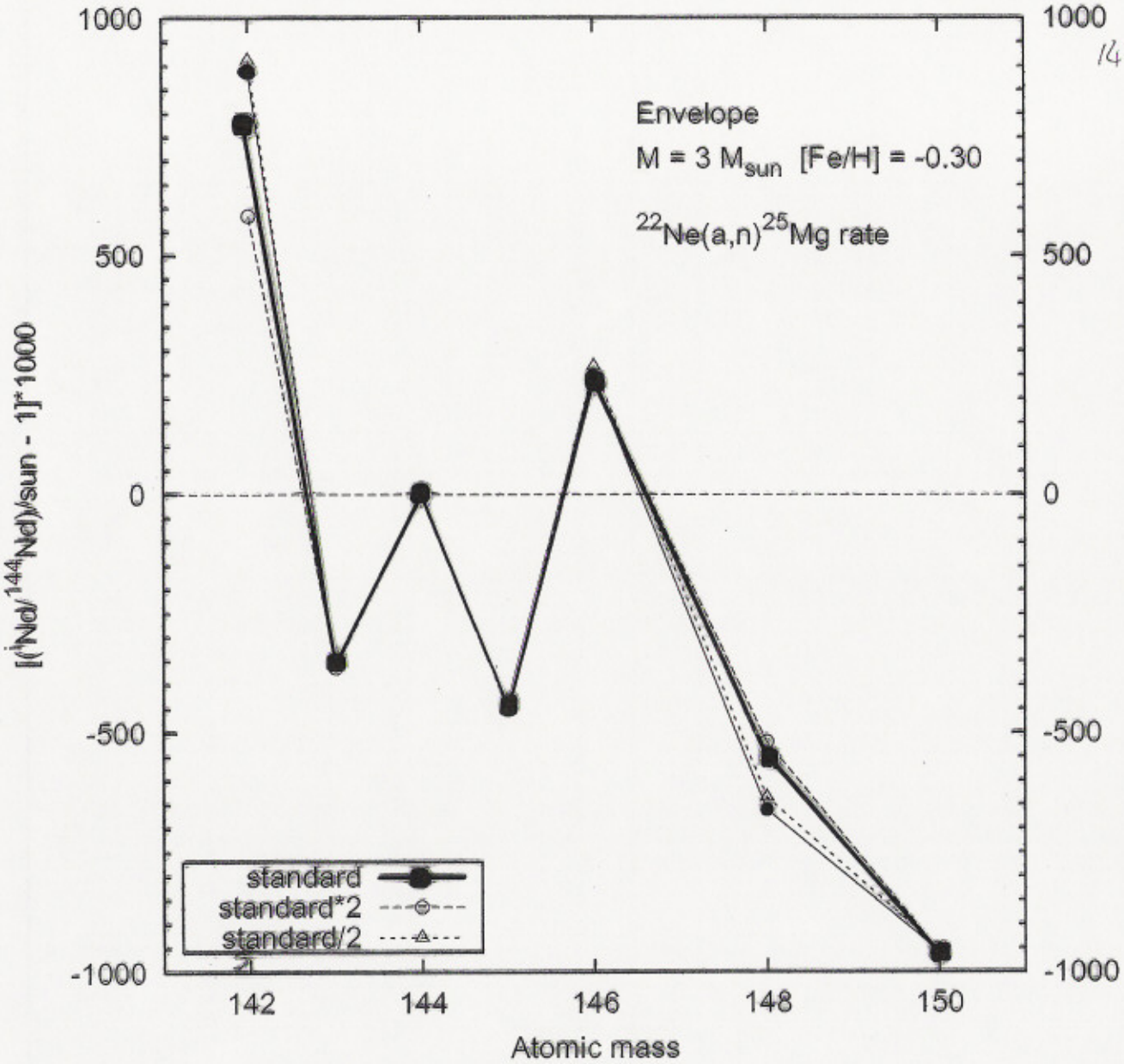

^{142}Nd → −11% (rate * 2)
+9% (rate / 2)

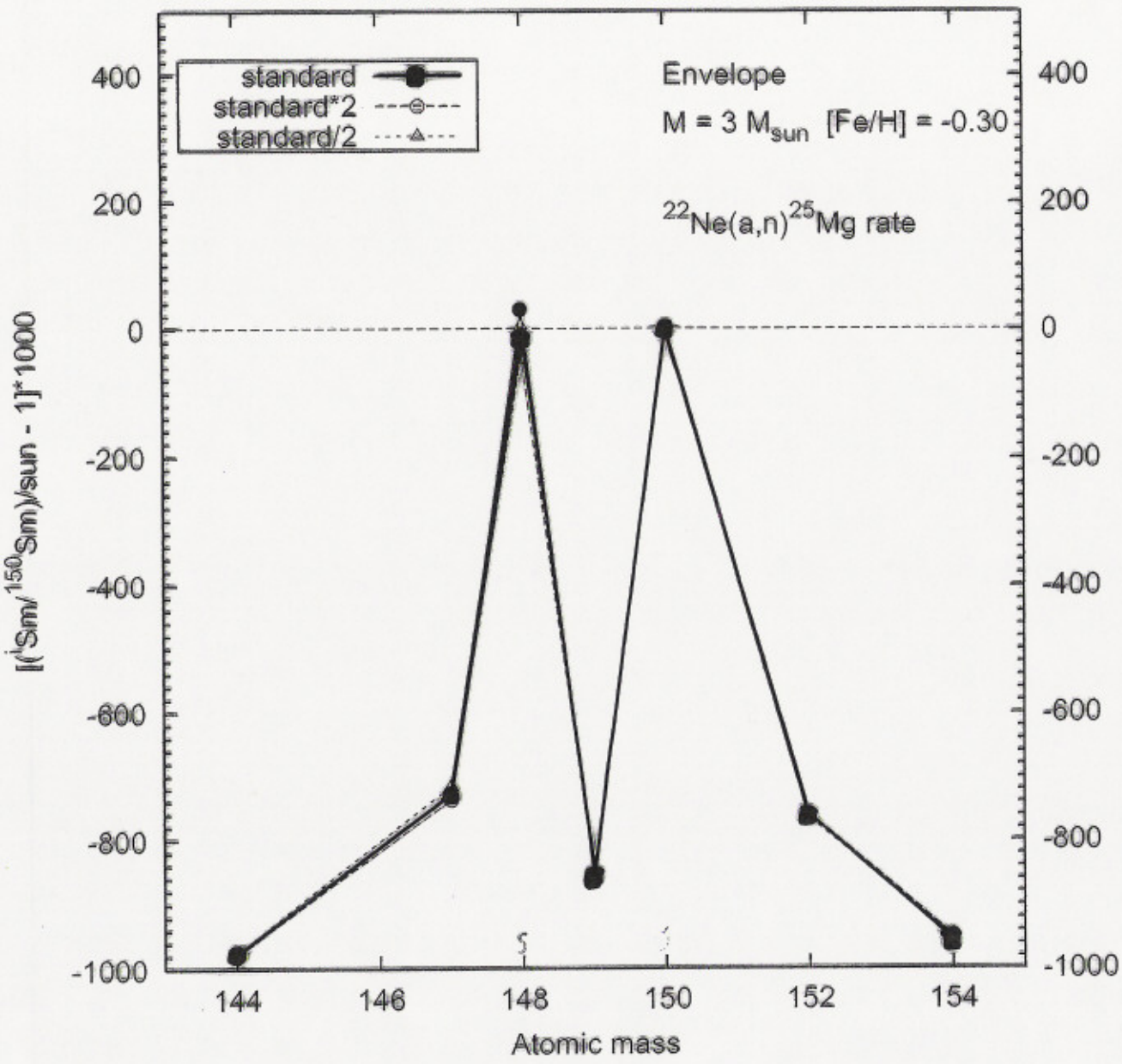
standard
standard*2
standard/2
Envelope
M = 3 M_sun [Fe/H] = -0.30
22Ne(a,n)25Mg rate
[(iSm/150Sm)/sun - 1]*1000
Atomic mass
400
200
0
-200
-400
-600
-800
-1000
144
146
148
150
152
154

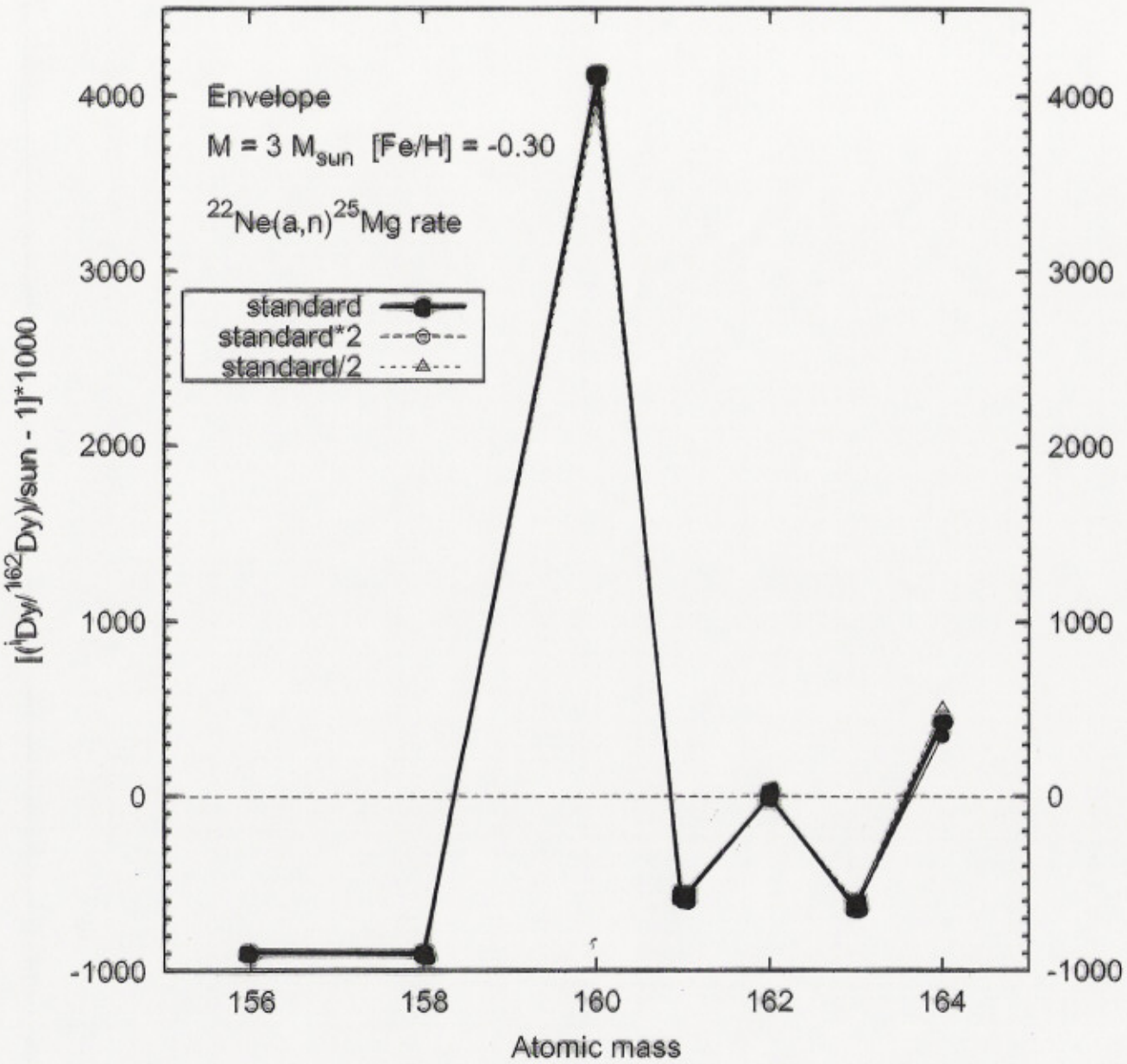
Envelope
M = 3 M_sun [Fe/H] = -0.30
22Ne(a,n)25Mg rate
standard
standard*2
standard/2
[(iDy/162Dy)/sun - 1]*1000
Atomic mass
4000
3000
2000
1000
0
-1000
156
158
160
162
164

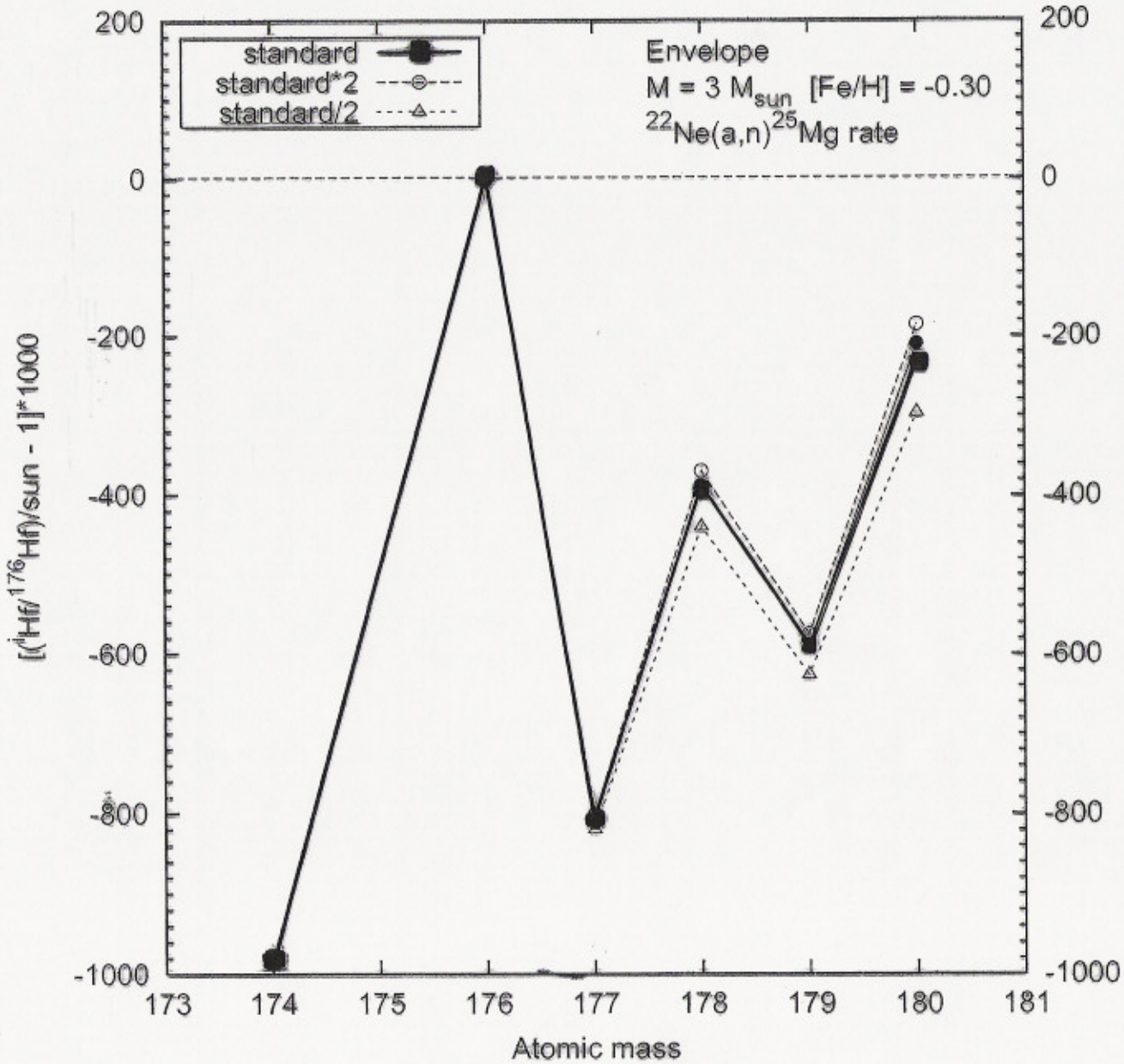
standard
standard*2
standard/2
Envelope
M = 3 M_sun [Fe/H] = -0.30
22Ne(a,n)25Mg rate
[(iHf/176Hf)/sun - 1]*1000
Atomic mass
200
0
-200
-400
-600
-800
-1000
173
174
175
176
177
178
179
180
181

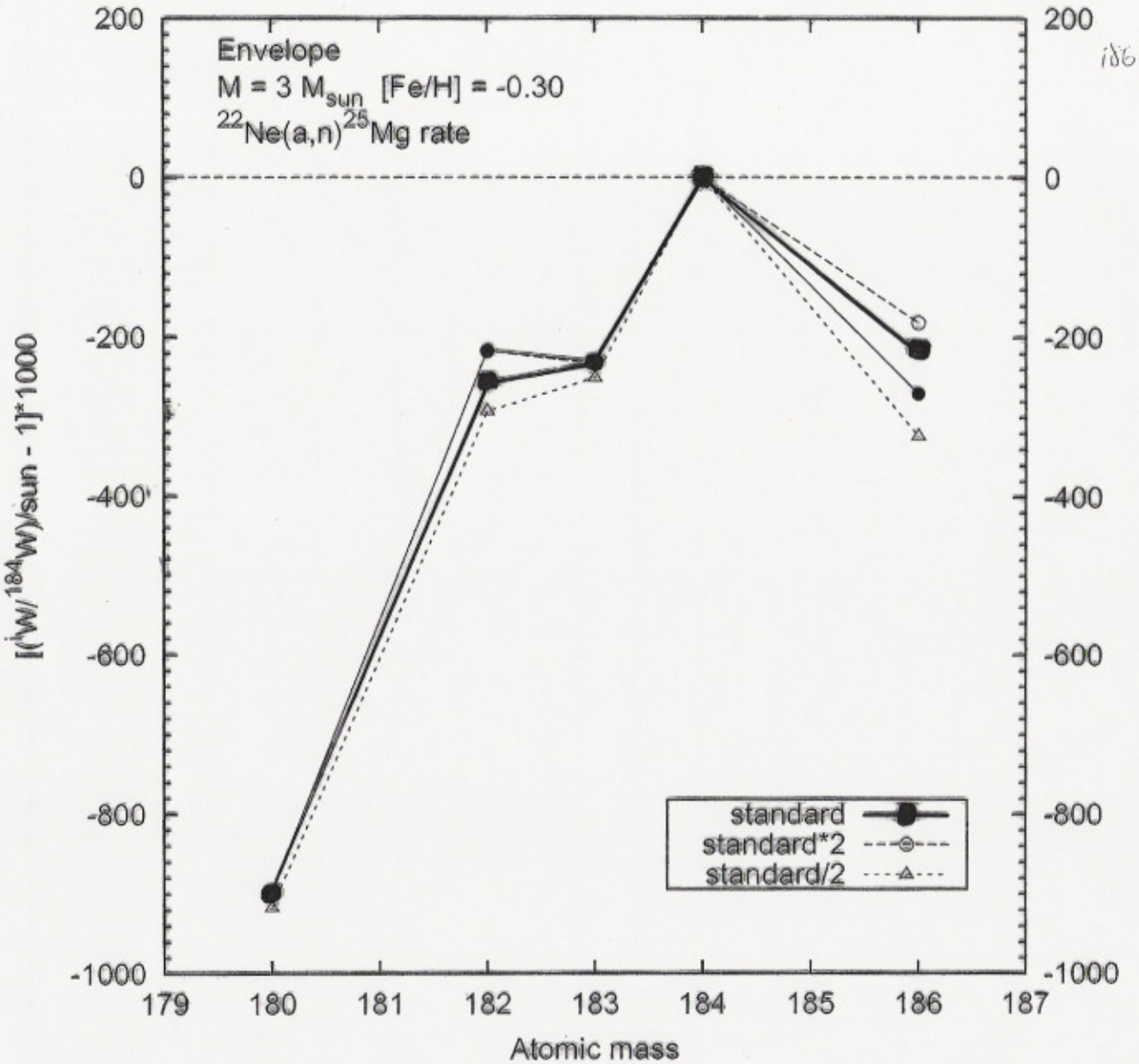

$^{186}W \rightarrow +4\%$ (rate *2)
-13% (rate/2)

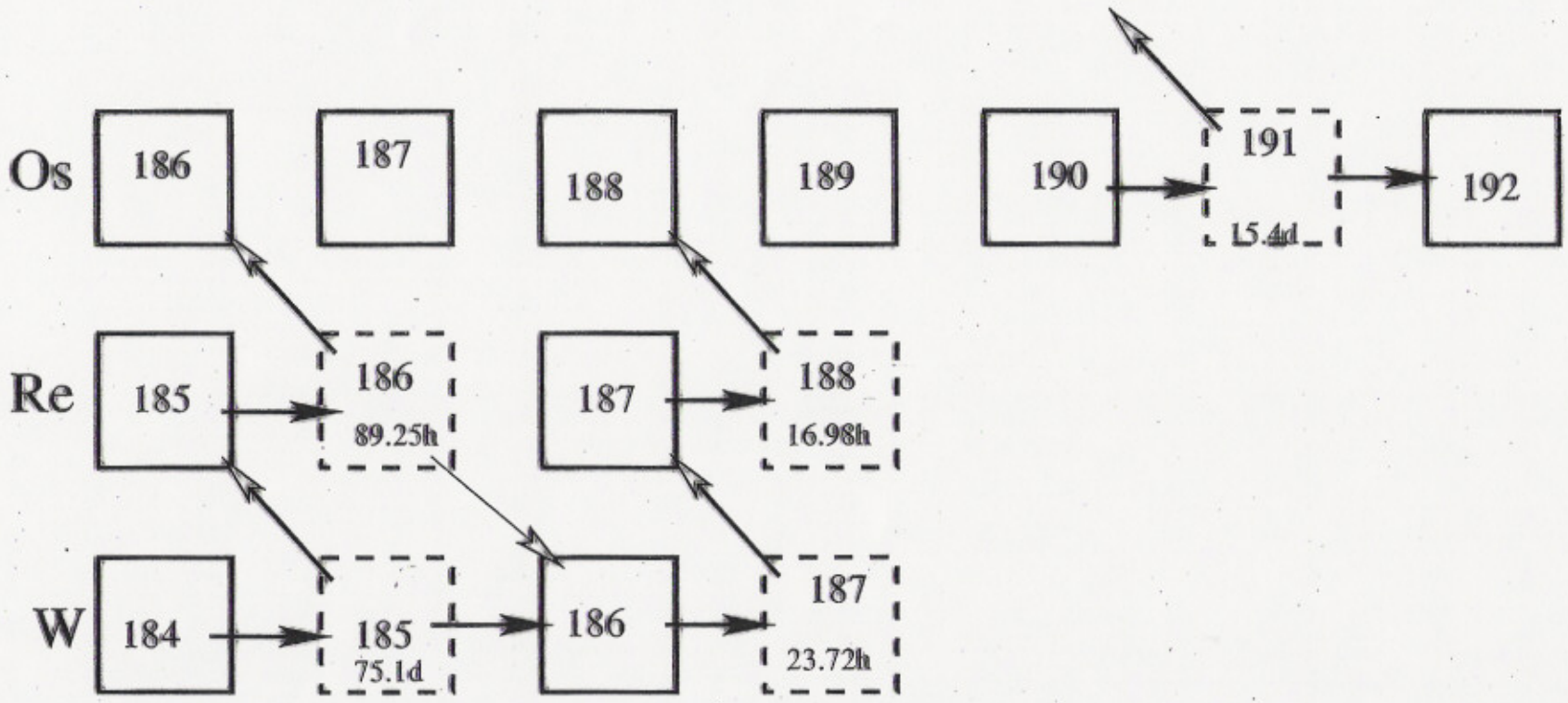
Os
186
187
188
189
190
191
15.4d
192
Re
185
186
89.25h
187
188
16.98h
W
184
185
75.1d
186
187
23.72h

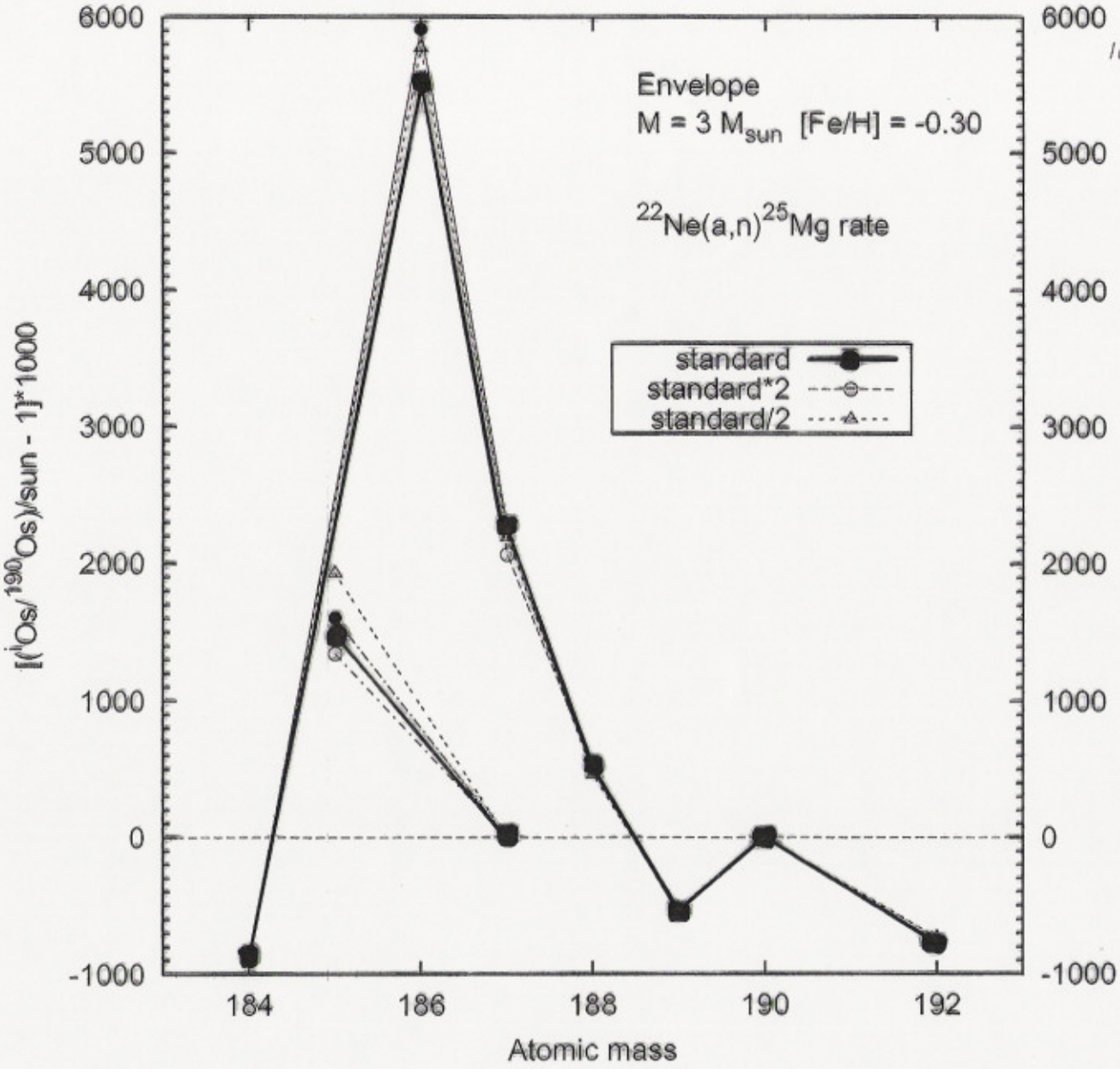

^{185}Re → +16% (rate/2)
−5% (rate*2)

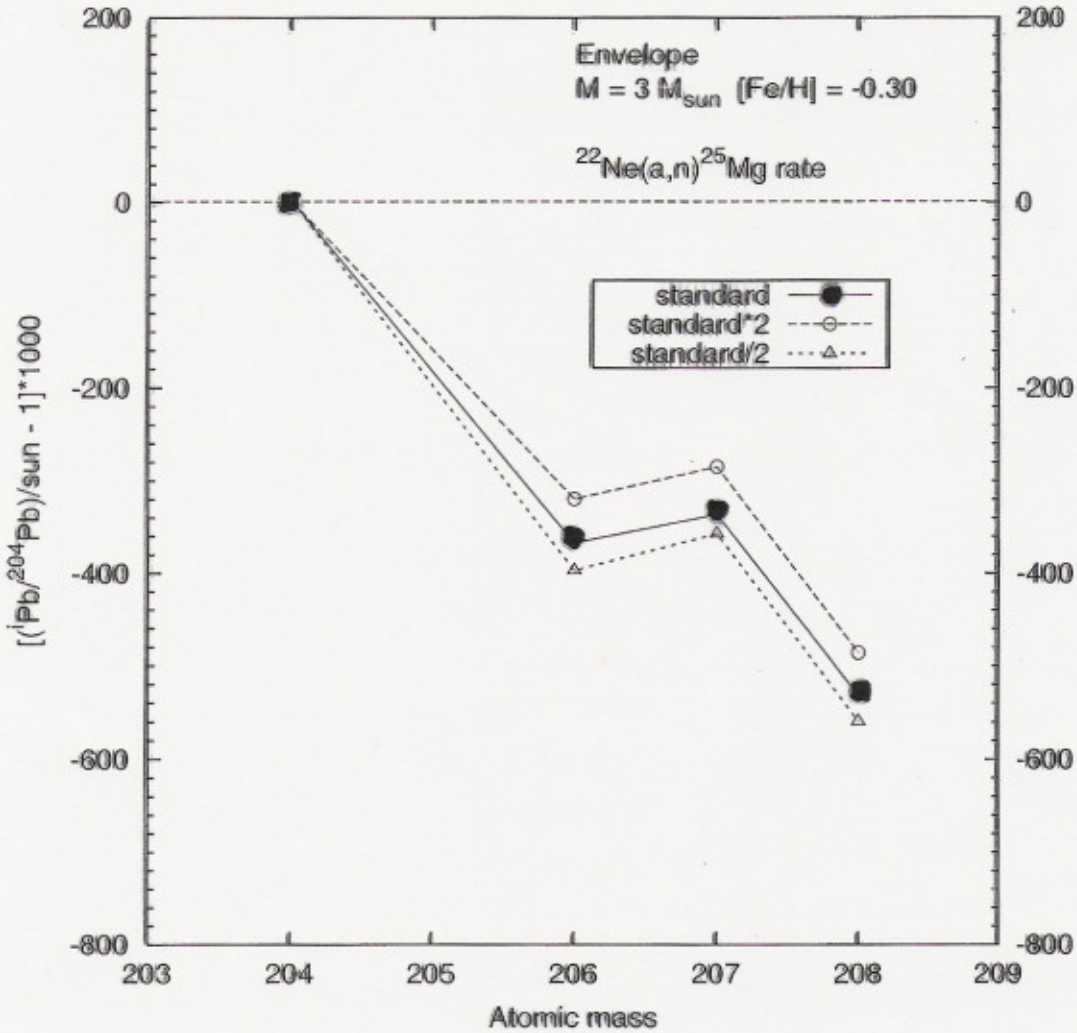

Figure 1:

Variations due to ^{204}Pb.

Contribution by

Michael Paul

Racah Inst. of Physics
paul@vms.huji.ac.il

22 pages

Cross Section of the $^{62}Ni(n,\gamma)^{63}Ni$ Reaction at Stellar Temperatures : Activation Measurement with Accelerator Mass Spectrometry (AMS)

1. Principle of the measurement
2. Uncertainties and discrepancies in estimates of the ^{62}Ni (n,γ) cross section.
3. Measurement and results

Collaborators :

Hebrew U. : S. Ghelberg, H. Nasar, M.P.
Forschungszentrum Karlsruhe : S. Dababneh, M. Heil, F. Kaeppeler, R. Plag
Argonne Nat. Lab. : I. Ahmad, J.P. Greene, D.J. Henderson, C.L. Jiang, R.C. Pardo, S. Sinha, T. Pennington, K.E. Rehm, R. Scott, X. Tang, R. Vondrasek
U. Jyvaskyla : H. Koivisto
Los Alamos Nat. Lab. : R. Reifarth
Soreq NRC : D. Berkovits, M. Bettan
U. Notre-Dame : P. Collon, S. O'Brien
U. Ioannina : N. Patronis

Principle :

- Activate enriched ^{62}Ni target with quasi-Maxwellian neutrons of $kT = 30$ keV (monitor neutron fluence $\langle \phi\, t \rangle$)

-Measure the isotopic abundance ^{63}Ni/^{62}Ni with accelerator mass spectrometry :
^{63}Ni : $t_{1/2} = 100$ yr, $Q_{\beta^-} = 70$ keV, no γ

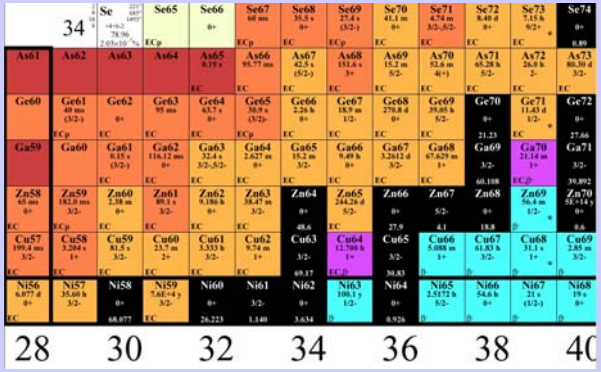

- Determine cross section from relation :

$$^{63}\text{Ni}/^{62}\text{Ni} = \sigma \langle \phi\, t \rangle$$

	34 (2, 8, 18, 6)	Se 221° 685° 1493° +4+6-2 78.96 2.03×10^{-7}%	Se65 ECp	Se66 0+	Se67 60 ms ECp	Se68 35.5 s 0+ EC	Se69 27.4 s (3/2-) ECp	Se70 41.1 m 0+ EC	Se71 4.74 m 3/2-,5/2- EC	Se72 8.40 d 0+ EC	Se73 7.15 h 9/2+ * EC	Se74 0+ 0.89
As61	As62	As63	As64	As65 0.19 s EC	As66 95.77 ms EC	As67 42.5 s (5/2-) EC	As68 151.6 s 3+ EC	As69 15.2 m 5/2- EC	As70 52.6 m 4(+) EC	As71 65.28 h 5/2- EC	As72 26.0 h 2- EC	As73 80.30 d 3/2- EC
Ge60	Ge61 40 ms (3/2-) ECp	Ge62 0+ EC	Ge63 95 ms EC	Ge64 63.7 s 0+ EC	Ge65 30.9 s (3/2)- ECp	Ge66 2.26 h 0+ EC	Ge67 18.9 m 1/2- EC	Ge68 270.8 d 0+ EC	Ge69 39.05 h 5/2- EC	Ge70 0+ 21.23	Ge71 11.43 d 1/2- * EC	Ge72 0+ 27.66
Ga59	Ga60	Ga61 0.15 s (3/2-) EC	Ga62 116.12 ms 0+ EC	Ga63 32.4 s 3/2-,5/2- EC	Ga64 2.627 m 0+ EC	Ga65 15.2 m 3/2- EC	Ga66 9.49 h 0+ EC	Ga67 3.2612 d 3/2- EC	Ga68 67.629 m 1+ EC	Ga69 3/2- 60.108	Ga70 21.14 m 1+ EC,β-	Ga71 3/2- 39.892
Zn58 65 ms 0+ EC	Zn59 182.0 ms 3/2- ECp	Zn60 2.38 m 0+ EC	Zn61 89.1 s 3/2- EC	Zn62 9.186 h 0+ EC	Zn63 38.47 m 3/2- EC	Zn64 0+ 48.6	Zn65 244.26 d 5/2- EC	Zn66 0+ 27.9	Zn67 5/2- 4.1	Zn68 0+ 18.8	Zn69 56.4 m 1/2- * β-	Zn70 5E+14 y 0+ 0.6
Cu57 199.4 ms 3/2- EC	Cu58 3.204 s 1+ EC	Cu59 81.5 s 3/2- EC	Cu60 23.7 m 2+ EC	Cu61 3.333 h 3/2- EC	Cu62 9.74 m 1+ EC	Cu63 3/2- 69.17	Cu64 12.700 h 1+ EC,β-	Cu65 3/2- 30.83	Cu66 5.088 m 1+ β-	Cu67 61.83 h 3/2- β-	Cu68 31.1 s 1+ * β-	Cu69 2.85 m 3/2- β-
Ni56 6.077 d 0+ EC	Ni57 35.60 h 3/2-	Ni58 0+ 68.077	Ni59 7.6E+4 y 3/2- EC	Ni60 0+ 26.223	Ni61 3/2- 1.140	Ni62 0+ 3.634	Ni63 100.1 y 1/2- β-	Ni64 0+ 0.926	Ni65 2.5172 h 5/2- β-	Ni66 54.6 h 0+ β-	Ni67 21 s (1/2-) β-	Ni68 19 s 0+ β-
28	30	32	34	36	38	40						

Principle :

- Activate enriched ^{62}Ni target with quasi-Maxwellian neutrons of $kT = 30$ keV (monitor neutron fluence $\langle \phi\, t \rangle$)

-Measure the isotopic abundance ^{63}Ni/^{62}Ni with accelerator mass spectrometry :
^{63}Ni : $t_{1/2} = 100$ yr, $Q_{\beta^-} = 70$ keV, no γ

- Determine cross section from relation :

$$^{63}\mathrm{Ni}/^{62}\mathrm{Ni} = \sigma \langle \phi\, t \rangle$$

Discrepancies in $^{62}Ni(n,\gamma)$ measurements and calculations :

- "Experimental" values extrapolated from $\sigma_{th}(n,\gamma)$
- Calculations :
  e.g. : T. Rauscher and K.H. Guber, preprint 2003
- Direct capture contribution
- Subthreshhold resonance

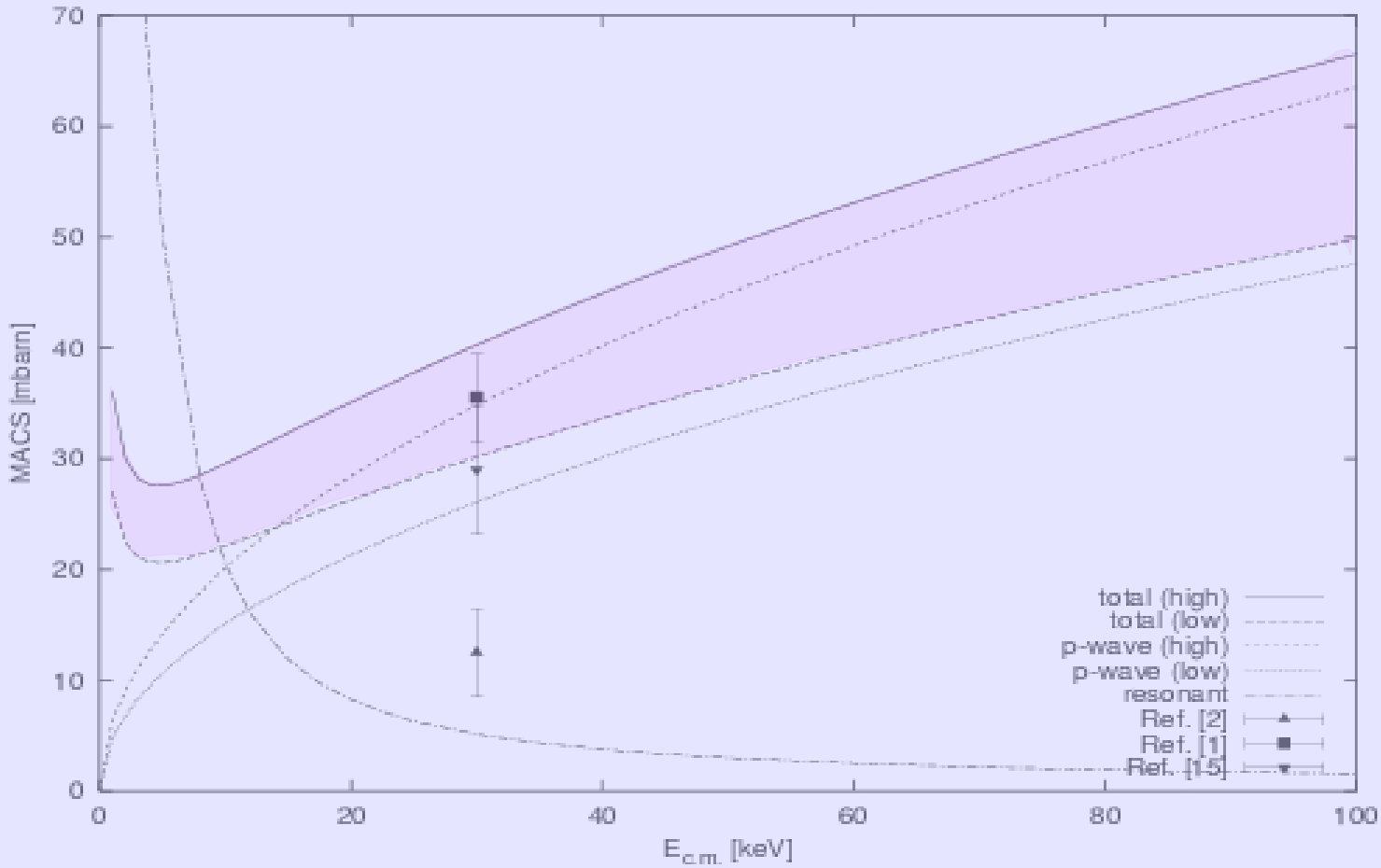

e.g. : massive star nucleosynthesis : overproduction of medium mass nuclei

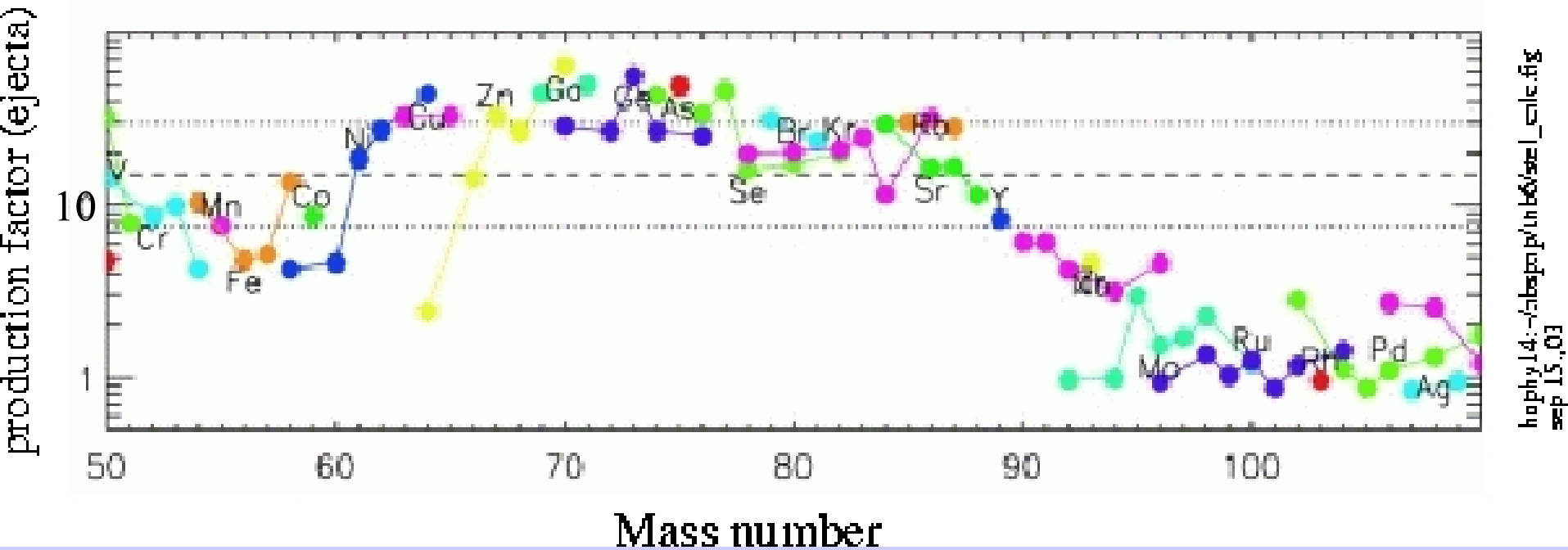

Ref. : T. Rauscher et al., Ap.J. 576 (2002) 323

Activation : 30 keV neutron flux (FZK)

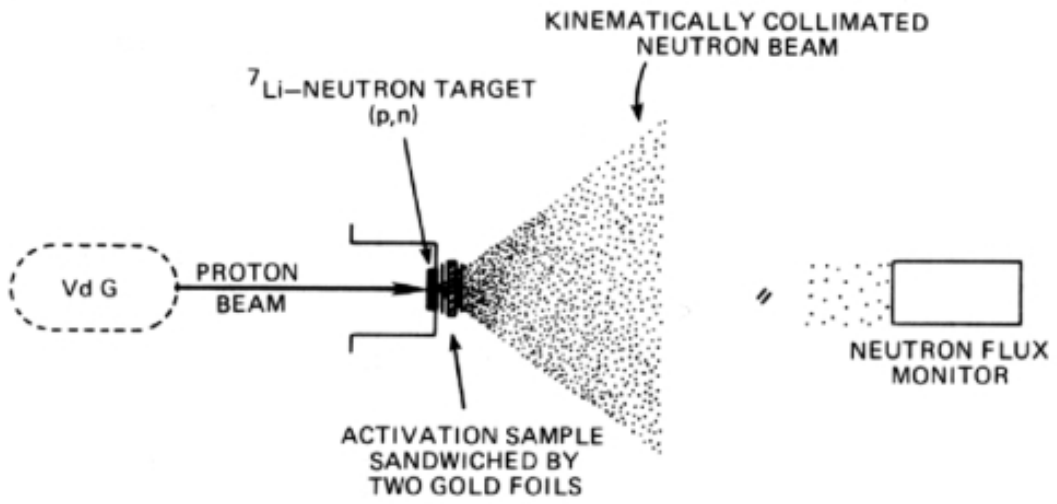

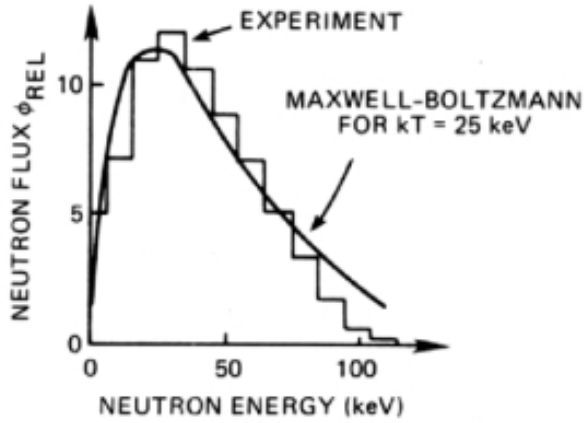

^{63}Ni/Ni measurement and ^{63}Ni separation from ^{63}Cu stable isobar :

1. Production of $^{63}Ni^{15+}$ ions in Electron Cyclotron Resonance Source (ECR), using nickelocene as source material

2. Acceleration to 9 MeV/nucleon at ATLAS (ANL)

3. Isobaric Separation in a Gas-Filled Enge Magnetic Spectrograph (GFM)

4. Isobaric Discrimination by E-multiple ΔE measurements in Focal Plane Detector and counting of ^{63}Ni ions

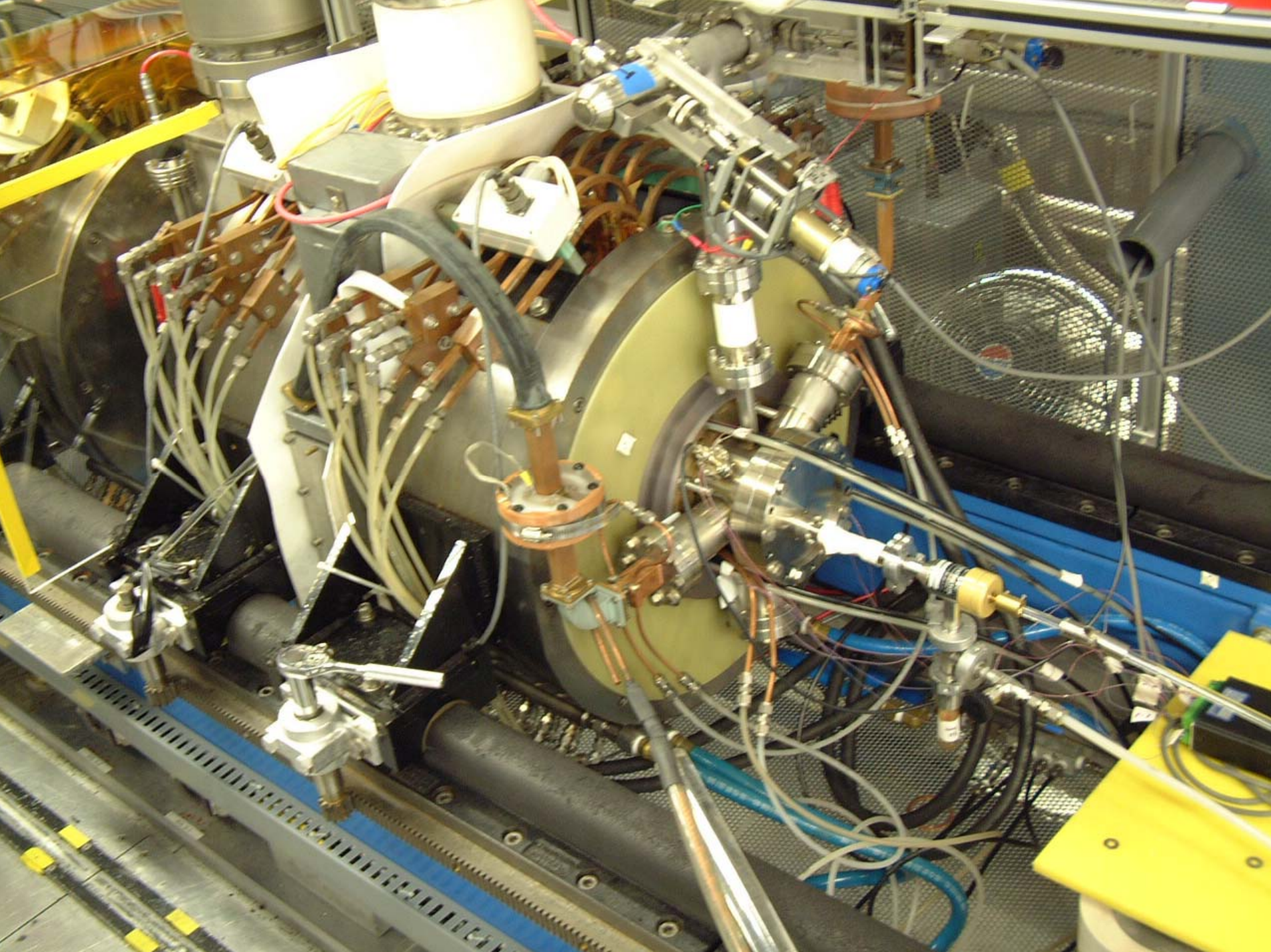

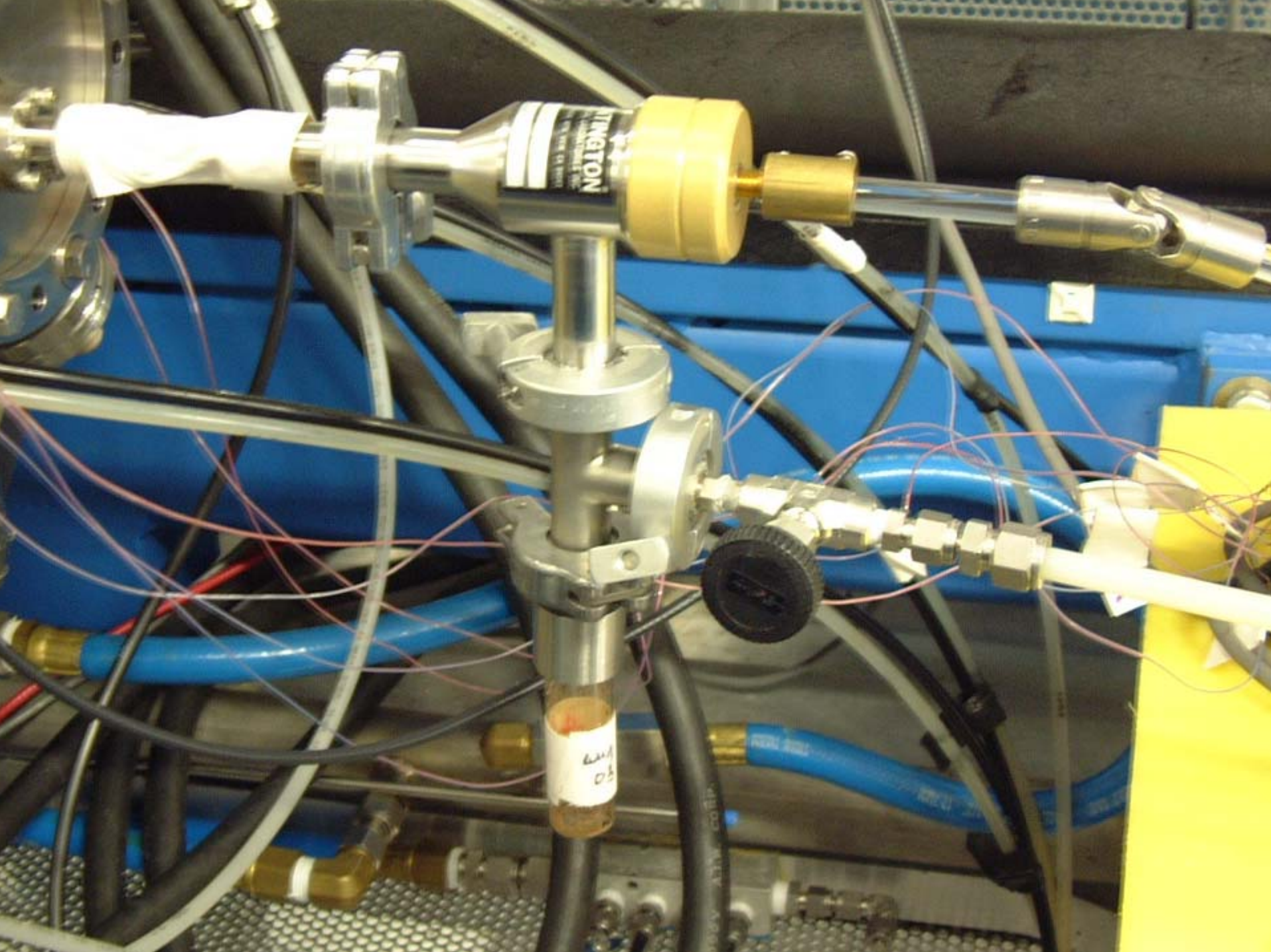
TINGLTON

Gas-filled magnetic spectrograph :

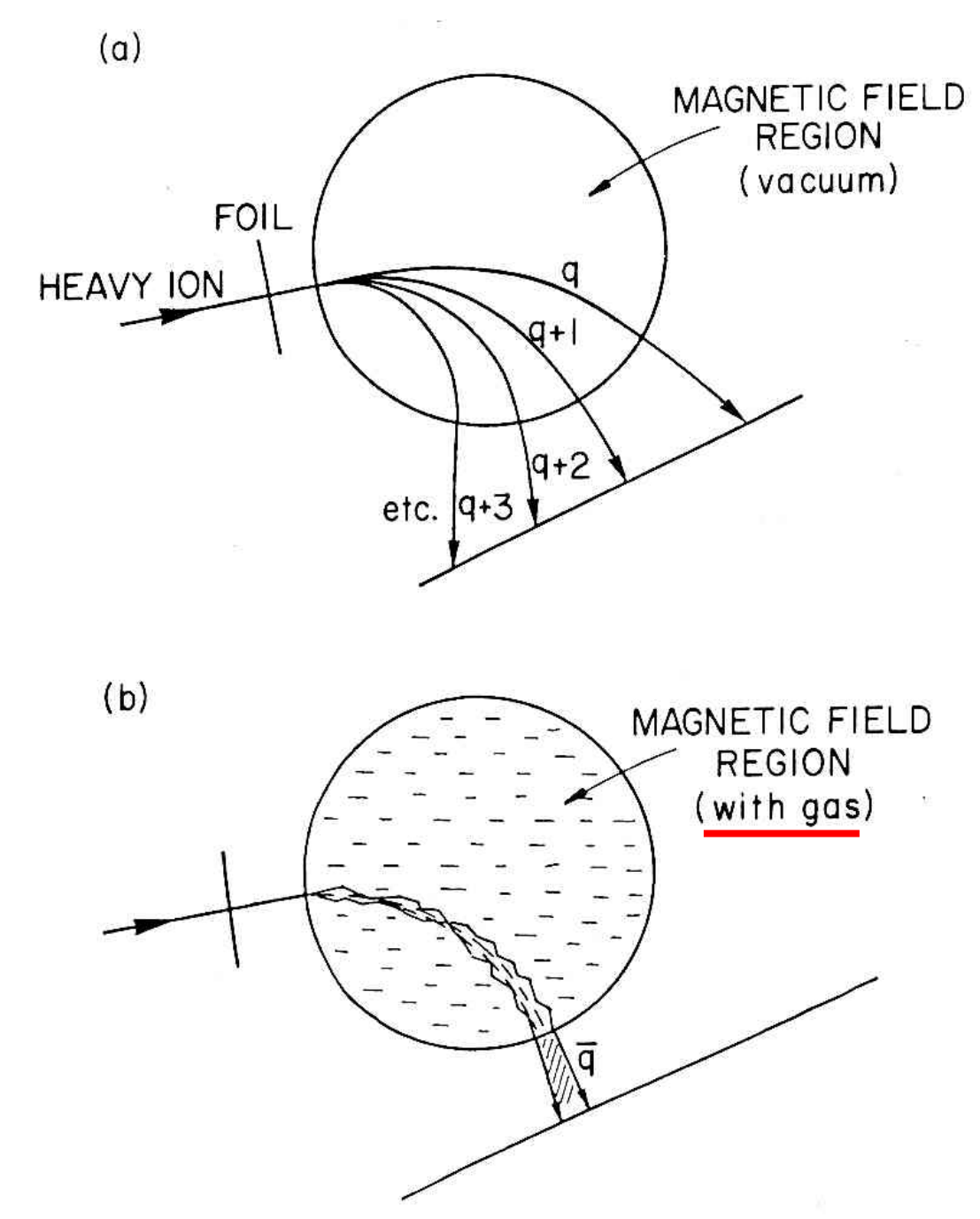

^{58}Ni (350 MeV)

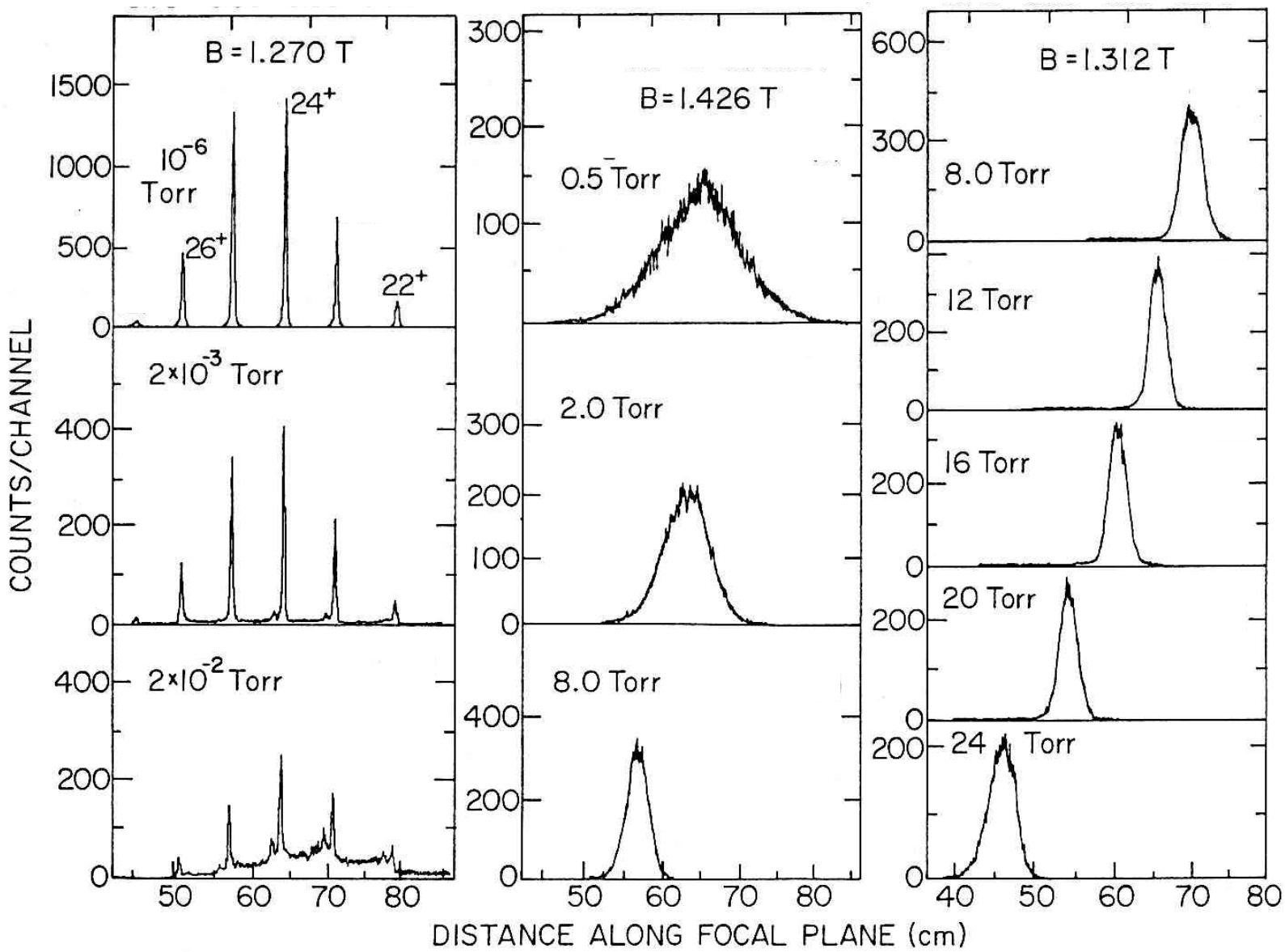
B = 1.270 T
10^{-6} Torr
26^+
24^+
22^+
2×10^{-3} Torr
2×10^{-2} Torr
B = 1.426 T
0.5 Torr
2.0 Torr
8.0 Torr
B = 1.312 T
8.0 Torr
12 Torr
16 Torr
20 Torr
24 Torr
COUNTS/CHANNEL
DISTANCE ALONG FOCAL PLANE (cm)

Isobaric separation in the gas-filled magnet

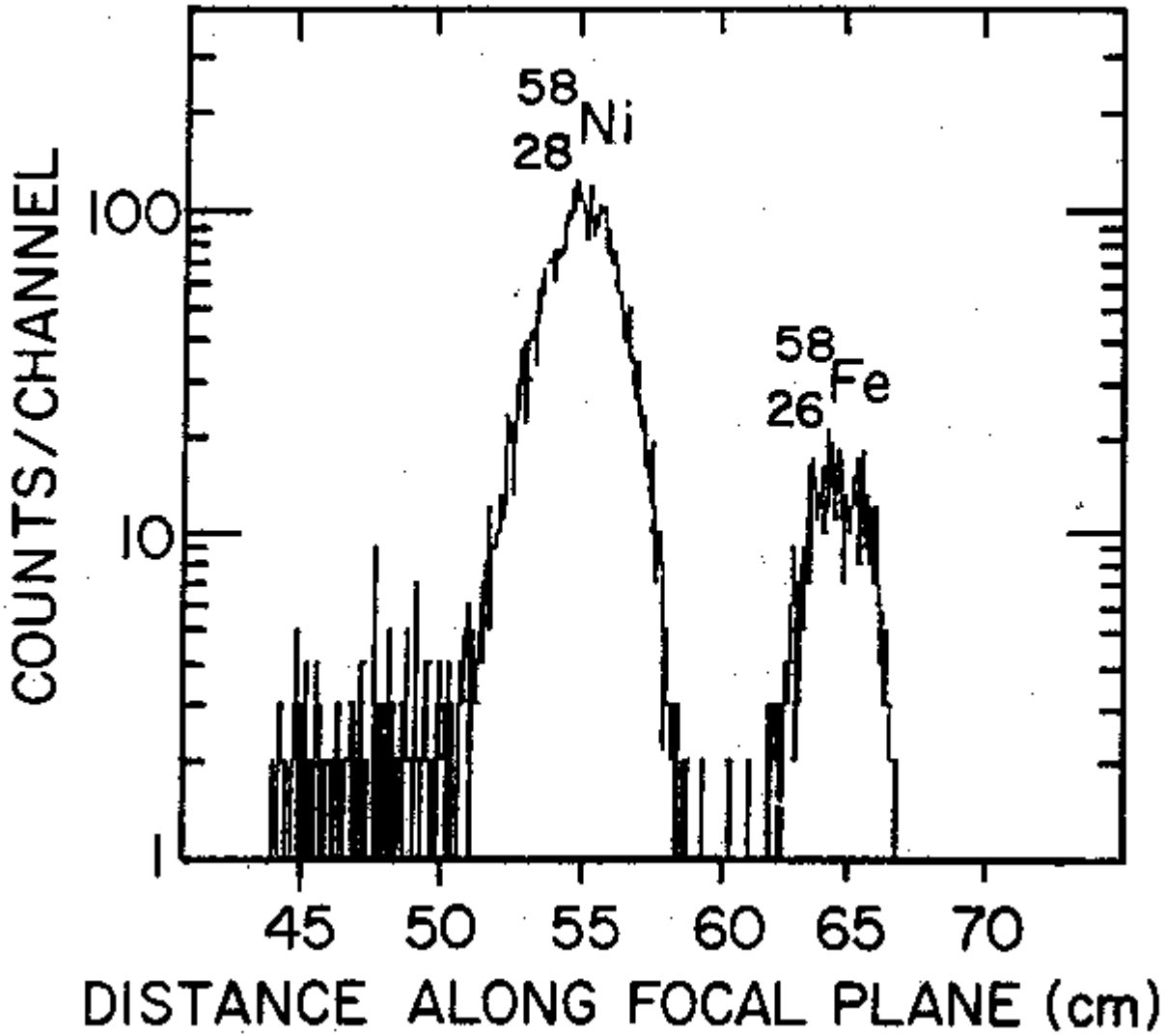

Ge59	Ge60	Ge61 40 ms (3/2-) ECp	Ge62 0+ EC	Ge63 95 ms EC	Ge64 63.7 s 0+ EC	Ge65 30.9 s (3/2)- ECp	Ge66 2.26 h 0+ EC	Ge67 18.9 m 1/2- EC	Ge68 270.8 d 0+ EC	Ge69 39.05 h 5/2- EC	Ge70 0+ 21.23
Ga58	Ga59	Ga60	Ga61 0.15 s (3/2-) EC	Ga62 116.12 ms 0+ EC	Ga63 32.4 s 3/2-,5/2- EC	Ga64 2.627 m 0+ EC	Ga65 15.2 m 3/2- EC	Ga66 9.49 h 0+ EC	Ga67 3.2612 d 3/2- EC	Ga68 67.629 m 1+ EC	Ga69 3/2- 60.108
Zn57 40 ms (7/2-) ECp	Zn58 65 ms 0+ EC	Zn59 182.0 ms 3/2- ECp	Zn60 2.38 m 0+ EC	Zn61 89.1 s 3/2- EC	Zn62 9.186 h 0+ EC	Zn63 38.47 m 3/2- EC	Zn64 0+ 48.6	Zn65 244.26 d 5/2- EC	Zn66 0+ 27.9	Zn67 5/2- 4.1	Zn68 0+ 18.8
Cu56	Cu57 199.4 ms 3/2- EC	Cu58 3.204 s 1+ EC	Cu59 81.5 s 3/2- EC	Cu60 23.7 m 2+ EC	Cu61 3.333 h 3/2- EC	Cu62 9.74 m 1+ EC	Cu63 3/2- 69.17	Cu64 12.700 h 1+ EC,β-	Cu65 3/2- 30.83	Cu66 5.088 m 1+ β-	Cu67 61.83 h 3/2- β-
Ni55 212.1 ms 7/2- EC	Ni56 6.077 d 0+ EC	Ni57 35.60 h 3/2-	Ni58 0+ 68.077	Ni59 7.6E+4 y 3/2- EC	Ni60 0+ 26.223	Ni61 3/2- 1.140	Ni62 0+ 3.634	Ni63 100.1 y 1/2- β-	Ni64 0+ 0.926	Ni65 2.5172 h 5/2- β-	Ni66 54.6 h 0+ β-
Co54 193.23 ms 0+ * EC	Co55 17.53 h 7/2- EC	Co56 77.27 d 4+ EC	Co57 271.79 d 7/2- EC	Co58 70.82 d 2+ * EC	Co59 7/2- 100	Co60 5.2714 y 5+ *	Co61 1.650 h 7/2- β-	Co62 1.50 m 2+ * β-	Co63 27.4 s (7/2)- β-	Co64 0.30 s 1+ β-	Co65 1.20 s (7/2)- β-
Fe53 8.51 m 7/2- * EC	Fe54 0+ 5.8	Fe55 2.73 y 3/2- EC	Fe56 0+ 91.72	Fe57 1/2- 2.2	Fe58 0+ 0.28	Fe59 44.503 d 3/2- β-	Fe60 1.5E+6 y 0+ β-	Fe61 5.98 m 3/2-,5/2- β-	Fe62 68 s 0+ β-	Fe63 6.1 s (5/2)- β-	Fe64 2.0 s 0+ β-
Mn52 5.591 d 6+ * EC	Mn53 3.74E+6 y 7/2- EC	Mn54 312.3 d 3+ EC,β-	Mn55 5/2- 100	Mn56 2.5785 h 3+ β-	Mn57 85.4 s 5/2- β-	Mn58 3.0 s 0+ * β-	Mn59 4.6 s 3/2-,5/2- β-	Mn60 51 s 0+ * β-	Mn61 0.71 s (5/2-) β-	Mn62 0.88 s (3+) β-	Mn63 0.25 s β-
Cr51 27.702 d 7/2- EC	Cr52 0+ 83.789	Cr53 3/2- 9.501	Cr54 0+ 2.365	Cr55 3.497 m 3/2- β-	Cr56 5.94 m 0+ β-	Cr57 21.1 s 3/2-,5/2-,7/2- β-	Cr58 7.0 s 0+ β-	Cr59 0.74 s β-	Cr60 0.57 s 0+ β-	Cr61	Cr62 0+

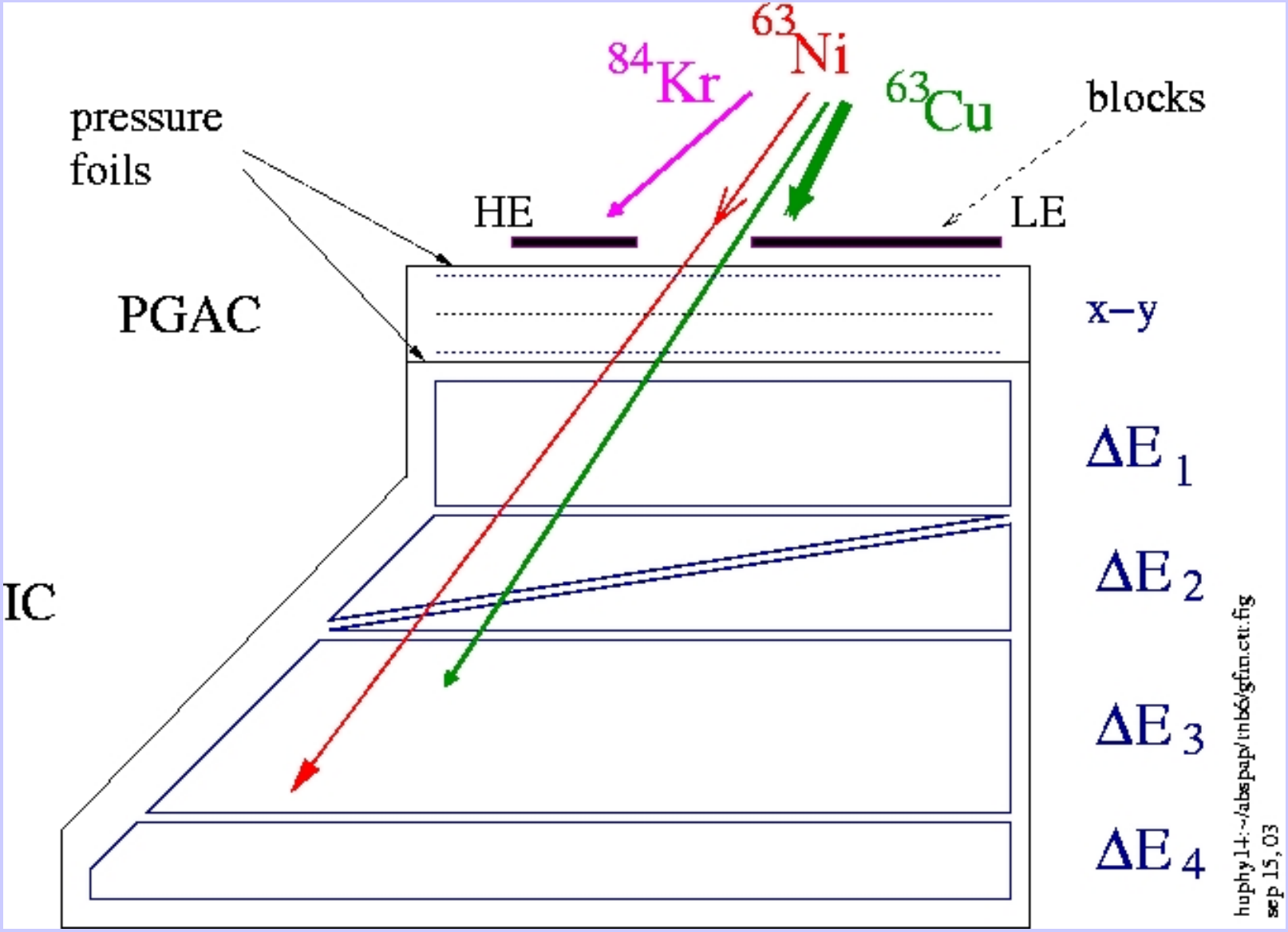
63Ni
84Kr
63Cu
pressure
foils
blocks
HE
LE
PGAC
x–y
ΔE 1
ΔE 2
IC
ΔE 3
ΔE 4
huphy14:~/abspap/inb6/gfin.ctt.fig
sep 15, 03

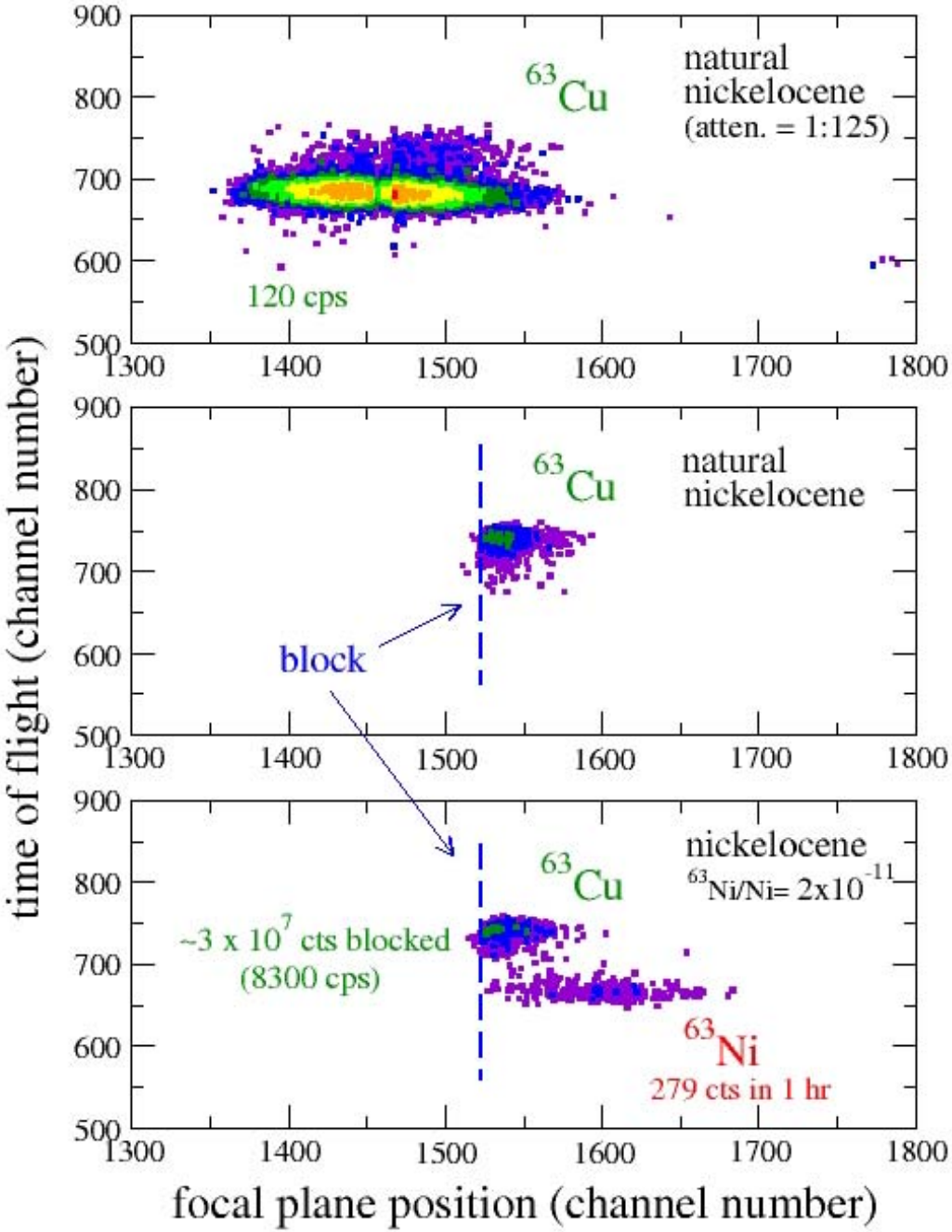
natural
nickelocene
(atten. = 1:125)
63Cu
120 cps
natural
nickelocene
63Cu
block
nickelocene
63Ni/Ni= 2x10-11
63Cu
~3 x 107 cts blocked
(8300 cps)
63Ni
279 cts in 1 hr
time of flight (channel number)
focal plane position (channel number)
900
800
700
600
500
1300
1400
1500
1600
1700
1800

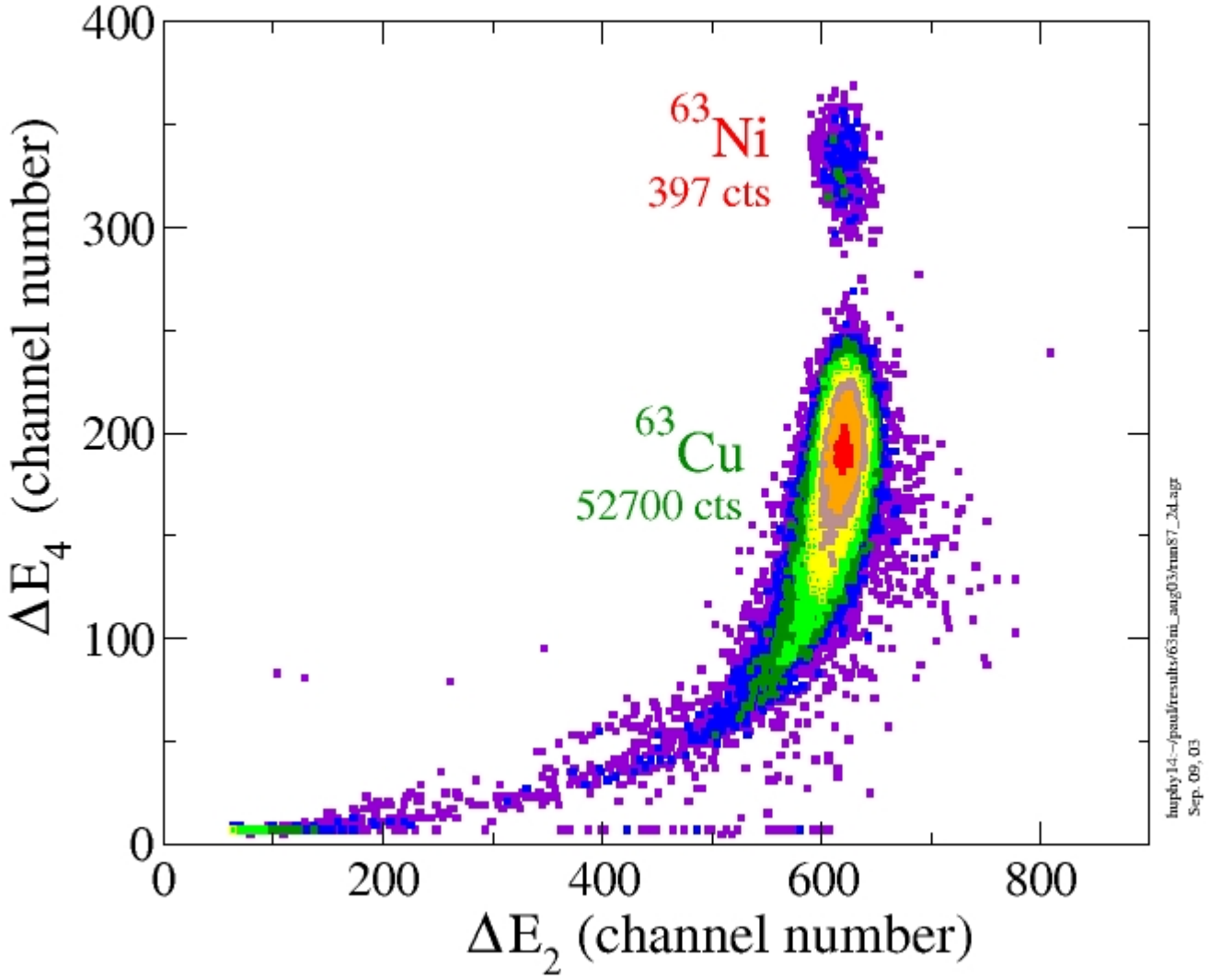
400
300
200
100
0
0
200
400
600
800
ΔE4 (channel number)
ΔE2 (channel number)
63Ni
397 cts
63Cu
52700 cts
hupby14:~/paul/results/63ni_aug03/run87_2d.agr
Sep. 09, 03

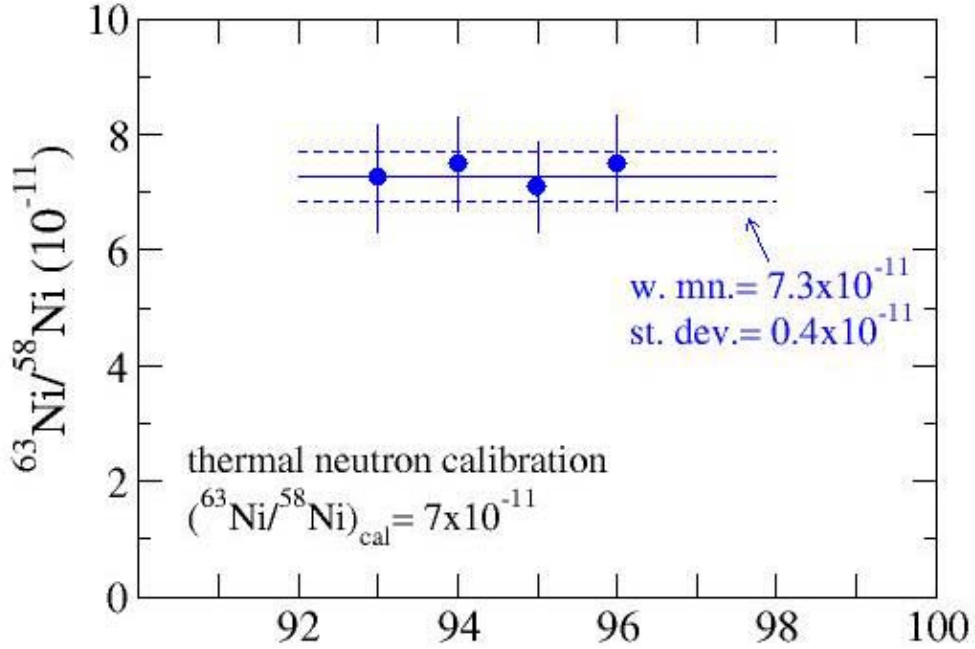
10
8
6
4
2
0
92
94
96
98
100
$^{63}Ni/^{58}Ni\ (10^{-11})$
w. mn.= 7.3x10^{-11}
st. dev.= 0.4x10^{-11}
thermal neutron calibration
$(^{63}Ni/^{58}Ni)_{cal}$= 7x10^{-11}

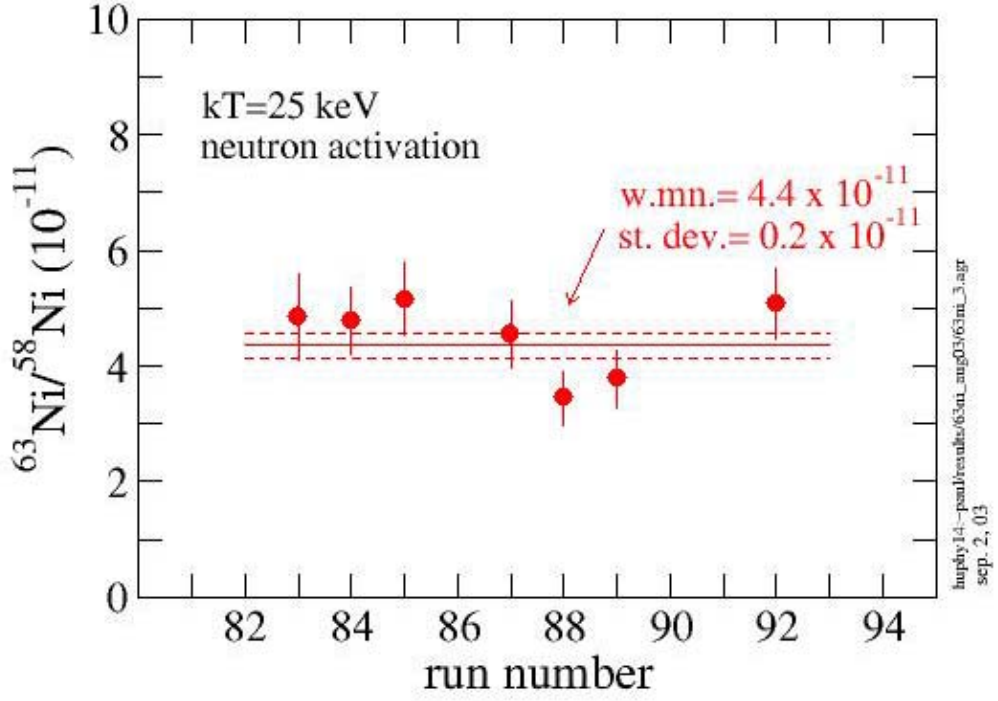
10
8
6
4
2
0
82
84
86
88
90
92
94
run number
$^{63}Ni/^{58}Ni\ (10^{-11})$
kT=25 keV
neutron activation
w.mn.= 4.4 x 10^{-11}
st. dev.= 0.2 x 10^{-11}
hupdy14:~paul/results/63ni_nug03/63ni_3.agr
sep. 2, 03

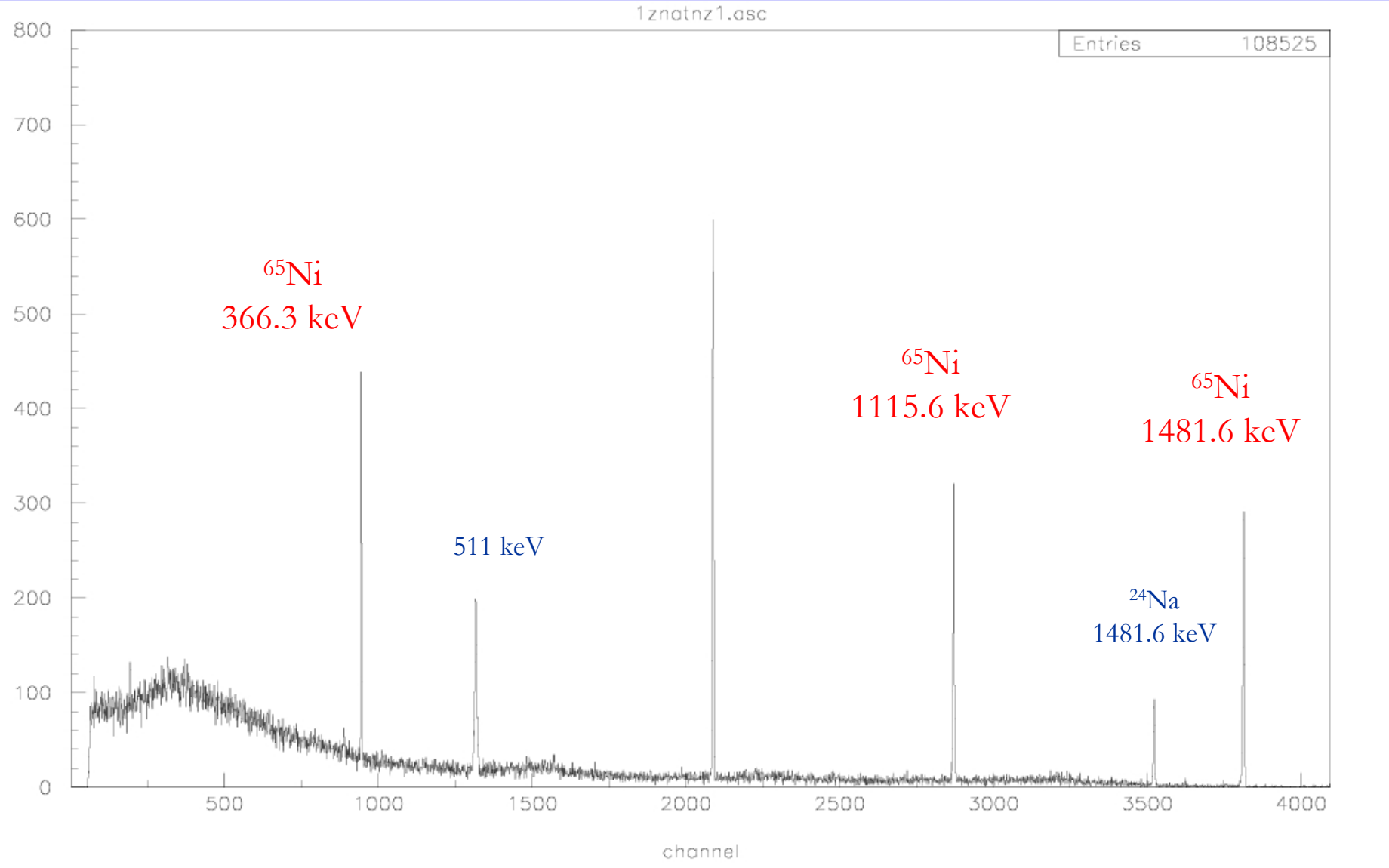
1znatnz1.asc
Entries 108525
800
700
600
500
400
300
200
100
0
500
1000
1500
2000
2500
3000
3500
4000
channel
65Ni
366.3 keV
511 keV
65Ni
1115.6 keV
65Ni
1481.6 keV
24Na
1481.6 keV

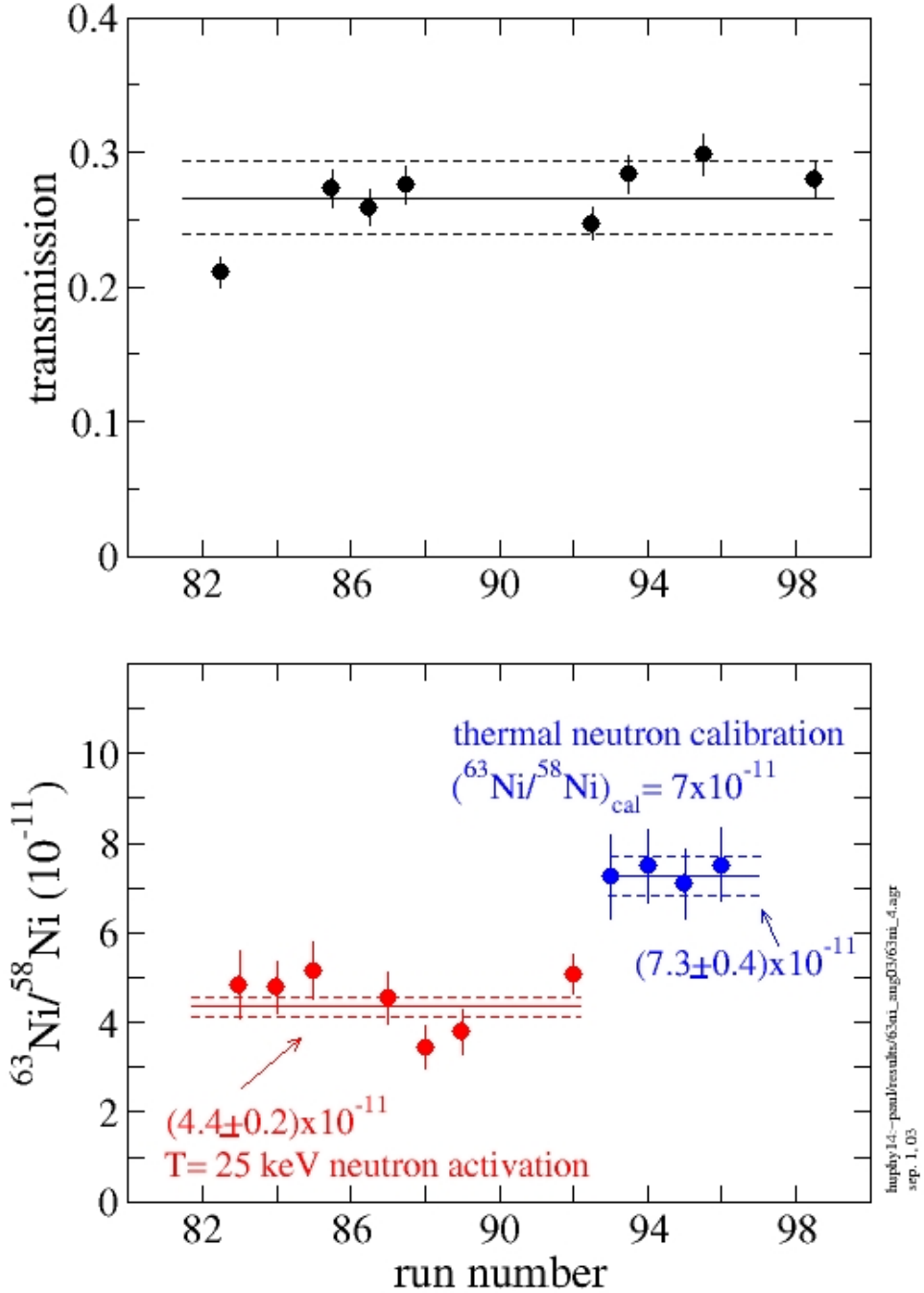
transmission
0.4
0.3
0.2
0.1
0
82
86
90
94
98
thermal neutron calibration
$(^{63}Ni/^{58}Ni)_{cal} = 7x10^{-11}$
$(7.3\pm0.4)x10^{-11}$
$(4.4\pm0.2)x10^{-11}$
T= 25 keV neutron activation
$^{63}Ni/^{58}Ni\ (10^{-11})$
10
8
6
4
2
0
run number
lurphy14:~paul/results/63ni_aug03/63ni_4.agr
sep. 1, 03

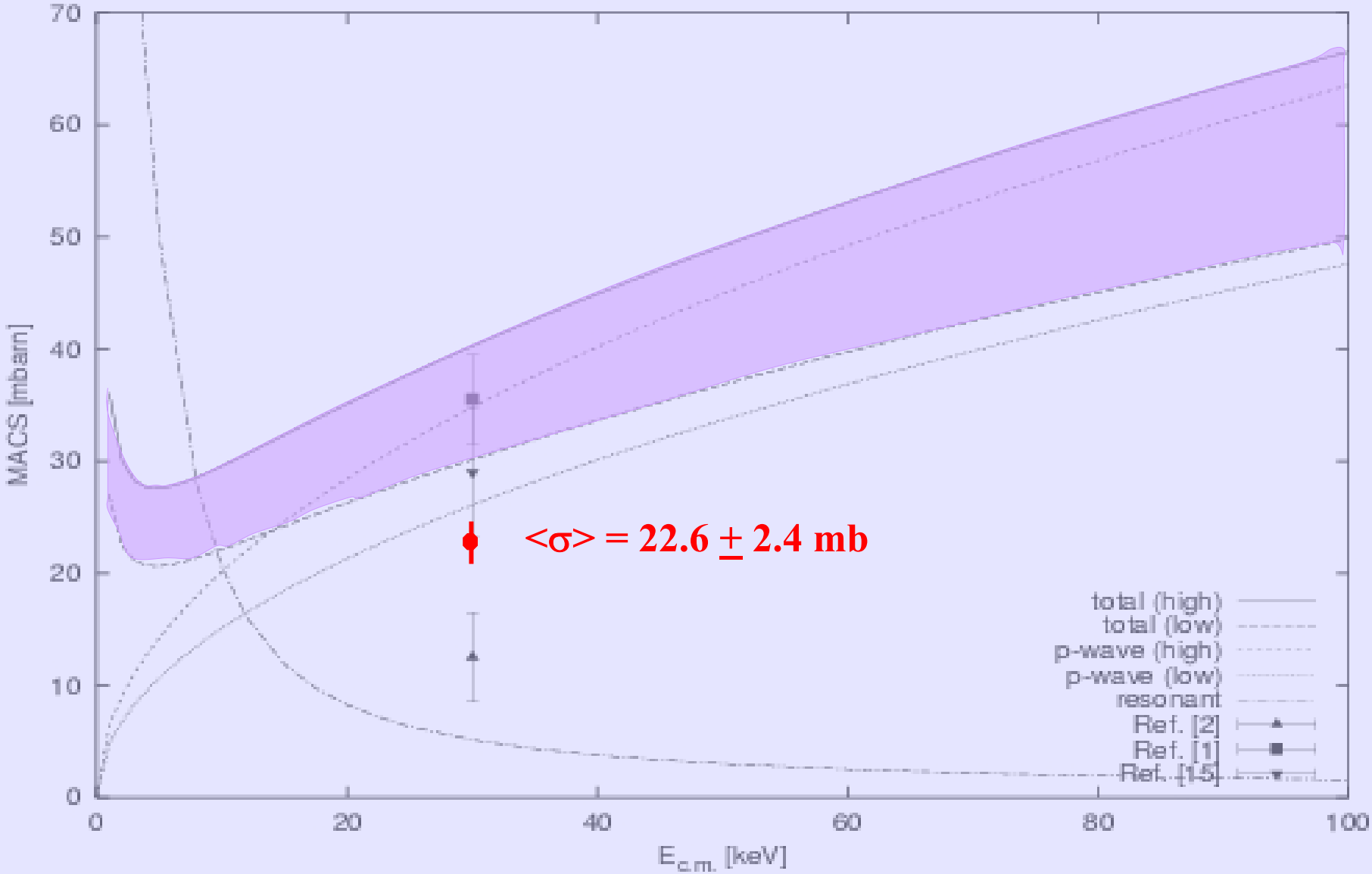
70
60
50
40
30
20
10
0
MACS [mbarn]
0
20
40
60
80
100
E c.m. [keV]
<σ> = 22.6 ± 2.4 mb
total (high)
total (low)
p-wave (high)
p-wave (low)
resonant
Ref. [2]
Ref. [1]
Ref. [15]

Contribution by

Goran Arbanas

Oak Ridge National Laboratory
arbanasg@ornl.gov

18 pages

UT-BATTELLE

Use of the direct-semidirect model to estimate capture between resonances

Goran Arbanas, ORNL

Frank Dietrich, LLNL

Arthur Kerman, MIT

DANCE Workshop, February 2-4, 2004, Santa Fe, NM

Topics to be covered

- Physics in direct-semidirect capture model
- Why direct-semidirect capture at low energies must be treated differently than at high energies
- Importance of single-particle resonances

Two interfering terms in direct-semidirect capture

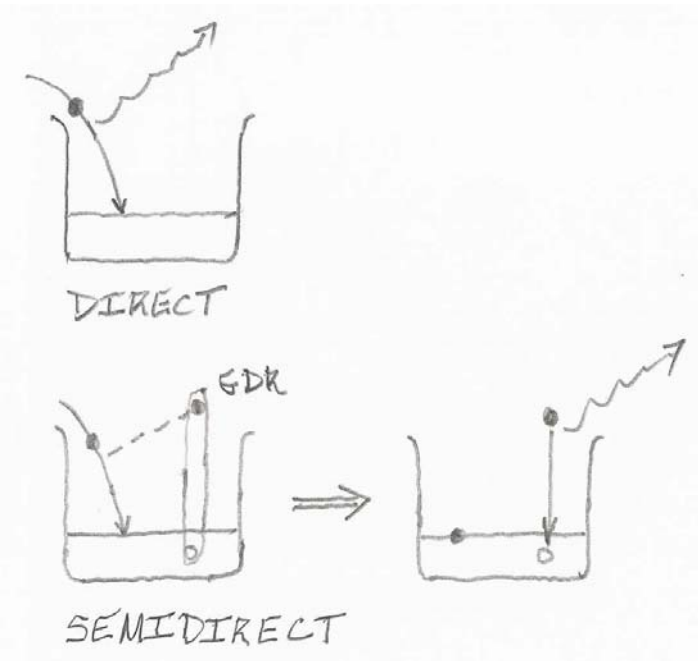

Projectile radiates and is captured into a well

1) Projectile excites giant dipole resonance and is captured;

2) Giant dipole collapses and emits the gamma ray

Effective radial electromagnetic operator:

$$Q_L = q_L r^L + \left(\frac{1}{E_\gamma - E_{res} + i\Gamma/2} - \frac{1}{E_\gamma + E_{res}} \right) h_L'(r)$$

direct **semidirect**

DSD describes data well at high energies

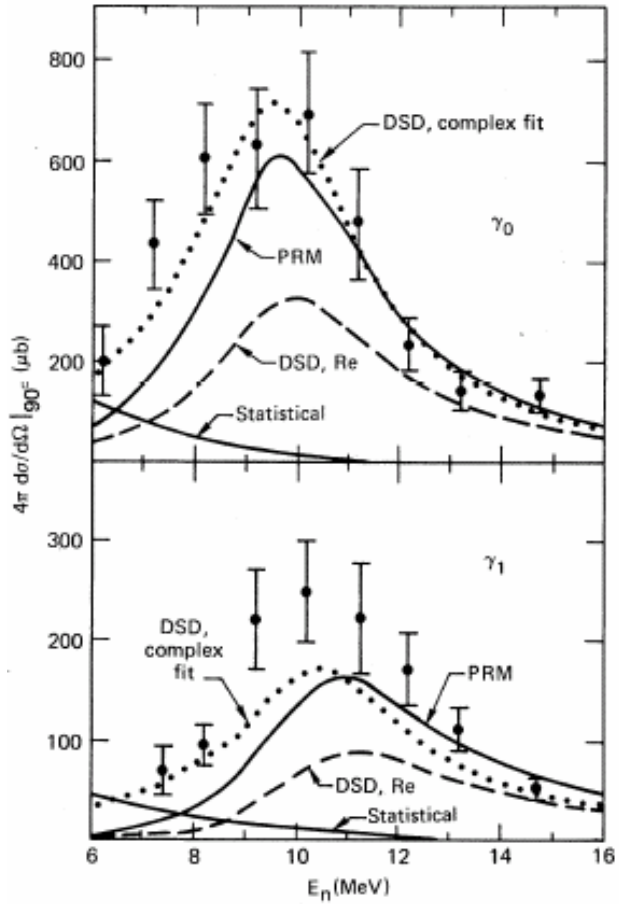

6 to 15 MeV neutrons on ^{208}Pb

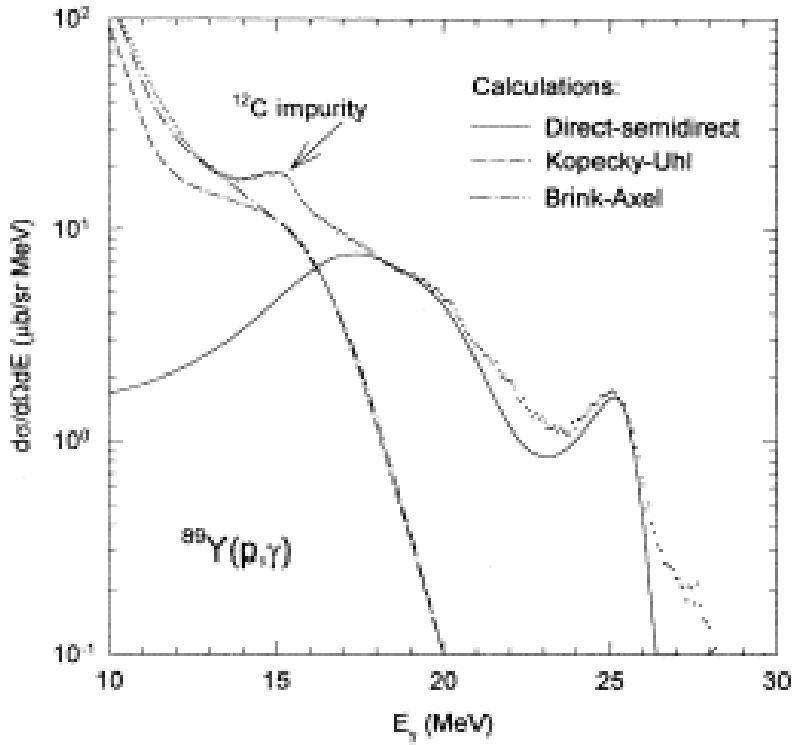

19.6-MeV protons on ^{89}Y

At low energies…

We seek neutron capture between resonances:

- **We are not energy averaging; therefore we must use a real potential.**
- **We find the DSD interference lowers the total cross section by 0 - 40% depending upon a transition**
- **We use the current form $\vec{j} \cdot \vec{A}$ of the EM operator which gives about 15% increase in cross-section compared to approximate, "density" form.**
- **We have additional complications, not entirely contained in direct (or direct-semidirect) model, namely fragmentation of single-particle resonances.**

Example: neutron capture on ^{19}F

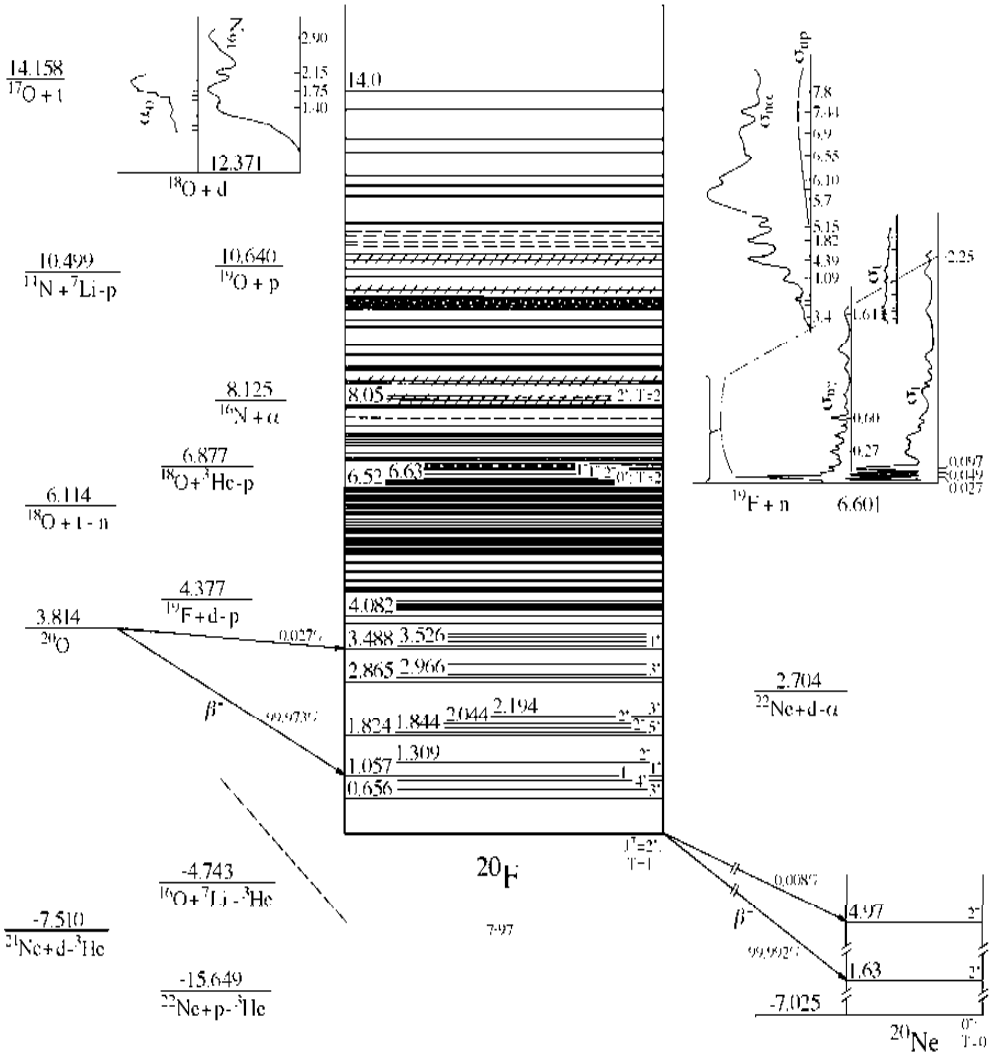

- Thermal capture cross section is very low, 10 mb
- Capture can occur to many final states in ^{20}F
- We look at (d,p) and (^{3}He,d) experiments on ^{19}F, and calculate direct-semidirect capture only to those states for which significant spectroscopic factors were seen
- We add the cross sections for all of the final states that were calculated to get the complete (n,γ) cross section

Integration with SAMMY

- **SAMMY uses Reich-Moore formalism and finds the best fit for neutron and gamma resonance parameters**
- **Our DC computation is submitted as an input to a SAMMY**
- **SAMMY then simultaneously fits resonance parameters and our DC via:**

$$\sigma_{total} = \sigma_{res}(\{E, \Gamma_n, \Gamma_\gamma\}) + c \cdot \sigma_{direct}$$

- **For** ^{19}F(n,γ), *c ≈ 0.5*

(Thanks to N. Larson and L. Leal of ORNL)

Direct capture exhibits single-particle resonances

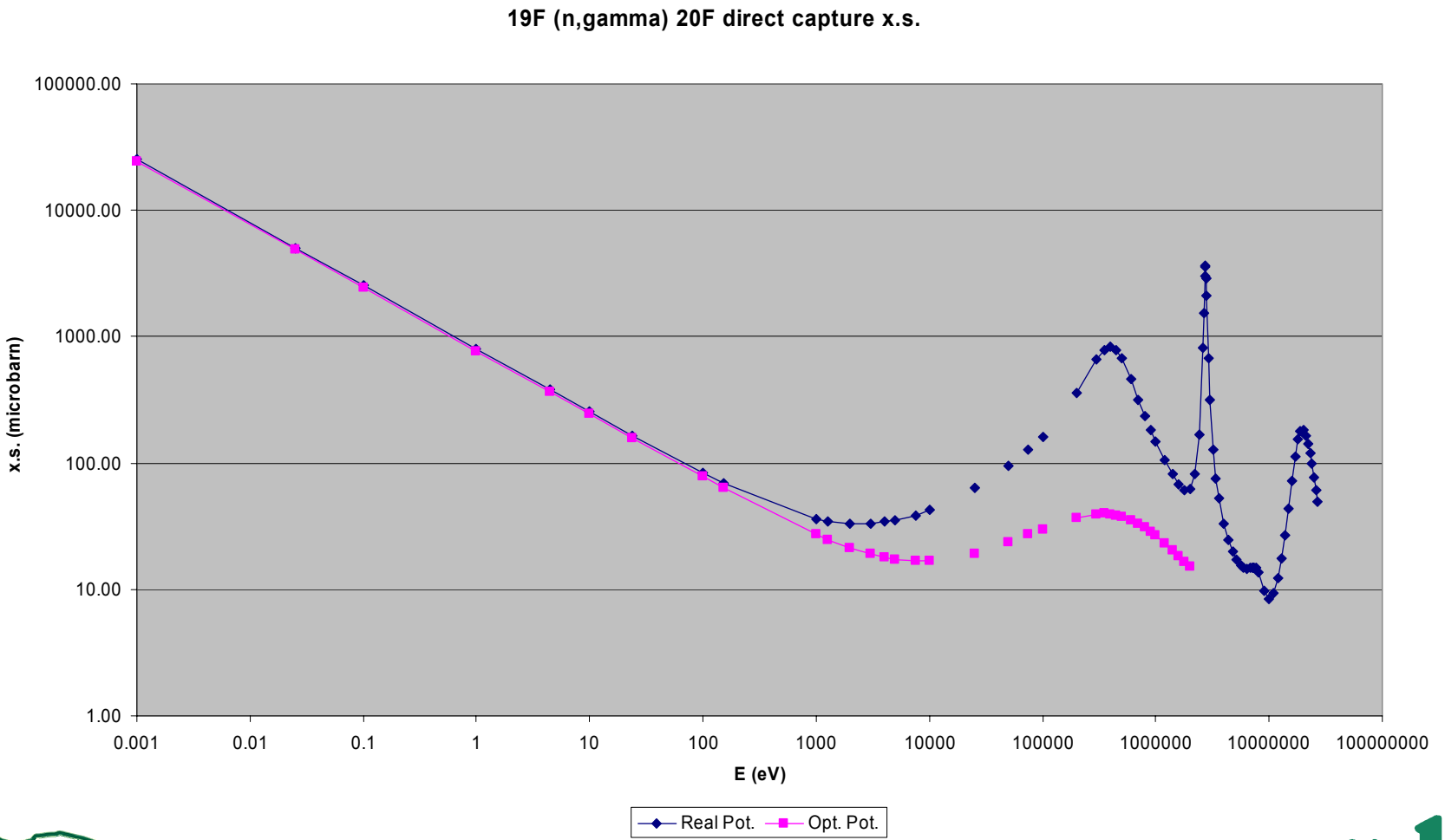

p-wave resonances in $^{19}F(n,\gamma)$ in 0-200 keV region are probably fragments of the $2p_{3/2}$ single particle state

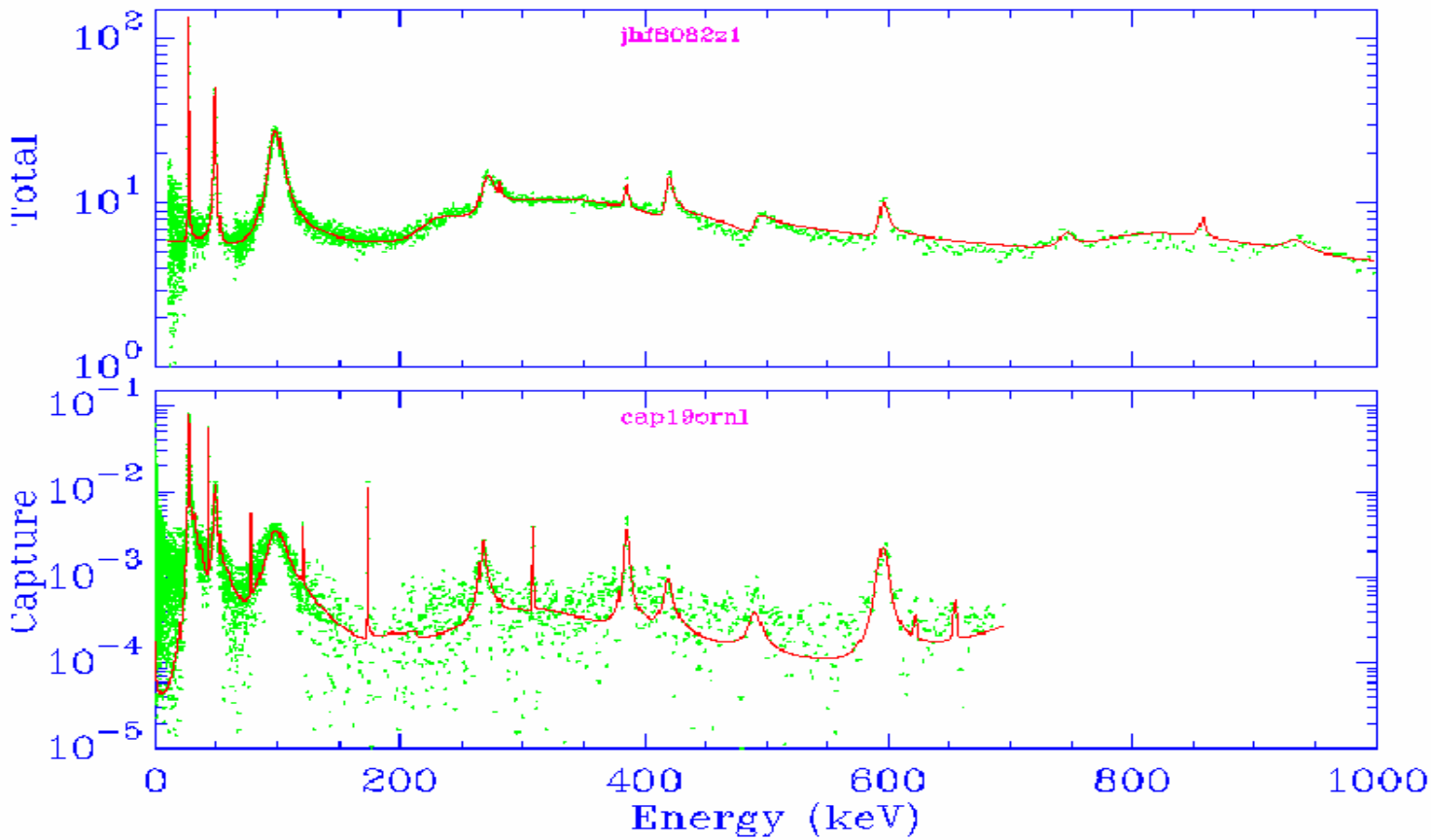

In some cases in light nuclei these resonances appear as a single resonance in nature

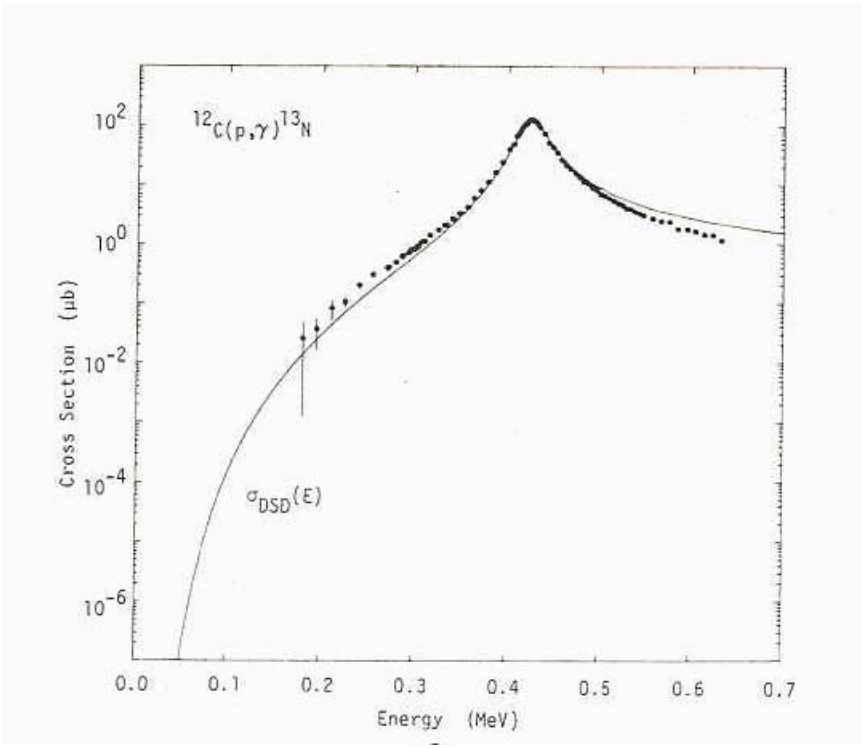

Mathews and Dietrich used a DSD calculation to calculate resonant $^{13}N(p,\gamma)^{14}O$ for hot CNO cycle

Projecting Single-particle resonances out

- We are supposed to be calculating a smooth background between experimentally visible resonances, not the resonances themselves
- Since our DSD calculations show SP resonances, we have a double-counting problem

- We are devising a method for dealing with this
  - Use projection operator techniques to remove resonances from the continuum

- In heavy nuclei (e.g. A~60) single particle resonances are spread among very many actual resonances
  - This leads to correlations between neutron and gamma widths of resonances (valence capture mechanism)

Conclusions

EXPECTATIONS FROM DANCE:

- For low energy neutrons there is little reliable data between resonances
- Such improved measurements at DANCE would be welcome, to guide and test our theory

TO DO:

- Project single particle resonance out of the continuum
- Apply to new ORELA data evaluations at NSTD-ORNL
- Coupled-channel analysis for D.C. on deformed nuclei.

The physics is in the radial integrals of the electromagnetic operators

- **For each final state, calculate:**

$$I_{fi}^{L} = \int_{0}^{\infty} dr\, u_f(r) Q_L(r) \psi_i(r)$$

Electromagnetic operator

Bound final state

Continuum initial state

- ***Solve single-particle Schrodinger equation to get initial, final states***
- **Cross section is a bilinear combination of these integrals**

$$d\sigma_{n,\gamma} / d\Omega = S_f \sum_{ii'LL'k} C_{ii'LL'fk}\, I_{fi'}^{L'*}\, I_{fi}^{L}\, P_k(\cos\theta)$$

- **The spectroscopic factor S_f is a measure of the amount of the simple configuration u_f in the actual final state. It may be calculated or gotten from stripping experiments such as (d,p).**

Example of direct-semidirect interference – semidirect lowers cross section by ~35%

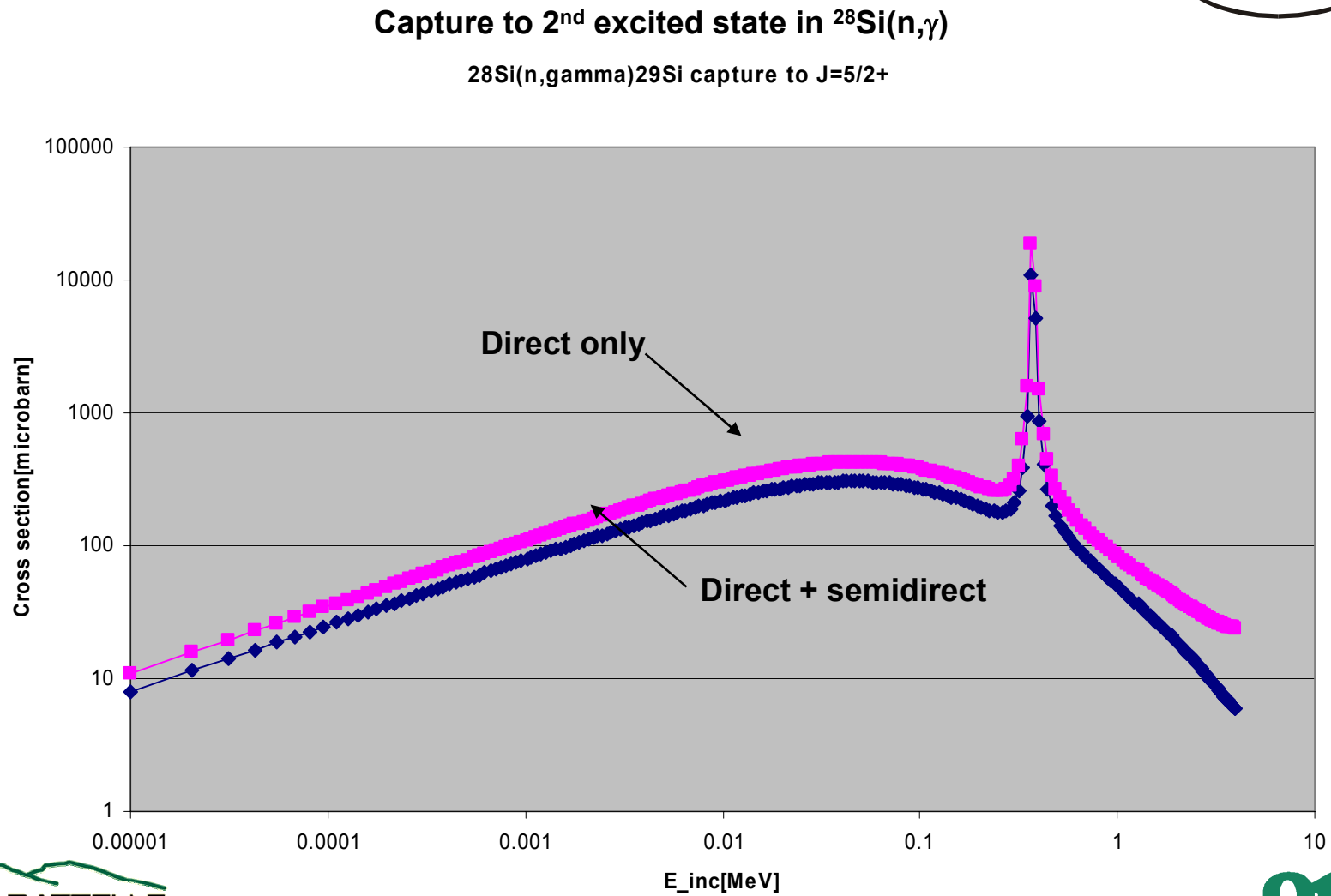

Example: cross section with exact (current) E1 operator ~20% larger than approximate (density) form

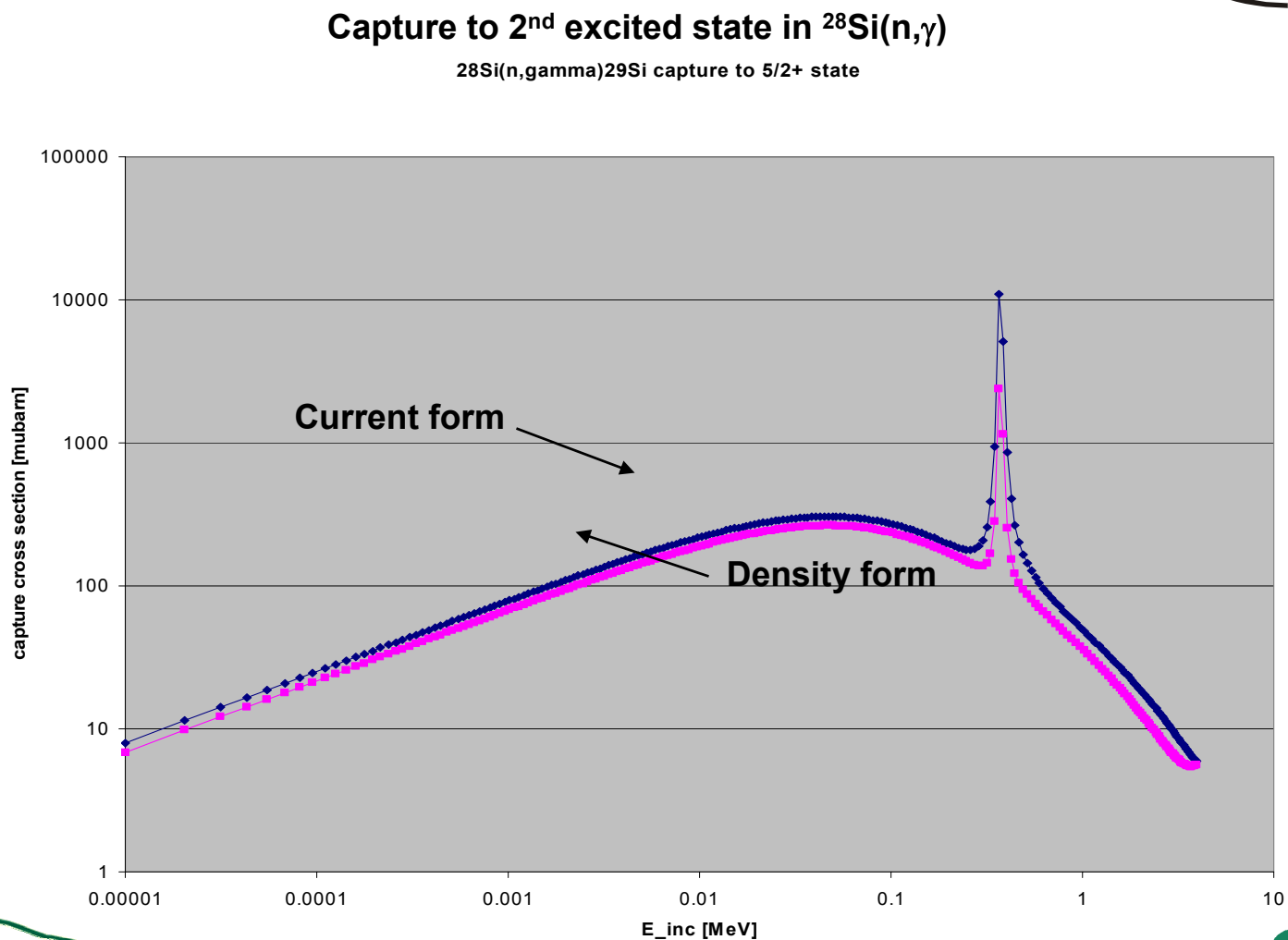

Similar physics in Dietrich and Rauscher codes, but there are some possibly significant differences

- Rauscher has direct only, Dietrich both direct and semidirect
  - Important for some gamma decays
- Multipolarities available: E1,E2,M1 (Rauscher), E1…E4,M1…M4 (Dietrich)
  - Not critical since E1 dominates for present application
- Direct electromagnetic operator: approximate ("density") form in Rauscher code, both this and exact "current" form in Dietrich code
  - Differences at ~15-20% level
- Potentials for initial and final states: conventional Woods-Saxon parameterizations in Dietrich; microscopic folding model in Rauscher
  - Differences probably not very great for nuclei near stability, where reasonable phenomenological parameterizations are available

When is semidirect term important (or not)?

- Semidirect term is dominant at energies near the giant resonance
- For low energy projectiles, the semidirect term always reduces the cross section (i.e., interference is destructive)
- If capture takes place well outside of the nucleus, semidirect capture is negligible
  - Always true for charged projectiles at sufficiently low energy
  - Sometimes true for neutrons; depends on target, energy, and angular momentum channel

Exact vs. approximate electromagnetic operator

- Interaction of nuclear system with electromagnetic field is:

$$H_\gamma = j \cdot A$$

Nuclear current

Radiation field

- Standard approximation for electric multipoles:
- Use Siegert's theorem to replace nuclear current by nuclear density

- Siegert's theorem is violated if initial and final state nuclear potentials are not identical. In fact, they are usually not identical

- It requires very little extra work to use the exact (current) form in direct calculations; the Dietrich code has this option

Contribution by

Toshihiko Kawano

Los Alamos National Laboratory
kawano@lanl.gov

25 pages

Neutron Capture Process for Astrophysics

T. Kawano

T-16, Los Alamos National Laboratory

Los Alamos, New Mexico 87545, USA

Los Alamos

Neutron Capture Cross Section

Energy Range for each Application

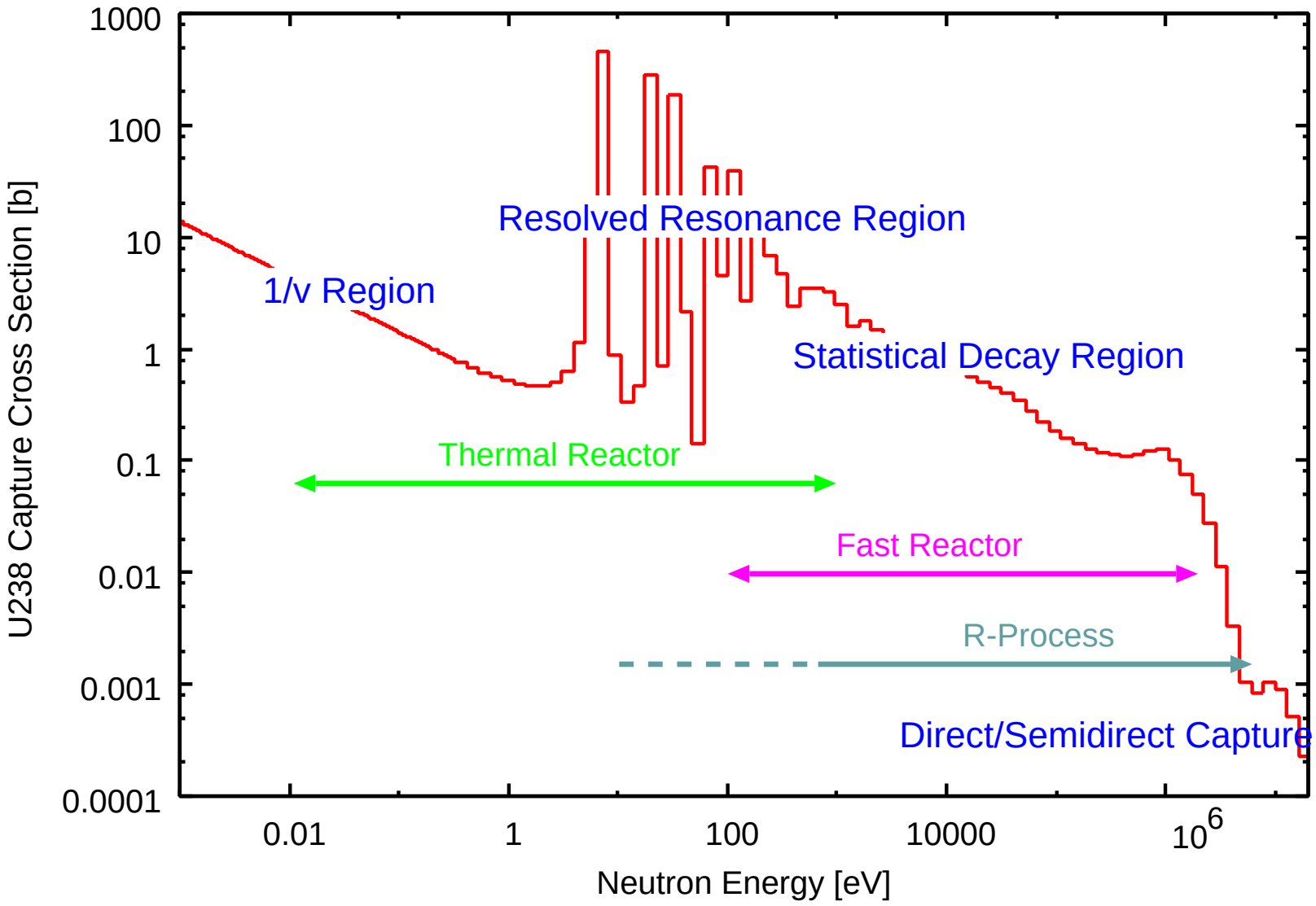

Los Alamos

Neutron Capture Process

Compound Reaction

- Incident neutron and target form a compound nucleus, and decay.
- Hauser-Feshbach model, with width fluctuation.
- Capture cross section decreases rapidly when many neutron inelastic channels open.

Direct/Semidirect Capture

- Direct transition to one of the single-particle state.
- Giant Dipole Resonance (GDR)

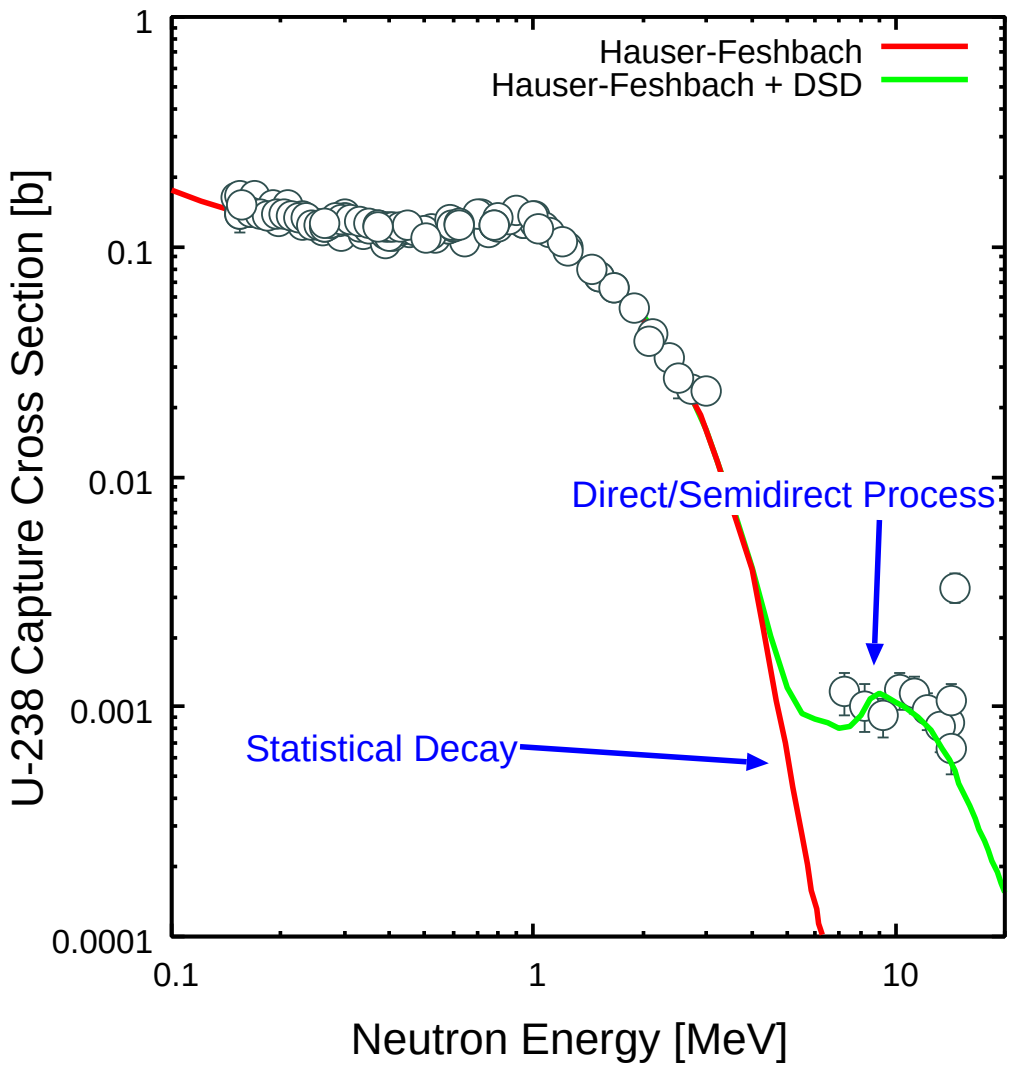

Los Alamos

Evaluated Nuclear Data and Astrophysics

- Nucleo-synthesis — r-process & s-process.
- Nuclear reactions under high neutron flux.
  — Capture process is important.
- Need a nuclear reaction rate at the temperature kT of 1–100 keV.
- Nuclear cross-section above the unresolved resonance region up to the fast region, those are expressed by a Maxwell-averaged value, $\langle \sigma v \rangle$.
- Procedure of the cross section evaluation is similar to that of usual nuclear data evaluation.
- The Hauser-Feshbach model which has been adopted to evaluate cross sections in those energy range can be applied to calculate the nuclear data for astrophysics.
- Many neutron-rich, unstable nuclides are involved.

R-Process Network Calculation and Nuclear Reaction Chain

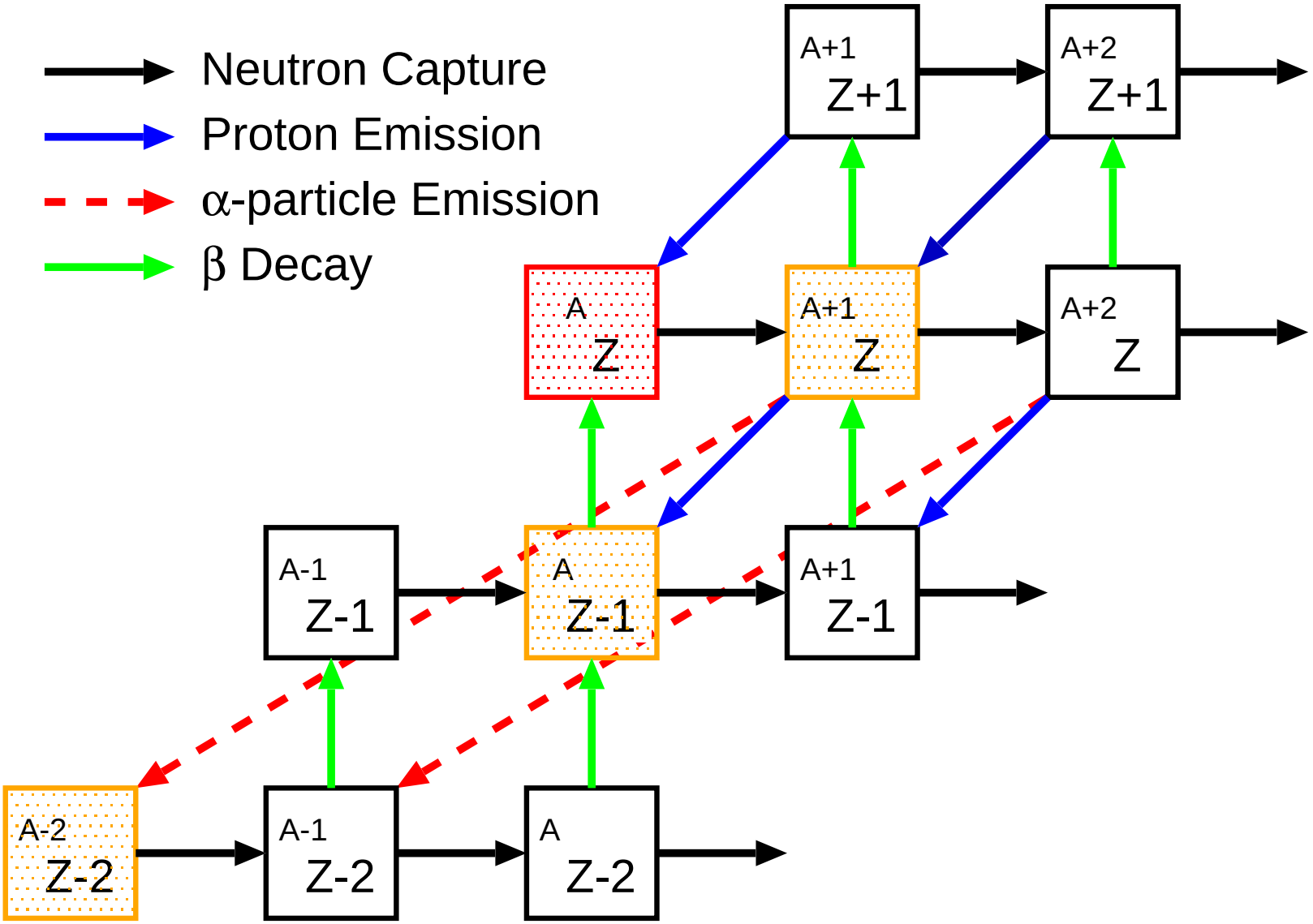

Strategies

Calculation of Cross Sections for Unstable Nuclei

- Microscopic Approach
  - Based on theoretical calculations, trying to remove any adjustable parameter.
  - Physical quantities needed — nuclear mass, ground state property, nuclear level density, E1 photoabsorption strength function, *etc.* — are calculated microscopically.
  - If successful, we can use the same method for any nuclides. (assuming we understand physics off-stability.)
- Theory with Systematics/Phenomenology Approach
  - Based on theoretical calculations, but with many systematic studies.
  - Model parameters are adjusted to observable quantities, and extrapolate into unstable region.
  - We can rely on this approach when the target nuclide is close to stability.

Objectives

Required Nuclear Data

- Cross sections for more than 3000 nuclides.
  — (n, p), (n, α), (n, γ)
- No experimental data / no nuclear structure data available
  — We rely on calculation (but having validated calculations to experiments when possible.)
- We need "a nuclear data production system" specialized for astrophysics to generate a large number of cross section data.
- Quality of our results depends on the input parameters.

Cross Section Calculation System

- A computer program to calculate the optical model, Hauser- Feshbach-Moldauer (HFM) statistical model, and Direct/Semidirect capture model.
- Interface to model parameter libraries, e.g. level densities, *etc.*

Hauser-Feshbach-Moldauer Calculation

Program CoH

- Spherical optical model
  - The global parameterization is adequate for cross section calculation of unstable nuclides.
  - Koning-Delaroche Global Potential for n and p
  - CoH also contains some potentials for α, d, t, and ^{3}He.
- Hauser-Feshbach model, width fluctuation by Moldauer
- Particle induced process, (n, pX), (α, nX), *etc.*
- Neutron capture, E_1 transition

Slave Programs and Database

- Interface mini-programs to retrieve input parameters.
- Mass excess data (KUTY00, KTUY03), and ground state $J\pi$

Reference Input Parameter Library

A library which contains nuclear model parameters, mainly for the statistical Hauser-Feshbach model calculation.

Masses	Experimental nuclear masses by Audi and Wapstra Mass excess calculated with several mass formulae
Levels	Energy, spin, parity, and γ-ray decay probabilities of excited states. (ENSDF-II)
Resonances	Average resonance parameters for s and p-waves.
Optical	Optical potentials for both spherical and deformed nuclei.
Densities	Level density parameters with several level density formulae, and numerical data calculated with a microscopic model.
Gamma	GDR parameters, and expressions of γ-ray strength functions.
Fission	Experimental / calculated fission barriers.

Code System for Astrophysics

T. Kawano and S. Chiba

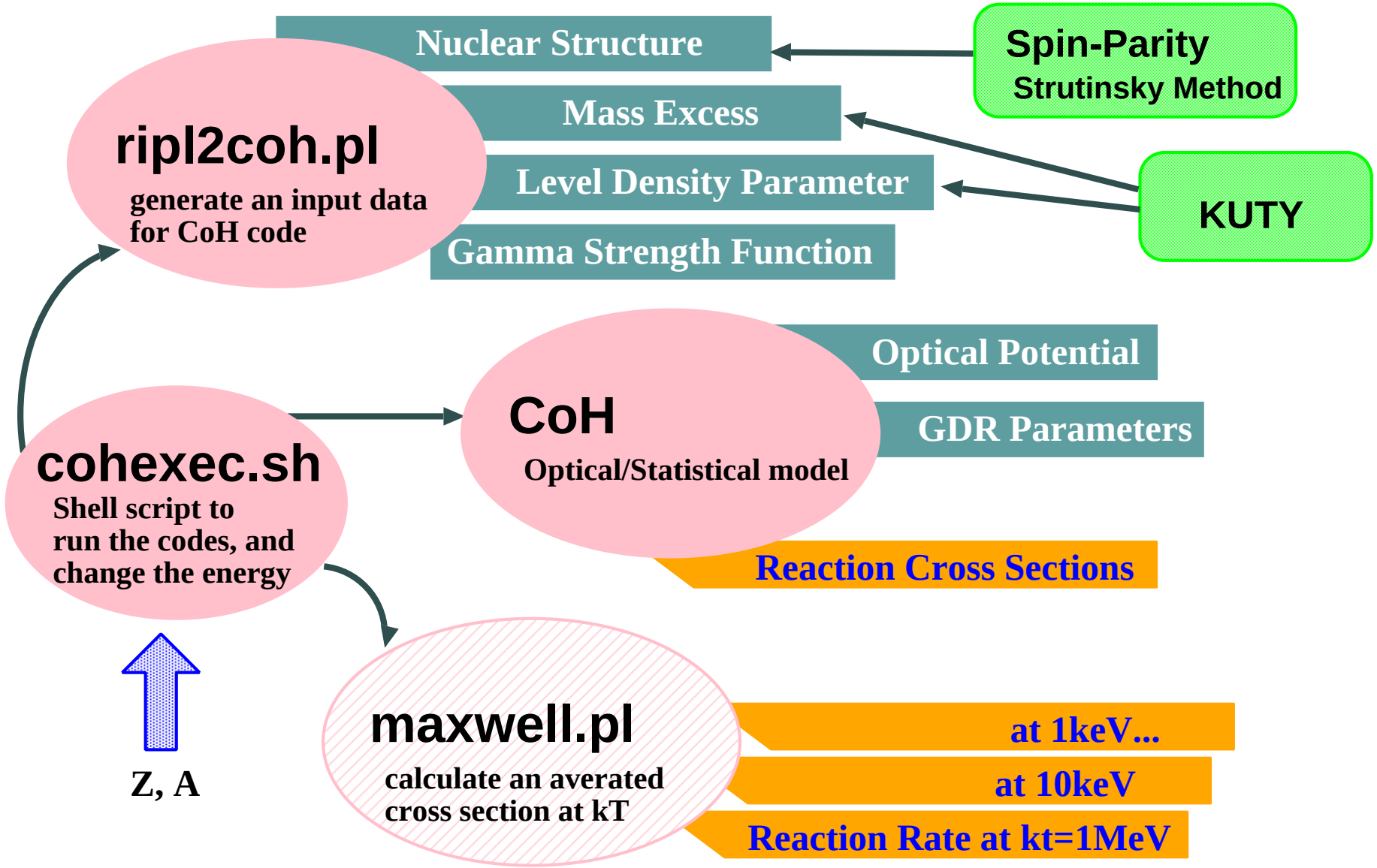

Los Alamos

γ-Ray Transmission

The γ-ray transmission coefficient is given by

$$T_{\mathrm{E1}}(E_\gamma) = 2\pi E_\gamma^3 f_{\mathrm{E1}}(E_\gamma)$$

where $f_{\mathrm{E1}}(E_\gamma)$ is the strength function.

γ-ray Strength Function

- Standard Lorentzian

$$f_{\mathrm{E1}}(E_\gamma) = C\sigma_0\Gamma_0 \frac{E_\gamma \Gamma_0}{(E_\gamma^2 - E_0^2)^2 + E_\gamma^2 \Gamma_0^2}$$

- Generalized Lorentzian
  finite value at low energies, energy dependent width

$$f_{\mathrm{E1}}(E_\gamma) = C\sigma_0\Gamma_0 \left\{ \frac{E_\gamma \Gamma(E_\gamma, T)}{(E_\gamma^2 - E_0^2)^2 + E_\gamma^2 \Gamma^2(E_\gamma, T)} + 0.7 \frac{\Gamma(E_\gamma = 0, T)}{E_0^3} \right\}$$

where $C = 8.68 \times 10^{-8}$ mb^{-1}MeV^{-2}, or can be obtained by normalization to an experimental value if available.

γ-ray Strength Function

Comparison of Standard-LO with Generalized-LO

Strength Function

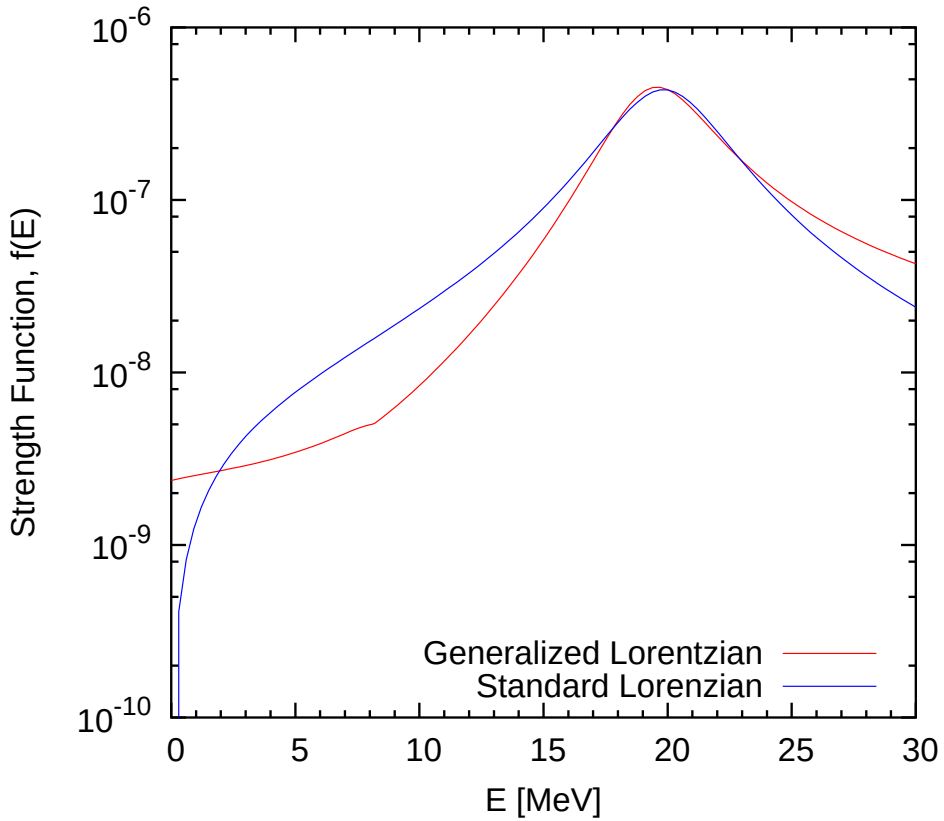

γ-ray Transmission Coeff.

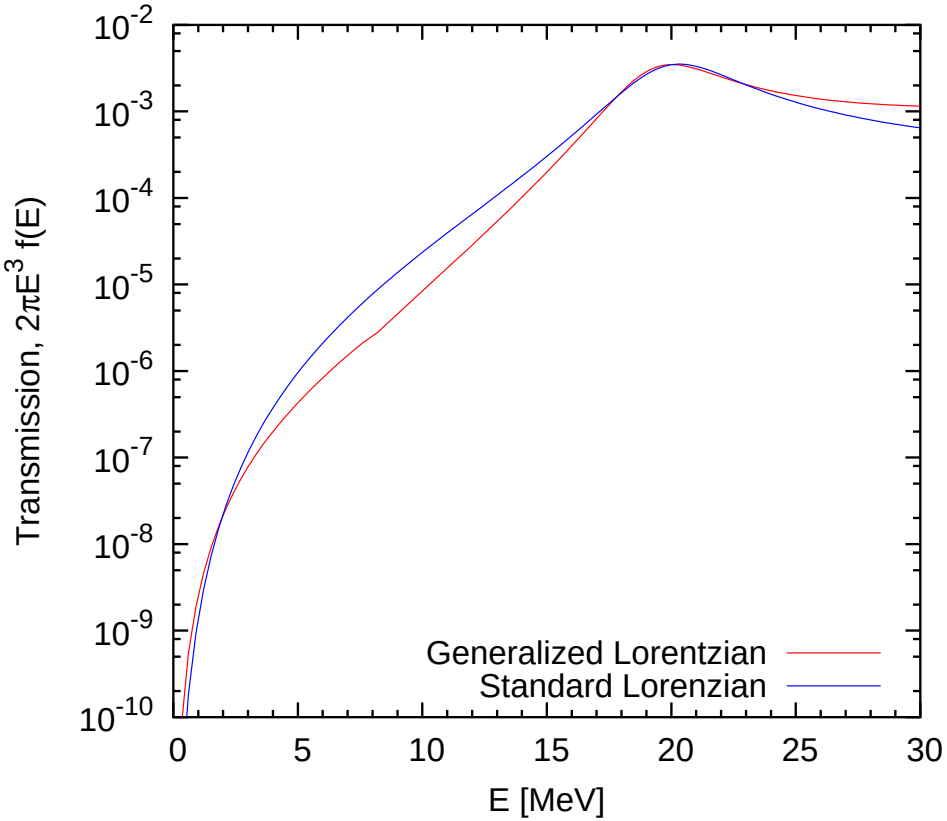

Model Parameters

Parameters Taken from RIPL2 (if available)

Level Density Parameter	Fermi gas, and Constant temperature model
Excited States $E_x(J^\pi)$	ENSDF
γ-ray strength function	$\langle\Gamma_\gamma\rangle$, D_0
GDR Parameter	D'Arigo *et al.* (systematics) $E_0 = (49.336 + 7.34\beta)A^{-0.2409}$ $\Gamma_0 = 0.3E_0$ $\sigma_0 = 10.6A/\Gamma_0$

Parameter Systematics for Unstable Nuclei

Level Density Parameter	Ignatyuk-type systematics constant temperature model
Ground State J^π	Nilsson-Strutinsky-BCS method
γ-ray strength function	Generalized Lorentzian

Level Density Parameter

Washing-out of Shell Effects

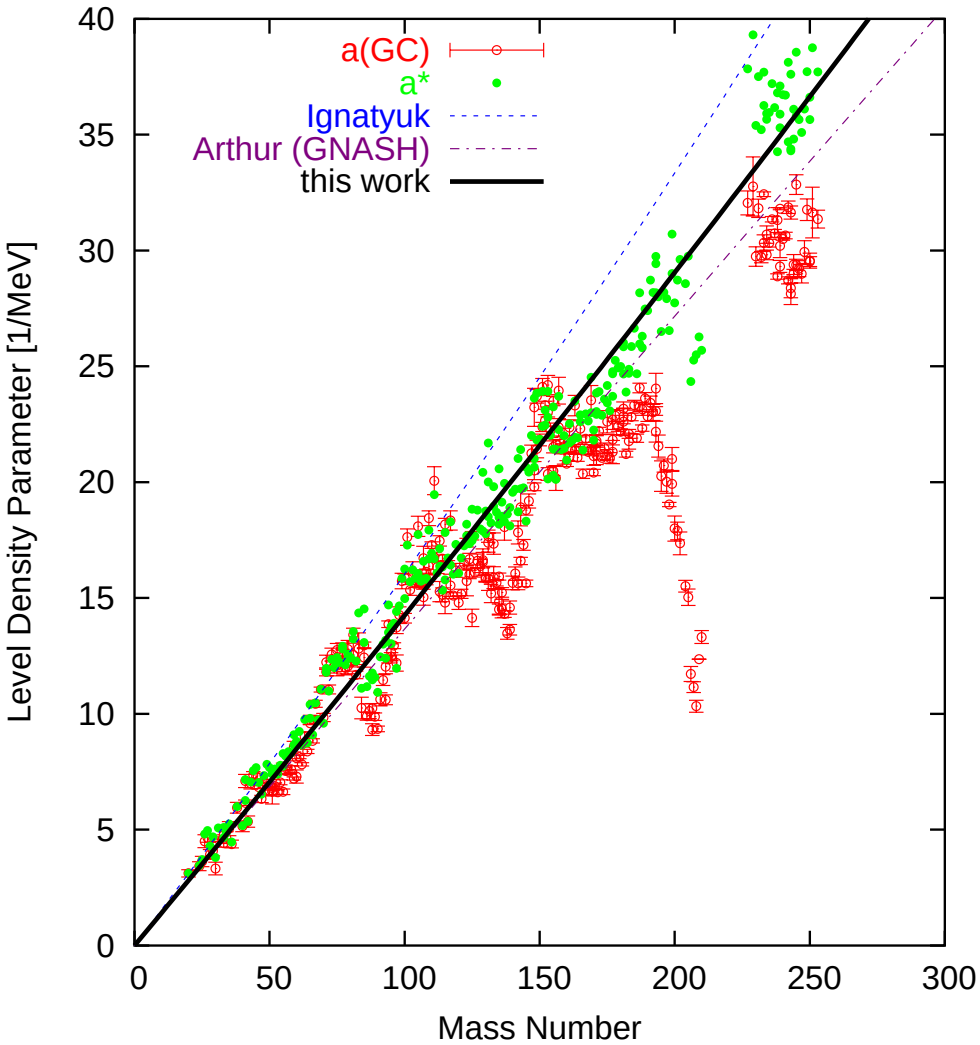

- Shell correction (δW) and pairing energies (Δ) taken from KUTY mass formula

$$a = a^* \left\{ 1 + \frac{\delta W}{U} \left(1 - e^{-\gamma U} \right) \right\}$$

$$a^* = 0.140 A + 2.65 \times 10^{-5} A^2$$

- At low excitation energies, the constant temperature model is used with

$$T = 28.0 A^{-0.8}$$

  - obtained from discrete level data of more than 1000 nuclei.

Los Alamos

^{99}Tc Capture Cross Section (I)

Calculated Capture Cross Section

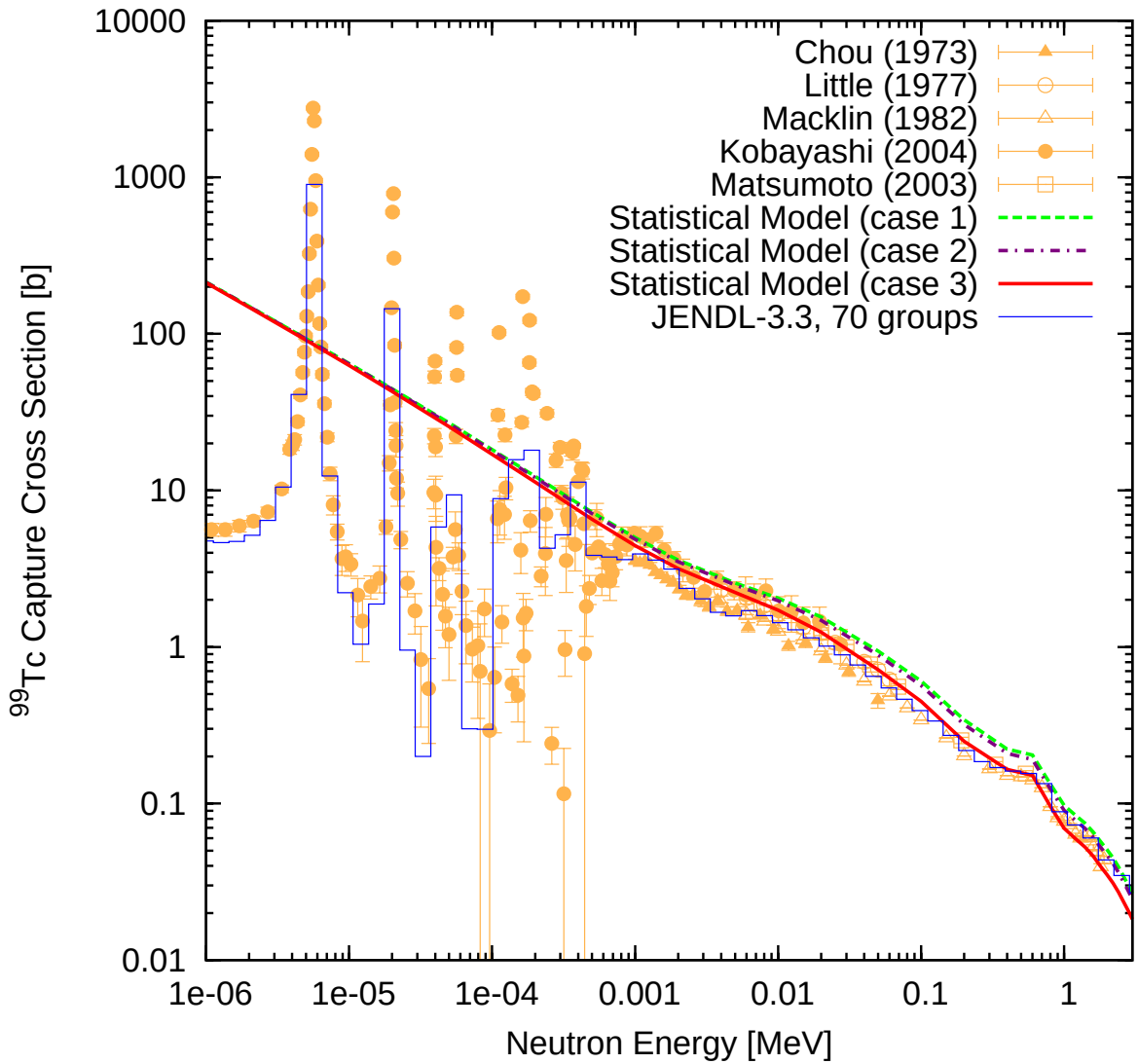

Los Alamos

^{99}Tc Capture Cross Section (II)

Magnified Plot in the Continuum Region

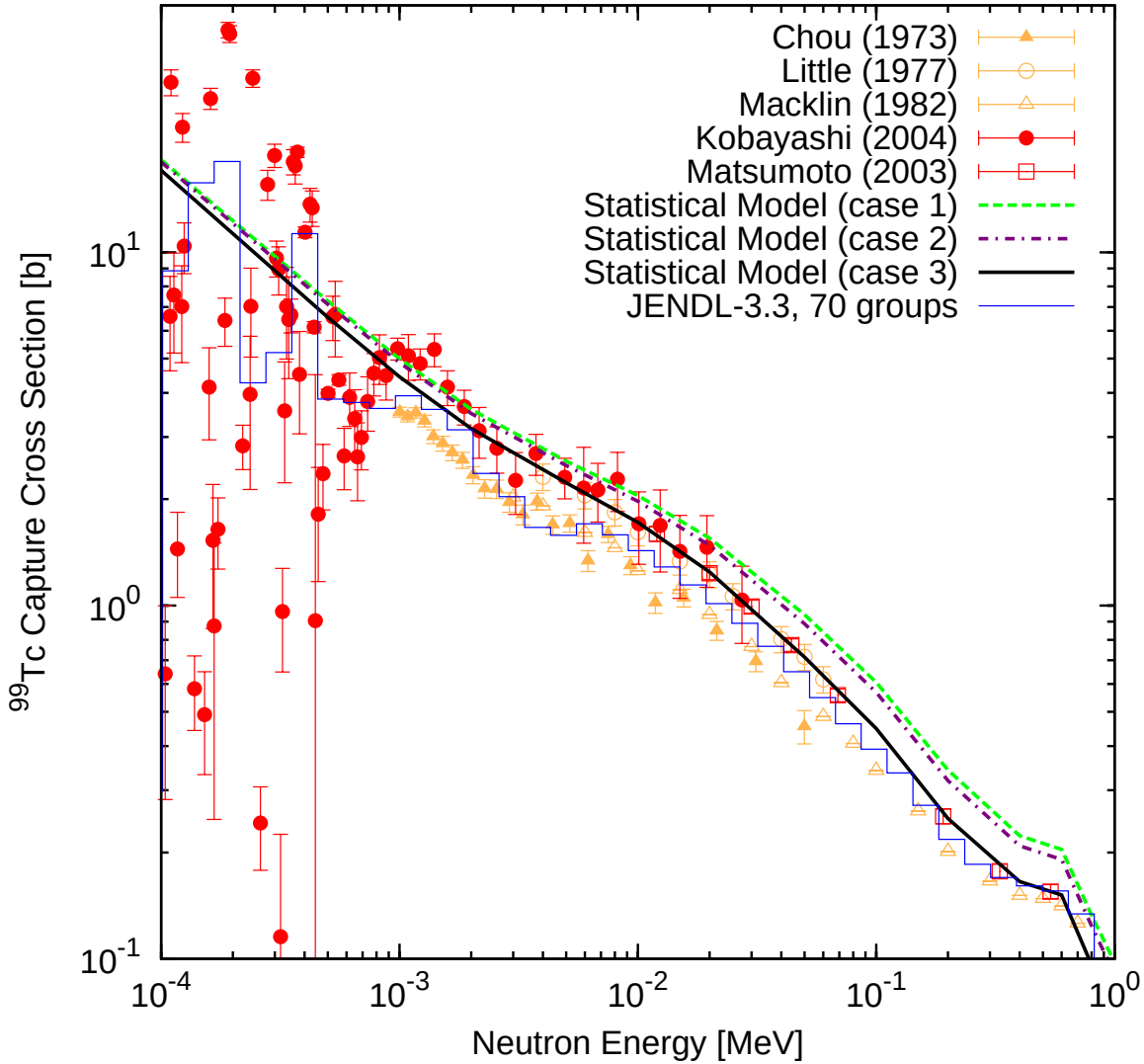

Case	$\langle\Gamma_\gamma\rangle/D_0$	
1	0.0133	RIPL-2 (default)
2	0.0123	Gunsing (Res. Analysis)
3	0.0091	fitted†

† Fitted to experimental data of Kobayashi *et al.* (Kyoto Univ., 2004) and Matsumoto *et al.* (Tokyo Inst. Tech., 2003) above 100 keV.

Los Alamos

Default Calc. to Test Predictive Capability

Gd Isotopes, Comparison with FZK Data

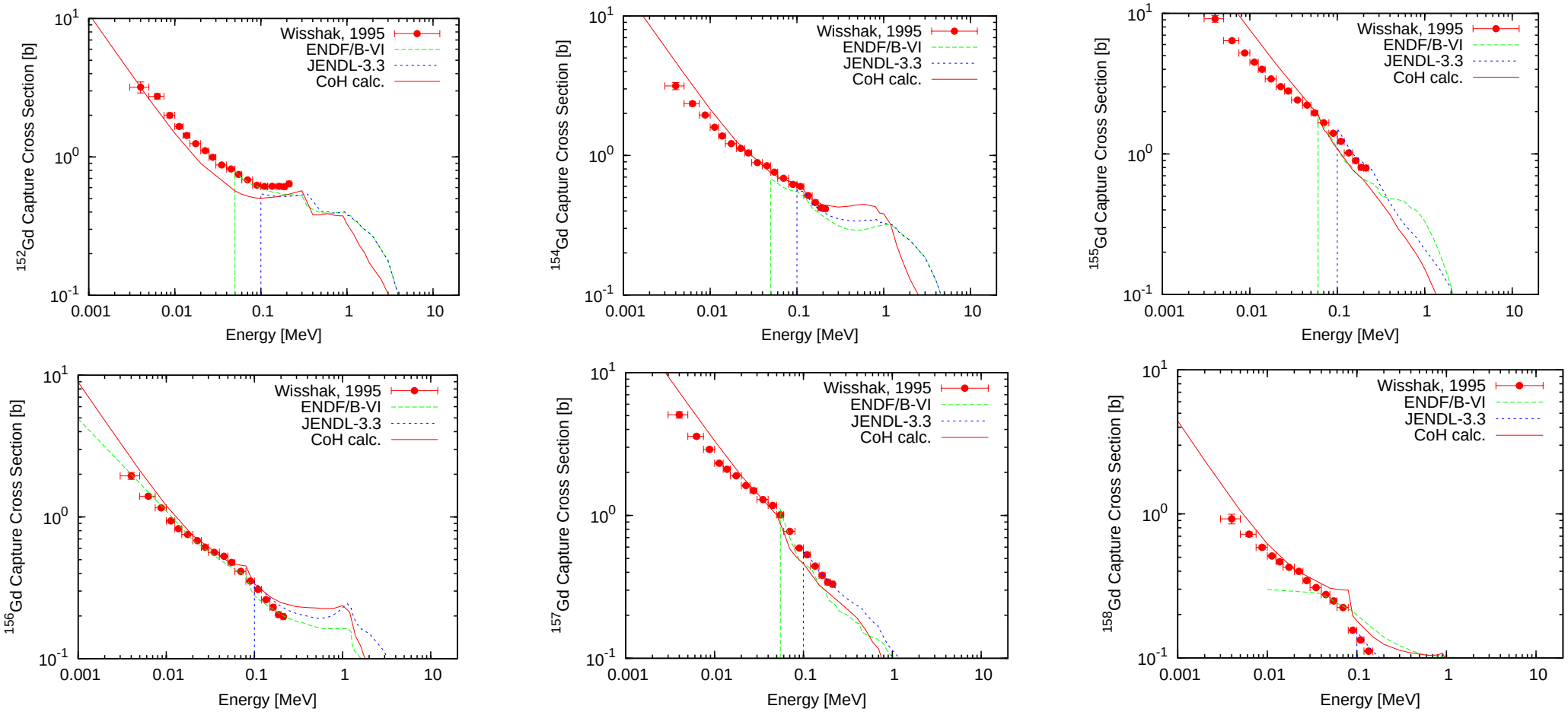

Los Alamos

Blind Calc. Using Global Parameters

Comparison with JENDL-3.3/Fission Products Region

- Capture cross sections at 100 keV were calculated with this system.
- from ^{69}Ga to ^{204}Hg (195 nuclides)
- Blind calculation, no adjustment.

Result

- Many of calculated σ_γ 's were from 0.1×(JENDL) to 2×(JENDL).
- CoH calc. tends to underestimate.
- Possible reasons —
  Level densities used, especially for nuclides with no available discrete level info. We need to improve the level density systematics for unstable targets.
- Cross section prediction can be improved by tuning parameters to measured data.

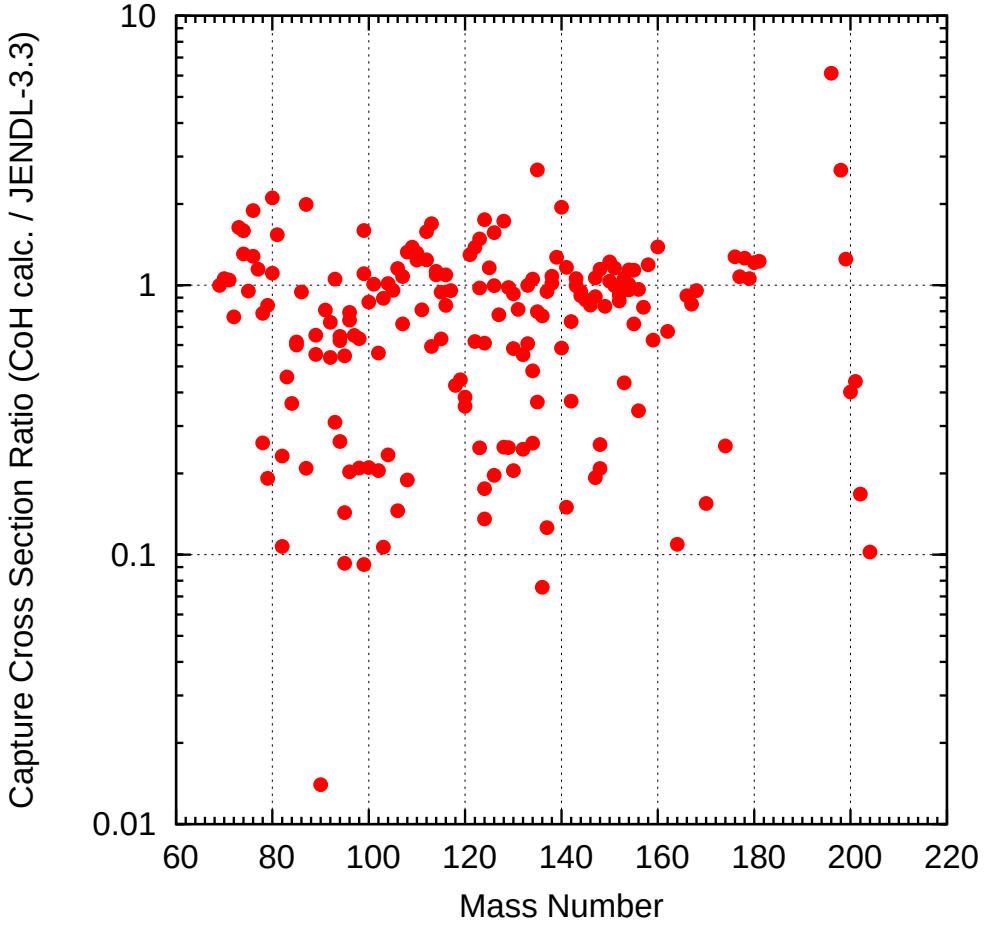

Los Alamos

Direct/Semidirect Capture Process

- For the capture cross section a compound nuclear reaction dominates up to 1 MeV.
- However, the Hauser-Feshbach model gives very small capture cross section when many particle emission channels open, because $\Gamma_{n,p,\cdots} \gg \Gamma_\gamma$, although the capture process is observed experimentally.
  - in the MeV energy region
    — typically $\sigma(n,\gamma) \sim 1$ mb.
  - resonance region (background between resonances)
    — by F. Dietrich, G. Arbanas, A. Kerman (this workshop)
- The direct/semidirect (DSD) model accounts for this.

DSD Theory

Direct Capture

- Electric dipole radiation transition from optical potential to single-particle state.
- Amplitude

$$T_d = C_d \times \langle U_{nl_1j_1} | r | \chi_{l_0j_0} \rangle$$

Semidirect (Collective) Capture

- Giant Dipole Resonance
- Optical Potential $\rightarrow$ GDR $\rightarrow$ S.P.
- Amplitude

$$T_{sd} = C_{sd} \times \langle U_{nl_1j_1} | V_1 r f(r) | \chi_{l_0j_0} \rangle \frac{|M_{GDR}|^2}{E_\gamma - E_{GDR} + i\Gamma_{GDR}/2}$$

Cross Section

$$\sigma(l_1j_1; l_0j_0) = \frac{8\pi\mu}{9k\hbar^2} \left(\frac{E_\gamma}{\hbar c}\right)^3 |T_d + T_{sd}|^2$$

Los Alamos

Resonance Analysis vs. Direct Capture

R-Matrix Analysis

- Cross sections in the resonance region are reproduced by a resonance formula.
  - Resonance parameters are fitted to experimental data.
  - Although it is phenomenological, it gives a very good fit to measured cross sections.
  - A big fictitious resonance is assumed at a negative energy, which represents contribution from all bound states, and its tail forms a $1/v$ slope.

Direct Capture

- Transition to the bound state is calculated explicitly.
- $1/v$ tendency can be obtained without the fictitious resonance.

^{99}Tc Capture in the Resonance Region

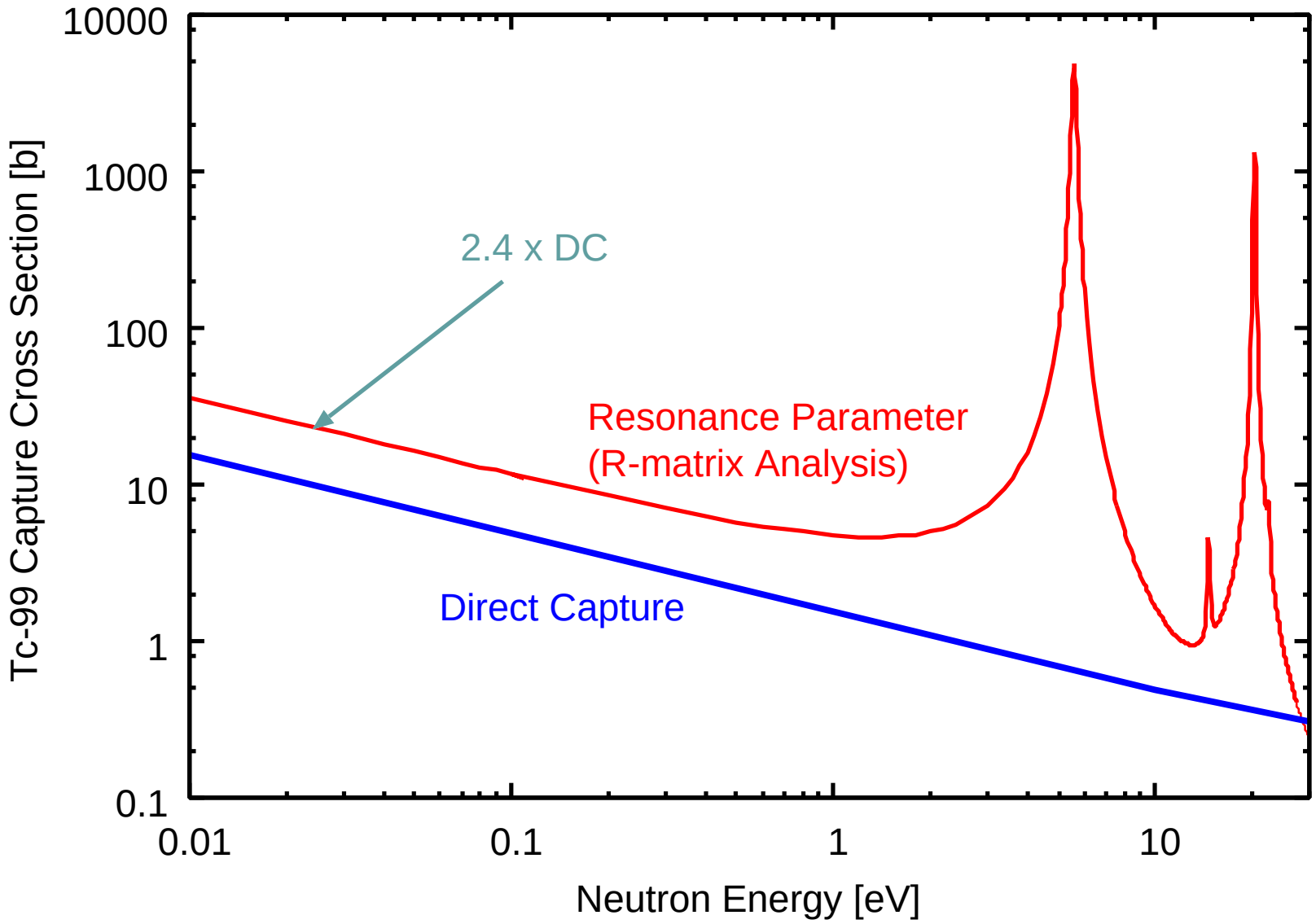

Los Alamos

Extension of Direct/Semidirect Model

DSD Capture of Nucleon in Deformed Nuclei

- Formulae
  - Boisson and Jang (1972).
  - Kitazawa *et al.* (1978).
- Single-particle state
  $U_{nl_1j_1}(r) \rightarrow R_{lj\Omega}(r)$
- γ-ray absorption cross section has two peaks in the GDR region.
- Additional angular momentum coupling coefficients.

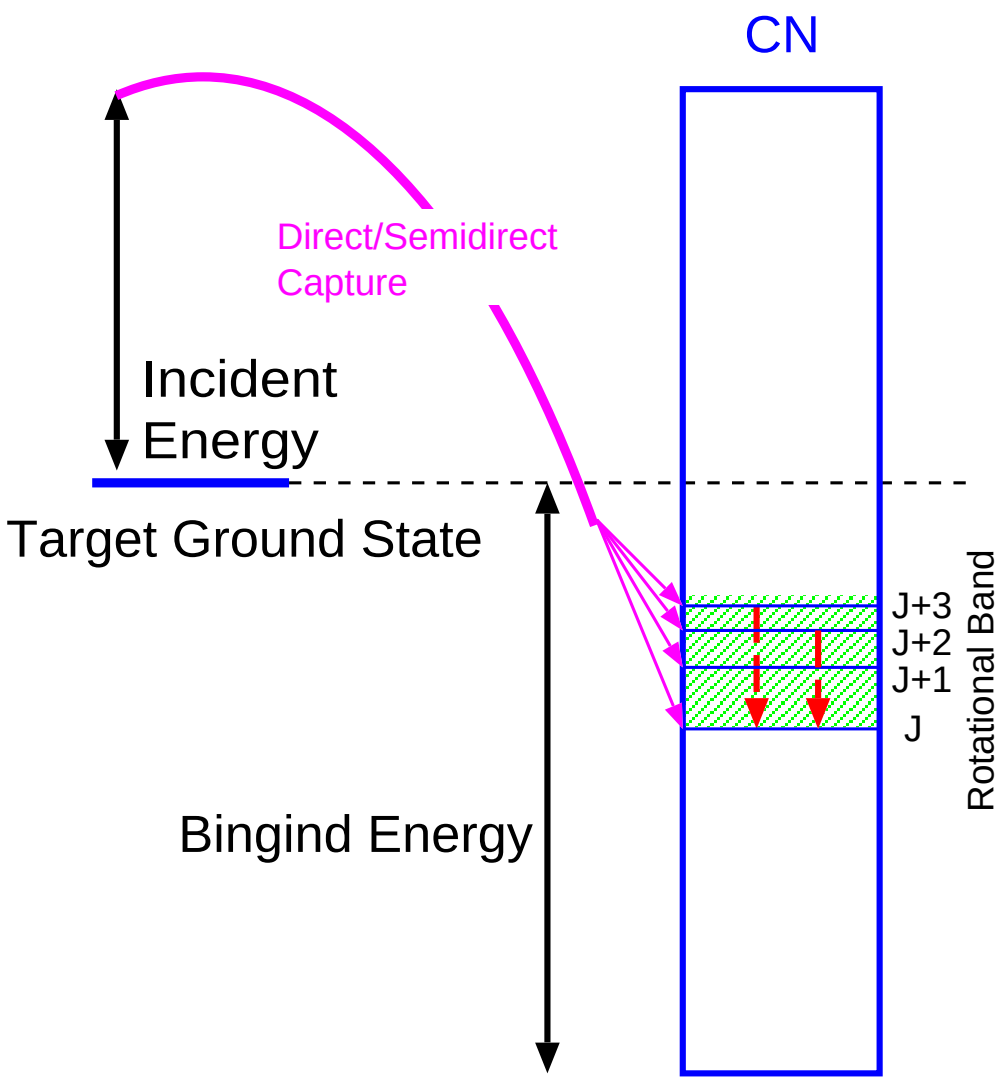

^{238}U Capture in the MeV Range

- DSD

$$|T_d + T_{sd}|^2$$

- Direct

$$|T_d|^2$$

- Semidirect

$$|T_{sd}|^2$$

- Direct + Semidirect

$$|T_d|^2 + |T_{sd}|^2$$

not correct since coherence not included

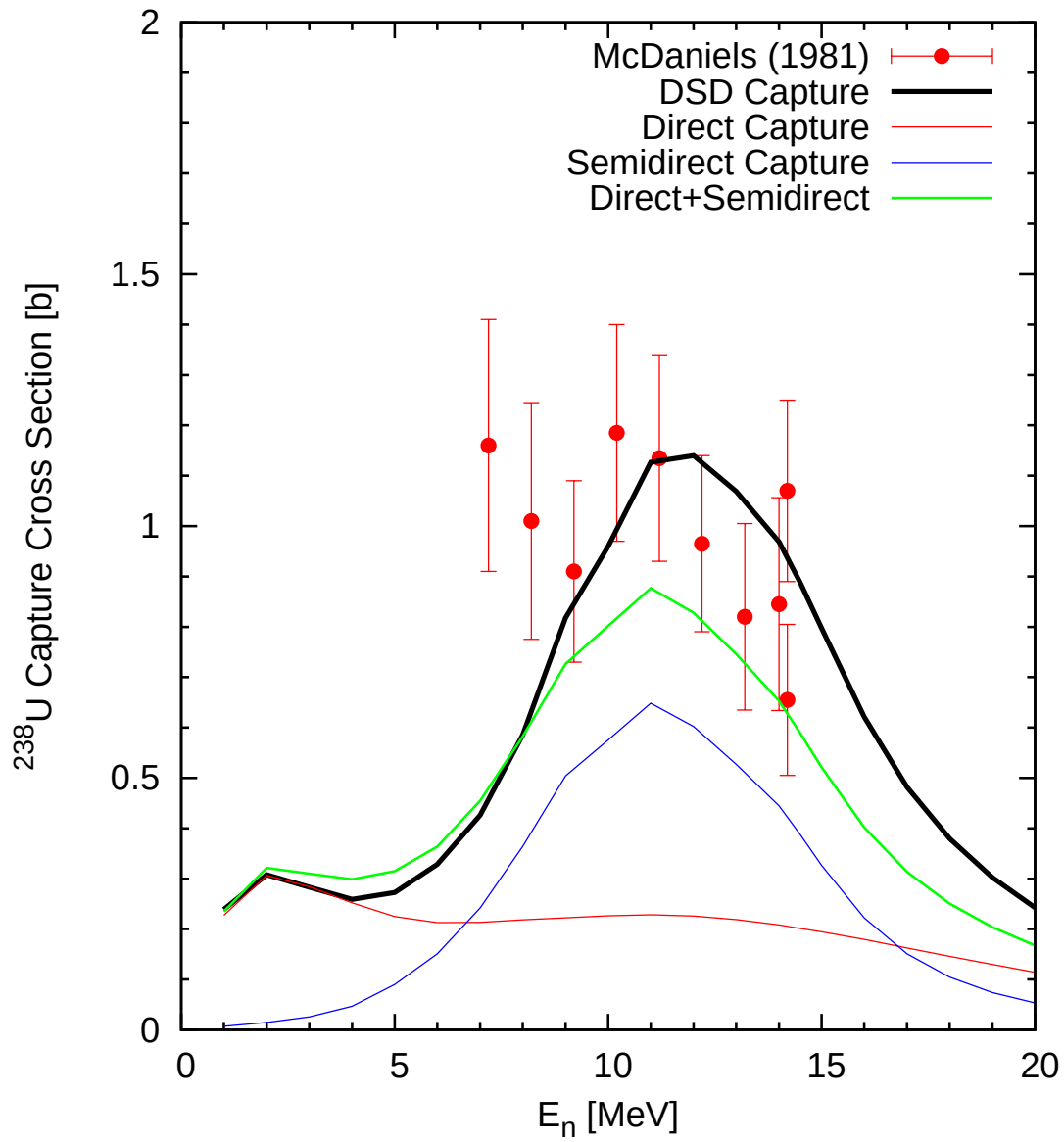

Los Alamos

Concluding Remarks

Theories Included

- Hauser-Feshbach statistical model with width fluctuation correction
- Direct-Semidirect capture process — spherical / deformed nuclei

Neutron Reaction Data for Astrophysics

- Development of an automated cross section calculation system
  - Optical Model and Hauser-Feshbach-Moldauer Theory
  - linked to nuclear structure information
    - KUTY00 and KTUY03 mass formula, ground state $J\pi$
  - linked to RIPL (input parameter library)
    - level density parameter, discrete level data, photo reaction data
  - systemtatics/phenomenology — new parametrization
- We have shown some examples; capture cross sections for Gd isotopes, and comparison with JENDL-3.3 FP data.
- Our goal is to generate cross sections more than 3000 nuclides.

Los Alamos

Contribution by

Alberto Mengoni

CERN

alberto.mengoni@cern.ch

70 pages

Neutron capture and exotic nuclei

A Mengoni (CERN)

- Neutron capture in light nuclei
- CERN n_TOF facility & status of the experimental programme

Neutron capture rates for light nuclei

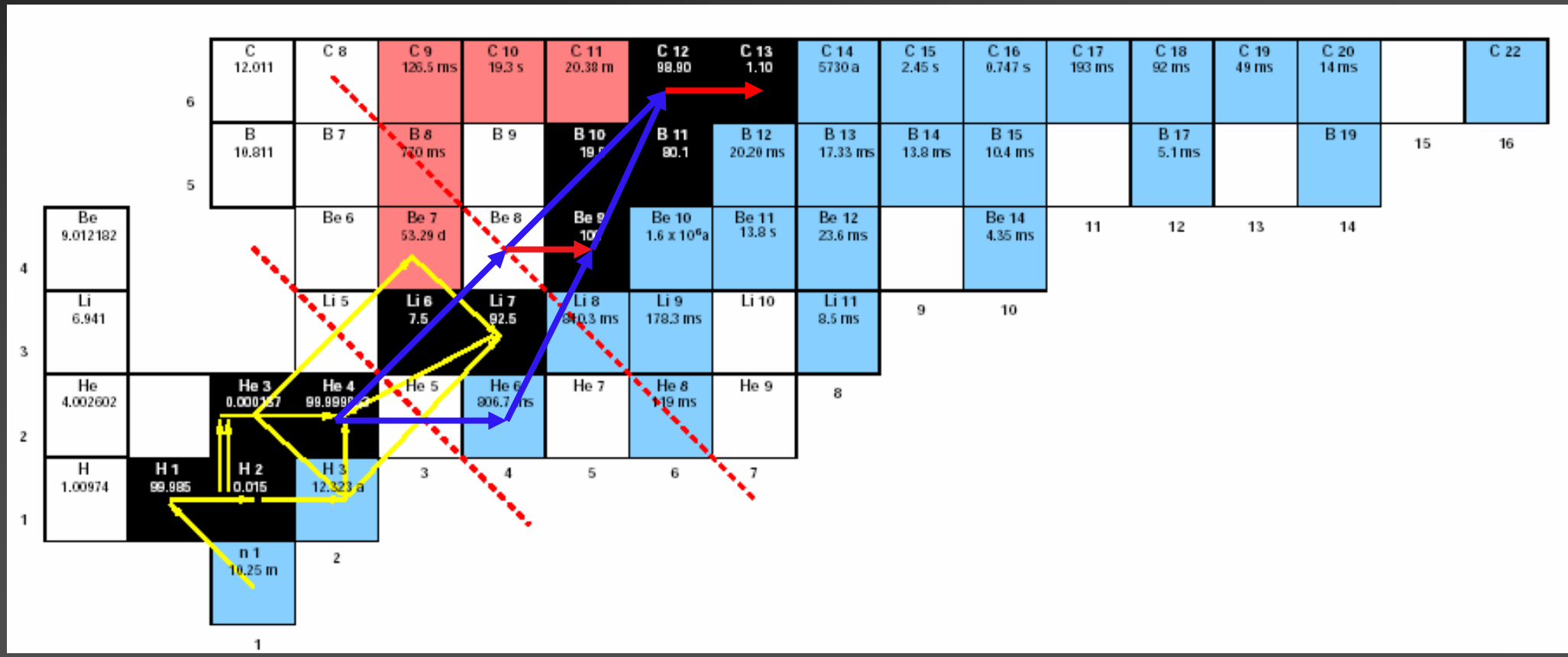

alberto.mengoni@cern.ch

Neutron capture rates

Capture reaction rates for kT ≈ 30 keV are the fundamental ingredient for understanding primordial as well as stellar nucleosynthesis

Direct methods

Direct measurements
- (n,γ)

Inverse measurements
- (γ,n)
- Coulomb dissociation

Indirect methods
(ANC, TH, etc.)

- Transfer reactions with stable beams

- Transfer reactions with radioactive beams

alberto.mengoni@cern.ch

Direct measurements: light nuclei

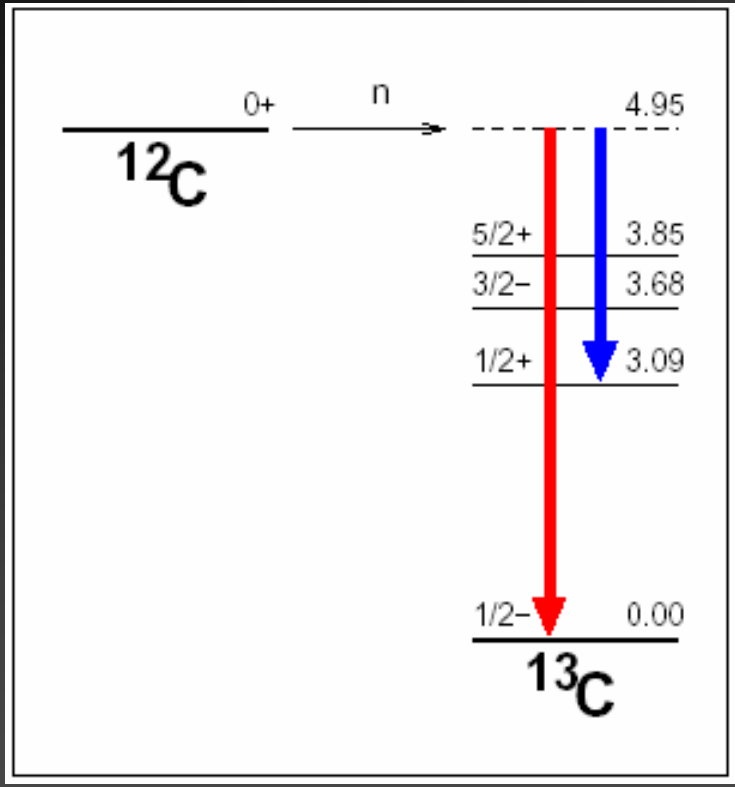

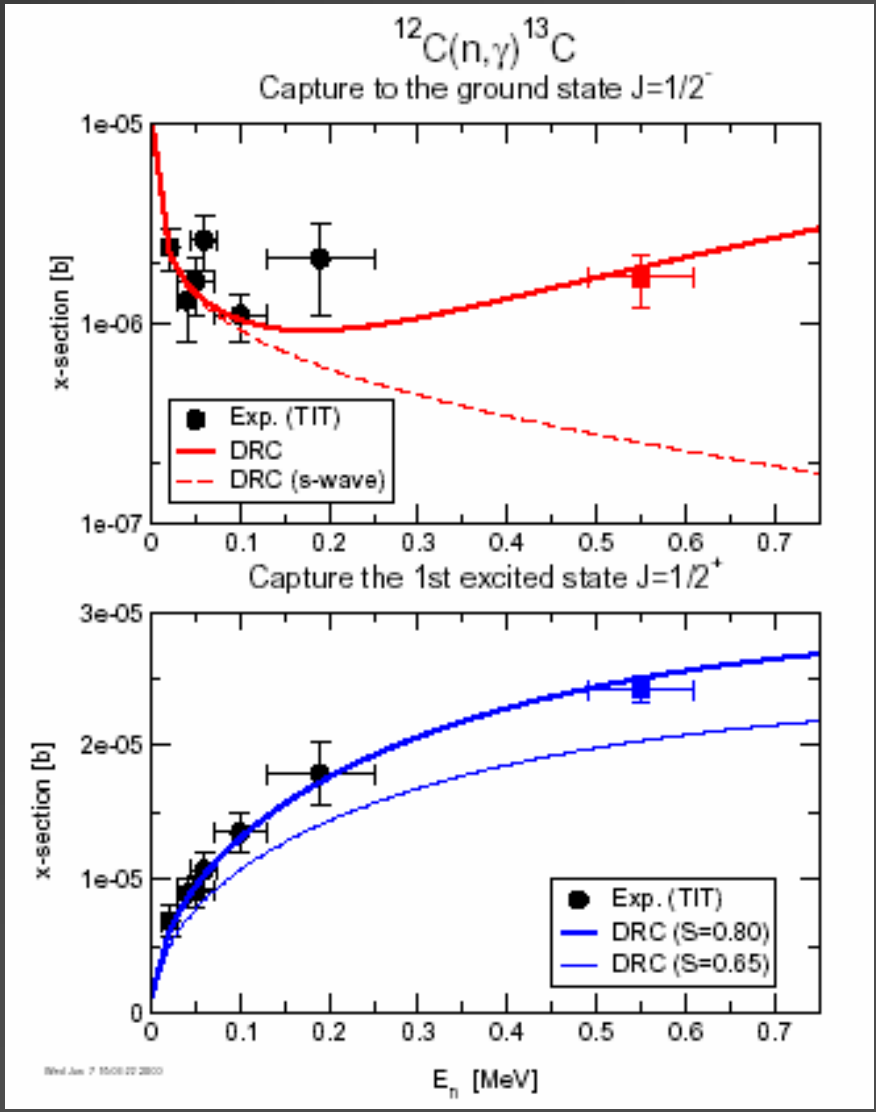

T Suzuki, Y Nagai, T Shima, M Igashira, A Mengoni, and T Otsuka
Phys. Rev. C **75** (1998) 2724.

alberto.mengoni@cern.ch

DRC

We start from the wave functions Ψ_c and Φ_b of the continuum and of the bound-state respectively given by

$$\Psi_c(r) = \sum_{l_c j_c} i^{l_c} \frac{\psi_{E_c l_c j_c}(r)}{r} [[\hat{Y}_{l_c} \times \hat{\chi}_s]^{j_c} \times \hat{\chi}_I]^{J_c}$$

and

$$\Phi_b(r) = \sum_{l_b j_b} B_{j_b, J_b \alpha_b, I\alpha} \frac{\phi_{n_b l_b j_b}(r)}{r} [[\hat{Y}_{l_b} \times \hat{\chi}_s]^{j_b} \times \hat{\chi}_I]^{J_b}$$

The radial wave functions $\psi_{E_c l_c j_c}(r)$ and $\phi_{n_b l_b j_b}(r)$ are obtained by solving the scattering and the bound state problem respectively, in a given potential.

The matrix elements $Q^{(\mathrm{EL})}_{c\to b} =< \Psi_c \,||\, \hat{T}^{\mathrm{EL}} \,||\, \Phi_b >$ may be written as a product of three terms

$$Q^{(\mathrm{EL})}_{c\to b} = \mathcal{I}_{cb} \cdot B_b \cdot A_{cb}$$

with $\hat{T}^{\mathrm{EL}}_M = r^L Y_{LM}$ and $\mathcal{I}_{cb} = \int \psi^*_{E_c l_c j_c}(r) r^L \phi_{n_b l_b j_b}(r) dr$.

The capture cross section is given by

$$\sigma^{(\mathrm{EL})}_{c\to b} = \frac{8\pi(L+1)}{L[(2L+1)!!]^2} \frac{k_\gamma^{2L+1}}{\hbar v} \frac{1}{2s+1} \frac{1}{2I+1} \bar{e}^2_{\mathrm{EL}} \sum_{l_c j_c, J_b j_b} | Q^{(\mathrm{EL})}_{c\to b} |$$

BW & DRC Interference

In the presence of a resonant state, the cross section contains a Breit-Wigner plus an interference term

$$\sigma(E) = \sigma_{DRC}(E) + \sigma_{BW}(E) + 2[\sigma_{DRC}(E) + \sigma_{BW}(E)]^{1/2} \cos[\delta_r(E)]$$

with

$$\sigma_{BW}(E) = \pi \lambda_n^2 g_J \frac{\Gamma_n \Gamma_\gamma}{(E_r - E)^2 + \frac{1}{4}\Gamma^2}$$

and

$$\delta_r(E) = \tan^{-1}\left[\frac{\Gamma(E)}{2(E - E_r)}\right]$$

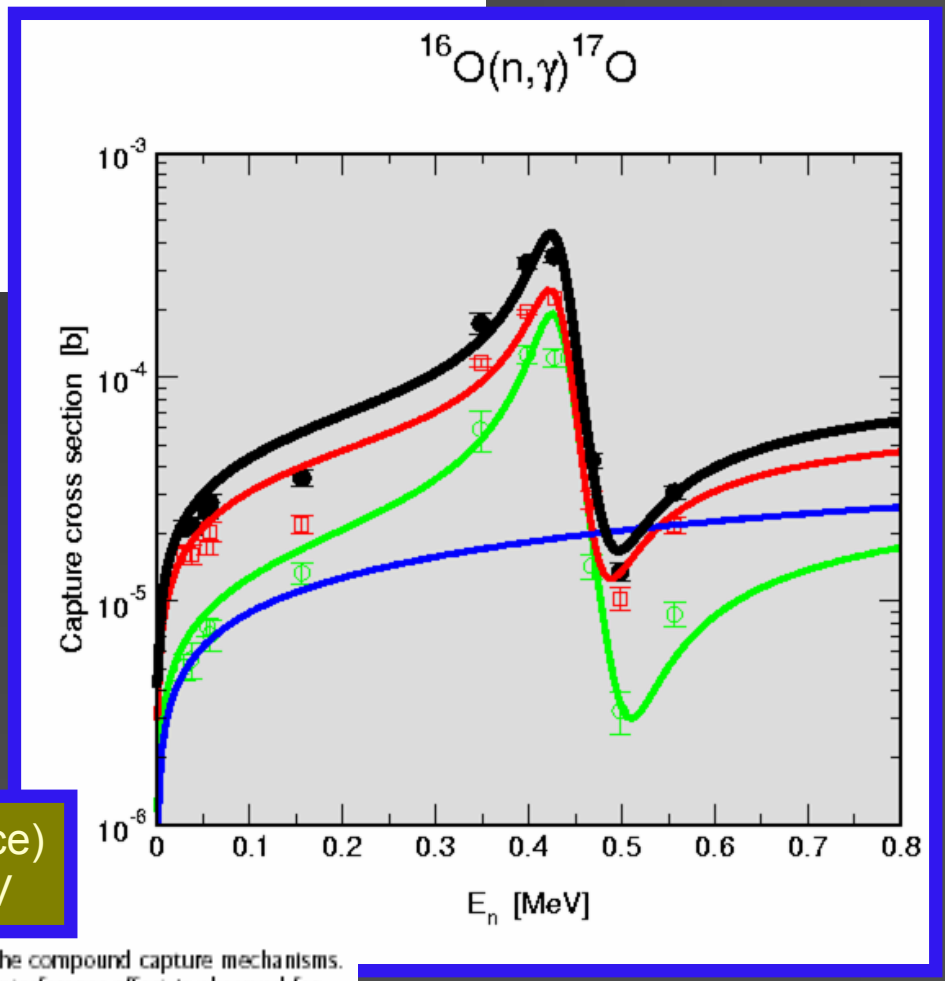

Model : DRC (p→s,d E1 transitions + BW interference)
Parameters : E_r = 434 keV, Γ_n = 45 keV, $\Gamma_{\gamma 0}$ = $\Gamma_{\gamma 1}$ = 0.5 eV

The p−wave resonance at 434 KeV in $n + {}^{16}O$ provides a nice example of interference between the DRC and the compound capture mechanisms. The interference occurs among the p−wave component of the DRC and the p−wave neutron resonance. The interference effect is observed for both the transitions to the ground-state ($J^\pi = 5/2^+$) and in the first excited state ($J^\pi = 1/2^+$) in ${}^{17}O$.

alberto.mengoni@cern.ch

Capture & Dissociation

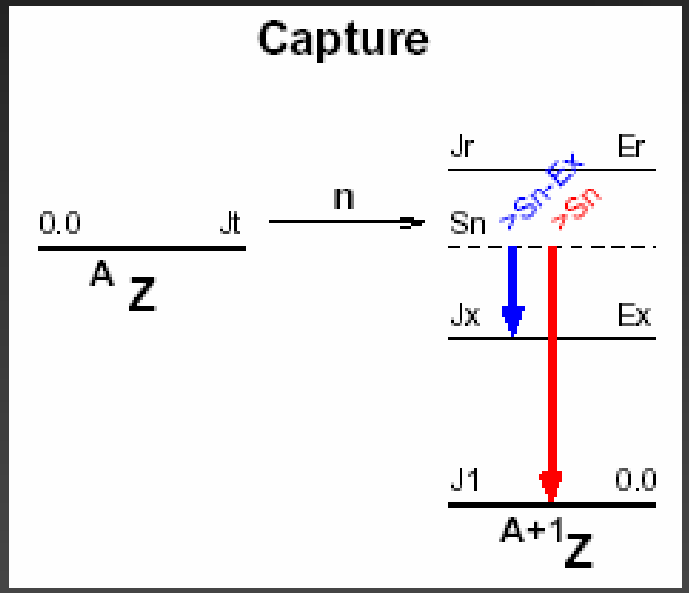

$$n + {}^{A}Z \rightarrow {}^{A+1}Z + \gamma$$

$$1 + 2 \rightarrow 3 + 4$$

$$\sigma_{n,\gamma} = \frac{k_\gamma^2}{k_n^2} \frac{2J_3 + 1}{2J_2 + 1} \sigma_{\gamma,n}$$

$$n + {}^{A}Z \leftarrow \gamma + {}^{A+1}Z$$

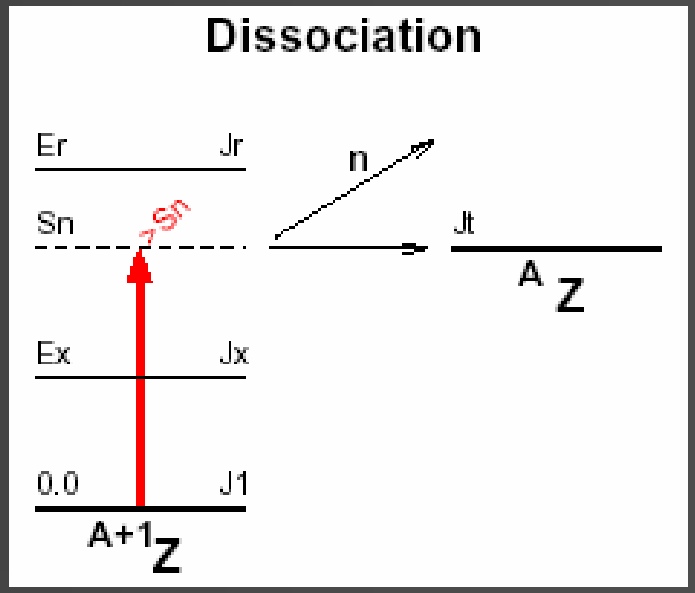

The time-reversal invariance for nuclear reactions allows for using the detailed balance

alberto.mengoni@cern.ch

Neutron capture rates: inverse

The time-reversal invariance for nuclear reactions allows for using the detailed balance

$^{8}Be(n,\gamma)^{9}Be$

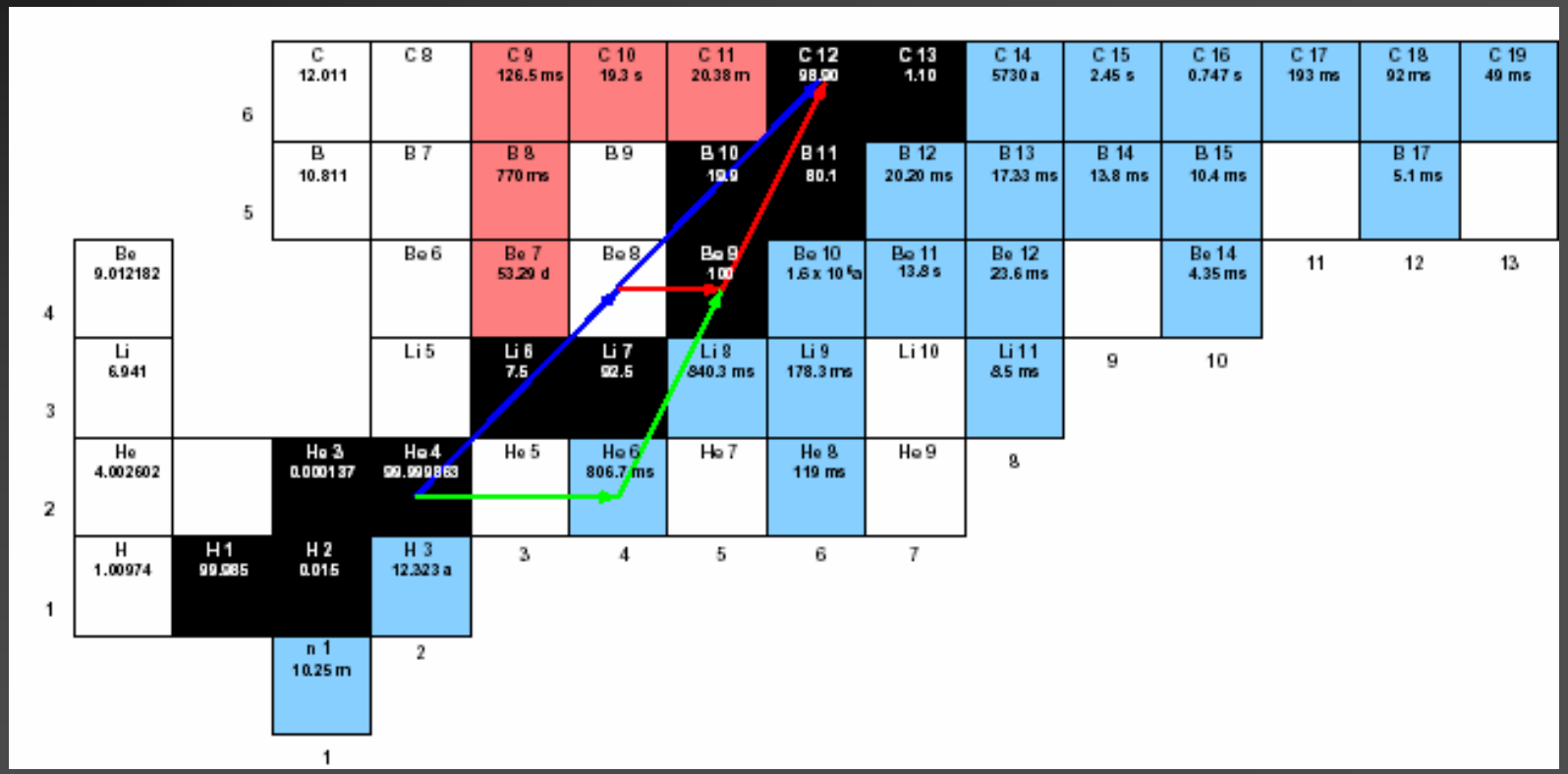

Phase: post-collaps phase of Type II sopernovae
Site: ν-heated high-entrpy bubble
Neutron density: $10^{20\text{-}30}$ n/cm^3
Status: NSE with α-induced re-combinations (high photon-to-baryon ratio)
Main quantities: expansion and cooling rates, reaction rates

alberto.mengoni@cern.ch

Neutron capture rates: inverse

The time-reversal invariance for nuclear reactions allows for using the detailed balance

$^{8}Be(n,\gamma)^{9}Be$

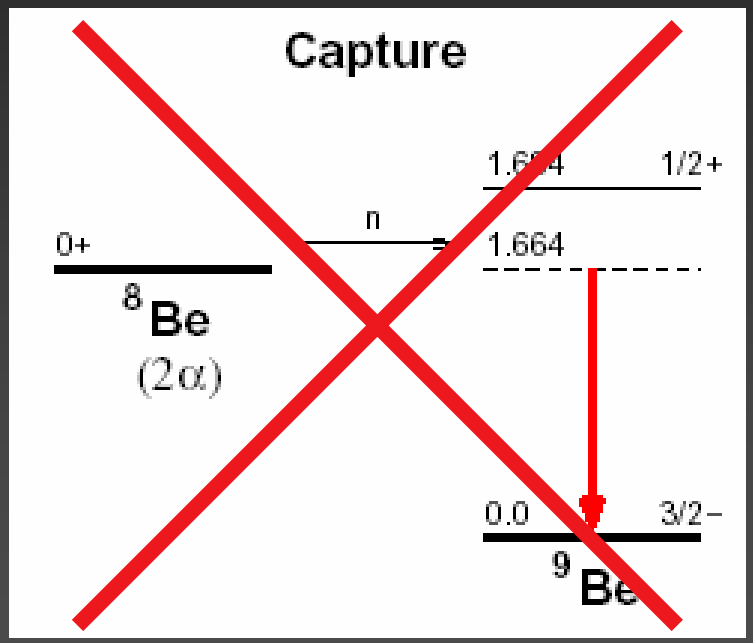

$^{9}Be(\gamma,n)^{8}Be \rightarrow \alpha\alpha$

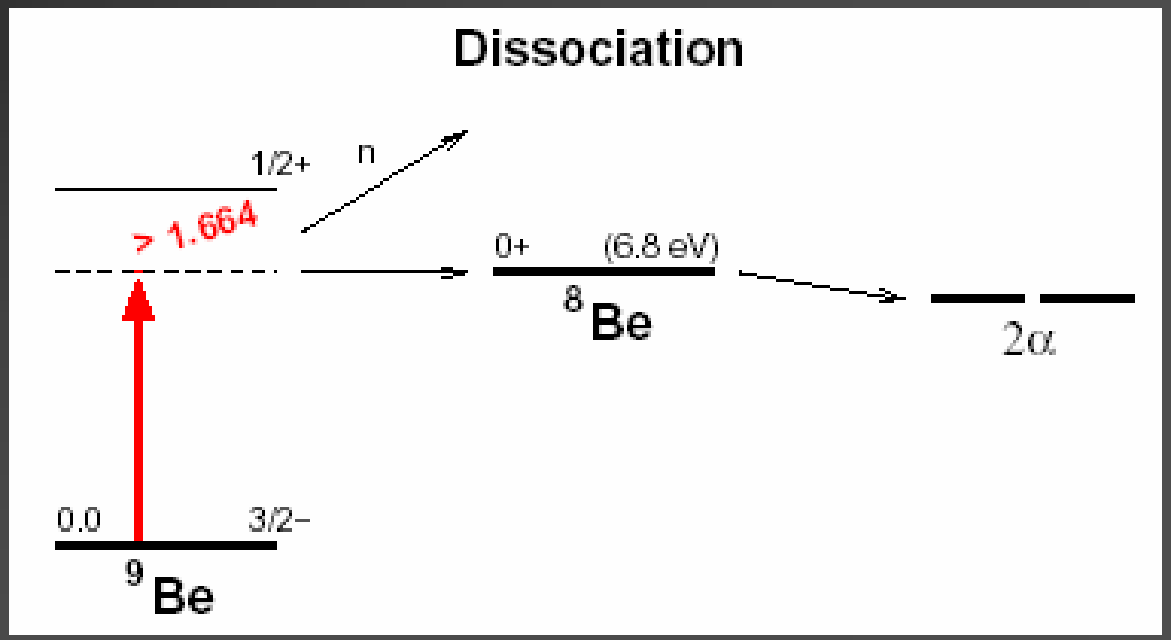

alberto.mengoni@cern.ch

Neutron capture rates: inverse

The time-reversal invariance for nuclear reactions allows for using the detailed balance

$^{8}Be(n,\gamma)^{9}Be$

Model	:	DRC ($s \rightarrow p$ E1 transition)
	:	Breit-Wigner single-level resonance term
	:	Interference term included
Parameters	:	$E_r = 73.4$ KeV, $\Gamma_n = 217$ KeV
	:	$\Gamma_\gamma = 0.45$ eV

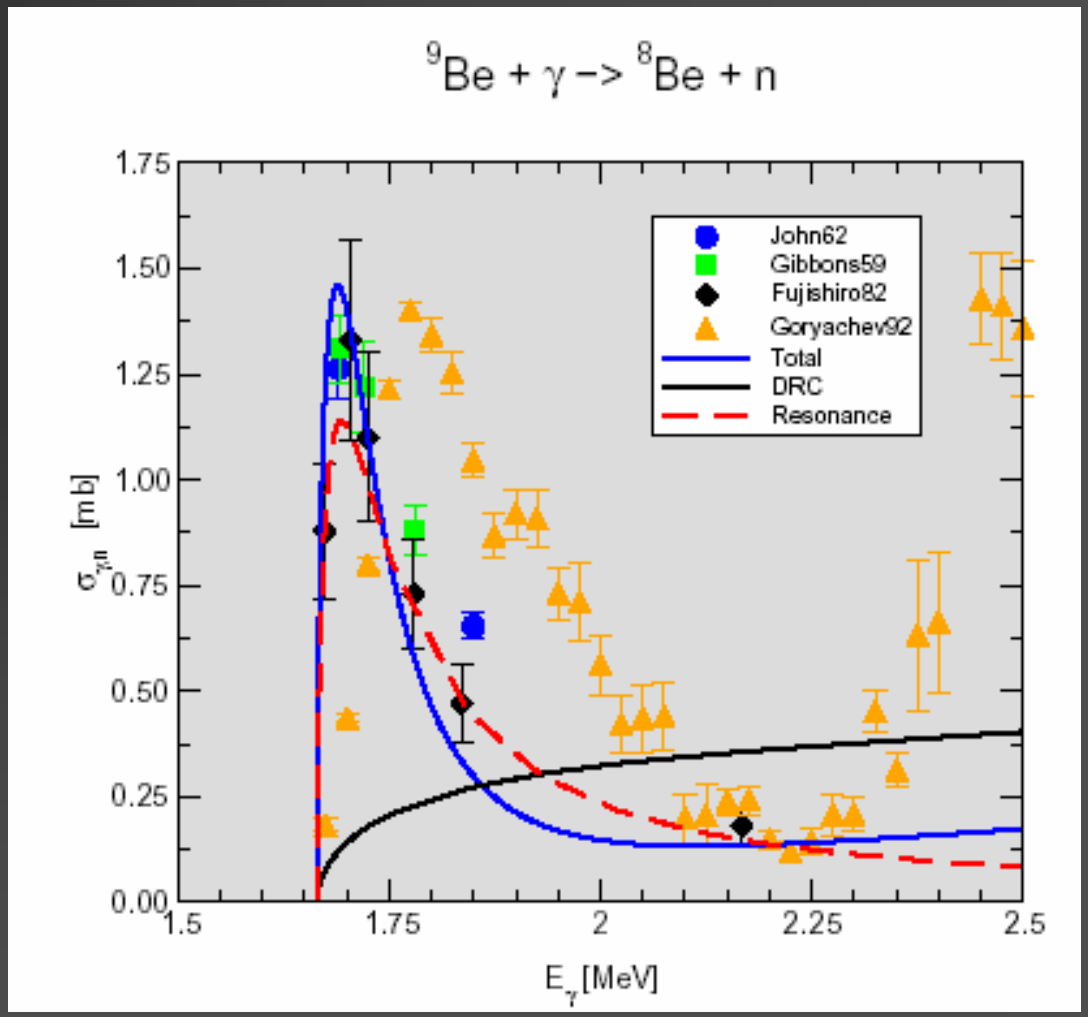

Phase: post-collaps phase of Type II sopernovae
Site: ν-heated high-entrpy bubble
Neutron density: $10^{20\text{-}30}$ n/cm^3
Status: NSE with α-induced re-combinations (high photon-to-baryon ratio)
Main quantities: expansion and cooling rates, reaction rates

alberto.mengoni@cern.ch

The $2s_{1/2}$ single-particle orbit in ^{9}Be

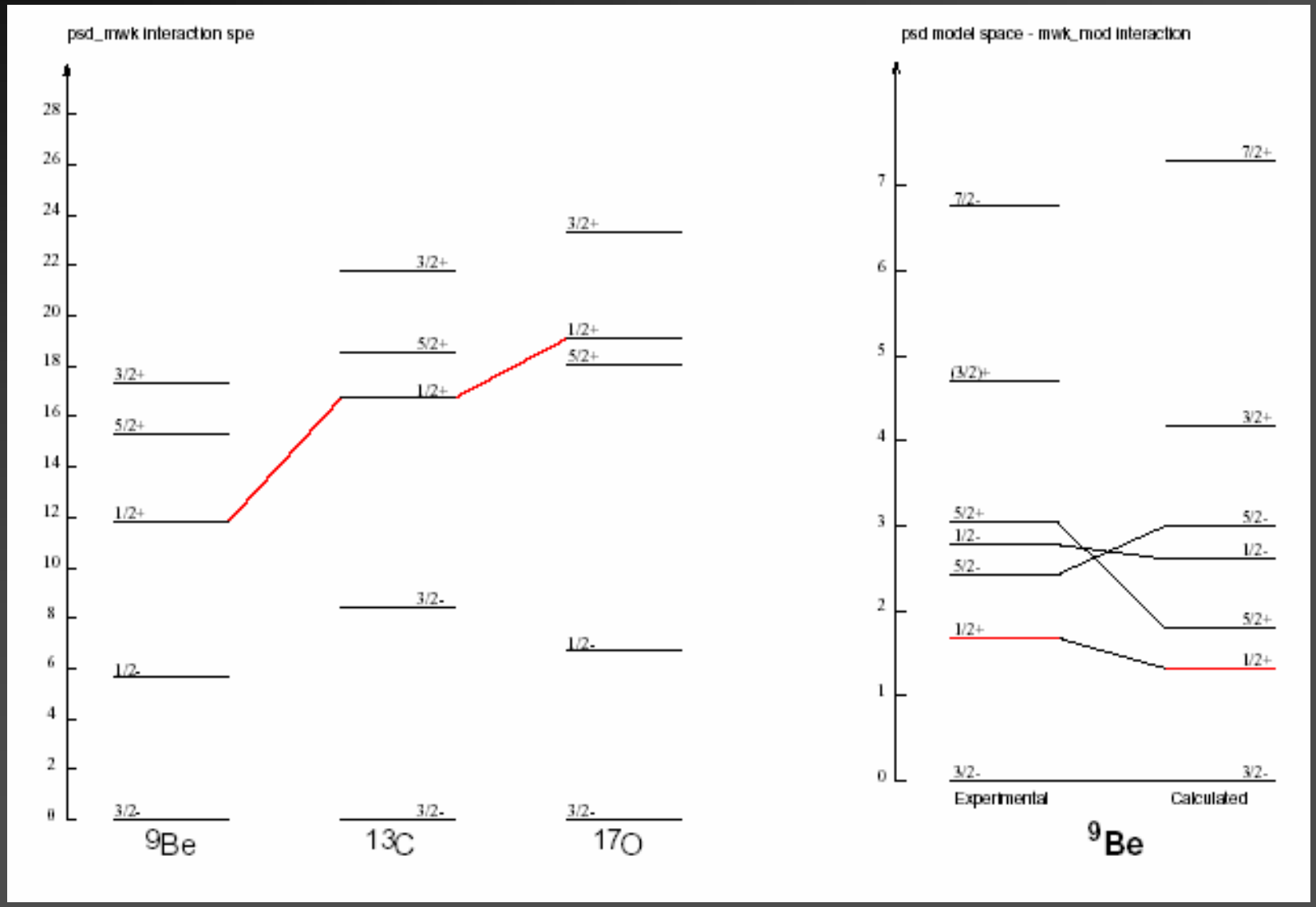

alberto.mengoni@cern.ch

Coulomb dissociation

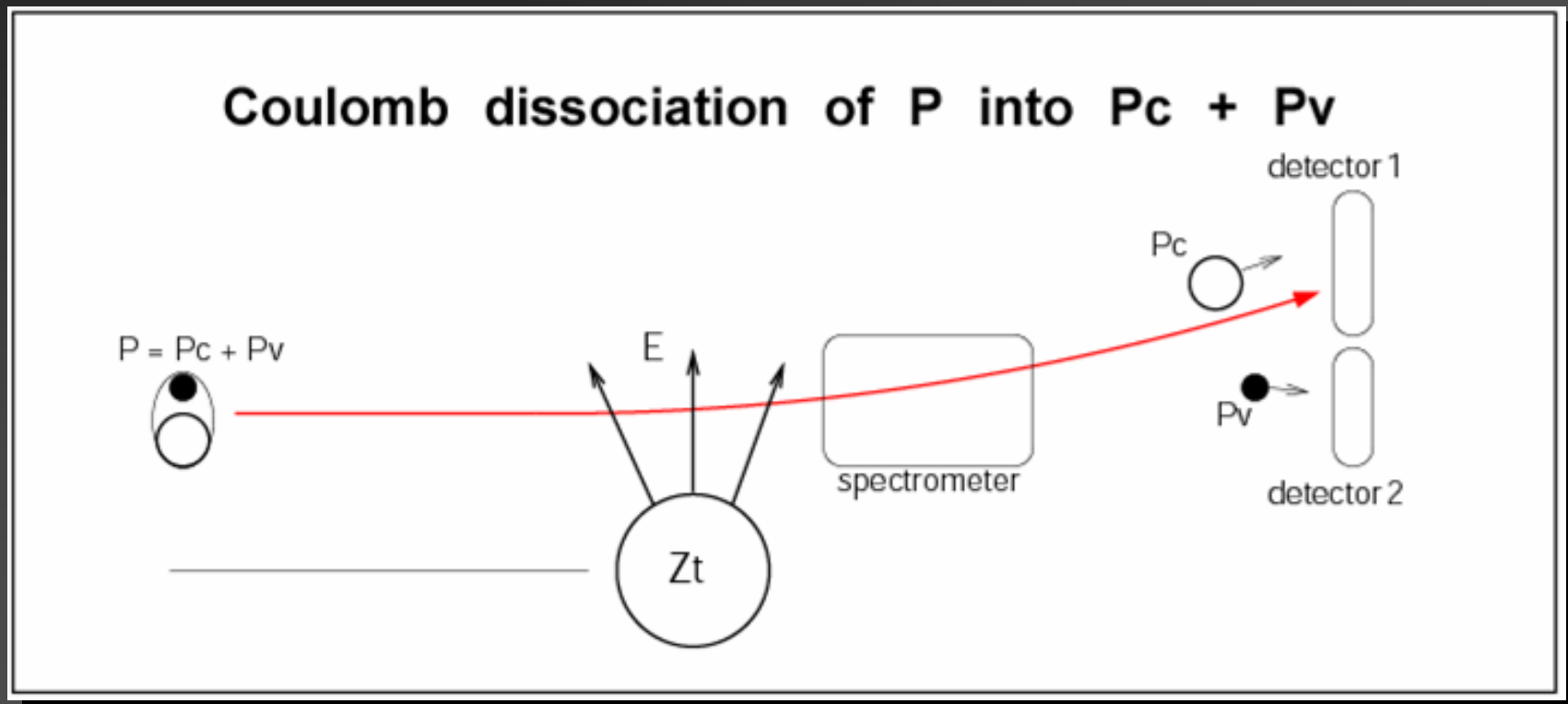

alberto.mengoni@cern.ch

^{11}Be Coulomb dissociation

The time-reversal invariance for nuclear reactions allows for using the detailed balance

^{10}Be(n,γ)^{11}Be

^{10}Be half-life: 1.6 x 10^6 a

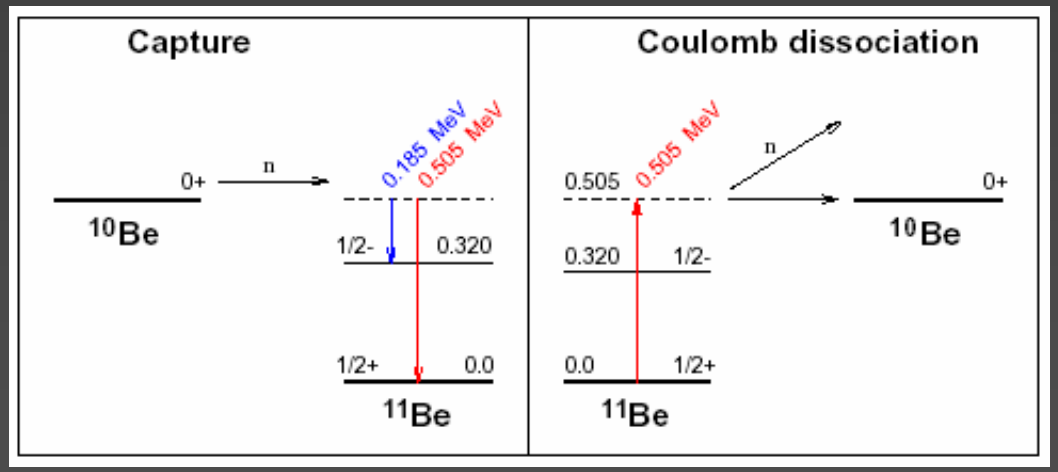

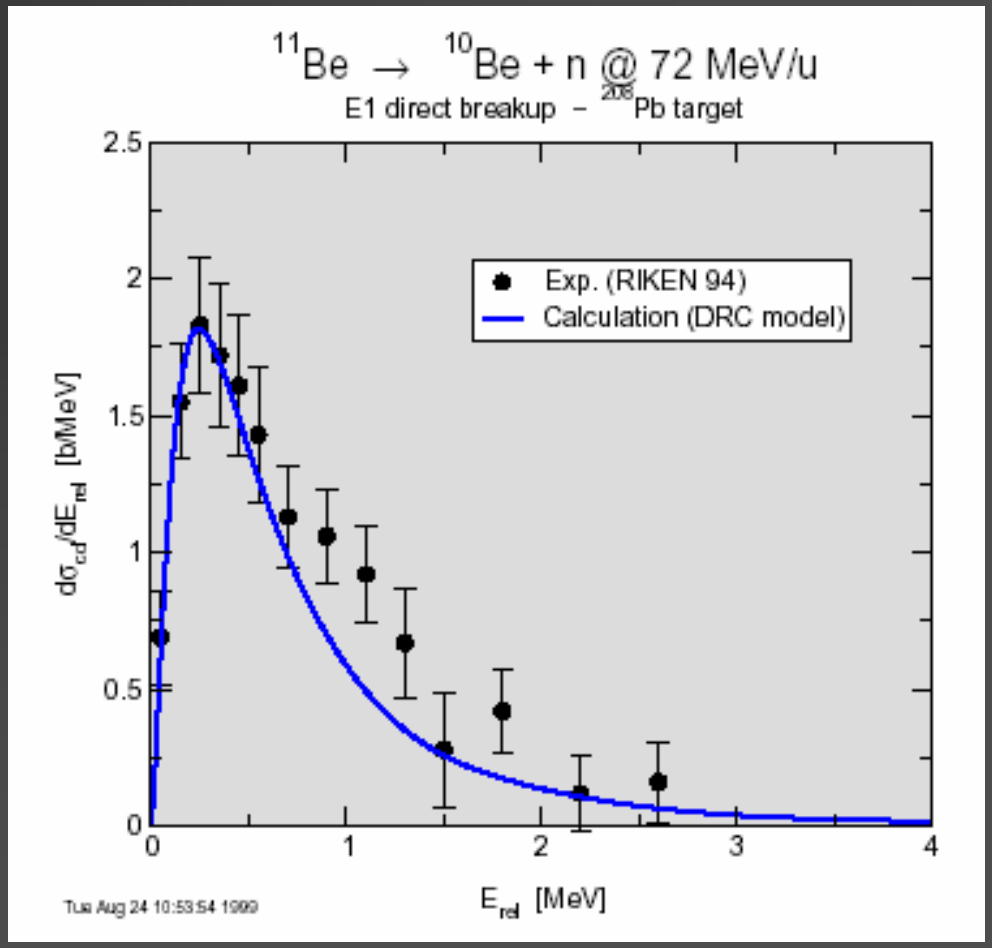

alberto.mengoni@cern.ch

$^{10}Be(n,\gamma)^{11}Be$: predictions

$^{10}Be(n,\gamma)^{11}Be$

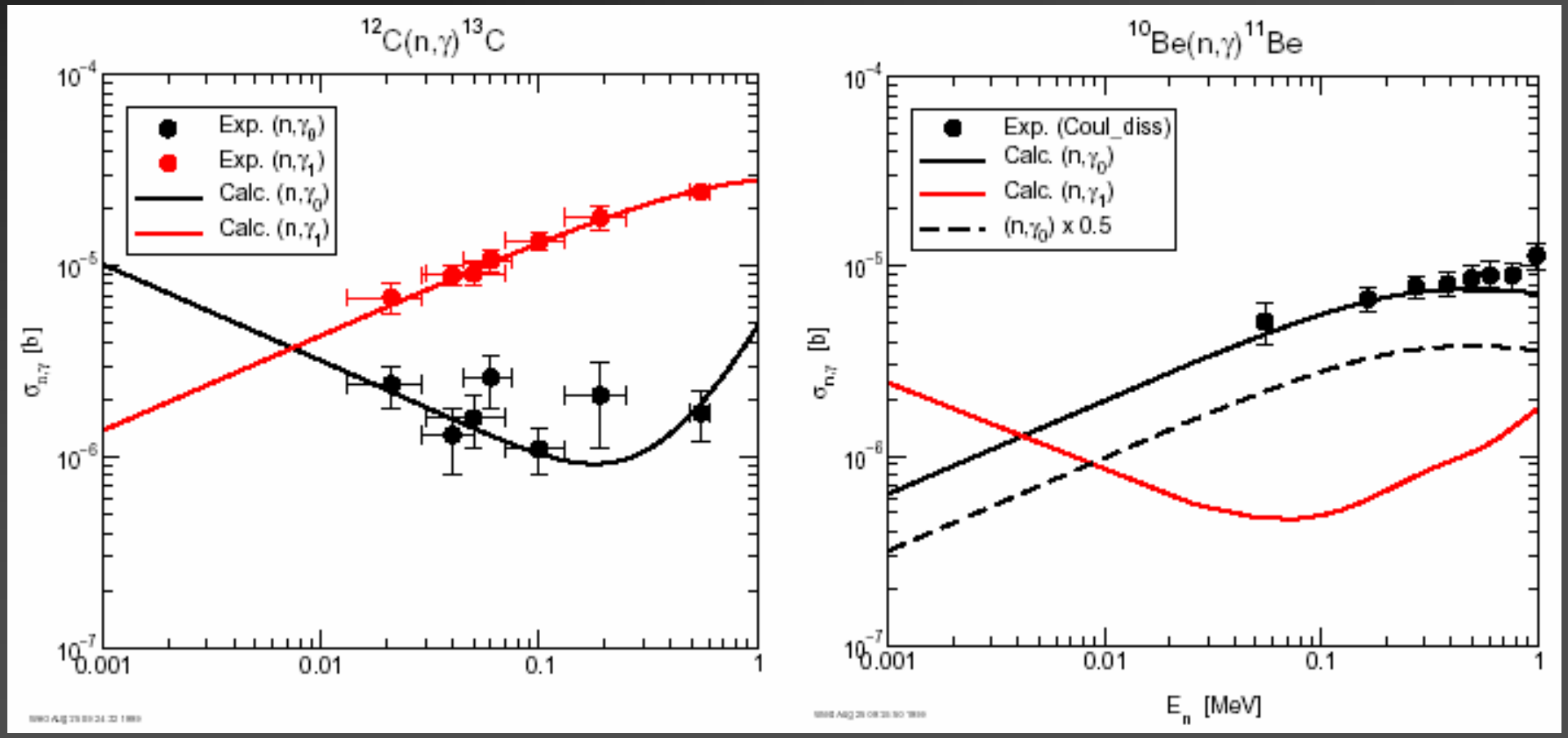

alberto.mengoni@cern.ch

$^{14}C(n,\gamma)^{15}C$

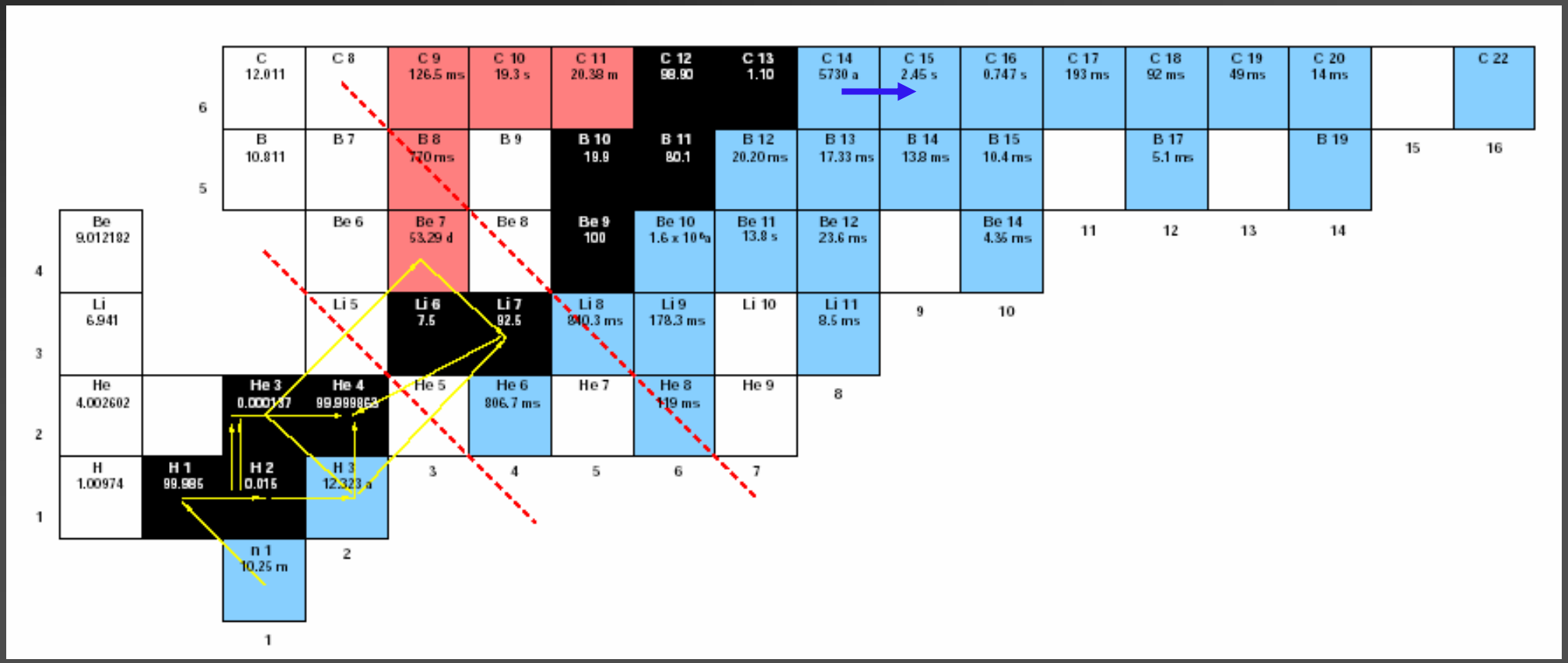

alberto.mengoni@cern.ch

$^{14}C(n,\gamma)^{15}C$ & ^{15}C Coul_diss

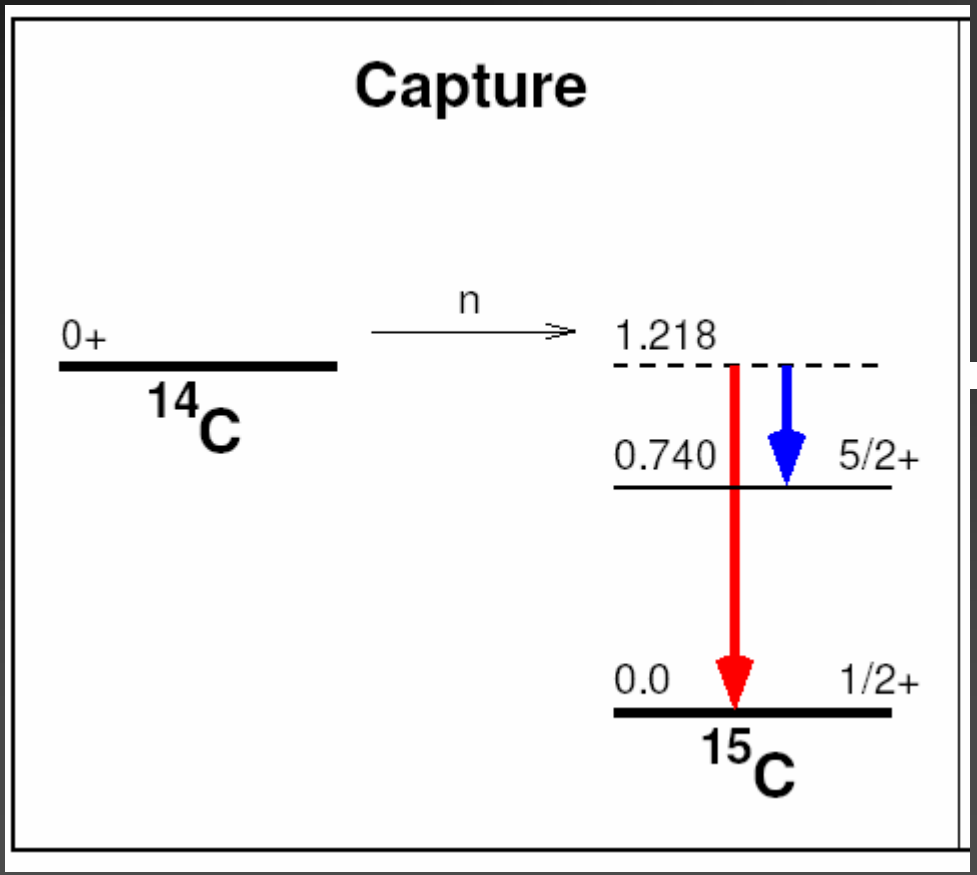

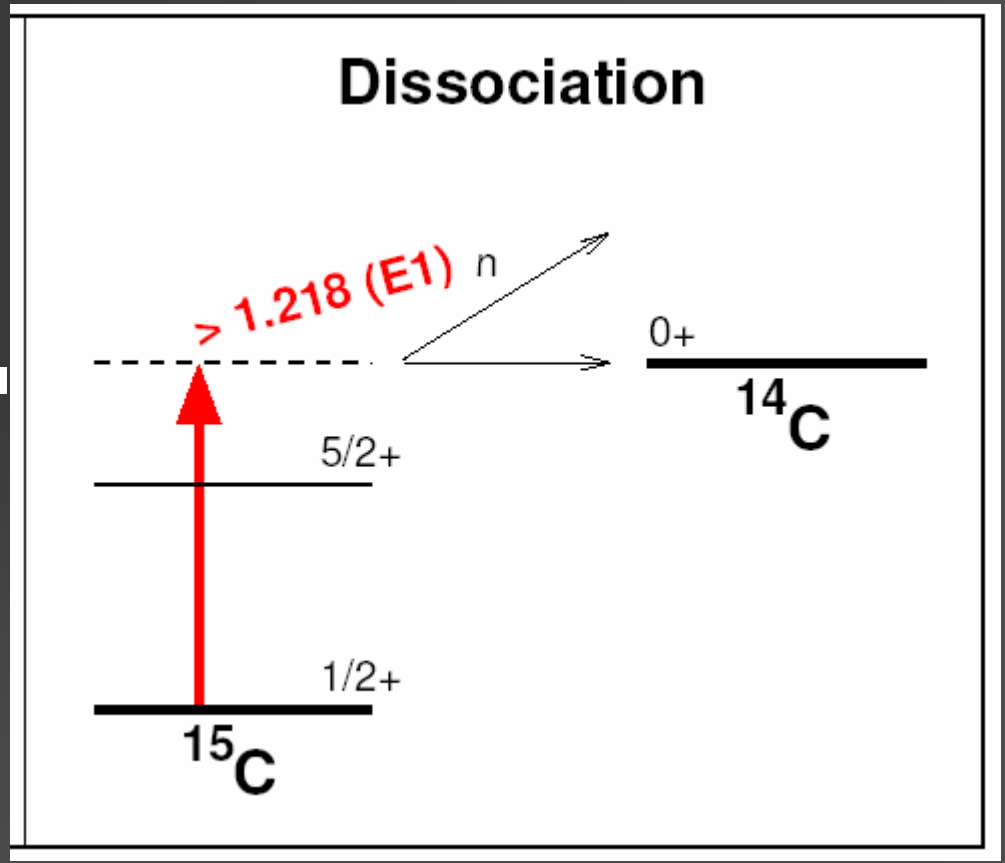

alberto.mengoni@cern.ch

$^{15}C \rightarrow {}^{14}C + n$

Coul_diss data: 20% reduction implies $S_{dp} \approx 0.7$ and

$$\left\langle \sigma_{n,\gamma} \right\rangle_{kT=25\,\mathrm{KeV}} = 6.0\,\mu b$$

To be compared with the activation measurement (H Beer et al. 1992):

$\langle\sigma\rangle = 1.7 \pm 0.4\ \mu b$

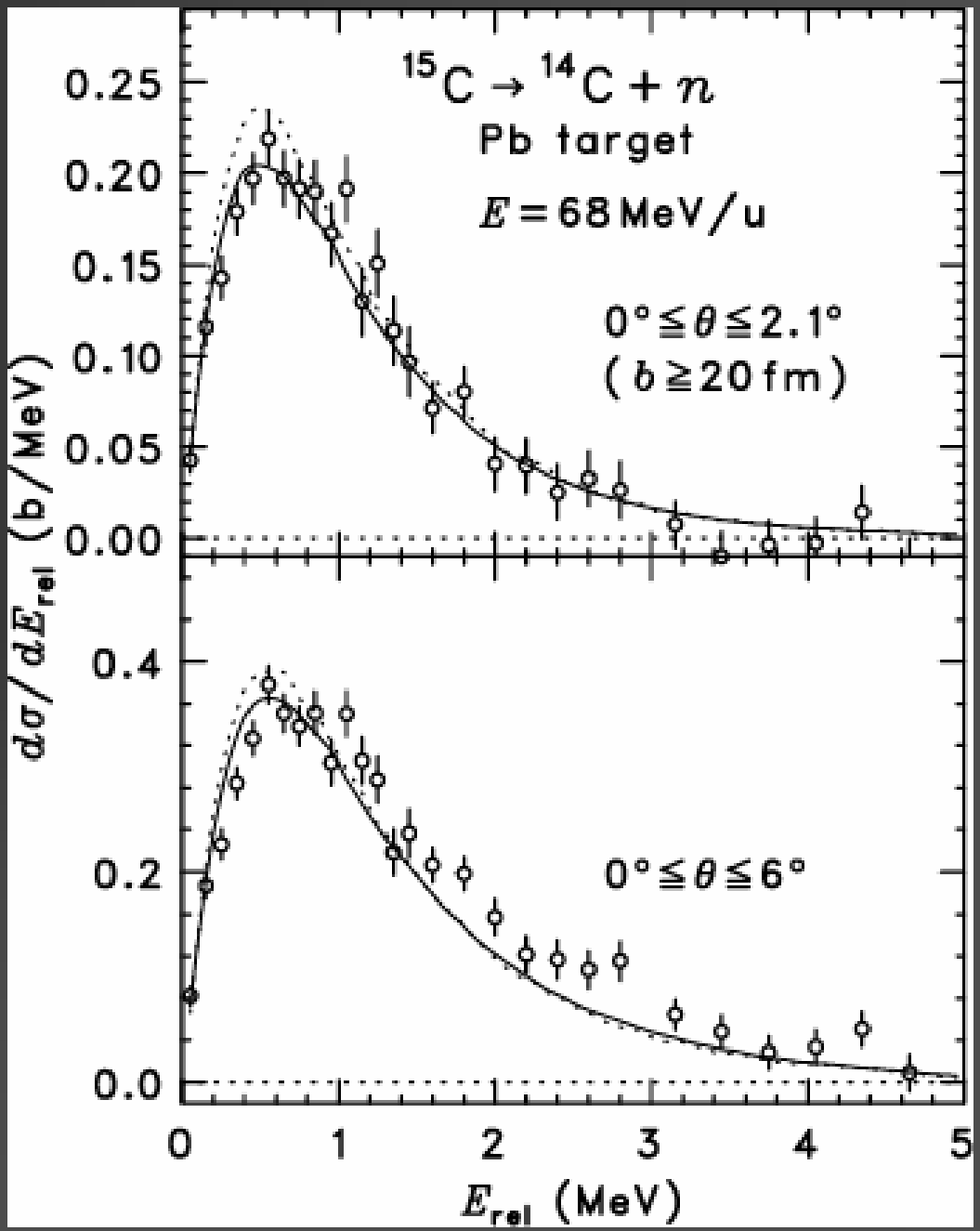

T Nakamura (private communication, 2004)

alberto.mengoni@cern.ch

Michael Wiescher visits CERN n_TOF

experimental device(?) set in operation
by A Mengoni (nuclear theorist)

alberto.mengoni@cern.ch

CERN accelerator Complex

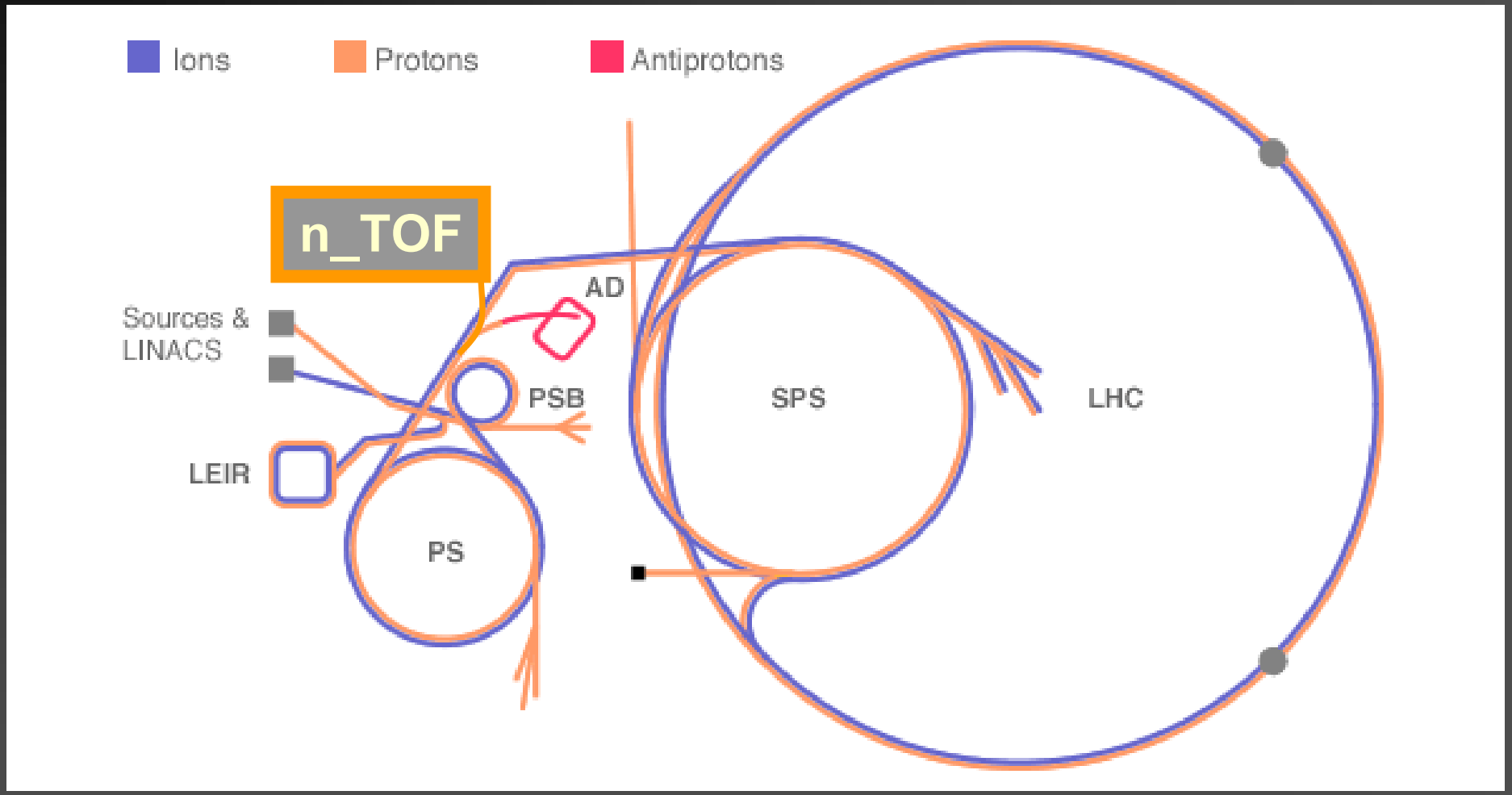

Linac(s): up to 50 MeV PSB: up to 1 GeV PS: up to 24 GeV

alberto.mengoni@cern.ch

CERN accelerator Complex: n_TOF

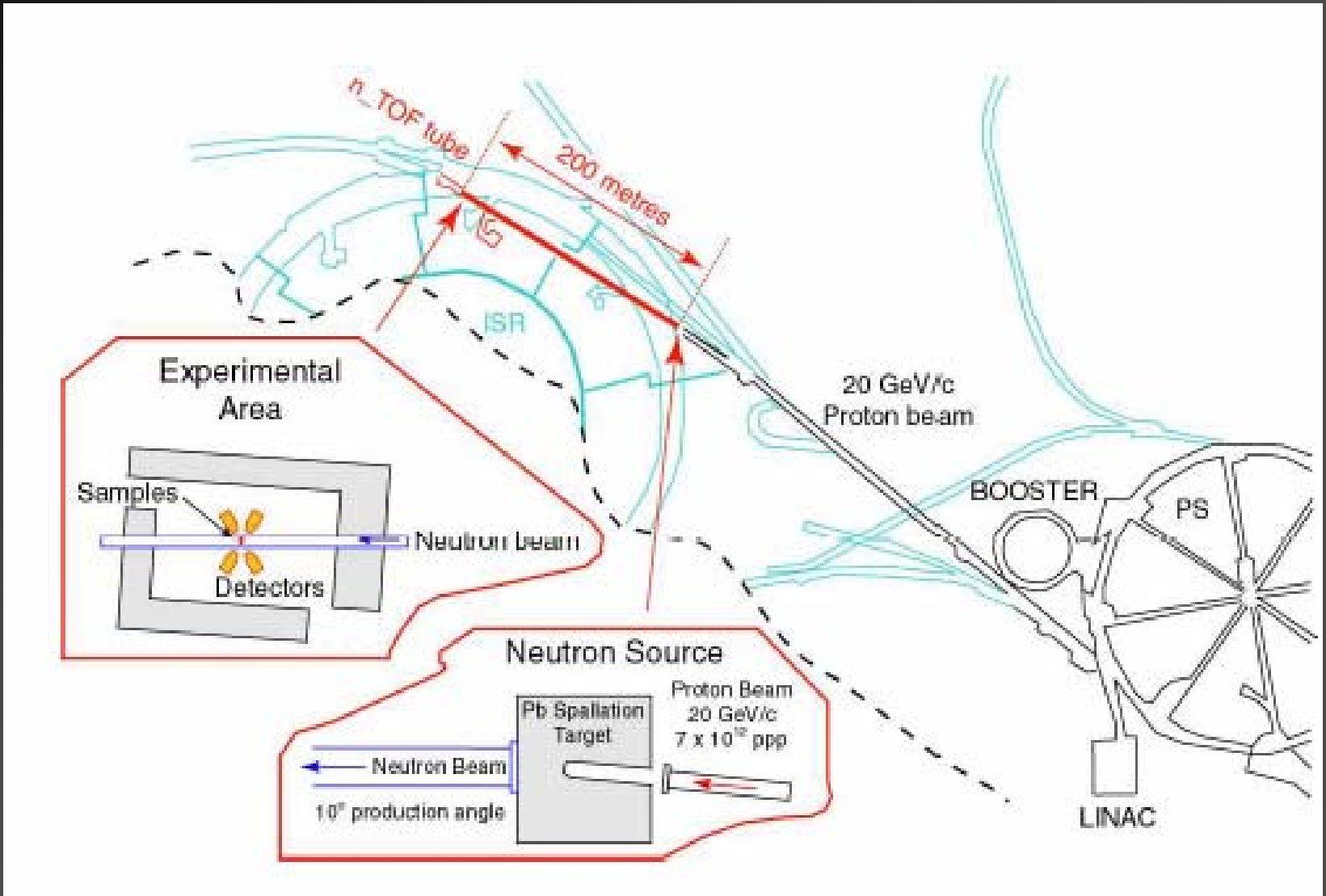

alberto.mengoni@cern.ch

CERN n_TOF Facility

- Design: the n_TOF Target
- The Tunnel

movie by V Vlachoudis

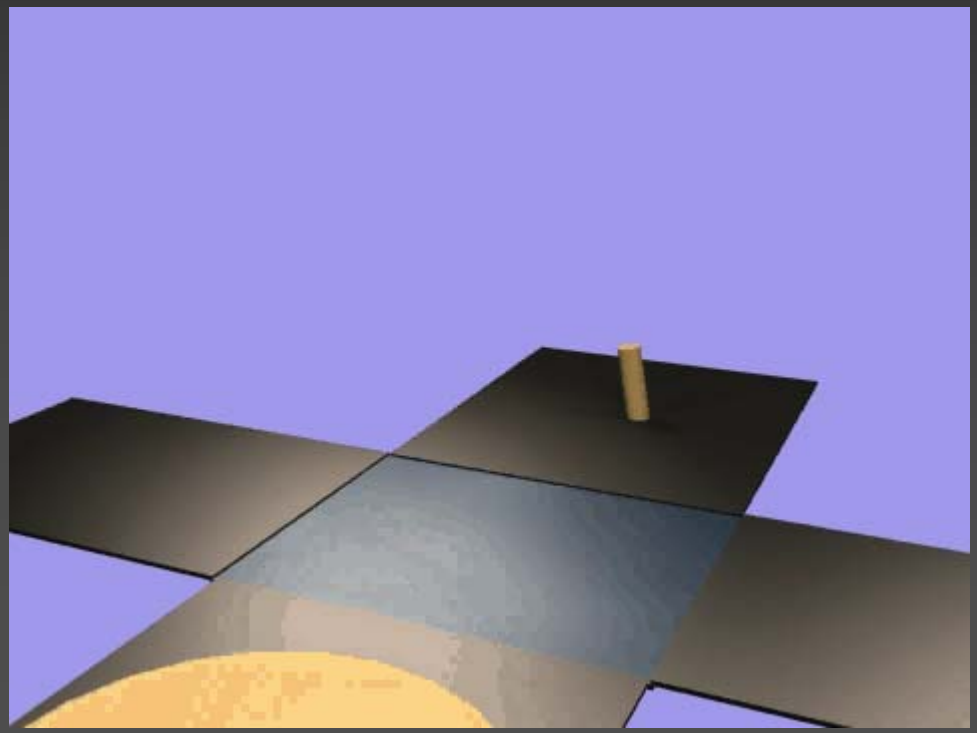

alberto.mengoni@cern.ch

n_TOF facility in operation

Main characteristics of the n_TOF neutron beam line:

- Exremely wide neutron energy range
- Extremely high istantaneous neutron flux
- High resolution
- Low background conditions for capture & fission measurements
- Low duty cycle expecially suited for measurements of radioactive samples

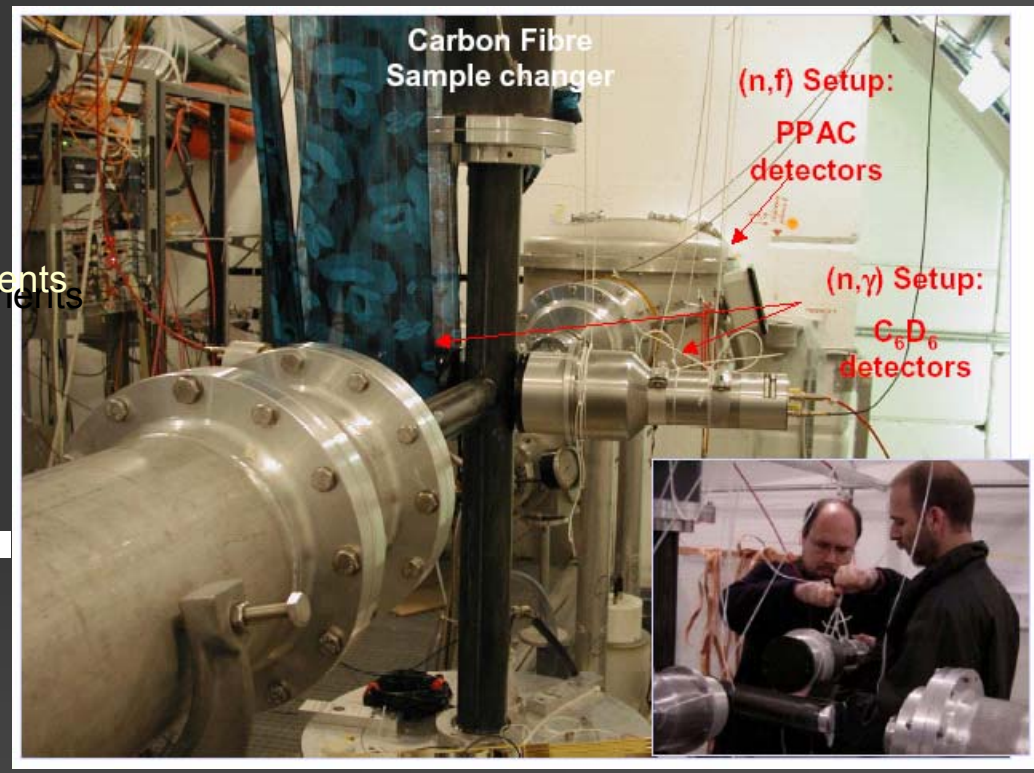

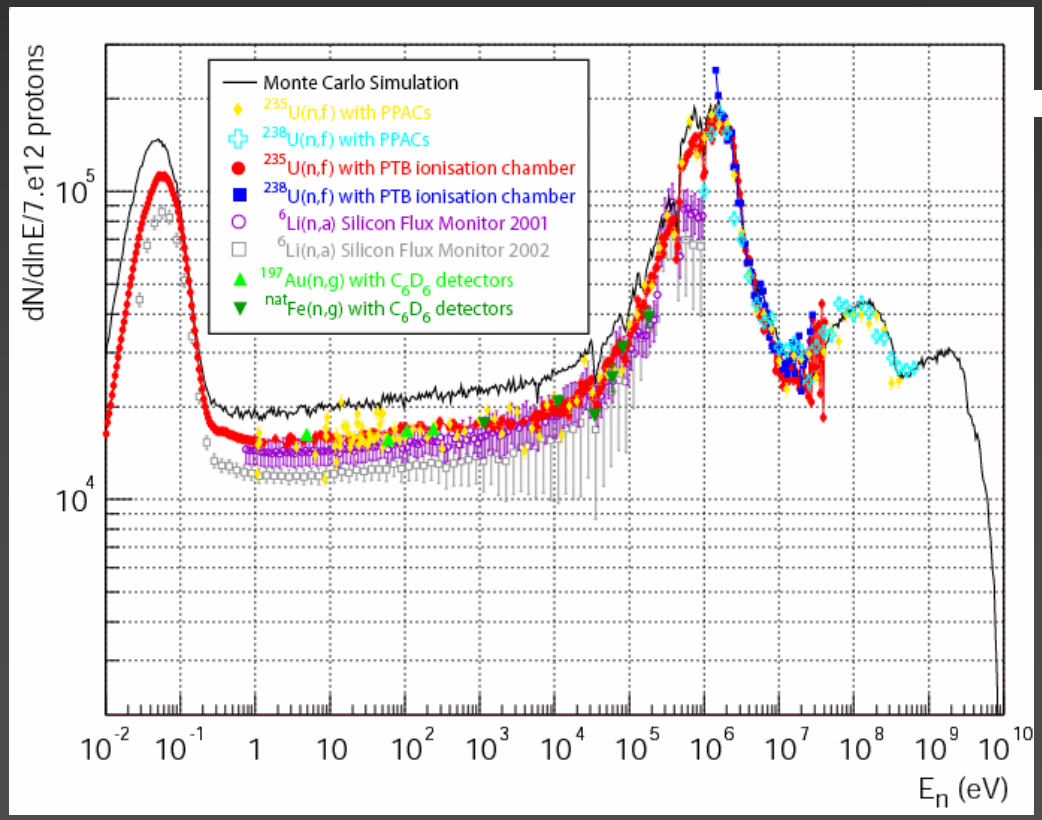

Experiments performed with:

- Innovative DAQ system
- Specialy developed detection systems for monitoring & measurements
- High efficiency 4π γ-ray detector array under construction (Total Absorption Calorimenter, n_TOF-TAC)

Why we do all this?

alberto.mengoni@cern.ch

Objectives

- Measurements of neutron cross sections relevant for Nuclear Waste Transmutation and related Nuclear Technologies
- Cross sections relevant for Nuclear Astrophysics
- Neutrons as probes for fundamental Nuclear Physics

alberto.mengoni@cern.ch

ADS (Accelerator Driven Systems)

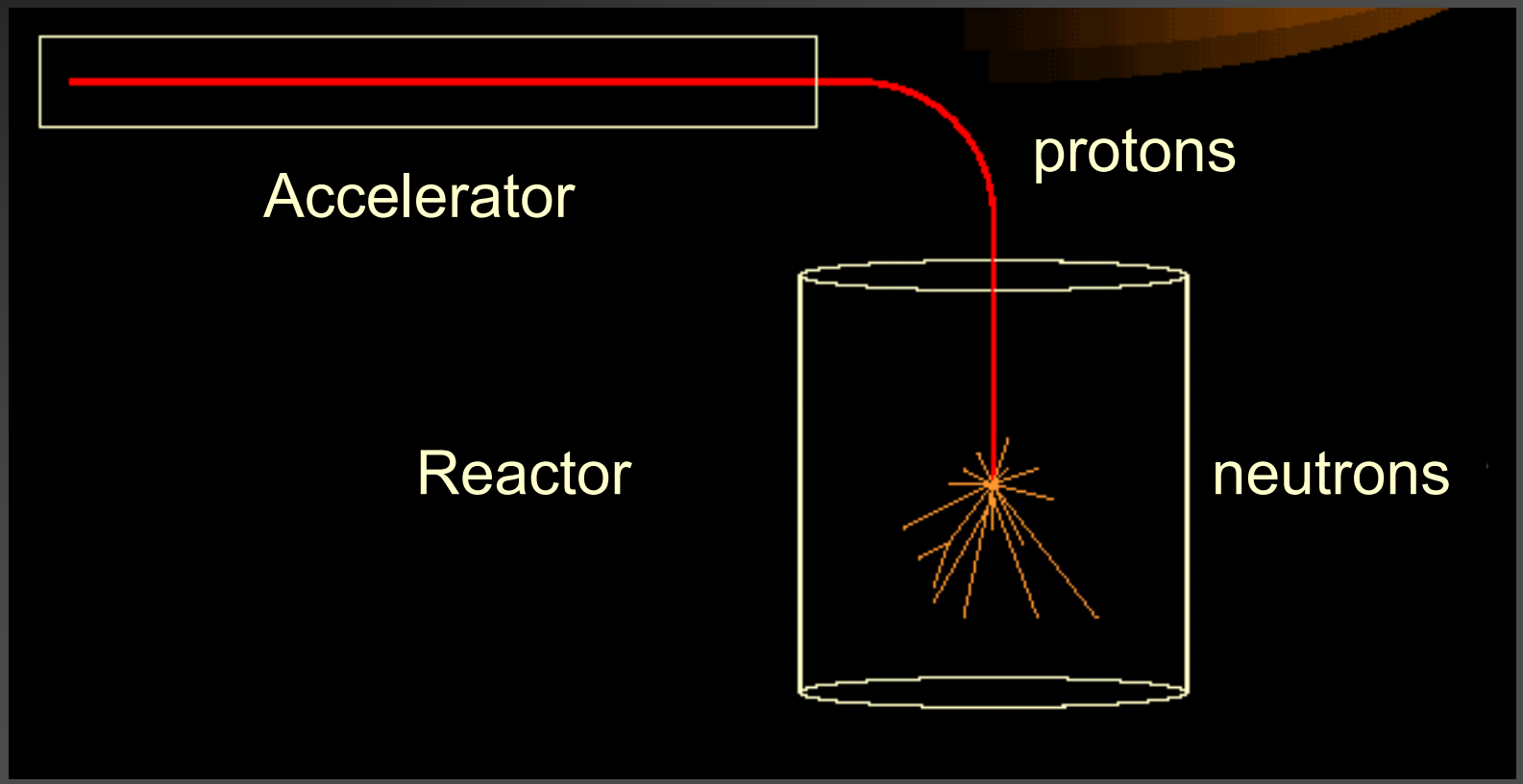

Zen-ADS

alberto.mengoni@cern.ch

Nucleosynthesis

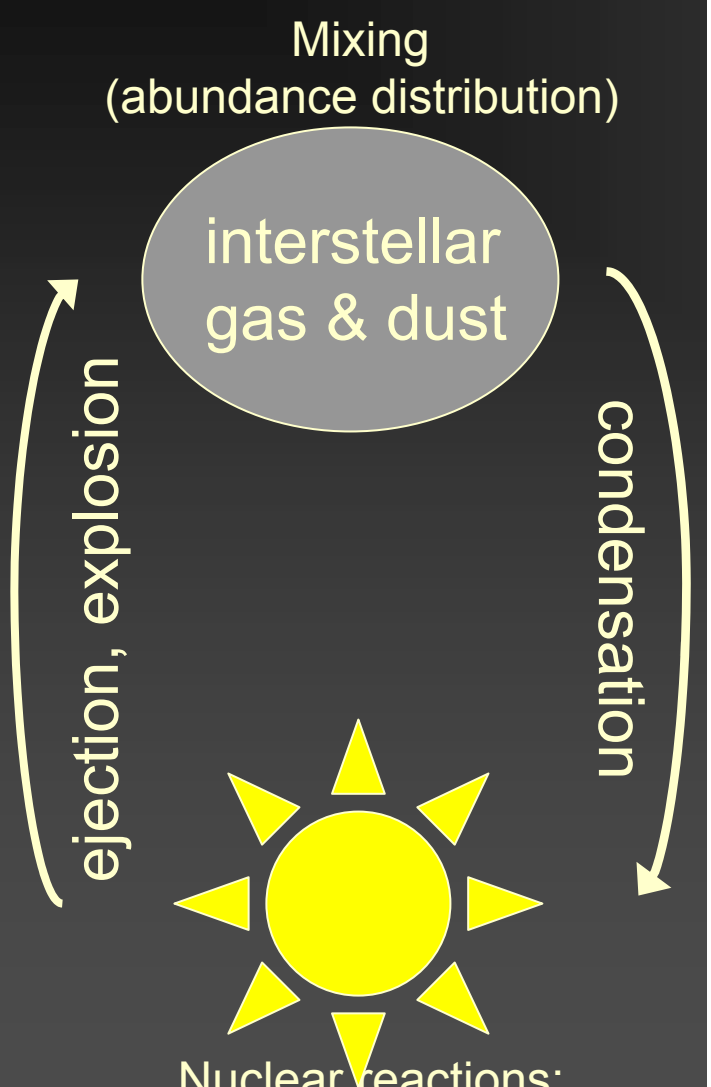

Nuclear reactions:
- energy generation
- nucleosynthesis

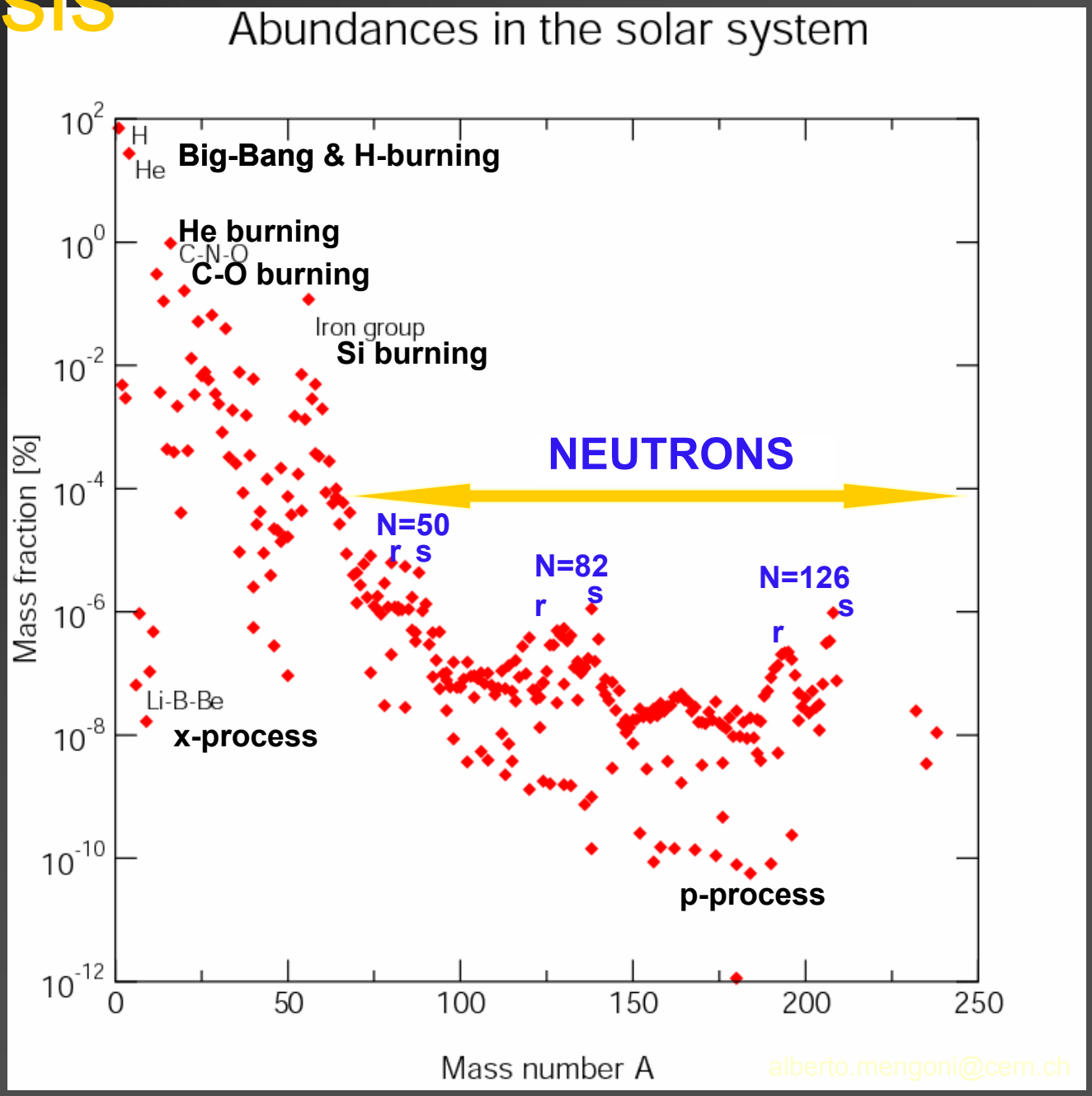

n_TOF experiments

Capture

^{151}Sm

^{204,206,207,208}Pb

^{209}Bi

^{232}Th

^{24,25,26}Mg

^{90,91,92,94,96}Zr

^{139}La

^{186,187,188}Os

Fission

^{233,234,235,236,238}U

^{232}Th

^{209}Bi

^{237}Np

^{241,243}Am

^{245}Cm

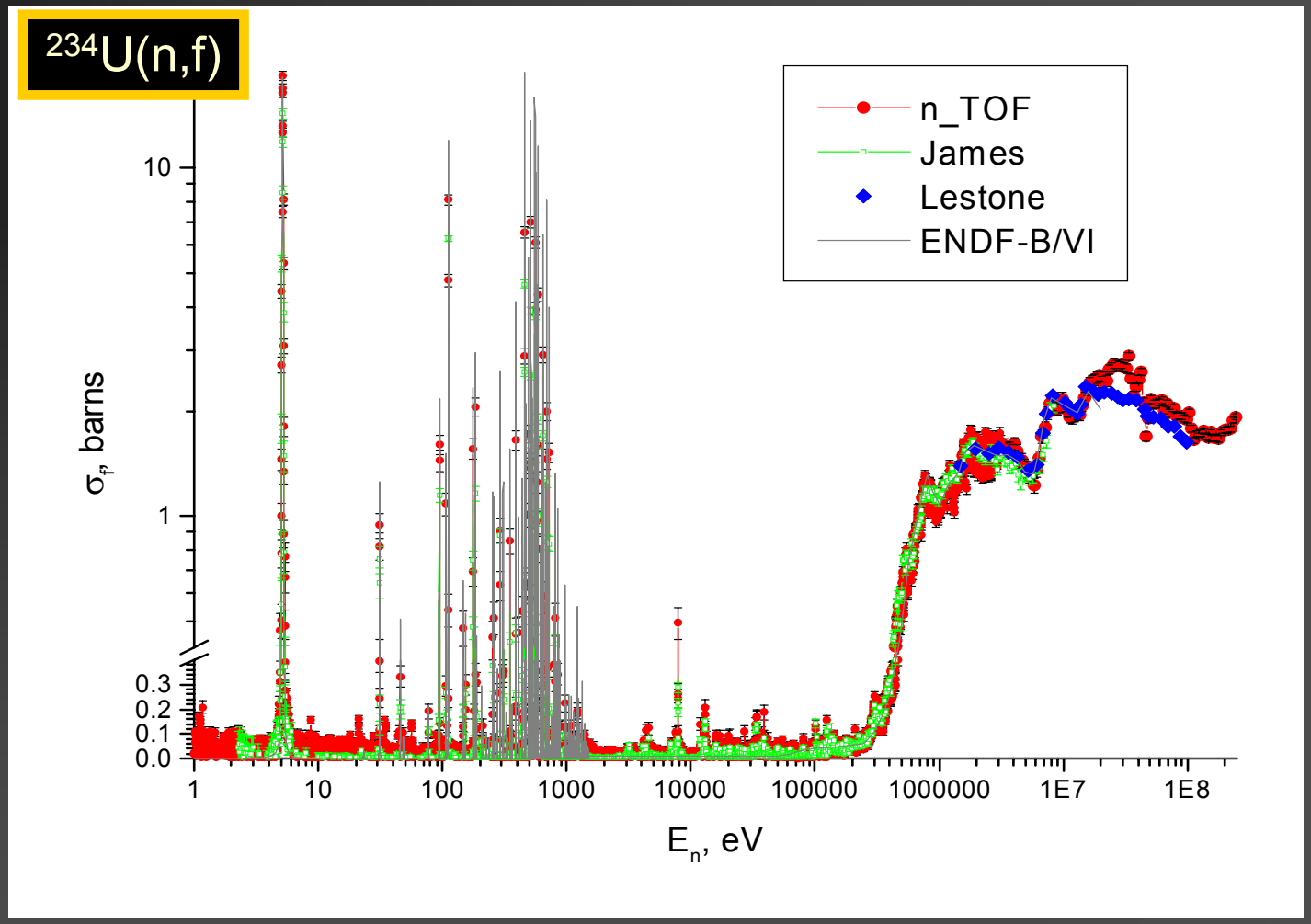

The n_TOF Collaboration (2003)

n_TOF-08: (n,γ) x-sections of Zr and La

probing the neutron exposure and neutron flux in Red Giant Stars

- Neutron magic, N=50 & 82
- Small x-sections (resonance dominated)
- Can be used for normalization of s-process abundance

- Fission products (stable ^{139}La and ^{90,91,92,94,96}Zr, radioactive ^{93}Zr)

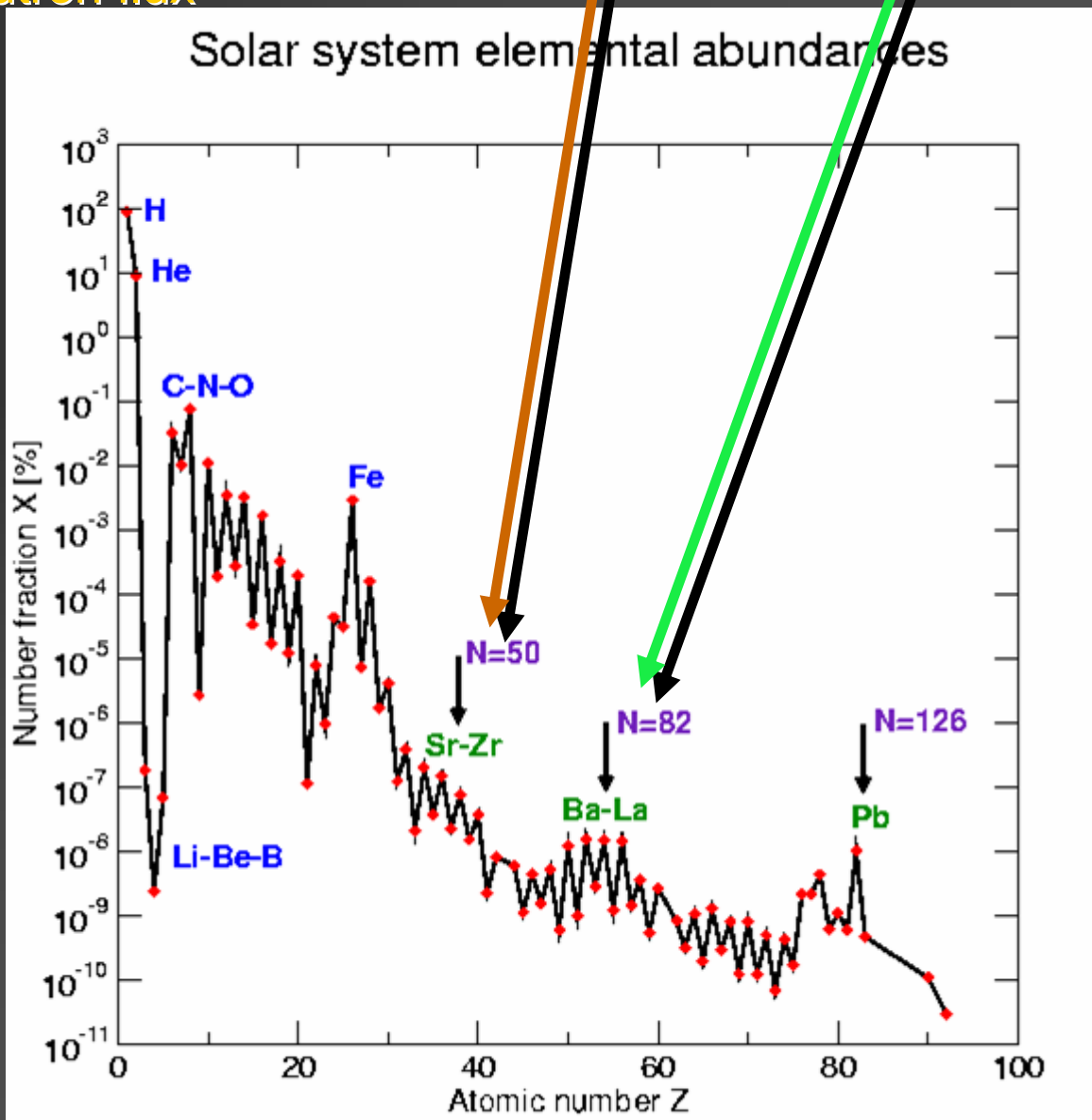

n_TOF-08: (n,γ) x-sections of Zr and La

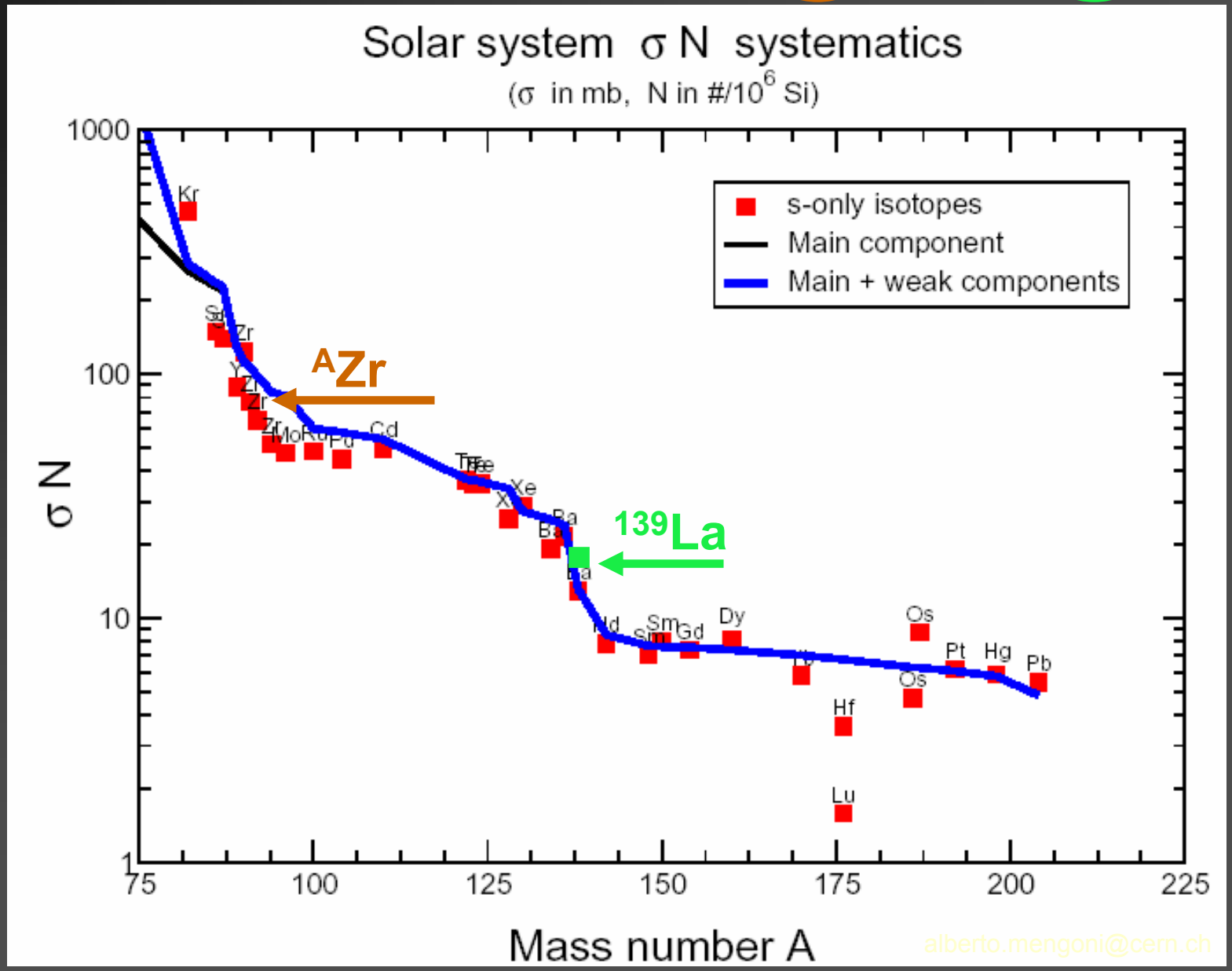

alberto.mengoni@cern.ch

n_TOF-08: $^{139}La(n,\gamma)$ measurement

Raw data: counts *vs* E_n

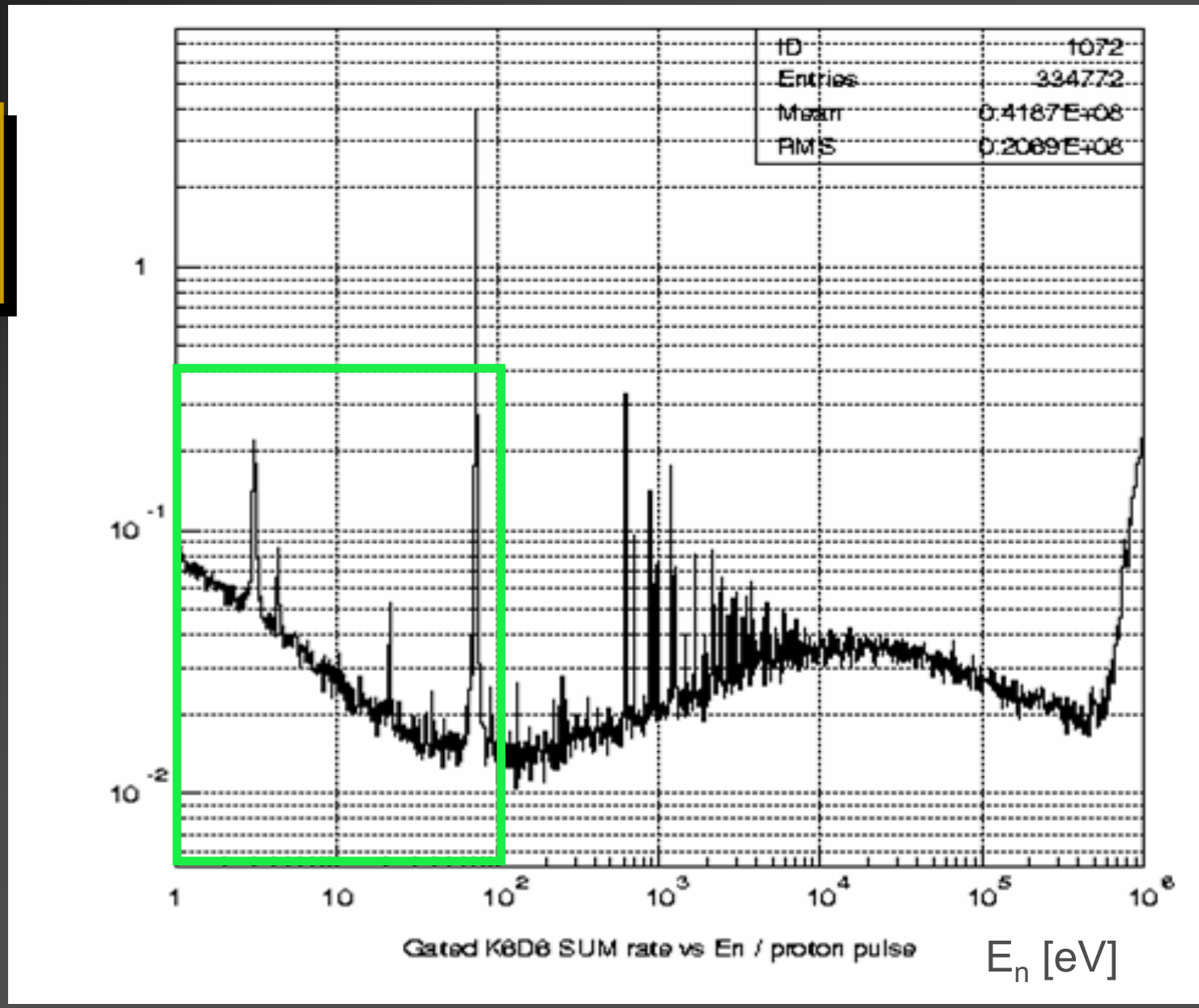

n_TOF-08: ^{139}La(n,γ) measurement

^{139}La: 99.91%
^{138}La: 0.09%

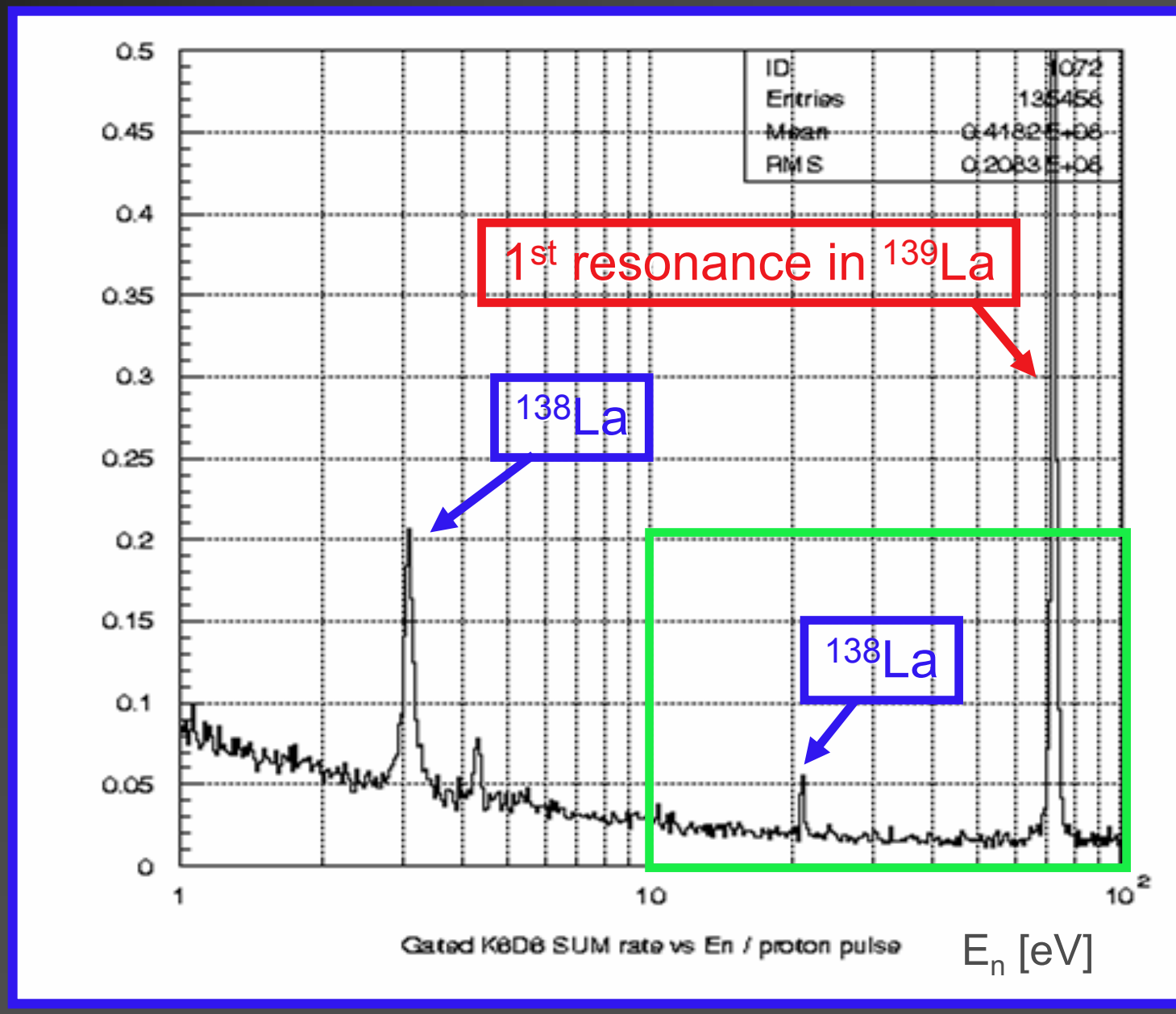

n_TOF-08: $^{139}La(n,\gamma)$ measurement

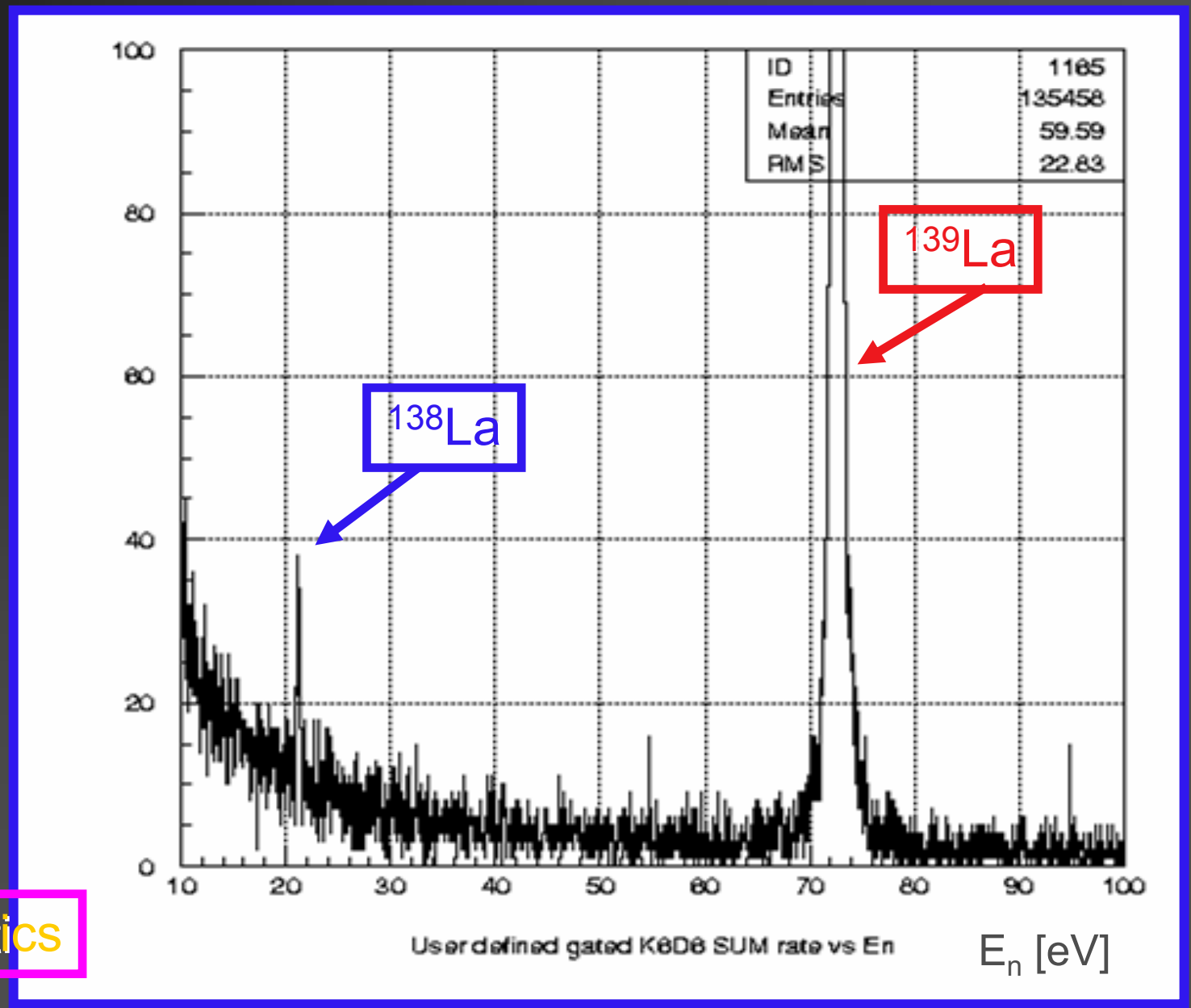

10% of statistics

n_TOF-08: $^{90,91,92,93,94,96}Zr(n,\gamma)$

- Neutron magic (^{90}Zr, N=50) or close to shell closure
- Small x-section (resonance dominated) → large abundances

- Zr is used in reactor's structural material (cladding of fuel elements)
- ^{93}Zr is one of the major long-lived fission product ($t_{1/2}$ = 1.5 Myr)

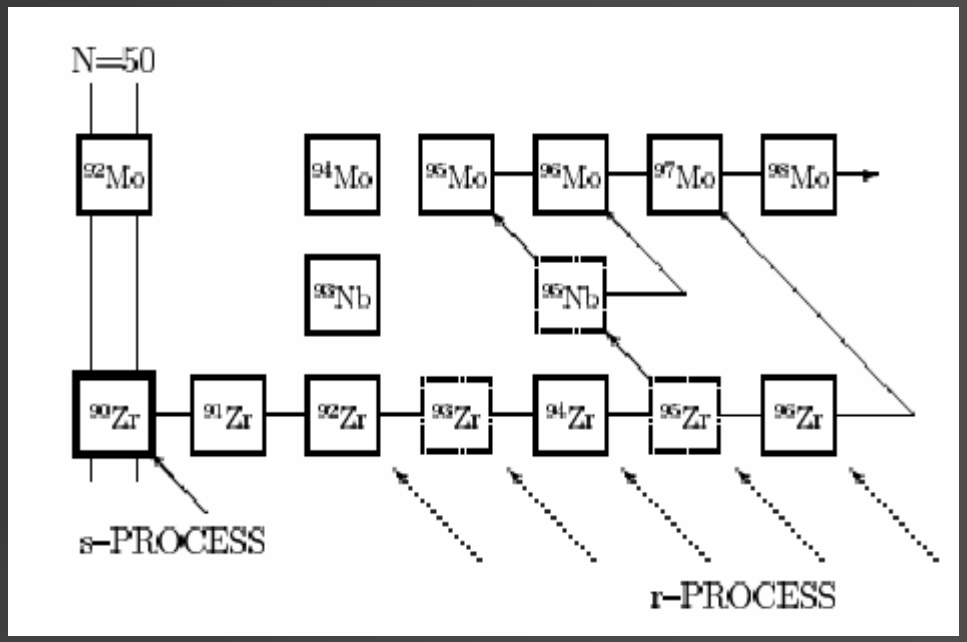

alberto.mengoni@cern.ch

n_TOF-08: $^{90}Zr(n,\gamma)$

$1\ KeV \leq E_n \leq 10\ KeV$

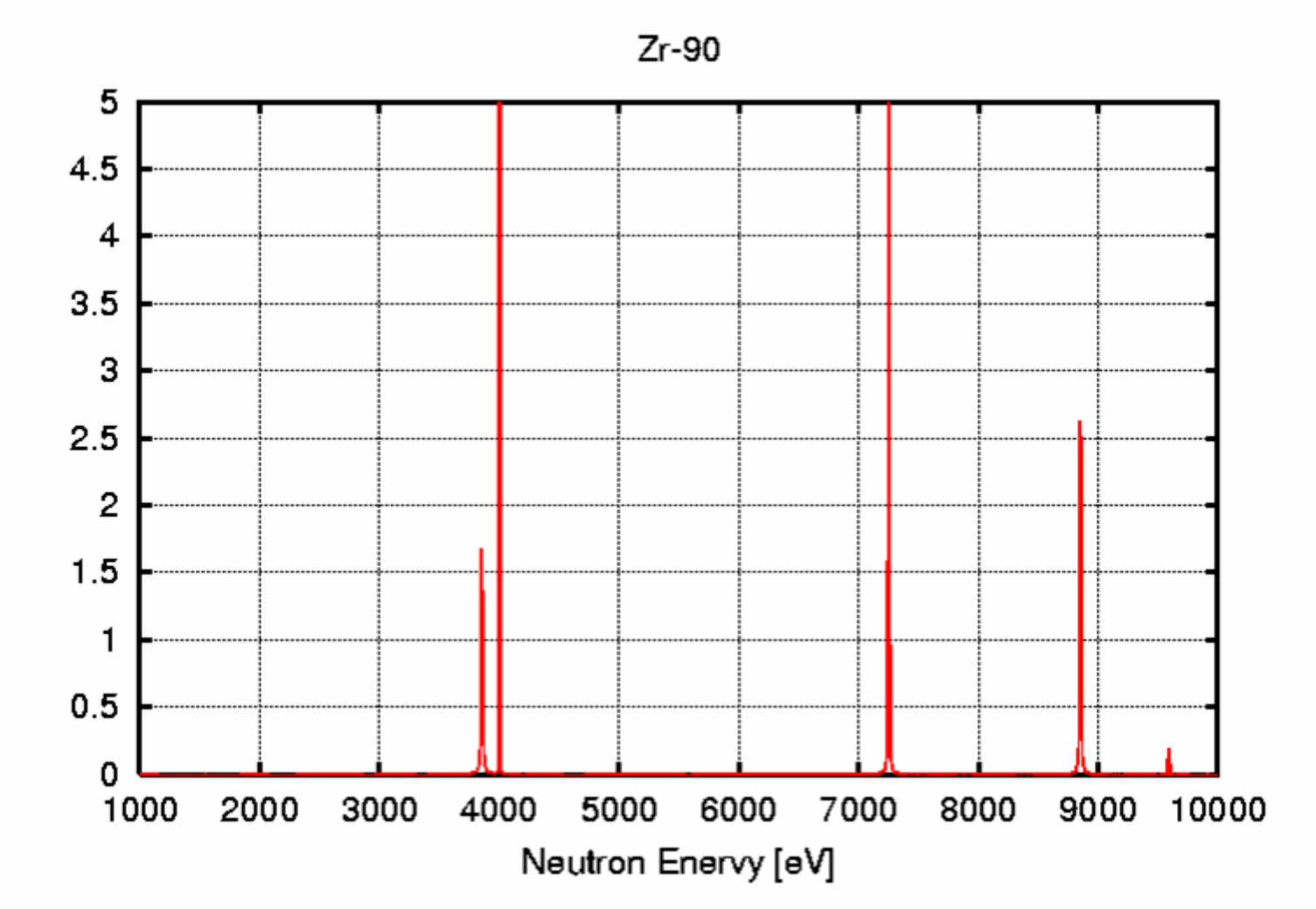

alberto.mengoni@cern.ch

n_TOF-08: $^{90}Zr(n,\gamma)$

$1\ KeV \leq E_n \leq 10\ KeV$

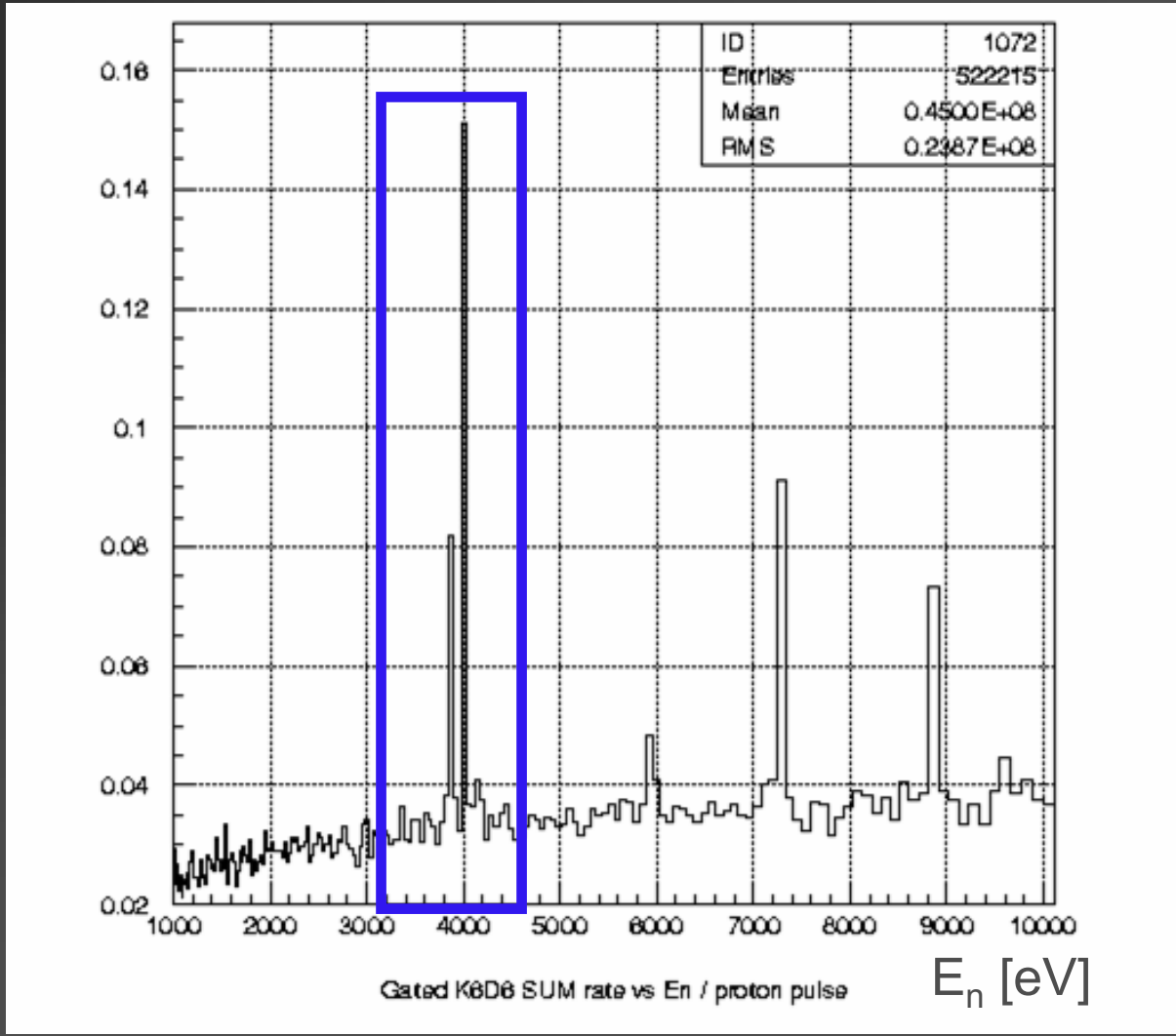

alberto.mengoni@cern.ch

n_TOF-08: $^{90}Zr(n,\gamma)$

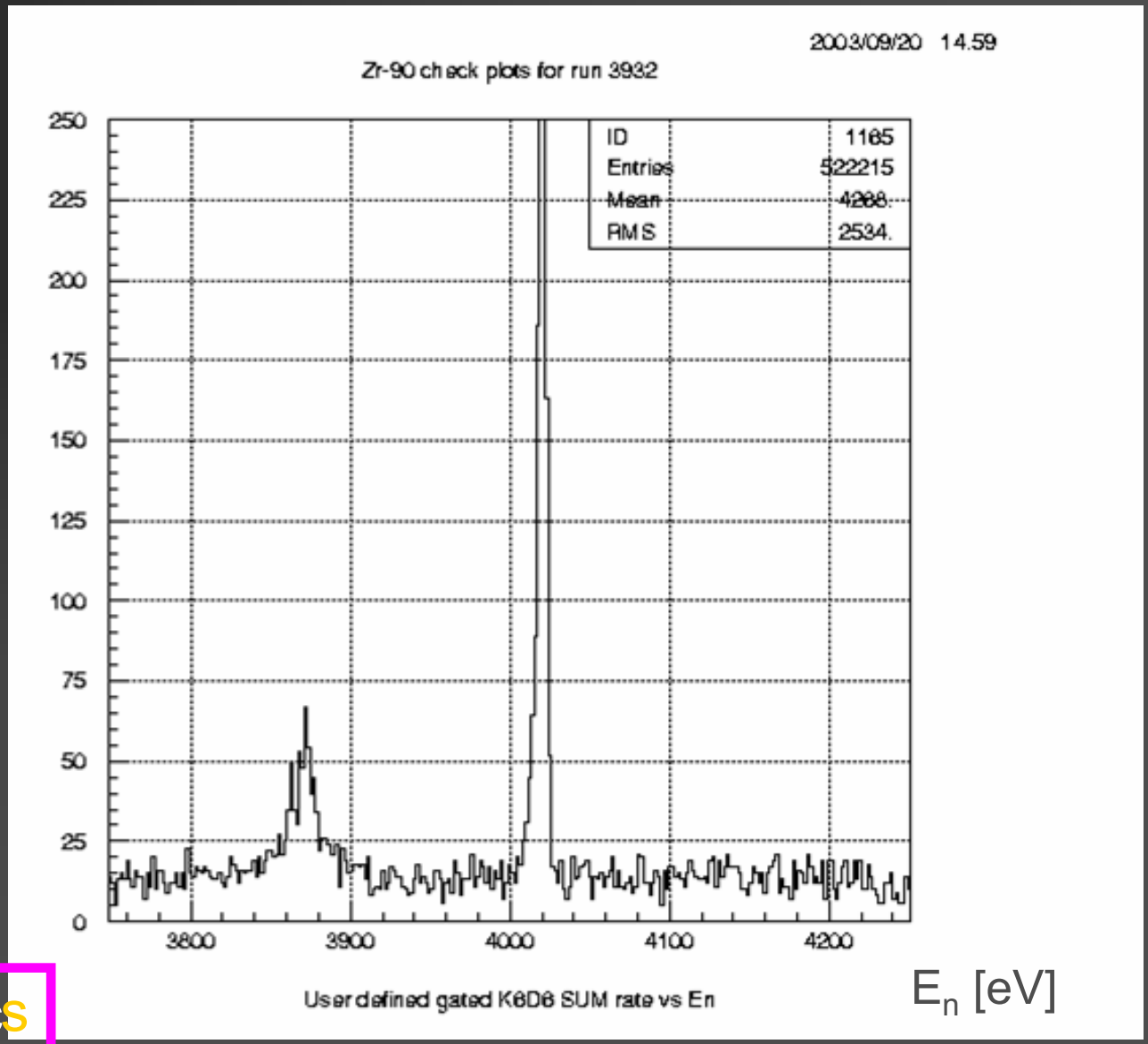

20% of statistics

n_TOF-08: $^{91}Zr(n,\gamma)$

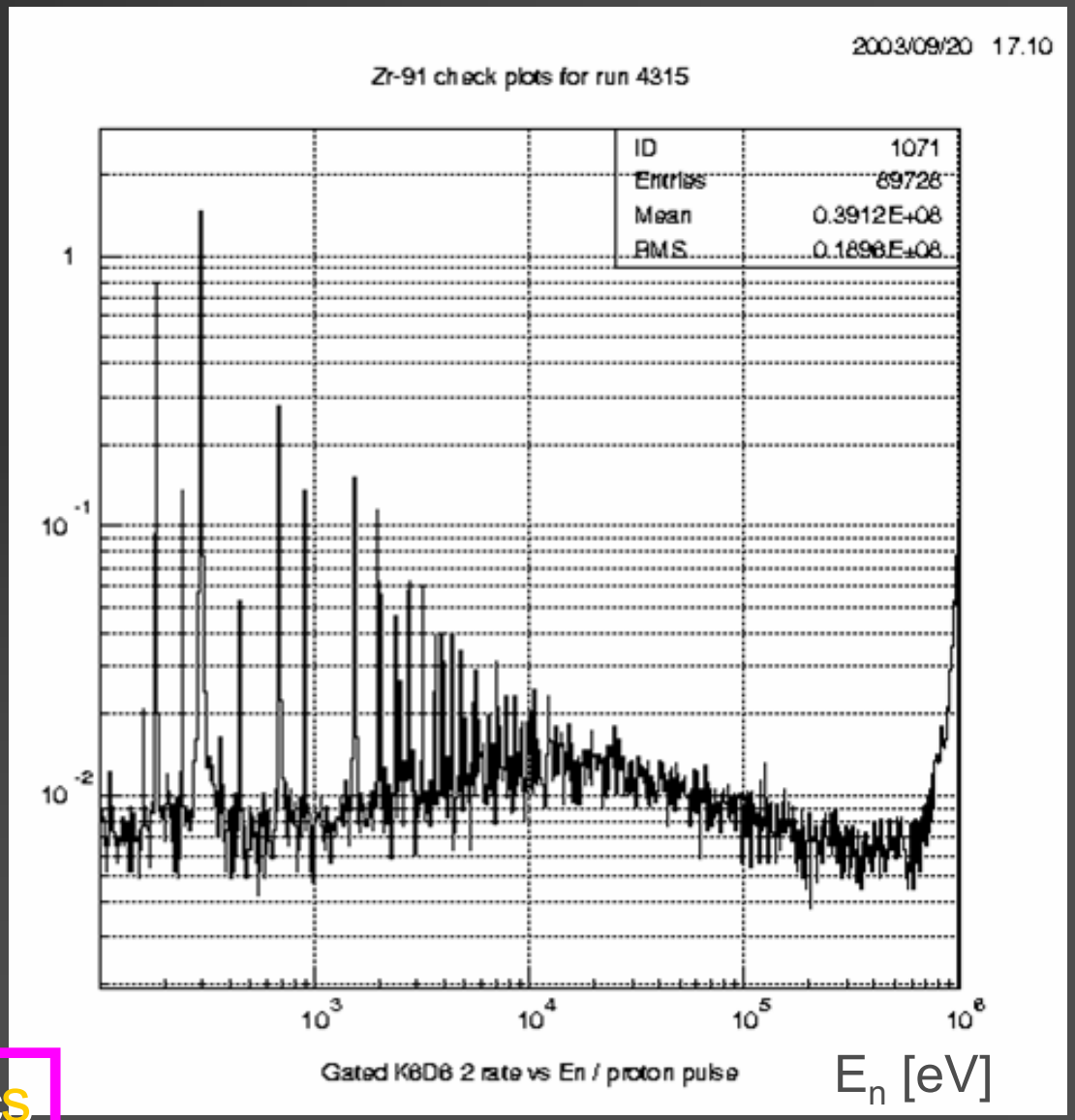

10% of statistics

alberto.mengoni@cern.ch

n_TOF-08: $^{92}Zr(n,\gamma)$

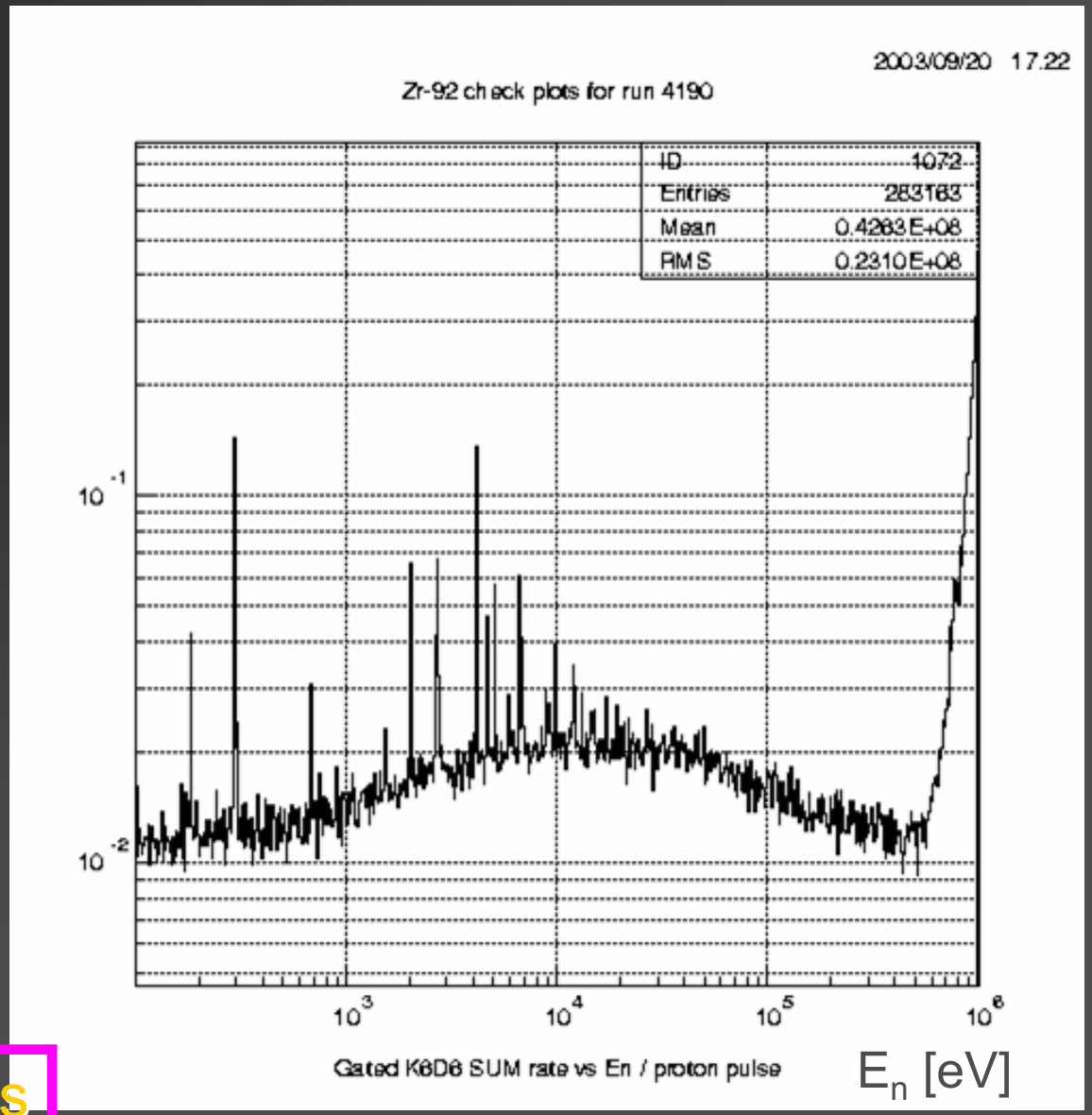

20% of statistics

alberto.mengoni@cern.ch

n_TOF-08: $^{93}Zr(n,\gamma)$

$t_{1/2}$ = 1.5 Myr
Mass = 0.66 g
Activity = 62.6 MBq
LA = 0.2 MBq

Problem:
^{241}Am (+ other MA & FP)
Mass ≈ 10 μg
Activity = 1.3 MBq
LA = 0.0002 MBq

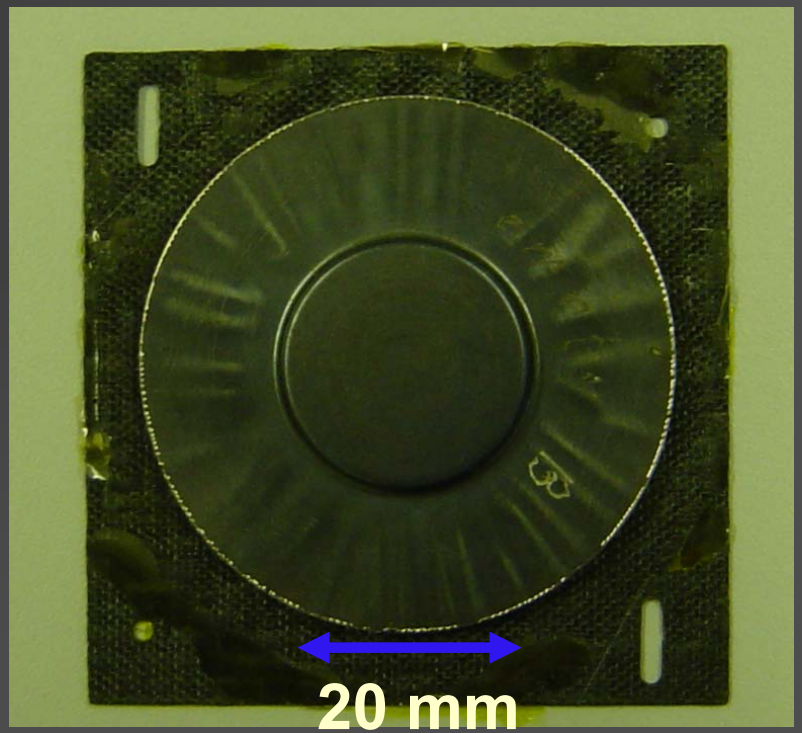

A plan for measurement in 2004 is in preparation.

alberto.mengoni@cern.ch

n_TOF-08: $^{94}Zr(n,\gamma)$

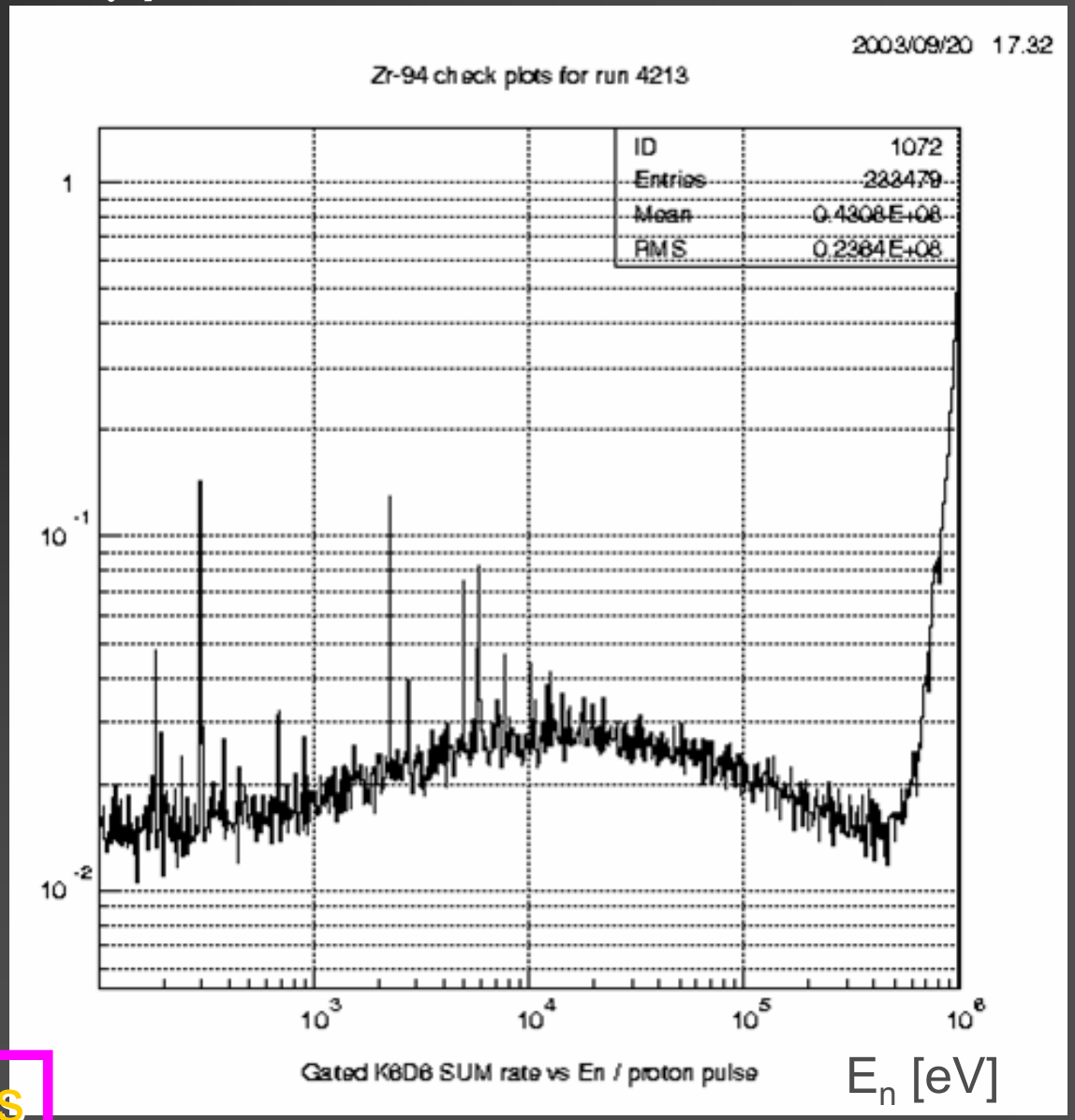

10% of statistics

alberto.mengoni@cern.ch

n_TOF-08: $^{96}Zr(n,\gamma)$

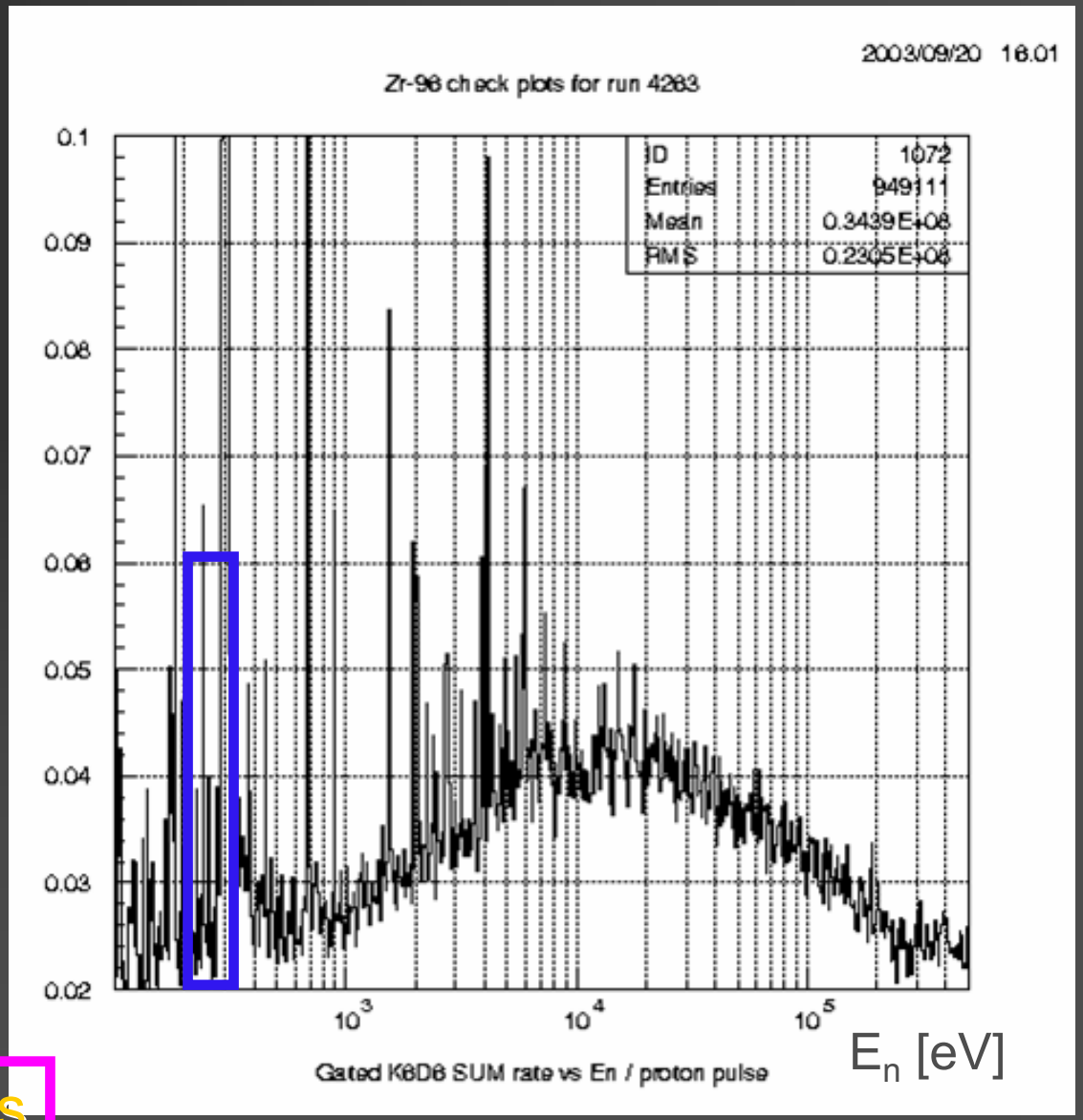

10% of statistics

alberto.mengoni@cern.ch

n_TOF-08: $^{96}Zr(n,\gamma)$

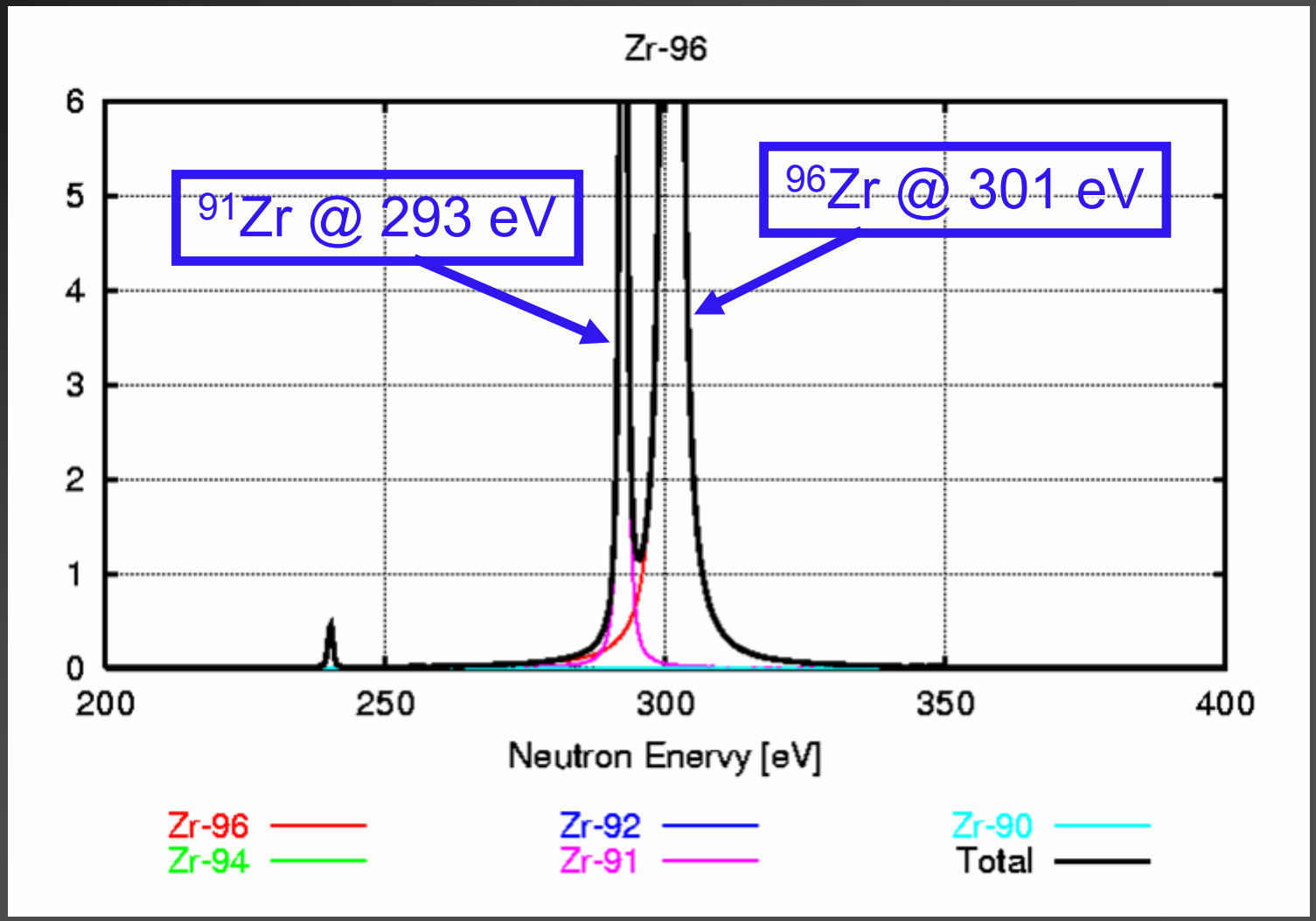

alberto.mengoni@cern.ch

n_TOF-08: $^{96}Zr(n,\gamma)$

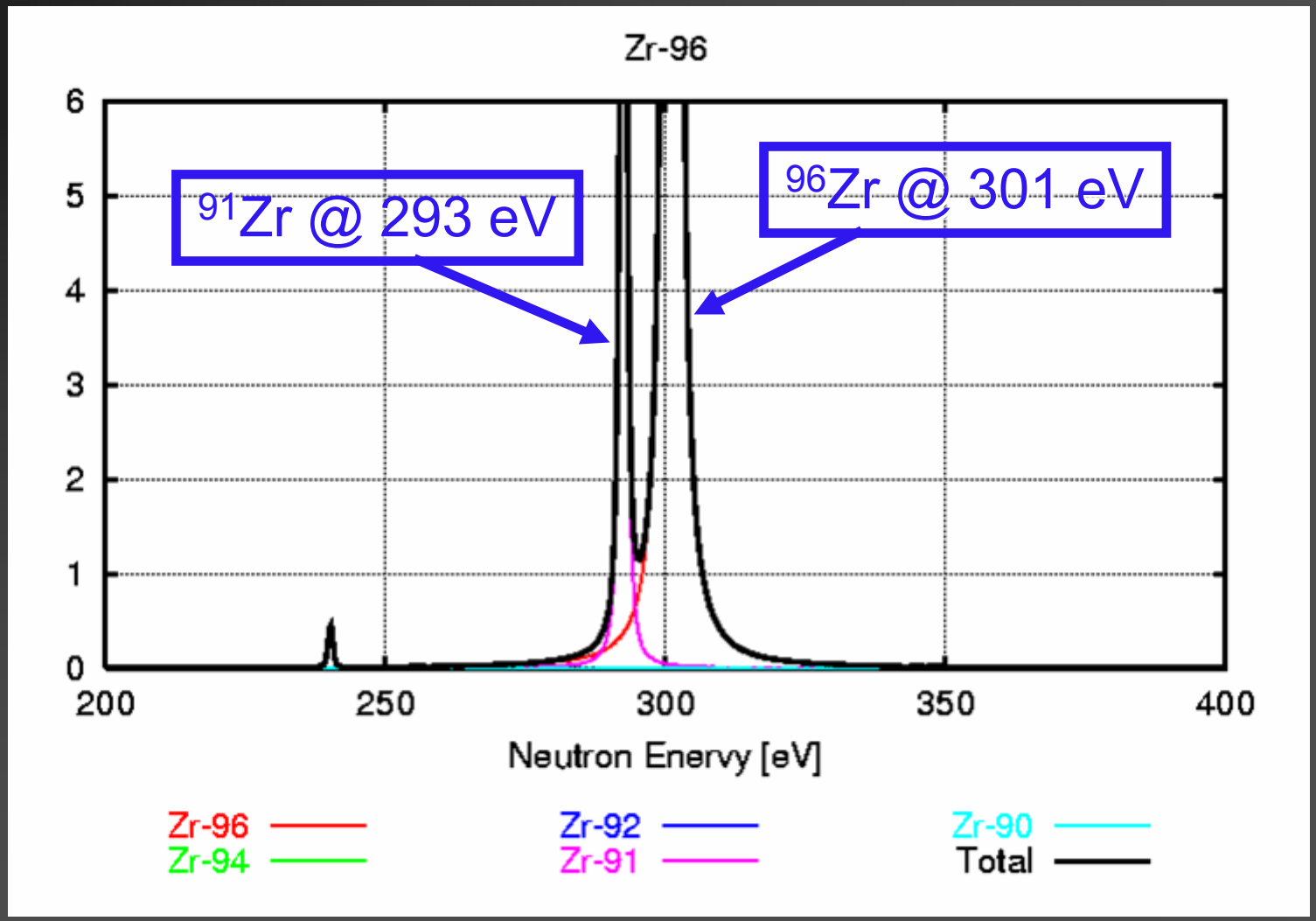

alberto.mengoni@cern.ch

n_TOF-08: $^{96}Zr(n,\gamma)$

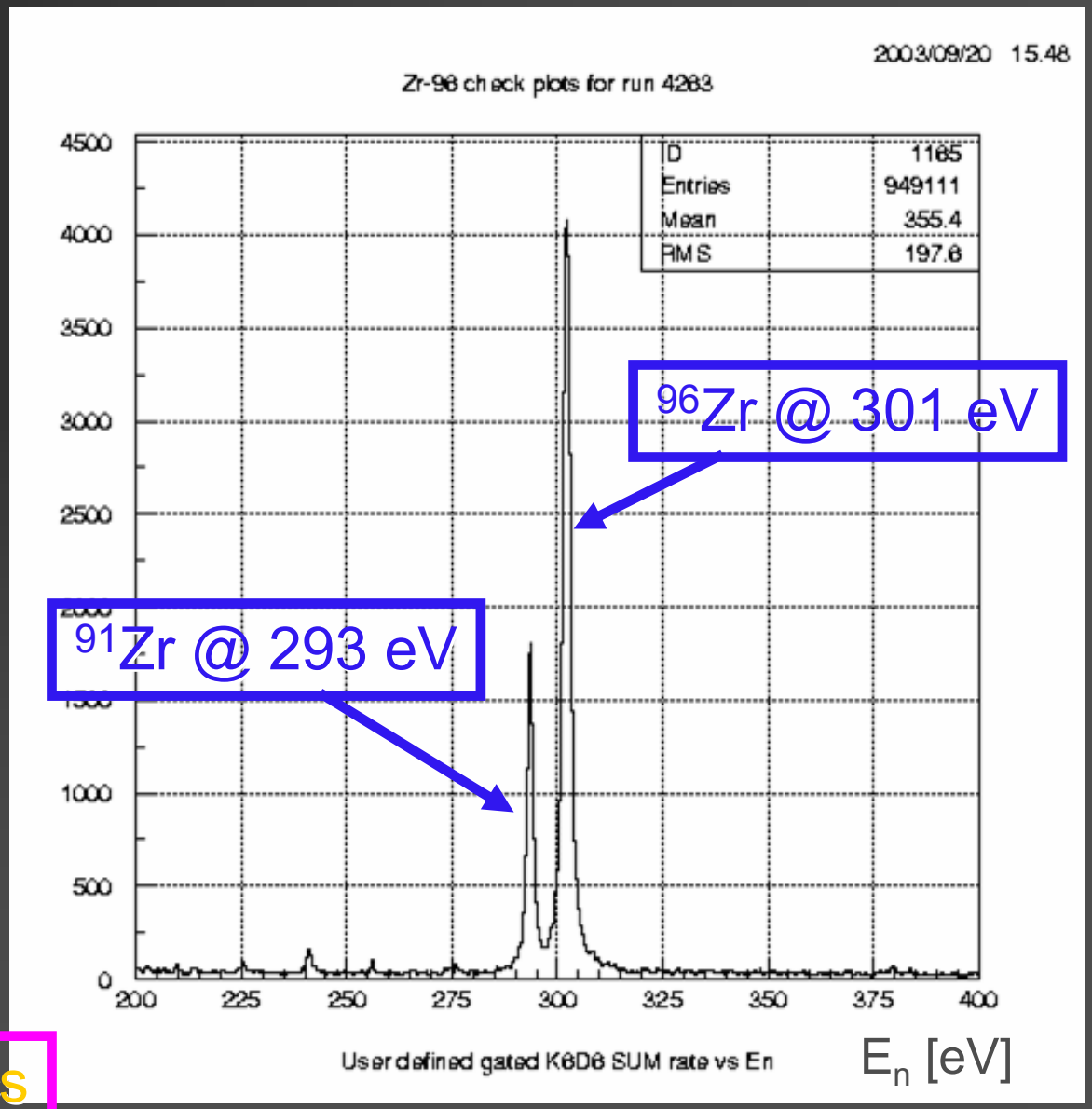

10% of statistics

alberto.mengoni@cern.ch

n_TOF-03: $^{24,25,26}Mg(n,\gamma)$

I. Abbundance ratios in presolar grains
II. Importance of the $^{22}Ne(\alpha,n)^{25}Mg$ as neutron source for the s-process

- Light nuclei: small cross sections
- Resonance dominated
- Capture/Scattering < 10^{-3}

alberto.mengoni@cern.ch

n_TOF-03: $^{nat}Mg(n,\gamma)$

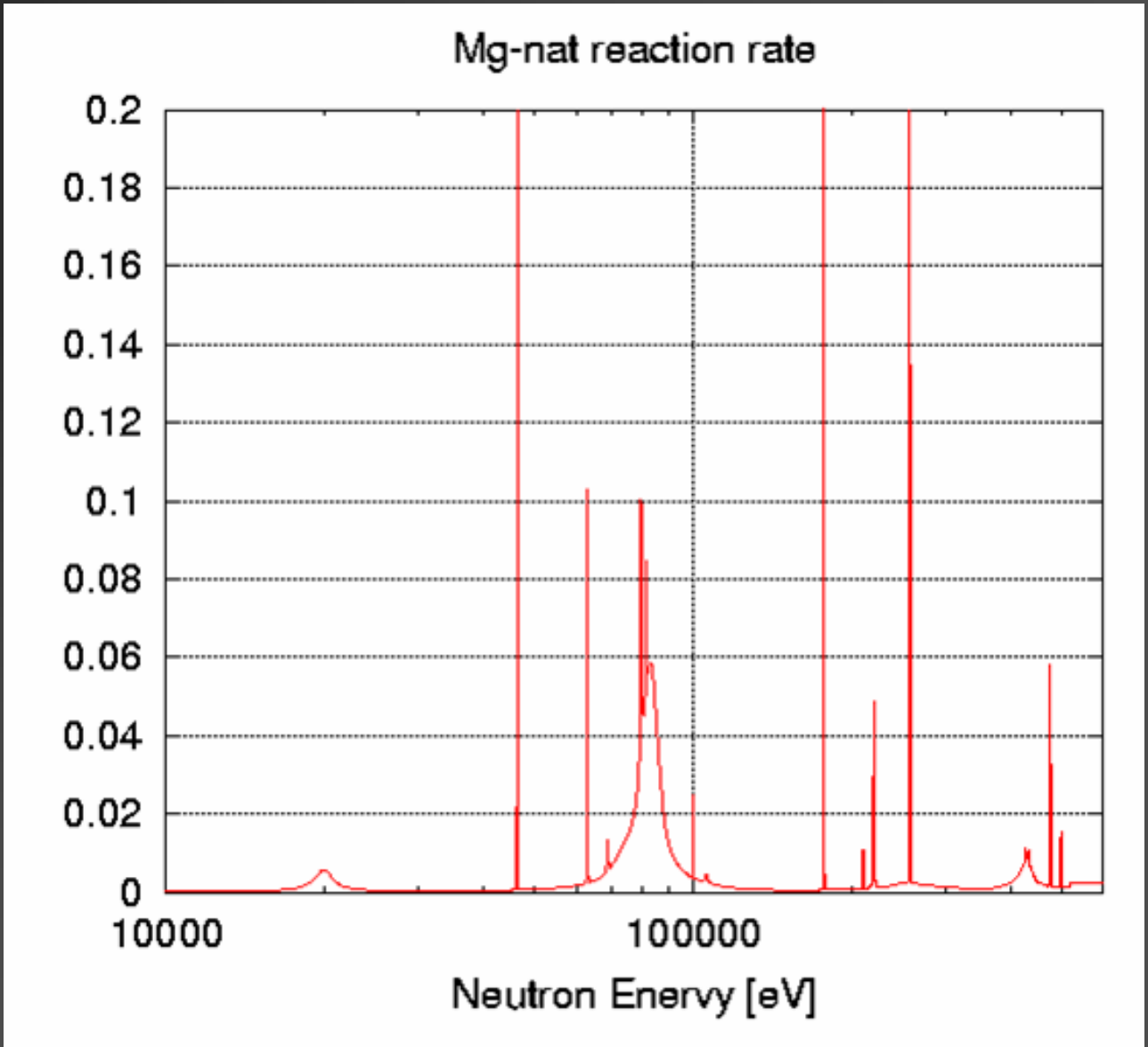

alberto.mengoni@cern.ch

n_TOF-03: $^{nat}Mg(n,\gamma)$

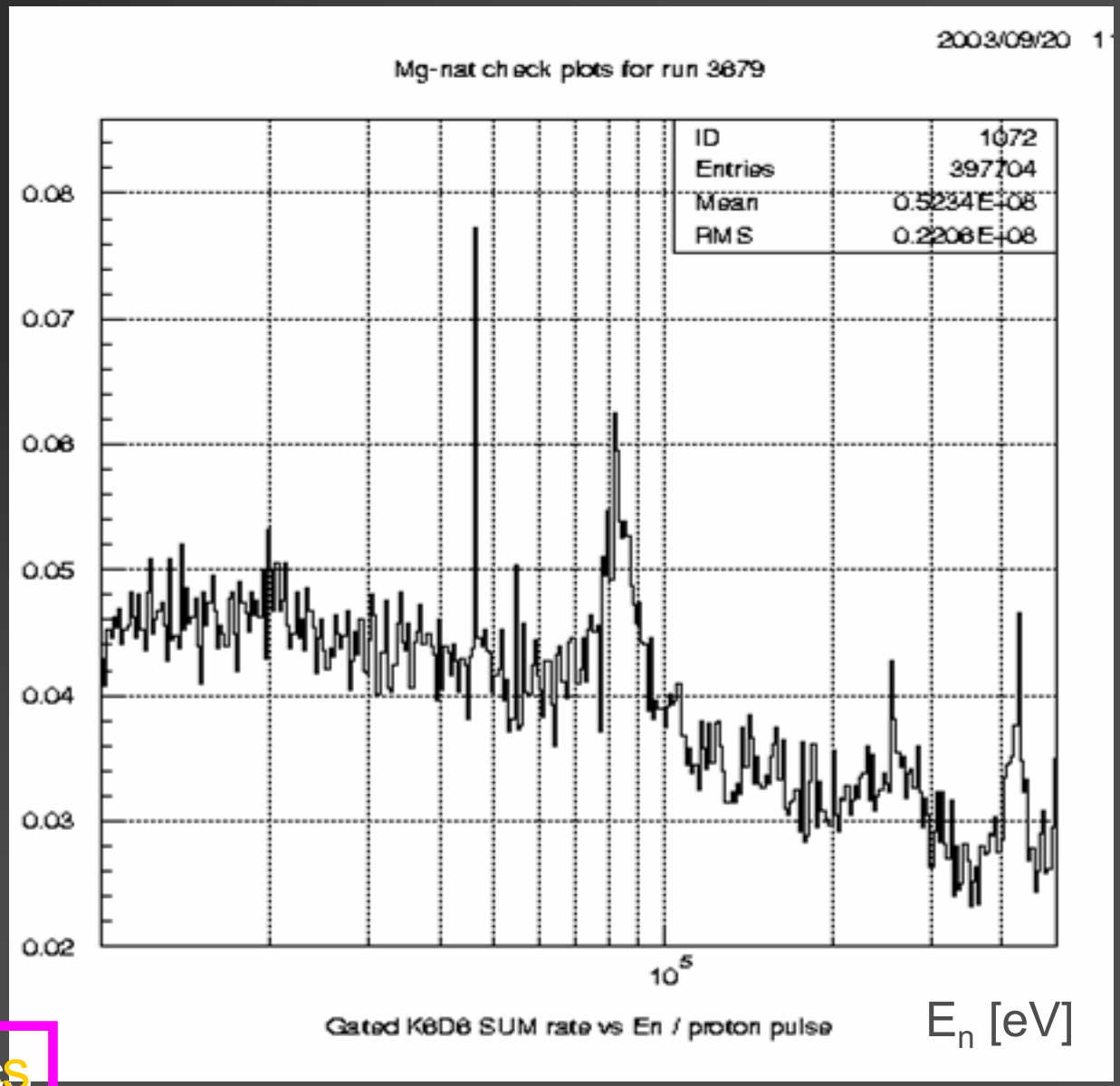

10% of statistics

alberto.mengoni@cern.ch

n_TOF-03: $^{25}Mg(n,\gamma)$

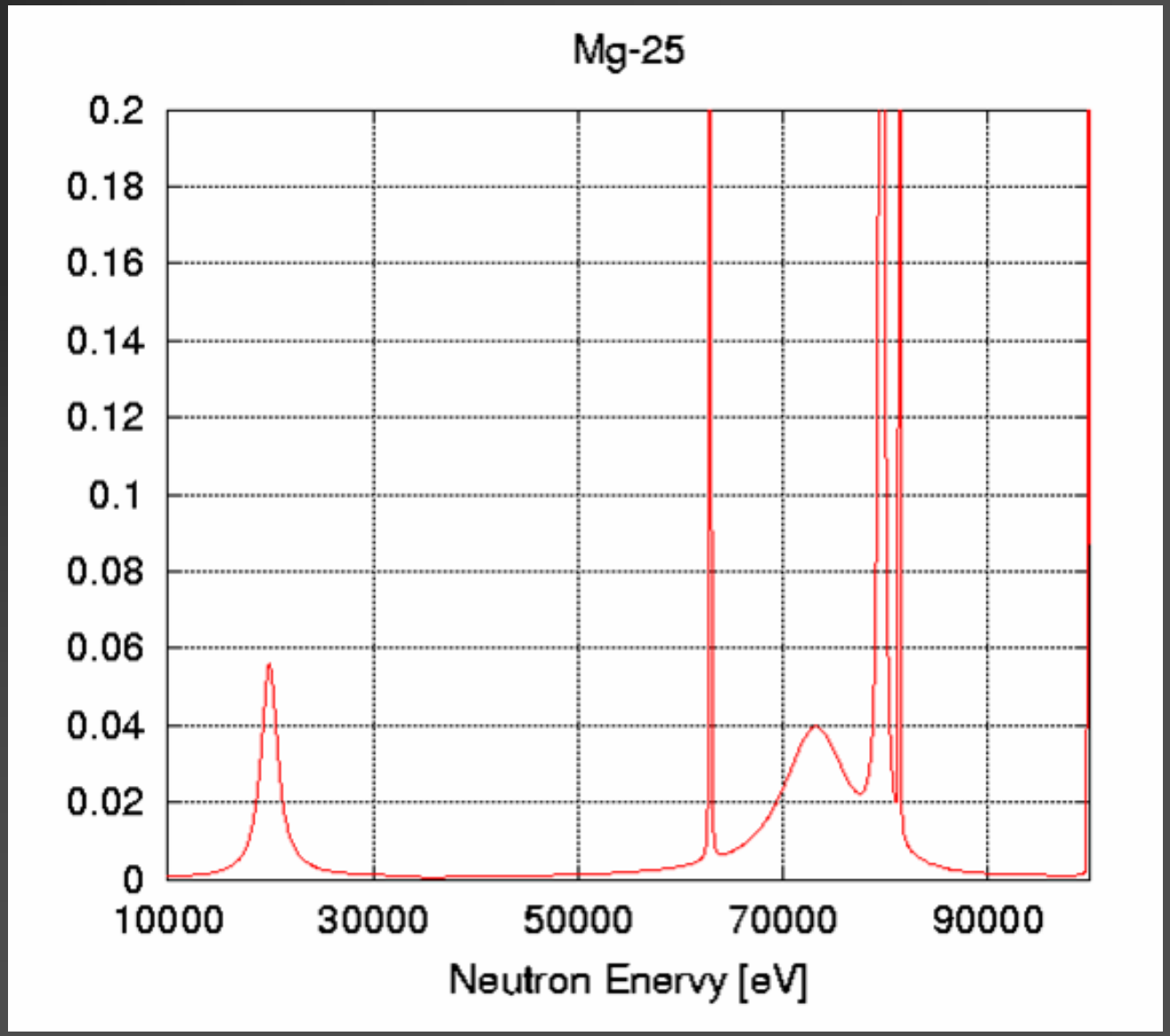

alberto.mengoni@cern.ch

n_TOF-03: $^{25}Mg(n,\gamma)$

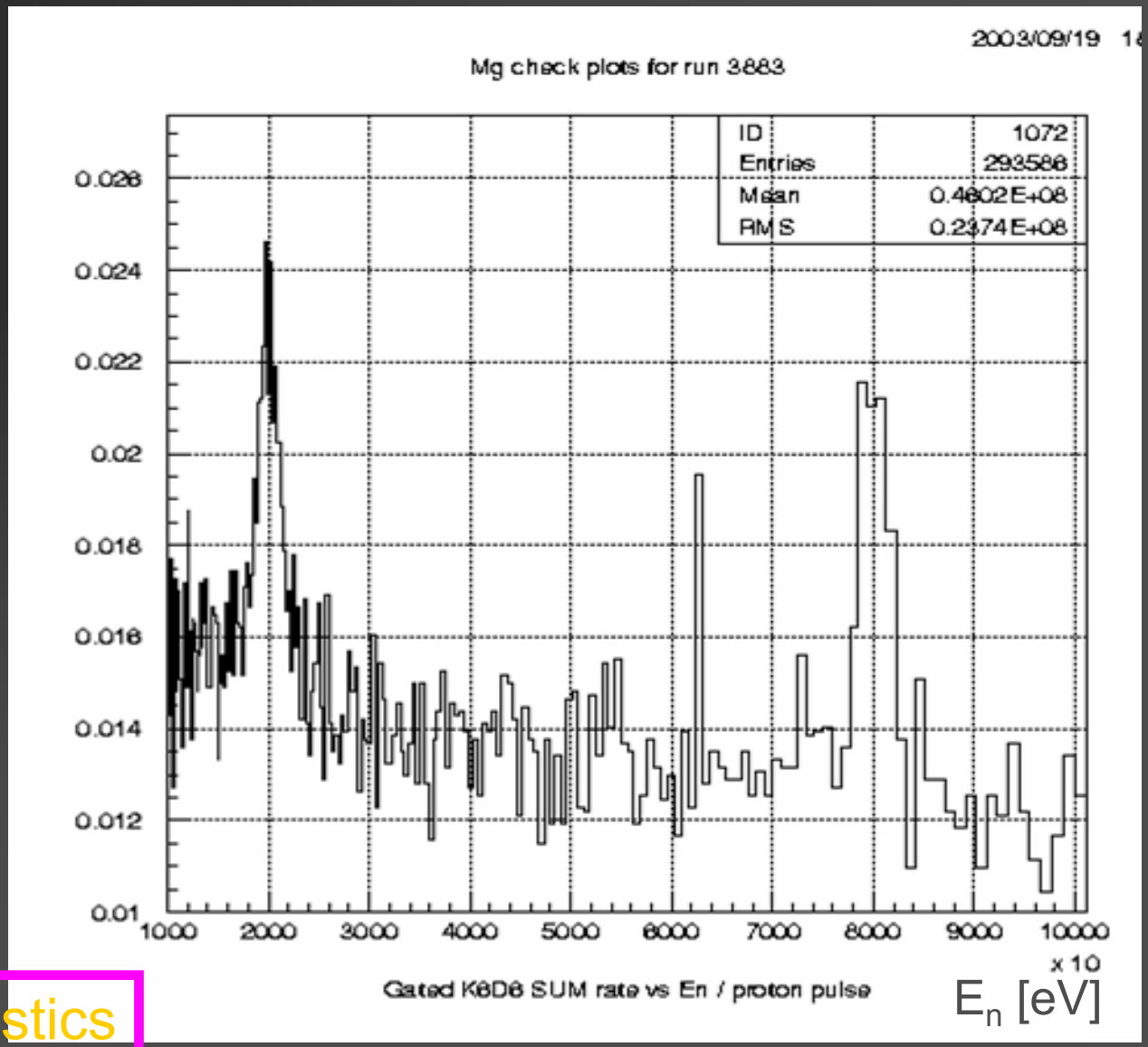

20% of statistics

alberto.mengoni@cern.ch

n_TOF-03: $^{26}Mg(n,\gamma)$

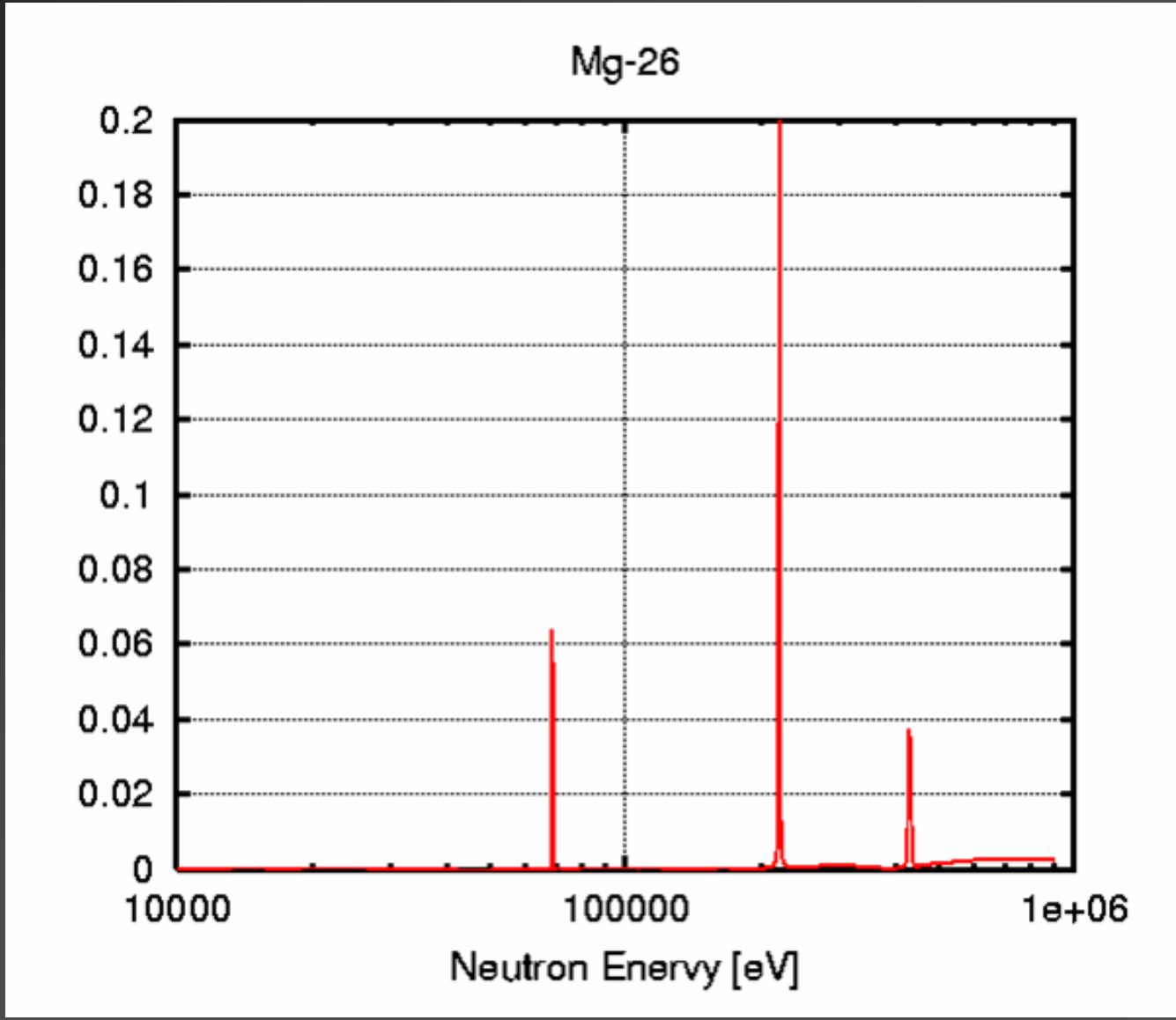

alberto.mengoni@cern.ch

n_TOF-03: $^{26}Mg(n,\gamma)$

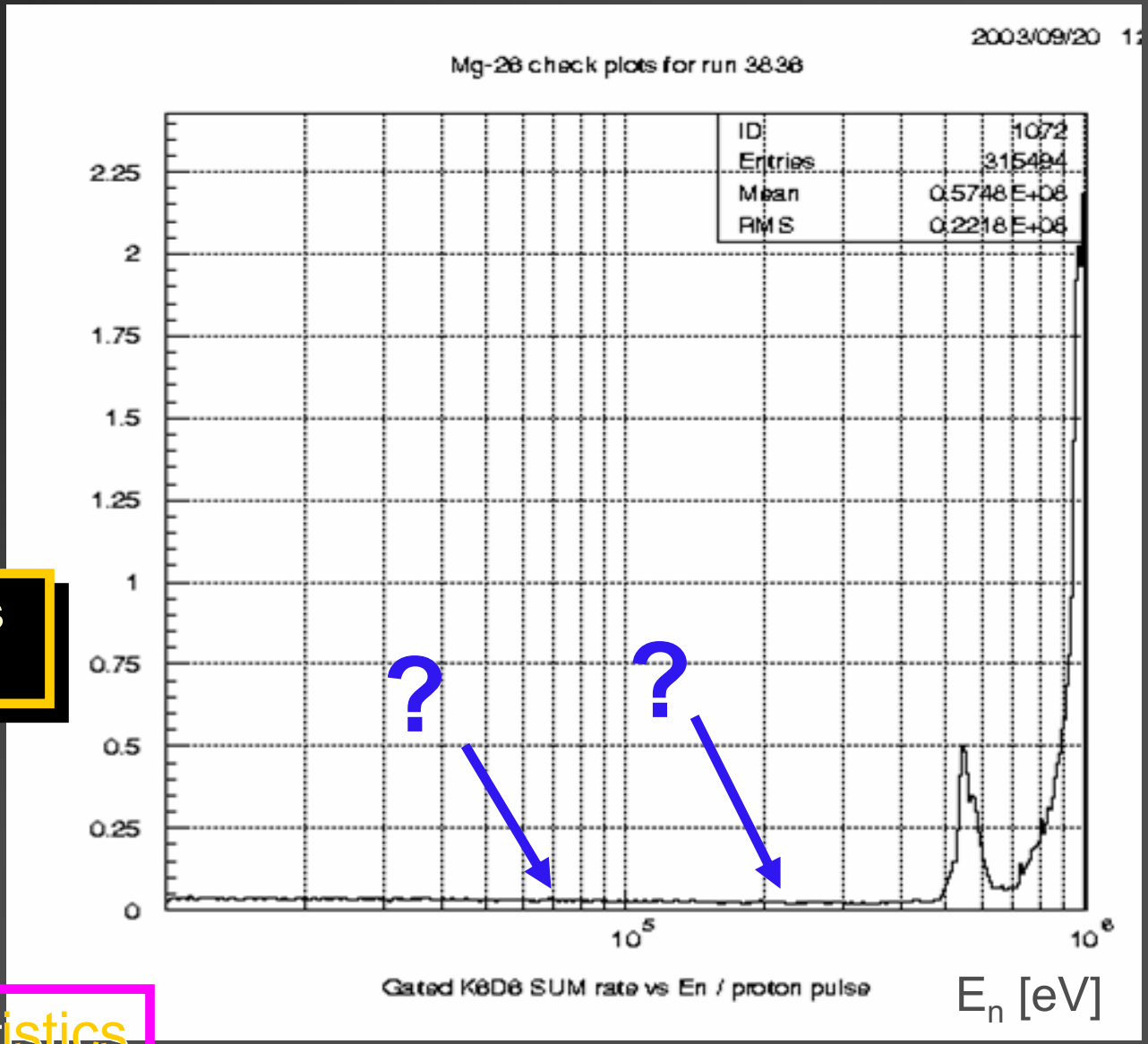

Where are the two resonances at 68 and 220 KeV ?

20% of statistics

alberto.mengoni@cern.ch

n_TOF-04: Re/Os clock

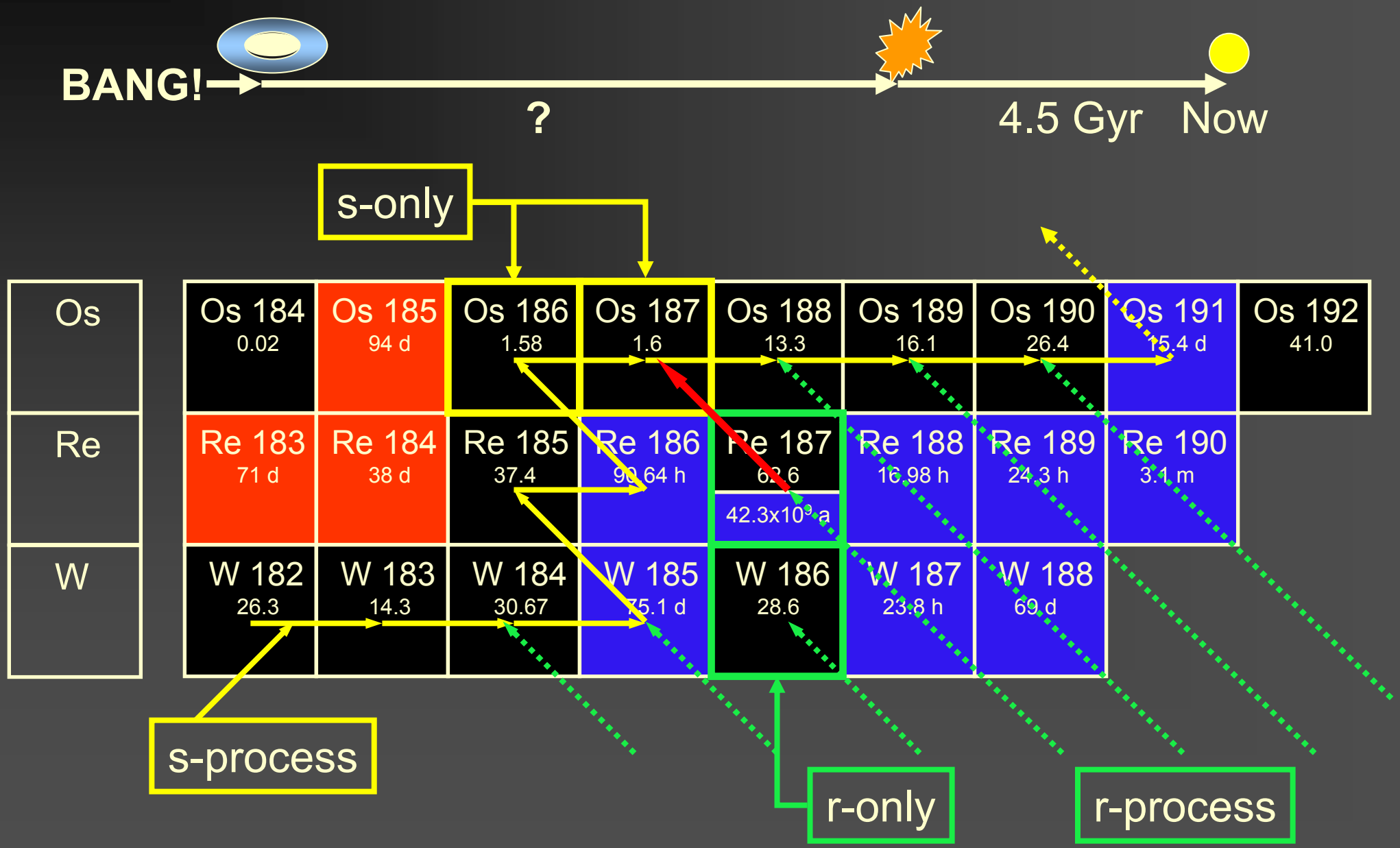

Nuclear & Astro issues

In addition to the particular conditions which allows to use the Re/Os abundance pair as a clock there are a number of complications:

- The β-decay half-life of ^{187}Re is strongly dependent on temperature
- The stellar neutron capture cross section of ^{187}Os is influenced by the population of low-lying excited levels (the 1st excited states is at 9.8 keV)
- Branching(s) at ^{185}W and/or at ^{186}Re

- The chemical evolution of the galaxy influences the history of the nucleosynthesis
- Re and Os abundances uncertainties

alberto.mengoni@cern.ch

Issue 1: $^{187}Re(\beta^-)$ decay

The β-decay half-life of ^{187}Re is τ_β = 43.2 ± 1.3 Gyr.
Under stellar conditions, the ^{187}Os and ^{187}Re atoms can be partly or fully ionized.
The β-decay rate can then proceed through a transition to bound-electronic states in ^{187}Os.
The rate for this process can be orders of magnitude faster than the neutral-atom decay.
The bound-state β-decay half-life of fully-ionized ^{187}Re has been measured @ GSI.

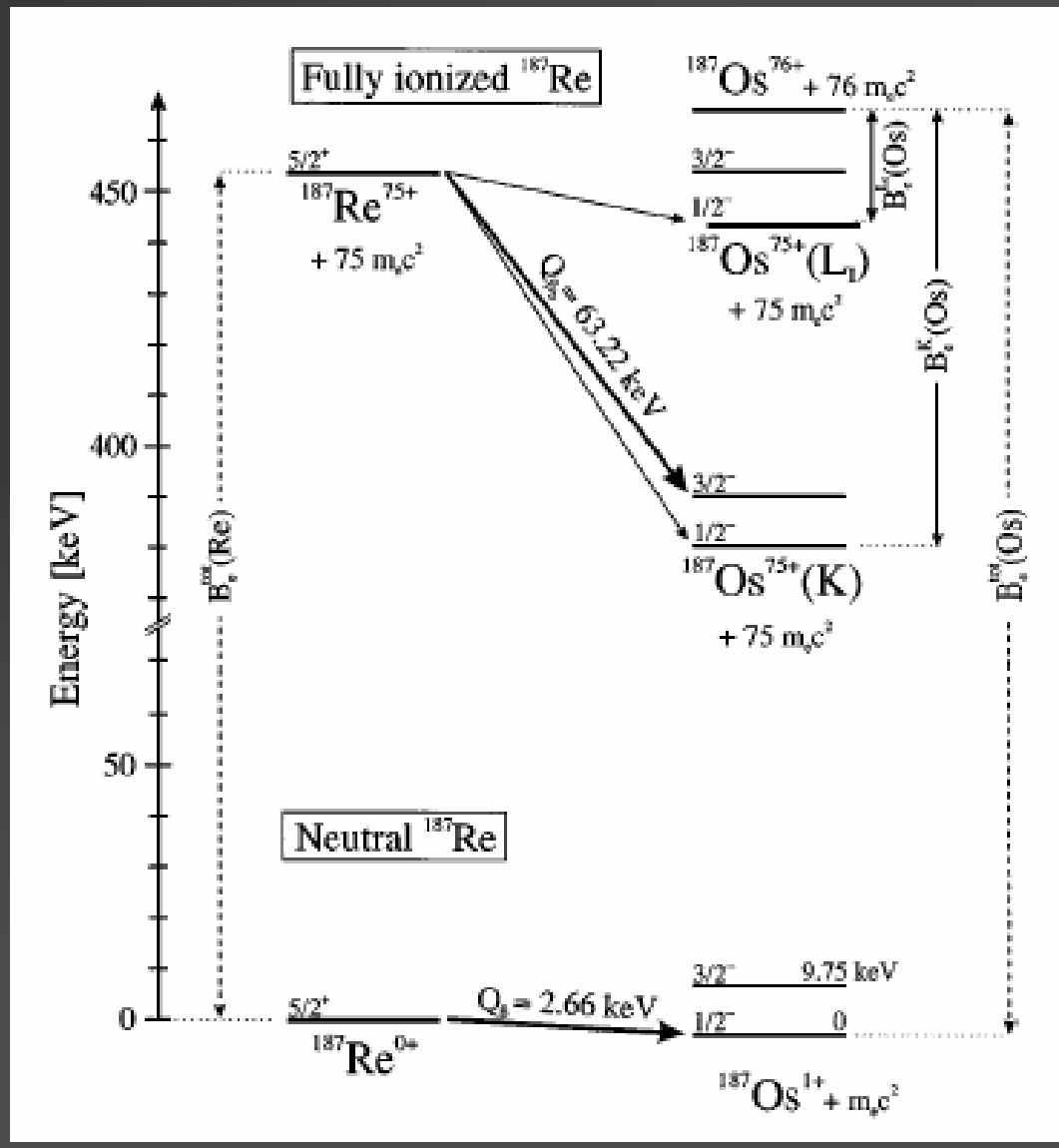

The half-life of fully-ionized ^{187}Re turns out to be: τ_β = 32.9 ± 2.0 yr.

(F. Bosch, *et al.*, PRL **77** (1996) 5190)

Impact on the age: ≈ 1 Gyr

Issue 2: stellar $^{187}Os(n,\gamma)$ rate

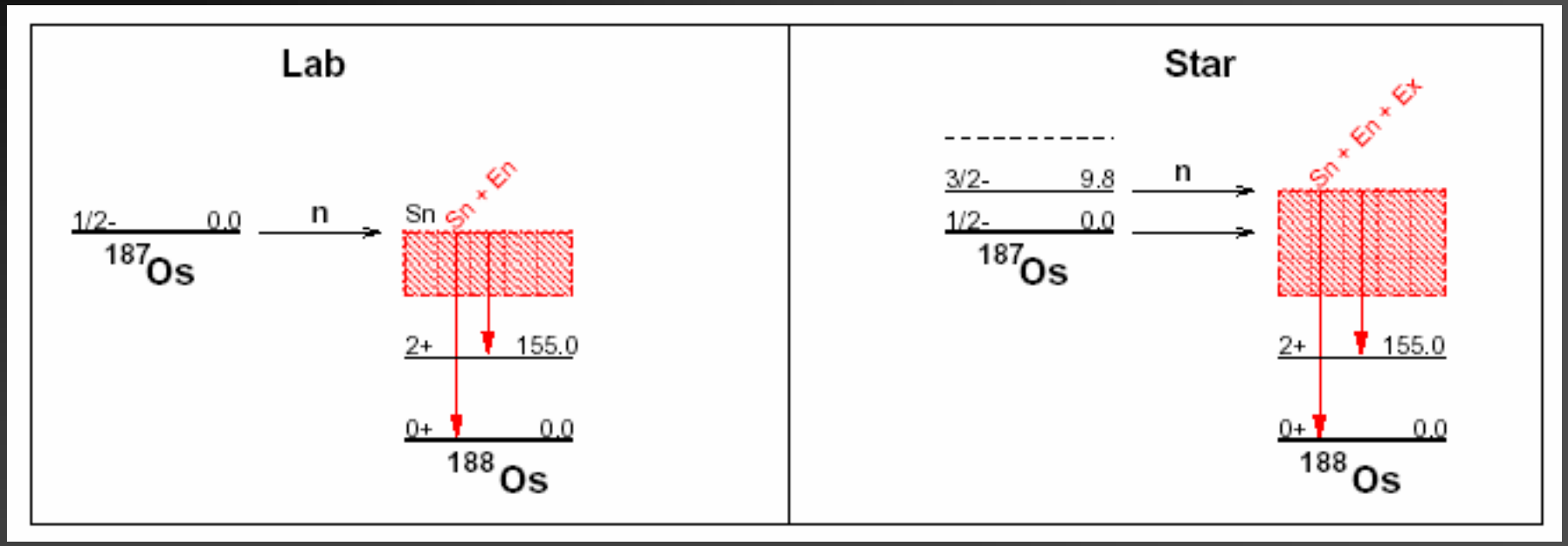

alberto.mengoni@cern.ch

Thermal population

$$P(E_k) = \frac{(2J_k + 1)e^{-E_k/kT}}{\sum_m (2J_m + 1)e^{-E_m/kT}}$$

For example, in ^{187}Os at kT = 30 keV it is:

P(gs) = 33%
P(1st) = 47%
P(all others) = 20%

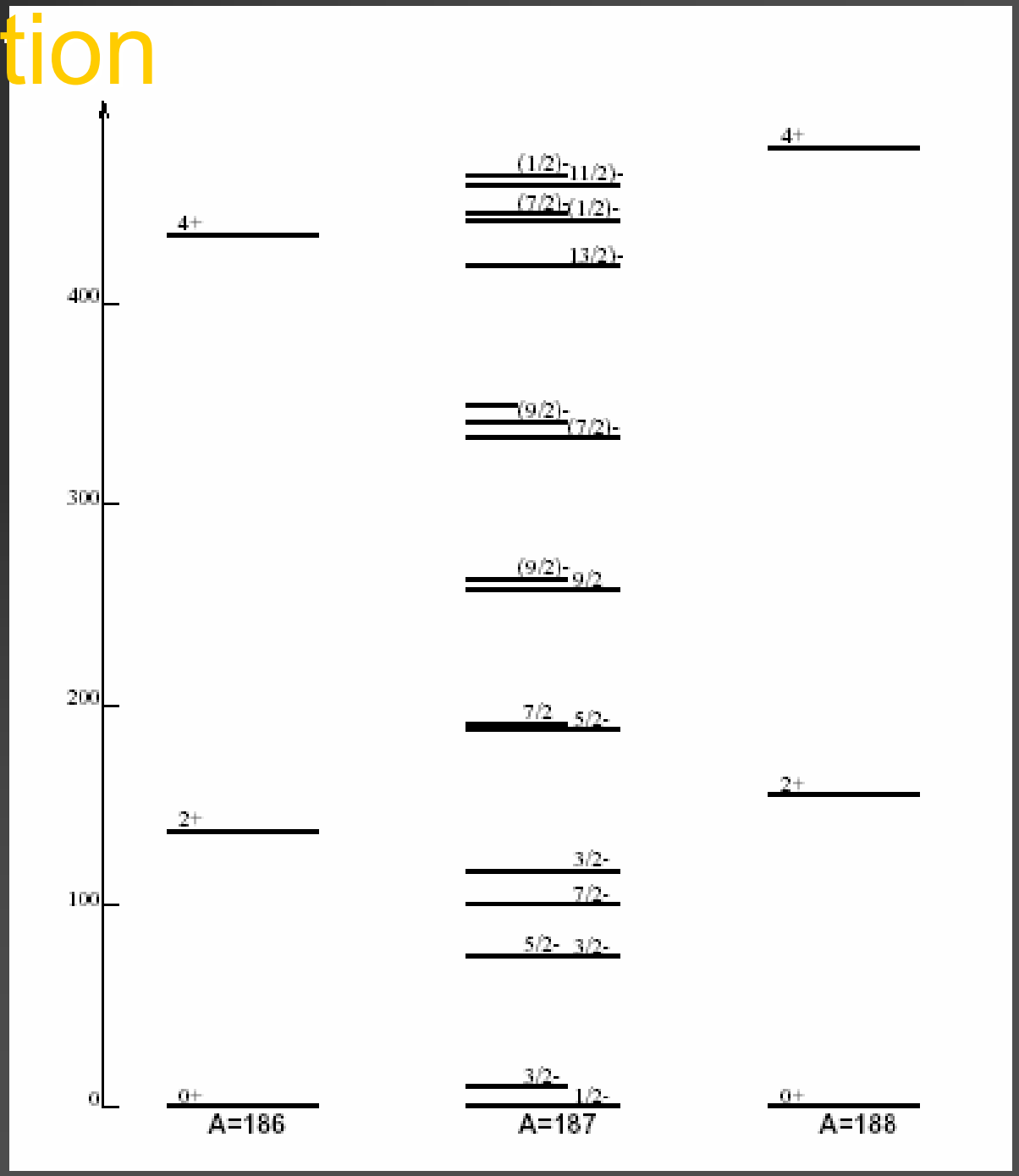

Issue 2: stellar $^{187}Os(n,\gamma)$ rate

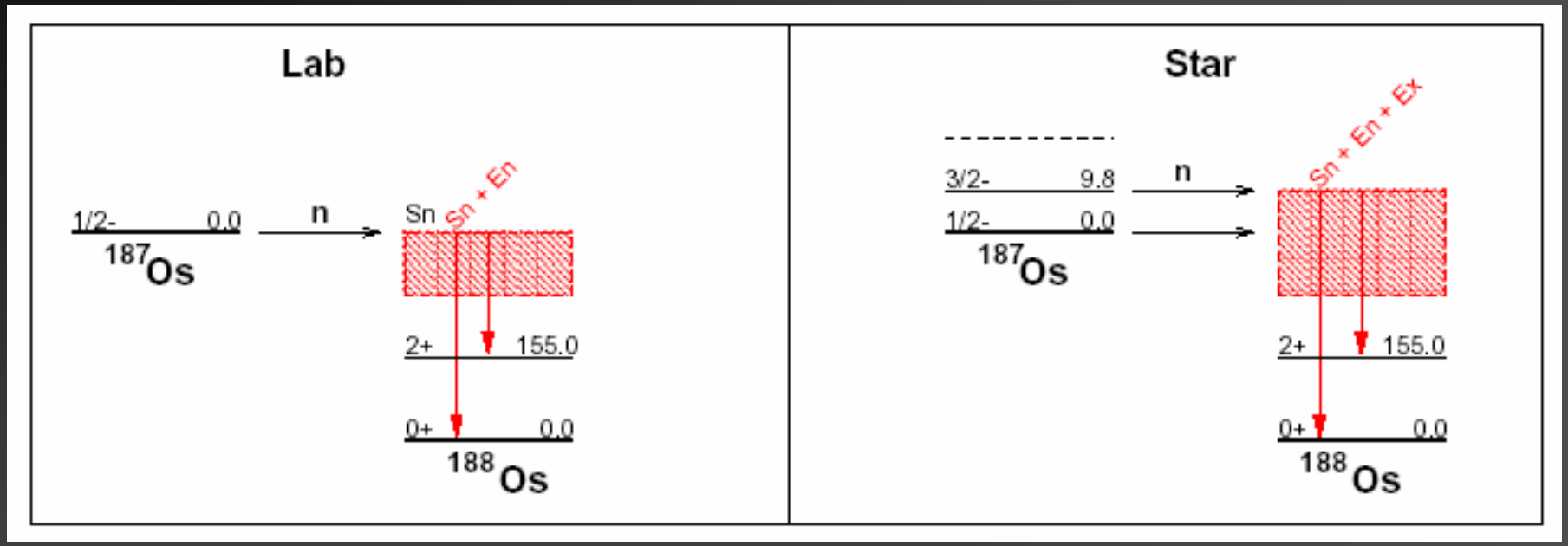

Calculation of the stellar correction factor $F_\sigma \equiv f_{186}/f_{187}$

Thermal energy KeV	$\langle\sigma(187)\rangle_{\rm Lab}$ mb	$\langle\sigma(187)\rangle_{\rm calc}$ mb	$\langle\sigma(187)\rangle_*$ mb	f_{187}	F_σ
10	1988 ± 100	2111	2324	1.10	0.91
20	1171 ± 39	1193	1402	1.18	0.85
30	874 ± 28	876	1059	1.21	0.86
40	715 ± 22	712	877	1.23	0.89
50	614 ± 12	610	766	1.26	0.93
100	—	395	571	1.45	1.03

alberto.mengoni@cern.ch

The ^{186}Os(n,γ) cross section: theory

Hauser-Feschbach theory:
(statistical model)

$$\sigma_{n,\gamma}(E_n) = \frac{\pi}{k_n^2} \sum_{J\pi} g_J \frac{\sum_{ls} T_{n,ls} T_{\gamma,J}}{\sum_{ls} T_{n,ls} + \sum_{ls} T_{n',ls} + T_{\gamma,J}} W_{\gamma,J}$$

- Neutron transmission coefficients, T_n : from OMP calculations

- γ-ray transmission coefficients, T_γ : from GDR (experimental parameters)

- Nuclear level densities: fixed at the neutron binding from $\langle D \rangle_{exp}$

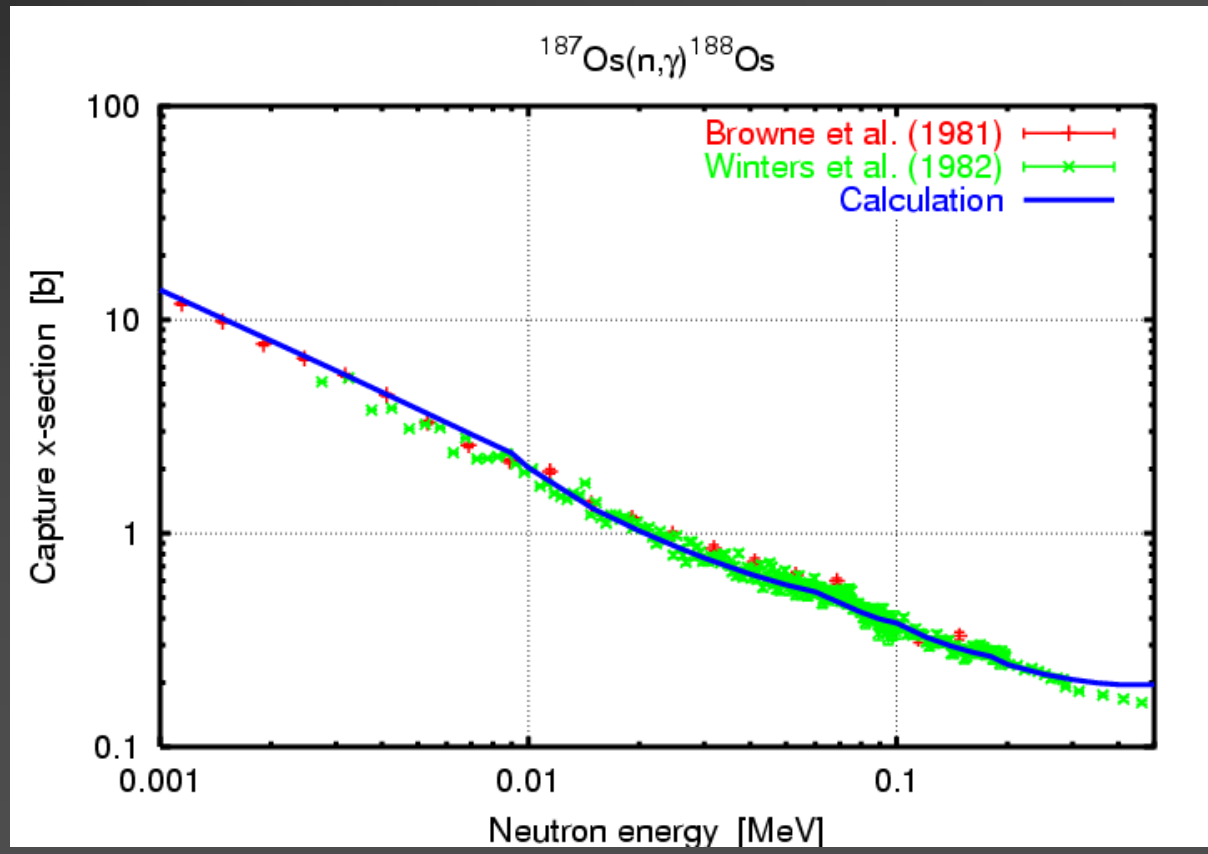

Issue 2: theory still needed

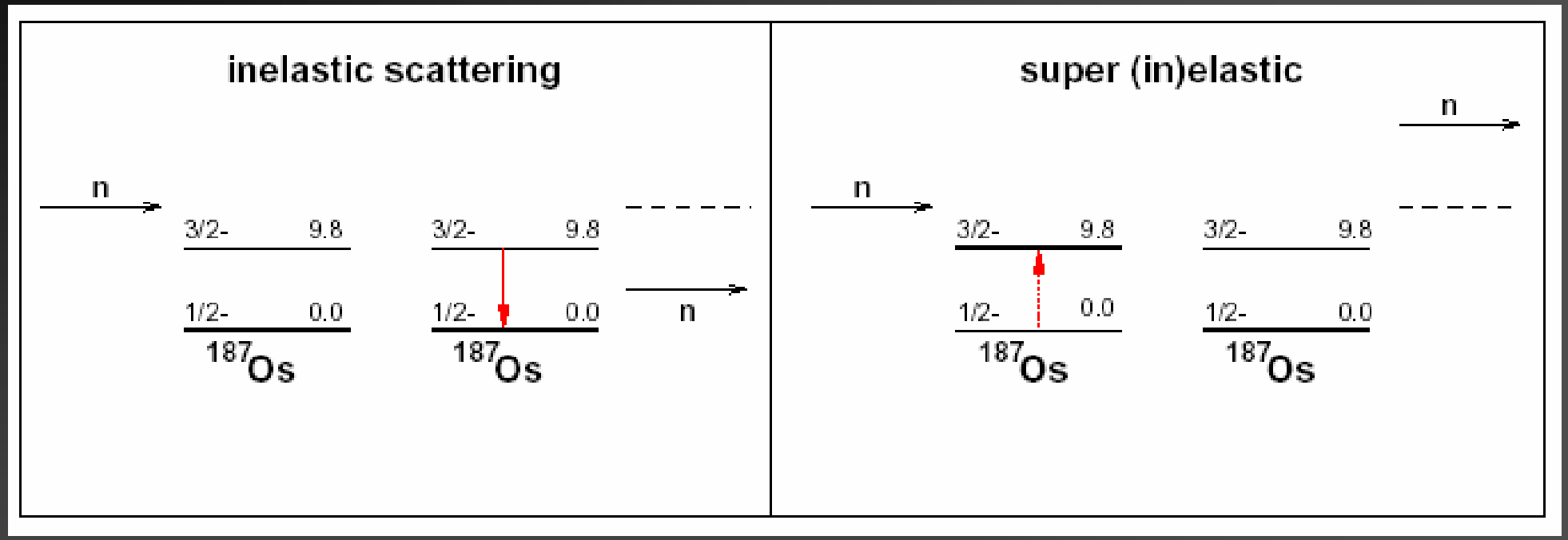

alberto.mengoni@cern.ch

Issue 2: theory still needed

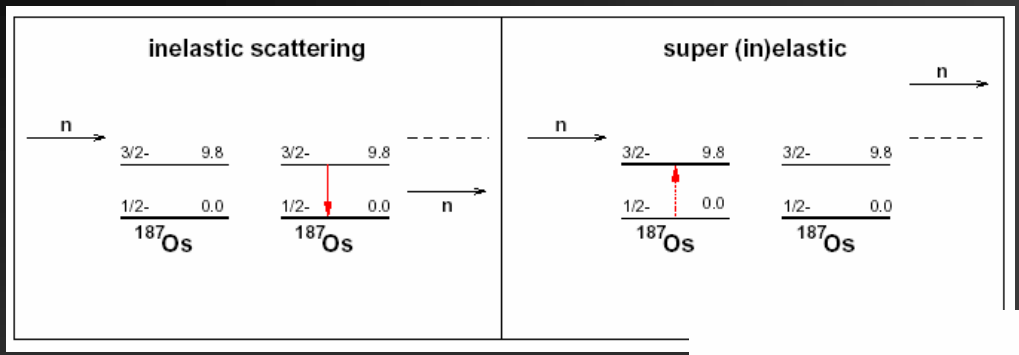

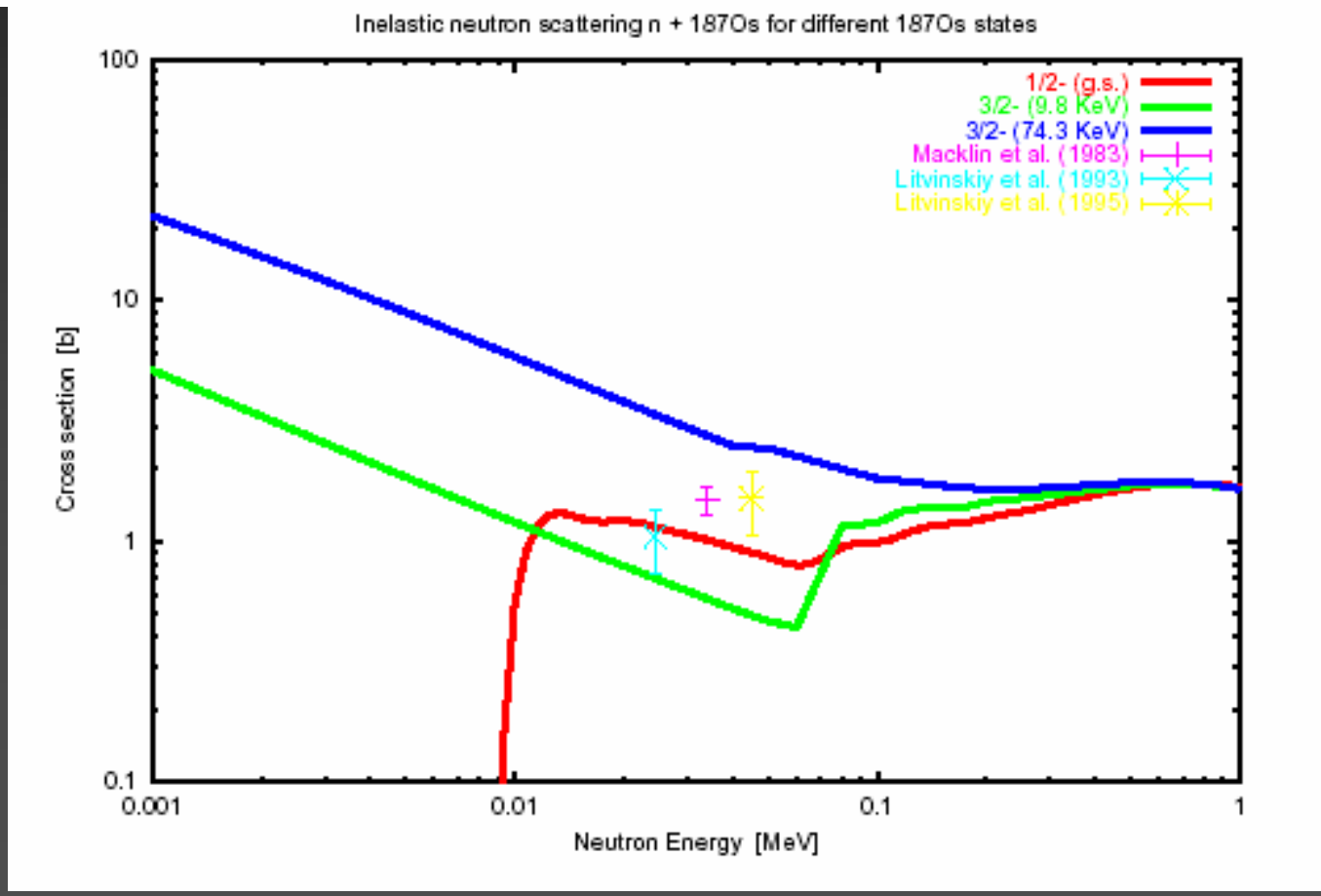

Stellar cross sections & the clock

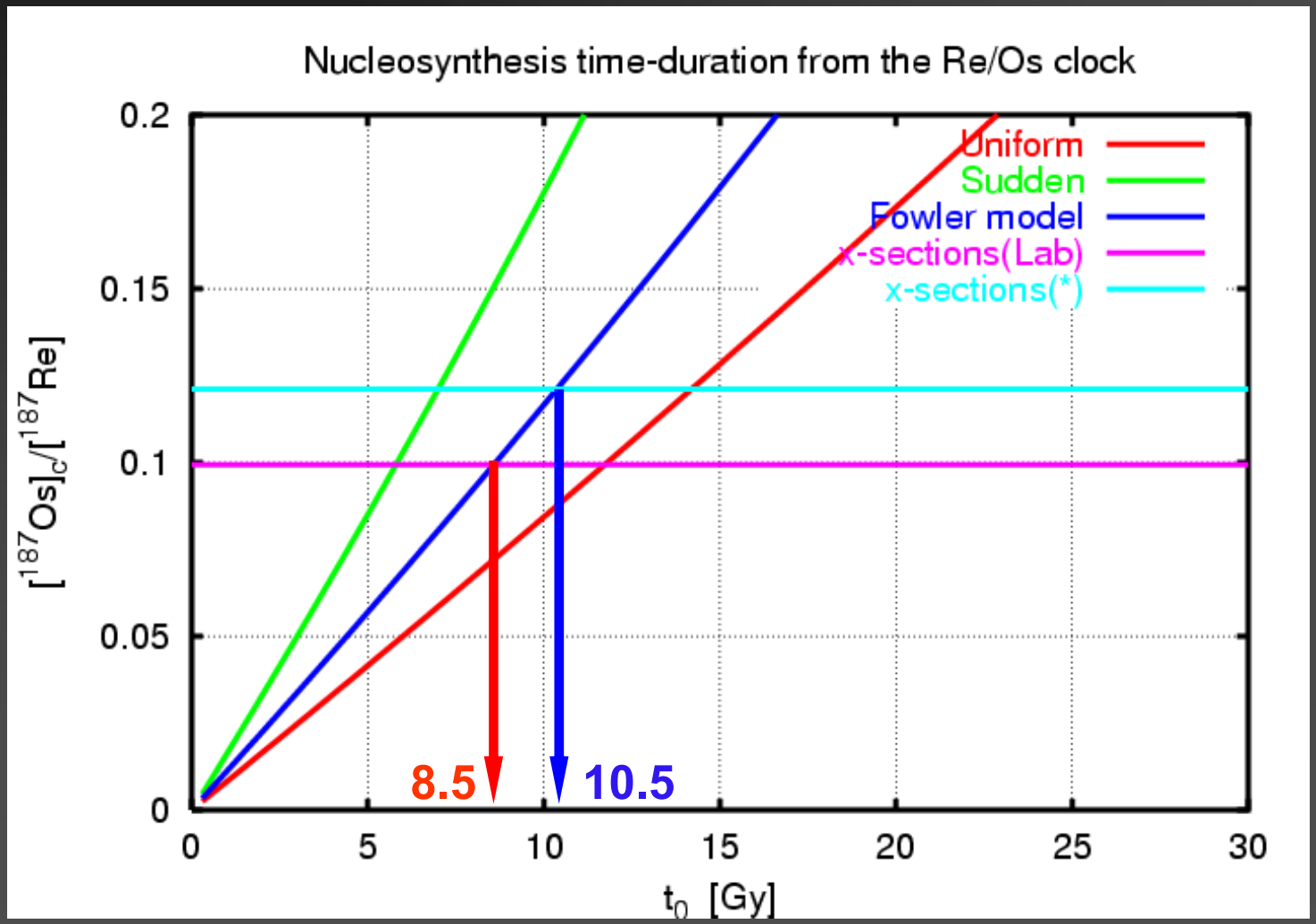

alberto.mengoni@cern.ch

n_TOF-04: the Re/Os revisited

The measurement is **completed**. The setup used is the standard for capture measurements with the FZK C_6D_6 detectors. The data taking has been performed during July/August.

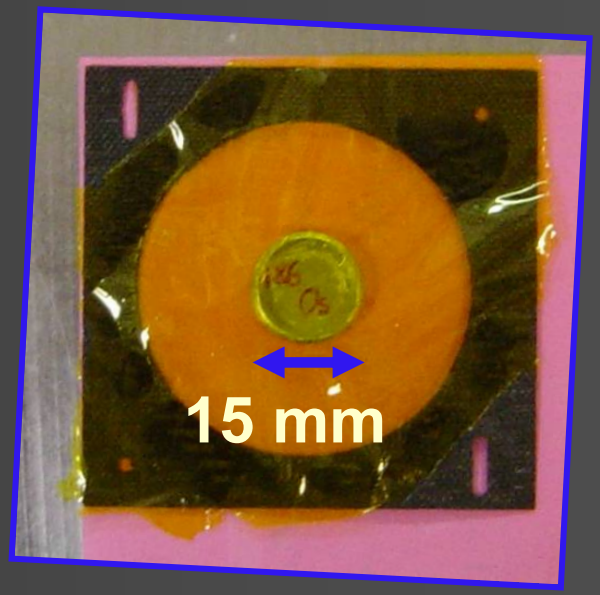

	Sample	Thickness [mm]	Diameter [mm]
1	186Os	1	15
2	187Os	1	15
3	188Os	1	15
4	Au	1	15

Isotope	Purity [%]
186Os	79.48
187Os	70.43
188Os	94.99
Supplier	ORNL
Metal powder	

Gamma-ray detector:	2 x C6D6
Neutron flux monitor:	SiMON

Total number of protons requested

1.4 x 1018**

n_TOF-04: $^{186}Os(n,\gamma)$

$0.1\ KeV \leq E_n \leq 500\ KeV$

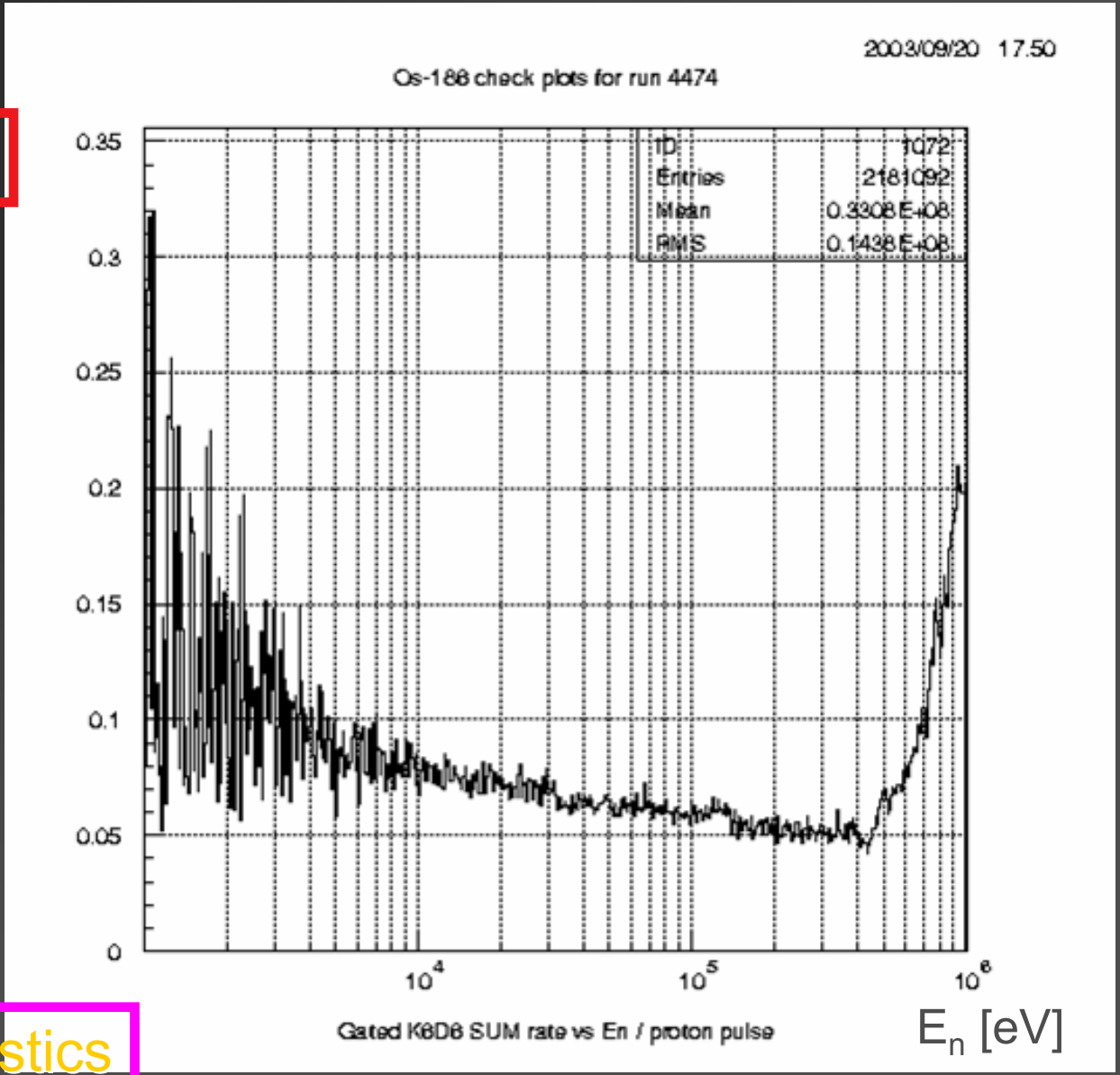

10% of statistics

alberto.mengoni@cern.ch

n_TOF-04: $^{187}Os(n,\gamma)$

$0.1\ KeV \leq E_n \leq 500\ KeV$

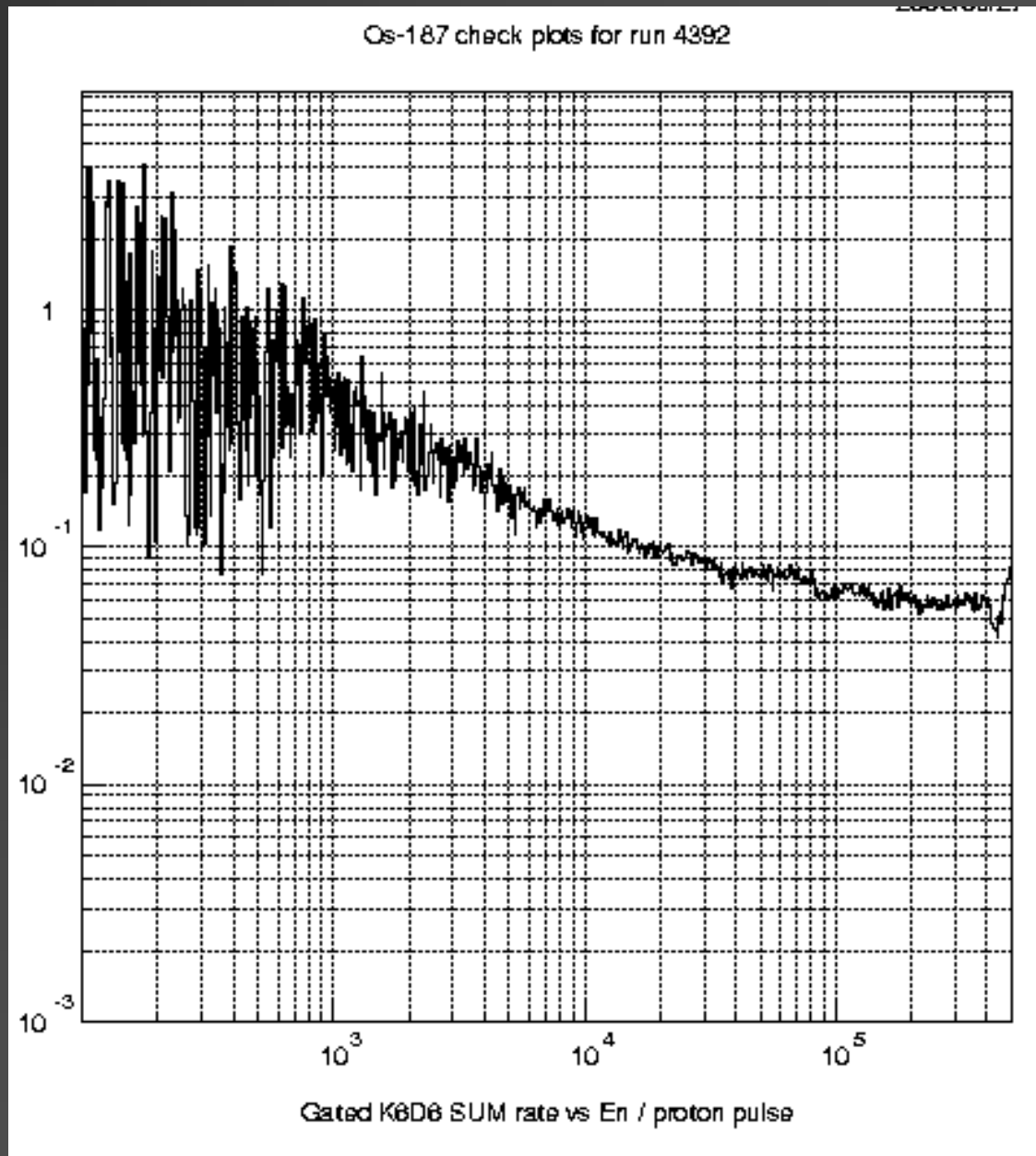

10% of statistics

n_TOF-04: $^{187}Os(n,\gamma)$

0.1 KeV ≤ E_n ≤ 500 KeV

in-beam γ-rays (Pb)

Al

10% of statistics

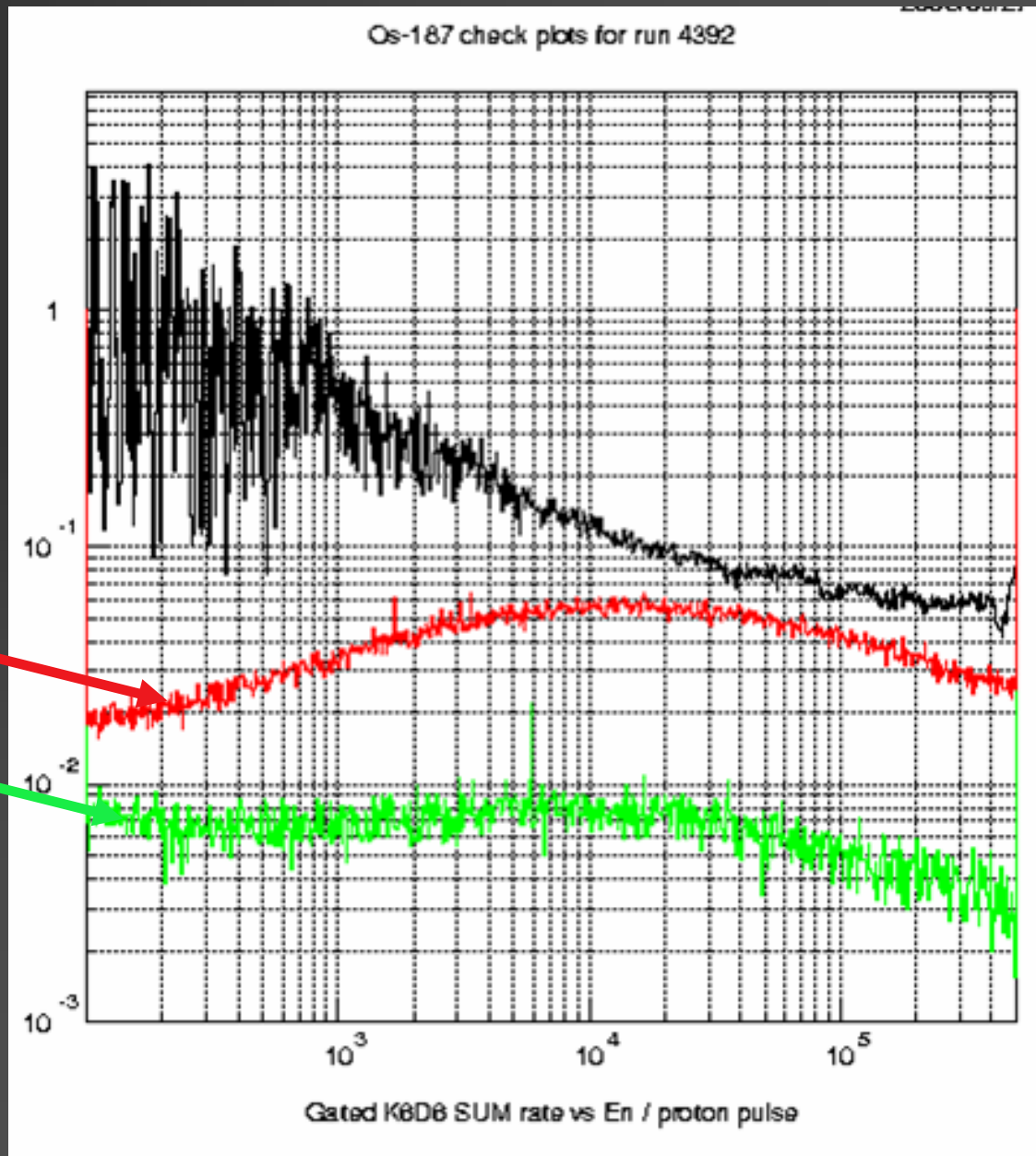

n_TOF-04: $^{188}Os(n,\gamma)$

$0.1\ KeV \leq E_n \leq 500\ KeV$

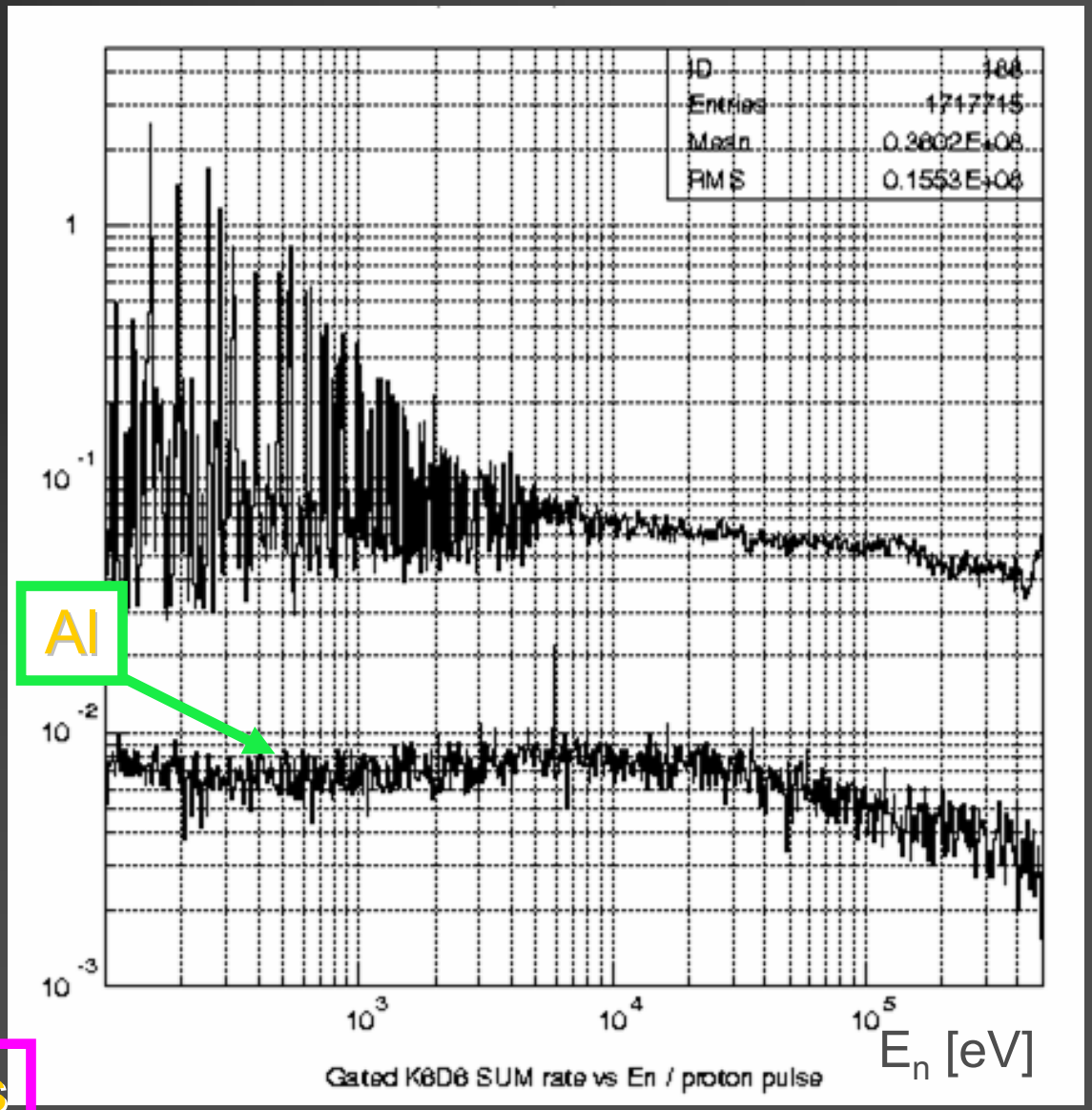

10% of statistics

alberto.mengoni@cern.ch

Brancing(s)

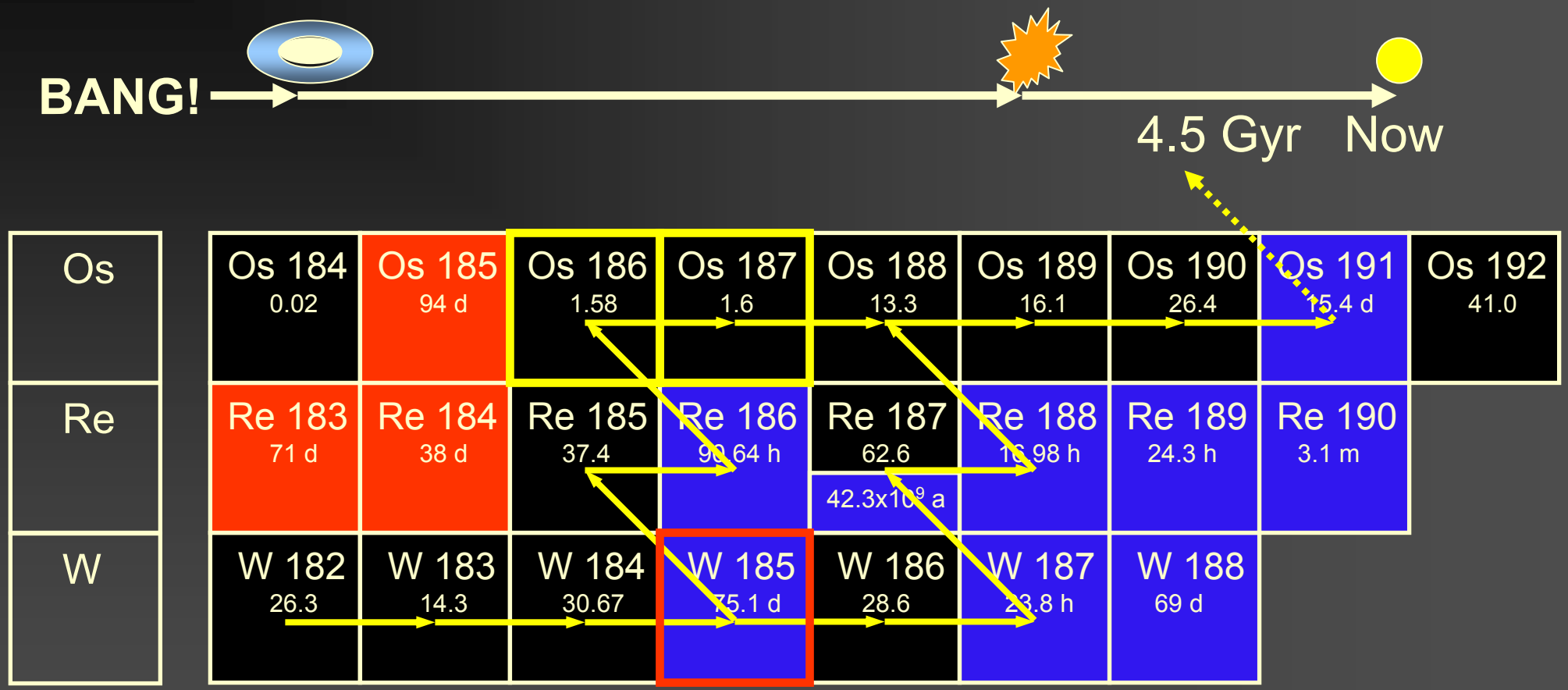

The $^{185}W(n,\gamma)^{186}W$ rate is needed

The inverse $^{186}W(\gamma,n)^{185}W$ cross section has been measured

K. Sonnabend *et al*. ApJ **583** (2003), 506-513.

Impact on the age: negligible

Th/U and Re/Os clocks: complementary

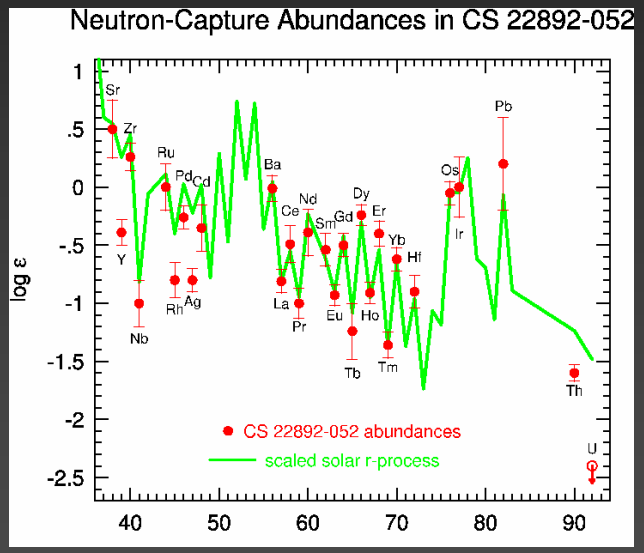

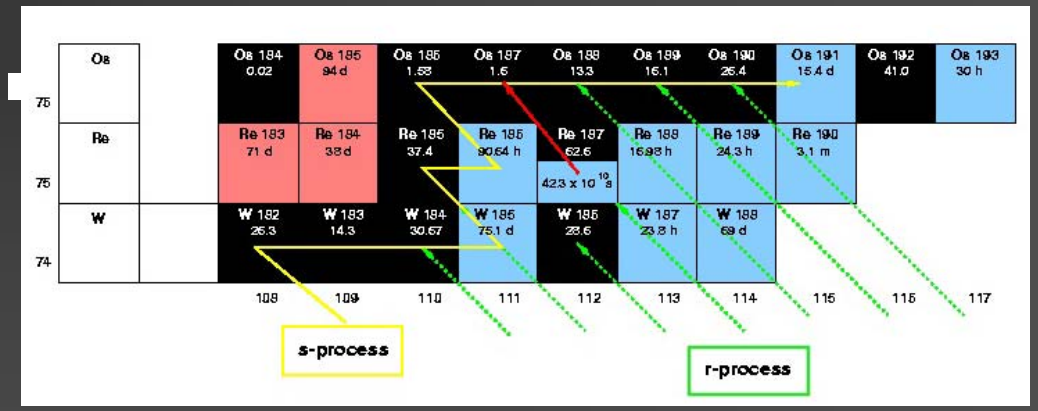

GCE	: independent
Primordial yields	: model-dependent

GCE	: dependent
Yield production	: well determined

alberto.mengoni@cern.ch

Conclusion

- n_TOF++
  - n_TOF at CERN is fully operational: performances as designed
- Neutron Cross section measurements
  - Measurement campaign in 2002 & 2003 completed. All but one of the planned measurements have been performed. Data analysis in progress.
  - 2004 measurement campaign is in preparation: TAC under construction
- Evaluation & Dissemination of Nuclear Data
  - Evaluation and dissemination plans produced

(not discussed in this presentation)

alberto.mengoni@cern.ch

Contribution by

David Vieira

Los Alamos National Laboratory

vieira@lanl.gov

2 pages

Fission (Charged Particle) Detector for DANCE

1. Actinides - low E_n fissioning isotopes

(n,γ) ---- (n,fission) competition

- need to extract (n,γ) cross section and the σ(n,γ)/σ(n,fission) ratio
- capture & fission processes are partially resolved based on total photon calorimetry $\Sigma E\gamma$ and γ multiplicity
- we need better separation
  → fission tagging detector
- different levels of fission-gamma data
  - 4π fission tagging
  - light / heavy fission fragment
  - fission fragment – γ correlations

Fission (Charged Particle) Detector for DANCE

2. Low energy (n,α) or (n,p) reactions (lighter Z species)

- requires a different charged particle detector?
- particle ID + energy (+ angle?)

I encourage an active discussion

Jerry Wilhelmy – fission-gamma exps.
Thierry Ethvignot – solar cell det. System
Demetrios Sarantites – thin scint. / Hercules
Yaron Danon – ion chamber
Lee Bernstein – Si detector system (light particle ID)

Contribution by

Jerry Wilhelmy

Los Alamos National Laboratory
j_wilhelmy@lanl.gov

17 pages

Fission Studies with DANCE

Dance Workshop

Santa Fe

February 2-3, 2004

Jerry Wilhelmy

Who Cares?

- National Security Programs - need to know fission cross sections and fission gamma emission
- Waste Transmutation - burning up actinide waste via fission is a desirable method for destroying long lived activities
- Astrophysics - need fission systematics to understand termination of nucleosynthesis

DANCE Characteristics

- 4π Detector
- High Granularity
- Fast Timing
- Calorimeter

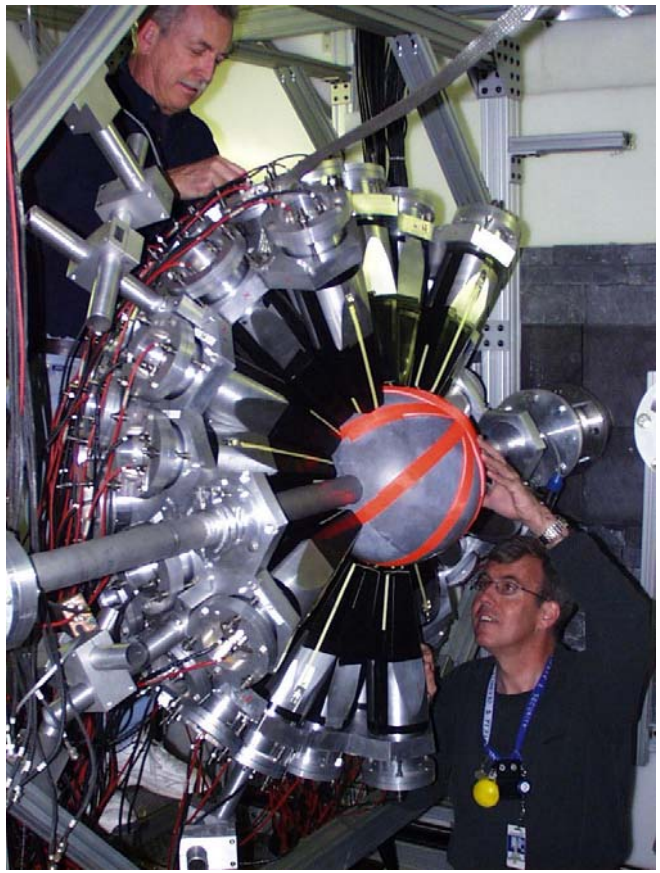

Fission Measurements

- $\sigma_{n,f}(E_n)/\sigma_{n,\gamma}(E_n)$ - Fission/Capture cross sections
- $\Sigma((E_\gamma)/f)$ - Total photon energy release per fission
- M_γ/f - Multiplicity of gammas/fission
- $\bar{E}_\gamma/f$ - Average energy of fission gammas
- $\Downarrow(f,\gamma)_t$ - Temporal distribution of fission gammas

Gamma Characteristics

- Fission
  - $\Sigma(E_\gamma) \sim 10$ MeV
  - $M_\gamma \sim 6\text{-}10$
  - $\overline{E}_\gamma \sim 1$ MeV
  - "Doppler" focusing
- Capture
  - $\Sigma(E_\gamma) \sim 6$ MeV
  - $M_\gamma \sim 3\text{-}5$
  - $\overline{E}_\gamma > 1$ MeV
  - No "Doppler" focusing

No Fission Trigger

- Simple - no additions to Dance
- Identify fission by differences between ΣE_γ and $<M_\gamma>$
- Not complete separation between capture/fission
- No fission mass information

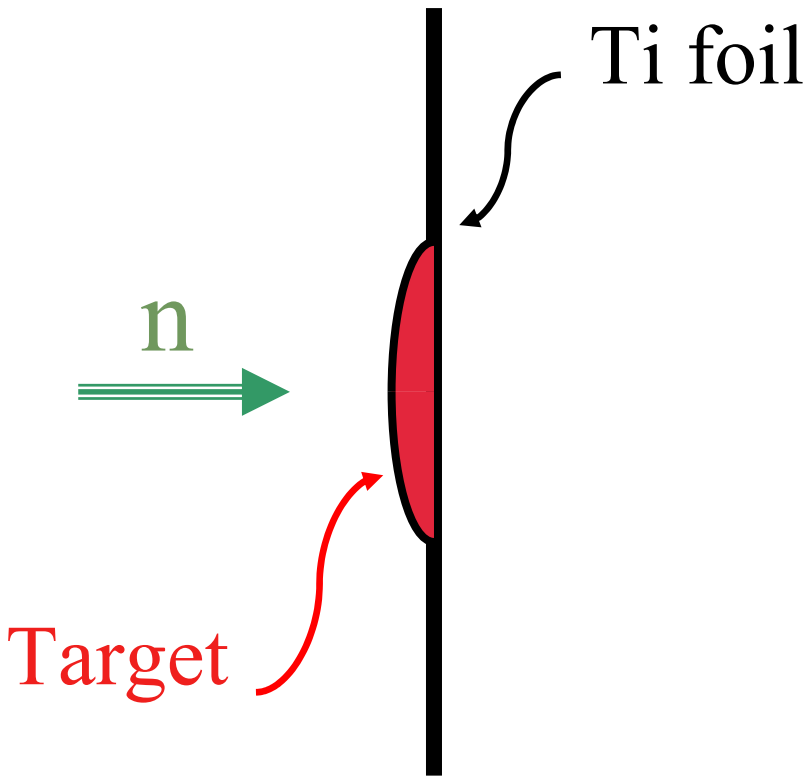

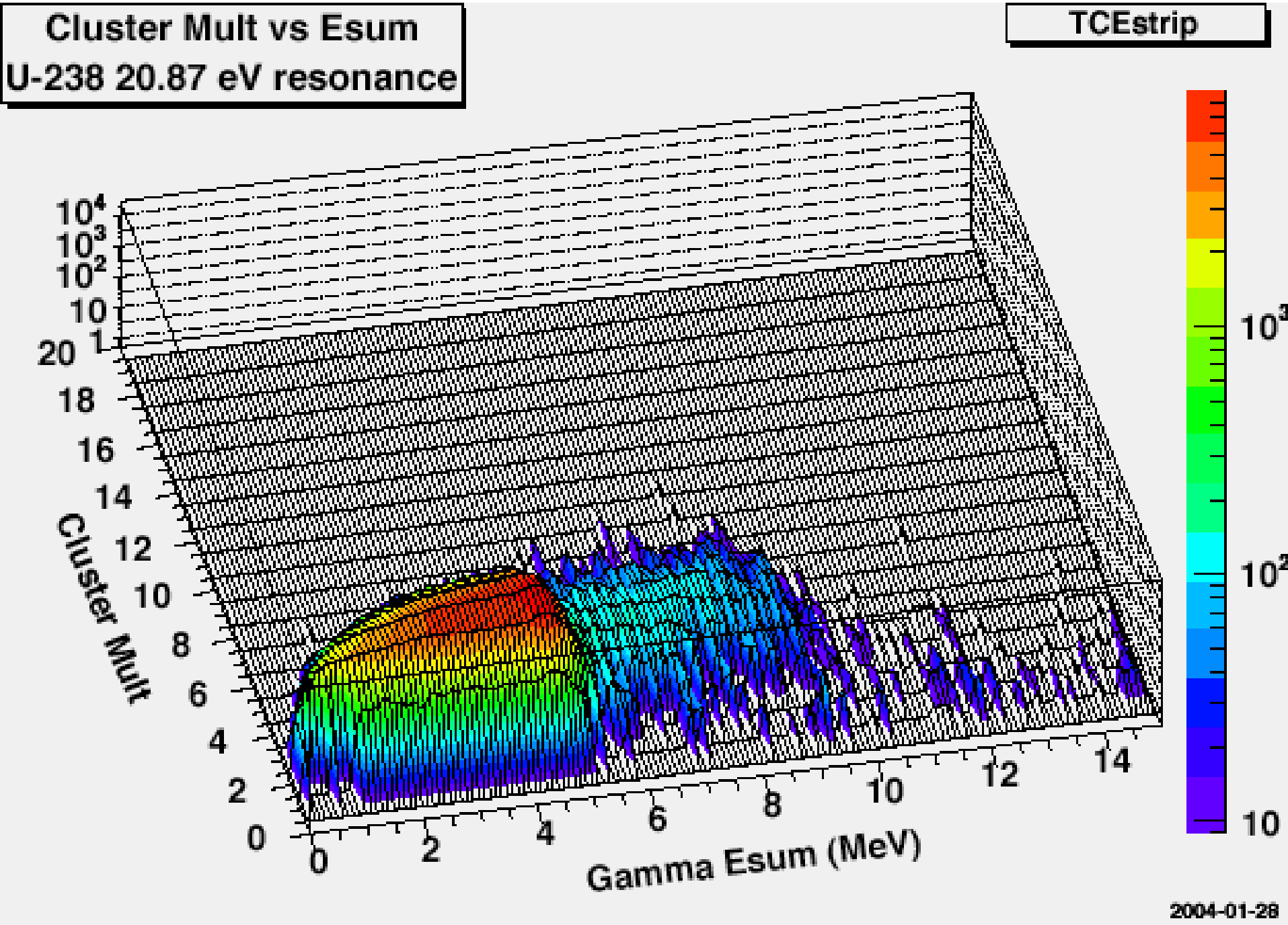
Cluster Mult vs Esum
U-238 20.87 eV resonance
TCEstrip
Cluster Mult
Gamma Esum (MeV)
2004-01-28

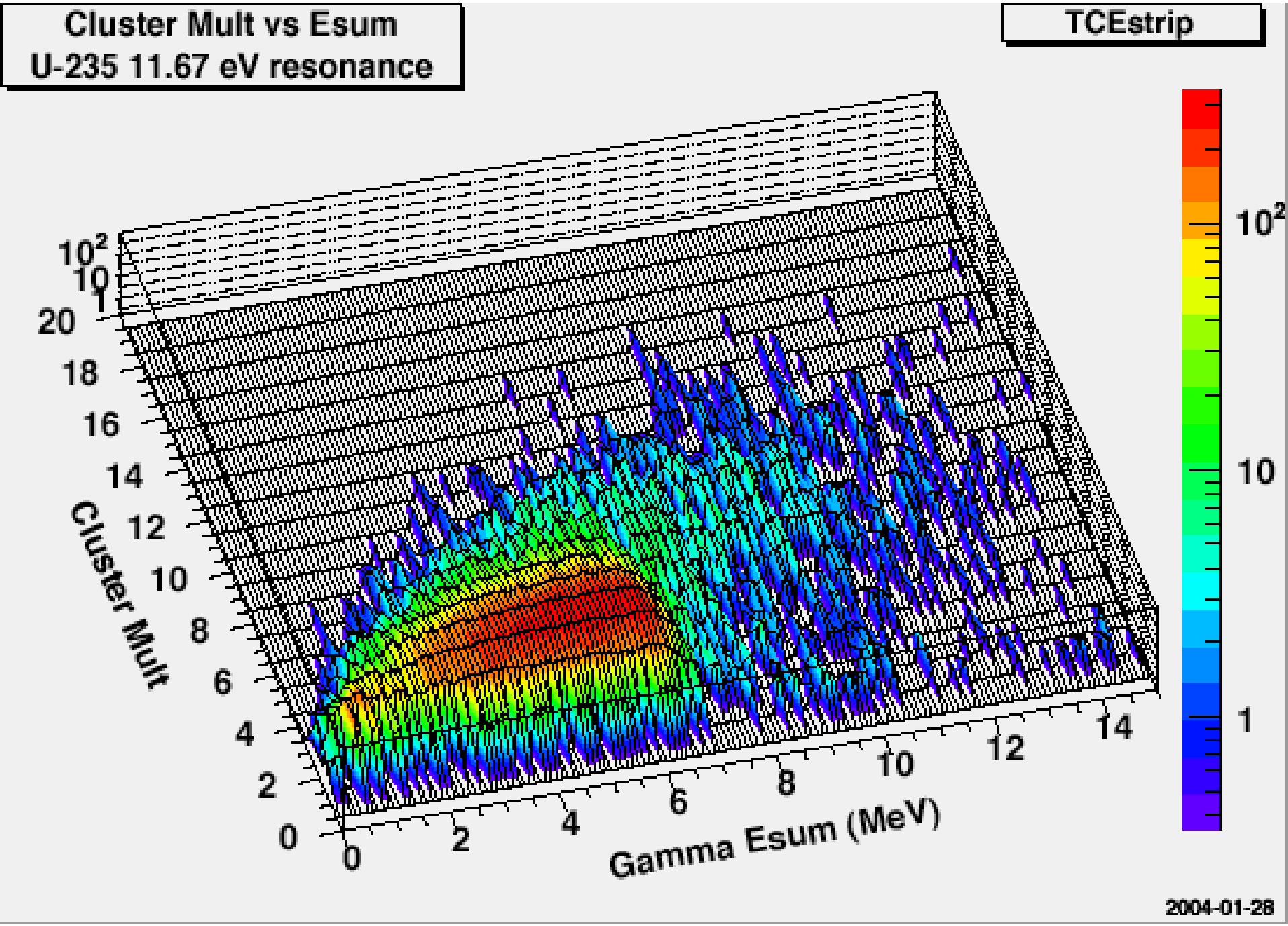
Cluster Mult vs Esum
U-235 11.67 eV resonance
TCEstrip
Cluster Mult
Gamma Esum (MeV)
2004-01-28

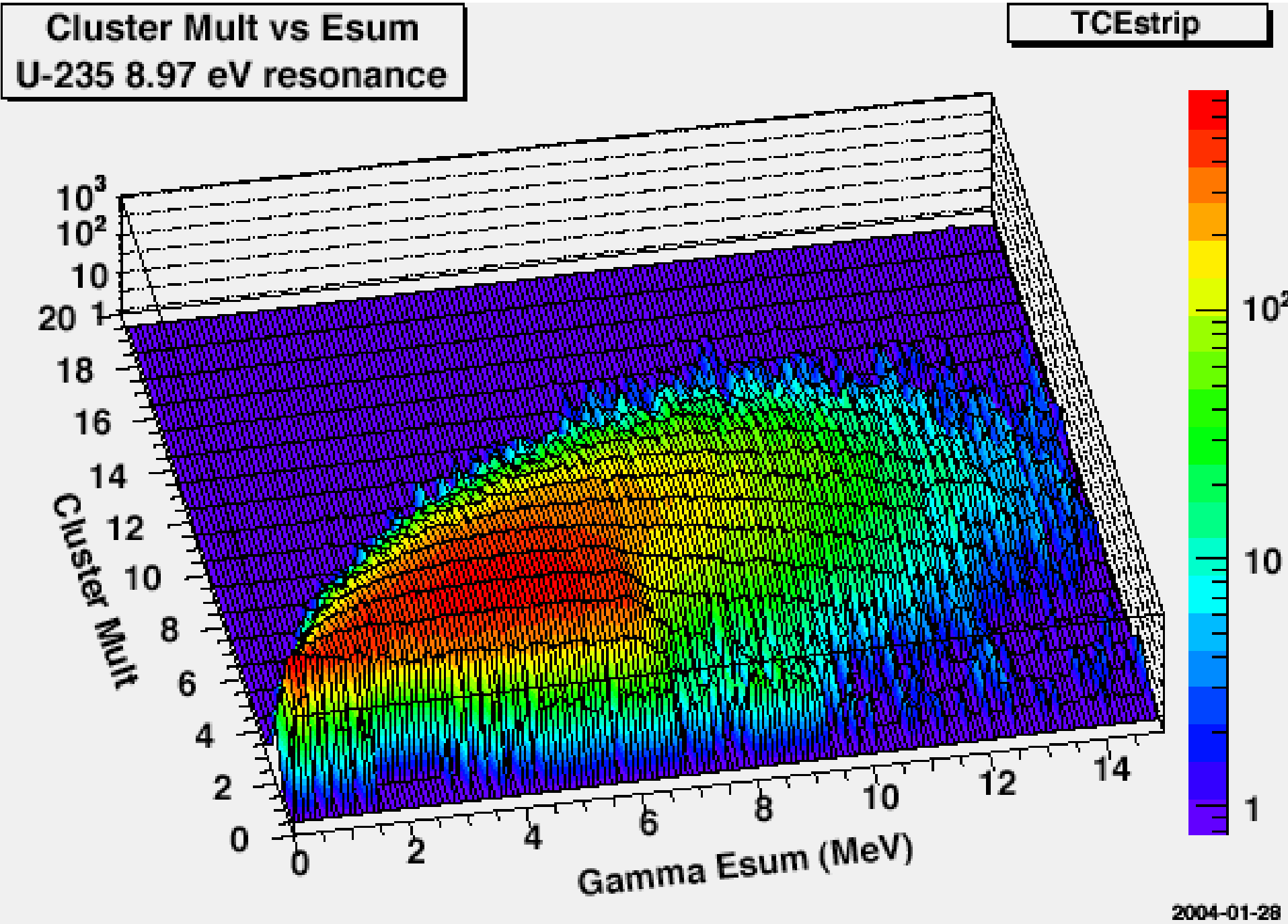
Cluster Mult vs Esum
U-235 8.97 eV resonance
TCEstrip
Cluster Mult
Gamma Esum (MeV)
2004-01-28

“Active” Detector

- Independent fission trigger
- Crude mass information
- More mass in beam
- Additional electronic signal to record/process

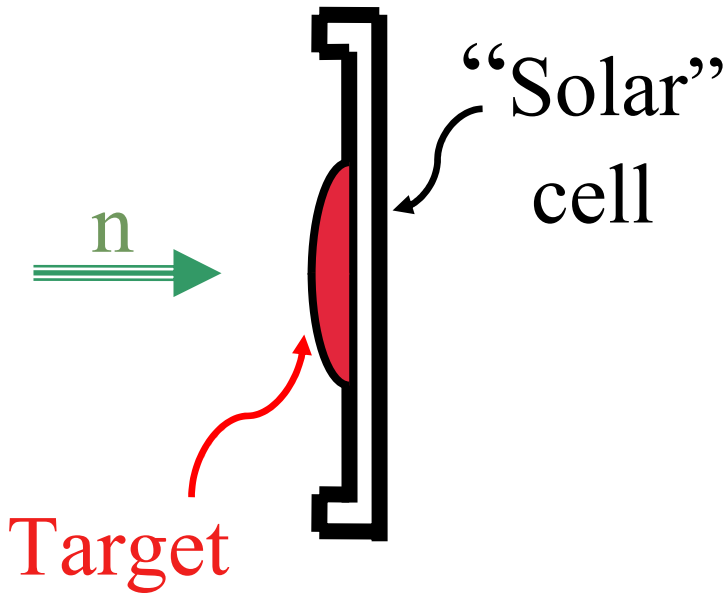

Two Sided Fission Detection

- Direct Fission Signal
- Fission Mass Determination
- Extensive Mass Exposed to Beam
- More Complex Electronics

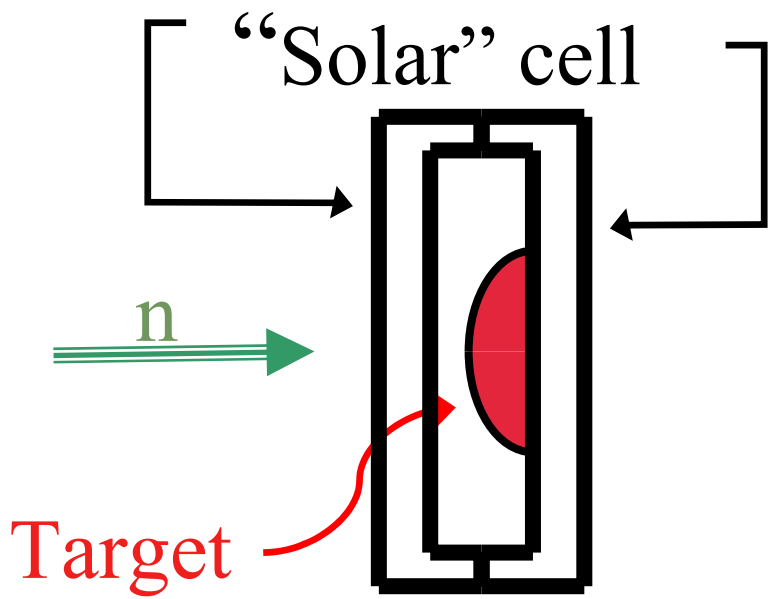

Fission Detector Array

- Fission Trigger
- Best Mass Resolution
- Minimal Additional Mass in Beam
- Complex
- Expensive
- Shields γ-Detectors

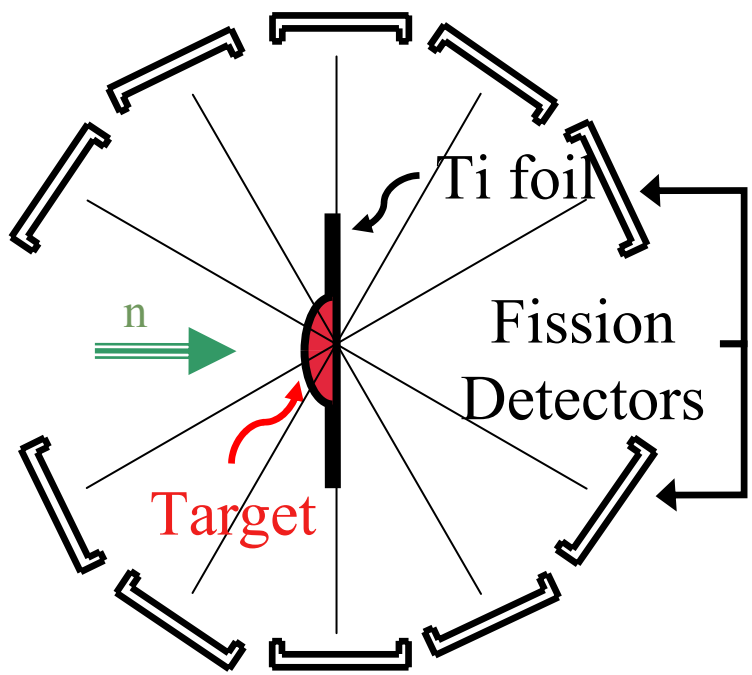

Off Line Testing

- Detection system could be developed/tested using ^{252}Cf(SF) - no neutron beam necessary
- Extensive Heidelberg Crystal Ball and Gammasphere data of ^{252}Cf(SF) gamma spectroscopy available

Isotope List

Isotope	$t_{(1/2)}$ (yrs)	σ_f-th (res int) (b)	σ_γ-th (res int) (b)
^{229}Th	7.3 E3	31 (500)	73 (280)
^{232}U	7.0 E1	75 (380)	73 (280)
^{233}U	1.6 E5	531 (760)	46 (140)
^{235}U	7.0 E8	585 (275)	99 (140)
^{236m}Np	1.5 E5	2500 (1000)	-
^{237}Np	2.1 E6	0.02 (7)	150 (650)
^{238}Pu	8.8 E1	18 (33)	540 (200)
^{239}Pu	2.4 E4	750 (300)	271 (200)
^{241}Pu	1.4 E1	1010 (570)	361 (160)
^{241}Am	4.3 E2	3 (14)	60 (150)
^{242m}Am	1.1 E3	7000 (1800)	1700 (200)
^{243}Am	7.4 E3	0.07 (0.06)	78 (1800)
^{243}Cm	2.9 E1	610 (1600)	130 (220)

Experimental Parameters

- FP-14 flux - Small
  - $(4 \times 10^4$ n/cm^2-eV-sec$)/E_n$(eV)
- With 10% $\Delta E/E$ energy bin
  - ~ 4,000 n/sec-energy bin
- With 1 mg/cm^2 target and $\sigma(n,f) = 1$ barn
  - ~ 1,000 f/day-energy bin

If $\sigma(n,f) \alpha 1/v$
(and $\sigma(n,f)$=1 barn @ 1 keV)

E_n (eV)	ΔE_n (eV)	$\sigma(n,f)$ (b)	f/day
1	0.1	30	24000
10	1	10	8000
100	10	3	2400
1000	100	1	800
10,000	1000	0.3	240
100,000	10,000	0.1	80

Conclusion

- Best technique to measure $\sigma(n,f)/\sigma(n,\gamma)$ as a function of E_n
- DANCE is well suited for studying (n,f) produced γ-rays
- LANL can provide suitable targets for fission studies with actinides.
- Fission detection techniques can be developed "off-line" using ^{252}Cf

Contribution by

Thierry Ethvignot

CEA
thierry.ethvignot@cea.fr

17 pages

Detection of fission fragments with solar cells for γ-fission or fission veto measurements with DANCE

Th. Ethvignot

Thierry.Ethvignot@cea.fr
CEA / Centre DAM Ile-de-France
Service de Physique Nucléaire,
BP 12, 91680 Bruyères-le-Châtel, France

Outline

- Using Solar Cells for Nuclear Physics (pulse mode)
- Performances
- Pros and Cons
- Work in progress
- 3 Set-up options

Using Solar Cells for Nuclear Physics (pulse mode)

The early days

G. Siegert *et al.* NIM **164** (1979)
→ fission fragment detection capability
→ concept of funneling

E. Liatard *et al.* NIM **A267** (1988)
→ low sensitivity to light ions
→ easiness to cut to any shape
→ fast timing with charge pre-amps (<10ns)

N.N. Ajitanand *et al.* NIM **A320** (1992)
→ nanobarn fission cross section measurements
→ detection of γ-rays in coinc. to increase sensitivity

S. Andriamonje *et al.* Phys. Lett. **B348** (1995)
→ used in sub-critical assembly (natural U)
→ 184 fission counters

Funeling in Solar Cells

energetic FFs increase the naturally
depleted zone from one micron to their range

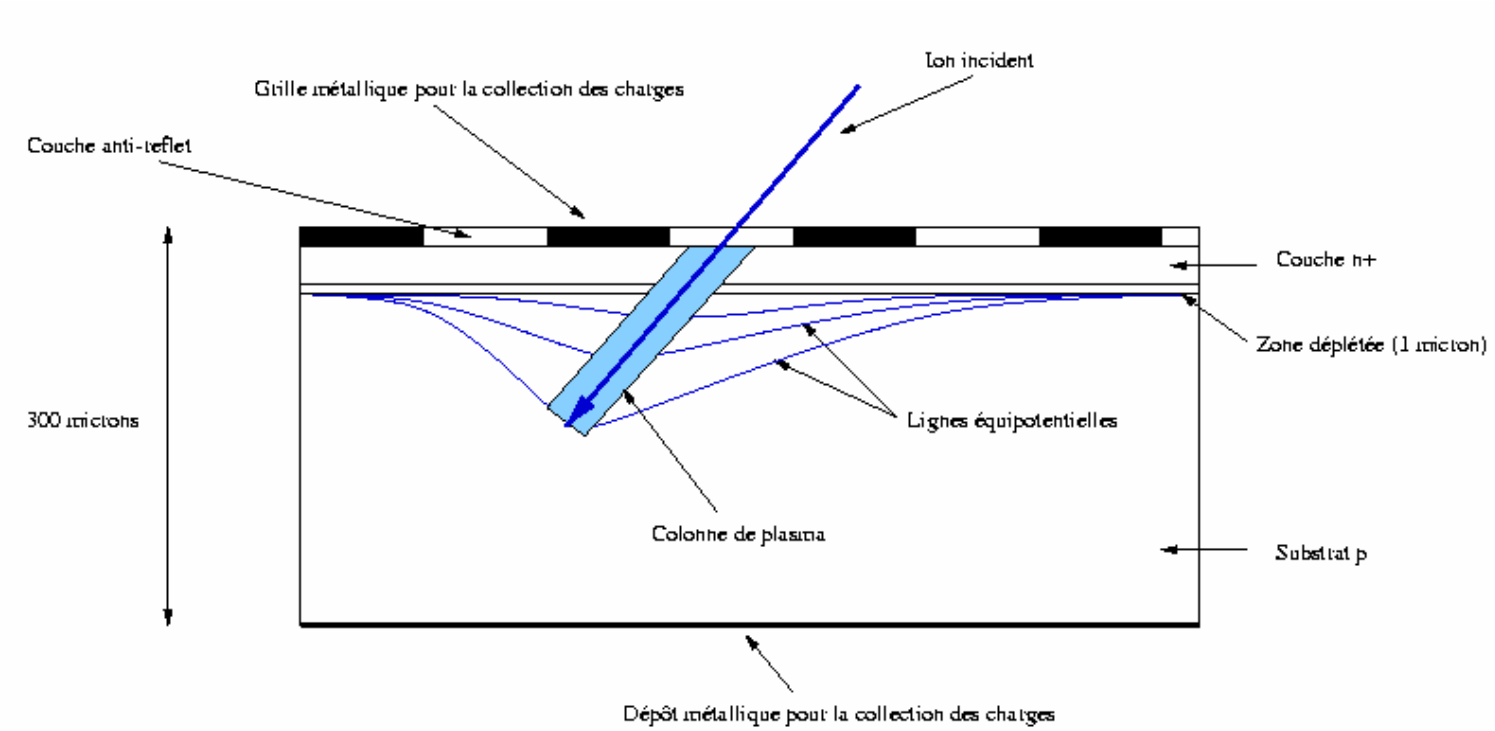

Ajitanand et al.

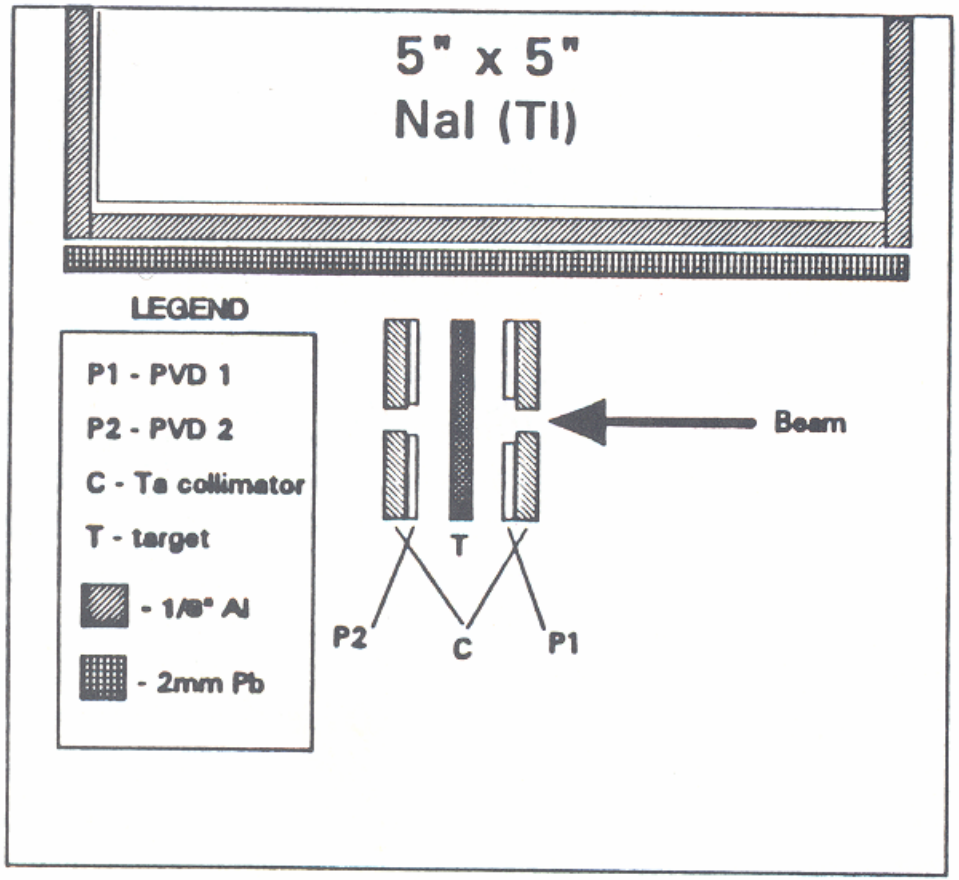

Fig. 1. Experimental arrangement used in the measurement of thick target fission yields for protons on ^{238}U.

Andriamonje et al.

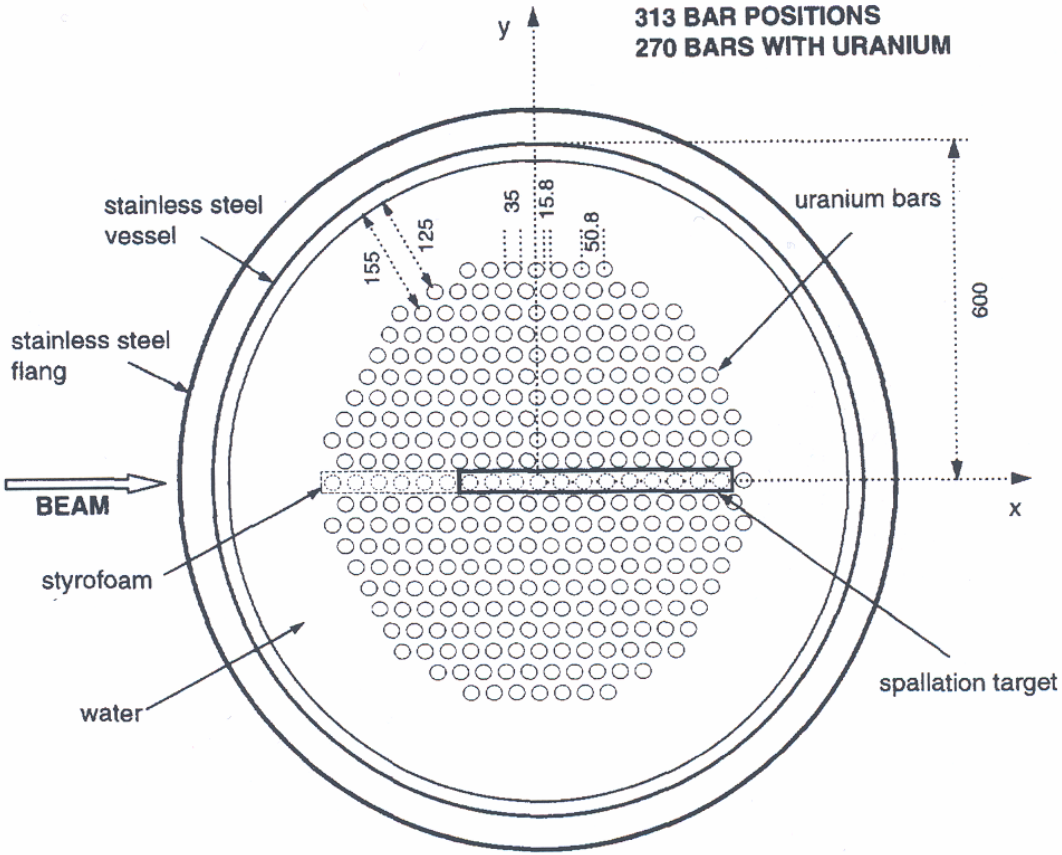

Fig. 1. Top view of the subcritical assembly. Distances are in mm.

More recently

Saphir Collaboration (~10 publications)

→ FF position and velocity for Doppler correction

→ FF γ-ray spectroscopy with EUROBALL

T. Ethvignot *et al.* NIM **A490** (2002)

→deposits on thin « space » cells to increase efficiency

→ FF X-ray spectroscopy with GEANIE

T. Granier *et al.* NIM **A506** (2003)

→ fission cross section of short lived actinides in LSDS

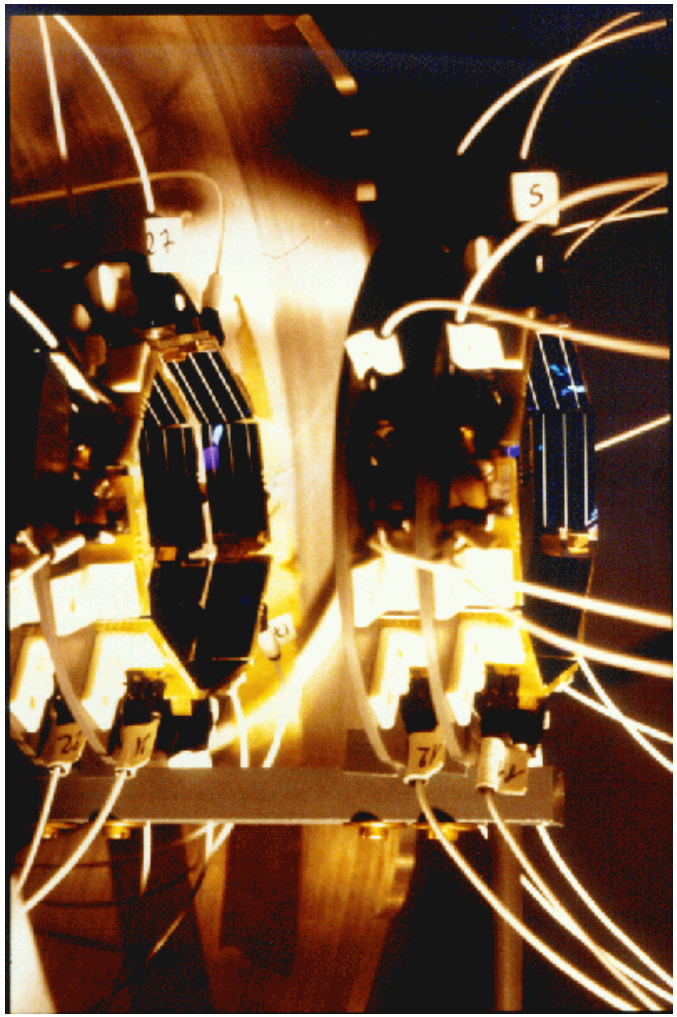

http://www-dapnia.cea.fr/Sphn/Deformes/Saphir/

16 cells

48 cells

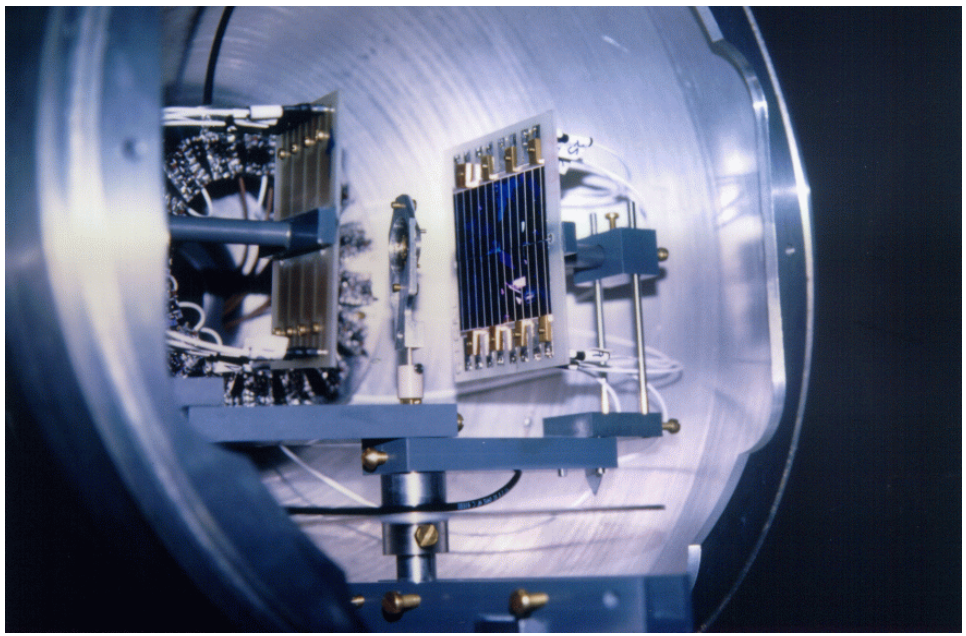

8 thin (100 μm) cells with ^{235}U deposits (1 mg/cm^2) in GEANIE

Quantity	Performance
Pulse linearity	good
Energy threshold	30 MeV
FF detection efficiency	65% (deposits) to 90% (SAPHIR)
Pulse height defect	higher than Si detectors
Energy resolution	2% (SAPHIR) to 20% (deposits)
Mass resolution	8 amu (SAPHIR)
Time resolution	10 ns (FWHM)
Position resolution	5 to 9 mm

Pulse height defect measurements at ILL (M. Petit PhD thesis, 2002)

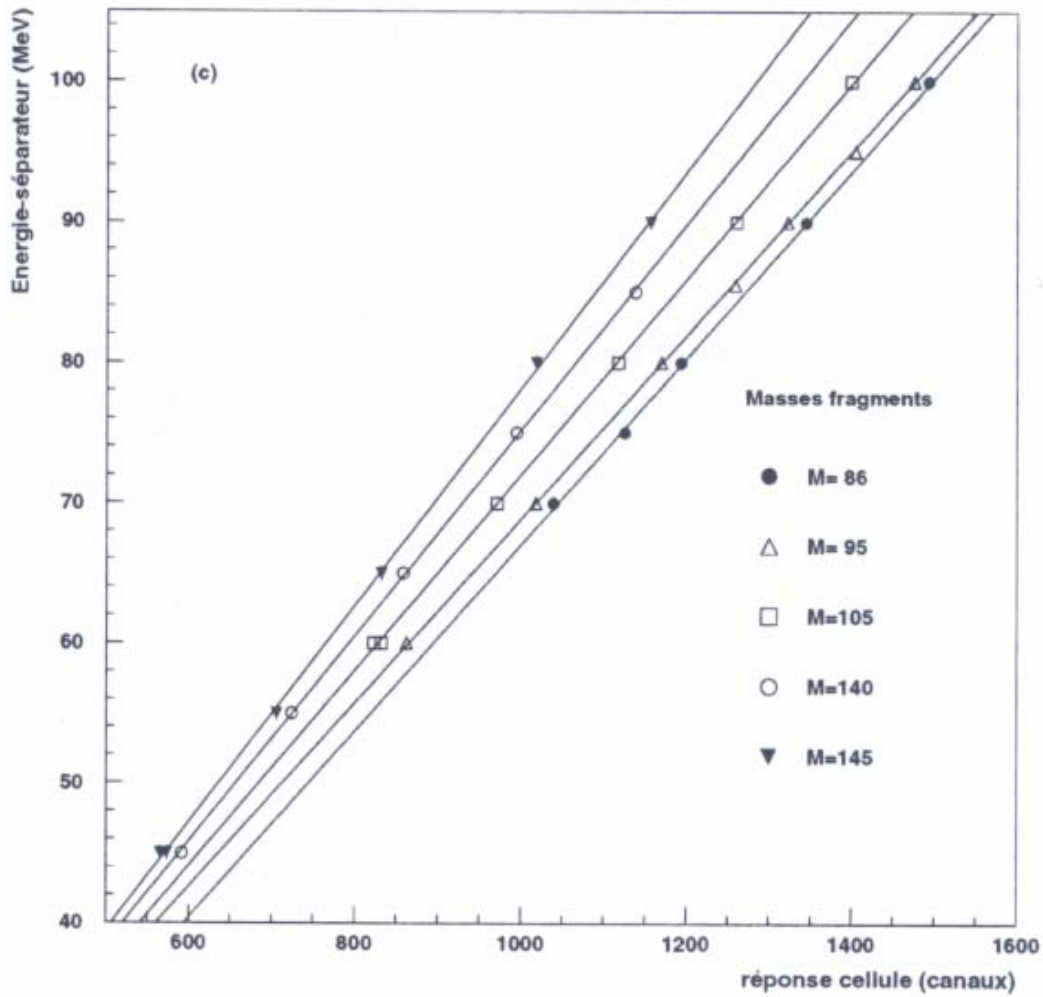

Energy spectrum with space solar cells and 1 mg/cm^2 ^{238}U deposit
(6% FF deposit no energy in cell, 16% deposit less than 30 MeV)

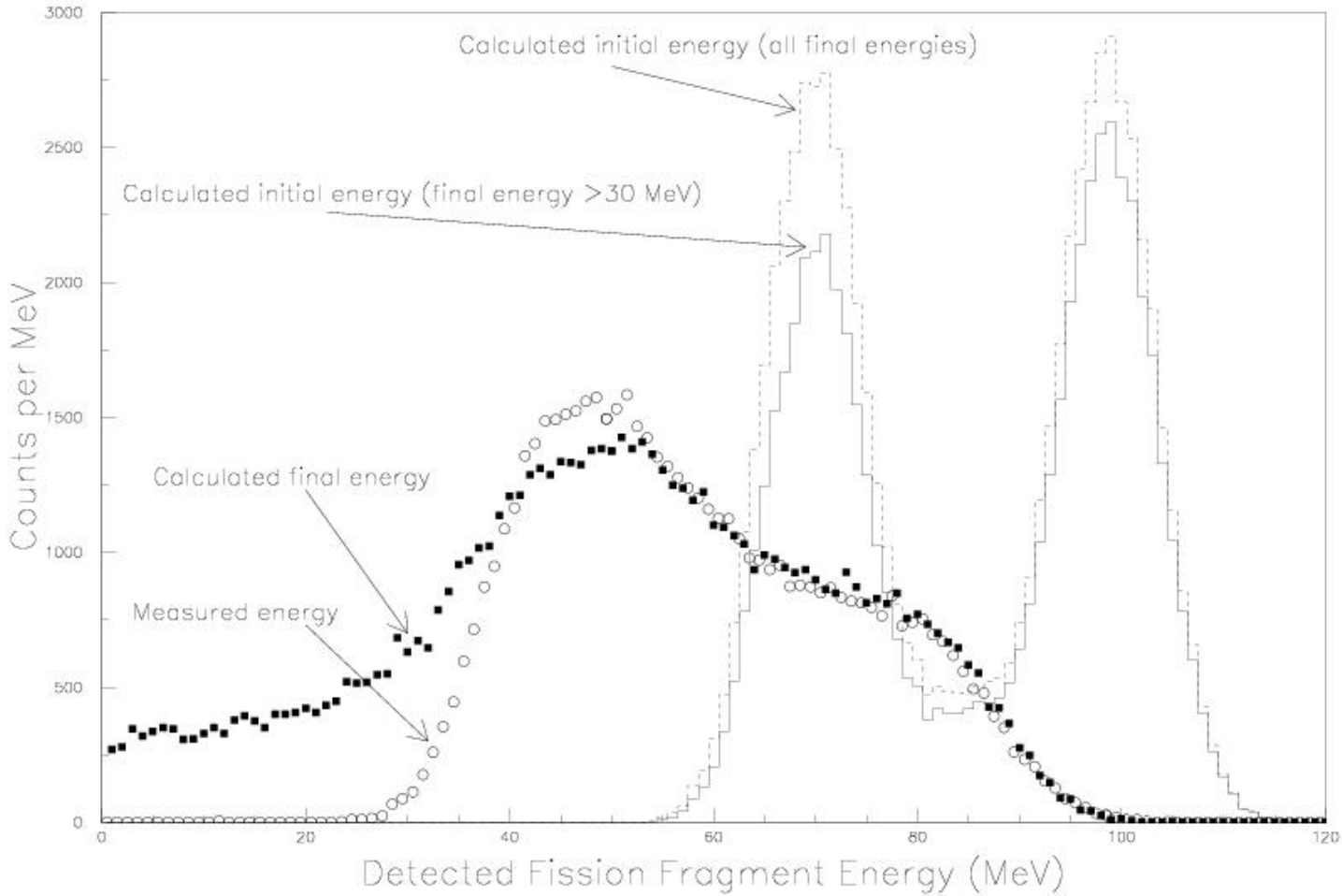

Advantages	Limitations
price	fragility
cut to any shape	noise/light sensitivity
no vacuum needed (deposits)	30 MeV threshold (deposits)
sustain high rates	low kinetic energy resolution
low sensitivity to n, α, β, γ	low mass resolution
no HV bias required	

Work in progress

Detection efficiency

Need to measure and increase efficiency for veto measurements

Lifetime vs. α dose

Cf point sources damage the cells – Need to establish the limit of α activity that can be deposited. Tests with α beams currently at B3.

Lifetime vs. n dose

no effect observed with WNR beam and LSDS.

Electronic oscillations vs. high intensity proton burst

phenomenon observed with LSDS experiment and high intensity proton bursts– compensation or isolation to be tested.

First Setup Option

Goal : measure (n,f), (n,γ) cross sections, Q_γ,photon multiplicity

How : detect fission or absence of fission (veto) simply and efficiently

Solution: (one cell + one mg/cm^2 deposit) x N

Count rate: for ten cells , 10 x 200 x 0.65 = 1300 fission/day-energy bin (Cf. Jerry)

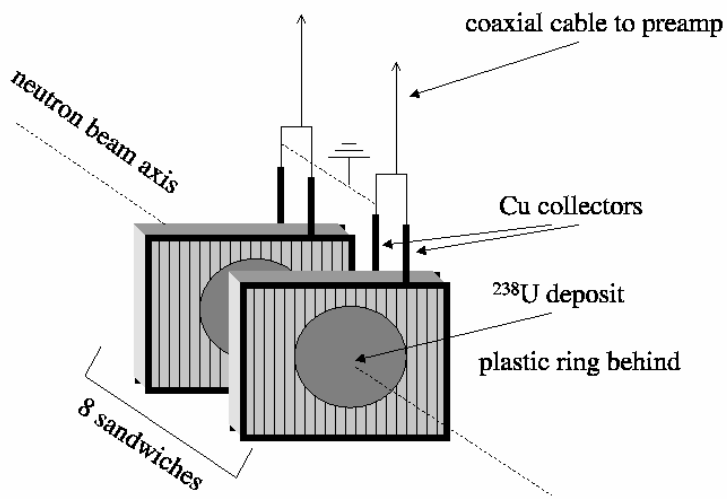

Second Setup Option

Goal : measure angular correlations between γs and fission axis

How : detect fission and fission angle

Solution: (one cell + one mg/cm^2 deposit) + PPAC or solar cell wall

Count rate: 200 x 0.65 = 130 fission/day-energy bin (Cf. Jerry)

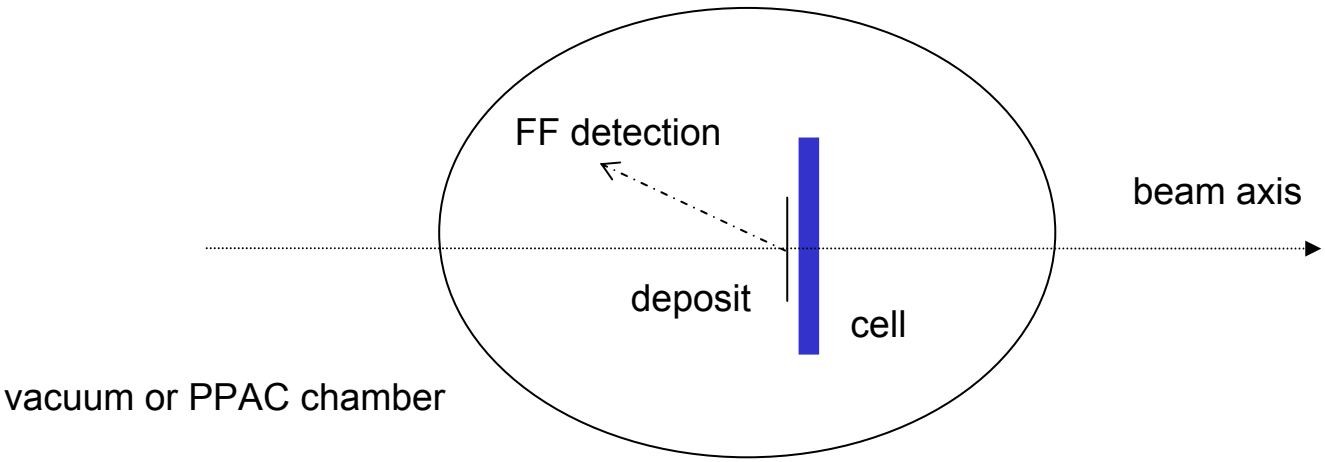

Third Setup Option

Goals : measure correlations between γs and mass asymmetry or TKE
investigate (n,γf) reactions

How : detect FF1 and FF2 energy

Solution: (one 0.01 mg/cm^2 deposit) + solar cell array

Count rate: 200 x 0.50 x 0.01 = 1 fission/day-energy bin (Cf. Jerry)

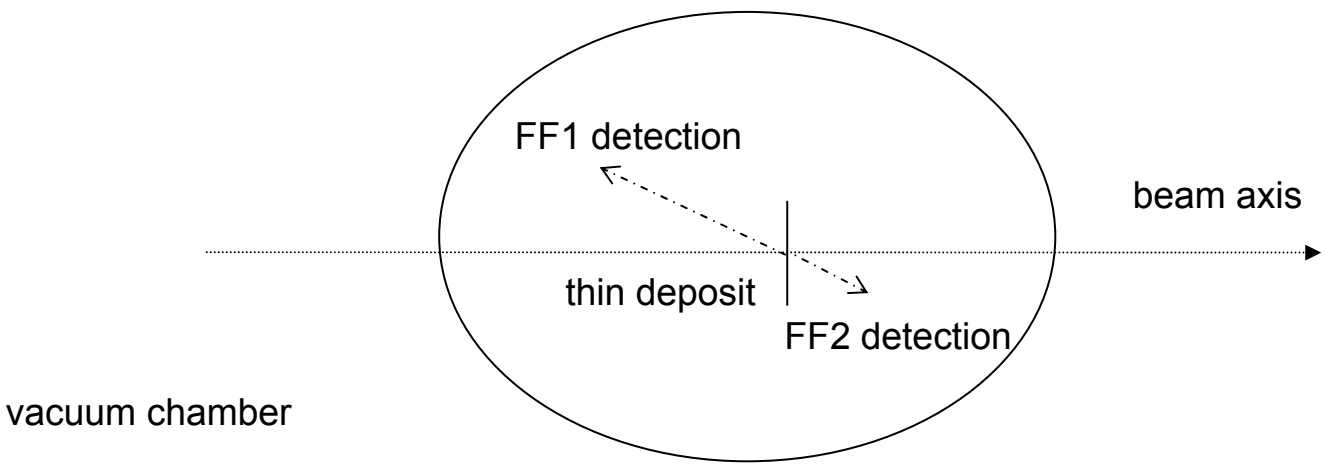

Contribution by

Demetrios Sarantites

Washington University
dgs@wuchem.wustl.edu

18 pages

Experiments with HERCULES

(High Efficiency Residue Counter Under Lots of Elastic Scattering)

Counting of Fission Fragments and Evaporation Residues with Very Thin Plastic Scintillators

Walter Reviol, D.G. Sarantites, C.J. Chiara, O. Pechenaya, J. Elson, M. Ferlotti, S.K.Ryu, and L.G. Sobotka
Washington University

Talk by D.G. Sarantites at the DANSE workshop,
Santa Fe, Feb. 2-3, 2004

The unfair fight

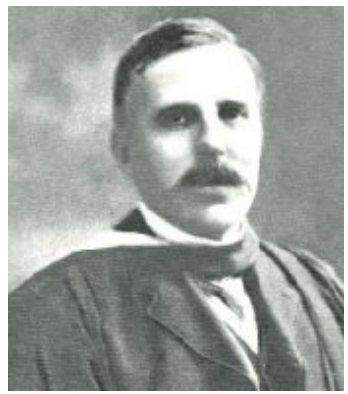

HERCULES

(A Demigod)

Rutherdford

(A Mortal Giant)

Detailed spectroscopy in actinides and light lead nuclei…

Problems:

- ~ A 100 mb fusion cross section but > 95 % of it lost in the fission channel;
  + ~ 500mb Coulex and transfer.
- Inner ball gating on multiplicity of evaporated protons, α's or neutrons
  is not selective (too many channels are open).
- Z-identification of residues by ΔExE (ion. chamber) does not work either.

We Need a "tag"…

Solutions (plural!):

1. **Recoil mass separation and Recoil Decay Tagging.**
   - Clean spectra – low cross sections – good identification capabilities!
     Limitations due to spectrograph angular acceptance:
     Low efficiency and choice of beam-target combination.
   - Limited applicability of RDT (500 ns ≤ $t_{1/2}(\alpha)$ ≤ 500 μs).

2. **Direct residue detection by ToF and Pulse Height. (HERCULES)**
   - Limitation due to presence of elastic scattering: "somewhat dirty".
   - Almost no identification capability.

3. **Isomer Tagging near the target.**
   - Applicability limited and no identification capability..

Design Considerations for HERCULES

- Fabrication of thin (1.0 mg/cm^2) and uniform plastic foils: *(Stop only the ER's)*
  - *(2.5 mg/cm^2 to stop Fission Fragments)*
- Response of scintillators to heavy evaporation residues: *(Ensure high trigger efficiency a low E_{kin} and high Z)*
- Radiation damage from elastics: *(Control loss in pulse height, compensate for it)*
- Fast electronics recovery: *(Achieve full recovery in 10 ns)*
- High segmentation in the array: *(Reduce rate in each detector)*
- Geometry: *(Must have ERs reach the detector before next beam burst)*

Parameters →

Ring	# Dets	Angular Range	Msr/Ring
1	8	3.2^o – 7.1^o	41.3
2	14	7.1^o – 11.2^o	73.8
3	18	11.2^o – 15.2^o	102.6
4	24	15.2^o – 19.1^o	128.4

Walter Reviol puts his toy together at GS

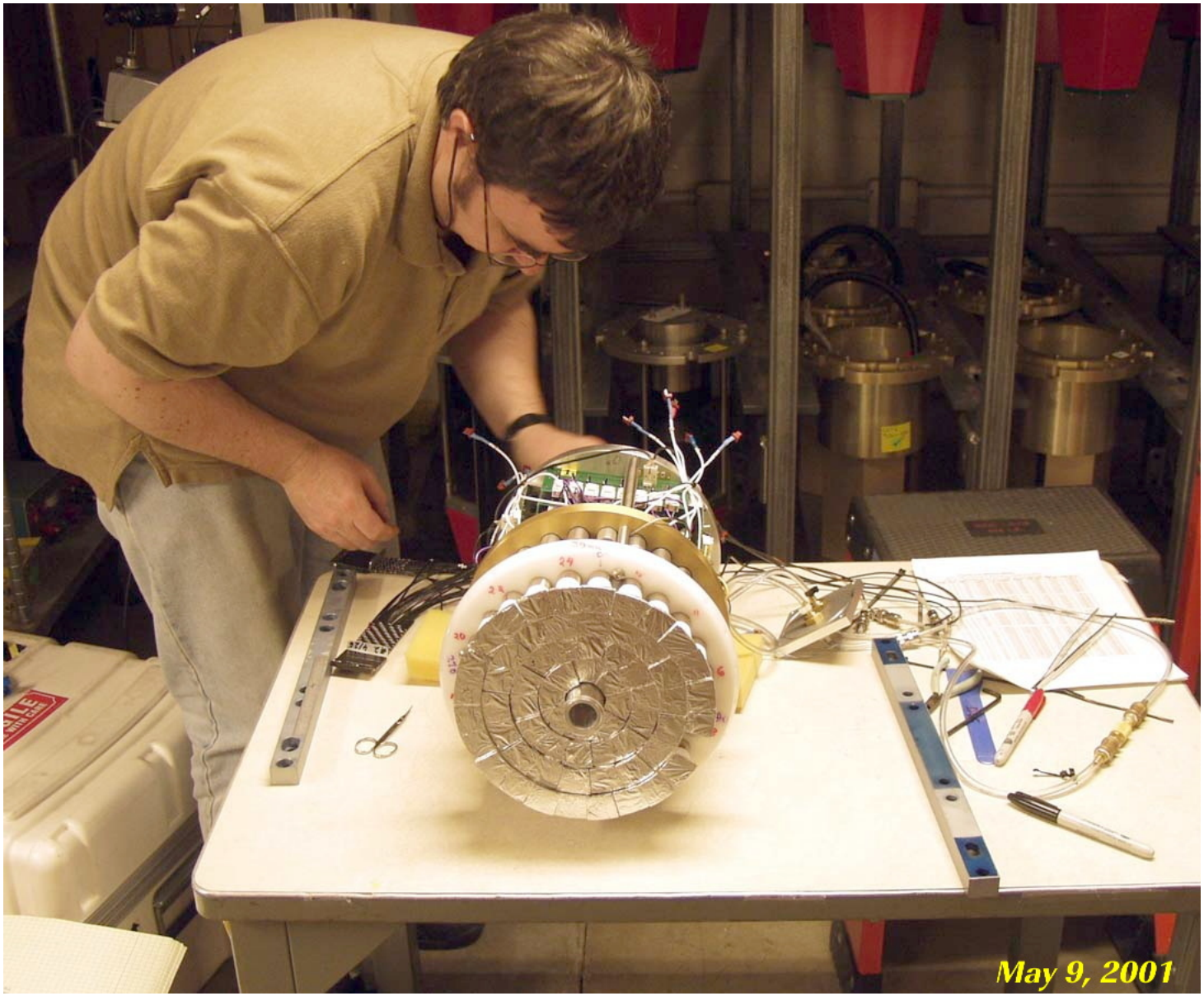

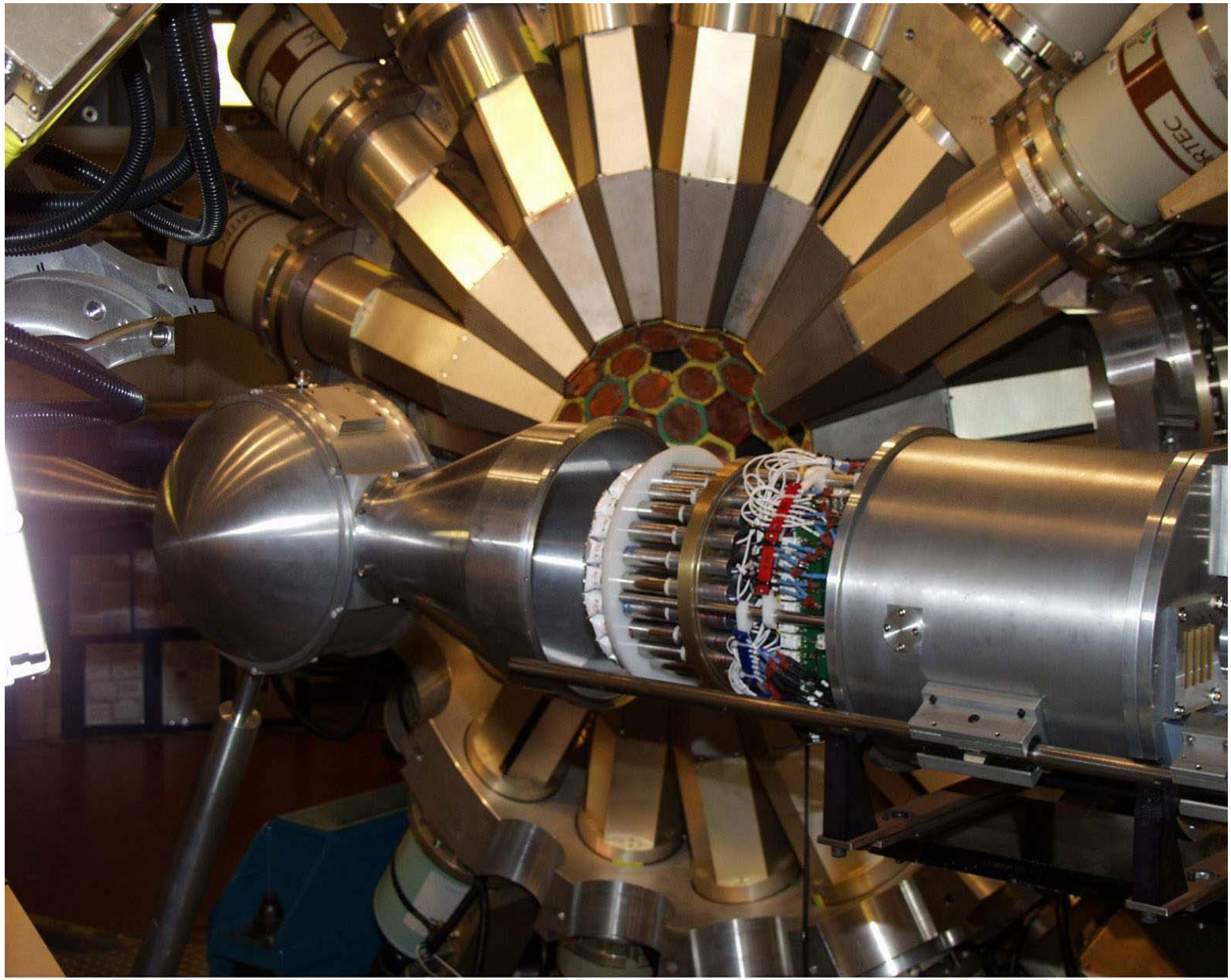

Washington University: HERCULES in Gammasphere, August 20, 2002

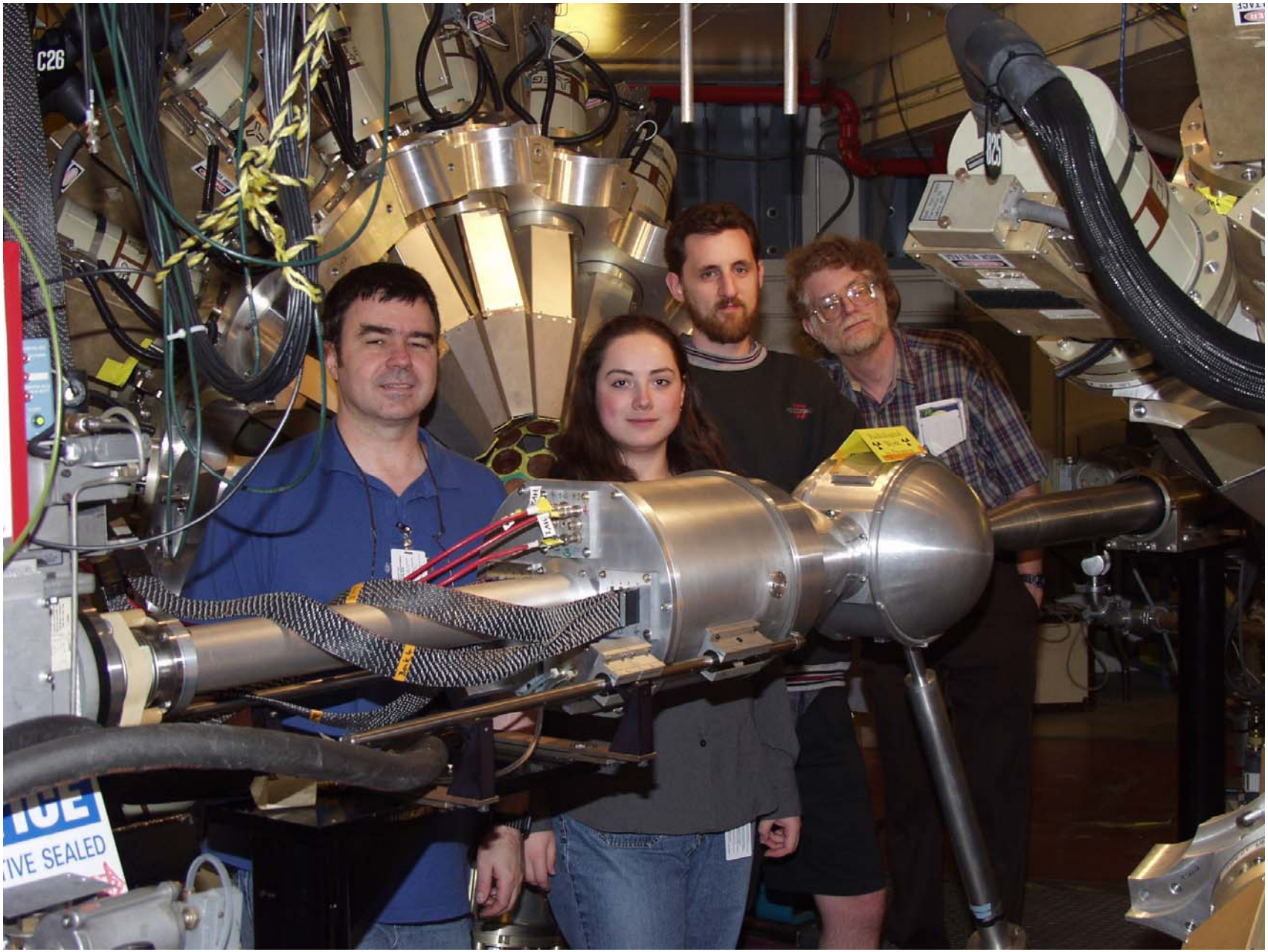
C26
IVE SEALED

Source Measurements

- **^{252}Cf: H.F. = Ba-like (Z=56), L.F. = Mo-like (Z=42)**
- **Detector thickness 0.97 to 2.5 mg/cm^2.**
  - Spin coating, uniformity ~1% !
- **Light output as a function of Z and E**
  - Source plain and with Al degrader foils from 0.25 → 2.92 mg/cm^2 : $E_{incident}$ = 82 – 6 MeV.
- **Identification of HF and LF for whole E range.**
  - Measured Pulse height and ToF at 20 cm source-detector distance
  - Use CsF γ-detector as trigger.

^{252}Cf tests

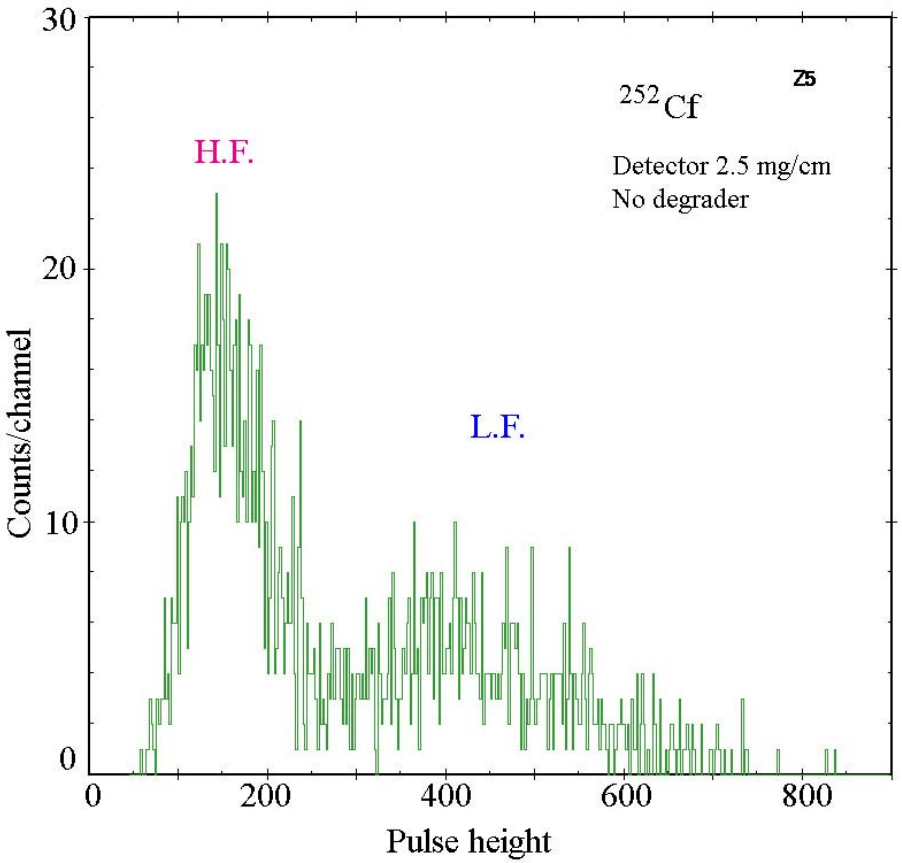

No degrader

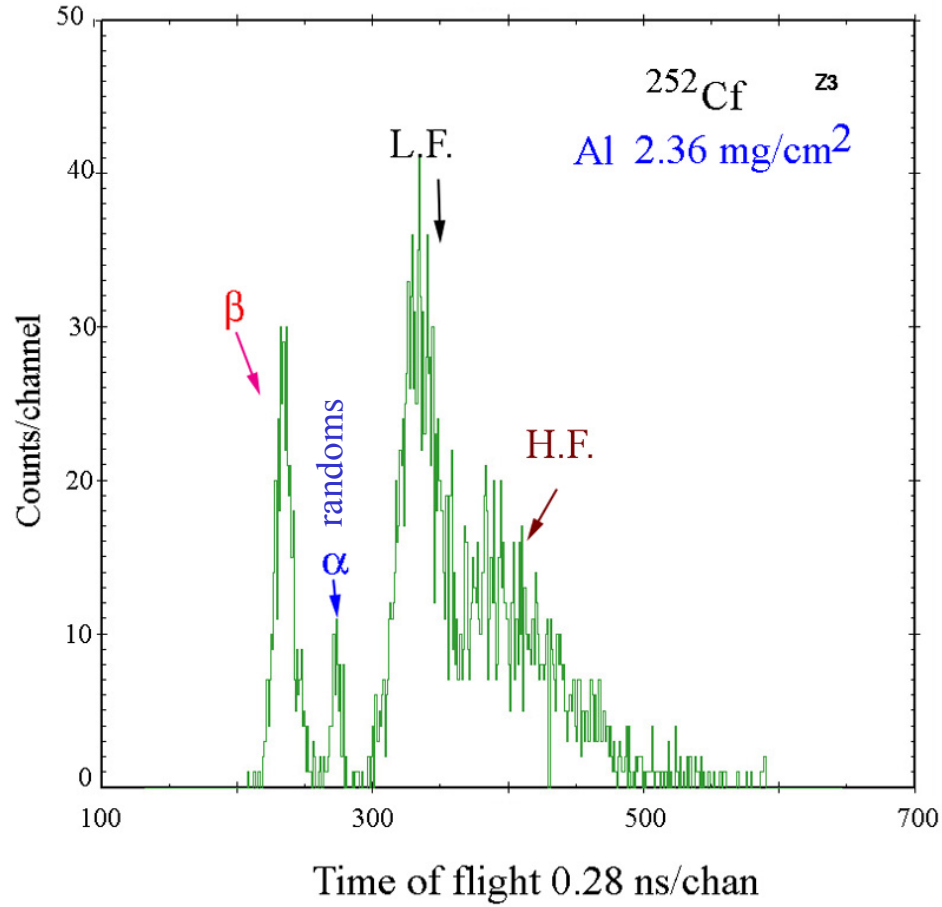

Degrader Al
2.36 mg/cm^2

Accelerator Experiments

- **Response to Heavy Evapor. Residues (6 hrs).**
  - Elastic Scattering of 160 MeV ^{197}Au on ^{197}Au (ATLAS). Prototype HERCULES detectors at angles $5^o < \Theta_{lab} < 120^o$, Si detectors at symmetric angles. See also ^{252}Cf source measurements!

- **Radiation Damage by Scattered Beam (2 d).**
  - ^{40}Ar + ^{170}Er at 210 MeV and 5 pnA (ATLAS). Prototype HERCULES detectors at 5° and 9°.

- **Test Run at Gammasphere (1 d).**
  - ^{48}Ca + ^{126}Te at 210 MeV (88-Inch). Full HERCULES device and 100 Compton-suppressed Ge detectors.

- **Commissioning Run at Gammasphere (6 d).**
  - For set up: ^{48}Ti + ^{126}Te at 230 and 238 MeV (6 hrs).
  - ^{48}Ti + ^{142}Nd at 230 and 238 MeV (88-Inch). Targets with various thicknesses. Blocked the first ring for $\theta \leq 6^o$. Trigger: γ^4.

The Commissioning Run for HERCULES at Gammasphere

A series of experiments were carried out at the 88-Inch Cyclotron at LBNL in a 6 day run:

(1) 215-MeV $^{48}Ti+^{126}Te$ (0.74 mg/cm^2 on 0.3 mg/cm^2 Au).
(2) 238-MeV $^{48}Ti+^{126}Te$ (same target).
(3) 230-MeV $^{48}Ti+^{142}Nd$ (1.1 mg/cm^2 ; 0.16, 0.48 mg/cm^2 Au).
(4) 230-MeV $^{48}Ti+^{142}Nd$ (0.46 mg/cm^2 ; 0.1, 0.37 mg/cm^2 Au).
(5) 238-MeV $^{48}Ti+^{142}Nd$ (same target).
(6) 238-MeV $^{48}Ti+^{142}Nd$ (1.0 mg/cm^2 ; 0.84 mg/cm^2 Au **target stack).**

The Setup:

HERCULES at 31 cm from the target; 5.6^o - 19.1^o coverage. **Gammasphere** with 102 detectors. Trigger: γ^4.

The nuclei of interest: $^{186}Pb+4n$ and $^{186}Tl+p3n$.

The Bass fusion cross section is ~ 180 mb and the evaporation residue (ER) cross section is ~ 1 mb. The ER's are selected by Time of Flight and Pulse Height.

$^{48}Ti+^{126}Te$ at 238 MeV
(0.74 mg/cm^2 Au backing)

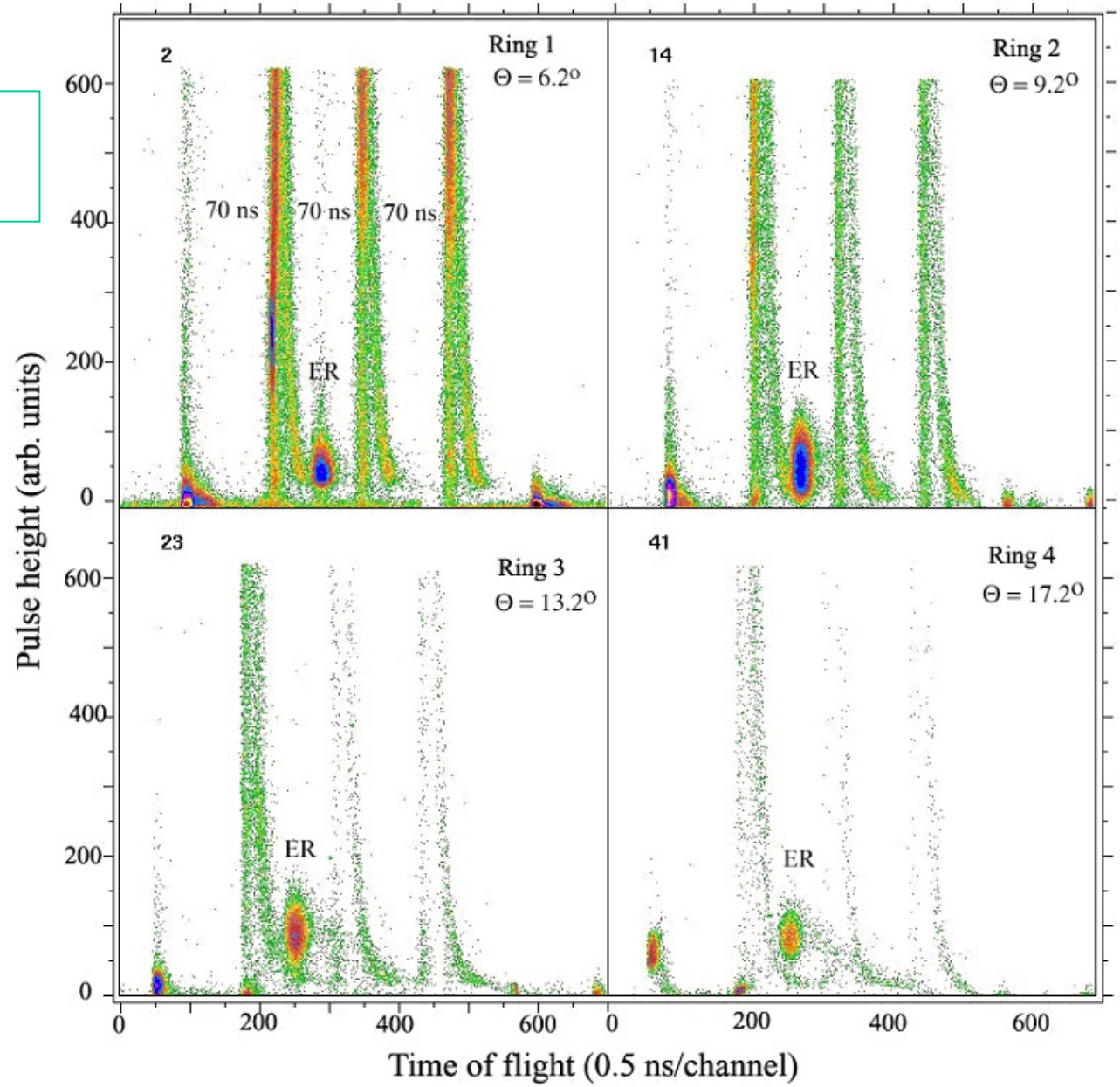

ER cross section ~100 mb

$^{48}Ti+^{142}Nd$ at 230 MeV
(0.46 mg/cm^2 Au backing)

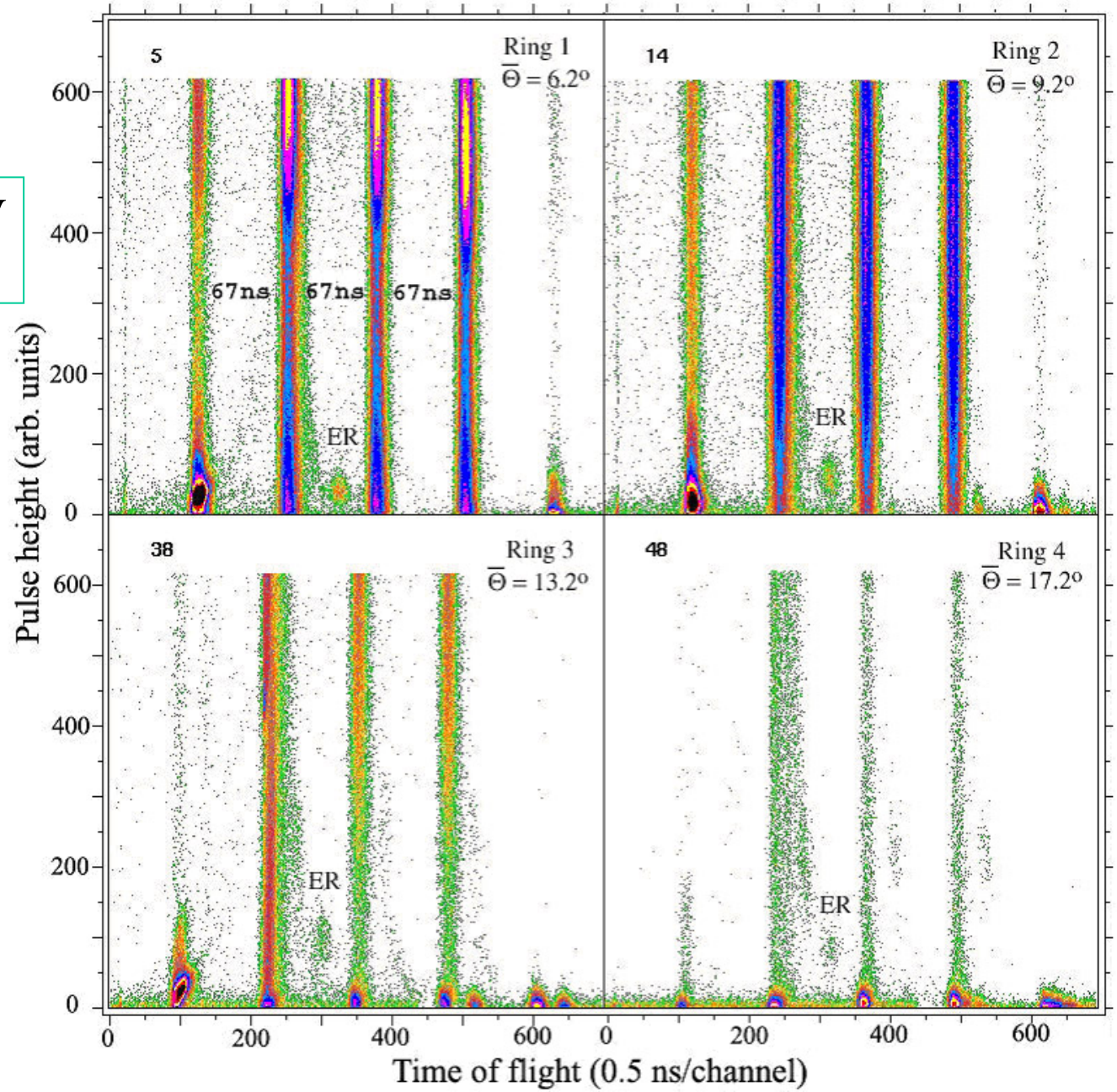

The Power of HERCULES !

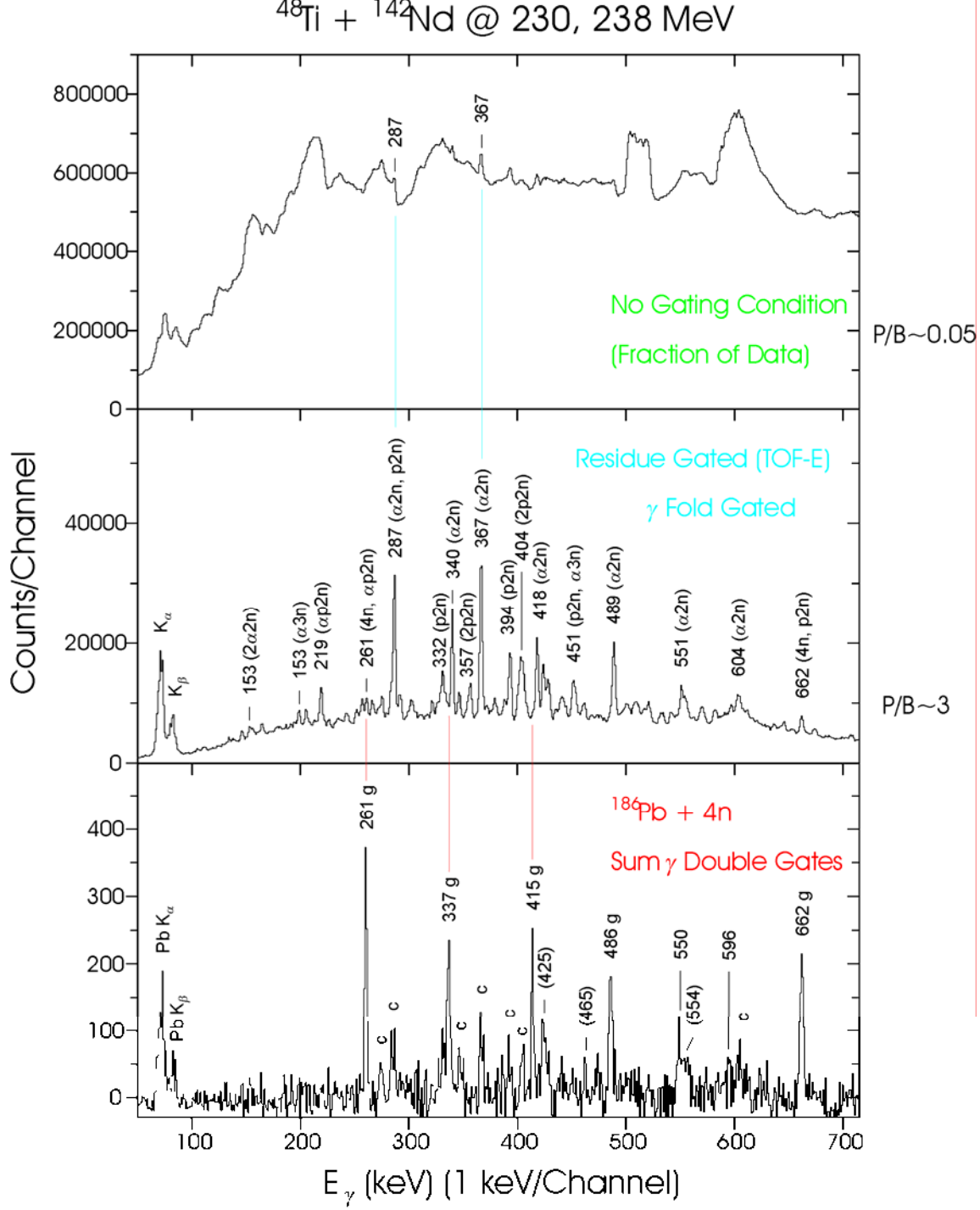

The Power of Gammasphere with HERCULES

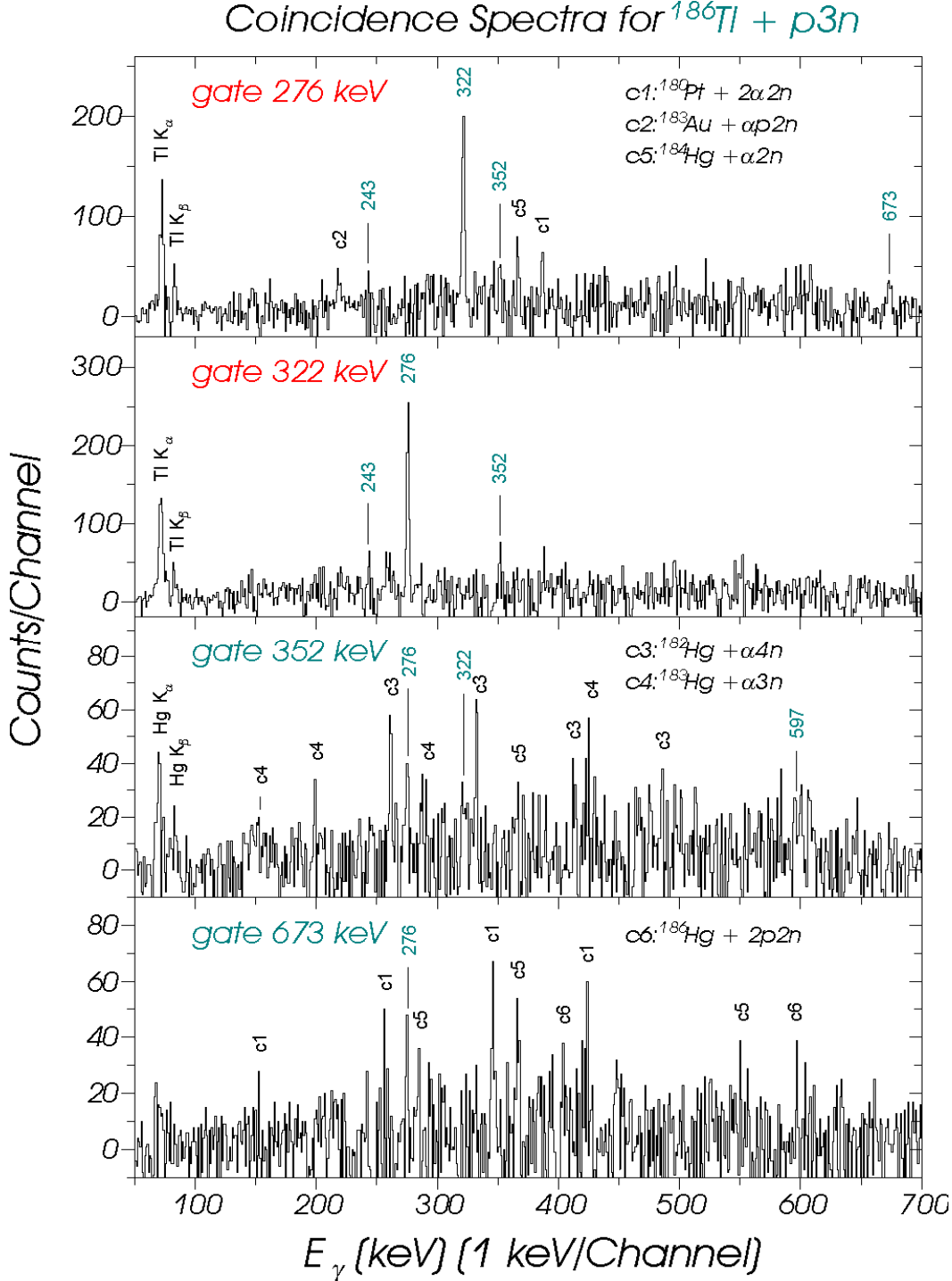

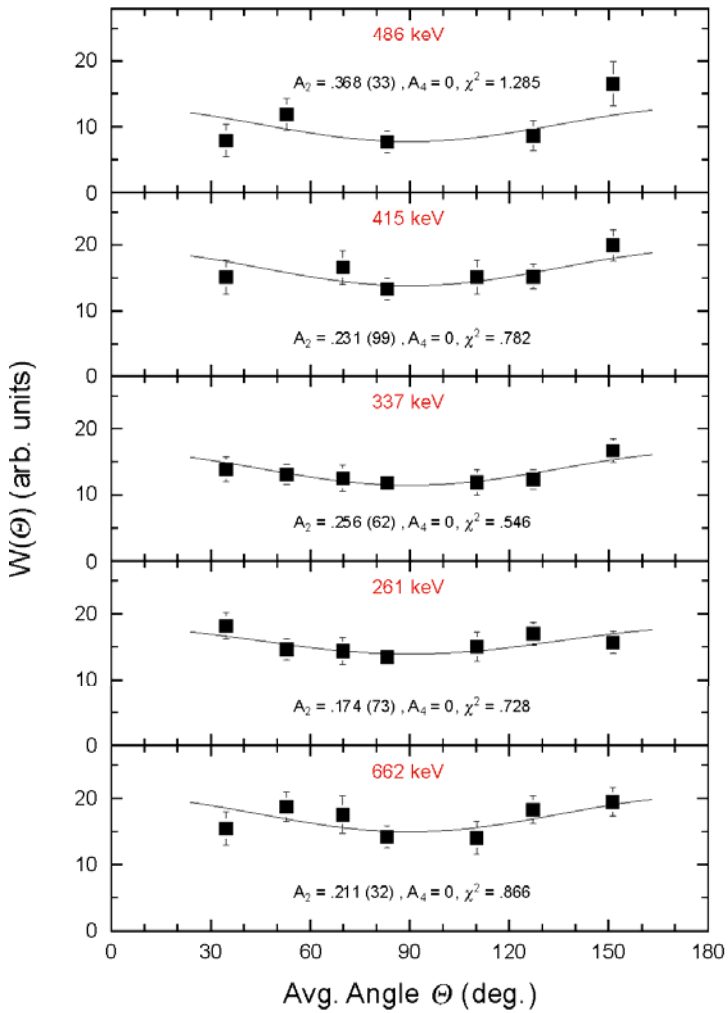
486 keV
A2 = .368 (33) , A4 = 0, χ2 = 1.285
415 keV
A2 = .231 (99) , A4 = 0, χ2 = .782
337 keV
A2 = .256 (62) , A4 = 0, χ2 = .546
261 keV
A2 = .174 (73) , A4 = 0, χ2 = .728
662 keV
A2 = .211 (32) , A4 = 0, χ2 = .866
W(Θ) (arb. units)
Avg. Angle Θ (deg.)

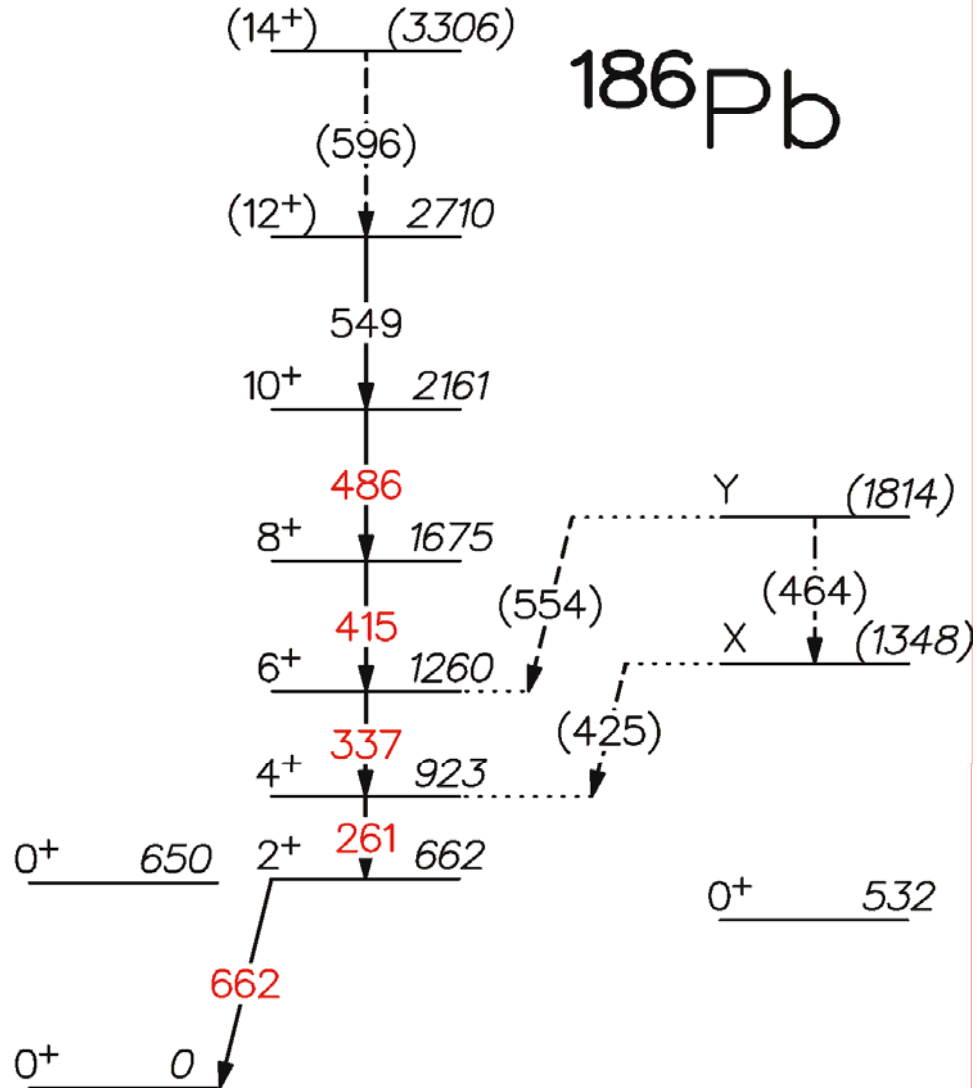
186Pb
(14+) (3306)
(596)
(12+) 2710
549
10+ 2161
486
8+ 1675
415
6+ 1260
337
4+ 923
261
2+ 662
662
0+ 0
0+ 650
0+ 532
Y (1814)
X (1348)
(554)
(464)
(425)

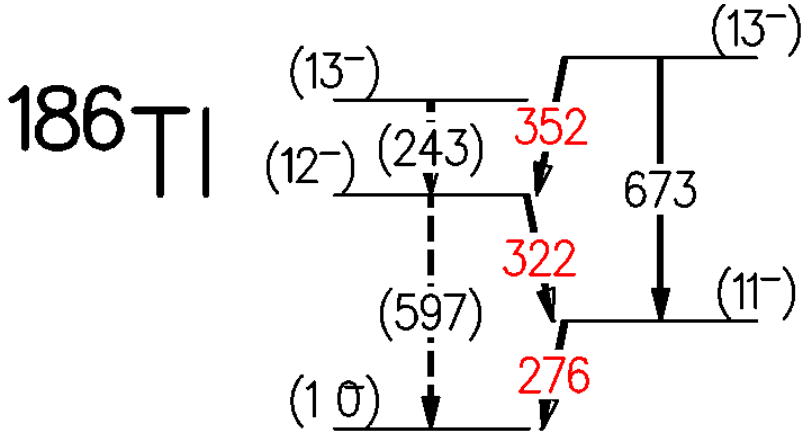

E_γ(keV)	A_2/A_0
243	-0.07 (17)
352	-0.25 (18)
322	0.02 (16)
276	-.038 (40)

Certain: multipolarities
Uncertain: bottom spin

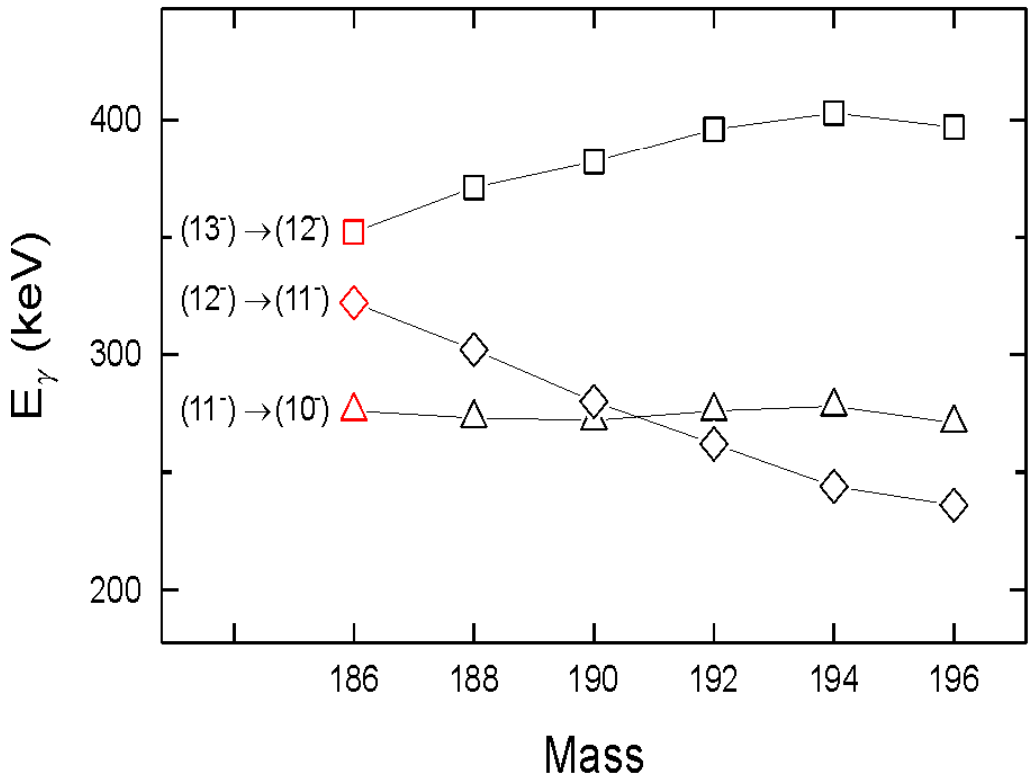

$\pi\, h_{9/2} \otimes \nu\, i_{13/2}$ (oblate)

Summary and Conclusion

- Showed that the residue detector **HERCULES** performs in experiments at **Gammasphere** as expected and presented first results from its commissioning run (^{186}Pb, ^{186}Tl).
- **^{186}Pb**: Established E2 character of prolate yrast band and saw candidate non-yrast states.
- **^{186}Tl**: Observed low-lying weakly-deformed (oblate) structure.
- For **detailed spectroscopy** in the presence of a large fission background, various, complimentary methods and setups are needed!

Contribution by

Yaron Danon

Rensselaer Polytechnic Inst.
danony@rip.edu

23 pages

Measurements with the RPI Multiplicity Detector

Rensselaer Polytechnic Institute, Troy, NY, 12180

D. Barry, R. C. Block, Y. Danon, N. Francis, M. Lubert, M. Trbovich

and

Lockheed Martin Corporation, Schenectady, NY 12301-1072

John Burke, Noel Drindak, Greg Leinweber

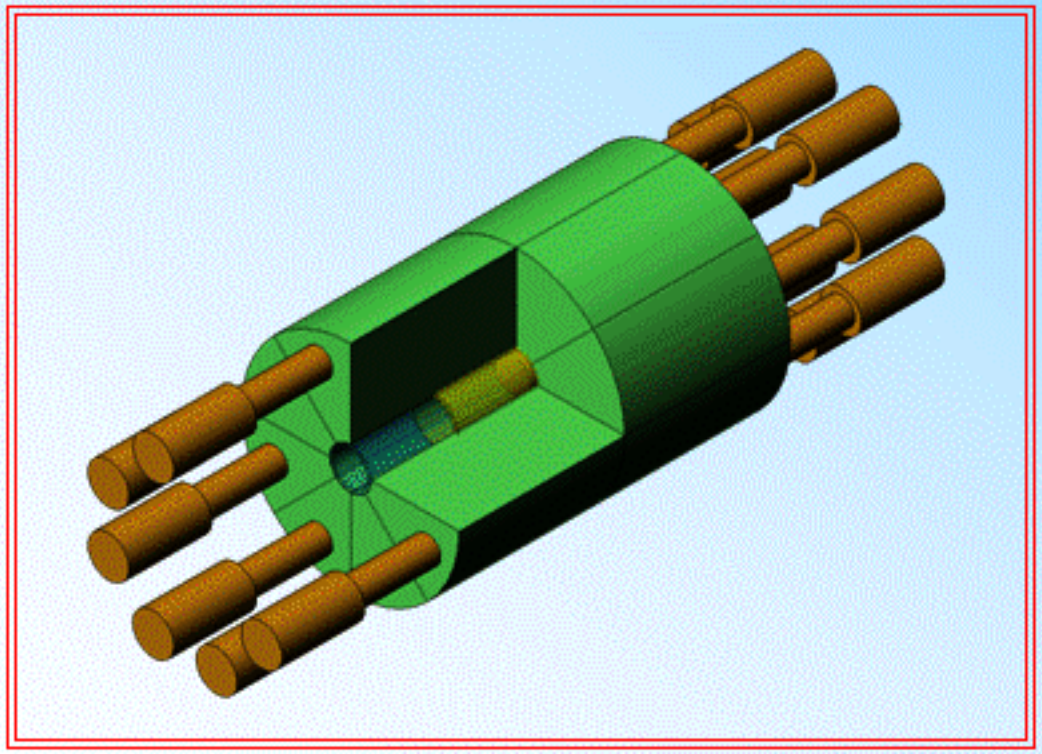

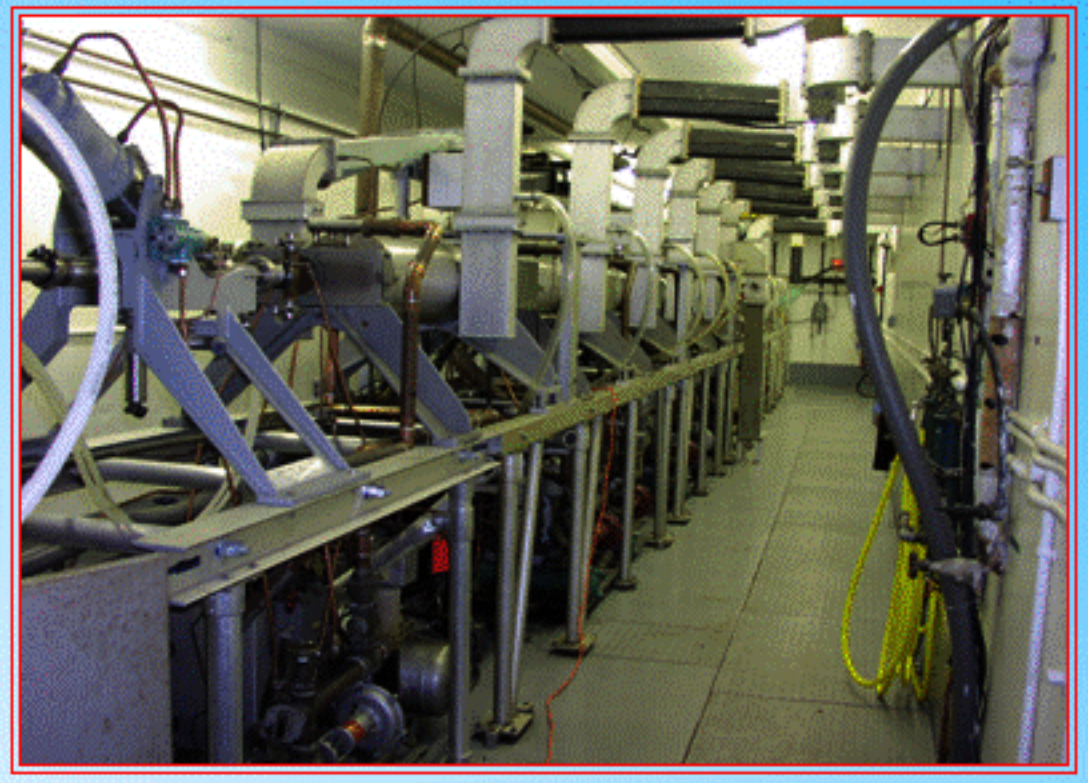

DANCE workshop February 2-4, 2004, Santa Fe, NM

Rensselaer

linac The Gaerttner Laboratory

The RPI LINAC
Gaerttner Laboratory

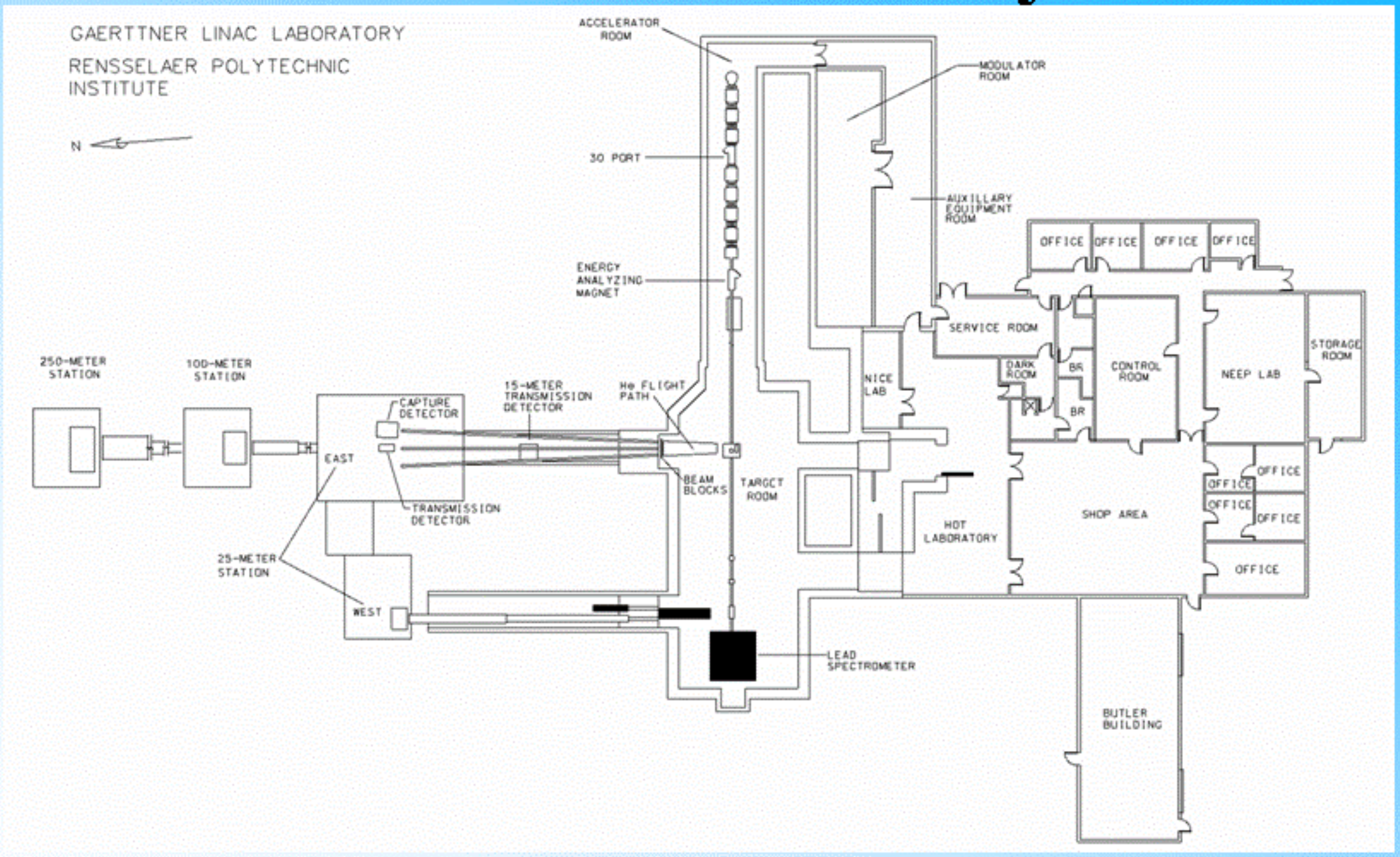

The Multiplicity Detector

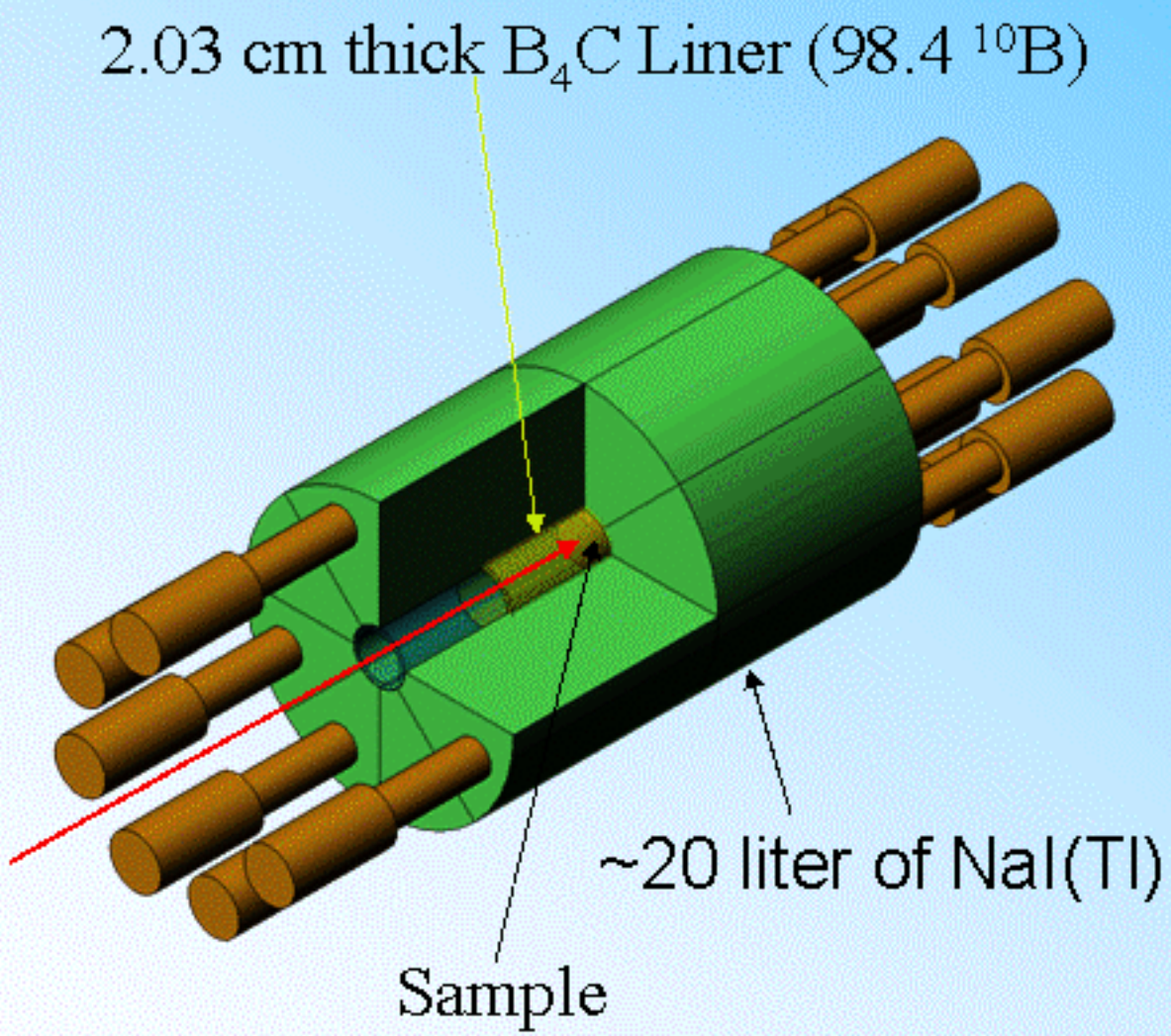

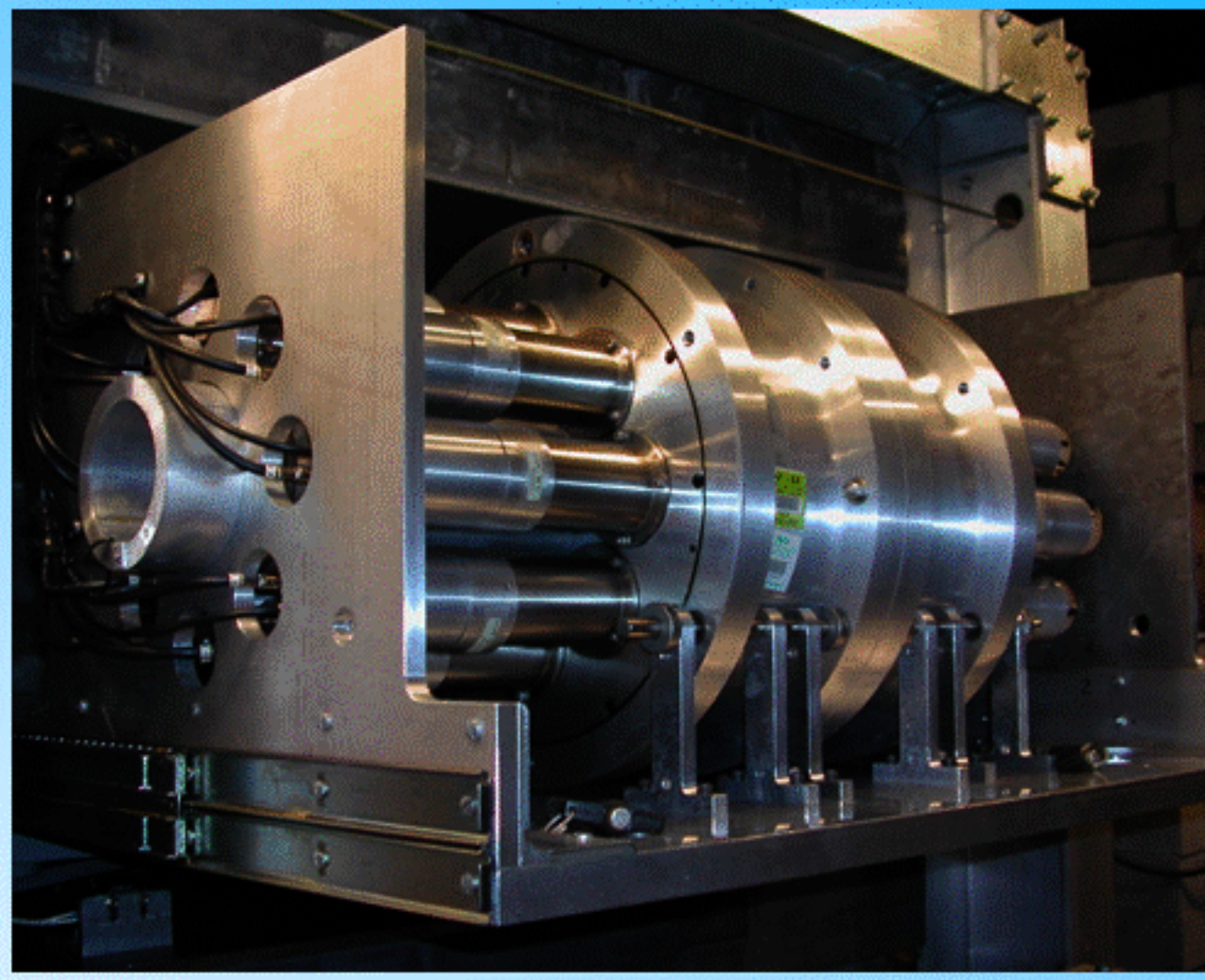

Rensselaer

linac The Gaerttner Laboratory

Electronics

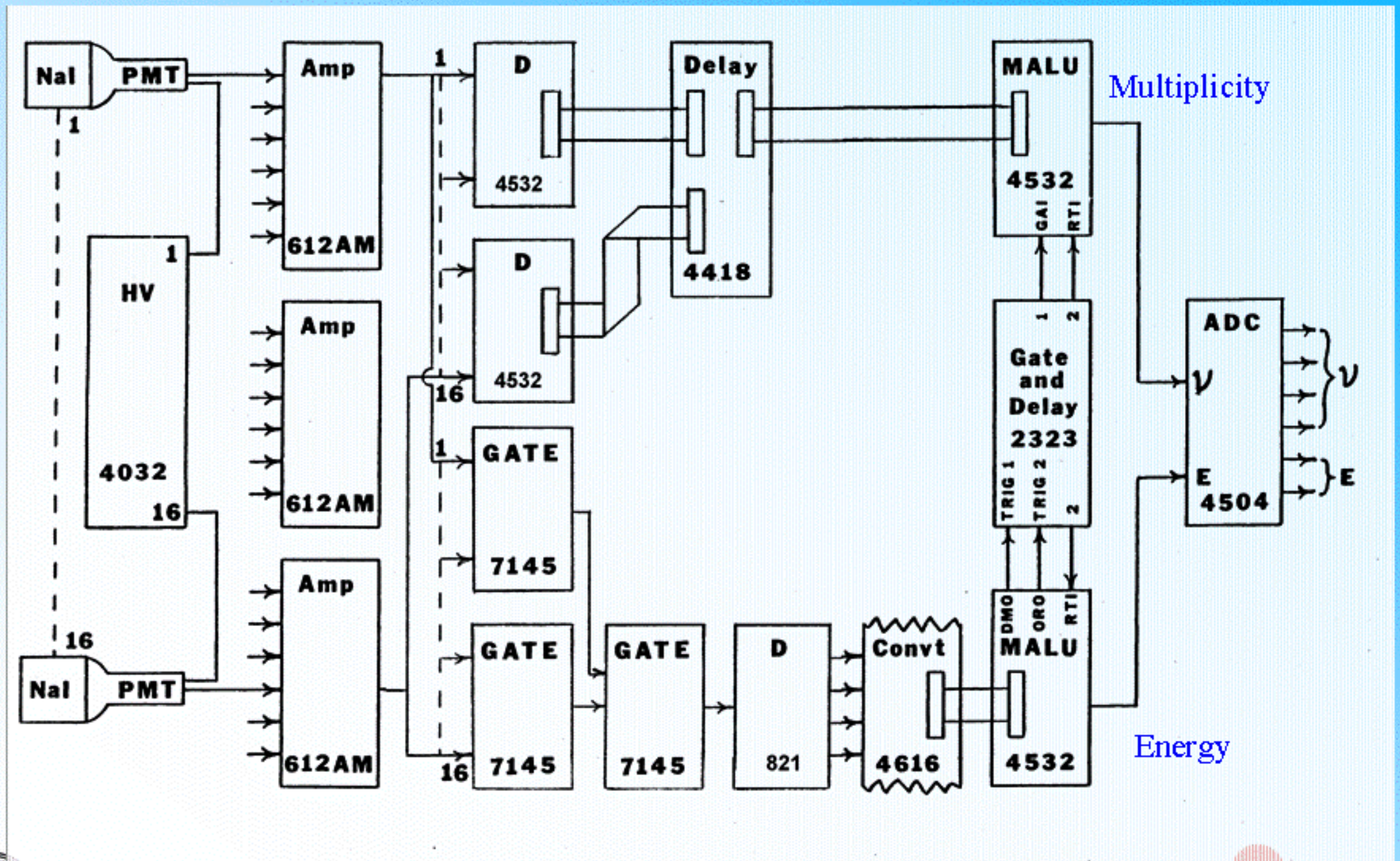

Applications

- Designed for capture cross section measurements in the energy range from 0.005 eV to 500 eV
- Neutron Scattering Measurements
- Spin-Meter – Use the multiplicity to determine resonance spins.
- Measurement of Alpha (capture to fission ratio) in U-235.

Nd Transmission and Capture

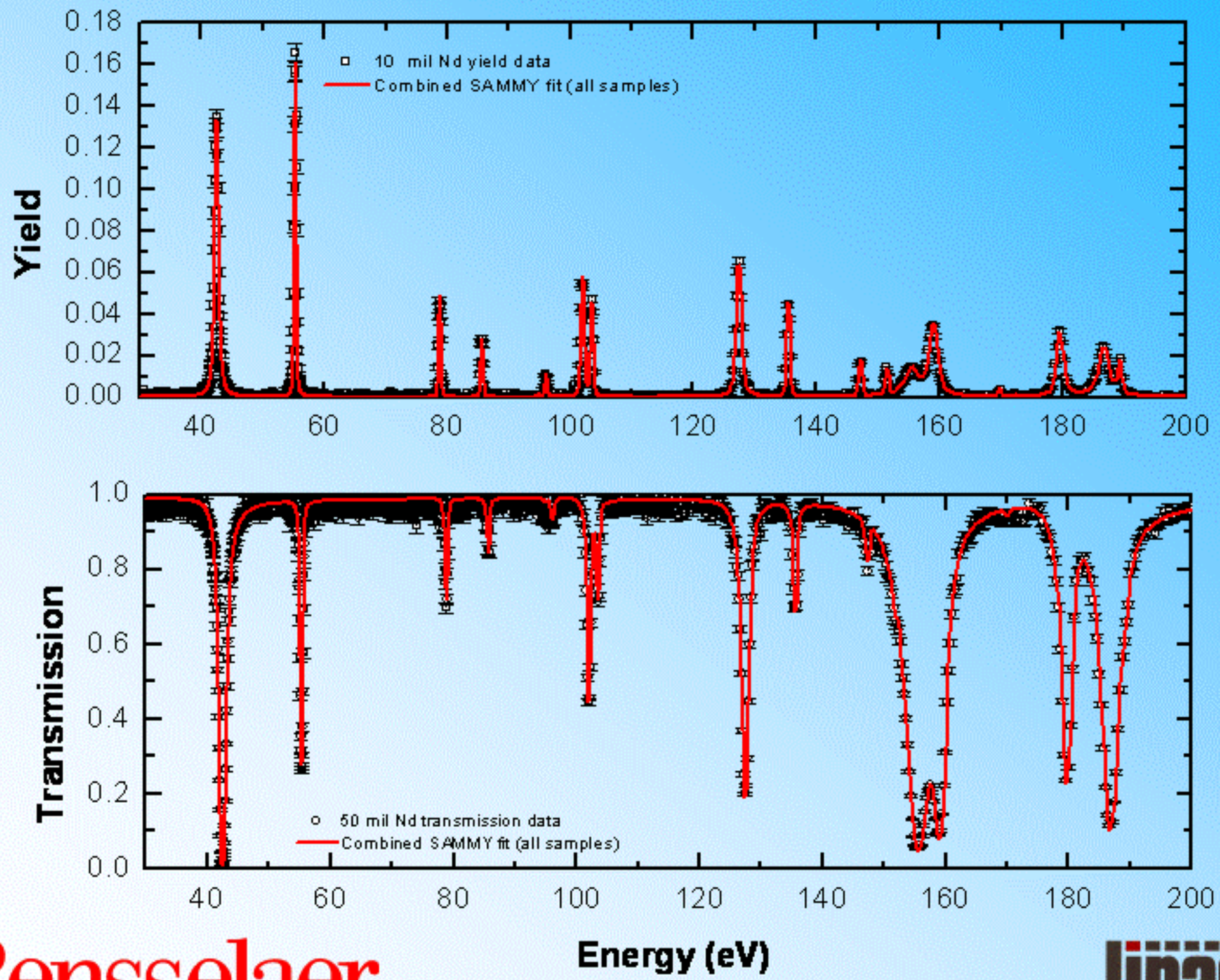

Rensselaer

linac The Gaerttner Laboratory

Cross Section Measurements

Hf Epithermal Data

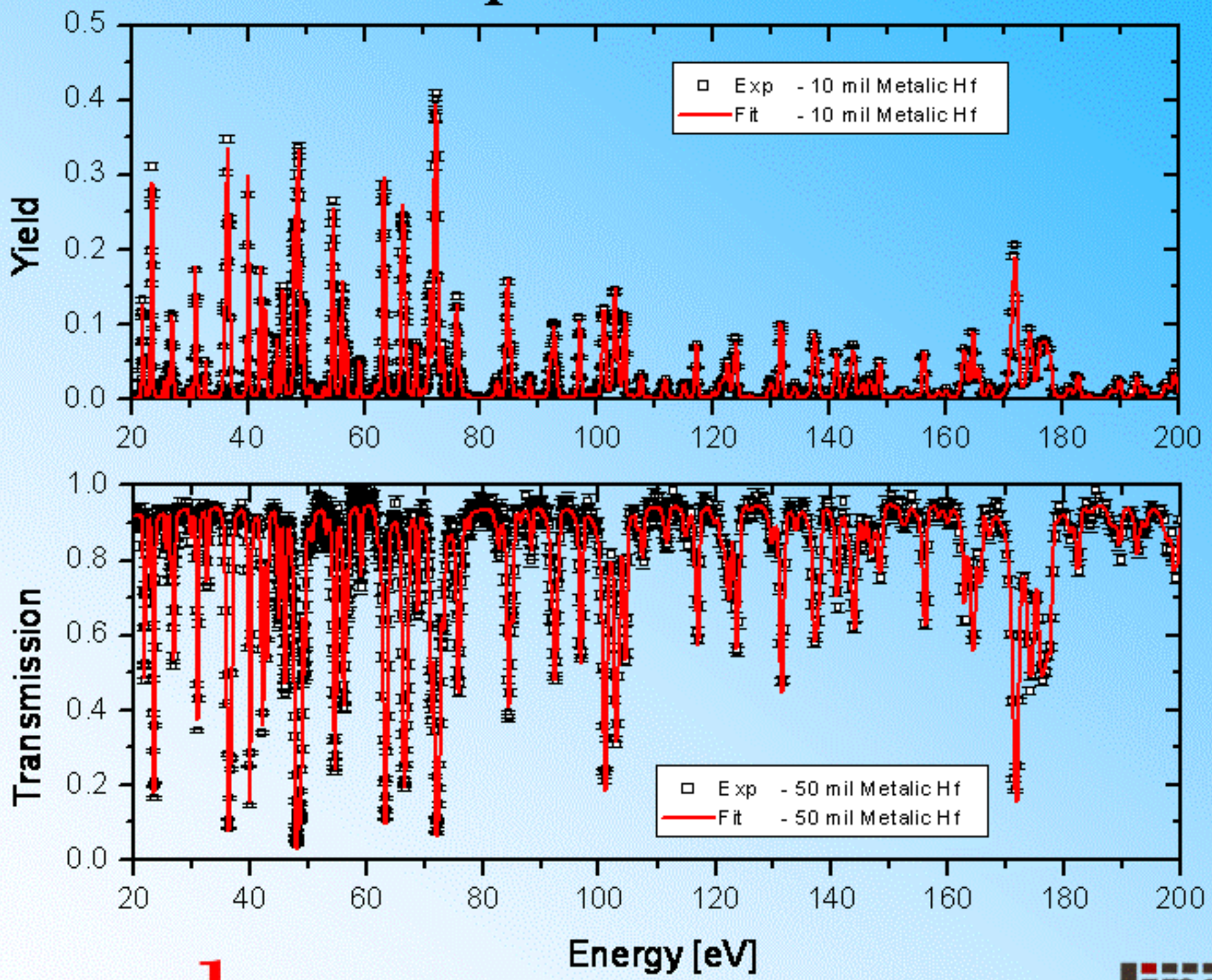

Rensselaer

linac The Gaerttner Laboratory

Cross Section Measurements

Hf Transmission and Capture Yield 95-115 eV

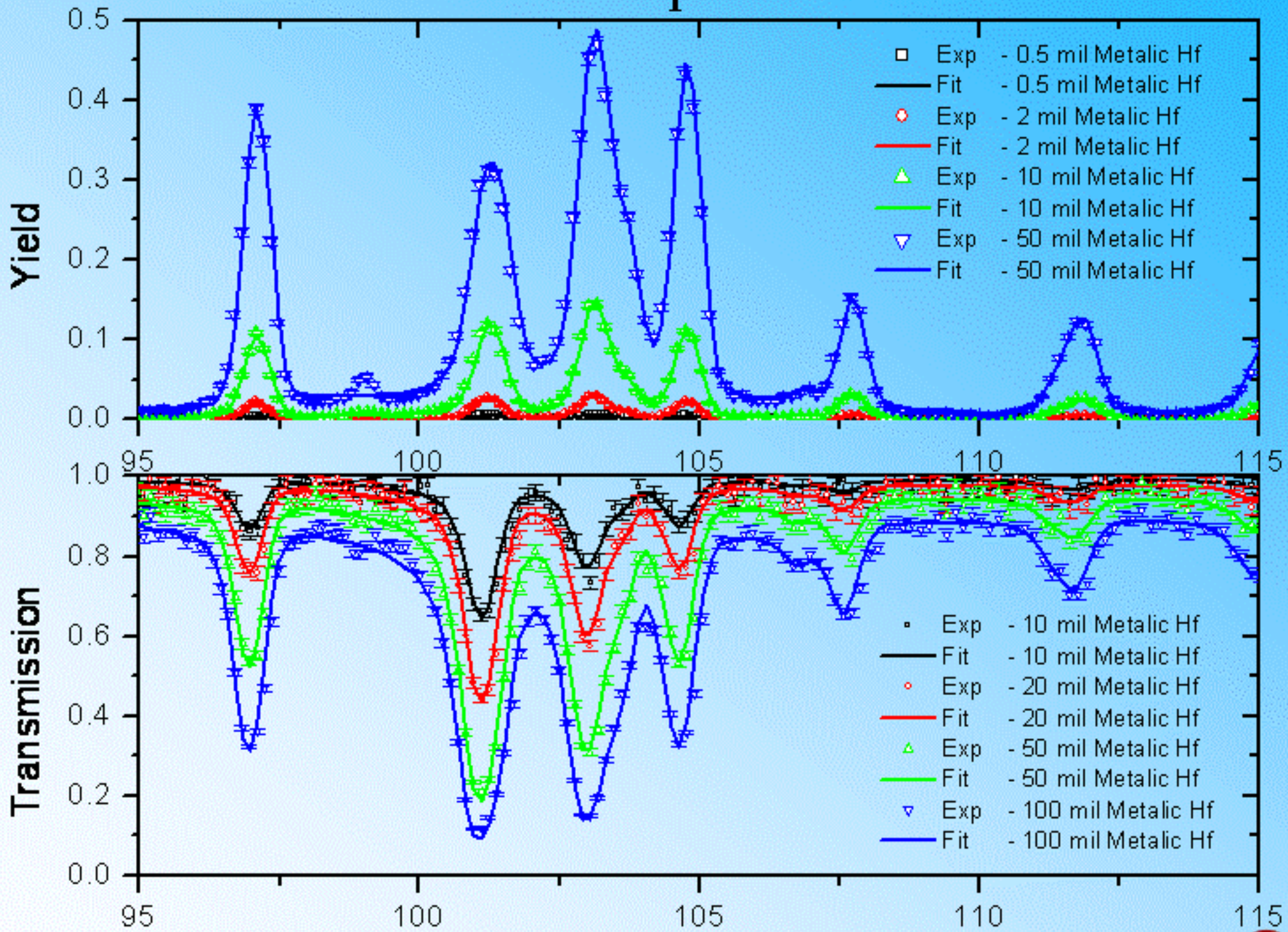

Rensselaer

linac The Gaerttner Laboratory

Cross Section Measurements

Hf Thermal Data and fits

Metallic Samples

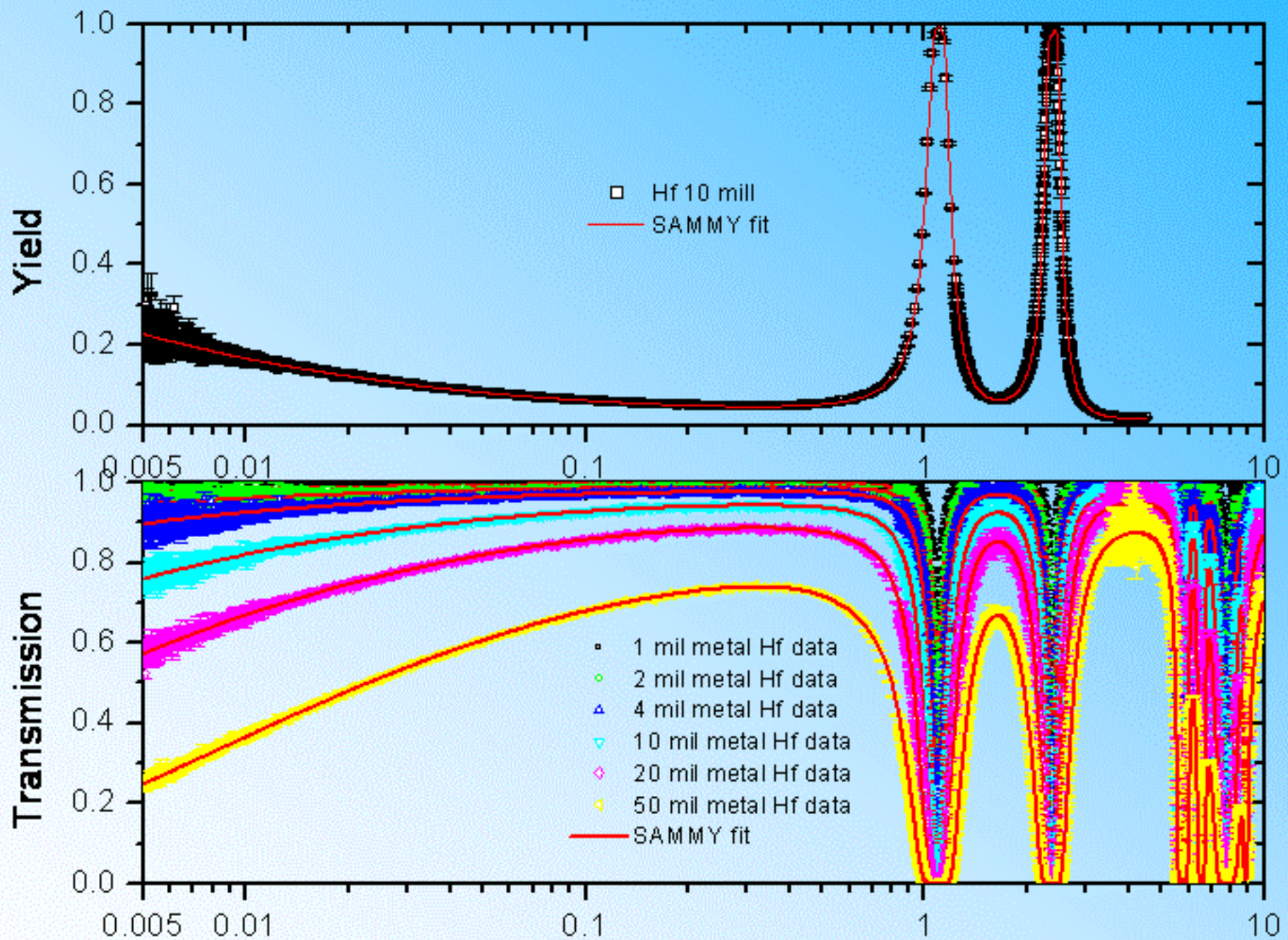

Rensselaer

linac The Gaerttner Laboratory

Observed Multiplicity Calculations

S. Wang, M. Lubert, Y. Danon, N. C. Francis, R. C. Block, F. Becvar, M. Krticka, *The RPI multiplicity detector response to γ-ray cascades following neutron capture in ^{149}Sm and ^{150}Sm*, Nuclear Instruments and Methods A 513/3 pp. 585-595, 2003

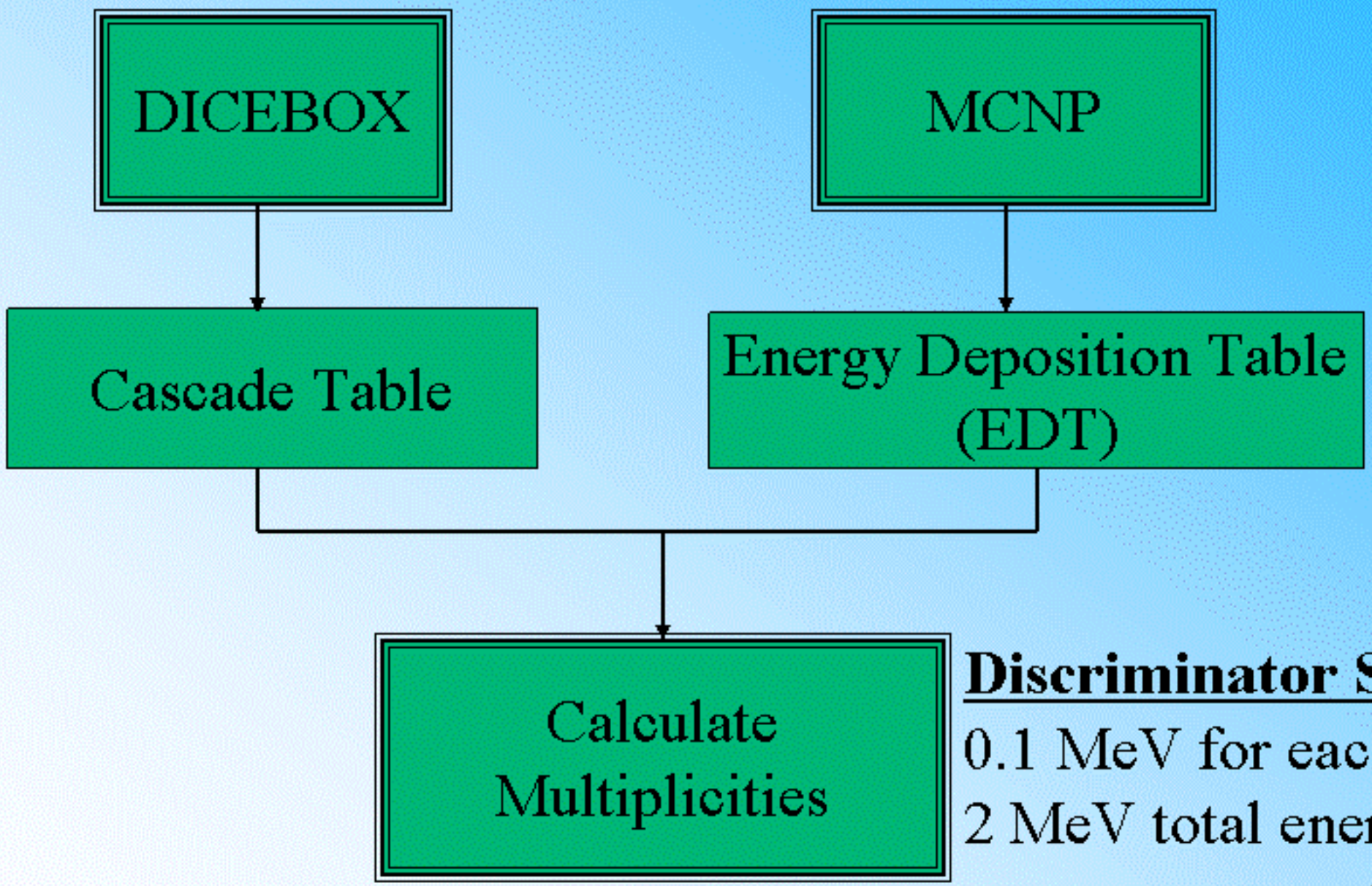

Discriminator Settings

0.1 MeV for each segment

2 MeV total energy

Comparison of Measured and Calculated Multiplicities for ^{149}Sm

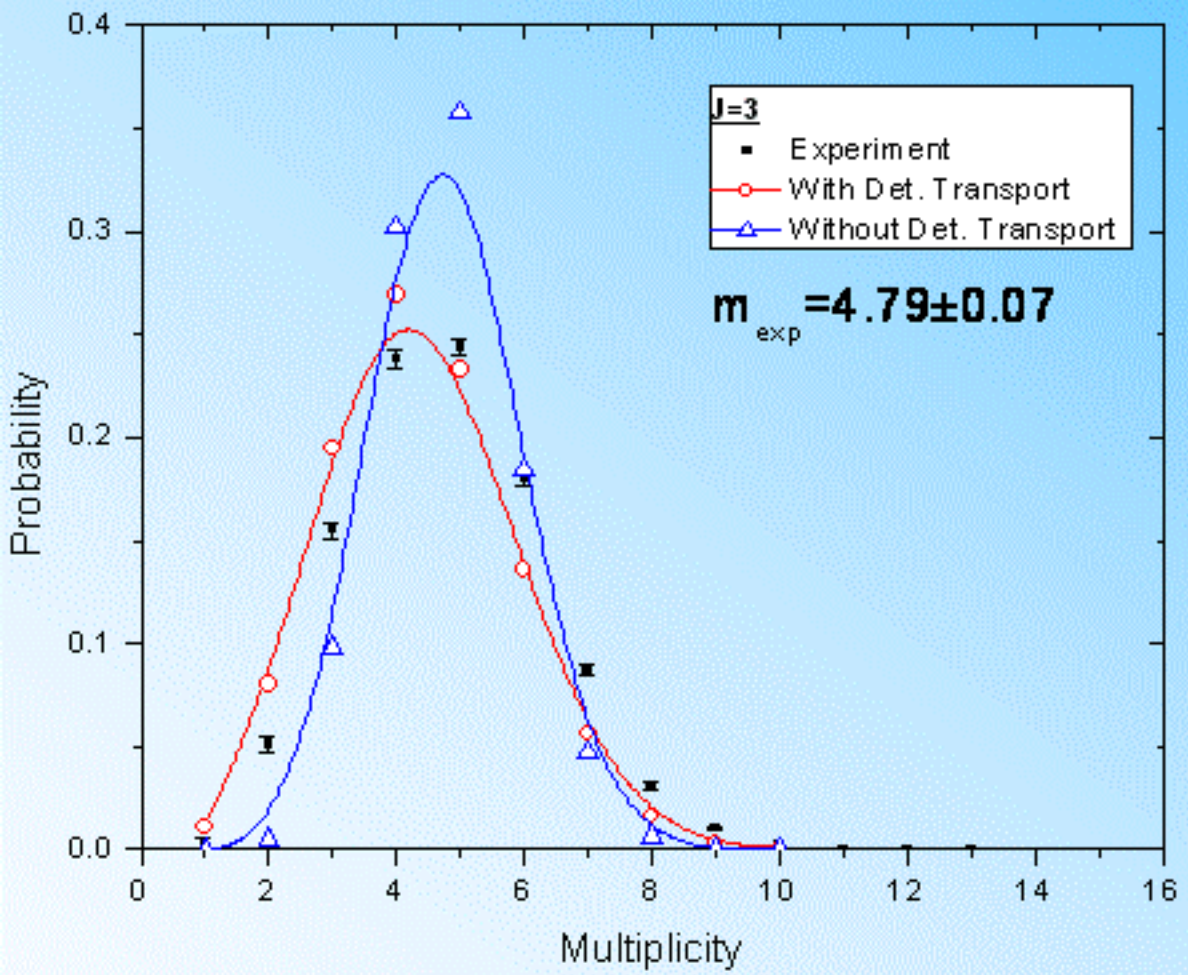

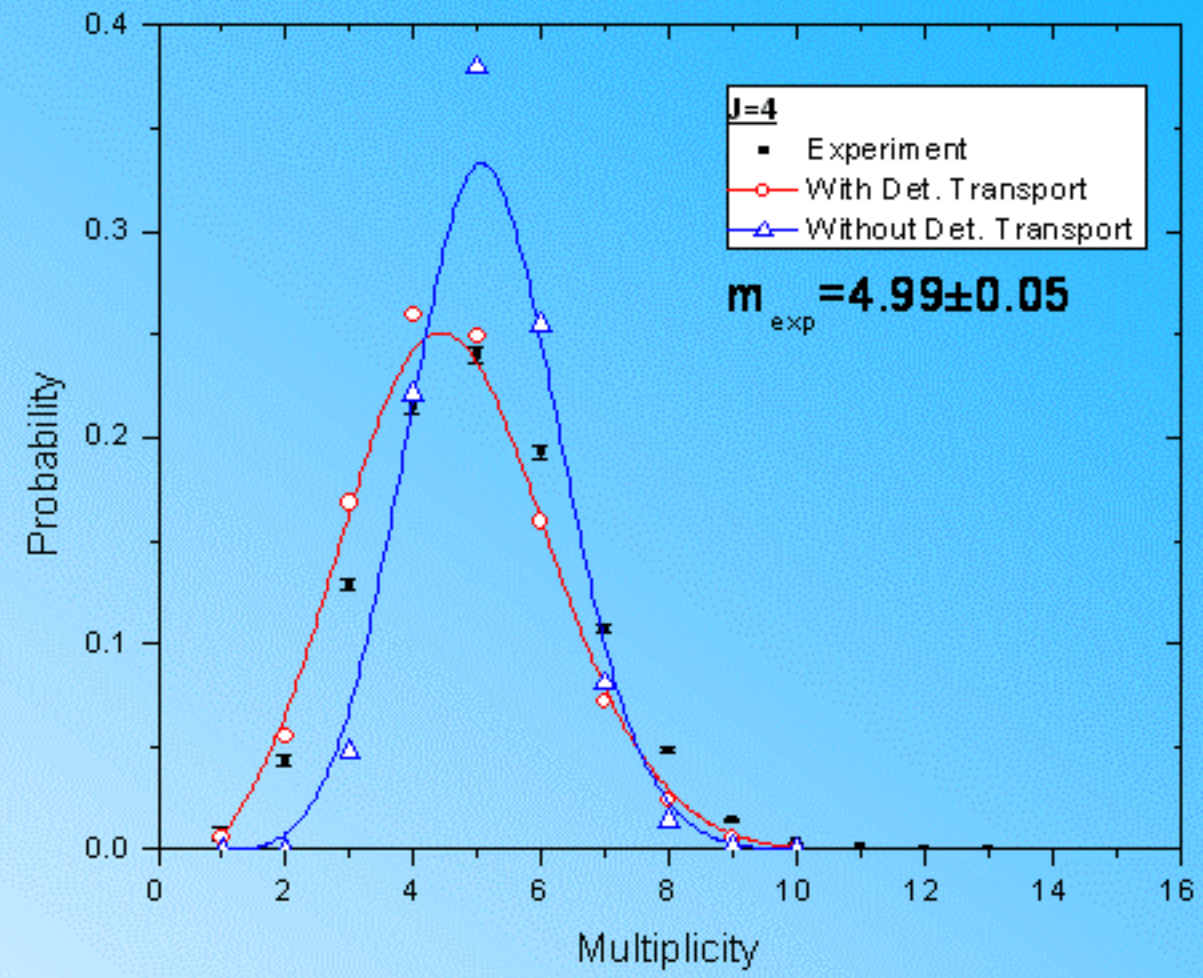

Table 1
The detector efficiency η of the RPI system and values of the parameters M and σ

Target	B_n (keV)	J^π	DICEBOX		DICEBOX/MCNP(4C)			Measured	
			M	σ	M	σ	η (%)	M	σ
^{149}Sm	7986	3^-	4.79[a]	1.07[a]	4.37	1.70	96.4±0.1	4.79±0.07	1.52
		4^-	5.20[b]	1.09[b]	4.66	1.70	96.7±0.1	4.99±0.05	1.62
^{150}Sm	5597	$1/2^+$	4.19[c]	1.10[c]	3.19	1.73	87.3±0.1	3.64±0.04	1.32

Rensselaer

linac The Gaerttner Laboratory

Spin Meter

- To find the spin, calculate the ratios S_i and $Snorm_i$ from the multiplicity spectra of each resonance.

$$S_i = \frac{\sum_{m=7}^{16} s_{i,m}}{\sum_{m=1}^{6} s_{i,m}} \qquad Snorm_i = 4\frac{S_i}{S_1}$$

Where

S_i – is the calculated ratio for resonance *i*

$s_{i,m}$ – is the multiplicity summed over *m* for resonance *i*

$Snorm_i$ – is the normalized multiplicity.

Spin Meter Plots for ^{149}Sm

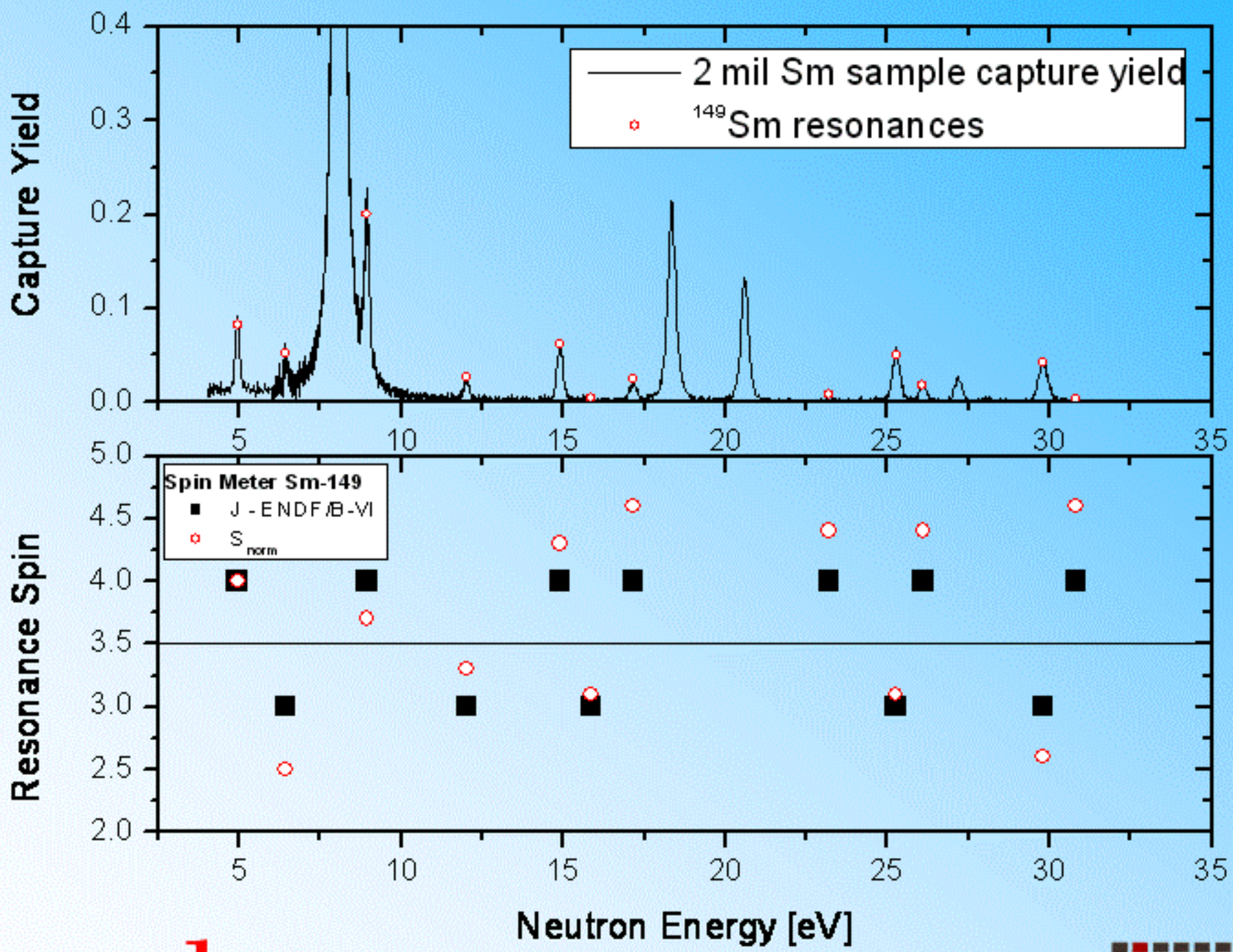

Rensselaer

linac The Gaerttner Laboratory

Spin Meter Plots for ^{147}Sm

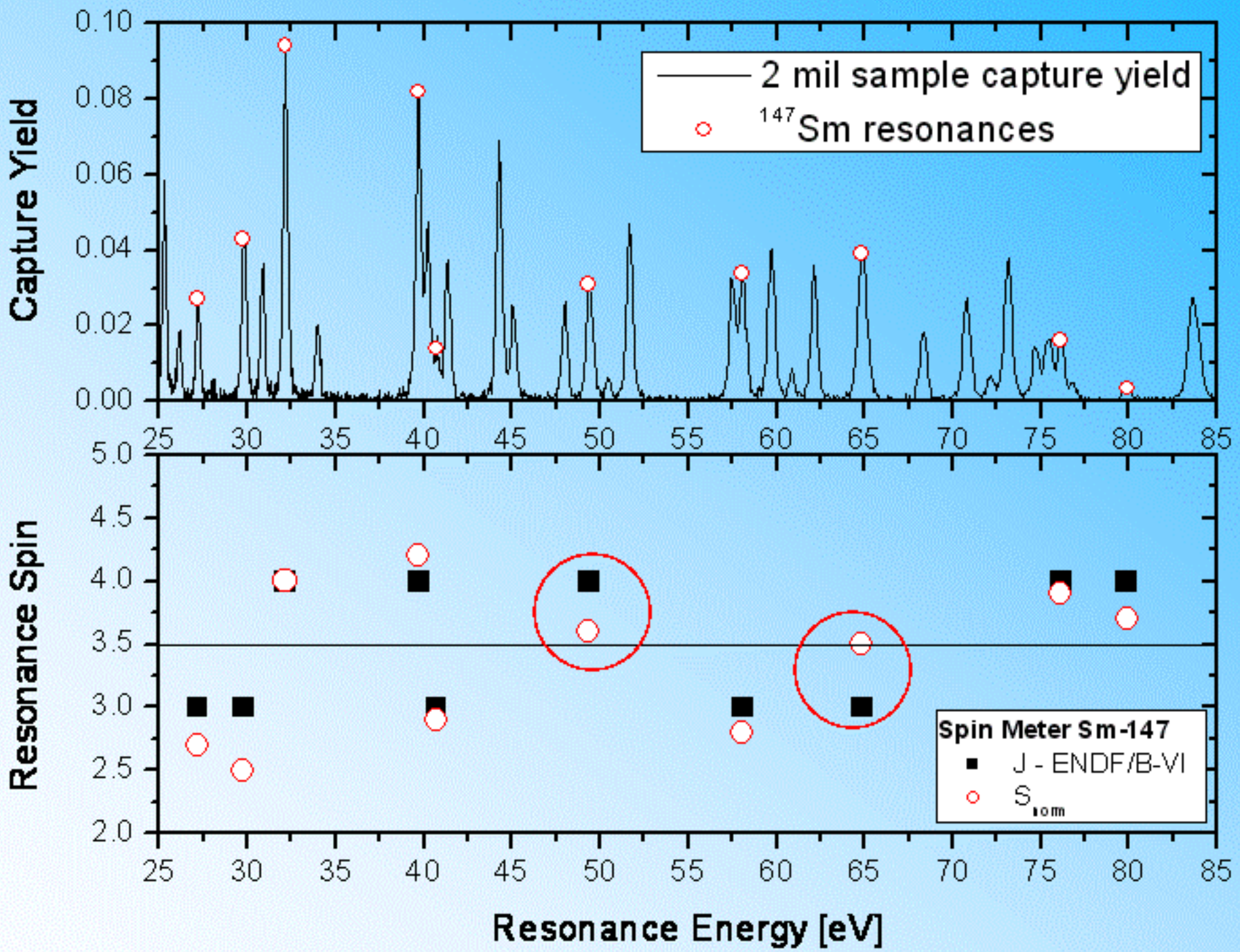

Rensselaer

linac The Gaerttner Laboratory

Alpha Measurement for U-235

- Alpha is the capture to fission ratio $\alpha(E) = \frac{\sigma_\gamma(E)}{\sigma_f(E)}$
- Two ways to measure
  - Use the difference in multiplicity and total energy.
  - Use coincidence (or anti) with a fission chamber.
- We are interested in the low energy region from 0.01 eV to 500 eV.

Gamma Emission From Fission

- Literature suggests (Valentine, 2001).

Isotope	$\bar{N}$	$\bar{E}$ [MeV]
^{235}U	6.51-7.45	0.96-1.06
^{252}Cf	7.5-10	0.85-0.96

$\bar{E}$ is the average gamma energy

$\bar{N}$ is the average number of gammas

For Capture $\bar{N} \approx 4, \quad \bar{E} \approx 1-2\,\text{MeV}$

Detector Multiplicity Response

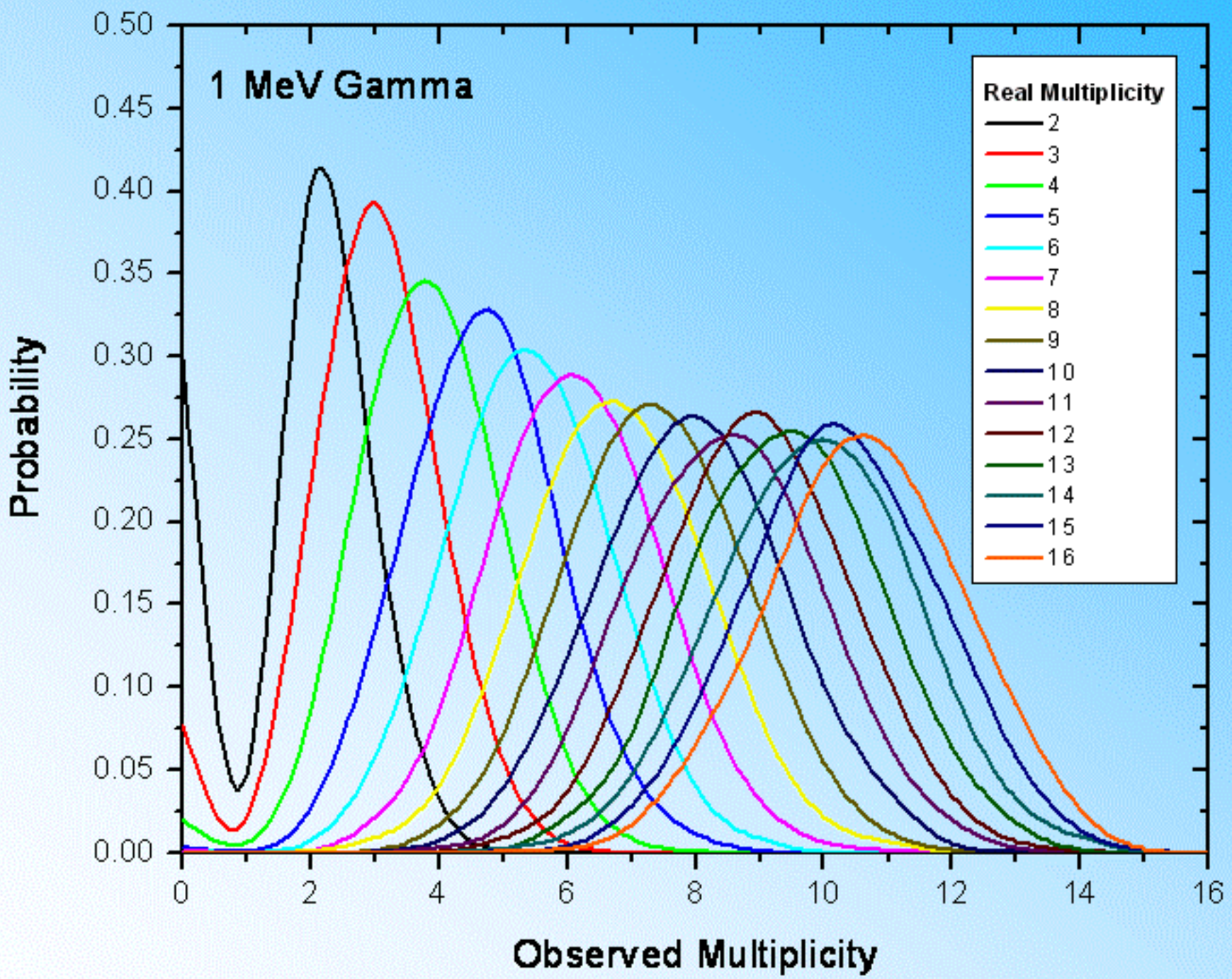

Discriminators

- 0.1 Mev each Segment
- 2 MeV total energy

Rensselaer

linac The Gaerttner Laboratory

Detector Multiplicity Response

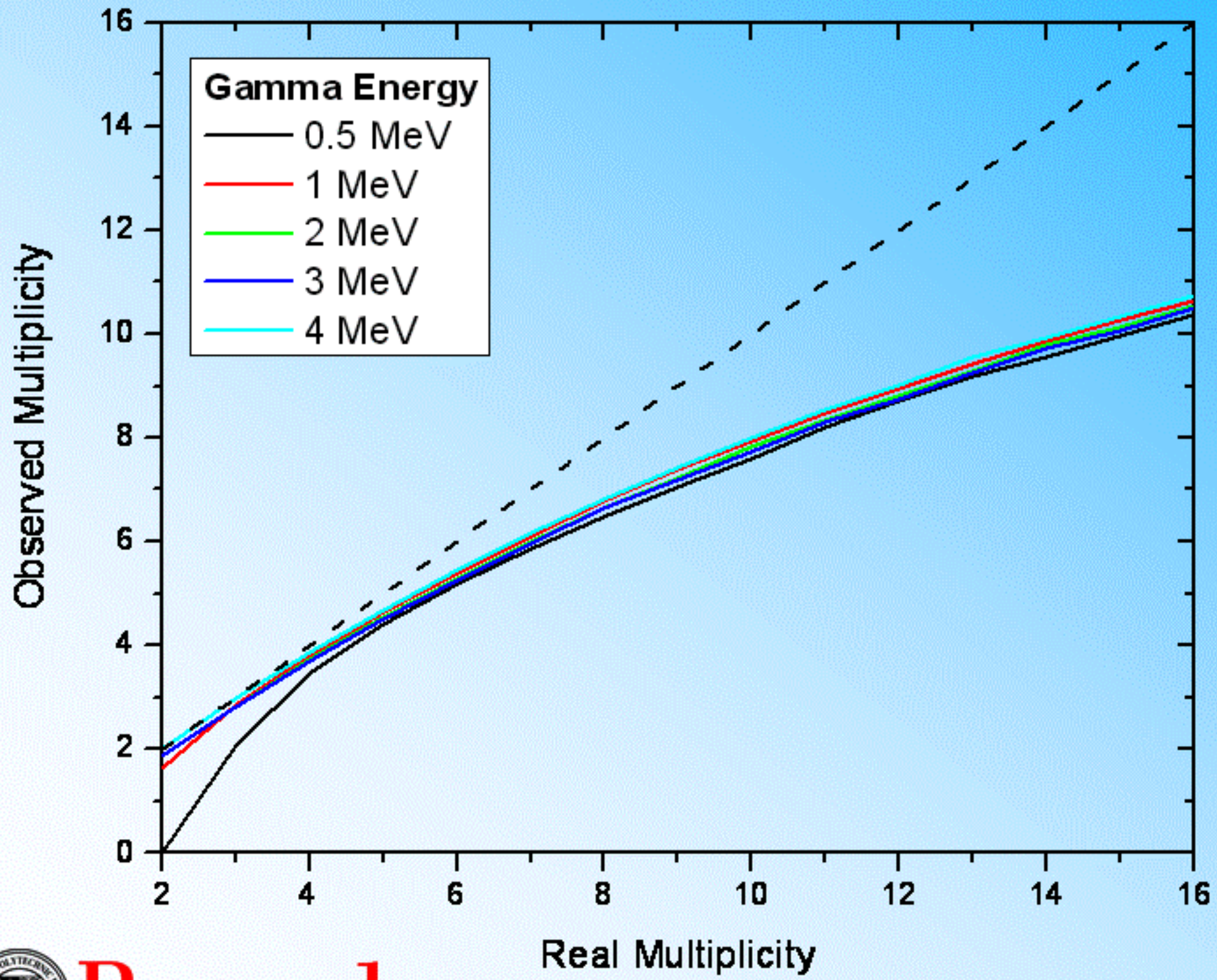

Discriminators
- 0.1 Mev each Segment
- 2 MeV total energy

Rensselaer

linac The Gaerttner Laboratory

Detector Efficiency

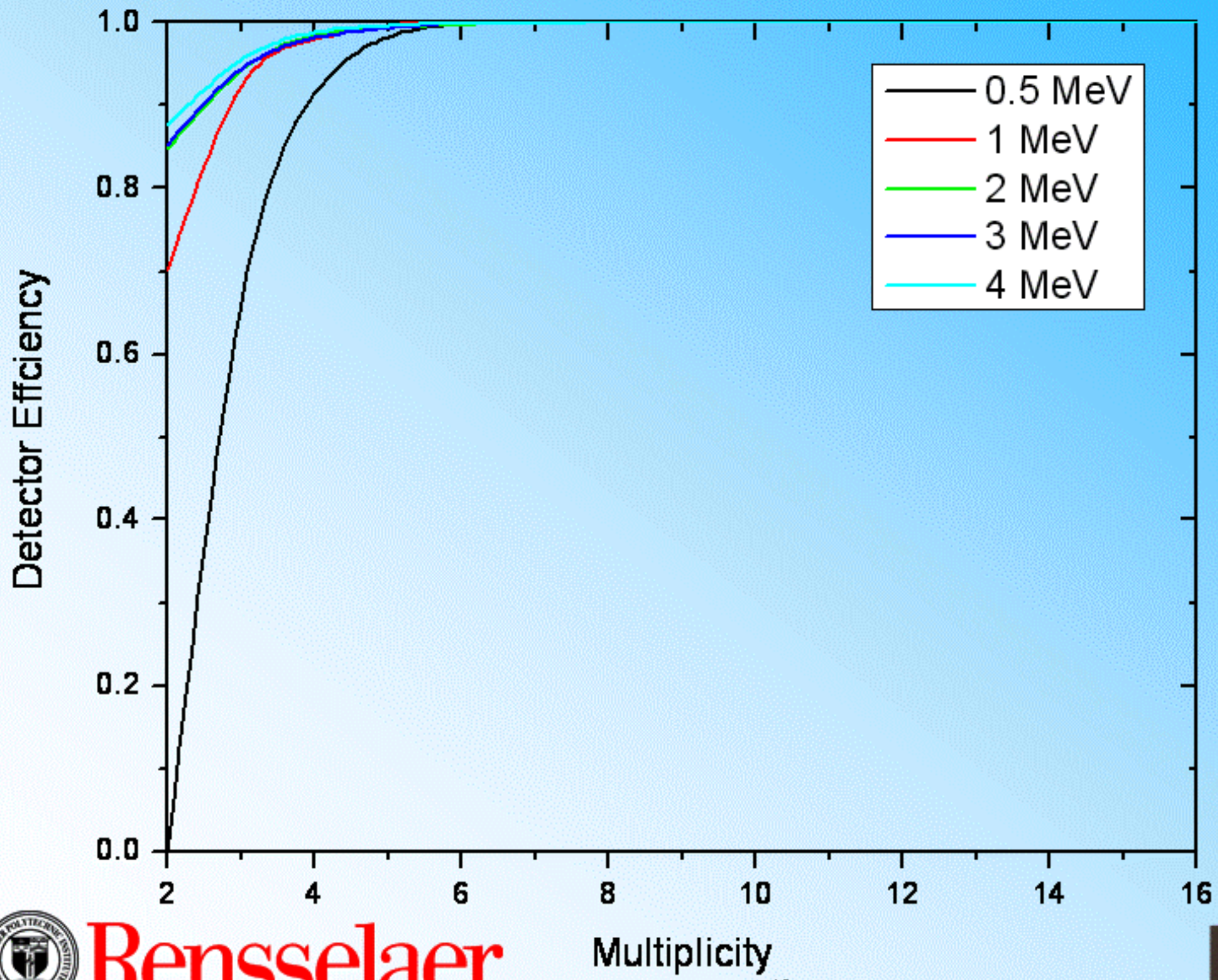

Discriminators
- 0.1 Mev each Segment
- 2 MeV total energy

Rensselaer

linac The Gaerttner Laboratory

Fission Multiplicity Measurements

Test Geometry

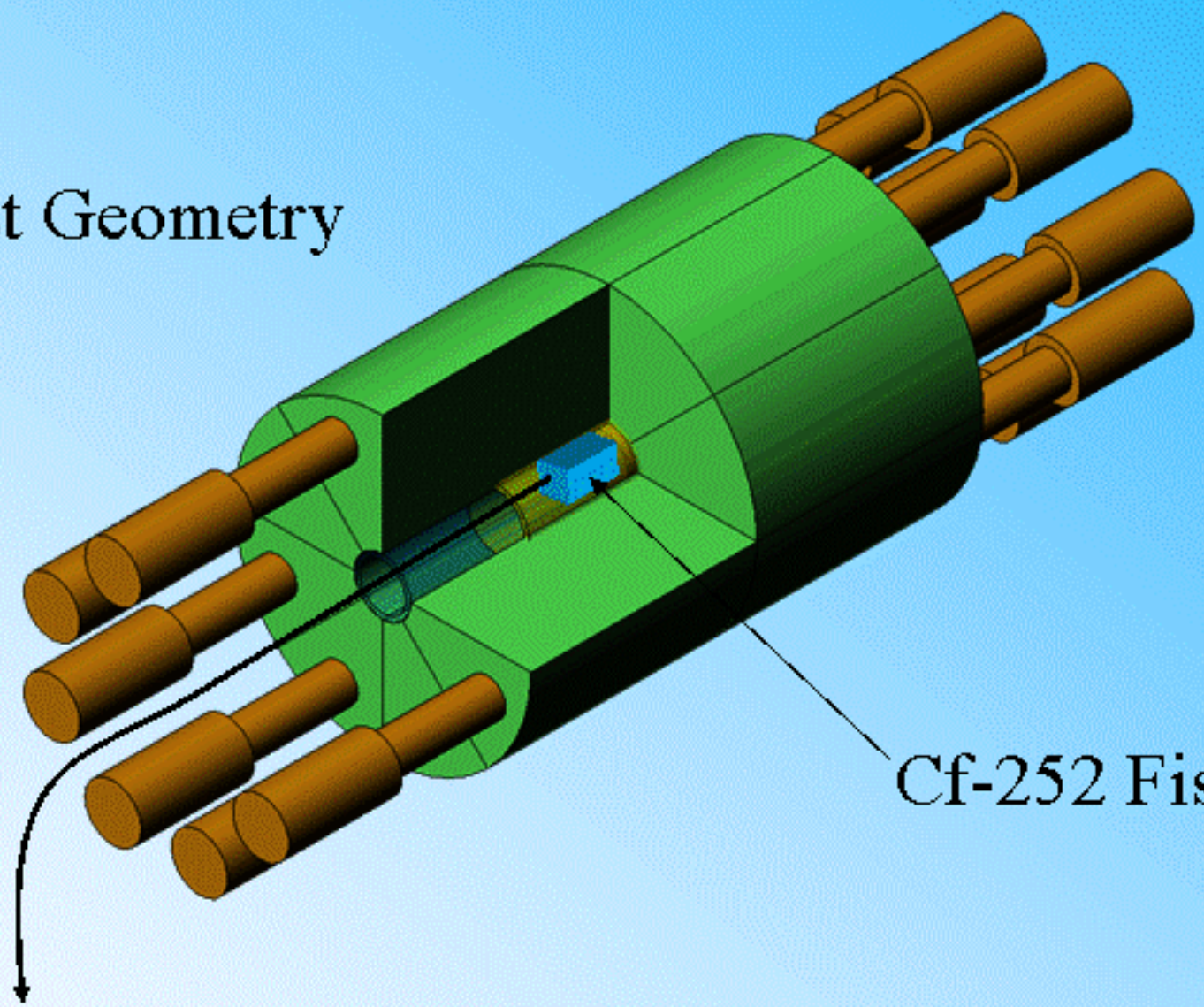

Cf-252 Fission Chamber

Coincidence with the capture detectors

Measurements Results

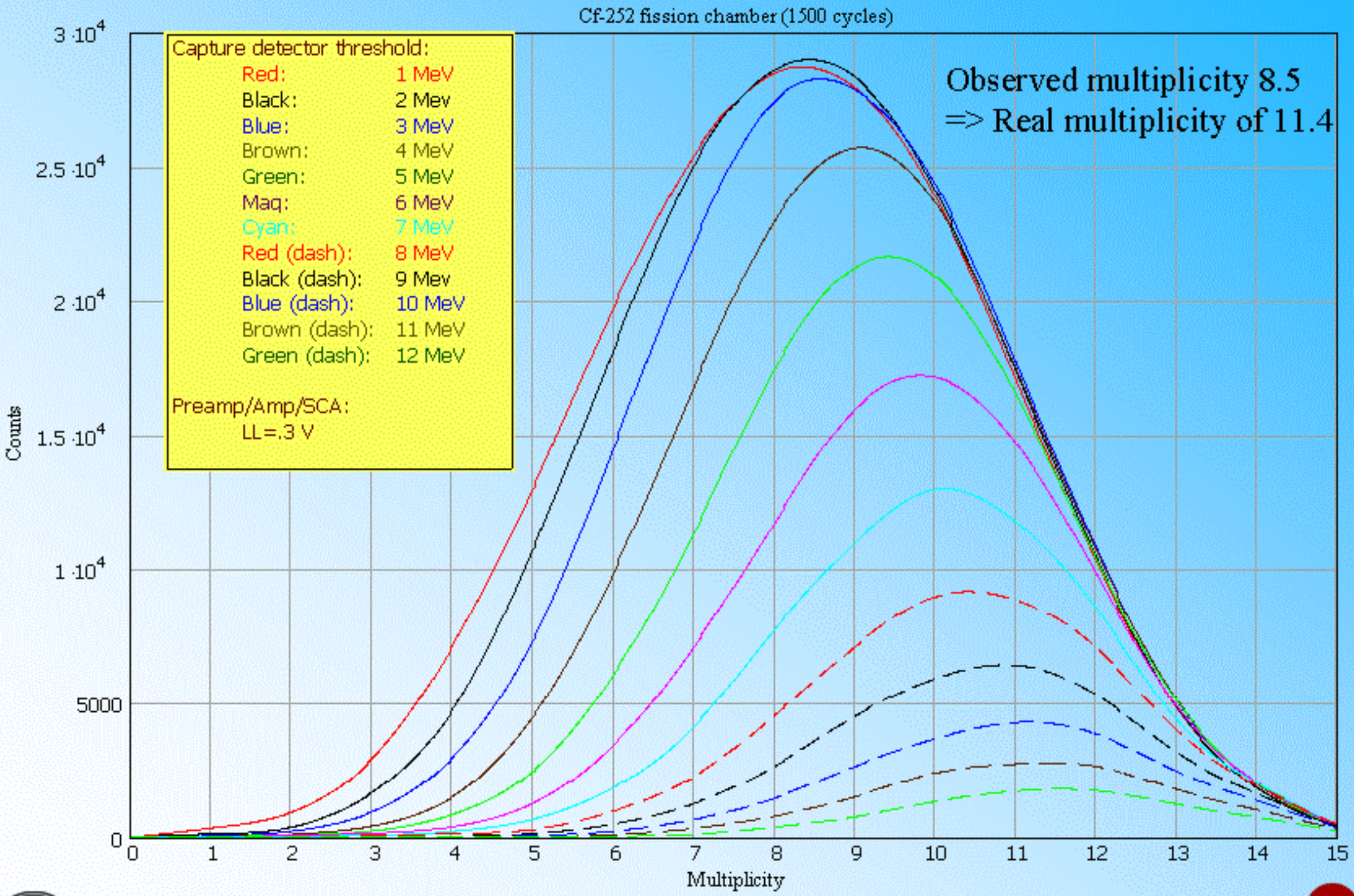

Rensselaer

linac The Gaerttner Laboratory

Future Plans

- Measure U-235 samples (~5-10 mil thick)
  - Obtain fission and capture multiplicities by integrating over resonances.
  - Estimate S/N ratios due to sample activity.
- Design a multi plate fission chamber with thin U-235 foils (~100 $\mu g/cm^2$)

^{235}U Fission and Capture Cross Sections

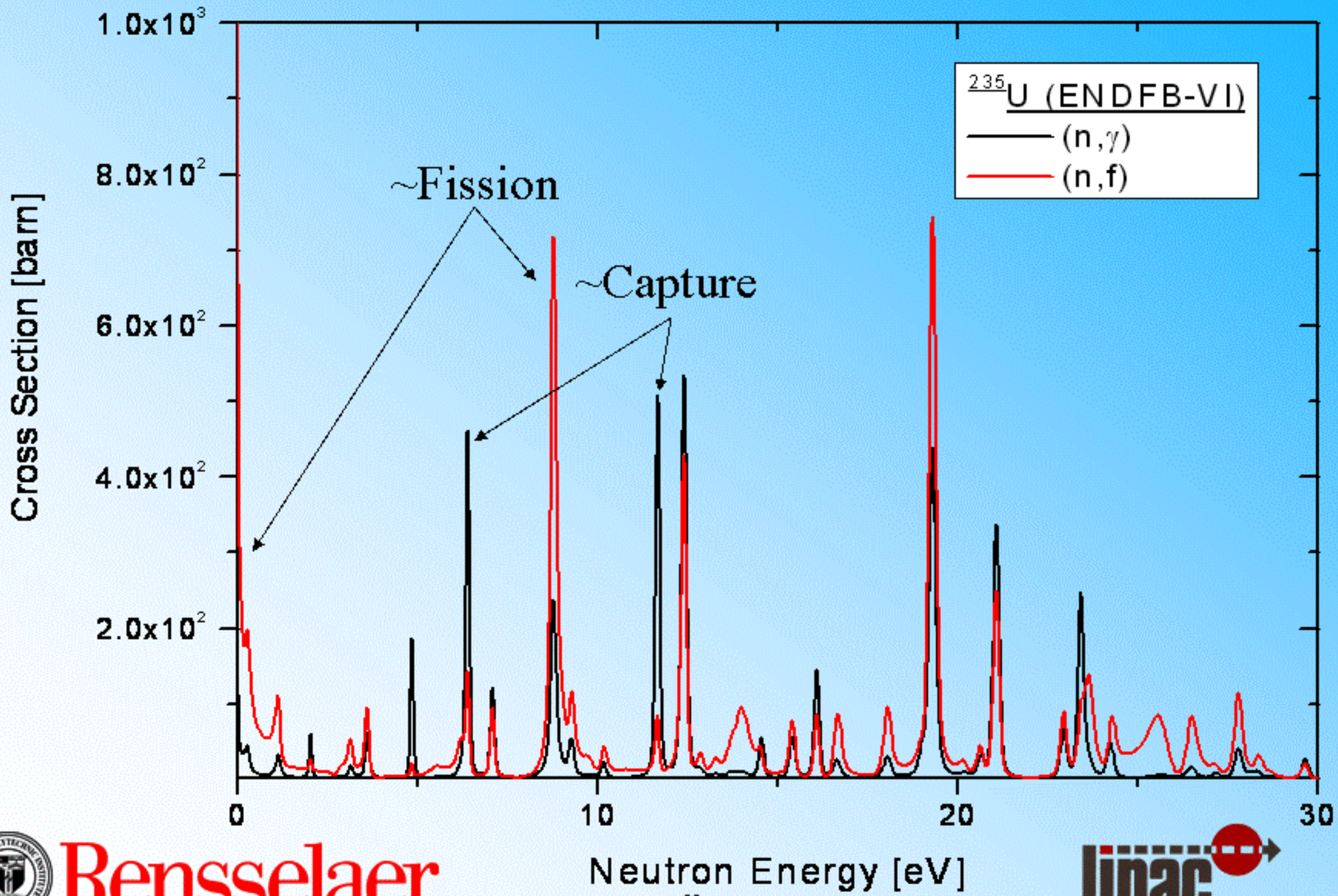

Rensselaer

linac The Gaerttner Laboratory

Contribution by

Lee Bernstein

Lawrence Livermore National Lab.
bernstein2@llnl.gov

19 pages

Measuring Charged Particles Using Silicon Detectors @ DANCE

L. A. Bernstein
LLNL

Workshop on New Opportunities and Research Challenges using DANCE
February 2-4, 2004

This work was performed under the auspices of the U.S. Department of Energy by the University of California, Lawrence Livermore National Laboratory under Contract No. W-7405-Eng-48.

Two major classes of experiments using particle detectors @ DANCE

- **Stand-alone measurements (no BaF data)**
  - **(n,p/α/e/f) ⇐ ^{48}V(n,p)**
- **Complementary measurements with γ-rays**
  - **(n,fγ) coincidence (Vieira, Wilhelmy, Ethvignot talks)**
  - **(n,p/α/e/f+γ) ⇐ ^{236}U(n,f), ^{236}U(n,e)**
- **Silicon might not be the right choice for p-, p-γ**
  - **High energy resolution might not be necessary**
  - **Expensive compared to Solar Cells**
  - **Large costs for new wafer designs**

The Basic Idea

- **Locate a particle detector array at DANCE for particle-TOF, particle-γ and fission-γ studies.**
- **Particles have a number of advantages for use with radioactive targets and neutron beams:**
  - **Largely insensitive to background from γ-rays.**
  - **Detectors tend to be resistant to neutron damage.**
  - **Target backing may not introduce any background.**
- **Particle detectors can be easily added as an "inner ball" to large γ-ray detector arrays (talk to Demetrios!).**
- **"Straw man" design for flexibility. Not ideal for all cases**

One option based on the detectors used in STARS (Silicon Telescope Array for Reaction Studies)

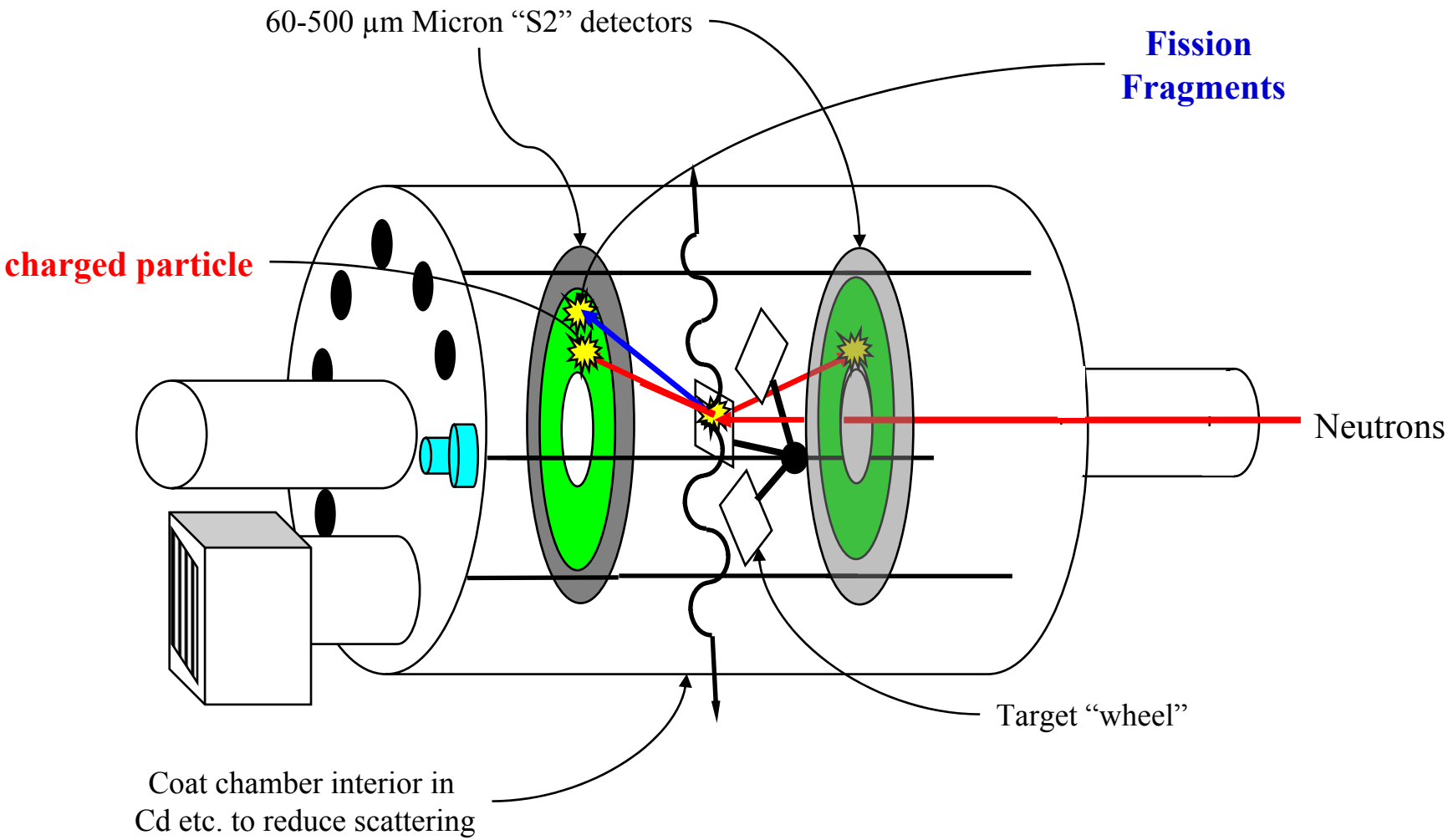

The Micron Double-sided "S2" Si detector

Characteristics:

- Inner(Outer) radius 11(35) mm
- 48 rings (0.5mm pitch)
- 16 sectors (22.5°/segment)
- Thickness = 60-1000 μm
- Resolution: 40 keV @ 5 MeV

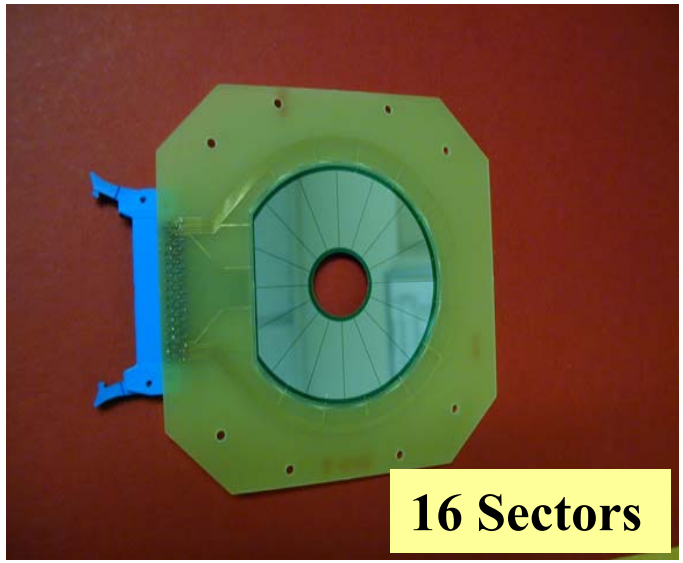

For a target-detector distance of 13.4 mm:

- Minimum angle front + back : 39.38°
- Maxímum angle front + back : 63.20°
- Solid angle coverage: 17.64% of 4π

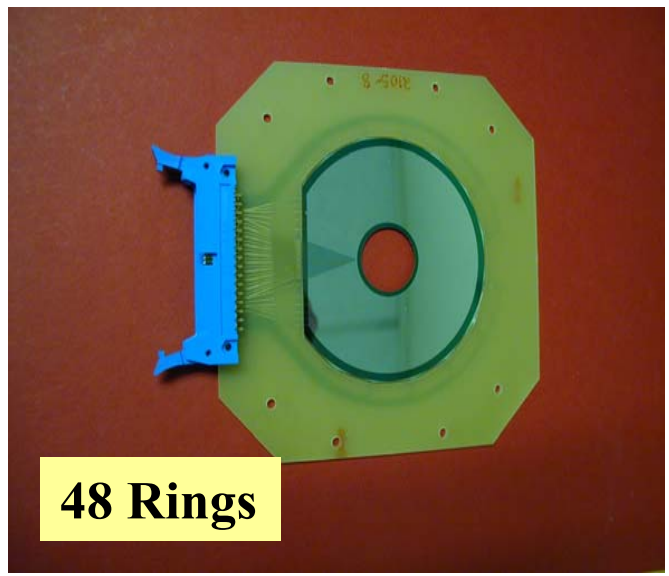

STARS at GAMMASHPERE

STARS at GAMMASPHERE

Back of STARS chamber

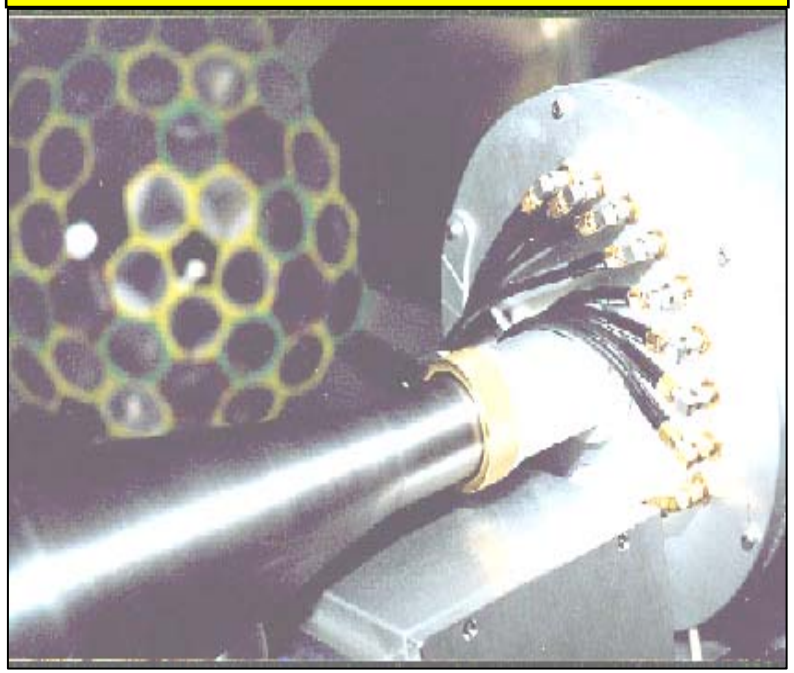

Currently located at Yale for use with YRAST ball

Silicon Detectors could last a long time at DANCE

Effects of Radiation in Silicon Detectors				
Threshold Doses (particles/cm^2)				
Electrons	Fast Neutrons	Protons	α's	Fission Fragments
10^{13}	10^{12}	10^{10}	10^{9}	10^{8}
Not an issue			Could be a problem for Actinide Targets	

For STARS (S2) detectors this equals

Protons	α's	Fission Fragments
3.48×10^{11}	3.48×10^{10}	3.48×10^{9}

First Example: $^{48}V(n,p)$, (n,α)

- The production of ^{48}V ($t_{1/2}$=16 days) by $^{48}Ti(p,n)$ is a charged-particle monitor.
- ^{48}V is destroyed by low-energy neutrons via:
  - $^{48}V(n,\gamma)^{49}V$ (Q=11.553 MeV)
  - $^{48}V(n,p)^{48}Ti$ (Q=4.795 MeV)
  - $^{48}V(n,\alpha)^{45}Sc$ (Q=2.241 MeV) (likely to be small)
- The last two cross sections cannot be determined radiochemically since they result in stable nuclei
- STAPRE calculations indicate that (n,p) is dominant at low energies.

Neutron-induced destruction of ^{48}V

(STAPRE calculations courtesy of R.D. Hoffman/F.S. Dietrich)

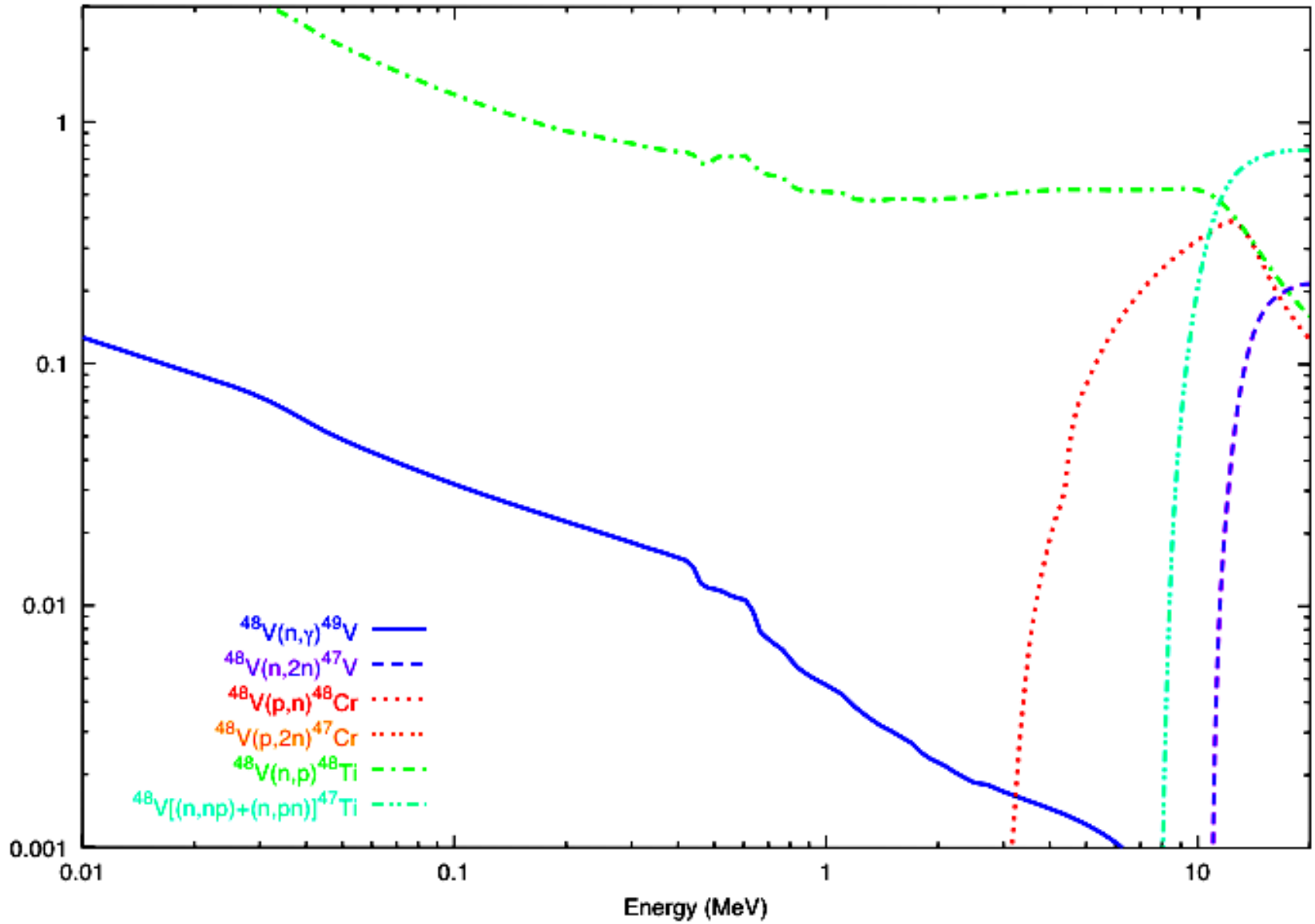

Neutron-induced Reactions on ^{48}V

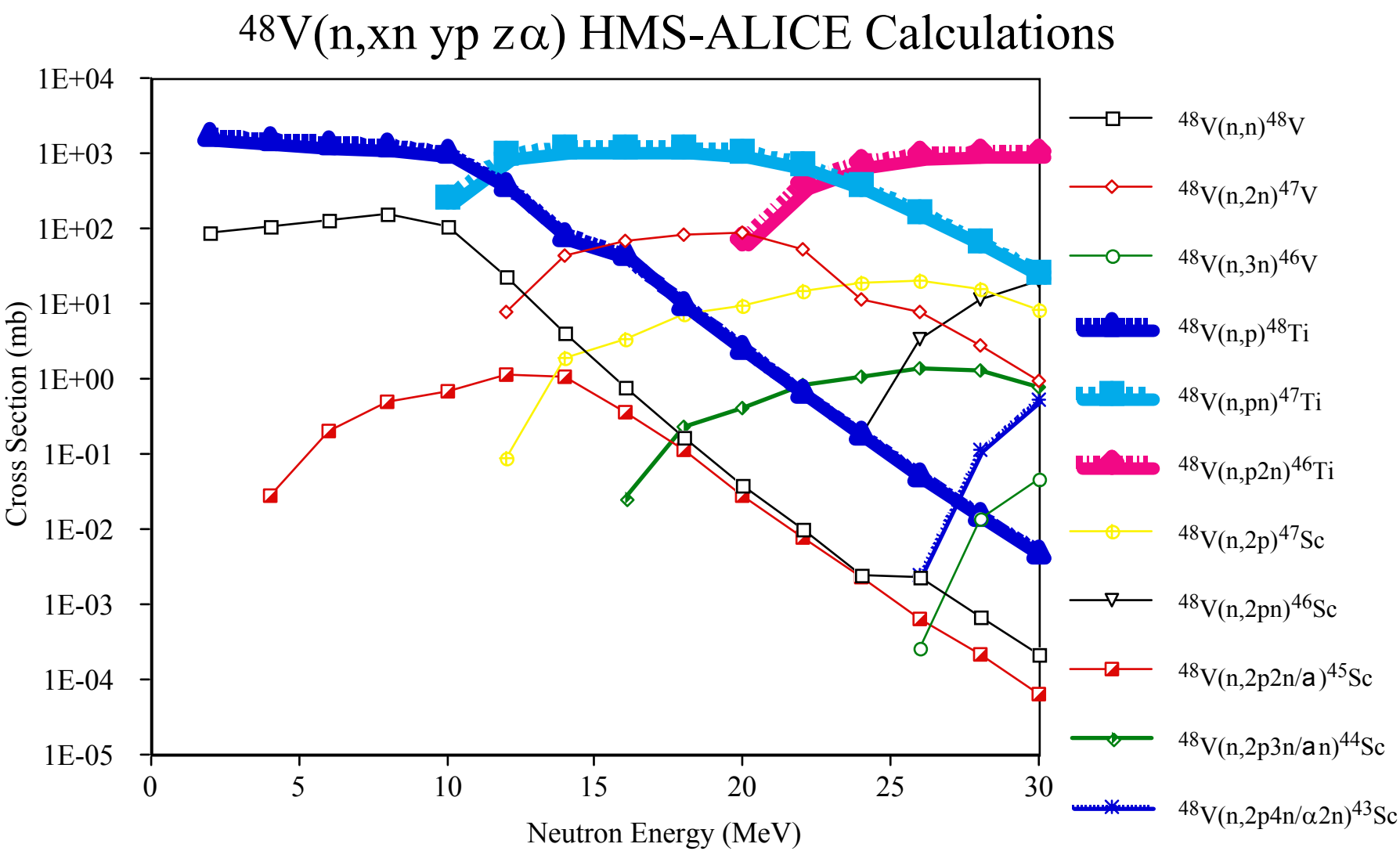

The ^{48}V Target

- Use a medical cyclotron to make the target via $^{48}Ti(p,n)^{48}V$.
  - A 5 day run @ 400 μa would produce 2 x 10^{18} atoms (0.2 mg)
  - Target Activity = 27 Ci (including a 1.3 MeV γ-ray) !!!
- The target need not be very pure (>90% desirable)
- The ^{48}V would be separated from the target chemically and electroplated (maybe?) on a high-Z backing (Au possibly).
- The LANSCE FP-14 irradiation would take place shortly after target preparation.
- Effect of the large γ-ray decay background on the Si detectors is uncertain.
- No charged-particle background from target backing

Clearly NOT a DANCE/BaF measurement

Statistics for $^{48}V(n,p)$

- **Assumptions:**
  - **10^{18} (10^{17}) atom target**
  - **5 day run**
  - **100 µa LANCE current**
  - **Flux = 1.4 x 10^4/E (eV) neutrons/cm^2 s eV**
  - **35% Particle Efficiency**
  - **1 keV energy bin**

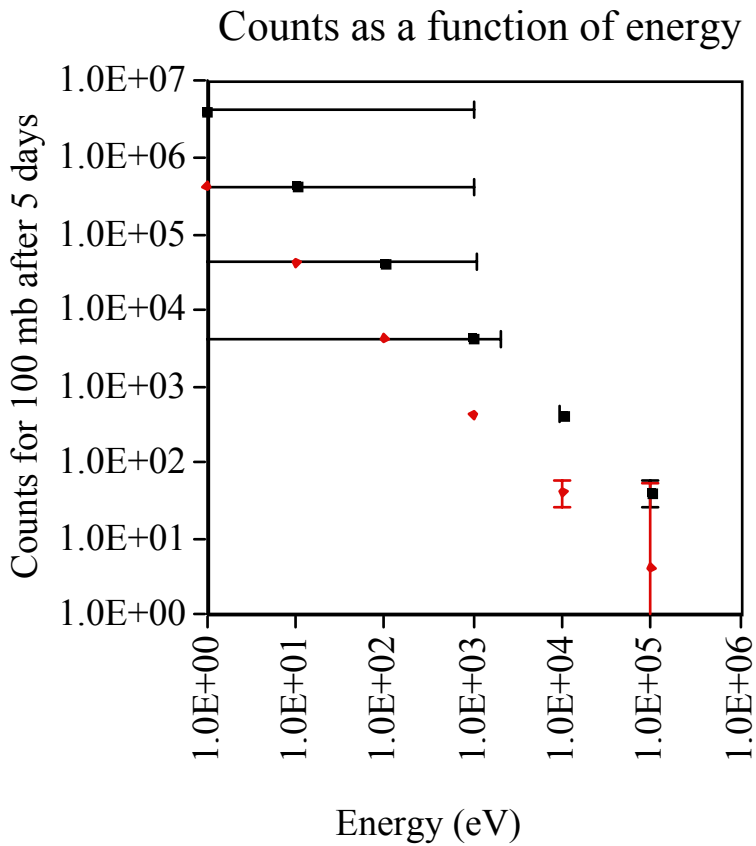

Reasonable Measurements could be made from 1-50 keV

Reactions with charged particle exit channels are strong competitors with (n,2n) for A=90 nuclei too

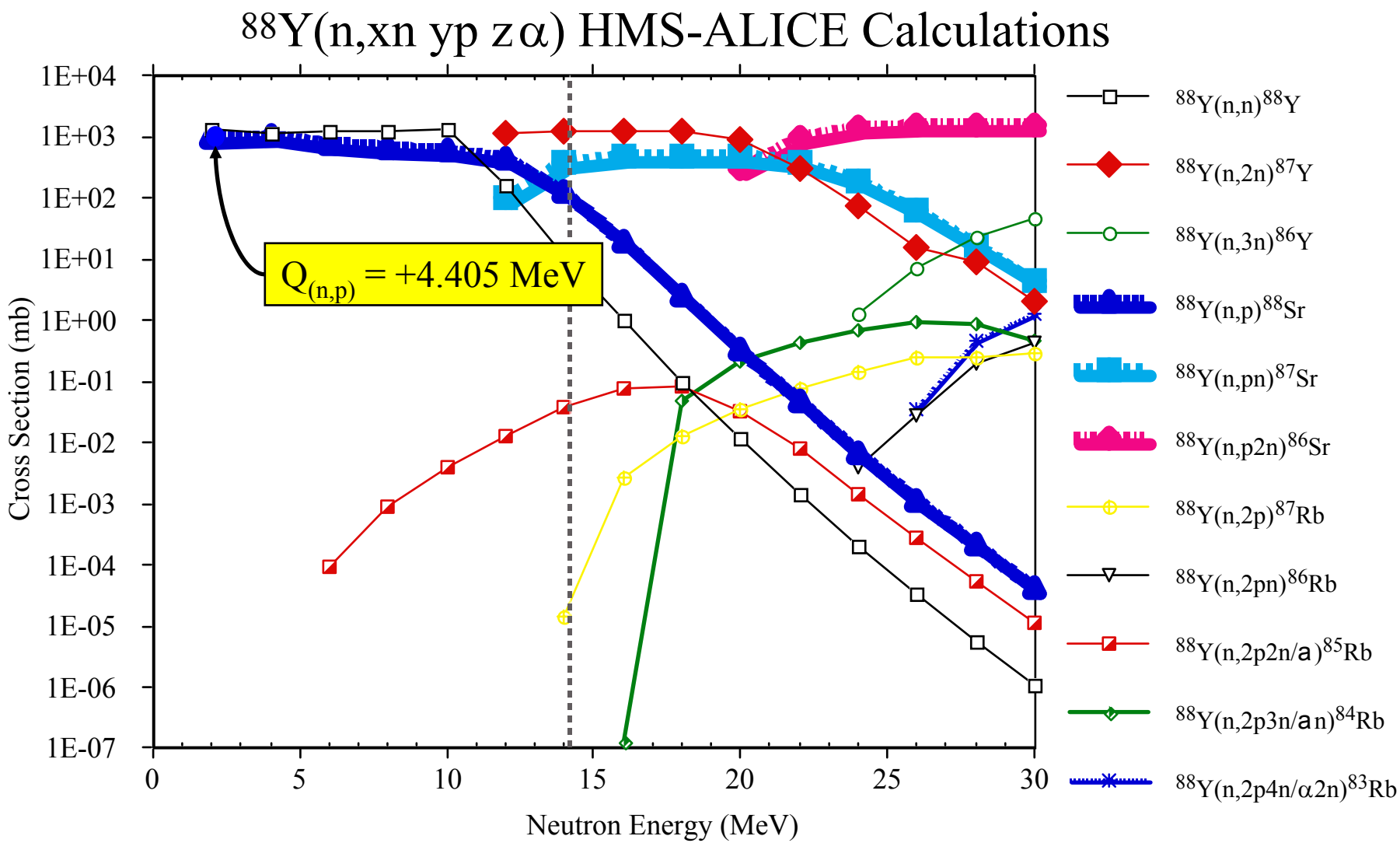

Second Example: $^{236}U(n,f)$

- **Background from α-decay is not an issue. For a 2 mg/cm^2 target:**
  - **Decay Rate = λN = (1.3×10^{-15} s^{-1})(5.0×10^{18} atoms) = 6.6×10^{3} s^{-1}**

Target lifetimes ≥ 10^4 years could be used

- **Mass of the fission fragments could be determined via p-γ "secondary" TOF:**
  - **Measure energy using the particle detector (≈$mv^2/2$)**
  - **Measure velocity using TOF and angular info ($\vec{v}$)**

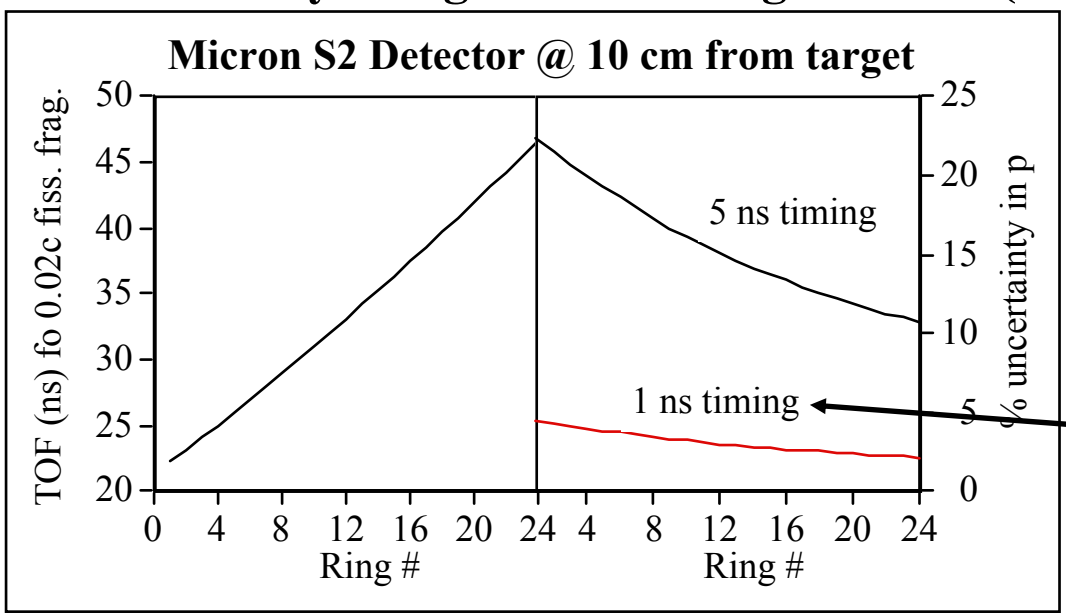

Good timing is a plus

Charged-particle detectors for conversion electron measurements

- **Actinides (especially odd-A, odd-odd) have highly converted low-lying transitions that could be measured using Si detectors**
- **These partial cross sections could be combined "GEANIE-style" to determine total (n,γ) using a Hauser-Feshbach reaction code.**
- **Conversion electrons from transitions following α-decay would be the primary source of background.**
- **DANCE γ-ray tag could help clean-up this data.**
- **Good resolution is essential.**

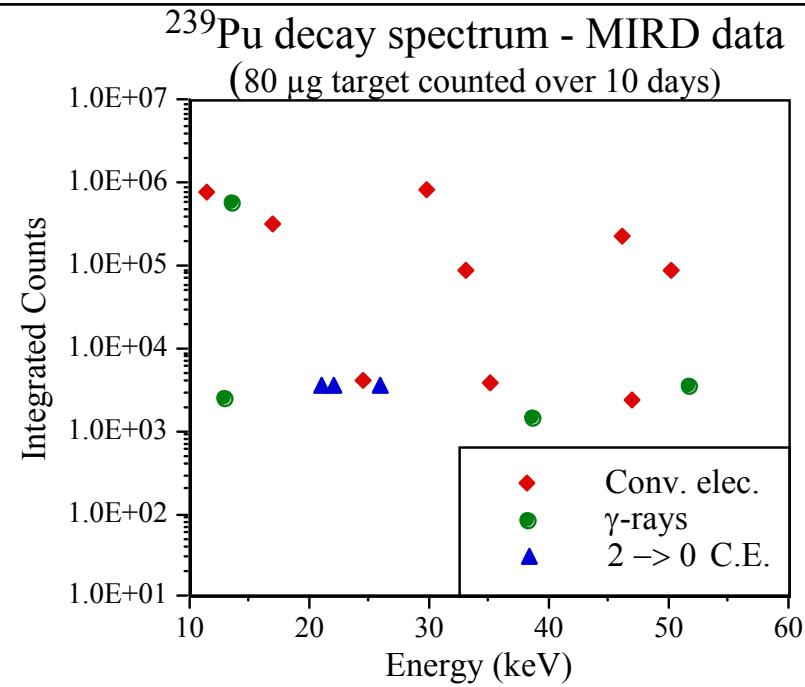

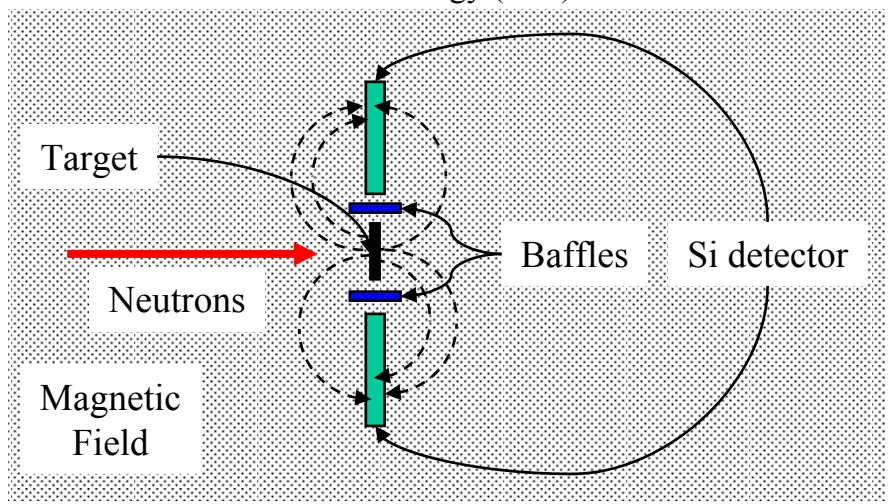

CERN-ISOLDE* γ-gated electron spectrum (^{229}Ra)

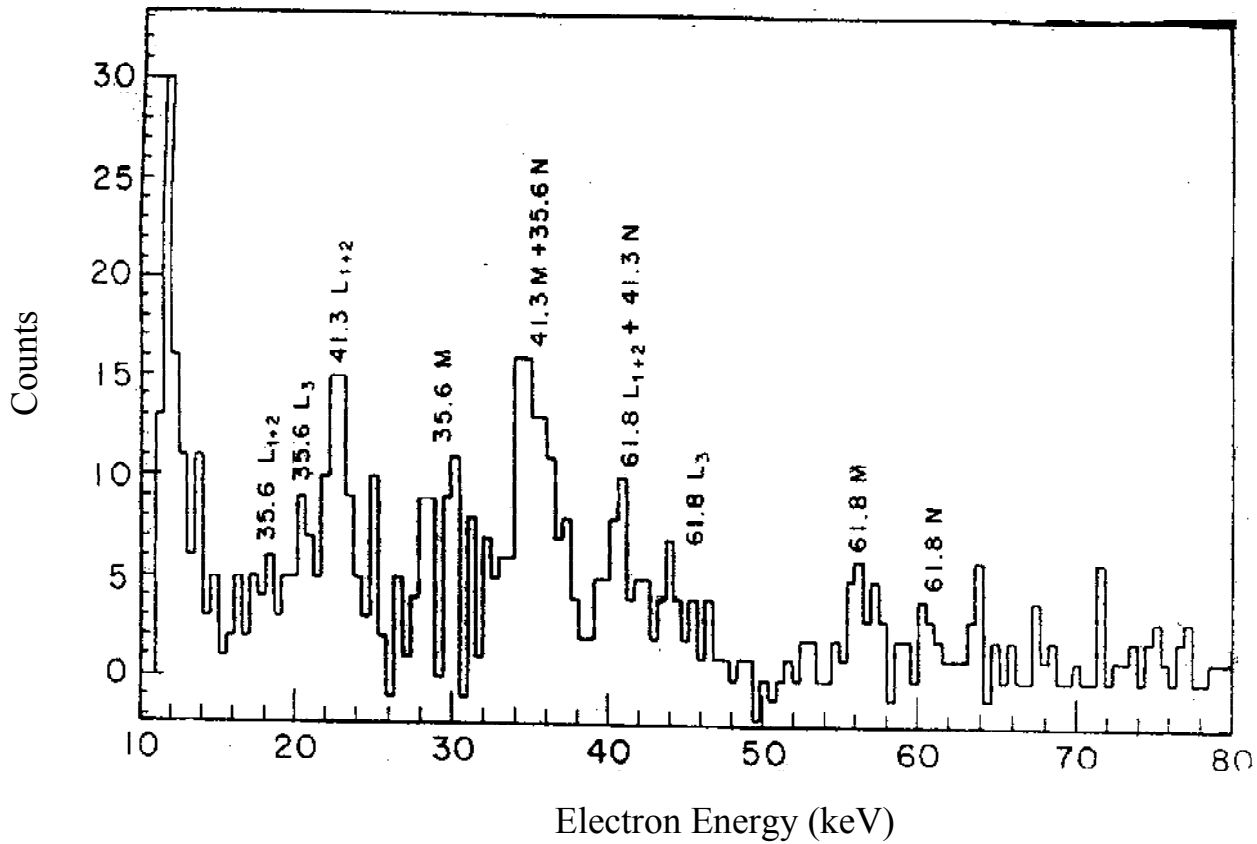

*L.M. Fraile et al., Nucl. Phys.A657 355 (1999)

Other Candidates

- **Radiochemistry:**
  - **Actinides: Pu, U, Np, Am (these have all been mentioned by others)**
  - **^{52g}Mn(n,p), ^{79,81}Kr(n,p)**
- **Questions:**
  - **What is the maximum γ-ray target background that DANCE can tolerate as a function of E_γ?**
  - **What safety requirements are there for highly radioactive targets (≈ 1-10 Ci)?**
  - **What is the effect of a large γ-ray background on Silicon/Solar Cell detectors?**

Converting Probability to Cross Section

Surrogate* vs. Measured $^{155}Gd(n,\gamma)^{156}Gd$

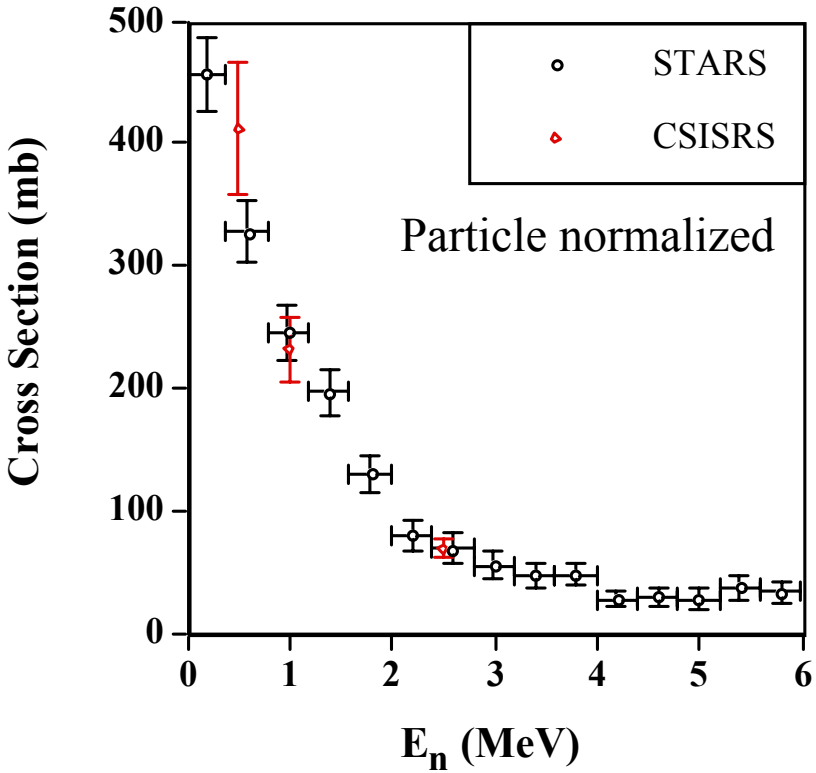

Surrogate* vs. Measured $^{155}Gd(n,2n)^{154}Gd$

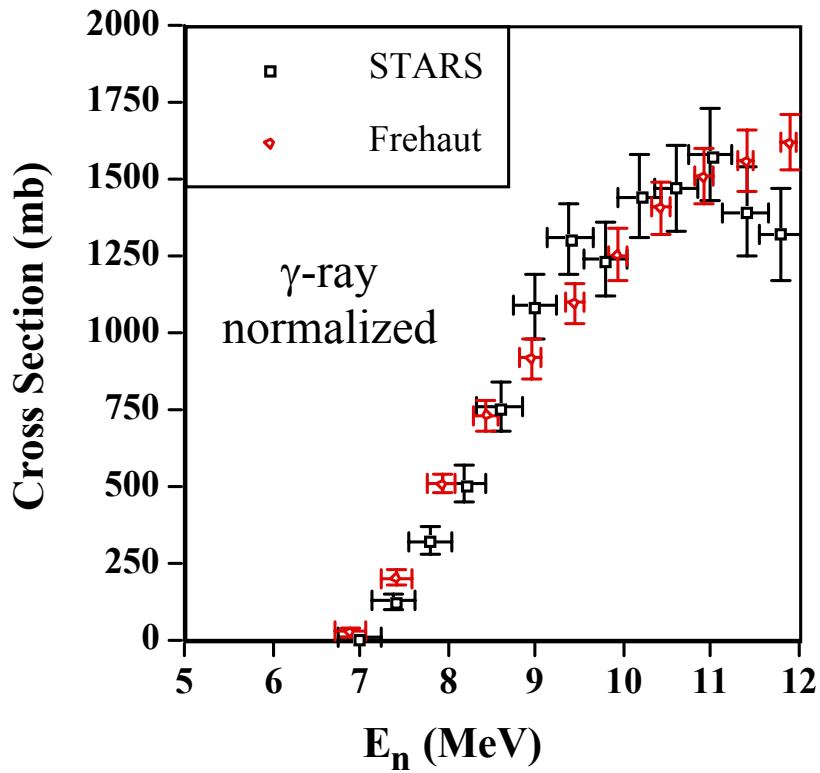

*based on ^{154}Gd and ^{156}Gd $2^+ \rightarrow 0^+$ transitions only

Weisskopf-Ewing Transformation

The Future: Surrogate Measurements at RIA

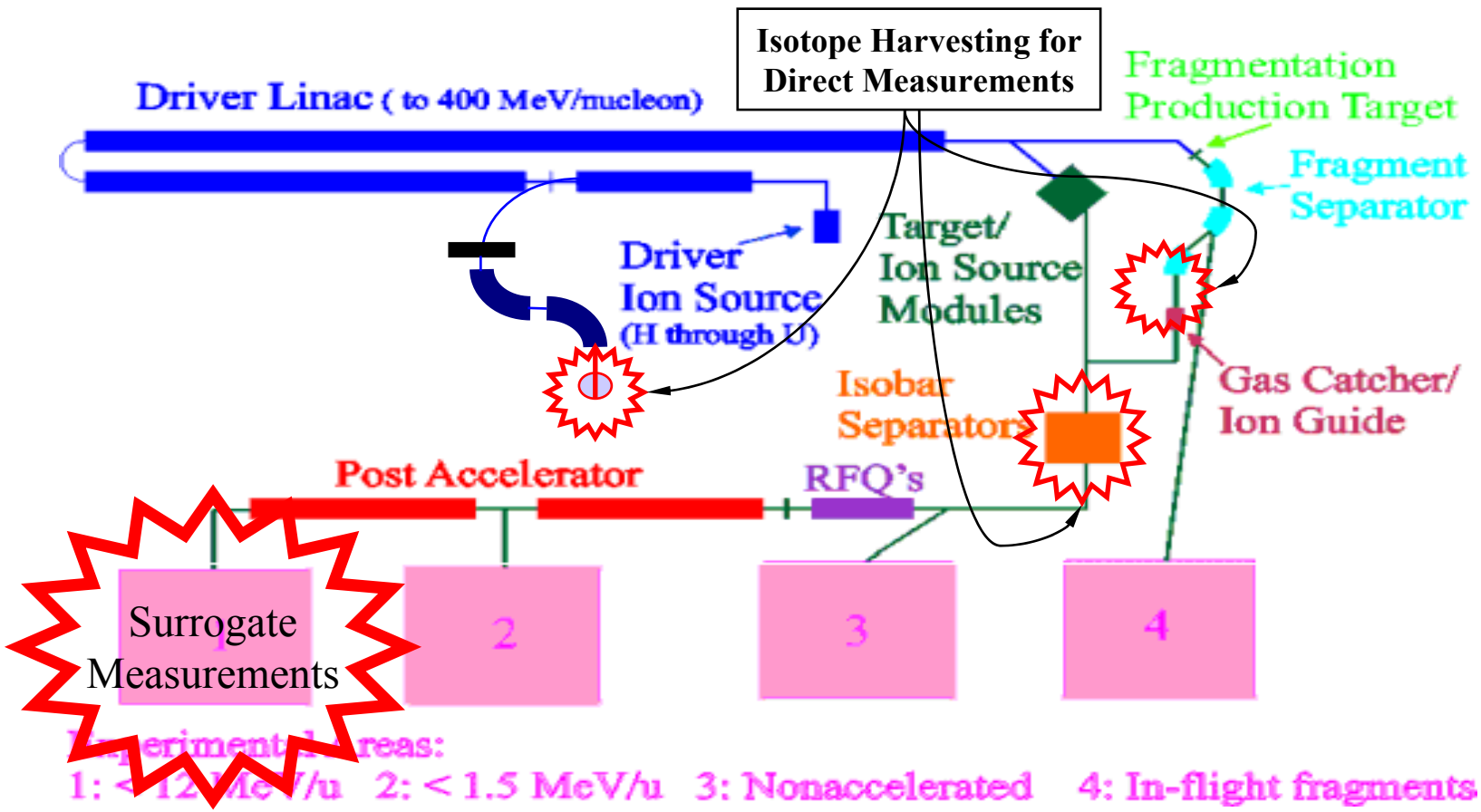

Develop now using stable (and some radioactive) beams

Contribution by

Undraa Agvaanluvsan

NCST / LLNL
agvaanluvsan1@llnl.gov

11 pages

Resonances and nuclear average properties using DANCE

U. Agvaanluvsan[1,2,3], L. Ahle[3], J.A. Becker[3],
L.A. Bernstein[3], P.E. Garrett[3], D. Hoffman[5], G.E. Mitchell[1,2],
W.E. Parker[3], R. Reifarth[4], J. Scwantes[5], J. Ullmann[4]
and the DANCE collaboration

[1]North Carolina State University, Raleigh, NC
[2]Triangle Universities Nuclear Laboratory, Durham, NC
[3]Lawrence Livermore National Laboratory, Livermore, CA
[4]Los Alamos National Laboratory, Los Alamos, NM
[5]University of California, Berkeley, CA

DANCE workshop, Feb 2-4, 2004, Santa-Fe, NM

Outline

- Objectives:
  - Neutron capture cross sections
  - Transmission coefficients
  - Resonance spacings, radiative widths
- Plan: start with simpler cases, proceed to more complicated systems
  - Light targets, e.g. ^{45}Sc, ^{55}Mn
  - Heavy targets, e.g. ^{151}Eu, ^{153}Eu, ^{nat}Eu
  - Unstable targets, e.g. ^{155}Eu

  All Eu targets are fabricated at UC Berkeley

  by J. Scwantes, D. Hoffman et al.

  Analysis will be joint effort of Academic Alliance projects

Neutron capture cross section

- Low energy -- resonance region
  - R-matrix fitting
    Energy, quantum numbers, widths
    - $D = \Delta E/N$
      Note: D subject to accuracy in N
    - $S_0 = \Sigma\Gamma/\Delta E$
      S_0 more reliable because of distribution, larger 50% N ~ 90% strengh
      - S_0 can be compared with model predictions which in turn can be used for normalization* at higher E
- High energy -- smooth region
  - Need to subtract background accurately
    *might rely on theoretical calculation

Target	Abund. % or Half-life	Q-value keV	$\sigma(n,\gamma)$ mb	Note
^{45}Sc	100	8760	69 ± 5	Data taken
^{151}Eu	47.9	6307	3775 ± 150	Run scheduled Feb 10 – 17
^{153}Eu	52.1	6442	2780 ± 100	Run scheduled Feb 10 – 17
^{Nat}Eu				Run scheduled Feb 10 – 17
^{155}Eu	4.9y	6338		Future

^{45}Sc

- Experiment performed in 2003
- $J^{\pi} = 7/2^{-}$, D = 1.33 ± 0.08 keV,
  Γ_{γ} = 0.84 ± 0.46 eV
- One of many data sets with stable targets
  ^{51}V, ^{55}Mn, ^{63,65}Cu, ^{85,87}Rb, ^{139}La, ^{169}Ho … of interest to astrophysics
- Isotopically pure, thus results may be simpler to interpret.

151, 153, Nat Eu

- Experiment scheduled for Feb 10 - 17, 2004
- Data relevant for stockpile stewardship science
- ^{151}Eu: $J^{\pi} = 5/2^{+}$, D = 0.73 ± 0.07 eV,

  Γ_{γ} = 0.092 ± 0.012 eV
- ^{153}Eu: $J^{\pi} = 5/2^{+}$, D = 1.1 ± 0.2 eV

  Γ_{γ} = 0.095 ± 0.012 eV
- Discrepancy in existing data, thus need for independent measurement

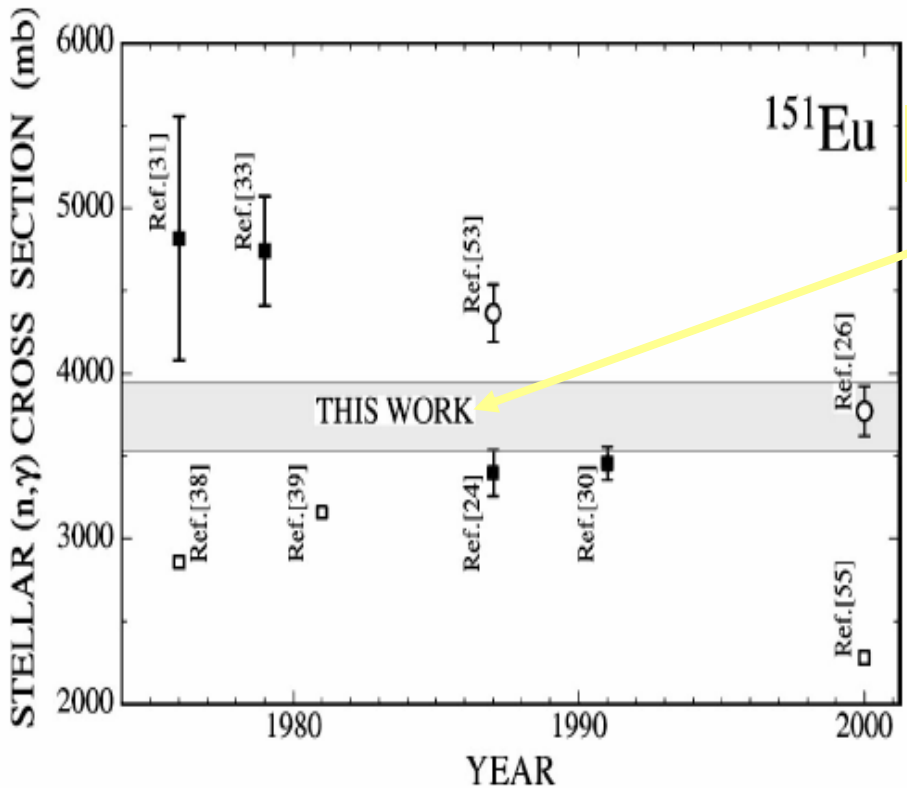

J. Best et al. PRC 64, 015801 (2001)

FIG. 7. The 30 keV (n,γ) cross section of ^{151}Eu (extrapolated from the measured 25 keV data, shaded band) compared to previous measurements (black squares), theoretical calculations (open squares), and evaluated data (open circles).

Properties of the γ – ray cascade

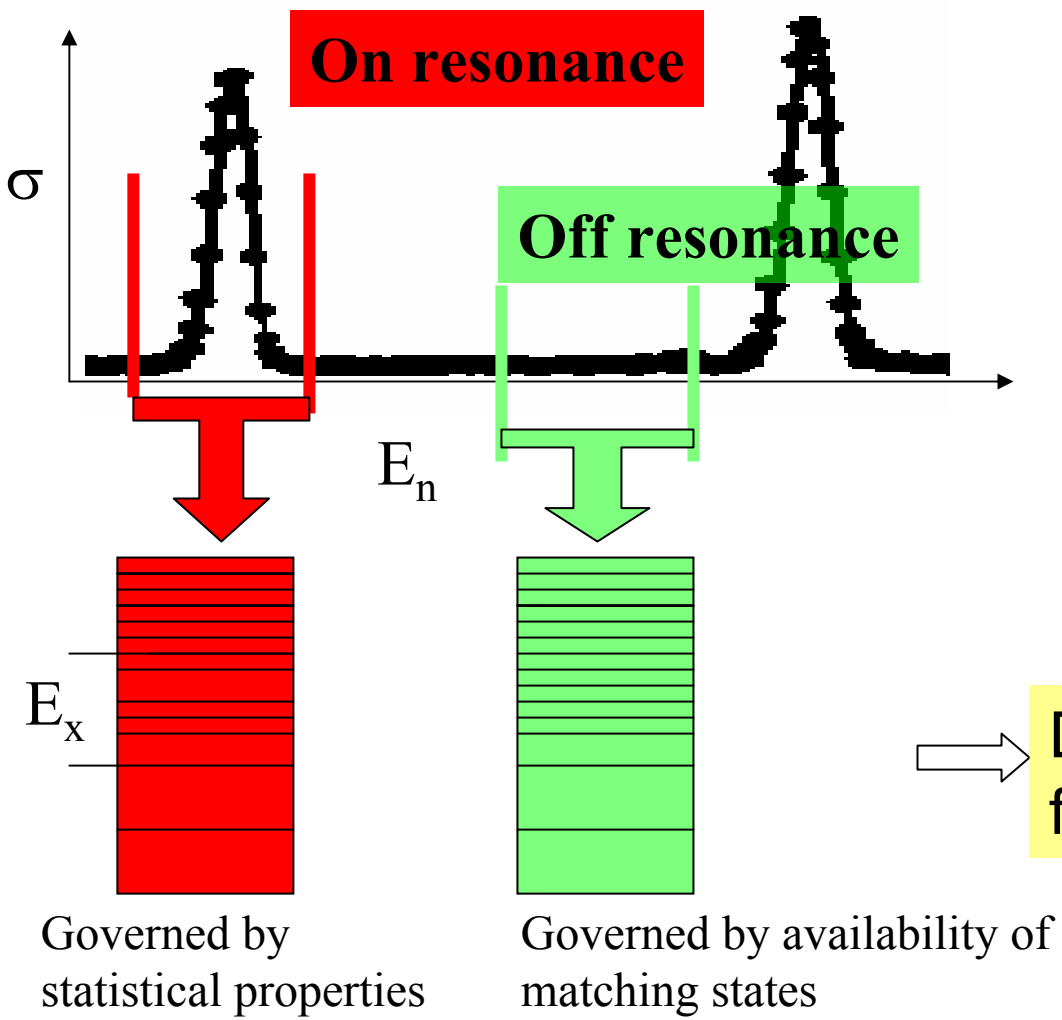

- Although cascades following resonant capture is widely studied, transition in the quasicontinuum not understood
- Cascades between resonances hardly investigated

DANCE may be suitable for such studies

Test and evaluate various possibilities

- Since γ-ray decay probability depend on nuclear level density and radiative strength functions, explore DANCE for suitable experiments

- Adding high resolution Ge detectors, coupled with DANCE calorimeter capacity, new methods to study cascade properties may be possible

- Multiplicity, correlation …

To obtain accurate radiative widths, neutron widths Γ_n needed

Resonance area $$A_\gamma = \frac{g\Gamma_n\Gamma_\gamma}{\Gamma_n + \Gamma_\gamma}$$ is determined from fit

Γ_n can be obtained from data or can be calculated.

Average capture cross section

$$\sigma_\gamma = \Sigma \text{ (capture area)} / \Delta E$$

where

$$\text{capture area} \sim A_\gamma / E_{resonance}$$

Outlook

- The first step is to understand the system, set necessary tools to facilitate the analysis (for this purpose, stable targets may be suitable)
- Obtain valuable cross section results for unstable nuclei
- Data contain wealth of information --> test and explore ways to use data to extract various quantities